

NUREG/CR-3208
LA-9700-MS

Los Alamos National Laboratory is operated by the University of California for the United States Department of Energy under contract W-7405-ENG-36.

TRAC-PD2
Developmental Assessment

Los Alamos Los Alamos National Laboratory
Los Alamos, New Mexico 87545

8504160087 850430
PDR NUREG
CR-3208 R PDR

An Affirmative Action/Equal Opportunity Employer

Prepared by N. Warnes, Group Q-9

NOTICE

This report was prepared as an account of work sponsored by an agency of the United States Government. Neither the United States Government nor any agency thereof, or any of their employees, makes any warranty, expressed or implied, or assumes any legal liability or responsibility for any third party's use, or the results of such use, of any information, apparatus, product or process disclosed in this report, or represents that its use by such third party would not infringe privately owned rights.

TRAC-PD2 Developmental Assessment

Compiled by
Thad D. Knight and Vera Metzger

Contributors

T. F. Bott
J. S. Gilbert
D. A. Mandell
J. K. Meier
J. M. Sicilian*

Manuscript submitted: February 1983
Date published: January 1985

Prepared for
Division of Accident Evaluation
Office of Nuclear Regulatory Research
US Nuclear Regulatory Commission
Washington, DC 20555

NRC FIN No. A7016

*Flow Science Inc., 1325 Trinity Drive, Los Alamos, NM 87544

CONTENTS

FIGURES	viii
TABLES	xvii
ABSTRACT	1
I. INTRODUCTION	2
II. EDWARDS' BLOWDOWN EXPERIMENT	6
A. Experiment Description	6
B. TRAC-PD2 Model	7
C. Data Comparisons	9
D. Conclusions	9
III. CISE BLOWDOWN EXPERIMENT	14
A. Experiment Description	14
B. TRAC-PD2 Model	16
C. Data Comparisons	16
D. Conclusions	20
IV. MARVIKEN FULL-SCALE CRITICAL-FLOW TESTS 4 AND 24	28
A. Experiment Description	28
B. TRAC-PD2 Model	28
C. Data Comparisons	35
D. Conclusions	43
V. THTF TEST 177 BLOWDOWN EXPERIMENT	44
A. Experiment Description	44
B. TRAC-PD2 Model	45
C. Data Comparisons	45
D. Conclusions	51
VI. BENNETT TUBE EXPERIMENTS	52
A. Experiment Description	52
B. TRAC-PD2 Model	52
C. Results	52
VII. CREARE COUNTERCURRENT-FLOW EXPERIMENTS	62
A. Experiment Description	62
B. TRAC-PD2 Model	62
C. Data Comparisons	64
D. TRAC-PD2 Features Tested	67
E. Input Data Decks	67
VIII. FLECHT FORCED-FLOODING EXPERIMENTS	68
A. Experiment Description	68
B. TRAC-PD2 Model	68
C. Results	70

CONTENTS (cont.)

IX.	SEMISCALE MOD-1 TEST S-02-8	74
	A. Experiment Description	74
	B. TRAC-PD2 Model	75
	C. Data Comparisons	77
	D. Conclusions	81
X.	SEMISCALE NOZZLE	85
	A. TRAC-PD2 Model	85
	B. Results	86
	C. Conclusions	89
XI.	SEMISCALE MOD-1 TEST S-06-3	90
	A. Experiment Description	90
	B. TRAC-PD2 Model	90
	C. Data Comparisons	91
	D. Conclusions	104
XII.	LOFT NONNUCLEAR EXPERIMENT L1-4	105
	A. Experiment Description	105
	B. TRAC-PD2 Model	106
	C. TRAC-Calculated Results	106
	1. Steady-State Results	106
	2. Transient Results	112
	D. Parametric Studies	122
	E. TRAC-PD2 Features Tested	122
	F. Input Data Decks	122
XIII.	LOFT NUCLEAR EXPERIMENT L2-2	123
	A. Experiment Description	123
	B. TRAC-PD2 Model	124
	C. TRAC-Calculated Results	128
	1. Steady-State Results	128
	2. Transient Results	128
	a. Fluid Results	136
	i. Intact-Loop Results	136
	ii. ECCS Results	140
	iii. Broken-Loop Results	143
	iv. Additional Calculated Results	149
	b. Rod Temperature Results	149
	i. Central Fuel Module	152
	ii. Second Radial Zone	161
	D. Parametric Studies	161
	E. TRAC-PD2 Features Tested	171
	F. Conclusions and Recommendations	171
	G. Input Data Decks	171
XIV.	CONCLUSIONS	172
	REFERENCES	174

CONTENTS (cont.)

APPENDIX A.	TRAC INPUT DECK FOR EDWARDS' BLOWDOWN EXPERIMENT	177
APPENDIX B.	TRAC INPUT DECKS FOR CISE BLOWDOWN EXPERIMENTS (TESTS 4 AND R)	179
I.	TRAC INPUT DECK FOR CISE UNHEATED BLOWDOWN EXPERIMENT (TEST 4)	179
II.	TRAC INPUT DECK FOR CISE HEATED BLOWDOWN EXPERIMENT (TEST R)	182
APPENDIX C.	TRAC INPUT DECKS FOR MARVIKEN TESTS 4 AND 24	185
I.	TRAC INPUT DECK FOR MARVIKEN TEST 4	185
II.	TRAC INPUT DECK FOR MARVIKEN TEST 24	187
APPENDIX D.	TRAC STEADY-STATE AND TRANSIENT INPUT DECKS FOR THTF TEST 177	189
I.	TRAC STEADY-STATE INPUT DECK FOR THTF TEST 177	189
II.	TRAC TRANSIENT INPUT DECK FOR THTF TEST 177	204
APPENDIX E.	TRAC STEADY-STATE INPUT DECKS FOR BENNETT RUNS 5442, 5431, 5336	207
I.	TRAC STEADY-STATE INPUT DECK FOR BENNETT RUN 5442	207
II.	TRAC STEADY-STATE INPUT DECK FOR BENNETT RUN 5431	208
III.	TRAC STEADY-STATE INPUT DECK FOR BENNETT RUN 5336	209
APPENDIX F.	TYPICAL TRAC STEADY-STATE AND RESTART INPUT DECKS FOR CREARE COUNTERCURRENT-FLOW EXPERIMENTS	210
I.	TYPICAL TRAC INPUT DECK FOR CREARE STEADY-STATE RUN	210
II.	TYPICAL TRAC RESTART INPUT DECK FOR CREARE TRANSIENT RUN	221
APPENDIX G.	TRAC TRANSIENT INPUT DECK FOR FLECHT TEST 17201	222
APPENDIX H.	TRAC STEADY-STATE AND TRANSIENT INPUT DECKS FOR SEMISCALE MOD-1 TEST S-02-8	237
I.	TRAC STEADY-STATE INPUT DECK FOR SEMISCALE MOD-1 TEST S-02-8	237
II.	TRAC TRANSIENT RESTART INPUT DECK FOR SEMISCALE MOD-1 TEST S-02-8	255
APPENDIX I.	TRAC STEADY-STATE AND TRANSIENT INPUT DECKS FOR SEMISCALE MOD-1 TEST S-06-3	259
I.	TRAC STEADY-STATE INPUT DECK FOR SEMISCALE MOD-1 TEST S-06-3	259
II.	TRAC TRANSIENT RESTART INPUT DECK FOR SEMISCALE MOD-1 TEST S-06-3	282
III.	TRAC TRANSIENT RESTART INPUT DECK WITH RENODED BROKEN-LOOP COLD LEG FOR SEMISCALE MOD-1 TEST S-06-3	287

CONTENTS (cont.)

APPENDIX J.	TRAC STEADY-STATE AND TRANSIENT INPUT DECKS FOR LOFT NONNUCLEAR EXPERIMENT L1-4	289
I.	TRAC STEADY-STATE INPUT DECK FOR LOFT NONNUCLEAR EXPERIMENT L1-4	289
II.	TRAC TRANSIENT INPUT DECK FOR LOFT NONNUCLEAR EXPERIMENT L1-4	318
APPENDIX K.	TRAC STEADY-STATE AND TRANSIENT INPUT DECKS FOR LOFT EXPERIMENT L2-2	319
I.	TRAC STEADY-STATE INPUT DECK FOR LOFT EXPERIMENT L2-2 . . .	319
II.	TRAC TRANSIENT INPUT DECK INCLUDING THE BLOWDOWN, REFILL, AND REFLOOD FOR LOFT EXPERIMENT L2-2	353

FIGURES

1. Edwards' blowdown-experiment configuration (adapted from Ref. 2)	6
2. TRAC component diagram for Edwards' blowdown experiment	7
3. TRAC noding diagram for components 2 and 3	7
4. TRAP-generated noding diagram of PIPE 2 for Edwards' blowdown experiment	8
5. TRAP-generated noding diagram of PIPE 3 for Edwards' blowdown experiment	8
6. Pressure at GS-1 for Edwards' blowdown experiment	10
7. Pressure at GS-5 for Edwards' blowdown experiment	10
8. Pressure at GS-6 for Edwards' blowdown experiment	11
9. Pressure at GS-7 for Edwards' blowdown experiment	11
10. Liquid temperature at GS-5 for Edwards' blowdown experiment	12
11. Void fraction at GS-5 for Edwards' blowdown experiment	12
12. CISE test section (adapted from Ref. 6)	14
13. CISE test-section geometry	15
14. TRAC model of CISE blowdown experiments	17
15. Typical TRAC noding of CISE blowdown experiments	17
16. TRAP-generated noding diagram of PIPE 2 for CISE blowdown experiment	17
17. TRAP-generated noding diagram of PIPE 3 for CISE blowdown experiment	18
18. TRAP-generated noding diagram of PIPE 4 for CISE blowdown experiment	18
19. TRAP-generated noding diagram of PIPE 5 for CISE blowdown experiment	19
20. Pressure at measurement station P7 for unheated CISE experiment	21
21. Pressure at measurement station P7 for heated CISE experiment	21
22. Pressure at measurement station P4 for unheated CISE experiment	22
23. Pressure at measurement station P4 for heated CISE experiment	22
24. Liquid temperature at measurement station TF7 for unheated CISE experiment	23
25. Liquid temperature at measurement station TF7 for heated CISE experiment	23
26. Liquid temperature at measurement station TF4 for unheated CISE experiment	24
27. Liquid temperature at measurement station TF4 for heated CISE experiment	24
28. Wall temperature at measurement station THW4 for unheated CISE experiment	25
29. Wall temperature at measurement station THW4 for heated CISE experiment	25
30. Test-section mass flow for unheated CISE experiment	26
31. Test-section mass flow for heated CISE experiment	26
32. Pressure vessel for Marviken Tests 4 and 24	29

FIGURES (cont.)

33.	Discharge pipe, test nozzle, and rupture-disk assembly for Marviken Tests 4 and 24	30
34.	TRAC nodding diagram of vessel and discharge pipe for Marviken Tests 4 and 24	31
35.	TRAC nodding diagram of nozzle and rupture-disk assembly for Marviken Test 4	31
36.	TRAC nodding diagram of nozzle and rupture-disk assembly for Marviken Test 24	32
37.	TRAP-generated nodding diagram of PIPE 2 for Marviken Test 4	32
38.	TRAP-generated nodding diagram of PIPE 3 for Marviken Test 4	33
39.	TRAP-generated nodding diagram of PIPE 2 for Marviken Test 24	33
40.	TRAP-generated nodding diagram of PIPE 3 for Marviken Test 24	34
41.	Mass flow for Marviken Test 4	36
42.	Mass flow for Marviken Test 24	36
43.	Pressure at measurement station P103 for Marviken Test 4	37
44.	Pressure at measurement station P106 for Marviken Test 4	37
45.	Pressure at measurement station P109 for Marviken Test 4	38
46.	Pressure at measurement station P103 for Marviken Test 24	38
47.	Pressure at measurement station P106 for Marviken Test 24	39
48.	Pressure at measurement station P109 for Marviken Test 24	39
49.	Liquid temperature at measurement station T401 for Marviken Test 4	40
50.	Liquid temperature at measurement station T402 for Marviken Test 4	40
51.	Liquid temperature at measurement station T405 for Marviken Test 4	41
52.	Liquid temperature at measurement station T401 for Marviken Test 24	41
53.	Liquid temperature at measurement station T402 for Marviken Test 24	42
54.	Liquid temperature at measurement station T405 for Marviken Test 24	42
55.	Oak Ridge National Laboratory THTF	44
56.	Single-channel test-section model of THTF (represents levels D, G, and M, identified in Ref. 9)	46
57.	TRAP-generated model of THTF VESSEL component	47
58.	Axial power profile for THTF Test 177	48
59.	Radial nodding diagram of the heater rod for THTF Test 177	49
60.	Comparison of the TRAC-calculated rod-surface temperatures with the THTF Test 177 measurements. The temperature was measured 1.20 m above the test-section base (level D, identified in Ref. 9)	49
61.	Comparison of the TRAC-calculated rod-surface temperatures with the THTF Test 177 measurements. The temperature was measured 2.22 m above the test-section base (level G, identified in Ref. 9)	50
62.	Comparison of the TRAC-calculated rod-surface temperatures with the THTF Test 177 measurements. The temperature was measured 3.44 m above the test-section base (level M, identified in Ref. 9)	50

FIGURES (cont.)

63.	TRAC model geometry	53
64.	Comparison of the TRAC-calculated wall temperatures with the Bennett Run 5442 data	53
65.	Comparison of the TRAC-calculated wall temperatures with the Bennett Run 5336 data	54
66.	Comparison of the TRAC-calculated wall temperatures with the Bennett Run 5431 data	55
67.	The effect of the boiling-curve interpolation on Bennett Run 5431	55
68.	Noding sensitivity for Bennett Run 5442	56
69.	CHF correlation sensitivity for Bennett Run 5442	57
70.	CHF correlation sensitivity for Bennett Run 5336	57
71.	CHF correlation sensitivity for Bennett Run 5431	58
72.	The effect of the CHF correlation and boiling-curve interpolation on Bennett Run 5336	58
73.	The effect of the CHF correlation and boiling-curve interpolation on Bennett Run 5431	59
74.	The effect of wall friction on Bennett Run 5442	60
75.	TRAC noding for Creare 1/15-scale vessel	63
76.	Comparison of calculated and measured flooding curves for Creare low-subcooling tests	65
77.	Comparison of calculated and measured flooding curves for Creare high-subcooling tests	65
78.	Calculated Creare downcomer liquid mass for the high-subcooling, high steam-flow test	66
79.	Lower-plenum liquid level for the high-subcooling, high steam-flow test	66
80.	TRAC noding diagram of FLECHT forced-flooding experiments	69
81.	Axial power profile for FLECHT Test 4831	69
82.	FLECHT Test 17201 rod-cladding temperatures at the 6-ft elevation compared with the TRAC-calculated temperatures	71
83.	FLECHT Test 17201 rod-cladding temperatures at the 8-ft elevation compared with the TRAC-calculated temperatures	71
84.	FLECHT Test 4831 rod-cladding temperatures at the 4-ft elevation compared with the TRAC-calculated temperatures	72
85.	FLECHT Test 4831 rod-cladding temperatures at the 6-ft elevation compared with the TRAC-calculated temperatures	72
86.	FLECHT Test 4831 total effluent mass compared with the TRAC-calculated effluent mass	73
87.	Isometric view of the Semiscale Mod-1 test apparatus (adapted from Ref. 18)	74
88.	TRAC noding and component diagram for Semiscale Mod-1 system	76
89.	Semiscale Mod-1 nozzle noding diagram	76
90.	Comparison of the calculated and measured lower-plenum pressures for Semiscale Mod-1 Test S-02-8	78
91.	Comparison of the calculated and measured mass flows at the inlet of the broken-loop hot leg for Semiscale Mod-1 Test S-02-8	78

FIGURES (cont.)

92.	Comparison of the calculated and measured mass flows at the outlet of the broken-loop hot leg for Semiscale Mod-1 Test S-02-8	79
93.	Comparison of the calculated and measured broken-loop cold-leg break flows for Semiscale Mod-1 Test S-02-8	79
94.	Comparison of the calculated and measured mass flows in the intact-loop pump for Semiscale Mod-1 Test S-02-8	80
95.	Comparison of the calculated and measured mass flows into the intact-loop hot leg for Semiscale Mod-1 Test S-02-8	80
96.	Comparison of the calculated and measured pressurizer flows for Semiscale Mod-1 Test S-02-8	82
97.	Comparison of the calculated and measured mass flows at the entrance to the core for Semiscale Mod-1 Test S-08-2	82
98.	Comparison of the calculated and measured cladding temperatures in the lower core for Semiscale Mod-1 Test S-02-8	83
99.	Comparison of the calculated and measured cladding temperatures in the middle core for Semiscale Mod-1 Test S-02-8	83
100.	Comparison of the calculated and measured cladding temperatures in the upper core for Semiscale Mod-1 Test S-02-8	84
101.	Volume diagram of Semiscale Test S-02-8 broken-loop cold-leg nozzle	85
102.	Comparison of the upstream pressure boundary condition and the measured pressure for the Semiscale nozzle study	86
103.	Comparison of the upstream void-fraction boundary condition and the measured void fraction for the Semiscale nozzle study	87
104.	Comparison of the upstream density boundary condition and the measured mixture density for the Semiscale nozzle study	87
105.	Comparison of the calculated and measured mass flows for the Semiscale nozzle study	88
106.	Comparison of the calculated and measured mixture velocities for the Semiscale nozzle study	88
107.	TRAC noding diagram of Semiscale Test S-06-3	90
108.	Finely noded break nozzle for Semiscale Test S-06-3	92
109.	Coarsely noded cold-leg break nozzle for Semiscale Test S-06-3	92
110.	Comparison of the TRAC-calculated and measured lower-plenum pressures for Semiscale Test S-06-3	93
111.	Comparison of the TRAC-calculated and measured mass flows at the entrance to the broken-loop cold leg for Semiscale Test S-06-3	94
112.	Comparison of the TRAC-calculated and measured volumetric flows at the entrance to the broken-loop cold leg for Semiscale Test S-06-3	95
113.	Comparison of the TRAC-calculated and measured mass flows at the entrance to the broken-loop hot leg for Semiscale Test S-06-3	95
114.	Volumetric flow at the entrance to the broken-loop hot leg for Semiscale Test S-06-3	96

FIGURES (cont.)

115.	Comparison of the TRAC-calculated and measured mass flows at the entrance to the intact-loop hot leg for Semiscale Test S-06-3	96
116.	Comparison of the TRAC-calculated and measured volumetric flows at the entrance to the intact-loop hot leg for Semiscale Test S-06-3	97
117.	Comparison of the TRAC-calculated and measured mass flows at the pressurizer exit for Semiscale Test S-06-3	97
118.	Comparison of the TRAC-calculated and measured mass flows at the pump exit for Semiscale Test S-06-3	98
119.	Comparison of the TRAC-calculated and measured volumetric flows at the pump exit for Semiscale Test S-06-3	98
120.	Comparison of the TRAC-calculated and measured mixture velocities at the accumulator exit for Semiscale Test S-06-3	99
121.	Comparison of the TRAC-calculated and measured mass flows at the core entrance for Semiscale Test S-06-3	100
122.	Comparison of the TRAC-calculated and measured cladding temperatures for the 32 low-power rods in the lower core	101
123.	Comparison of the TRAC-calculated and measured cladding temperatures for the 32 low-power rods in the midcore	101
124.	Comparison of the TRAC-calculated and measured cladding temperatures for the 32 low-power rods in the upper core	102
125.	Comparison of the TRAC-calculated and measured cladding temperatures for the high-power rods in the lower core for Semiscale Test S-06-3	102
126.	Comparison of the TRAC-calculated and measured cladding temperatures for the high-power rods in the midcore for Semiscale Test S-06-3	103
127.	Comparison of the TRAC-calculated and measured cladding temperatures for the high-power rods in the upper core for Semiscale Test S-06-3	103
128.	Major LOFT components	105
129.	TRAC model of LOFT L1-4	107
130.	LOFT L1-4 reactor-vessel horizontal nodding diagram for level 8	107
131.	LOFT L1-4 reactor-vessel axial nodding diagram	108
132.	LOFT L1-4 intact-loop cold-leg nodding diagram	108
133.	LOFT L1-4 intact-loop hot-leg nodding diagram	109
134.	LOFT L1-4 broken-loop hot-leg nodding diagram	109
135.	LOFT L1-4 broken-loop cold-leg nodding diagram	110
136.	LOFT L1-4 ECCS nodding diagram	110
137.	LOFT L1-4 steady-state intact-loop pressure	111
138.	LOFT L1-4 steady-state intact-loop mixture velocity	111
139.	LOFT L1-4 steady-state intact-loop liquid temperature	112
140.	Comparison of the LOFT L1-4 steady-state mass flows on the steam-generator secondary side	113
141.	Comparison of the TRAC-calculated and measured broken-loop cold-leg mass flows for LOFT L1-4	114
142.	Comparison of the TRAC-calculated and measured broken-loop hot-leg mass flows for LOFT L1-4	114

FIGURES (cont.)

143.	Comparison of the TRAC-calculated and measured broken-loop cold-leg average densities for LOFT L1-4	115
144.	Comparison of the TRAC-calculated and measured broken-loop hot-leg average densities for LOFT L1-4	115
145.	Comparison of the TRAC-calculated and measured broken-loop cold-leg liquid temperatures for LOFT L1-4	116
146.	Comparison of the TRAC-calculated and measured broken-loop cold-leg pressures for LOFT L1-4	117
147.	Comparison of the TRAC-calculated and measured pressurizer pressures for LOFT L1-4	117
148.	Comparison of the TRAC-calculated and measured intact-loop cold-leg pressures for LOFT L1-4	118
149.	Comparison of the TRAC-calculated and measured pressurizer liquid levels for LOFT L1-4	118
150.	Comparison of the TRAC-calculated and measured differential pressures across the steam-generator simulator for LOFT L1-4	119
151.	Comparison of the TRAC-calculated and measured differential pressures across the pump simulator for LOFT L1-4	119
152.	Comparison of the TRAC-calculated and measured differential pressures across the cold-leg break plane for LOFT L1-4	120
153.	Comparison of the TRAC-calculated and measured downcomer liquid levels near the broken-loop cold leg for LOFT L1-4	120
154.	Comparison of the TRAC-calculated and measured downcomer liquid levels near the intact-loop cold leg for LOFT L1-4	121
155.	Comparison of the TRAC-calculated and measured vessel liquid mass inventories for LOFT L1-4	121
156.	LOFT core 1 configuration showing the instrumented rod designations and the TRAC nodding	123
157.	LOFT L2-2 VESSEL nodding diagram (level 11) and rod locations	125
158.	LOFT L2-2 VESSEL axial nodding diagram	126
159.	LOFT L2-2 core axial nodding diagram and power profile	127
160.	LOFT L2-2 fuel-rod radial nodding diagram	128
161.	LOFT L2-2 steady-state pressure in the intact-loop cold leg	129
162.	LOFT L2-2 steady-state mixture velocity in the intact-loop cold leg	129
163.	LOFT L2-2 steady-state mass flow in the intact-loop cold leg	130
164.	LOFT L2-2 steady-state liquid temperature in the intact-loop cold leg	130
165.	LOFT L2-2 steady-state pressure differential across pump 6	131
166.	LOFT L2-2 steady-state pressure differential across pump 7	131

FIGURES (cont.)

167.	LOFT L2-2 steady-state steam-generator primary-side liquid temperatures	132
168.	LOFT L2-2 steady-state steam-generator secondary-side liquid temperatures	133
169.	LOFT L2-2 steady-state steam-generator secondary-side void fractions	133
170.	LOFT L2-2 steady-state steam-generator secondary-side mass flows	134
171.	LOFT L2-2 steady-state fuel-rod cladding-surface temperatures	134
172.	Comparison of the TRAC-calculated and measured intact-loop hot-leg pressures for LOFT L2-2	137
173.	Comparison of the TRAC-calculated and measured intact-loop hot-leg mixture densities for LOFT L2-2	137
174.	Comparison of the TRAC-calculated and measured intact-loop hot-leg liquid temperatures for LOFT L2-2	138
175.	Comparison of the TRAC-calculated and measured intact-loop cold-leg pressures for LOFT L2-2	138
176.	Comparison of the TRAC-calculated and measured intact-loop cold-leg mixture densities for LOFT L2-2	139
177.	Comparison of the TRAC-calculated and measured intact-loop cold-leg liquid temperatures for LOFT L2-2	139
178.	Comparison of the TRAC-calculated and measured pressurizer liquid levels for LOFT L2-2	140
179.	Comparison of the TRAC-calculated and measured HPIS flows for LOFT L2-2	141
180.	Comparison of the TRAC-calculated and measured LPIS flows for LOFT L2-2	141
181.	Comparison of the TRAC-calculated and measured accumulator flows for LOFT L2-2	142
182.	Comparison of the TRAC-calculated and measured accumulator pressures for LOFT L2-2	142
183.	Comparison of the TRAC-calculated and measured accumulator liquid levels for LOFT L2-2	143
184.	Comparison of the TRAC-calculated and measured broken-loop hot-leg mixture densities for LOFT L2-2	144
185.	Comparison of the TRAC-calculated and measured broken-loop hot-leg mass flows for LOFT L2-2	144
186.	Comparison of the TRAC-calculated and measured broken-loop hot-leg liquid temperatures for LOFT L2-2	145
187.	Comparison of the TRAC-calculated and measured broken-loop cold-leg mixture densities for LOFT L2-2	145
188.	Comparison of the TRAC-calculated and measured broken-loop cold-leg mass flows for LOFT L2-2	146
189.	Comparison of the TRAC-calculated and measured broken-loop cold-leg liquid temperatures for LOFT L2-2	146
190.	The calculated broken-loop cold-leg liquid vs the calculated saturation temperatures for LOFT L2-2	147
191.	Comparison of the pressure differentials across the hot-leg break plane for LOFT L2-2	147

FIGURES (cont.)

192.	Comparison of the pressure differentials across the cold-leg break plane for LOFT L2-2	148
193.	Comparison of the pressure differentials across the pump simulator for LOFT L2-2	148
194.	LOFT L2-2 calculated vessel liquid mass	150
195.	LOFT L2-2 calculated core liquid mass	150
196.	LOFT L2-2 calculated total rod heat transfer	151
197.	LOFT L2-2 calculated total slab heat transfer	151
198.	LOFT L2-2 calculated core vapor fractions	152
199.	Axial comparison of the calculated central-rod cladding-surface temperatures for LOFT L2-2	154
200.	Azinuthal comparison of the calculated central-rod midplane cladding-surface temperatures for LOFT L2-2	155
201.	Comparison of the calculated central-rod midplane cladding-surface temperatures and group 1 data for LOFT L2-2 . . .	155
202.	Comparison of the calculated central-rod midplane cladding-surface temperatures and group 2 data for LOFT L2-2 . . .	156
203.	Comparison of the calculated central-rod midplane cladding-surface temperatures and group 3 data for LOFT L2-2 . . .	156
204.	Comparison of the calculated central-rod midplane cladding-surface temperatures and group 4 data for LOFT L2-2 . . .	157
205.	Comparison of the calculated central-rod midplane cladding-surface temperatures and group 5 data for LOFT L2-2 . . .	157
206.	Comparison of the calculated vessel void fractions for LOFT L2-2	158
207.	Azinuthal comparison of the calculated central-rod low-plane cladding-surface temperatures for LOFT L2-2	159
208.	Comparison of the calculated central-rod low-plane cladding-surface temperatures and the group 6 data for LOFT L2-2	159
209.	Azinuthal comparison of the calculated central-rod high-plane cladding-surface temperatures for LOFT L2-2	160
210.	Comparison of the calculated central-rod high-plane cladding-surface temperatures and the group 7 data for LOFT L2-2	160
211.	Comparison of the calculated second radial-zone midplane cladding-surface temperatures for LOFT L2-2	161
212.	Comparison of the calculated second radial-zone midplane cladding-surface temperatures and group 8 data for LOFT L2-2 . . .	162
213.	Comparison of the calculated second radial-zone midplane cladding-surface temperatures and group 9 data for LOFT L2-2 . . .	162
214.	Comparison of the calculated second radial-zone midplane cladding-surface temperatures and group 10 data for LOFT L2-2 . .	163
215.	Comparison of the calculated second radial-zone midplane cladding-surface temperatures and group 11 data for LOFT L2-2 . .	163
216.	Comparison of the calculated second radial-zone midplane cladding-surface temperatures and group 12 data for LOFT L2-2 . .	164
217.	Comparison of the calculated second radial-zone midplane cladding-surface temperatures and group 13 data for LOFT L2-2 . .	164

FIGURES (cont.)

218.	Comparison of the calculated second radial-zone midplane cladding-surface temperatures and group 14 data for LOFT L2-2 . .	165
219.	Comparison of the calculated second radial-zone midplane cladding-surface temperatures and group 15 data for LOFT L2-2 . .	165
220.	Azimuthal comparison of calculated outer radial-zone midplane cladding-surface temperatures for LOFT L2-2	166
221.	Comparison of calculated outer radial-zone midplane cladding-surface temperatures and group 16 data for LOFT L2-2 . .	166
222.	LOFT L2-2 parametric-study pressures	168
223.	LOFT L2-2 parametric-study mass flows	169
224.	LOFT L2-2 parametric-study void fractions	169
225.	LOFT L2-2 calculated radial temperature distribution at the midplane of rod 1	170
226.	LOFT L2-2 transient response of the fuel-rod surface at the axial midplane of rod 1	170

TABLES

I.	TRAC-PD2 DEVELOPMENTAL ASSESSMENT ANALYSES	4
II.	LOCATION OF MEASURED AND CALCULATED QUANTITIES FOR THE EDWARDS' BLOWDOWN EXPERIMENT	9
III.	CISE TEST-SECTION DIMENSIONS	15
IV.	LOCATION OF MEASURED AND CALCULATED QUANTITIES FOR CISE BLOWDOWN EXPERIMENTS	19
V.	LOCATION OF MEASURED AND CALCULATED QUANTITIES FOR MARVIKEN BLOWDOWN EXPERIMENTS (TESTS 4 AND 24)	34
VI.	MARVIKEN CRITICAL-FLOW TEST CONDITIONS	35
VII.	LOCATION OF MEASURED AND CALCULATED QUANTITIES FOR THTF TEST 177 BLOWDOWN EXPERIMENT	48
VIII.	TEST CONDITIONS	52
IX.	TRAC WALL FRICTION OPTIONS	59
X.	COMPUTER REQUIREMENTS FOR BENNETT PREDICTIONS	61
XI.	CALCULATED AND MEASURED INITIAL PARAMETERS FOR SEMISCALE MOD-1 TEST S-02-8	75
XII.	CALCULATED AND MEASURED INITIAL CONDITIONS FOR SEMISCALE MOD-1 TEST S-06-3	93
XIII.	CALCULATED AND MEASURED INITIAL CONDITIONS FOR LOFT L1-4	113
XIV.	CALCULATED AND MEASURED INITIAL CONDITIONS FOR LOFT L2-2	135
XV.	LOFT L2-2 STATISTICS	135
XVI.	SEQUENCE OF EVENTS FOR LOFT L2-2	136
XVII.	FUEL-ROD TEMPERATURE MEASUREMENTS	153
XVIII.	LOFT L2-2 FUEL-ROD MODELS FOR SENSITIVITY STUDY	168

TRAC-PD2 DEVELOPMENTAL ASSESSMENT

Compiled and Edited by

Thad D. Knight

and

Vera B. Metzger

Contributors: T. F. Bott, J. S. Gilbert, D. A. Mandell,
J. K. Meier, and J. M. Sicilian

ABSTRACT

The Los Alamos National Laboratory is developing the Transient Reactor Analysis Code (TRAC) to provide advanced, best-estimate predictions of postulated accidents in light water reactors. The TRAC-PD2 program provides this analysis capability for pressurized water reactors and for many thermal-hydraulic test facilities. The code features a three-dimensional treatment of the pressure vessel and its associated internals; two-phase, nonequilibrium hydrodynamic models; flow-regime-dependent constitutive relations; optional reflood tracking capability for bottom-flood and falling-film quench fronts; and consistent treatment of entire accident sequences including the generation of consistent steady-state conditions. The Los Alamos report, "TRAC-PD2: An Advanced Best-Estimate Computer Program for Pressurized Water Reactor Loss-of-Coolant Accident Analysis," LA-8709-MS (NUREG/CR-2054), provides a detailed code description.

This report describes the final results of the developmental assessment analyses conducted during the later stages of the TRAC-PD2 development. The calculations discussed in this report used the released version of TRAC-PD2 and cover separate-effects blowdown, heat transfer, and downcomer penetration tests together with integral tests from the Loss-of-Fluid Test and Semiscale facilities. Although these calculations are not an exhaustive test of the code, they demonstrate its capabilities, including automatic steady-state initialization and the complete transient from blowdown through refill and reflood. The results show good agreement between the calculated parameters and the data and indicate that the code is applicable to large-break loss-of-coolant accident analyses.

I. INTRODUCTION

The Transient Reactor Analysis Code (TRAC) is an advanced, best-estimate systems code for analyzing light water reactor (LWR) accidents. The Office of Nuclear Regulatory Research of the US Nuclear Regulatory Commission (NRC) sponsors the code development at the Los Alamos National Laboratory. We released TRAC-PD2 (Ref. 1) to the National Energy Software Center (NESC) at the Argonne National Laboratory (ANL) in October 1980. This TRAC version is the third in a series of publicly released codes intended primarily to analyze large-break loss-of-coolant accidents (LOCAs) in pressurized water reactors (PWRs). However, because of the generality incorporated into the thermal-hydraulic modeling, TRAC-PD2 can be applied directly to small-break LOCAs and some non-LOCA transients. The generality of the code also permits direct application to a large variety of analyses ranging from blowdowns in simple pipes to integral LOCA tests in multiloop test facilities to separate-effects tests. The Idaho National Engineering Laboratory (INEL) is developing a TRAC version for application to boiling-water reactors (BWRs). We will improve various models and the numerical techniques in future TRAC versions to facilitate and to enhance applications to small-break LOCAs and non-LOCA transients and to expand applications to a much wider range of non-LOCA transients.

Reference 1 describes the TRAC-PD2 code. The code is completely modular by component and by function. One-dimensional components (PIPE, TEE, VALVE, PUMP, PRIZER, ACCUM, and STGEN) describe pipes, tees, valves, pumps, pressurizers, accumulators, and steam generators. The VESSEL component provides a two-dimensional, Cartesian-geometry or a three-dimensional, cylindrical-geometry hydraulic description for a vessel and its related internals, including the reactor core. The FILL and BREAK components provide velocity and pressure boundary conditions, respectively. The one-dimensional components use a five-equation, drift-flux hydraulic model. The VESSEL component implements a complete, two-fluid, six-equation hydraulic model; thus, the code can model nonhomogeneous, nonequilibrium fluid conditions. The required constitutive relations are dependent upon the flow regime. The code also provides a comprehensive heat-transfer capability. The one-dimensional components, except for the ACCUM and the PRIZER, represent pipe walls with a one-dimensional heat-conduction solution. Lumped-parameter heat slabs represent the structural mass in the VESSEL component. The core fuel rods (or fuel-rod simulators) are represented by a two-dimensional conduction solution with dynamic fine-mesh rezoning in the axial direction to resolve large temperature gradients associated with both bottom-reflood and falling-film quench fronts. These combined code attributes provide a consistent code input and thermal-hydraulic analysis capability for generating the steady-state initial conditions and for calculating the entire LOCA sequence, including blowdown, refill, and reflood. Although the code permits renoding on restart, renoding is not required. The TRAC-Plot (TRAP) graphics program produced most of the graphics in this report.

Code assessment is a two-stage process. The first stage is the developmental assessment that is coupled closely to the code-development process. Developmental assessment principally involves posttest analyses of various thermal-hydraulic experiments. The developmental assessment primary objectives are to define the validity limits for the methods, models, and correlations in the developmental version of the code and to establish values for various empirical parameters; these objectives are achieved by comparing

the calculated results with experiment data. Other objectives include the determination of code sensitivity to input data, model assumptions, and solution techniques; the recommendation of standard calculational procedures for various classes of problems; and the identification of code and model improvements or additional experiments needed to assess the advanced TRAC models.

Independent assessment is the second stage of the assessment process. Independent assessment uses publicly available, documented TRAC versions and pretest and posttest analyses. The primary objective is to determine the predictive capability of the code when applied to new tests involving different scales and facility configurations. All of the developmental assessment objectives also apply to independent assessment; however, in independent assessment, the results are factored into the future code development without updating the current, released code. Discrepancies between the calculations and the data are resolved by performing additional posttest analyses, as required. Guidance for future code development and recommendations for future experiments also are provided.

The final TRAC-PD2 developmental assessment results are reported here. We performed these analyses with the released TRAC-PD2 version; therefore, these analyses provide the initial independent assessment results for TRAC-PD2. Table I summarizes the experiments analyzed and the code areas tested. Six of the analyses in Table I involved only the one-dimensional capability of TRAC-PD2, and the remaining analyses invoked the TRAC-PD2 VESSEL component in a two-dimensional Cartesian geometry or a three-dimensional cylindrical geometry in combination with one-dimensional components. The developmental assessment analyses included separate-effects tests that generally involved one type of component; systems-effects tests that coupled several components in a single LOCA transient phase (either blowdown, refill, or reflood); and integral tests that involved several components through multiple LOCA transient phases.

The order in which Table I lists the tests reflects the order in which the tests are discussed in this report. The Edwards' pipe blowdown is relatively simple to model and provides a test of many constitutive relations in the code. The two Centro Informazioni Studi Esperienze (CISE) tests are slightly more complicated than the Edwards' pipe blowdown and test the wall friction and heat-transfer correlations. The Marviken vessel blowdown tests are really very large scale critical-flow tests that also check the slip correlations.

The Thermal-Hydraulic Test Facility (THTF) provides a good test of the heat-transfer correlations in a rod bundle during blowdown. The Bennett tube experiments investigated critical heat flux (CHF) and tested the wall heat transfer in the code. The Creare tests provided data on emergency core-cooling (ECC) bypass, an important phenomenon in the LOCA blowdown phase; we used these tests to check the calculated flooding behavior in the vessel downcomer. The Full-Length Emergency Core Heat-Transfer (FLECHT) analyses tested the heat-transfer correlations and quench-front tracking during slow and fast refloods.

The Semiscale Mod-1 Test S-02-8 provided data during the blowdown phase in an integral PWR simulator with an electrically heated core. We conducted the Semiscale-nozzle critical-flow analyses primarily to investigate the nodding sensitivity of the critical-flow calculation. Test S-06-3 was similar to Test S-02-8 but continued the transient through the refill and reflood phases of the large-break LOCA transient. The Loss-of-Fluid Test (LOFT) facility is a 50-MWt PWR designed to simulate the large-break LOCA. LOFT L1-4, without the nuclear core, provided blowdown and refill data at a much larger scale than the

TABLE I

TRAC-PD2 DEVELOPMENTAL ASSESSMENT ANALYSES

<u>Number</u>	<u>Experiment</u>	<u>Thermal-Hydraulic Effects</u>
1	Edwards' Horizontal-Pipe Blowdown (Standard Problem 1)	Separate effects, one-dimensional critical flow, phase change, slip, and wall friction
2	CISE Unheated-Pipe Blowdown (Test 4)	Same as (1) plus wall heat transfer, flow-area changes, and gravitational effects
3	CISE Heated-Pipe Blowdown (Test R)	Same as (2) plus CHF
4	Marviken Full-Scale Vessel Blowdown (Tests 4 and 24)	Same as (1) plus full-scale effects
5	THTF (Test 177)	Systems effects, two-dimensional Cartesian-geometry vessel model with rod heat transfer and rewet models
6	Bennett Tube Experiments	Separate effects, wall heat transfer, CHF, phase change, and slip
7	Creare Countercurrent Flow Tests	Systems effects, countercurrent flow, interfacial drag and heat transfer, and condensation with the VESSEL component
8	FLECHT Forced-Flooding Tests (Tests 17201 and 4831)	Systems effects, reflood heat transfer, quench-front propagation, and liquid entrainment and carryover
9	Semiscale Mod-1 Test S-02-8	Integral synergistic effects, one-dimensional flow, phase change, slip, wall friction, nozzle critical flow, three-dimensional vessel with rod heat transfer including nucleate boiling, departure from nucleate boiling (DNB), and post-DNB

TABLE I (cont.)

<u>Number</u>	<u>Experiment</u>	<u>Thermal-Hydraulic Effects</u>
10	Semiscale-Nozzle Critical Flow	Separate effects, one-dimensional critical flow with area change
11	Semiscale Mod-1 Test S-06-3	Same as (9) plus reflood heat transfer, quench-front propaga- tion, and liquid entrainment and carryover
12	LOFT Nonnuclear L1-4	Integral effects during blowdown and refill, larger scale than Semiscale
13	LOFT Nuclear L2-2	Same as (11) at larger scale

Semiscale facility. LOFT L2-2, with the nuclear core installed and operating at 50% power, provided data throughout the entire LOCA. We used these integral tests in Semiscale and LOFT basically to check the entire code, including the constitutive relations, the thermal-hydraulic modeling, the numerical techniques, all of the components, and the coupling of the components into a system model.

All of the analyses in Table I are discussed in the following chapters. For each we briefly describe the facility, test, and TRAC-PD2 input. We compare the calculated results with data and discuss the results and conclusions. Section XIV summarizes the overall conclusions.

II. EDWARDS' BLOWDOWN EXPERIMENT

A. Experiment Description

The Edwards' horizontal-pipe blowdown experiment studied depressurization phenomena of initially nonflowing subcooled water.² The test apparatus, a 4.096-m straight steel pipe with a 0.073-m i.d., was designed for a maximum 17.24-MPa pressure at temperatures to 616.5 K. The discharge end of the horizontal pipe was sealed with a 0.0127-m-thick glass disk.

The pipe was evacuated by a vacuum pump before it was filled with demineralized water. A hydraulic pump and a control valve regulated the system pressure. Before the glass disk was ruptured, the pipe was isolated from the supply tank to prevent the discharge of cold water into the pipe during blowdown. The pipe, which was insulated with asbestos, was heated electrically. Figure 1 shows the gauge stations GS-1 to GS-7 where the pressure transducers were located. Also located at GS-5 were two aluminum-alloy disk windows that were used to measure transient void fractions through an x-ray absorption system and a temperature transducer.

The operating procedure required that degassed water completely fill the pipe. The cold pipe was checked for leaks after the initial pressurization to the 7-MPa test pressure. Next, the pressure was reduced to 3.45 MPa and heat was applied gradually for ~1.5 h. Although the water temperature increased, the system pressure was maintained at ~3.45 MPa above the saturation pressure to prevent liquid flashing. Each heater had a voltage control that was used to control the temperature variation along the pipe. Initially, the system was brought to an approximately uniform 515 K and 7 MPa. Because the isolating valve between the pipe and the storage tank was closed, the glass disk ruptured and the data were recorded automatically.

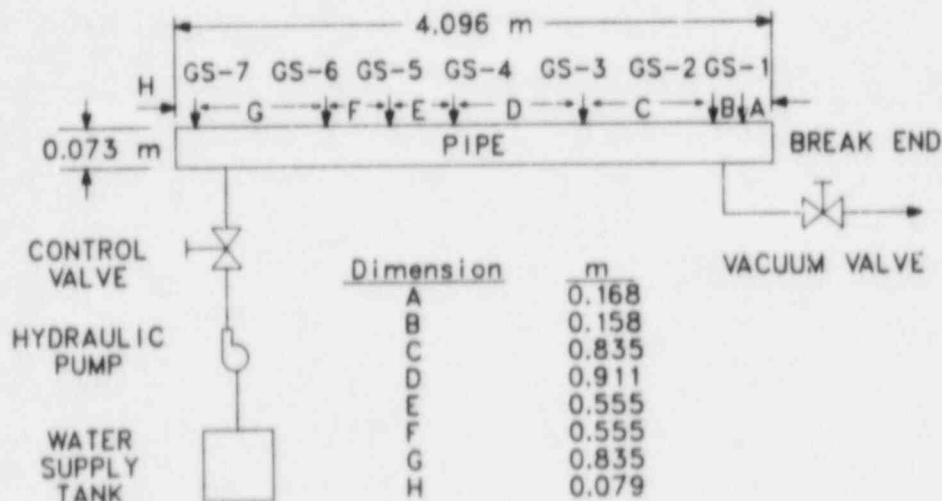


Fig. 1.

Edwards' blowdown-experiment configuration (adapted from Ref. 2).

B. TRAC-PD2 Model

The test apparatus was a straight horizontal pipe with one abrupt area change at its exit. Figure 2 shows the one-dimensional components used to model this experiment. The model included three types of components (BREAK, PIPE, and FILL) coupled in series. The 2 PIPEs were subdivided into 46 fluid cells. We performed a noding sensitivity study³ to determine the TRAC noding (Figs. 3-5). Table II lists the locations of the measured and the calculated quantities. After a parametric study,³ we set the annular-flow friction-factor correlation option (NFF = 4). Also, we selected an additive loss coefficient (FRIC), equal to 1.436, for the exit flow cell. This FRIC value accounted for form losses at the break caused by the two-dimensional effects that could not be simulated by the one-dimensional model. For the TRAC-PD2 developmental assessment, we used the best-estimate model developed for TRAC-PLA.

With initial conditions of uniform pressure, approximately uniform temperature, and zero-flow velocity, no steady-state calculations were required. Because the temperature distribution along the pipe may have varied as much as 9 K, an adjusted temperature distribution was used, as suggested by

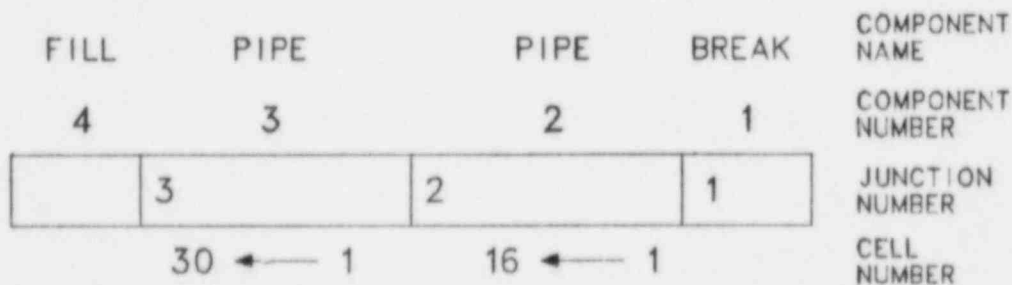


Fig. 2.

TRAC component diagram for Edwards' blowdown experiment.

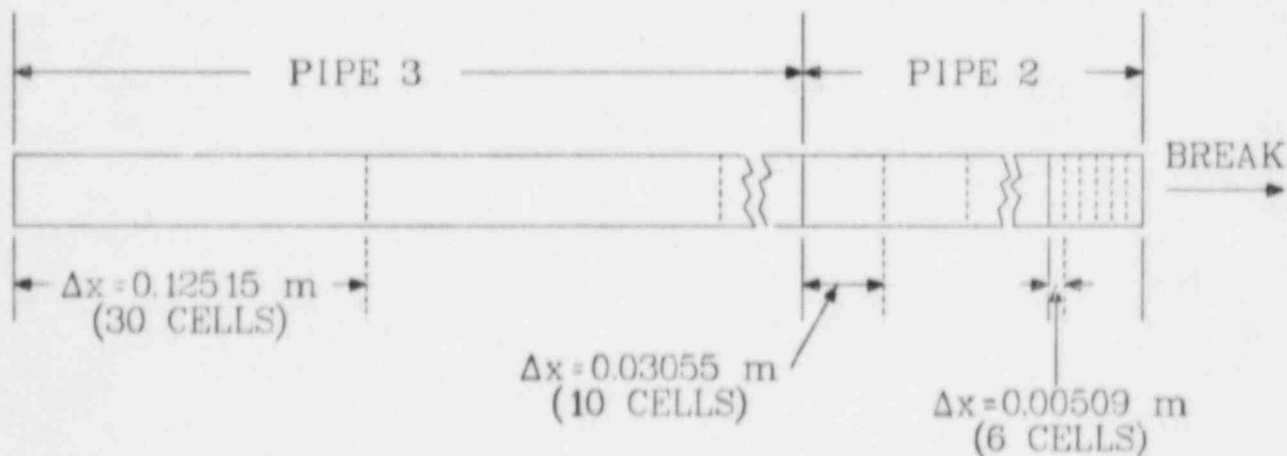


Fig. 3.

TRAC noding diagram for components 2 and 3.

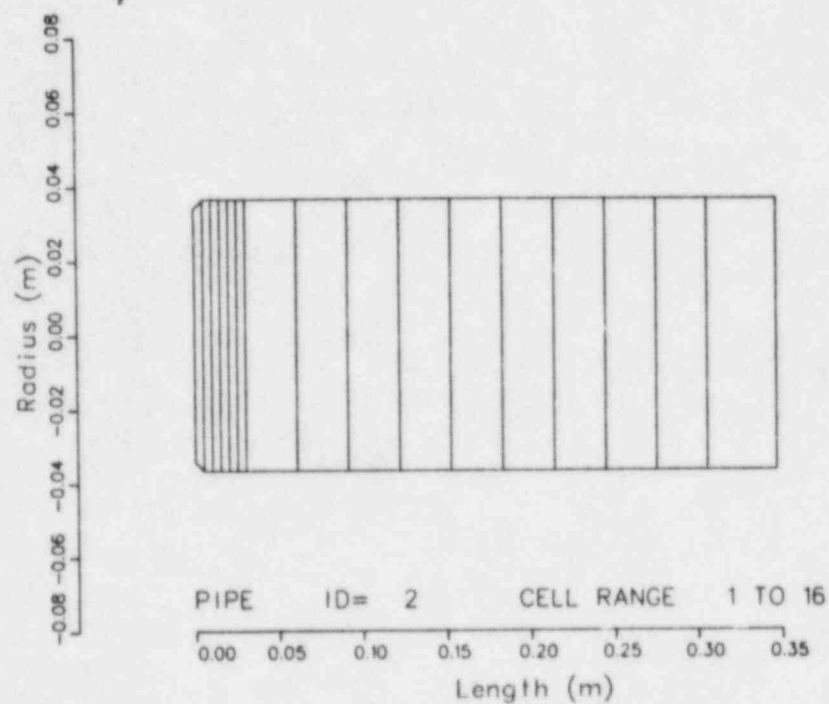


Fig. 4.

TRAP-generated noding diagram of PIPE 2 for Edwards' blowdown experiment.

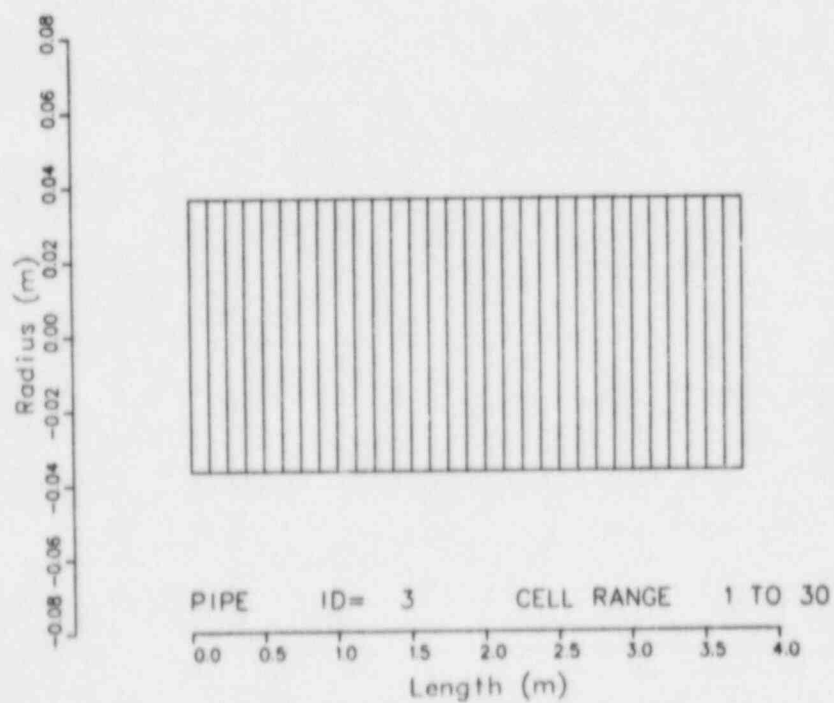


Fig. 5.

TRAP-generated noding diagram of PIPE 3 for Edwards' blowdown experiment.

TABLE II

LOCATION OF MEASURED AND CALCULATED QUANTITIES
FOR THE EDWARDS' BLOWDOWN EXPERIMENT

<u>Measured</u>		<u>Calculated</u>	
<u>Gauge Station</u>	<u>Parameter</u>	<u>Component</u>	<u>Cell</u>
GS-7	Pressure (Pa)	PIPE 3	30
GS-6	Pressure (Pa)	PIPE 3	23
GS-5	Pressure (Pa)	PIPE 3	19
GS-5	Temperature (K)	PIPE 3	19
GS-5	Void fraction	PIPE 3	19
GS-1	Pressure (Pa)	PIPE 2	11

Garner.⁴ Linear interpolation was used to obtain initial temperatures at locations other than those given for the initial temperature distribution.

The FILL imposed a zero-velocity boundary condition at the closed end of the pipe. The BREAK specified a fixed 0.10-MPa boundary condition at the broken end of the pipe. The PIPE adjacent to the BREAK used the fully implicit hydrodynamics option (IHYDRO = 1) to model the high-flow velocities at the break. The other PIPE used the more efficient, partially implicit hydrodynamics option (IHYDRO = 0).

Appendix A lists the TRAC input data deck for the Edwards' blowdown experiment.

C. Data Comparisons

The calculated pressures for GS-1, GS-5, GS-6, and GS-7 (Figs. 6-9, respectively) were similar to the test results. The following observations apply to all the pressure results. From 0.0-0.2 s, the calculated pressures were within ~10% of the test values. During the midrange of the transient, 0.2-0.4 s, a faster depressurization rate was predicted than was observed. The maximum difference between the calculation and the experiment was 0.7 MPa at 0.25 s for GS-6. For the balance of the transient, 0.4-0.6 s, the calculated results agreed well with the test results. Experiment uncertainty information was not available; however, an uncertainty of ~0.3 MPa was suggested.⁴

Figure 10 compares the calculated fluid temperature with the fluid temperature measured at GS-5. After 0.2 s, the calculated saturation, liquid, and vapor temperatures were equal. The agreement with the measured temperature was excellent from 0.0-0.2 s; after 0.2 s, the calculated results dropped ~6% below the test results. Figure 11 compares the calculated and measured void fractions. The comparison was fair from 0.0-0.3 s and good after 0.3 s. The void fraction was greater than 90% after 0.3 s. The deviations between the calculated and the test results may have occurred partially because the void fraction was difficult to measure when the x-ray absorption technique was used.

D. Conclusions

This problem included some important thermal-hydraulic effects such as one-dimensional critical flow, flashing, slip, wall friction, and break flow-area reduction. Code components tested included the PIPE, FILL, and BREAK.

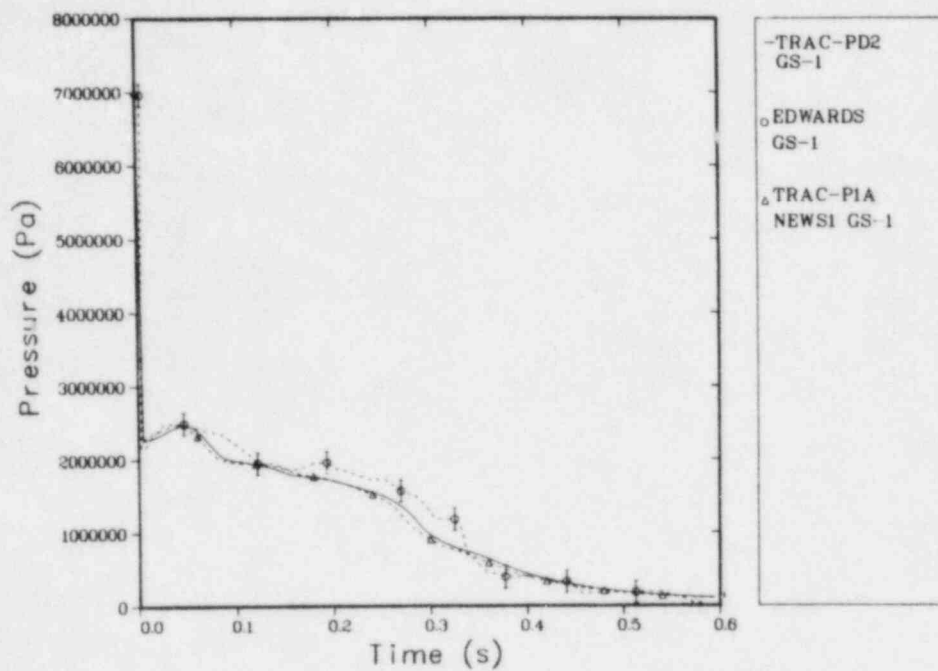


Fig. 6.
Pressure at GS-1 for Edwards' blowdown experiment.

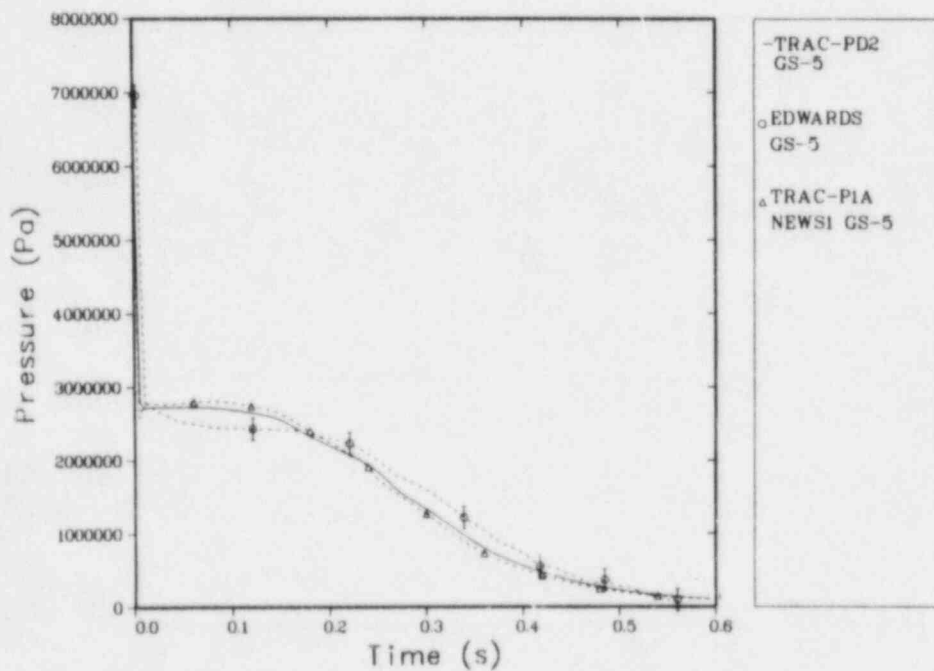


Fig. 7.
Pressure at GS-5 for Edwards' blowdown experiment.

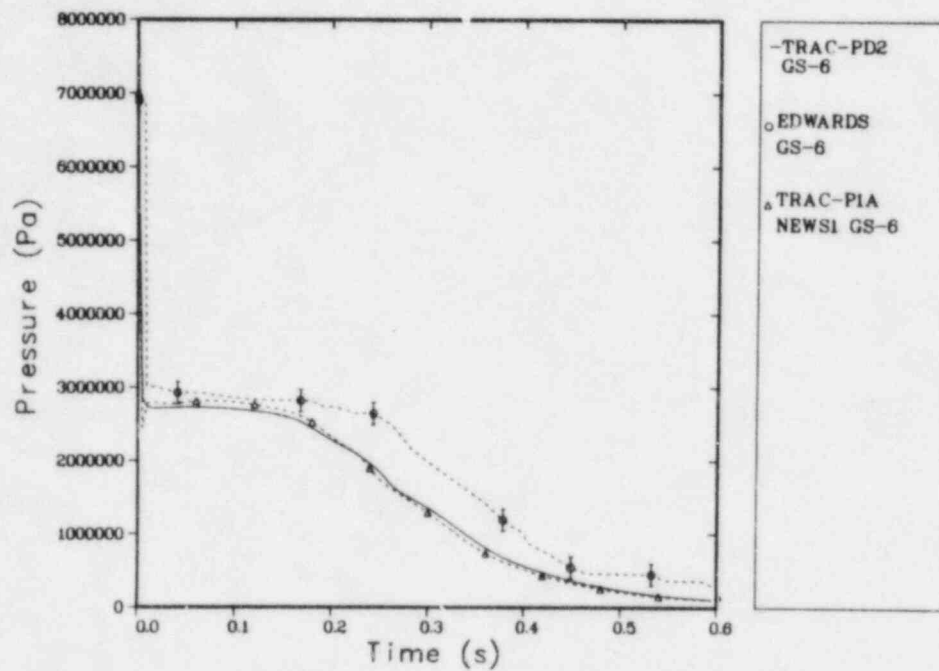


Fig. 8.
Pressure at GS-6 for Edwards' blowdown experiment.

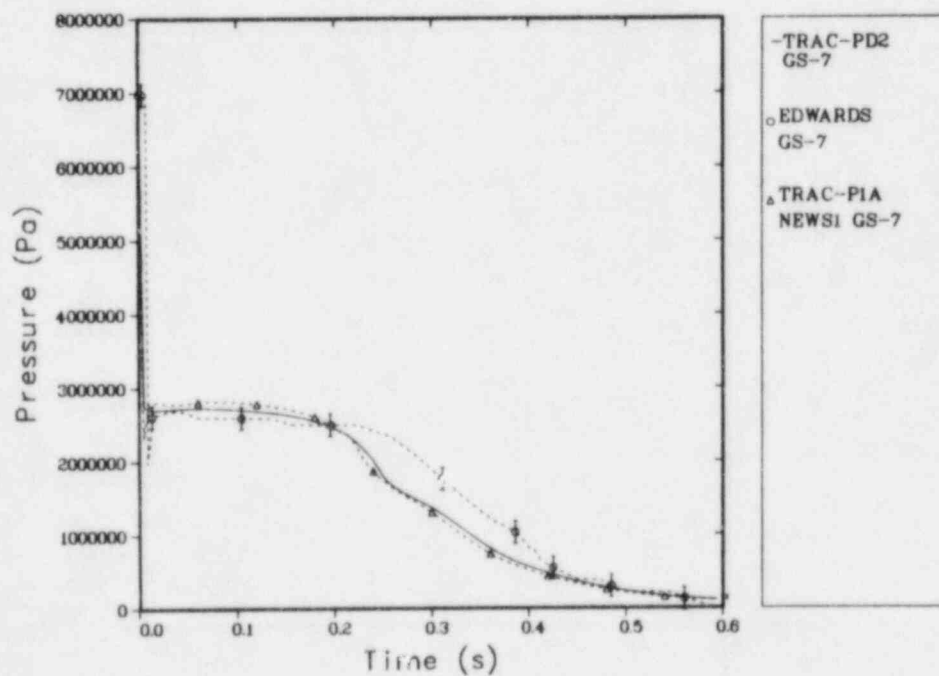


Fig. 9.
Pressure at GS-7 for Edwards' blowdown experiment.

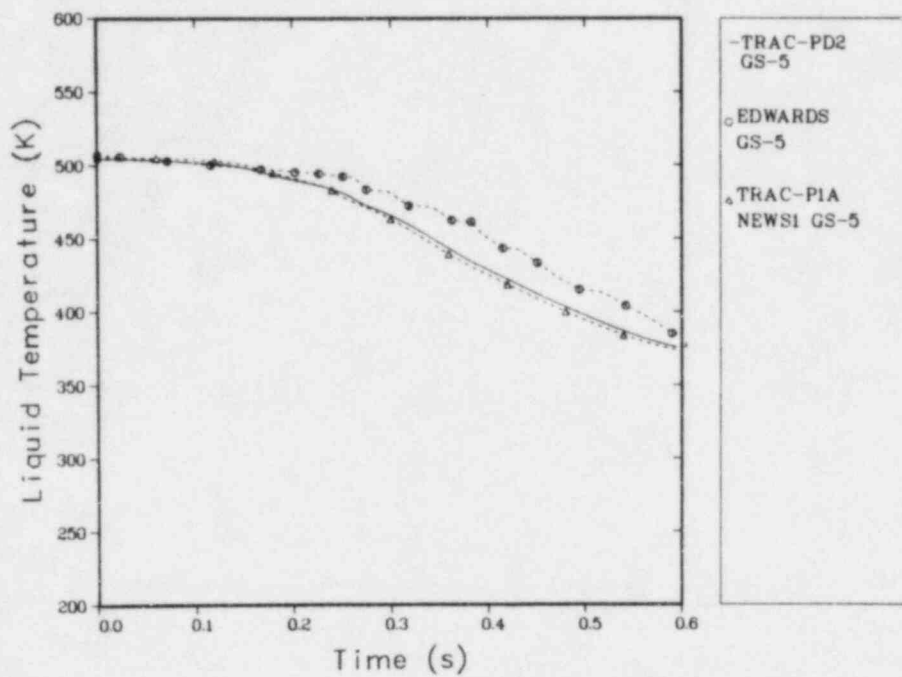


Fig. 10.
Liquid temperature at GS-5 for Edwards' blowdown experiment.

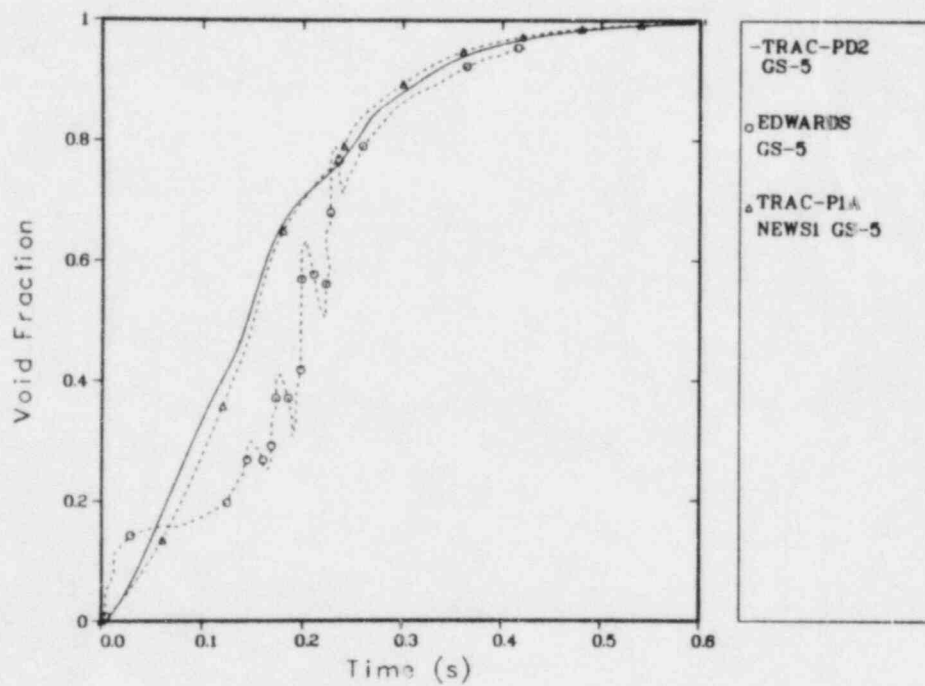


Fig. 11.
Void fraction at GS-5 for Edwards' blowdown experiment.

The TRAC-PD2 results were similar to the TRAC-PlA calculated values and, in general, were in slightly better agreement with the measurements than those from TRAC-PlA. The TRAC-PD2 calculations were in reasonable agreement with the test measurements. The mass flows and the pipe-wall temperatures were not measured. Also, there were uncertainties in the initial temperature distribution, the rupture-disk dynamics, and the effect of residual disk fragments on the flow field. Because of these factors, we cannot recommend code model improvements based on our developmental assessment analysis of the Edwards' experiment.

The transient calculation required 31 s of central-processor-unit (CPU) time on a Control Data Corporation (CDC) 7600 computer.

III. CISE BLOWDOWN EXPERIMENTS

A. Experiment Description

The CISE vertical-pipe blowdown experiment studied depressurization and heat-transfer phenomena of initially flowing subcooled water.⁵ Figure 12 shows the CISE blowdown-loop test section. Stations P4 and P7 measured the pressure, stations TF4 and TF7 measured the fluid temperature, and station THW4 measured the temperature of the heated wall. The loop consisted of the feeder, heater, and riser sections. Table III lists the test-section dimensions. Figure 13 shows a test-section schematic. The internal diameters of the loop tubing ranged from 0.01694 m for the feeder to 0.02618 m for the riser. The blowdown portion of the loop was 24.06 m long. The heated section was vertical, whereas the feeder and riser tubes were coiled helically with a ~ 1 -m radius resulting in elevation changes of 3.6 m and 1.455 m, respectively. Tests were run with and without heat in the heater section so that comparisons could be made. We performed calculations for unheated Test 4 and heated Test R. All tubing was

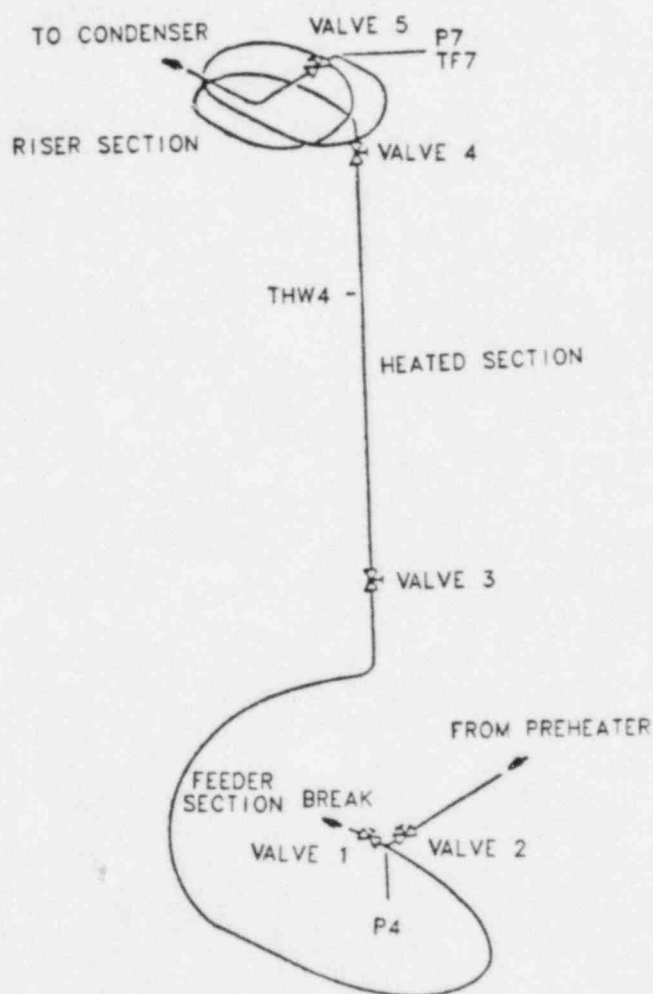


Fig. 12.
CISE test section (adapted from Ref. 6).

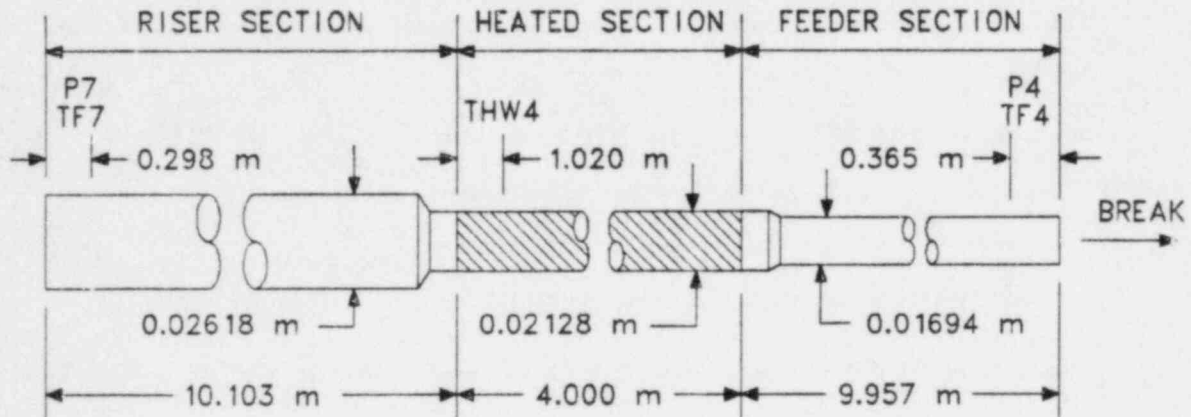


Fig. 13.
CISE test-section geometry.

TABLE III
CISE TEST-SECTION DIMENSIONS

Tube Section	Length (m)	Diameter (m)	Volume (m ³)	Wall Thickness (m)	Elevation Change (m)
Feeder	9.848	0.01694	2.22×10^{-3}	0.0015	3.600
Transition	0.072	0.01694	1.62×10^{-5}	0.0015	4.222
Transition	0.042	0.02128	1.49×10^{-5}	0.0020	4.222
Heated	4.000	0.02128	1.42×10^{-3}	0.0020	4.222
Transition	0.108	0.02128	3.84×10^{-5}	0.0020	4.222
Riser	9.995	0.02618	5.38×10^{-3}	0.0020	1.455

AISI-304 stainless steel. Only the feeder and riser tubes were insulated to reduce heat loss.

One quick-closing or quick-opening valve (valve 1) and four quick-closing valves (valves 2-5) were used to isolate not only the test section from the loop during blowdown but also the contents of the feeder, heated section, and riser. All valves were gas activated and closed or opened within 10 ms. These valves when fully opened offered no additional resistance to the flow. A 300-kW controllable power supply generated uniform axial heat in the heated section of the tube wall. For the heated test, 109.5 kW were supplied to the heater section during blowdown.

Pressure and temperature transducers were located along the test section, as indicated in Fig. 12. All transducers were connected to a digital data-acquisition system, but only selected transducers were connected to the analog strip-chart recorders.

The operating procedure required that the experiment begin with subcooled water flowing under steady-state conditions through the test loop. At time zero, depressurization was initiated by closing valves 2 and 5 and

simultaneously opening valve 1, the discharge valve. Thus, the test section was isolated from the remainder of the loop in less than 20 ms. The test section discharged the liquid to the atmosphere; however, the energy input to the heater section was maintained at the initial rate. Pressure, fluid temperature, and heater wall temperatures were recorded continuously. The mass inventory was determined at selected stages of the blowdown by simultaneously closing valves 1, 3, and 4. This procedure not only isolated the contents of the feeder, heated section, and riser, but also allowed the contents to be drained through a condenser and to be weighed. The experiment was terminated when the heated-section wall temperature exceeded ~873 K.

B. TRAC-PD2 Model

The test section, composed of three tubes of different sizes connected by gradual area transitions, was modeled with the one-dimensional TRAC-PD2 components shown in Fig. 14. The model included three types of components (BREAK, FILL, and PIPE) coupled in series. The noding given in Figs. 15-19 was based on our noding sensitivity study.³ As a result of this noding, the 4 PIPES were subdivided into 38 fluid cells. Table IV lists the locations of the measured and calculated quantities. We set NFF to 4, based on our parametric study.³ Gravitational effects and flow-area changes were included in the modeling. For the heated-pipe blowdown experiment, the CHF option, ICHF, was set to 1 and the outer-wall heat-transfer coefficient (HTC) to vapor, HOUTV, was set to $50 \text{ W} \cdot \text{m}^{-2} \cdot \text{s}^{-1}$ in PIPE3. Again, we used the best-estimate model developed for TRAC-PlA in this assessment.

The initial velocities, pressures, coolant temperatures, and wall temperatures approximated the steady-state test conditions for the heated and the unheated experiments. Five pipe-wall nodes with a linear 20-K temperature drop across the wall were used to model Test R. For both tests, the feeder and the riser pipe walls were modeled with two nodes using a flat initial temperature distribution across the pipe wall. Linear interpolation was used to obtain the initial fluid-cell temperatures.

Also, for both tests, four PIPES located between a FILL and a BREAK represented the CISE facility. The FILL located at the closed end of the riser section specified a zero-velocity boundary condition. The BREAK imposed a fixed 0.1-MPa boundary condition at a distance approximately one cell away from its adjacent PIPE.

The PIPE adjacent to the BREAK used the fully implicit hydrodynamics option (IHYDRO = 1) because of the large flow velocities at the break. The other PIPES used the partially implicit hydrodynamics option (IHYDRO = 0). For Test R, the input for the PIPE that represented the heated test section used several features that were not included in the other PIPES. These features specified a HTC between the outer boundary of the pipe wall and the ambient air and a CHF test.

Appendix B lists the TRAC input data decks for CISE Tests 4 and R, respectively.

C. Data Comparisons

Calculated results for both tests were compared with test data from Ref. 6 and data supplied by the NRC.*

*This information was provided by W. T. Hancox to L. Shotkin, US NRC (August 31, 1976).

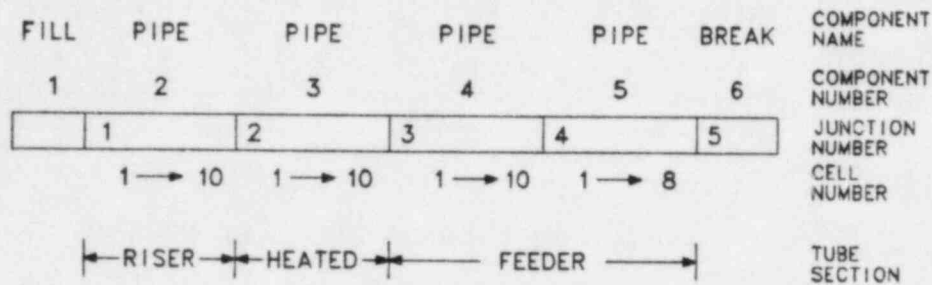


Fig. 14.
TRAC model of CISE blowdown experiments.

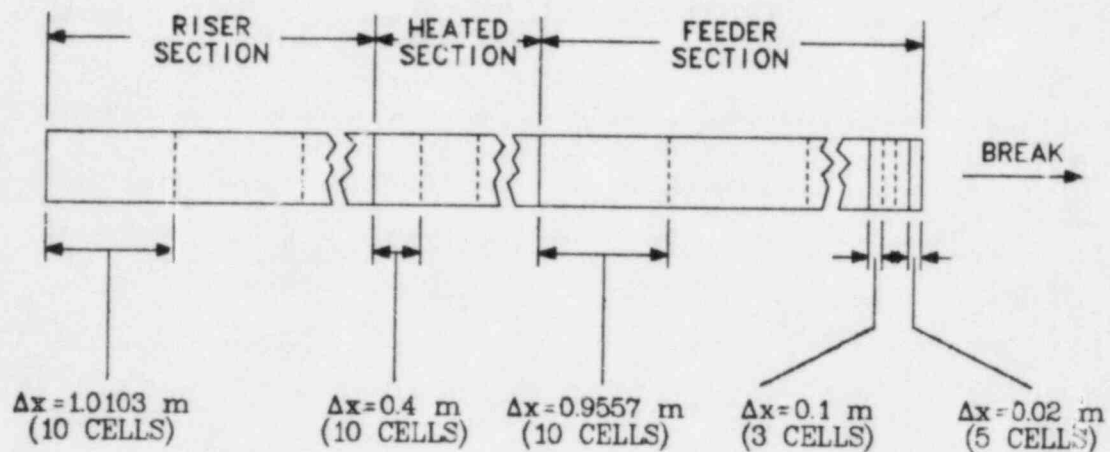


Fig. 15.
Typical TRAC noding of CISE blowdown experiments.

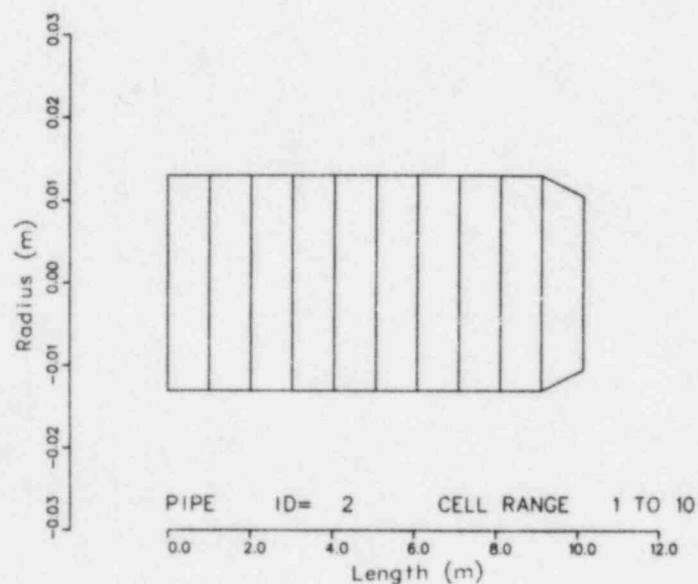


Fig. 16.
TRAP-generated noding diagram of PIPE 2 for CISE blowdown experiment.

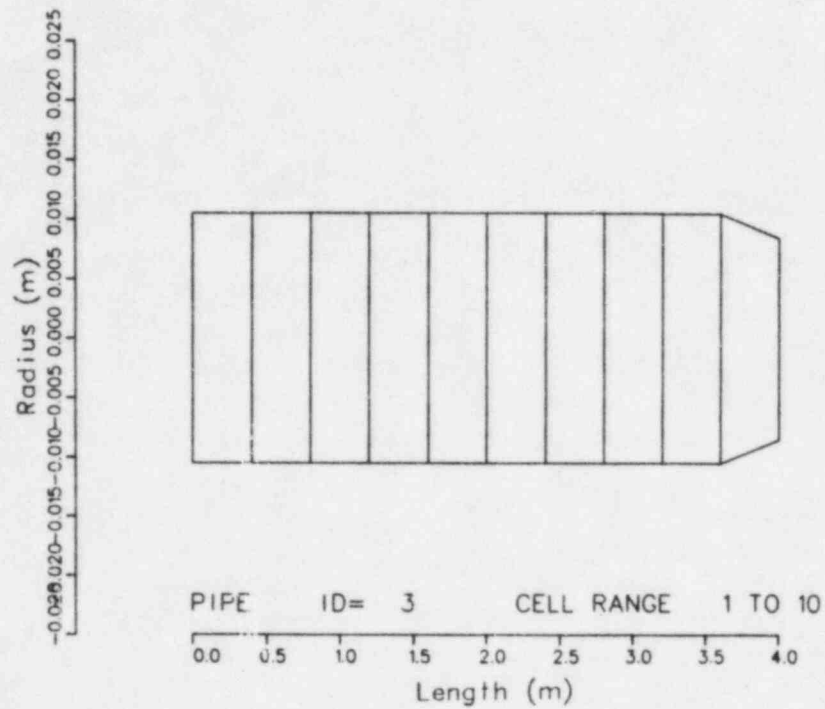


Fig. 17.
TRAP-generated noding diagram of PIPE 3 for CISE blowdown experiment.

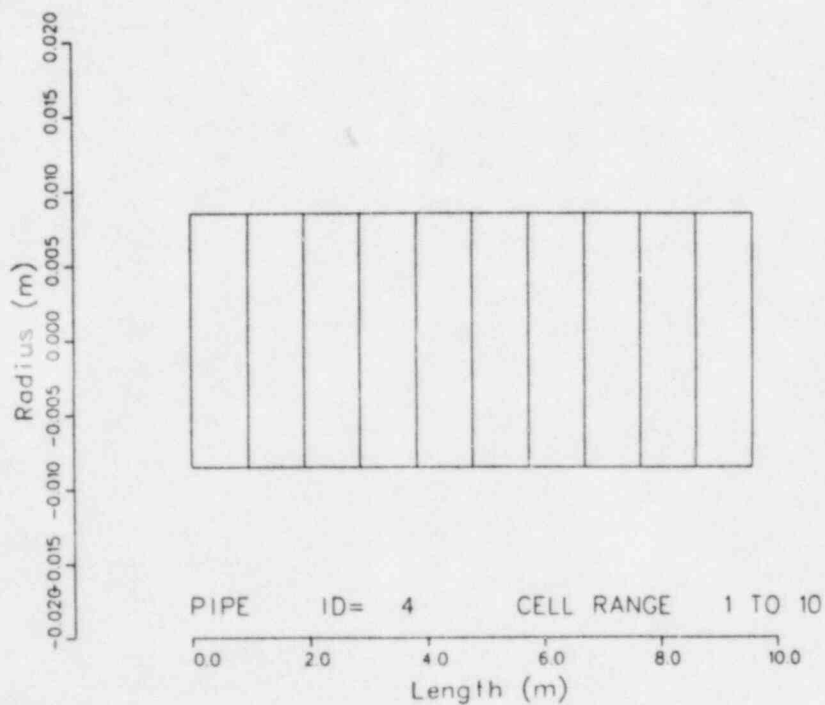


Fig. 18.
TRAP-generated noding diagram of PIPE 4 for CISE blowdown experiment.

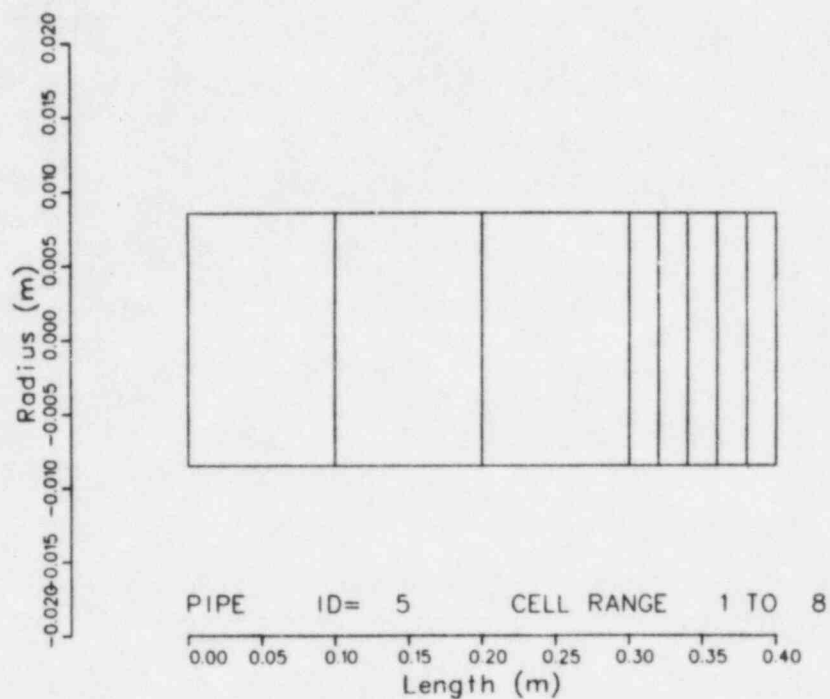


Fig. 19.

TRAP-generated noding diagram of PIPE 5 for CISE blowdown experiment.

TABLE IV

LOCATION OF MEASURED AND CALCULATED QUANTITIES
FOR CISE BLOWDOWN EXPERIMENTS

<u>Measured</u>		<u>Calculated</u>	
<u>Measurement Station</u>	<u>Parameter</u>	<u>Component</u>	<u>Cell</u>
P7	Pressure (Pa)	PIPE 2	1
TFT	Temperature (K)	PIPE 2	1
THW4	Wall temperature (K)	PIPE 3	3 (node 3)
P4	Pressure (Pa)	PIPE 5	1
TF4	Temperature (K)	PIPE 5	1
--	Mass flow ($\text{kg} \cdot \text{s}^{-1}$)	BREAK 6	--

Figure 20 compares the test fluid pressure at measurement station P7 for Test 4 with the pressures calculated by TRAC-P1A and TRAC-PD2. The comparisons were good but the calculated pressures slightly exceeded the measured results. Similar results (Fig. 21) were obtained for Test R except that agreement during the latter part of the transient was fair.

Figures 22 and 23 show that the calculated fluid pressures at measurement station P4 for Tests 4 and R, respectively, are in good overall agreement with the test results. The discrepancies early in the transient may have been caused by the assumption in the calculations that the blowdown valve opened instantaneously. Actually, this valve required ~ 0.01 s to open completely.

Figures 24 and 25 compare the calculated and measured fluid temperatures at measurement station TF7 for Tests 4 and R, respectively. Agreement was excellent for Test 4. For Test R, agreement was excellent for the first 1.5 s of the transient. Then, the measured temperature dipped sharply at 2 s and recovered at 2.5 s. The cause of this dip is unknown as there was no corresponding dip in the pressure, and the fluid reached saturation at this point in the transient.

The calculated fluid temperatures at measurement station TF4 were in good agreement with the test data after 1 s for Test 4 (Fig. 26) and after 2 s for Test R (Fig. 27). In both cases, the temperature response was consistent with the calculated pressures (Figs. 22 and 23).

Figures 28 and 29 compare the calculated and measured pipe-wall temperatures near the top of the heater section and at the radial midpoint of the wall, THW4, for Tests 4 and R, respectively. Agreement was good throughout the transient for Test 4. However, for Test R, the calculated time to dryout was delayed ~ 1 s after the measured time and the calculated temperature at dryout was ~ 20 K below the measured temperature. Figures 30 and 31 show the mass flows as a function of time for Tests 4 and R, respectively. The measured mass flows were determined by differencing the measured total test-section mass as a function of time; thus, measurement uncertainty may be high. Although the agreement was good for Test 4, the measurements were available only to 2 s. For this case, the calculated initial total test-section mass was slightly less than the test value. For Test R, the calculated mass flow agreed well with the data after 1 s; however, measured values were unavailable after 4 s. Because the initial fluid conditions were matched better, the calculated and measured initial total test-section masses agreed more closely than for Test 4.

Experiment uncertainty information was not provided; however, accuracy data⁵ for various transducers were available. The pressure-transducer accuracy for the range of 0-11 MPa was 0.25 MPa, and the temperature-measurement uncertainty was ± 2 K up to 543 K.

D. Conclusions

The CISE experiments involved the same thermal-hydraulic effects as the Edwards' experiment (Sec. II.A) plus additional ones. These additional effects included wall heat sources, flow-area changes in the multisection pipes, and gravitational effects in the vertical-pipe sections. The CISE and the Edwards' experiments used the same code components; that is, no new code components were necessary.

Because the CISE test section was longer and had a smaller diameter than the one in the Edwards' experiment, the results were more sensitive to the wall friction-factor correlation. The generally good agreement between the calculations and the test data for Test 4 indicated that the annular

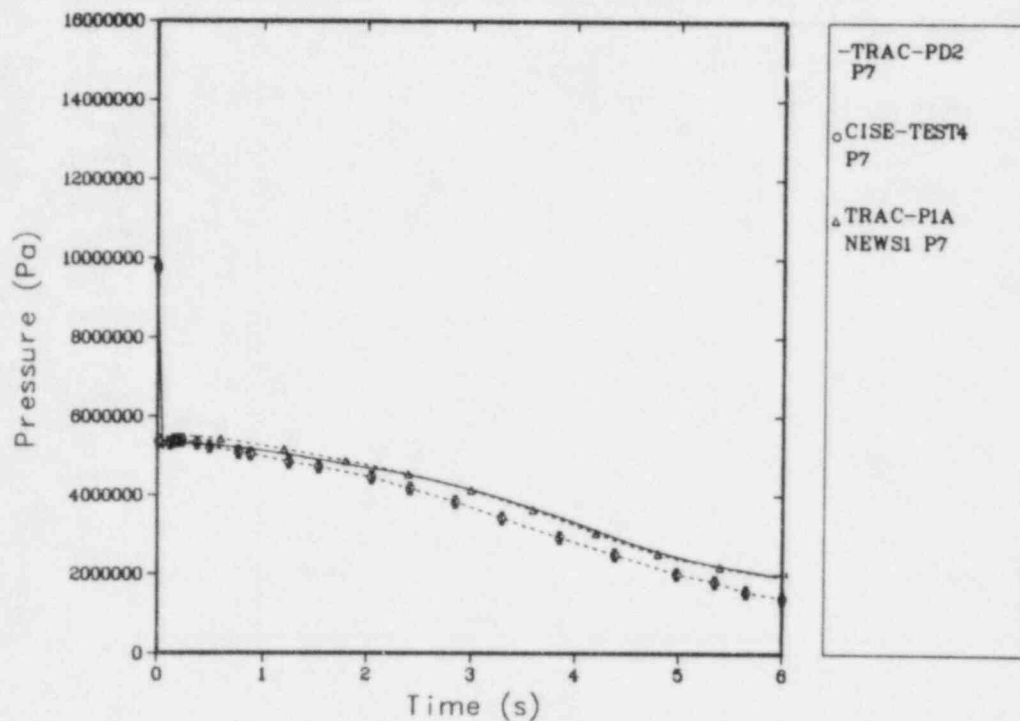


Fig. 20.
Pressure at measurement station P7 for unheated CISE experiment.

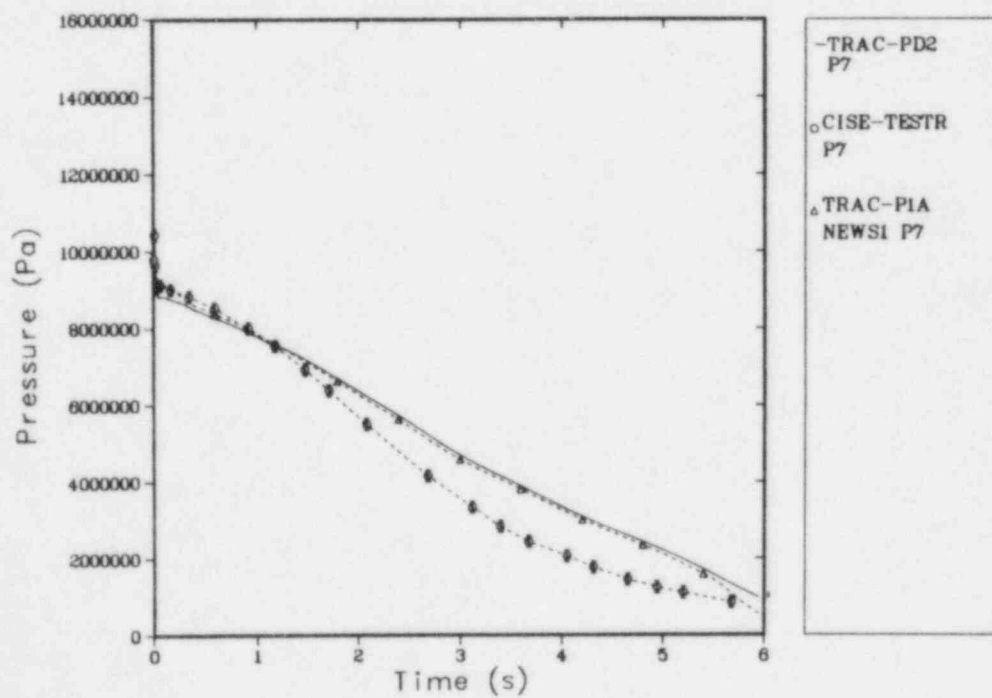


Fig. 21.
Pressure at measurement station P7 for heated CISE experiment.

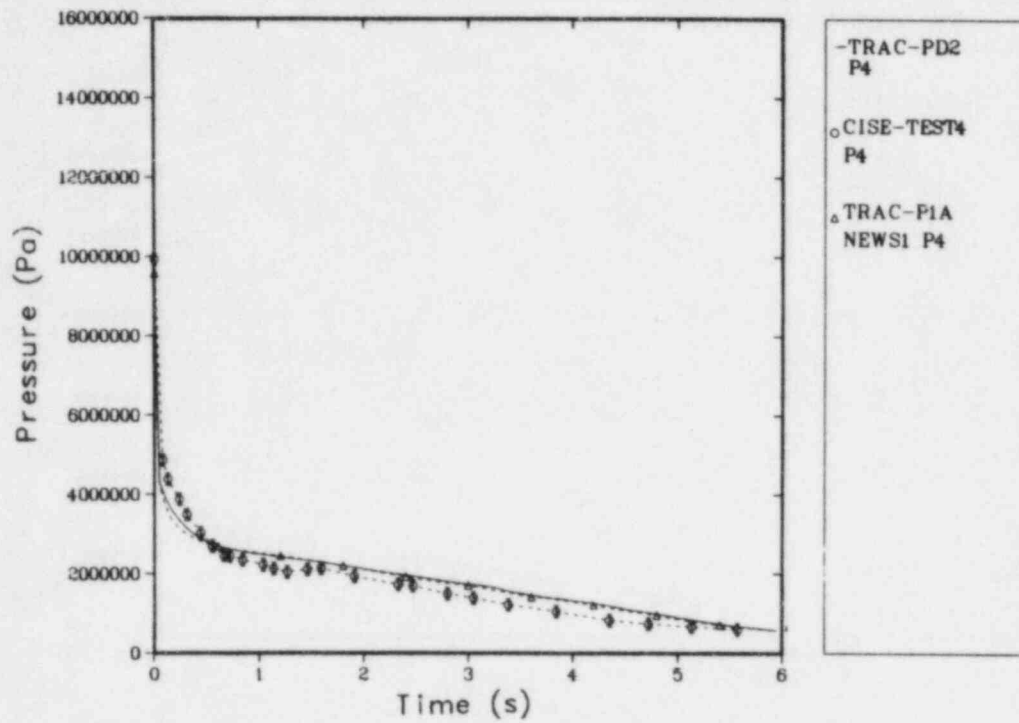


Fig. 22.
Pressure at measurement station P4 for unheated CISE experiment.

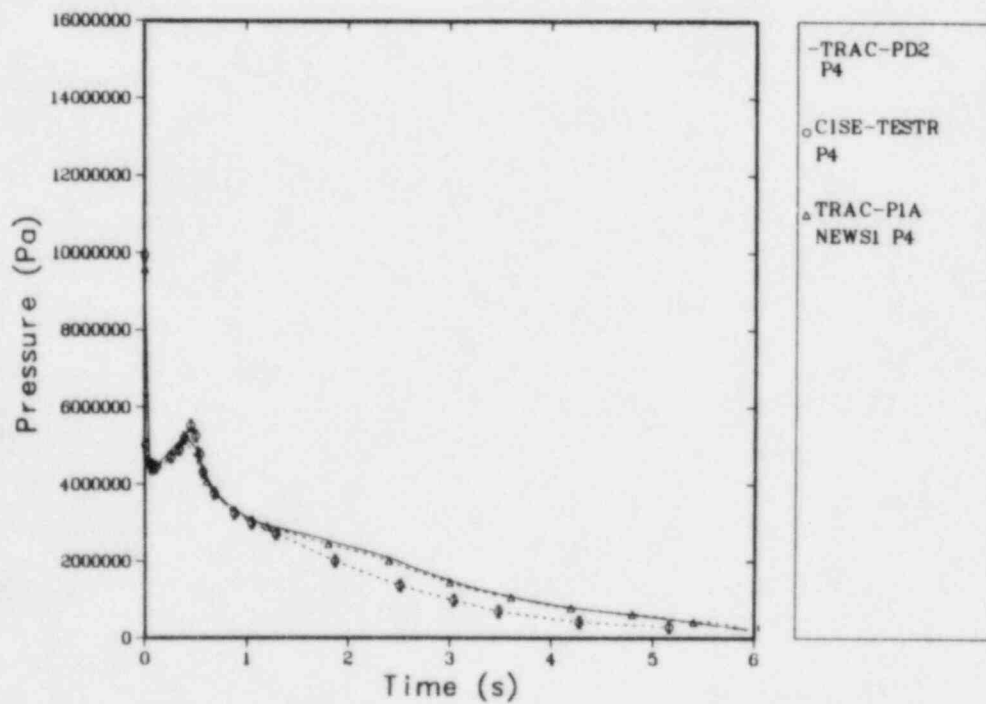


Fig. 23.
Pressure at measurement station P4 for heated CISE experiment.

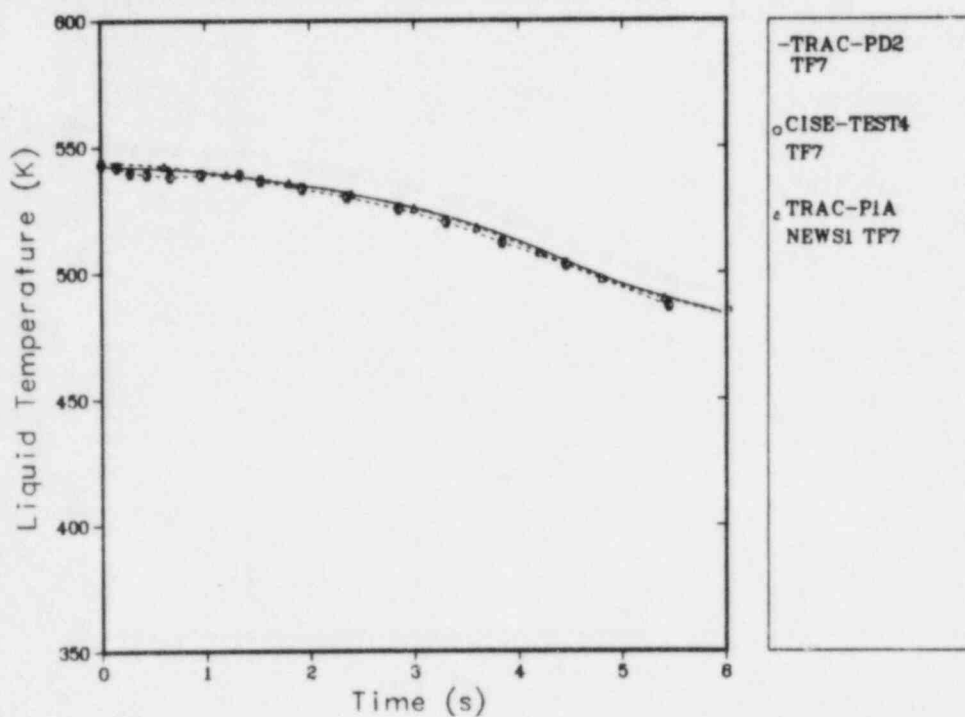


Fig. 24.

Liquid temperature at measurement station TF7 for unheated CISE experiment.

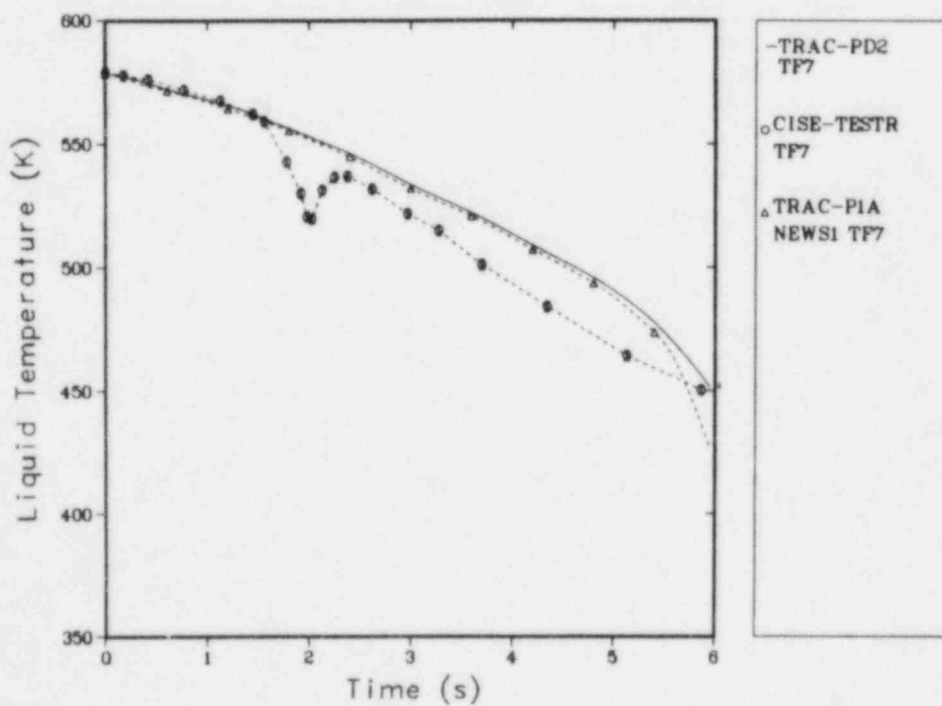


Fig. 25.

Liquid temperature at measurement station TF7 for heated CISE experiment.

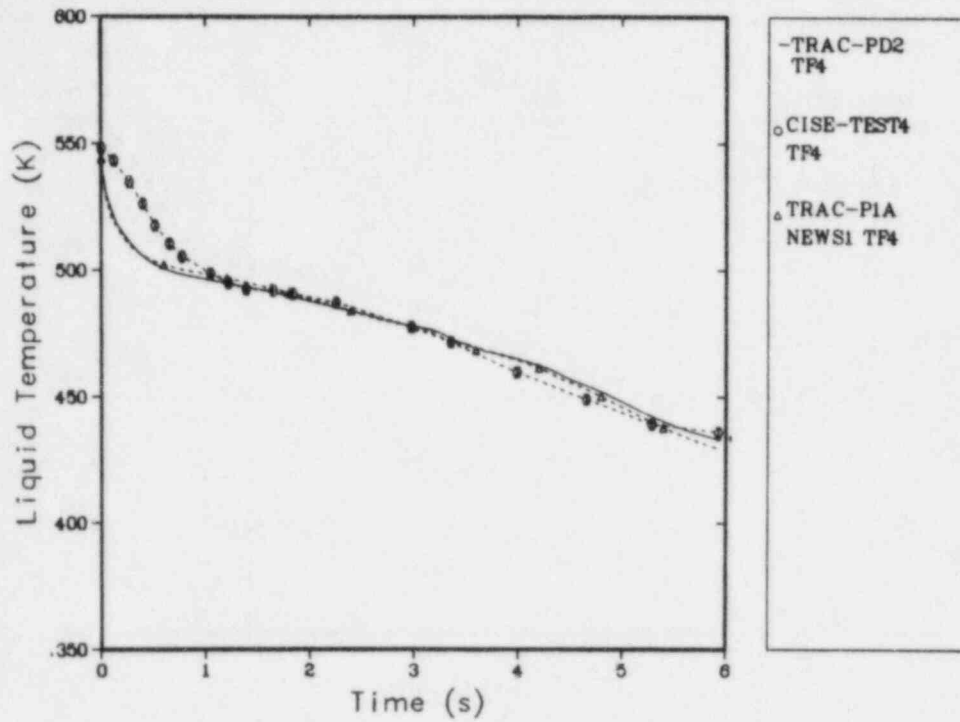


Fig. 26.
Liquid temperature at measurement station TF4 for unheated CISE experiment.

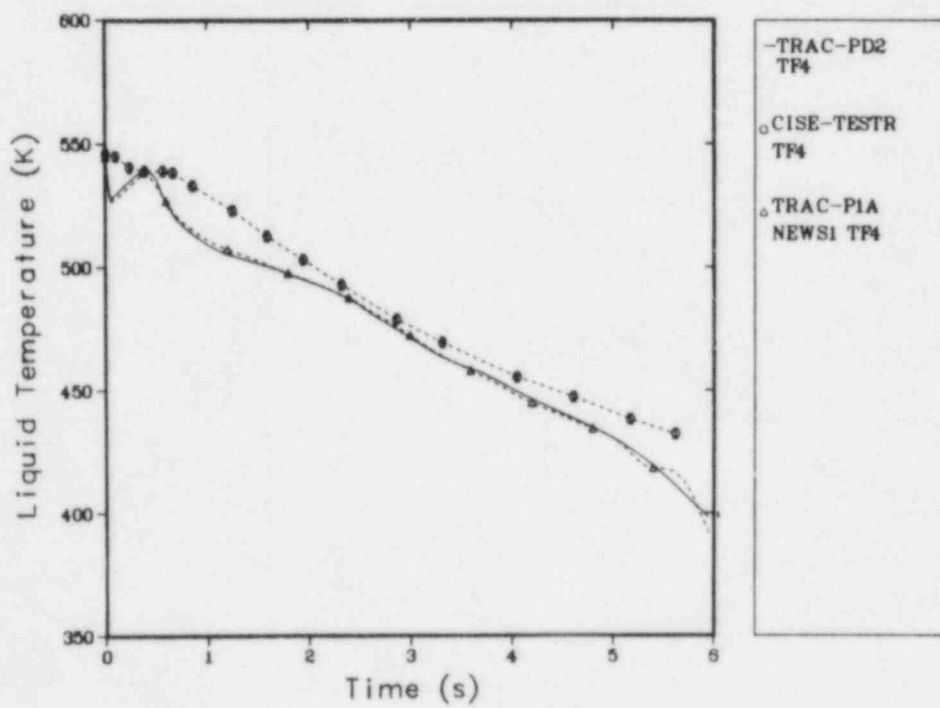


Fig. 27.
Liquid temperature at measurement station TF4 for heated CISE experiment.

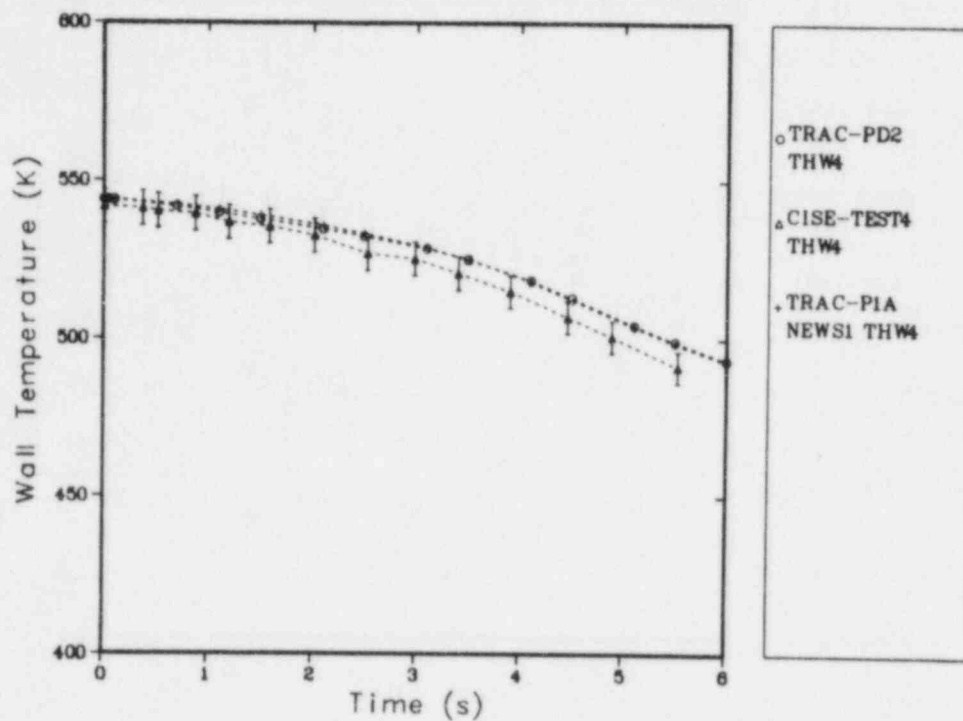


Fig. 28.

Wall temperature at measurement station THW4 for unheated CISE experiment.

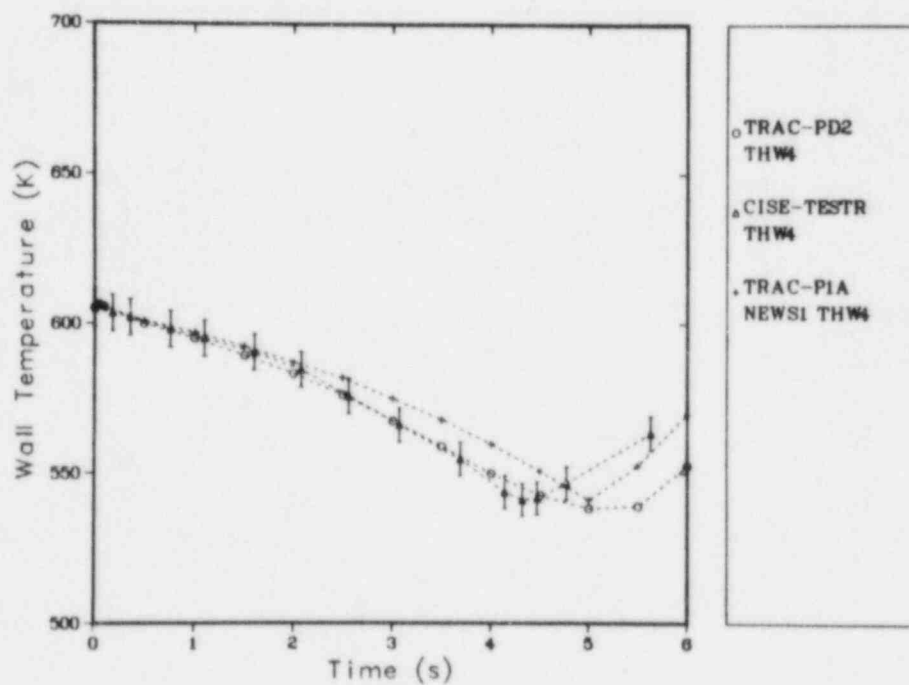


Fig. 29.

Wall temperature at measurement station THW4 for heated CISE experiment.

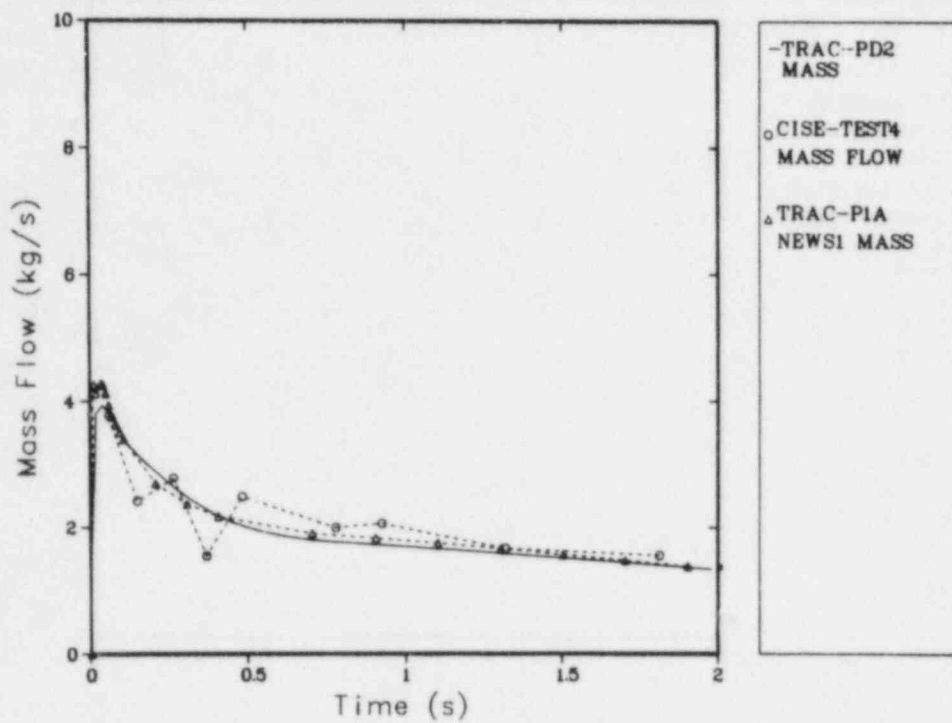


Fig. 30.
Test-section mass flow for unheated CISE experiment.

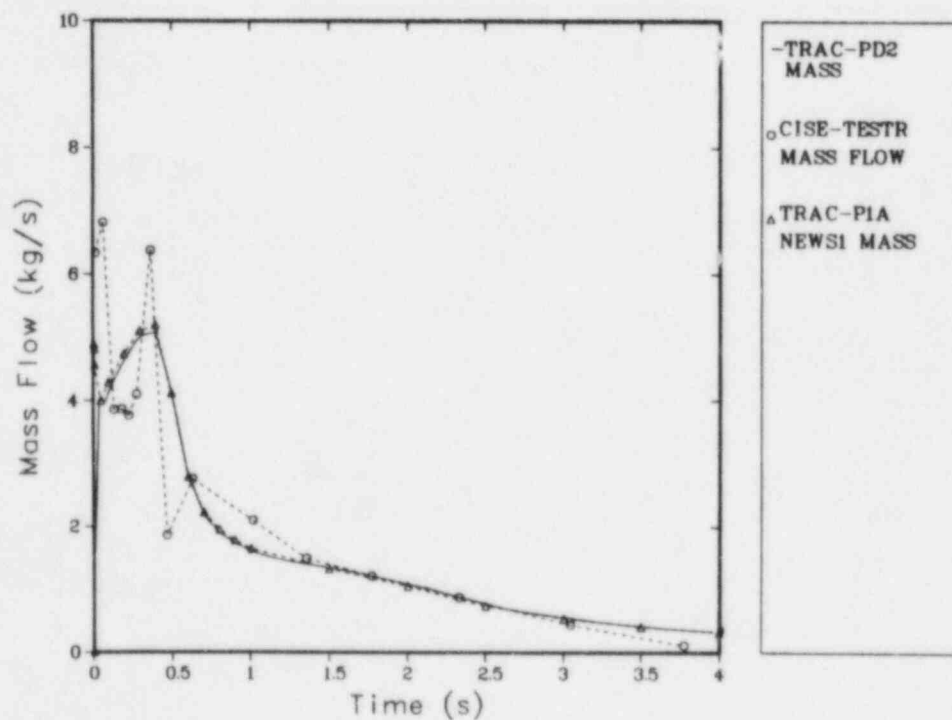


Fig. 31.
Test-section mass flow for heated CISE experiment.

friction-factor correlation ($NFF = 4$) was appropriate for this experiment. However, it would be desirable to incorporate flow-regime dependence into the wall-friction correlations and to specify pipe roughness through user input. Then, the code would select an appropriate friction-factor correlation based on local flow conditions and pipe roughness just as it uses local conditions for other constitutive relations.

The agreement between the TRAC-PD2 and the test results for Test R was not as good as that for Test 4. Perhaps some discrepancies were caused by measured and assumed initial conditions that were inconsistent with a calculated steady-state solution. Test R also provided a more stringent test of wall heat-transfer effects during blowdown. For both cases, the TRAC-PD2 results were very similar to TRAC-PLA calculated values except for the heated, radial midpoint wall temperature.

The transient calculations required 71 s of CPU time on a CDC 7600 computer for Test 4 and 255 s for Test R.

IV. MARVIKEN FULL-SCALE CRITICAL-FLOW TESTS 4 AND 24

A. Experiment Description

The Marviken full-scale critical-flow tests^{7,8} were designed to assess the ability of computer codes to predict large pressure-vessel blowdowns. The four major components were a pressure vessel, originally designed to be part of the Marviken nuclear power plant; a discharge pipe; a test nozzle with the minimum flow area in the system; and a rupture-disk assembly. Figure 32 shows the pressure vessel. Figure 33 shows the discharge pipe, test nozzle, and the rupture-disk assembly. The elevations in both figures were measured relative to the bottom of the vessel. Stations P103, P106, and P109 measured the pressure; stations T401, T402, and T405 measured the temperature. In Test 4, the nozzle had a minimum 0.509-m diameter with a length-to-diameter (L/D) ratio of 3.1; in Test 24, the nozzle had a minimum 0.500-m diameter with an L/D ratio of 0.33.

Figures 32 and 33 show the locations of the pressure and temperature transducers along the vessel and the discharge pipe. The transducer signals were processed through a signal-conditioning unit whose channels were connected to a pulse code-modulation system.

Before both tests, the vessel was filled partially with deionized water, which was heated by removing it from the bottom of the vessel through an electric heater and adding it to the steam dome at the top of the vessel. This procedure produced a complicated initial temperature distribution in the vessel. A saturated steam dome filled the vessel region above the initial water level and the water at the nozzle inlet was subcooled substantially (60 K). Both tests were initiated by releasing the rupture disks and were terminated by closing a ball valve in the discharge pipe after 49 s for Test 4 and after 54 s for Test 24.

B. TRAC-PD2 Model

The TRAC models of Marviken Tests 4 and 24 included four components. A zero-velocity FILL modeled the vessel upper boundary; a semi-implicit PIPE modeled the vessel above the 2.6-m elevation including the maximum diameter region plus the top cupola; a fully implicit PIPE modeled the lower part of the vessel, discharge pipe, nozzle, and rupture-disk assembly; and a BREAK component provided a pressure boundary condition at the rupture-disk-assembly lower boundary.

In Test 4, the semi-implicit pipe used 15 cells, whereas the fully implicit pipe used 45. In Test 24, 15 and 27 cells were used, respectively. Parametric studies³ for both tests that reduced the number of cells in PIPE 3 and kept the same number of cells in PIPE 2 yielded virtually identical results. Figure 34 shows the noding for the vessel and the discharge pipe. Figures 35 and 36 show the noding for the nozzle and the rupture-disk assembly for Tests 4 and 24, respectively. Figures 37-40 show the TRAP-generated noding diagrams. The calculated results were sensitive to the initial, nonuniform temperature distribution. Although the experimenters specified this temperature distribution, some averaging was necessary to describe the system with discrete fluid cells. Because it was difficult to represent accurately the steep initial temperature ramps in the vessel, we recommended that the minimum number of cells in PIPE 1 should be 15. Table V lists the locations of the measured and calculated quantities.

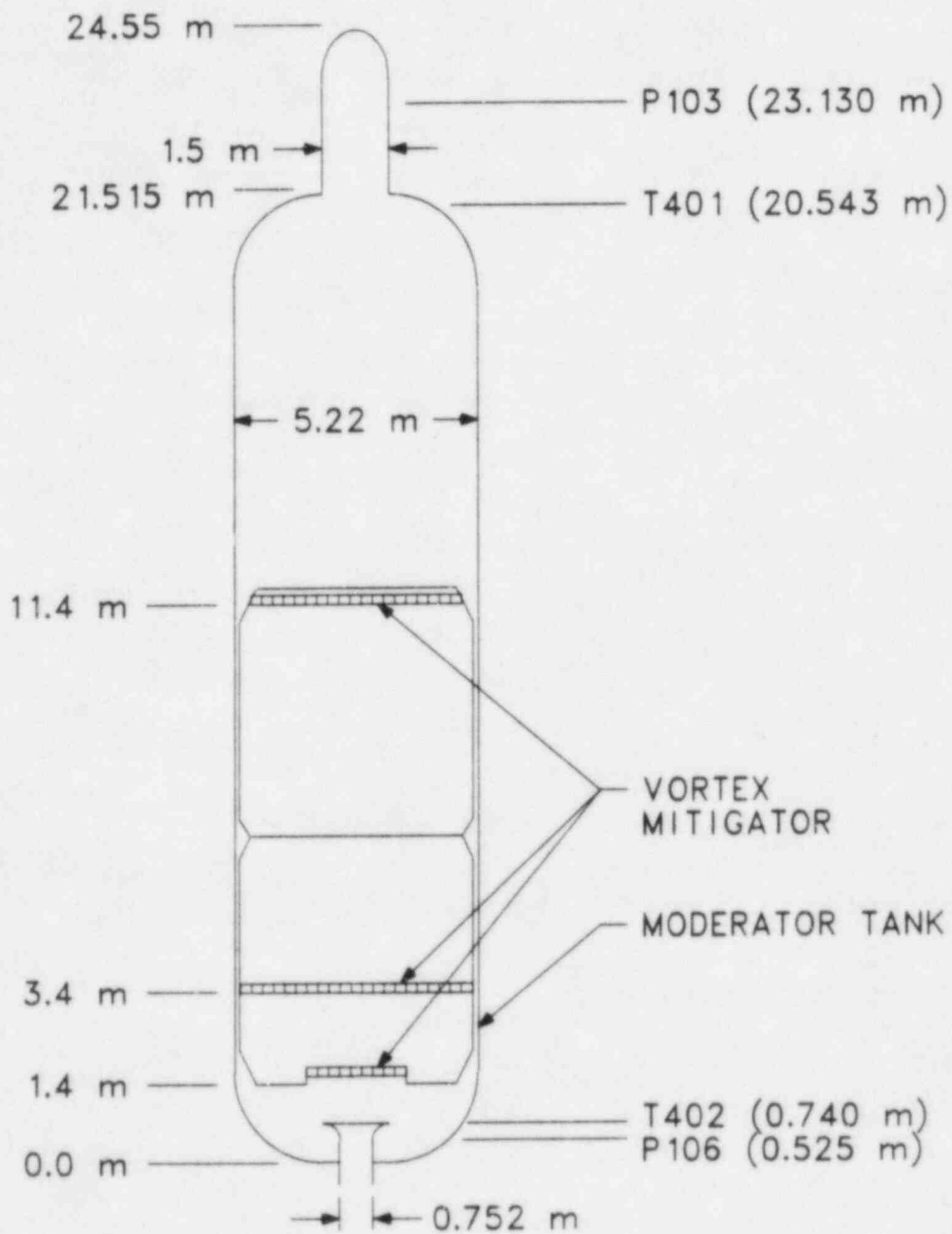


Fig. 32.
Pressure vessel for Marviken Tests 4 and 24.

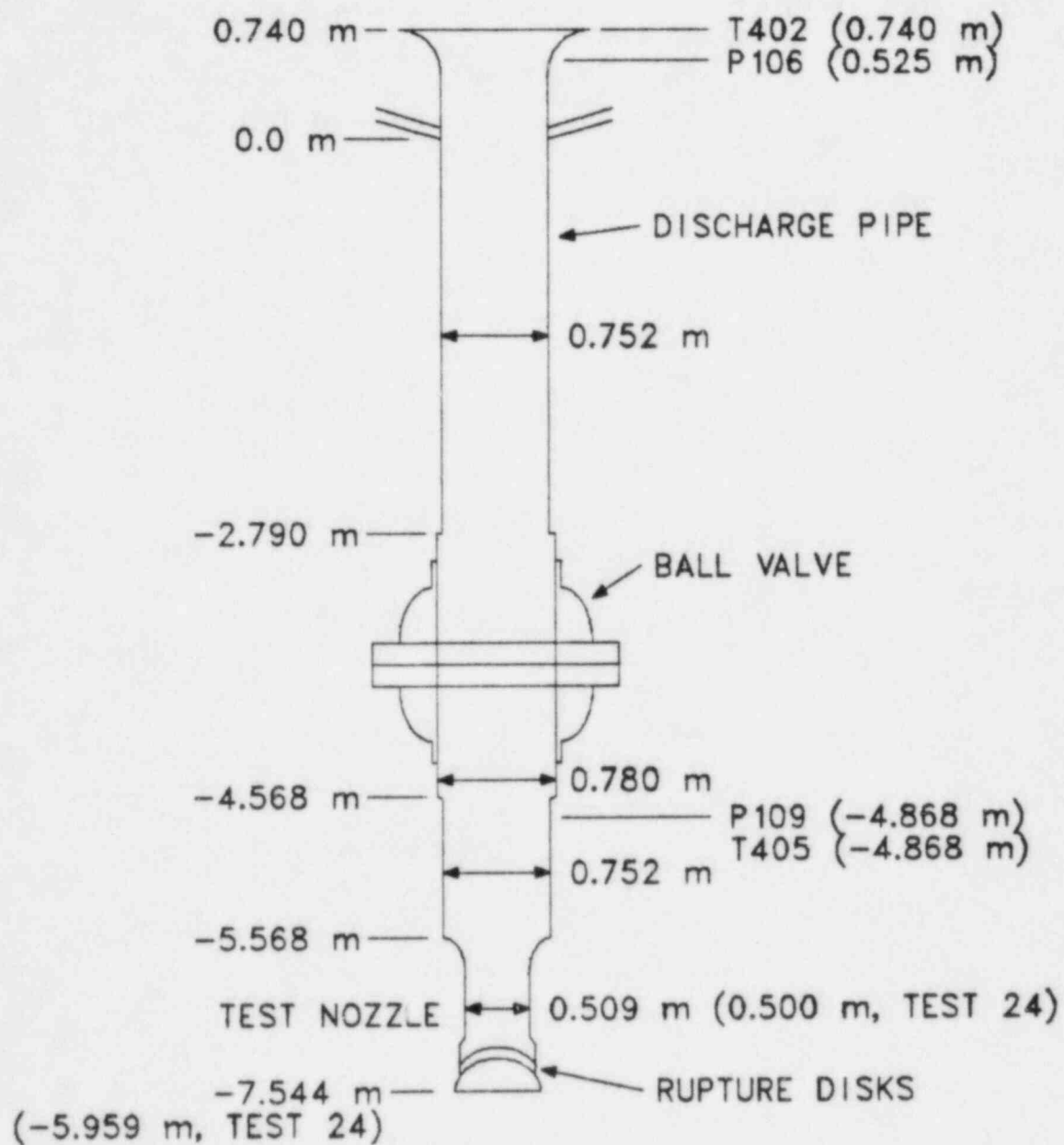


Fig. 33.

Discharge pipe, test nozzle, and rupture-disk assembly for Marviken Tests 4 and 24.

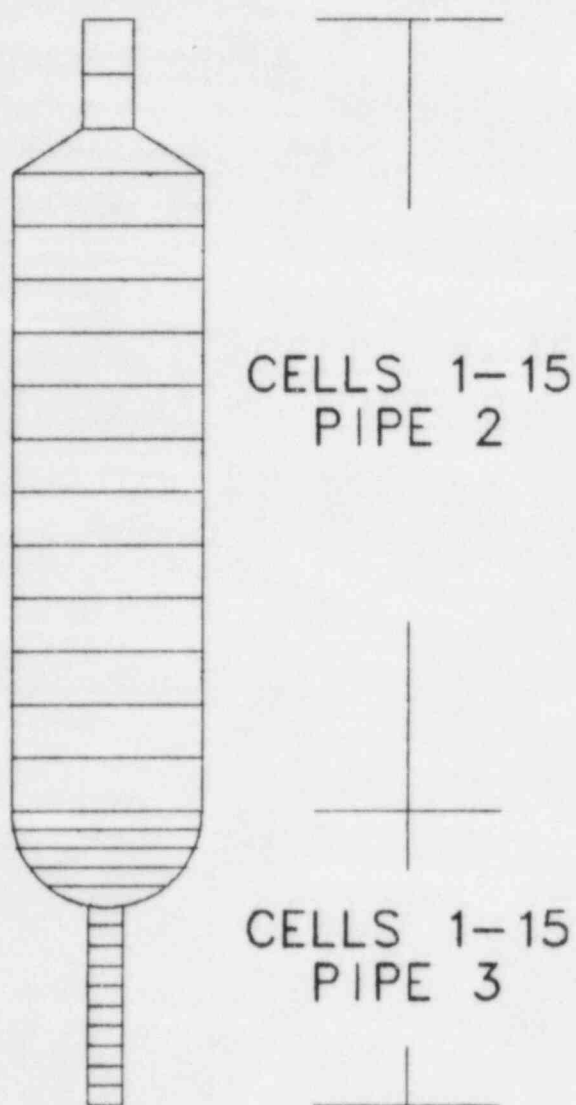


Fig. 34.
TRAC noding diagram of vessel and
discharge pipe for Marviken Tests 4
and 24.

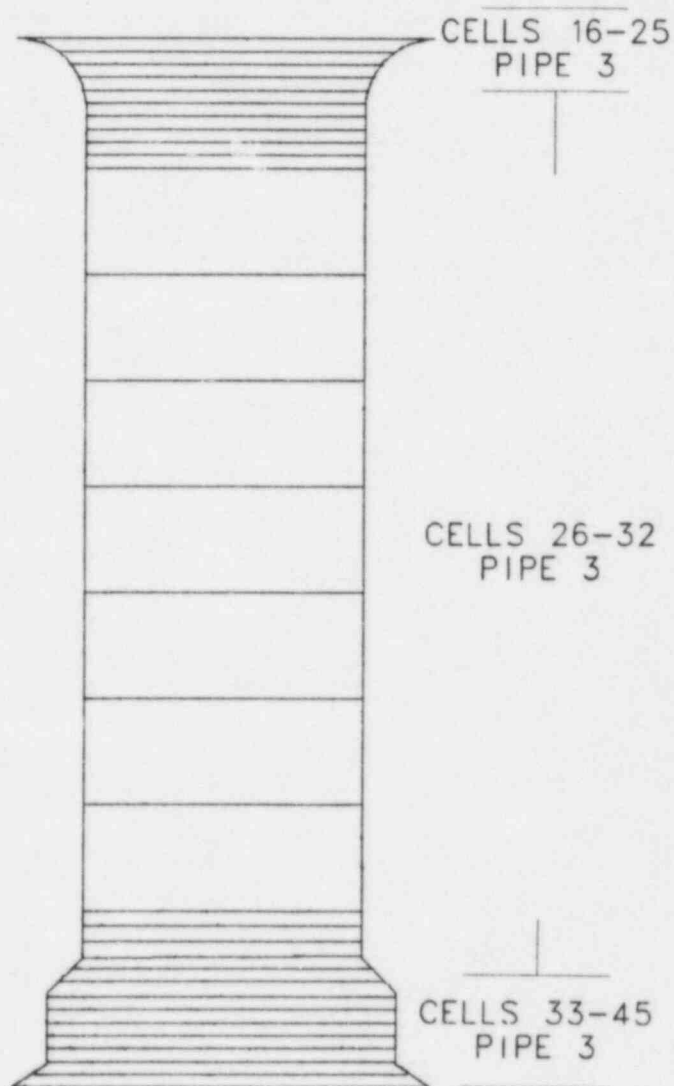


Fig. 35.
TRAC noding diagram of nozzle and
rupture-disk assembly for Marviken
Test 4.

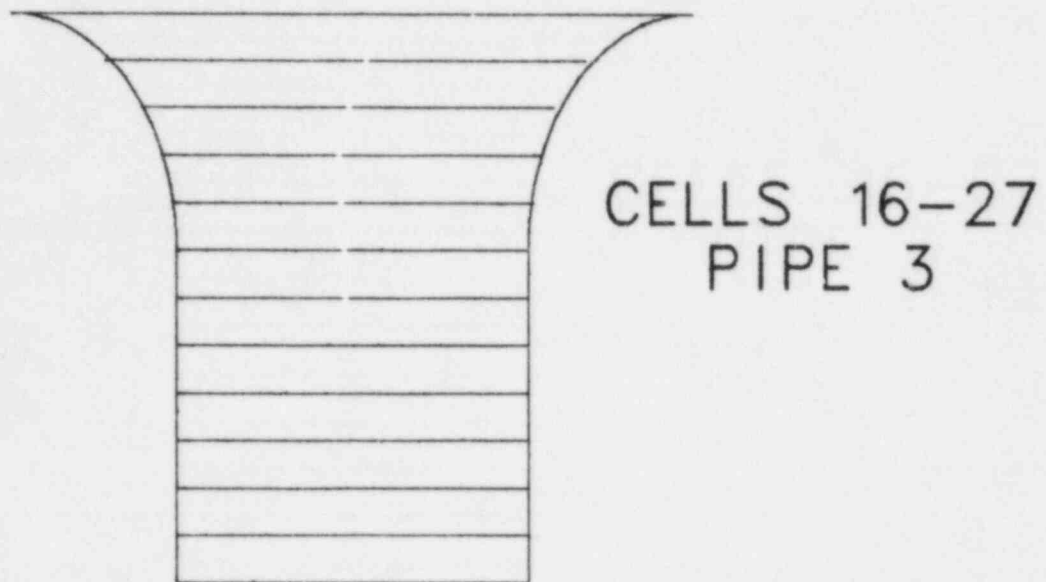


Fig. 36.

TRAC noding diagram of nozzle and rupture-disk assembly for Marviken Test 24.

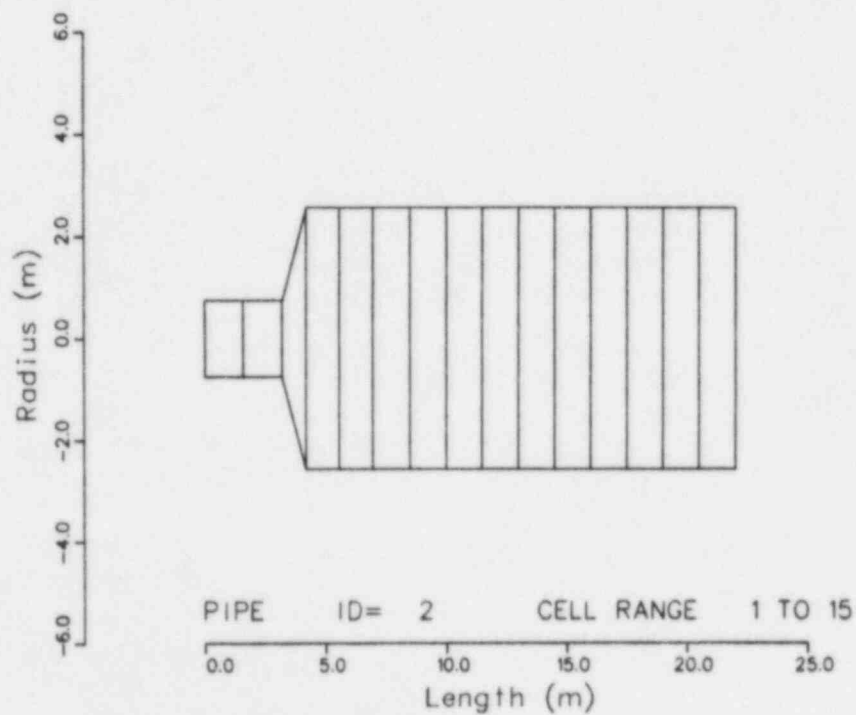


Fig. 37.

TRAP-generated noding diagram of PIPE 2 for Marviken Test 4.

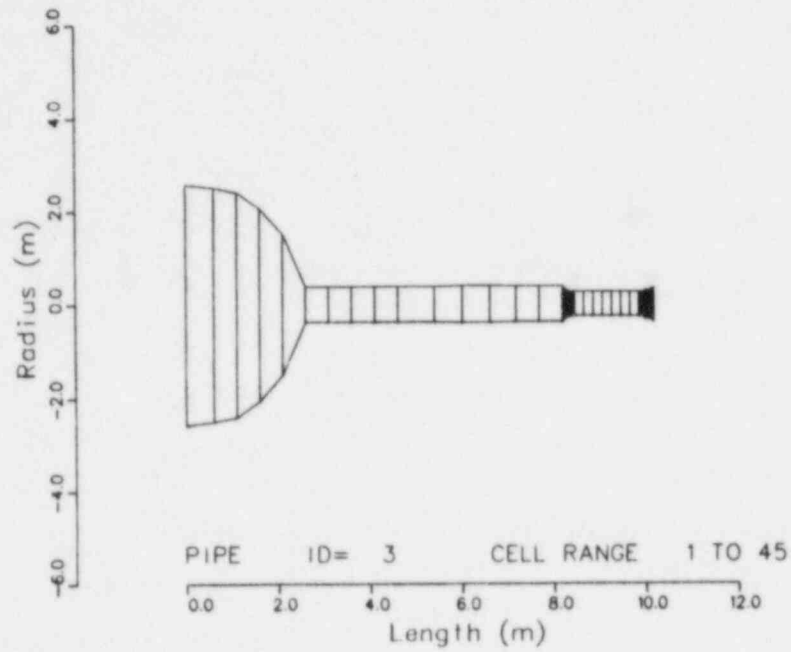


Fig. 38.

TRAP-generated noding diagram of PIPE 3 for Marviken Test 4.

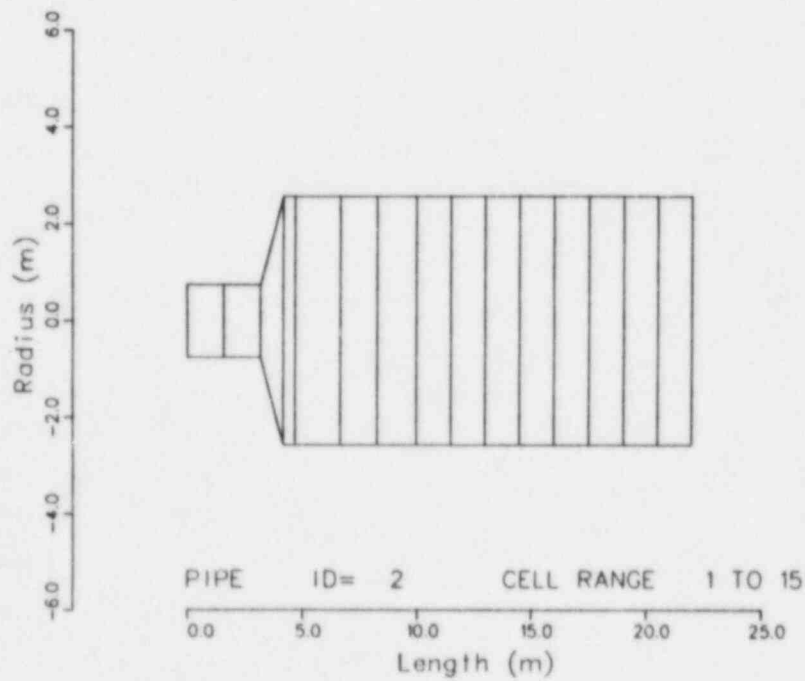


Fig. 39.

TRAP-generated noding diagram of PIPE 2 for Marviken Test 24.

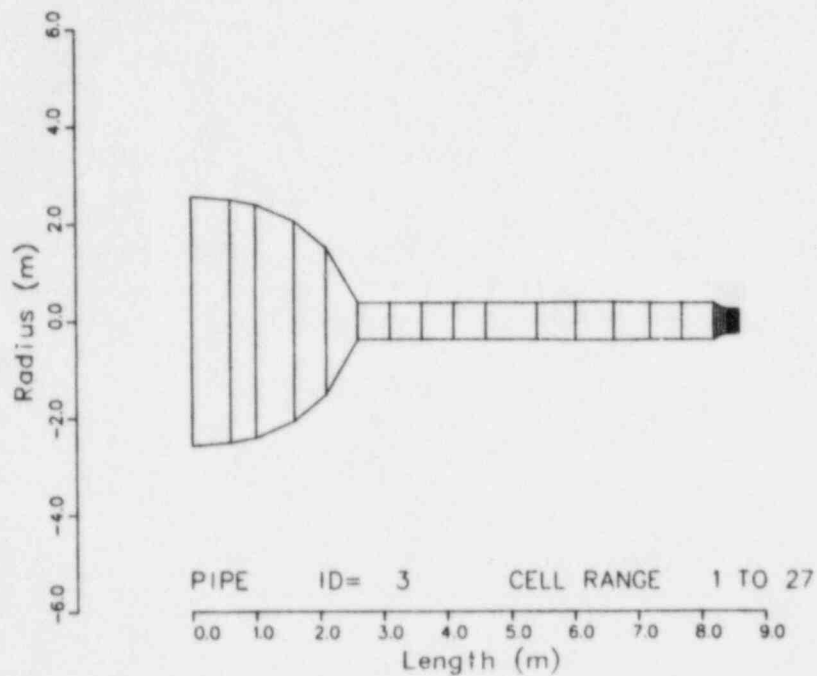


Fig. 40.

TRAP-generated noding diagram of PIPE 3 for Marviken Test 24.

TABLE V

LOCATION OF MEASURED AND CALCULATED QUANTITIES
FOR MARVIKEN BLOWDOWN EXPERIMENTS (TESTS 4 AND 24)

<u>Measured</u>		<u>Calculated</u>	
<u>Measurement Station</u>	<u>Parameter</u>	<u>Component</u>	<u>Cell</u>
P103	Pressure (Pa)	PIPE 2	2
T401	Temperature (K)	PIPE 2	3
P106	Pressure (Pa)	PIPE 3	5
T402	Temperature (K)	PIPE 3	4
P109	Pressure (Pa)	PIPE 3	14
P405	Temperature (K)	PIPE 3	14
--	Mass flow ($\text{kg} \cdot \text{s}^{-1}$)	BREAK 4	--

Because the vessel included some internal structure, the actual 5.220-m diameter was reduced to 5.136 m in the TRAC model to obtain the correct initial water mass and net available internal volume. The discharge pipe was modeled as if it were located at the vessel bottom. The annular-flow friction-factor correlation option, $NFF = 4$, was specified. For the TRAC-PD2 developmental assessment, we used the best-estimate model developed for TRAC-PlA. Appendix C lists the input decks for Marviken Tests 4 and 24, respectively.

C. Data Comparisons

The TRAC results were compared with the blowdown flow rate and the pressures and temperatures at several locations for Tests 4 and 24. Table VI lists the important critical-flow test conditions. The table shows that the tests were similar except the nozzle length in Test 24 was one-tenth the nozzle length in Test 4. Because the test results were qualitatively the same, the same discussion applies to both experiments.

Figures 41 and 42 compare the TRAC mass flow with the flow derived from the pitot-static velocity and the vessel differential-pressure measurements. The pitot-static data curve was valid throughout the transient, whereas the vessel differential-pressure curve was valid only after ~ 5 s. The TRAC results agreed closely with the initial peak, somewhat underpredicted the subcooled part of the blowdown, and agreed well when saturation occurred at the nozzle (17 s for Test 4 and 25 s for Test 24). The differences between the calculations and the data at the end of the transient resulted from the different emptying times. Figures 43-48 compare the pressures for the upper and lower vessel and the discharge pipe for both tests. During the first 3 s, there was a dip in the test data that did not appear in the calculations; the code did not calculate the dip because the constitutive relations do not permit delayed nucleation. After the dip, the code slightly underpredicted the pressure at all three locations during the subcooled depressurization. After the system reached saturation, the pressure comparisons were very good. The discrepancies at the end of the transient reflected different emptying times.

Figures 49-54 compare the fluid temperatures for Tests 4 and 24 at two locations in the vessel and one location in the discharge pipe. In Figs. 50, 51, 53, and 54 the temperature increased above the initial subcooling because the warm liquid near the top of the mixture level moved downward in the vessel and in the discharge pipe as the vessel emptied. The code did not calculate as sharp a rise in the temperature as shown in the data because the fluid conditions in a hydraulic cell were averaged as warm liquid mixed with the

TABLE VI
MARVIKEN CRITICAL-FLOW TEST CONDITIONS

Test Number	Initial Sub-cooling near Vessel Bottom (K)	Initial Sub-cooling at Nozzle Inlet (K)	Water Level (m)	Initial Pressure (MPa)	Nozzle Diameter (m)	L/D
4	36	60	17.6	4.94	0.509	3.1
24	33	76	19.88	4.96	0.500	0.3

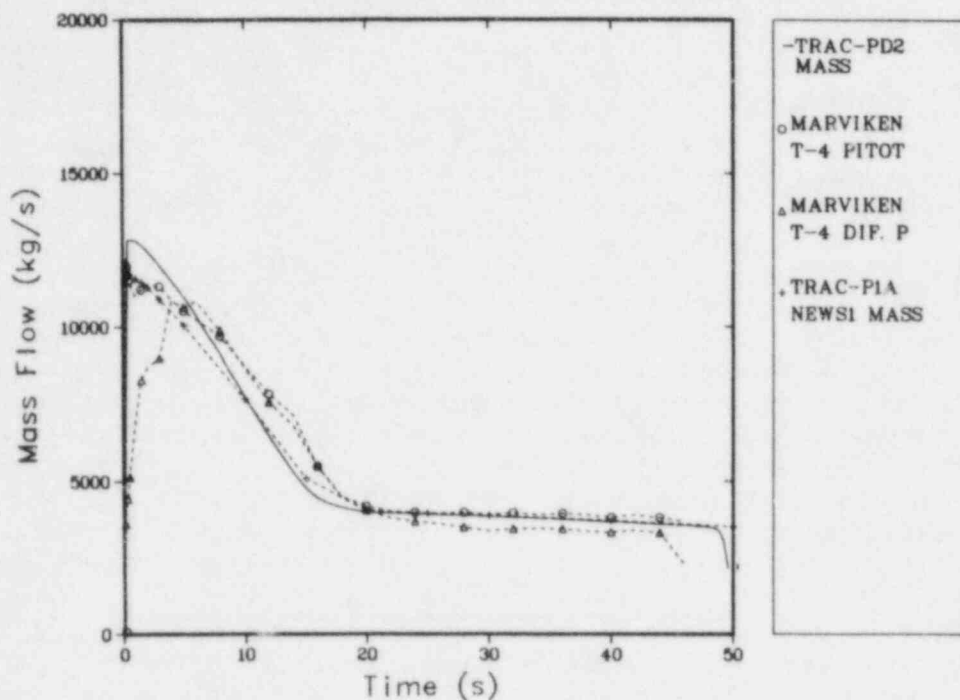


Fig. 41.
Mass flow for Marviken Test 4.

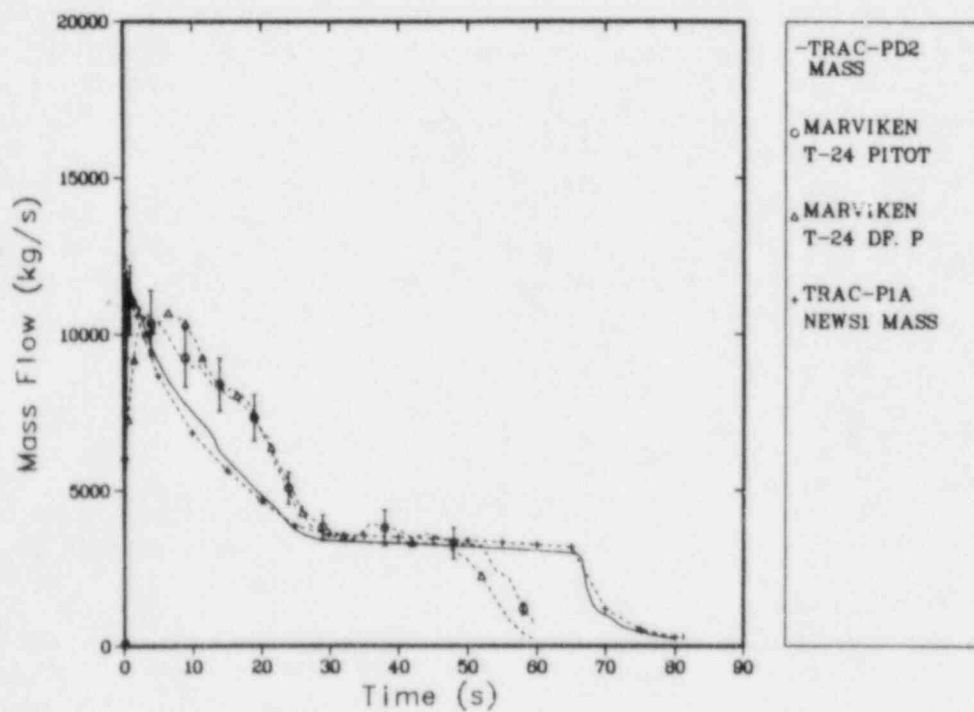


Fig. 42.
Mass flow for Marviken Test 24.

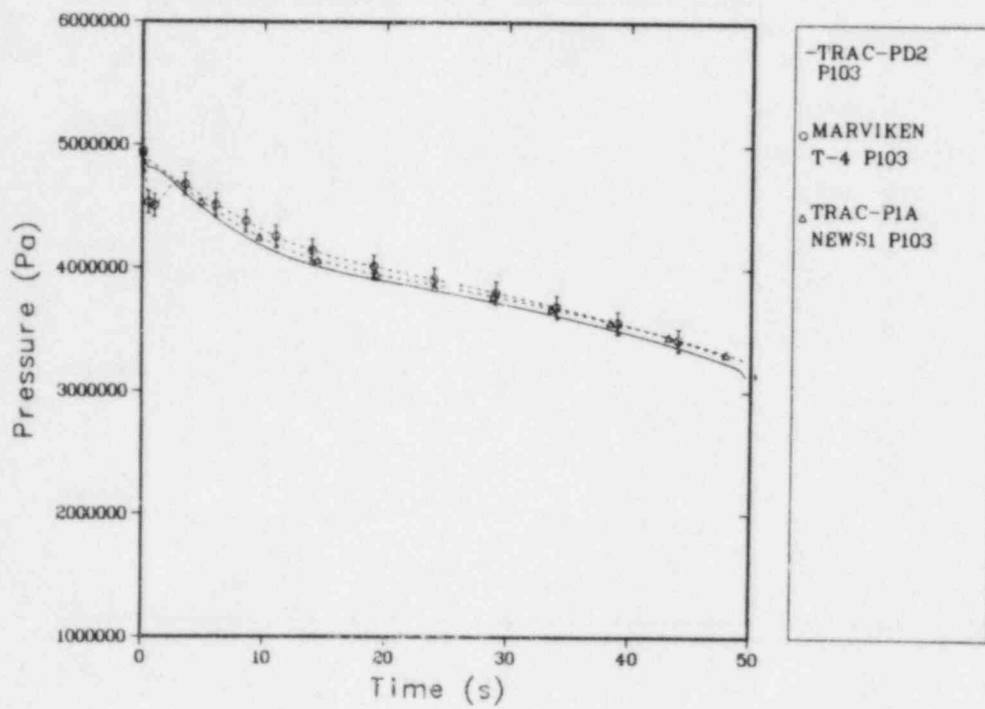


Fig. 43.
Pressure at measurement station P103 for Marviken Test 4.

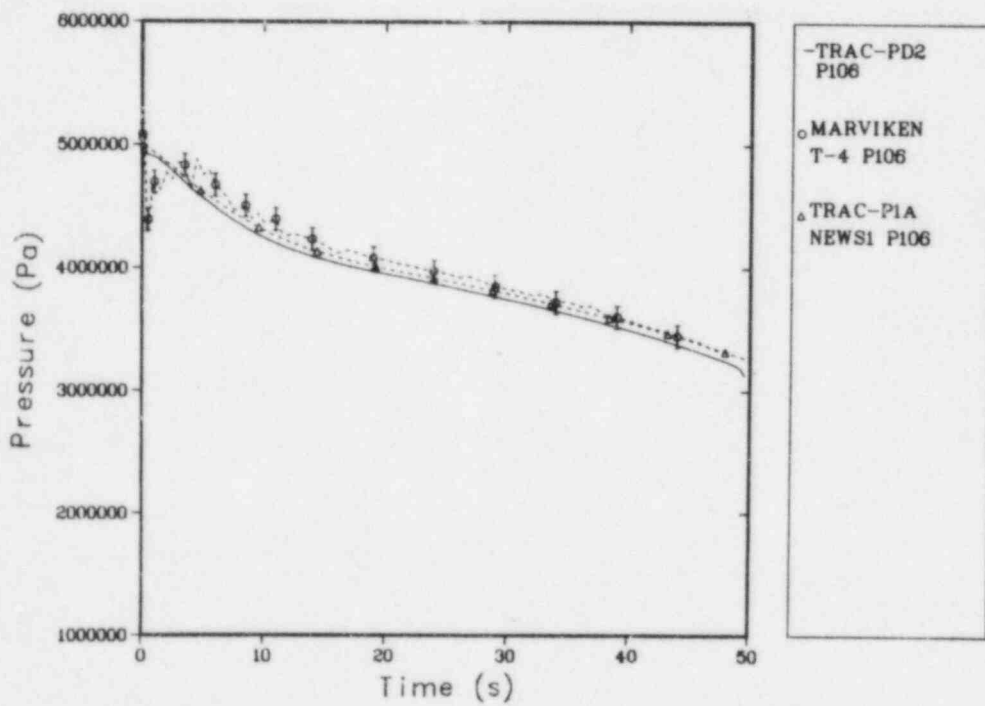


Fig. 44.
Pressure at measurement station P106 for Marviken Test 4.

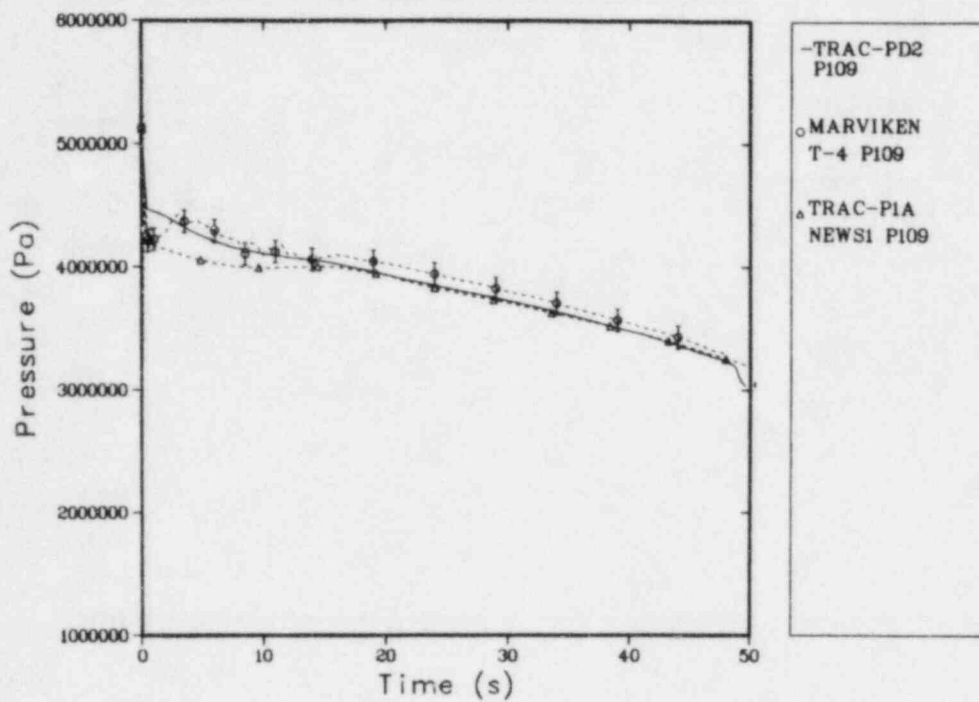


Fig. 45.
Pressure at measurement station P109 for Marviken Test 4.

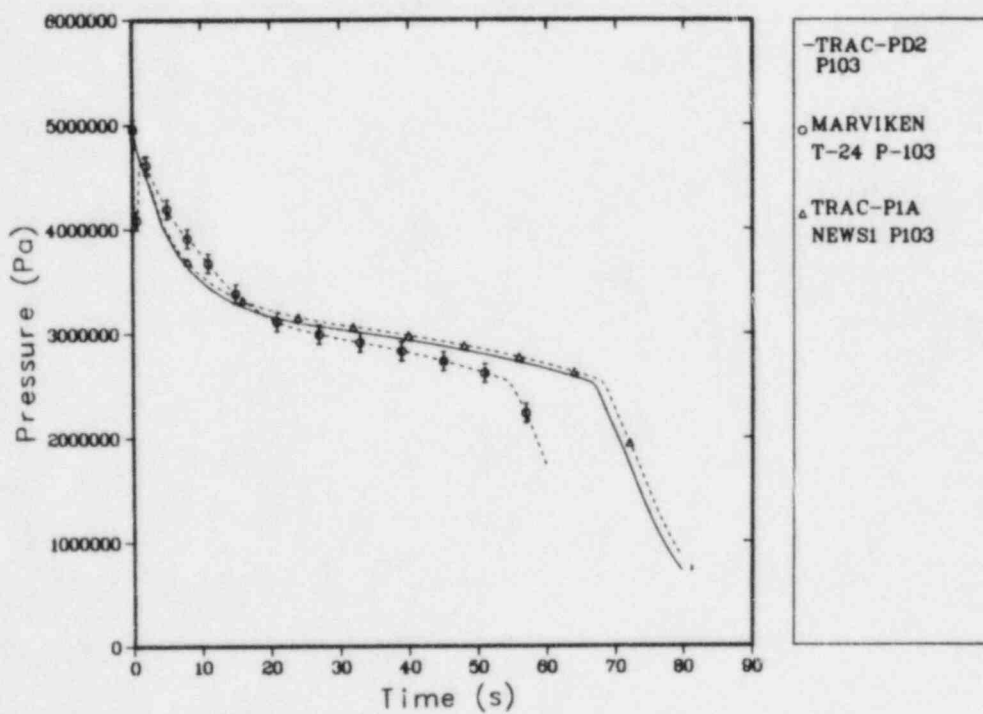


Fig. 46.
Pressure at measurement station P103 for Marviken Test 24.

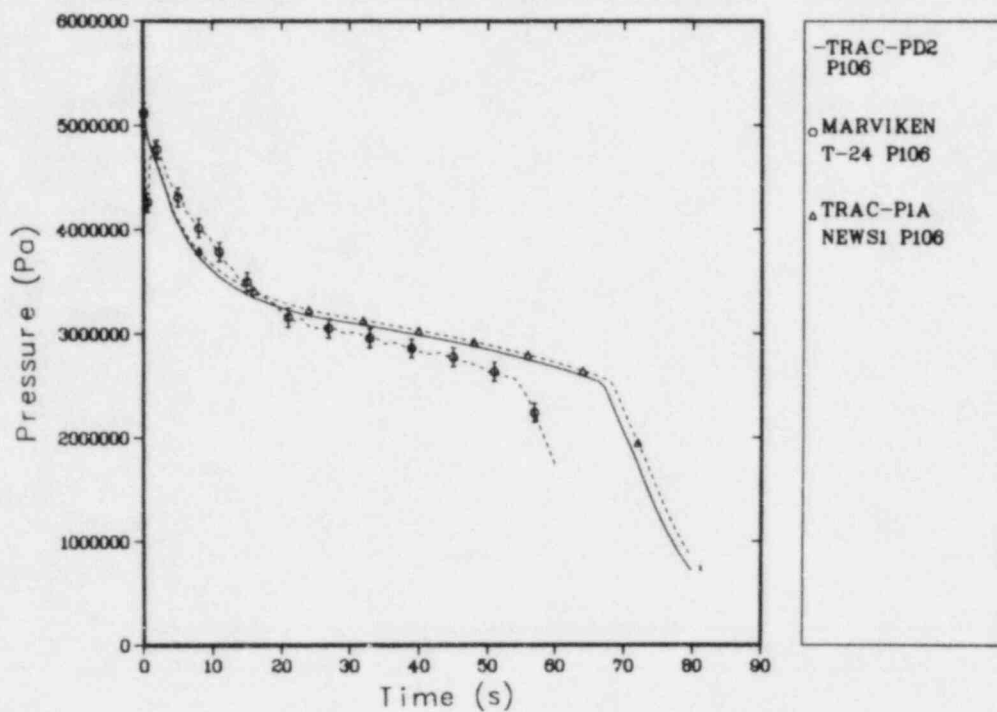


Fig. 47.
Pressure at measurement station P106 for Marviken Test 24.

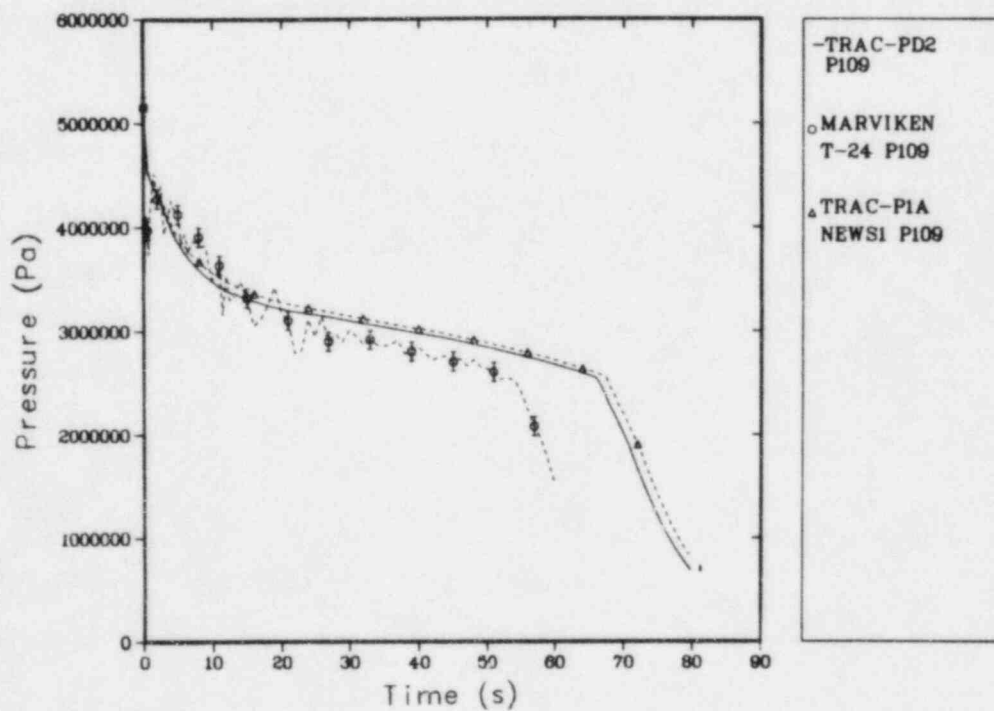


Fig. 48.
Pressure at measurement station P109 for Marviken Test 24.

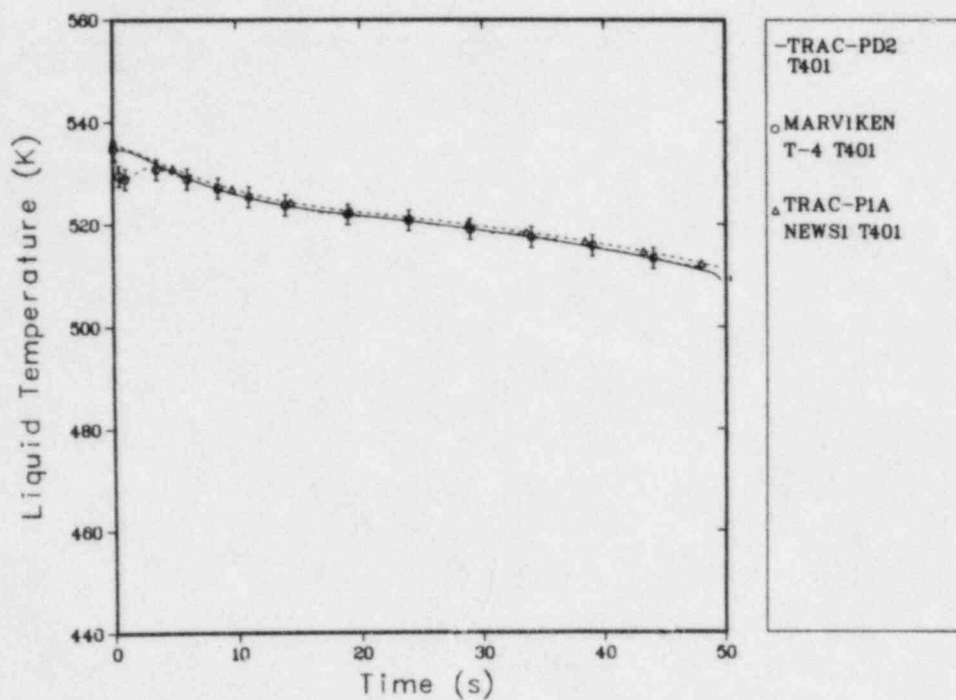


Fig. 49.
Liquid temperature at measurement station T401 for Marviken Test 4.

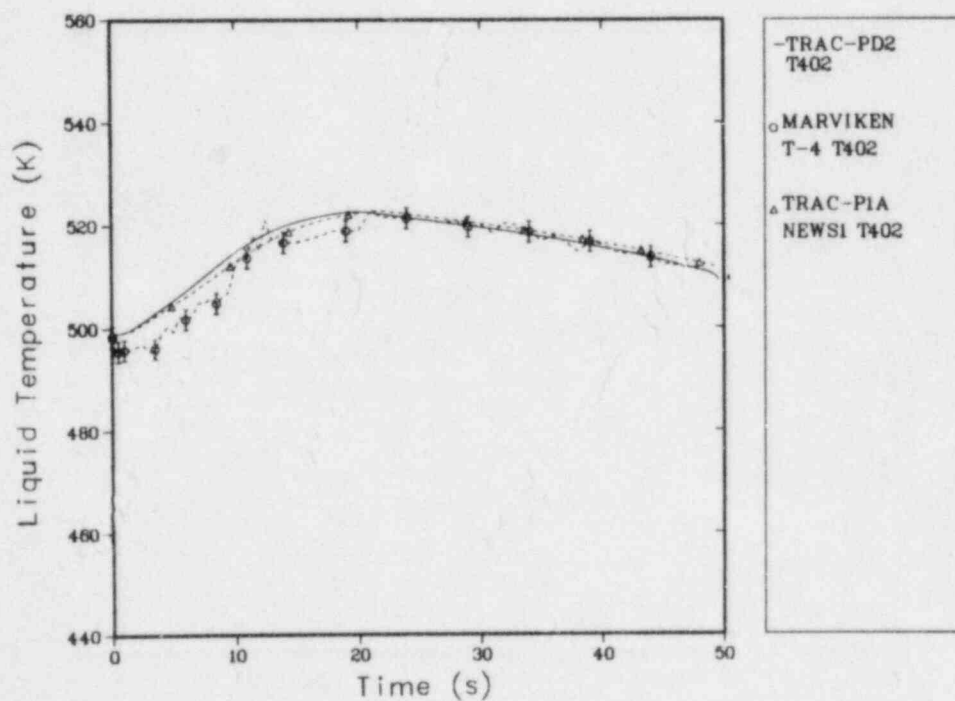


Fig. 50.
Liquid temperature at measurement station T402 for Marviken Test 4.

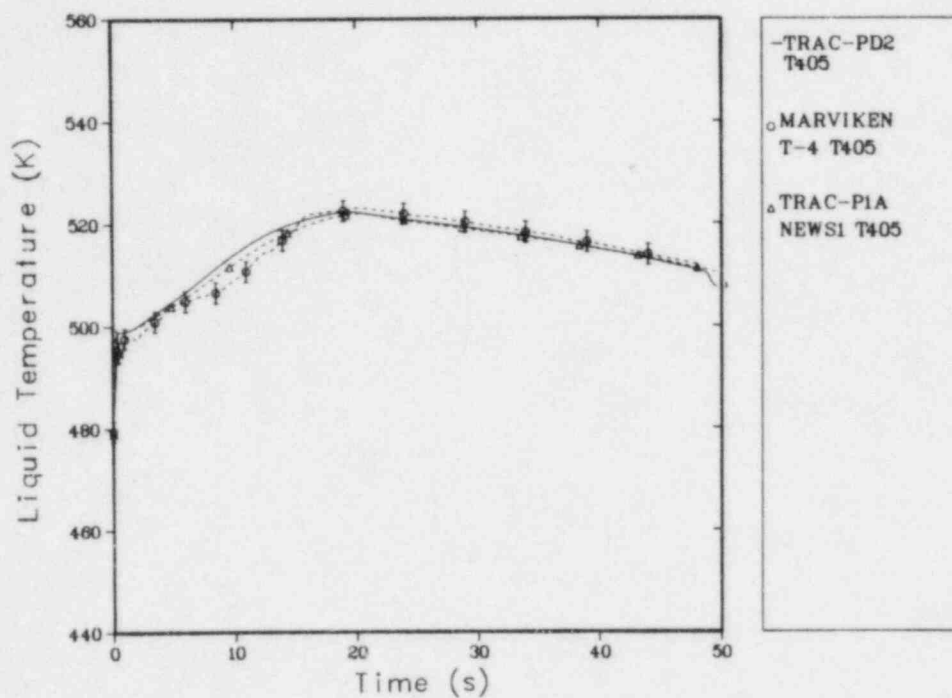


Fig. 51.
Liquid temperature at measurement station T405 for Marviken Test 4.

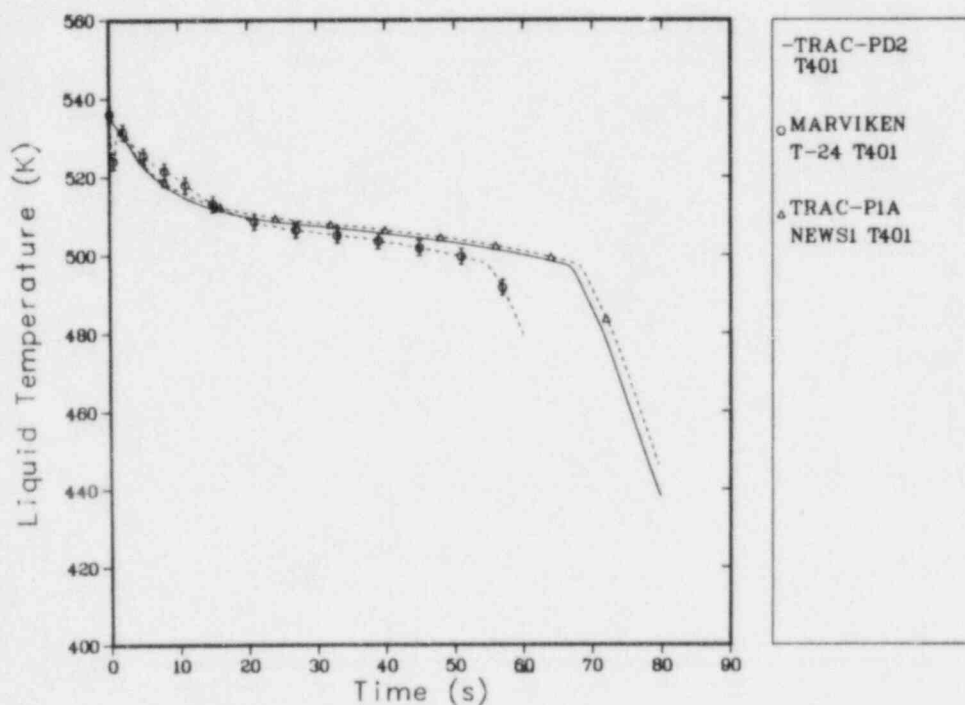


Fig. 52.
Liquid temperature at measurement station T401 for Marviken Test 24.

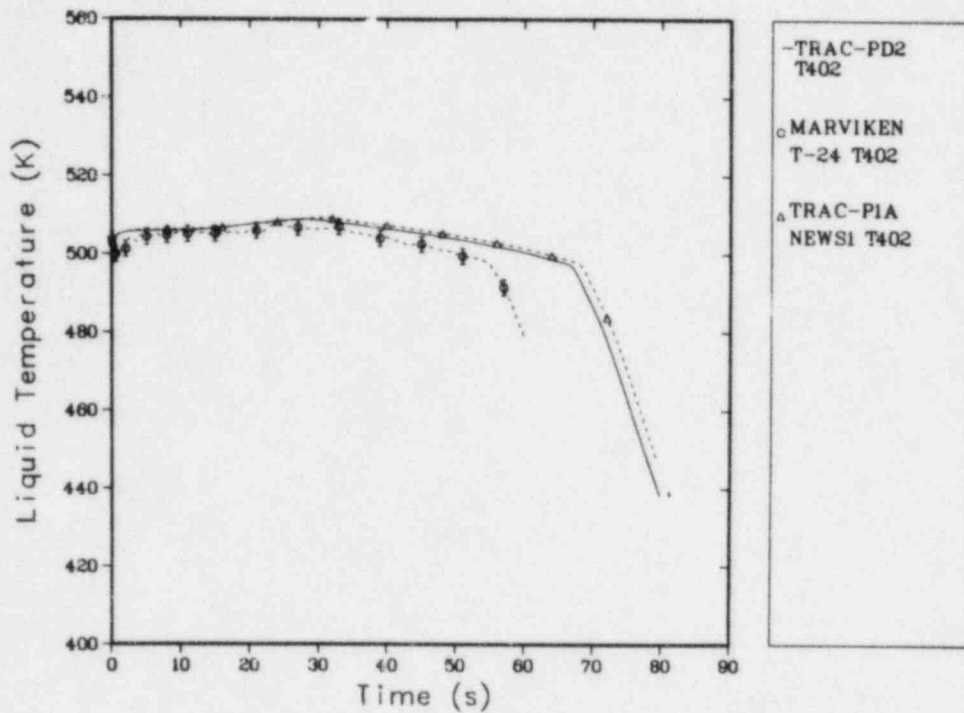


Fig. 53.
Liquid temperature at measurement station T402 for Marviken Test 24.

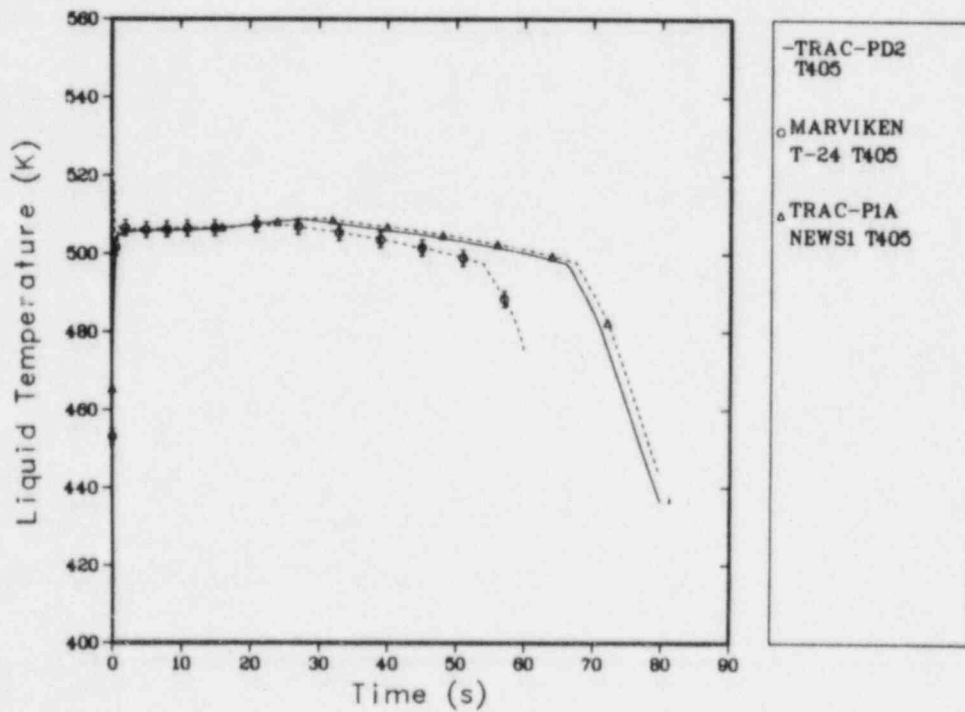


Fig. 54.
Liquid temperature at measurement station T405 for Marviken Test 24.

cooler liquid. The mixing process in a cell diffused the thermal stratification in the liquid. After the peak temperature was reached, the temperature, although slightly delayed, corresponded to the saturation curve.

In summary, when we related the data comparisons to the information in Table VI, we found that the quality of the comparisons degraded as the L/D ratio decreased. The discrepancy between emptying times increased as the mass-flux underprediction became more severe. The quality of the comparisons for other parameters such as temperature, pressure, and density was related directly to the quality of the mass-flux comparisons.

Experiment uncertainty information was provided.^{7,8} For pressure data, the uncertainty was ± 90 kPa; for temperature data, ± 2 K. For mass-flow comparisons, the pitot-static data uncertainty was $\pm 15\%$ and the vessel differential-pressure data uncertainty was $\pm 10\%$ after 5 s.

D. Conclusions

The Marviken calculations used the same code components (PIPE, FILL, and BREAK) that the other blowdown calculations used. In addition to most of the effects present in the Edwards' and CISE experiments, the Marviken experiment included full-scale effects and large flow-area variations.

For both tests, the TRAC-PD2 results were similar to the TRAC-PLA calculated values. The comparison between the calculated and measured results indicated that the code underpredicted the flow and did not calculate correctly the nonequilibrium effects when the upstream conditions were subcooled and the critical flow was controlled by nonequilibrium effects. The longer nozzle, because of frictional effects, tended to drive the flow toward equilibrium and, thus, accounted for the improved comparisons at large L/D ratios. Once the system reached saturation, the code generally calculated the correct critical flows. The results were sensitive to the initial system temperature distribution.

The discrete nature of the hydraulic cells caused the artificial mixing of the hotter liquid near the top of the liquid region with the colder liquid farther down in the vessel and, ultimately, propagated the higher enthalpy fluid to the break earlier than demonstrated in the tests. The constitutive relations in TRAC-PD2 do not permit delayed nucleation; thus, the code did not calculate the initial dip in pressure at the beginning of the tests and forced the critical-flow calculation toward equilibrium.

In conclusion, after the early portion of the transient, the good agreement between the calculated and measured results indicated that TRAC-PD2 properly treats scale effects in one-dimensional critical-flow configurations. Also, because of these calculations we identified the possible need for a delayed-nucleation model.

The calculations for Tests 4 and 24 required 130 s of CPU time on a CDC 7600 computer.

V. THTF TEST 177 BLOWDOWN EXPERIMENT

A. Experiment Description

The THTF was designed to investigate heat transfer in an electrically heated rod bundle that simulates a PWR core. Test 177 simulated the core thermal-hydraulic response during a blowdown. Figure 55 is a schematic of the THTF.

This blowdown experiment is a nonnuclear pressurized water loop containing a 7×7 array of fuel-pin simulators.⁹ The fuel-pin simulators had a 3.66-m heated length, a 0.010 77-m diameter, and a 82-kW input per pin. In this test, 45 of the 49 pins were electrically heated. During steady-state operation, water was pumped through the system at a nominal rate of $23 \text{ kg} \cdot \text{s}^{-1}$ and at an inlet pressure of 16 MPa. The coolant inlet and outlet temperatures were 551 and 581 K, respectively.

The transient was initiated by simultaneously opening the inlet and outlet rupture disks. Flow from both the inlet and outlet piping returned to the pressure-suppression system. During the transient, power to the electrically heated rods decreased sharply during the first 4 s then recovered to ~62% full power at 5 s, after which it decayed to zero power at 10 s. The measured volumetric flow rate at the inlet reversed direction early in the transient (<1 s) and decreased to a low flow rate after 5 s. The TRAC-PD2 program calculated that only ~8% of the initial system mass remained at 6 s. Three-dimensional flow patterns in the test section were observed frequently.

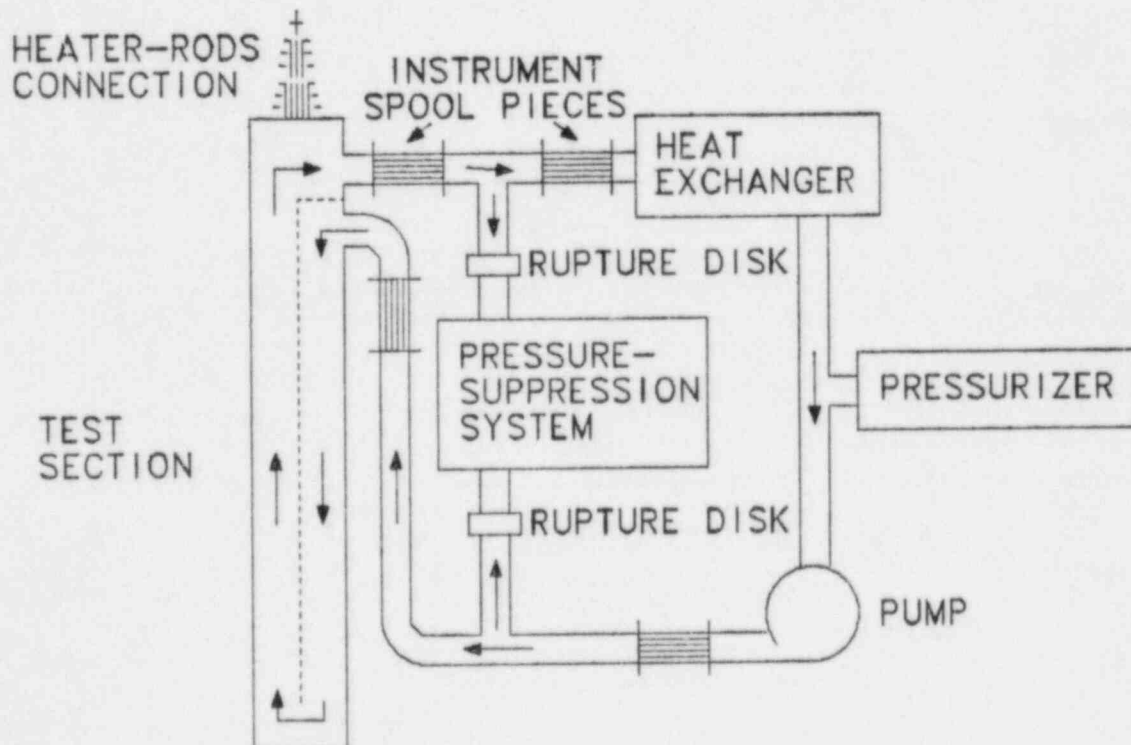


Fig. 55.
Oak Ridge National Laboratory THTF.

Pressure and temperature transducers were located in the instrument spool pieces near the inlet and the outlet (Fig. 55) to the test section. Also located there were turbine meters to measure volumetric flow and gamma densitometers to measure density. Temperatures determined by the thermocouples inside the heater rods at the lower, middle, and upper portions of the test section (levels D, G, and M, respectively) were compared with the calculated temperatures. Figure 56 shows the thermocouple locations.

B. TRAC-PD2 Model

The test facility was modeled with three types of TRAC components. In the nonnuclear pressurized water loop, the VESSEL modeled the 7×7 test-section array of fuel-pin simulators. A 36-cell two-dimensional Cartesian vessel geometry approximated the test-section array of fuel-pin simulators. The PIPEs were connected to the VESSEL for the inlet and outlet flows. The FILLS were connected to the PIPEs and the test velocity conditions were specified both at the inlet and at the outlet.

Four PIPEs were used, two at the inlet and two at the outlet. The component adjacent to the VESSEL used the partially implicit hydrodynamics option, whereas the component adjacent to the FILL used the fully implicit hydrodynamics option.

Because the test-section array of fuel-pin simulators was square, a VESSEL with a two-dimensional Cartesian geometry was used. Figures 56 and 57 show the 36-cell noding. The outer cells modeled the downcomer and the inner cells modeled the upward flow past the fuel-pin simulators. Table VII lists the locations of the measured and the calculated rod temperatures. Figure 56 shows their locations. Each PIPE used 10 cells of equal size.

The axial power profile was modeled with the axial cells shown in Fig. 58. The power steps do not coincide with the cell edges except at the beginning of the profile. Figure 59 displays the radial noding of a rod and a cross section of the rods that shows the thermocouple locations.

Because dryouts and rewets were measured in the test section, two rewet correlations were studied. A rewet correlation deals with the minimum stable film-boiling temperature (T_{min}). The homogeneous-nucleation, minimum, stable film-boiling temperature is the TRAC-PD2 default option. The T_{min} correlation by Iløeje et al.¹⁰ also was considered.

We performed a steady-state calculation to establish the initial conditions and then performed the transient calculation.

Appendix D lists the steady-state and transient input decks for THTF Test 177.

C. Data Comparisons

Figures 60-62 compare the calculated rod-surface temperatures with the measured values from the lower, middle, and upper levels of the test section, respectively. The temperature scales differ for each plot (note expanded scale in Fig. 62). During the first 6 s, several rewets occurred (Figs. 60 and 62). The main rewet in Fig. 60 was calculated accurately. The rewet in Fig. 62 was not calculated because TRAC-PD2 determined that the upper test section dried out. The TRAC-PD2 calculations using the homogeneous-nucleation, minimum, stable film-boiling temperature in place of the Iløeje correlation yielded virtually identical results. No spurious rewets were observed in either case.

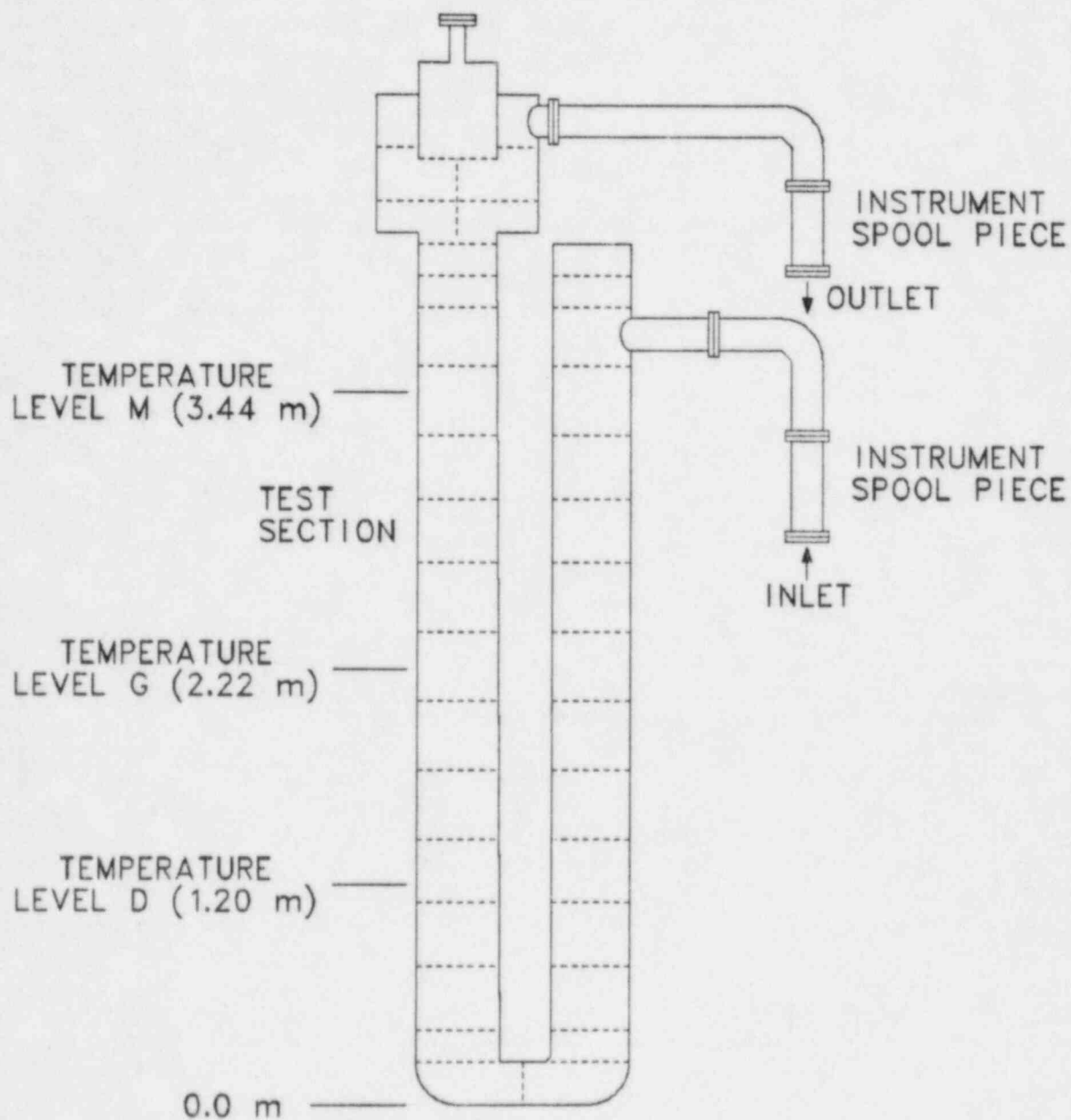


Fig. 56.

Single-channel test-section model of THTF (represents levels D, G, and M, identified in Ref. 9).

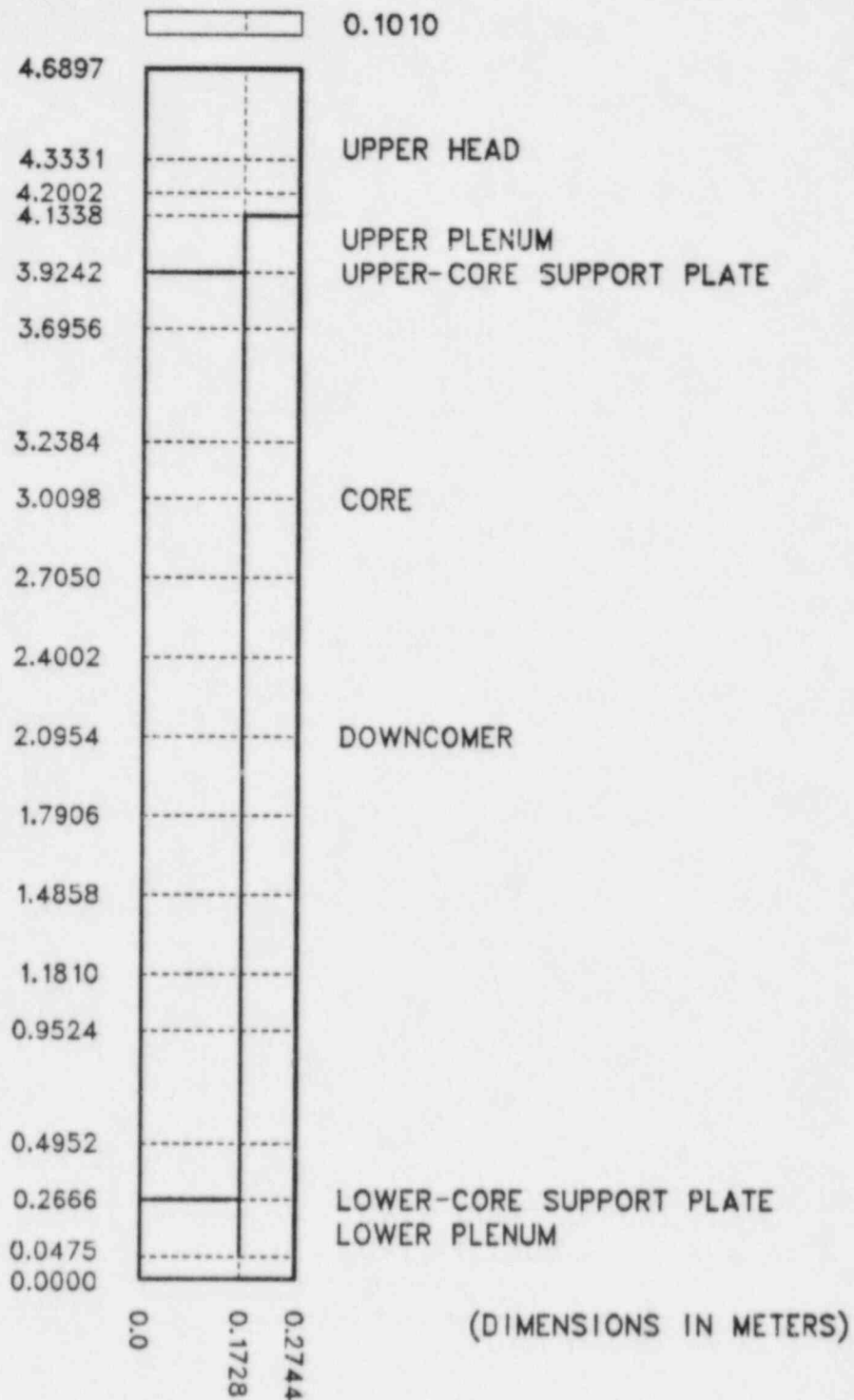


Fig. 57.
TRAP-generated model of THTF VESSEL component.

TABLE VII

LOCATION OF MEASURED AND CALCULATED QUANTITIES
FOR THTF TEST 177 BLOWDOWN EXPERIMENT

<u>Measured</u>		<u>Calculated</u>	
<u>Level</u>	<u>Parameter</u>	<u>Component</u>	<u>Cell</u>
Temperature level D	Temperature (K)	VESSEL 1	1 (axial level 5)
Temperature level G	Temperature (K)	VESSEL 1	1 (axial level 8)
Temperature level M	Temperature (K)	VESSEL 1	1 (axial level 12)
--	Mass flow ($\text{kg} \cdot \text{s}^{-1}$)	FILL 3	--
--	Mass flow ($\text{kg} \cdot \text{s}^{-1}$)	FILL 7	--

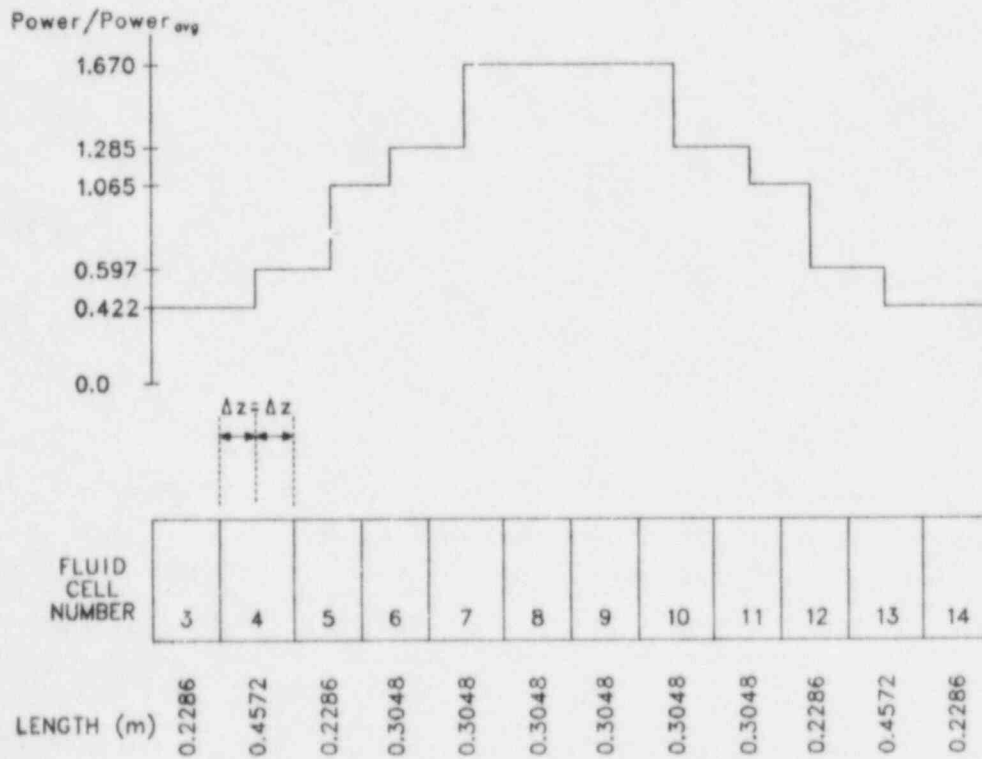


Fig. 58.
Axial power profile for THTF Test 177.

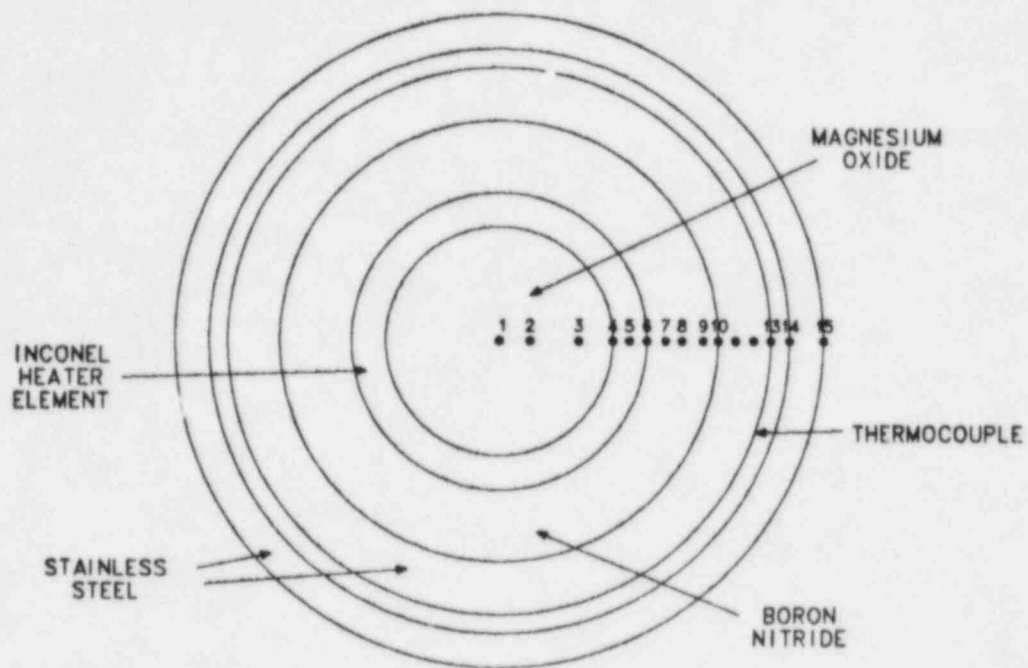


Fig. 59.
Radial noding diagram of the heater rod for THTF Test 177.

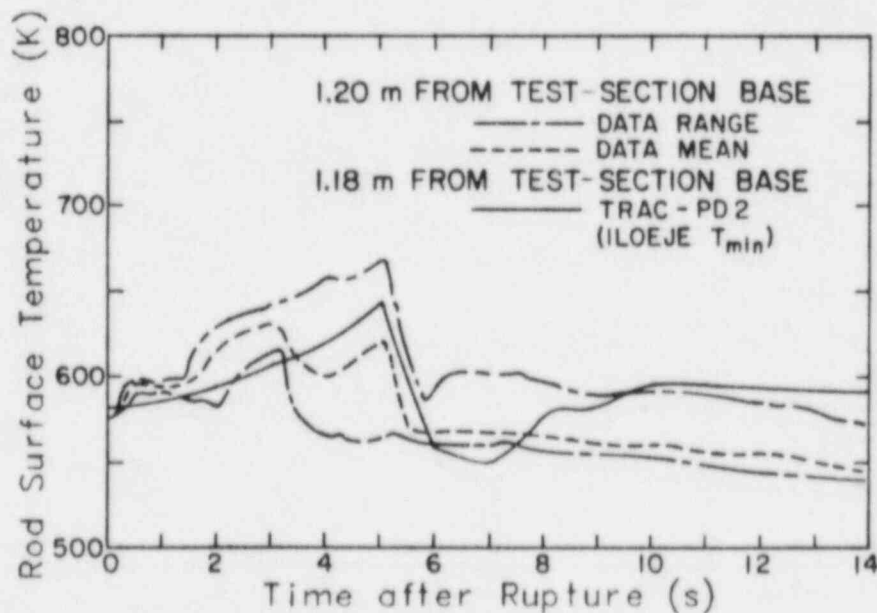


Fig. 60.
Comparison of the TRAC-calculated rod-surface temperatures with the THTF Test 177 measurements. The temperature was measured 1.20 m above the test-section base (level D, identified in Ref. 9).

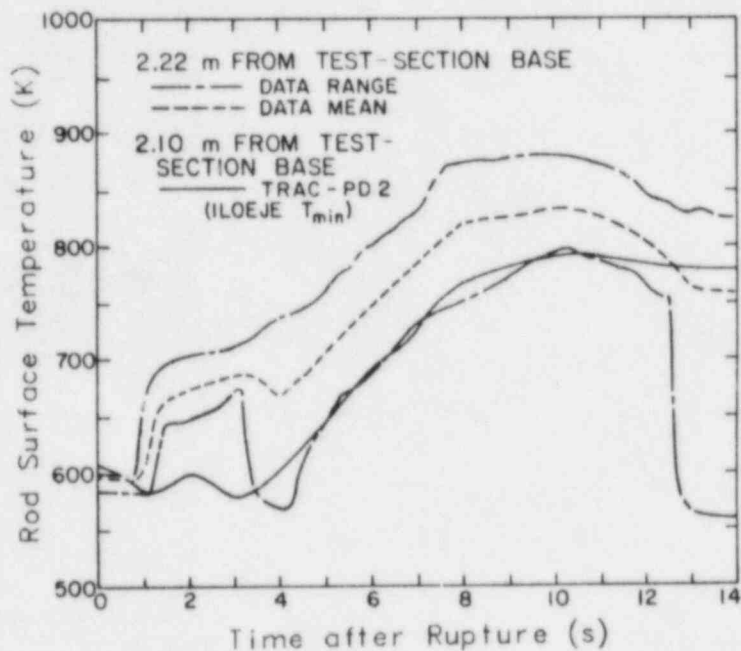


Fig. 61.

Comparison of the TRAC-calculated rod-surface temperatures with the THTF Test 177 measurements. The temperature was measured 2.22 m above the test-section base (level G, identified in Ref. 9).

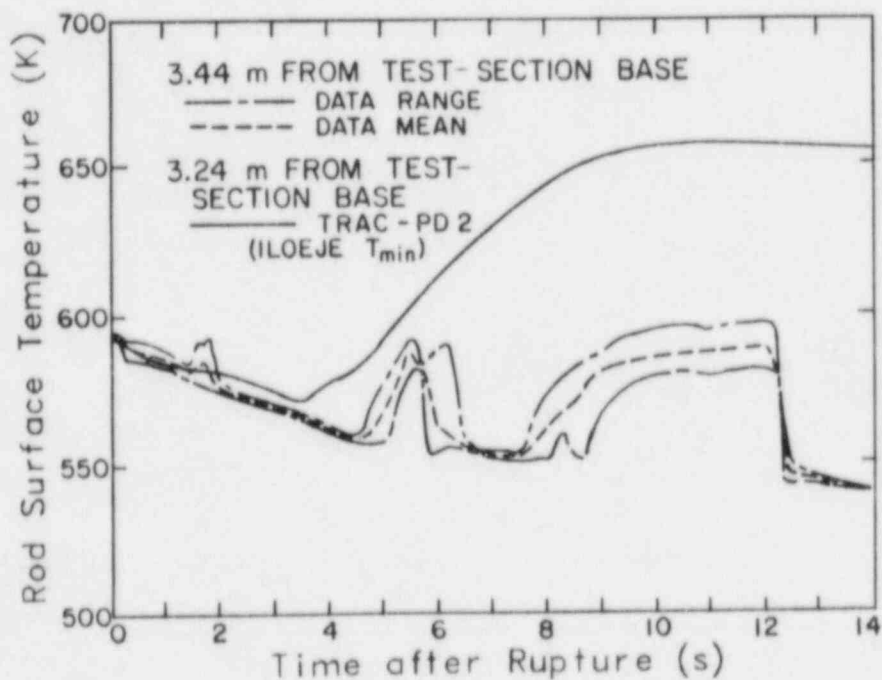


Fig. 62.

Comparison of the TRAC-calculated rod-surface temperatures with the THTF Test 177 measurements. The temperature was measured 3.44 m above the test-section base (level M, identified in Ref. 9).

D. Conclusions

Thermal-hydraulic effects assessed by Test 177 included a two-dimensional Cartesian-geometry vessel model with rod heat transfer including rewet models. Code components tested in this problem were VESSEL, PIPE, and FILL. In general, TRAC-PD2 rewet calculations were in reasonable agreement with the available measurements. Three-dimensional flow patterns in the test section were observed frequently. A one-dimensional flow model was used in the test section. The homogeneous-nucleation, minimum, stable film-boiling temperature correlation gave virtually identical results to the Iloeje correlation.

The steady-state calculation required 388 s of CPU time on a CDC 7600 computer; the transient calculation, 480 s.

VI. BENNETT TUBE EXPERIMENTS

A. Experiment Description

For the TRAC assessment, the TRAC-PD2 results were compared with data from the steady-state experiments performed by A. W. Bennett et al.¹¹ The data determined the variation of wall temperatures in the region beyond the dryout point for various coolant flow rates, wall heat fluxes, and coolant inlet subcoolings. The experiments consisted of circulating preheated water through a tubular test section that was heated by passing direct current through its walls.

The test section was a 5.8-m length of Nimonic 80A alloy tubing, which had a 12.6-mm i.d. and a 1.63-mm wall thickness. Busbars attached to the test section provided heated lengths of 3.66 and 5.56 m. The inside wall temperatures were determined by 27 thermocouples attached to the outer wall of the test section.

In this study we analyzed three typical test Runs 5336, 5431, and 5442. Table VIII lists the test conditions for these three experiments. In all cases the pressure was 6.895 MPa (1000 psia).

B. TRAC-PD2 Model

The facility was modeled by three TRAC components, a FILL, a PIPE, and a BREAK (Fig. 63). The FILL provided the inlet boundary conditions for the PIPE, whereas the BREAK provided the outlet boundary conditions. The specified inlet boundary conditions were a void fraction equal to zero, liquid mass flow, pressure, and temperature. The vapor pressure and temperature were specified at the pipe outlet. Appendix E lists the TRAC-PD2 steady-state input decks for Bennett Runs 5442, 5431, and 5336, respectively. Because TRAC does not permit steady-state CHF, the transient runs were made until the wall temperatures approached steady-state conditions (25 s).

C. Results

Figure 64 shows the results from Bennett Run 5442, TRAC-P1A (Ref. 12), TRAC-P1A/NEWS1, and TRAC-PD2. The TRAC-P1A program greatly overestimated the wall temperatures because it contained an interfacial heat-transfer error. Errors found after TRAC-P1A was released were described in the first TRAC

TABLE VIII
TEST CONDITIONS

Run Number	Mass Flux ($\text{kg} \cdot \text{m}^{-2} \cdot \text{s}^{-1}$)	Power (kW)	Heat Flux ($\text{W} \cdot \text{m}^{-2}$)	Inlet Subcooling (K)	Tube Length (m)
5336	664	181	8.18×10^5	26.3	5.56
5431	651	115	7.96×10^5	23.9	3.66
5442	4814	302	2.07×10^6	16.4	3.66

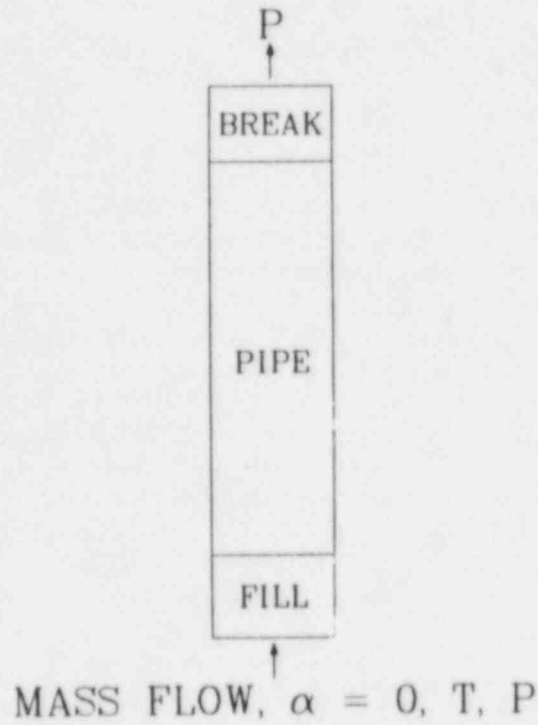


Fig. 63.
TRAC model geometry.

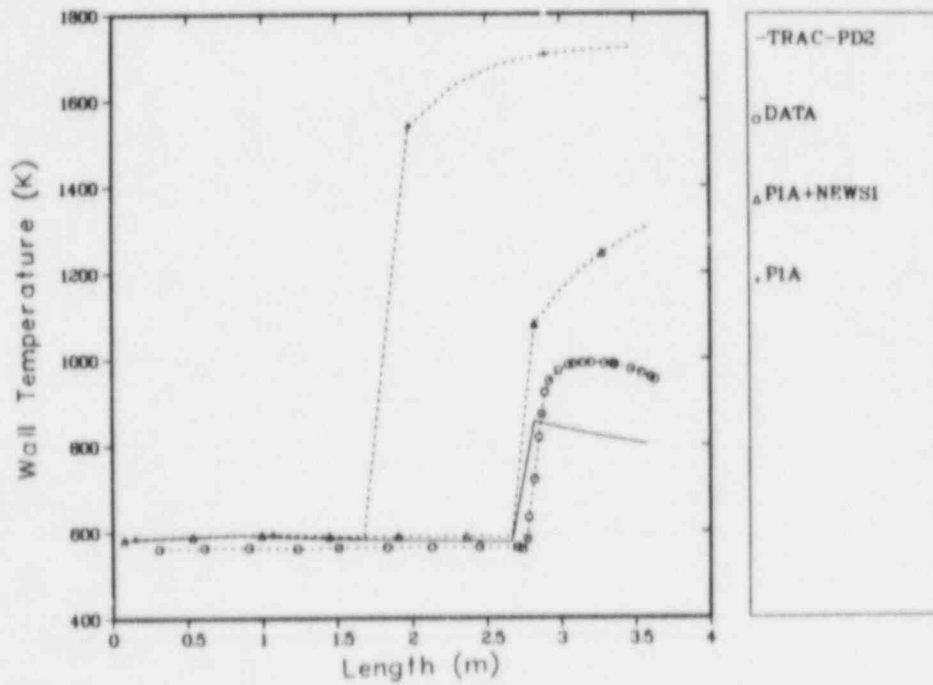


Fig. 64.
Comparison of the TRAC-calculated wall temperatures with the Bennett Run 5442 data.

newsletter,¹³ and the modified code was designated TRAC-PIA/NEWS1. The TRAC-PIA/NEWS1 results (Fig. 64) agreed better with the data than the TRAC-PIA results, but the data still overpredicted the wall temperatures. Although the TRAC-PD2 results underpredicted the data, they agreed better with the data than previous predictions.

Figure 65 compares the data for Bennett Run 5336 and the TRAC predictions. The TRAC-PIA/NEWS1 version predicted the CHF point better than TRAC-PD², but the temperature gradient near the top of the tube was steeper than indicated by the data. The difference in CHF points between the two TRAC predictions is discussed below.

Figure 66 shows the results for Bennett Run 5431. As in Run 5336, TRAC-PD2 predicted the CHF at too low an elevation in the tube. Figure 67 explains this CHF prediction. To obtain a smooth boiling curve, interpolation is used in TRAC between correlations. For void fractions between 0.96 and 1.0, linear interpolation was used to obtain the liquid and vapor HTC's. When the void-fraction cutoff point (ALPCUT) was changed from 0.96 to 0.99, much better agreement with the data was obtained for Run 5431 (Fig. 67). No change occurred in the TRAC-PD2 prediction for Run 5442 when ALPCUT was changed from 0.96 to 0.99. A value of ALPCUT equal to 0.96 was used in the code because the predicted HTC gradients were too steep for other test facilities.

Figure 68 shows a noding sensitivity study for Run 5442. Six fluid cells were too few, but 12 or 24 fluid cells resulted in approximately the same wall temperatures.

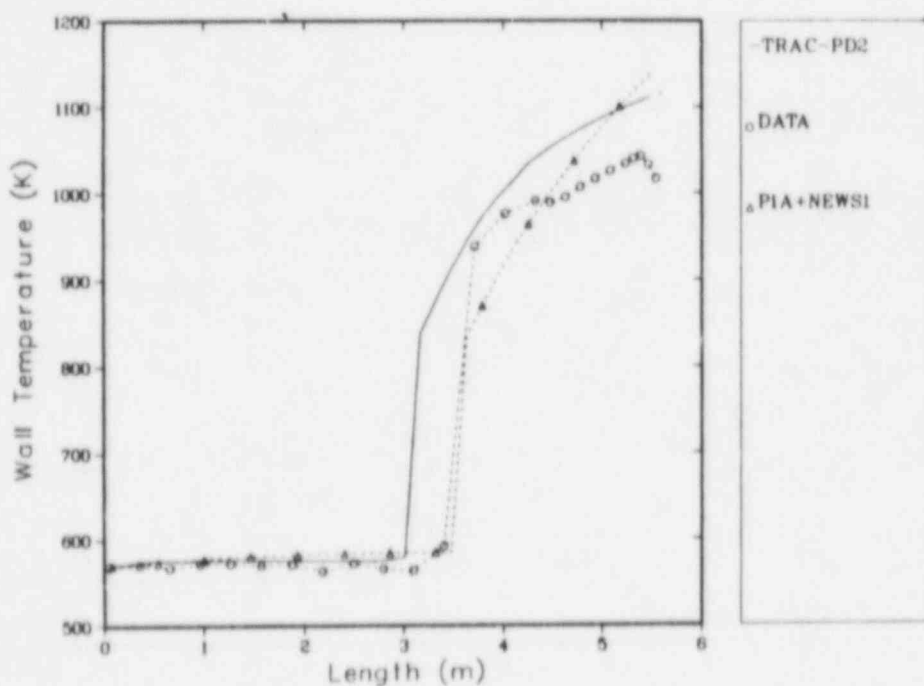


Fig. 65.

Comparison of the TRAC-calculated wall temperatures with the Bennett Run 5336 data.

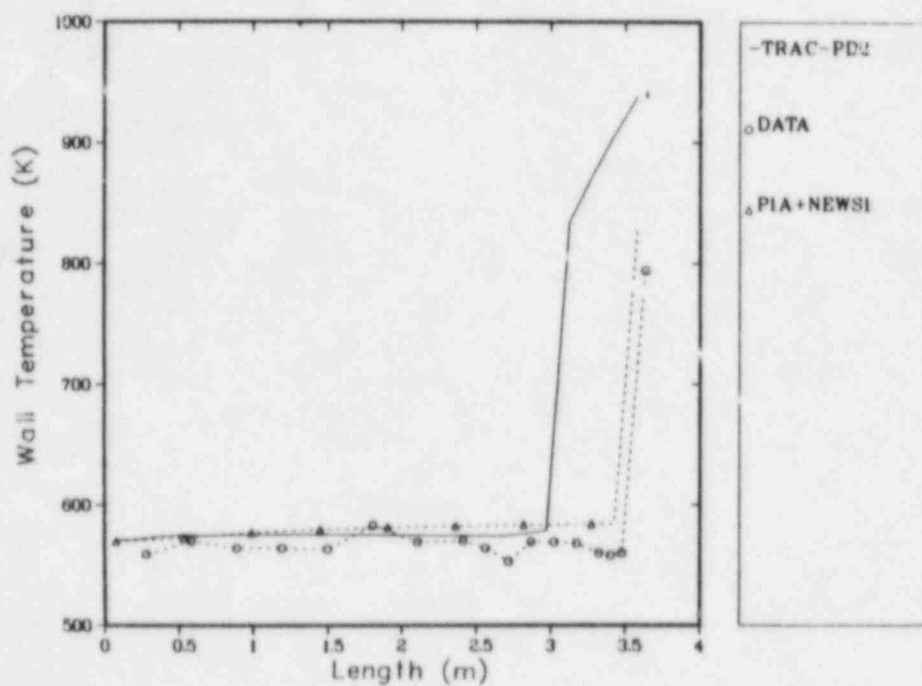


Fig. 66.

Comparison of the TRAC-calculated wall temperatures with the Bennett Run 5431 data.

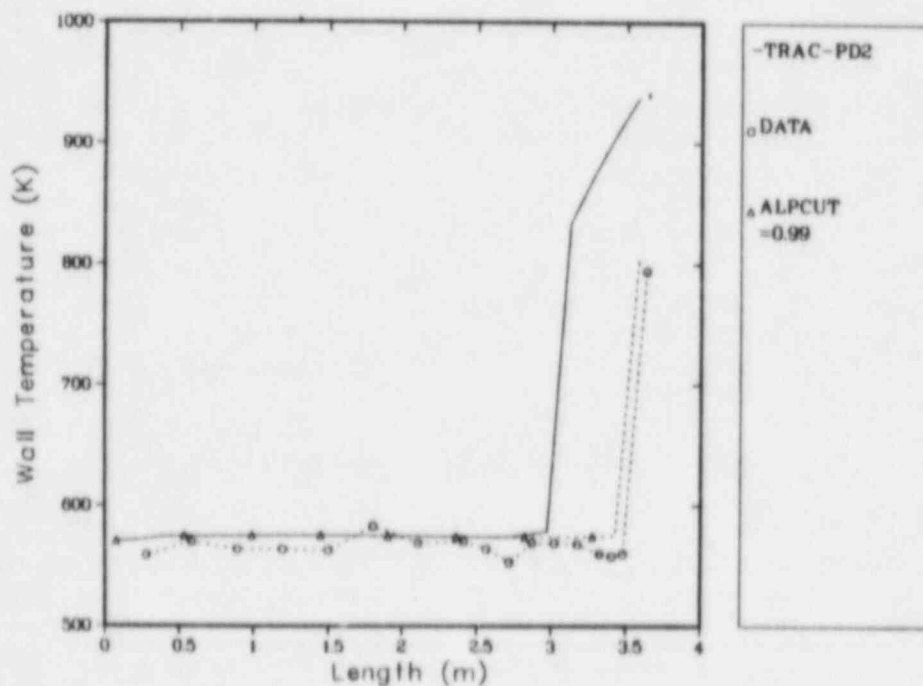


Fig. 67.

The effect of the boiling-curve interpolation on Bennett Run 5431.

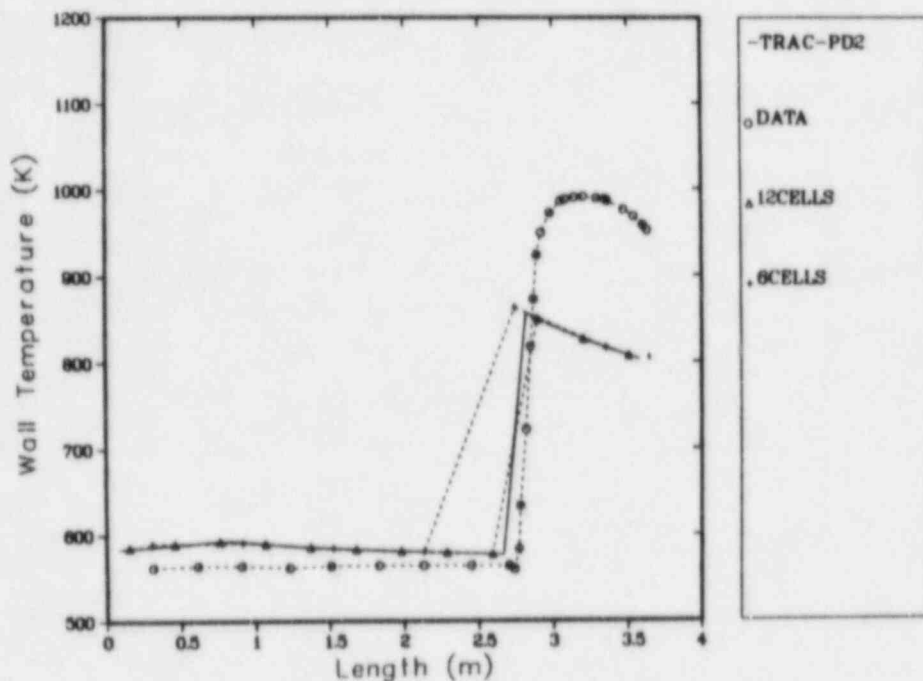


Fig. 68.
Noding sensitivity for Bennett Run 5442.

The TRAC-PIA program¹² allowed three CHF options: the Biasi correlation for high flow and the Zuber correlation for low flow, the Biasi correlation for both high and low flows, and the Bowring correlation for both high and low flows.

In TRAC-PD2 only the Biasi correlation was used but, at mass fluxes between -200 and $200 \text{ kg} \cdot \text{m}^{-2} \cdot \text{s}^{-1}$, the Biasi correlation was evaluated at $200 \text{ kg} \cdot \text{m}^{-2} \cdot \text{s}^{-1}$. Figures 69-71 show that the Bowring CHF correlation gave significantly worse results than the Biasi CHF correlation for Run 5442 (high mass flux), but the predictions using the Bowring correlation were better for Runs 5336 and 5431 (low mass flux). When the Bowring correlation was used and ALPCUT was changed from 0.96 to 0.99, the Run 5442 results were unchanged, but the CHF occurred later than in the data for Runs 5336 and 5431 (Figs. 72 and 73). The low mass-flux runs were very sensitive to the boiling curve interpolation and, overall, the Biasi correlation gave better results than the Bowring correlation.

Five options for the wall friction, in addition to an input constant, are available in TRAC-PD2. Table IX lists these options (see Ref. 1 for model details).

The value $\text{NFF} = 1$ was used in the base runs. Figure 74 shows the results for Bennett Run 5442 when $\text{NFF} = 1, 2$, or 3 . Predictions using $\text{NFF} = 4$ were identical to those using $\text{NFF} = 2$; the predictions using $\text{NFF} = 5$ were identical to those using $\text{NFF} = 1$ or 3 . The CHF point (Fig. 74) was slightly lower in the tube and the maximum wall temperature was a few degrees higher when the Armand correlation or the modified annular-flow model was used.

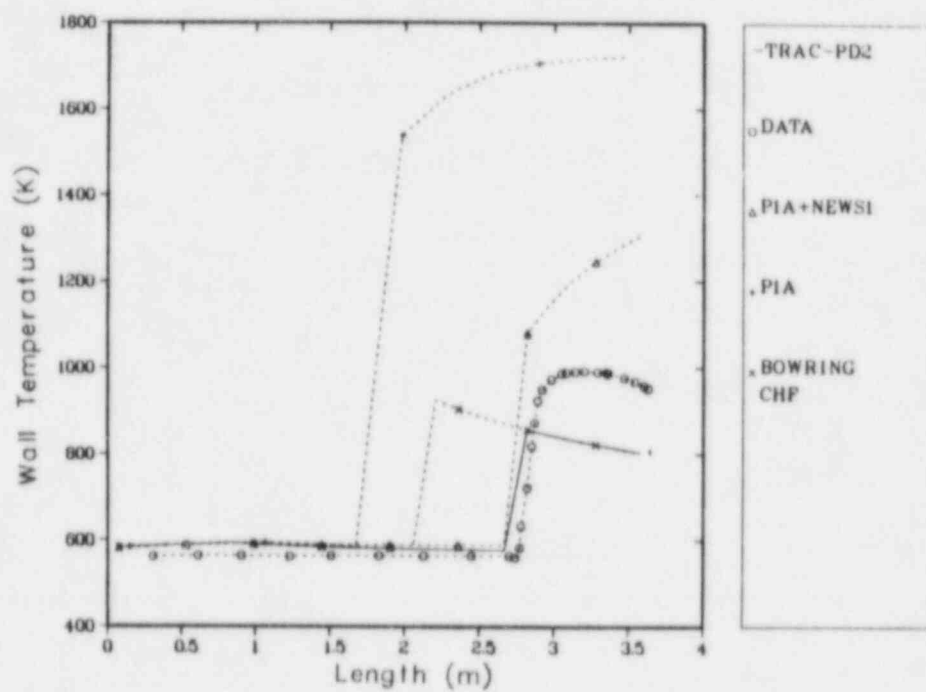


Fig. 69.
CHF correlation sensitivity for Bennett Run 5442.

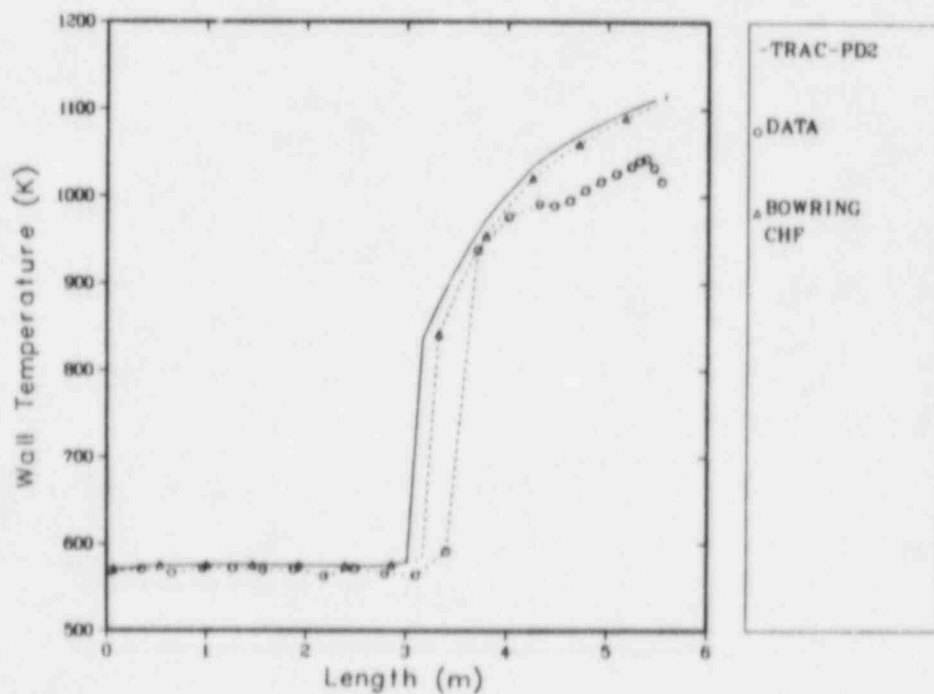


Fig. 70.
CHF correlation sensitivity for Bennett Run 5336.

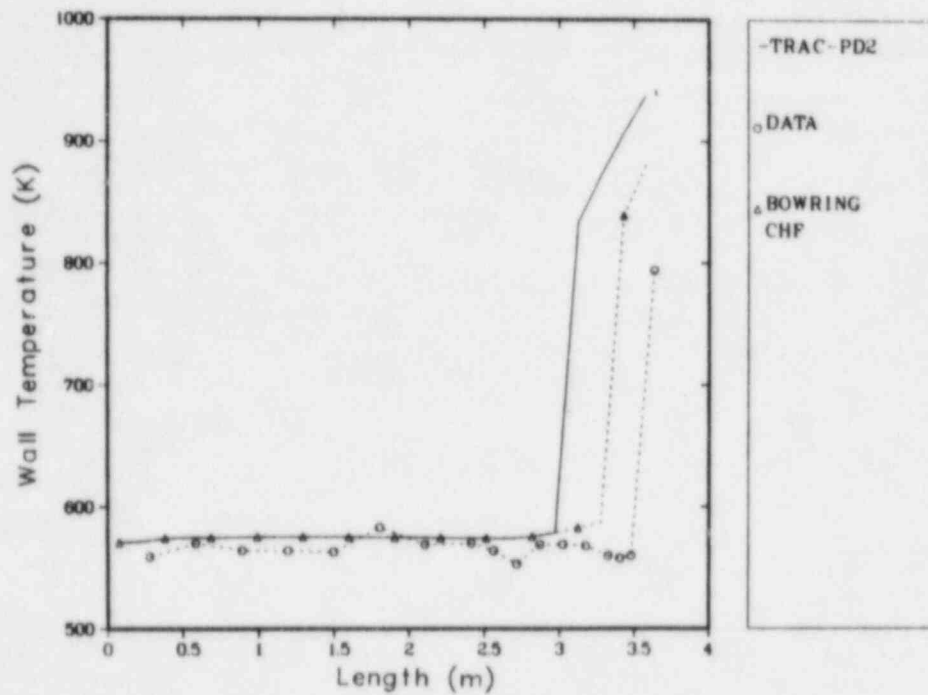


Fig. 71.
CHF correlation sensitivity for Bennett Run 5431.

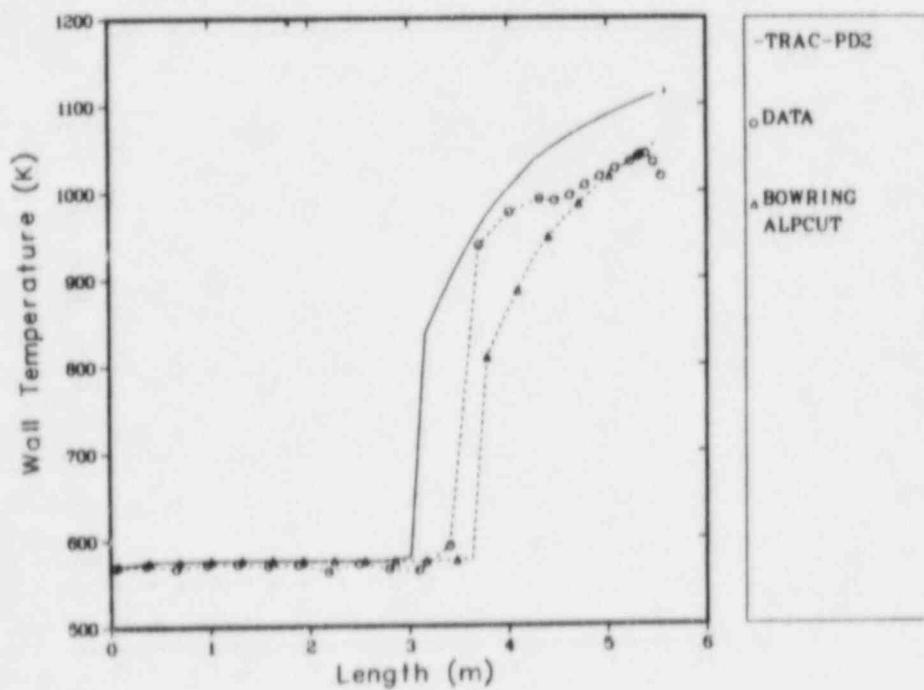


Fig. 72.
The effect of the CHF correlation and boiling-curve interpolation on Bennett Run 5336.

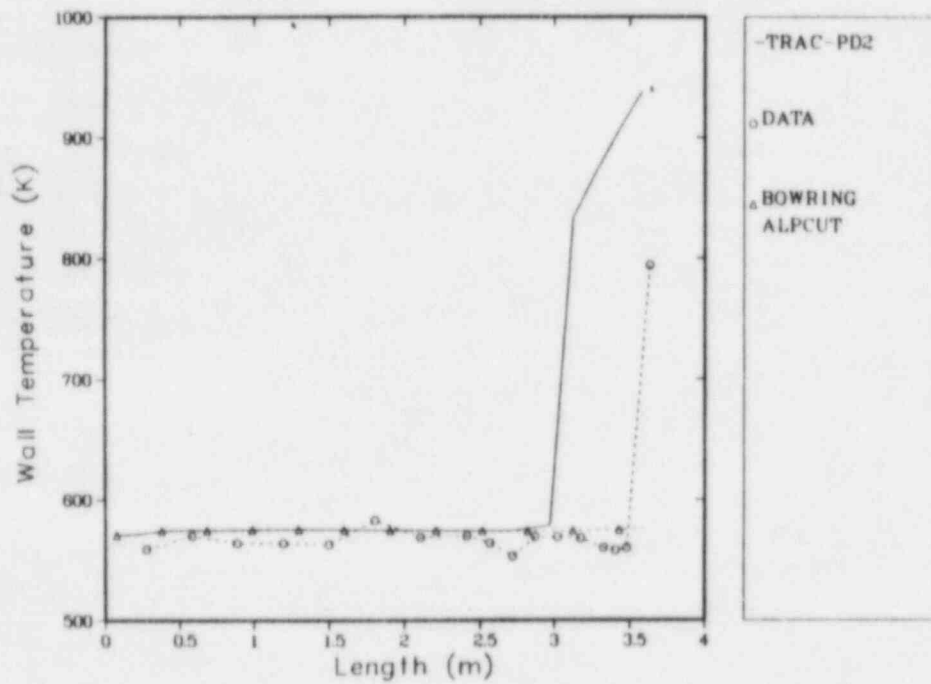


Fig. 73.

The effect of the CHF correlation and boiling-curve interpolation on Bennett Run 5431.

TABLE IX

TRAC WALL FRICTION OPTIONS

<u>NFF</u> <u>Value</u>	<u>Option</u>
1	Homogeneous model
2	Armand correlation
3	CISE correlation
4	Modified annular-flow model
5	Chisholm correlation

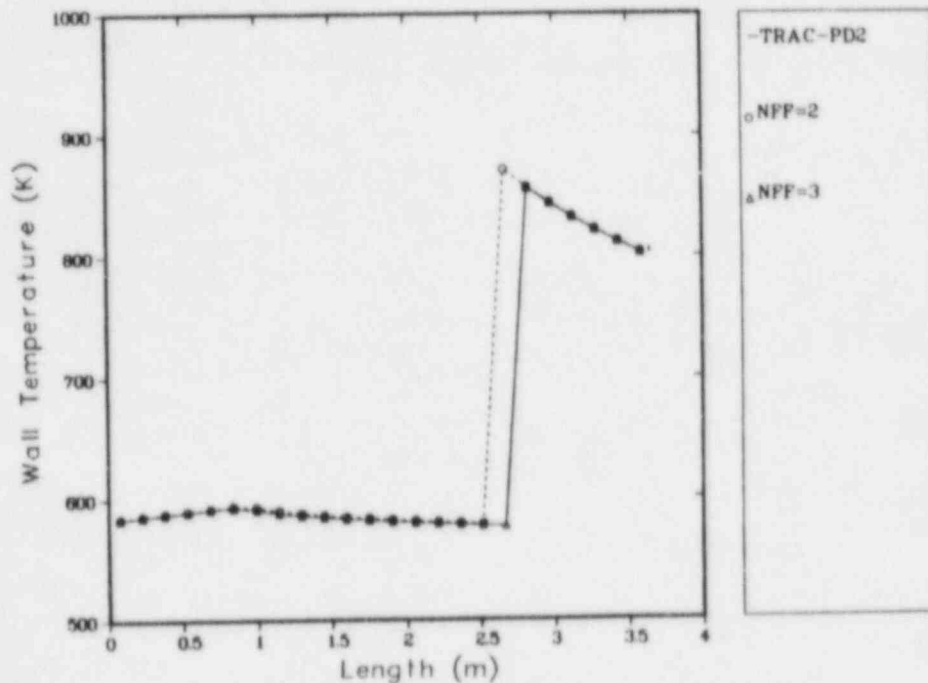


Fig. 74.
The effect of wall friction on Bennett Run 5442.

Table X lists the computer storage requirements and the computer times required for the Bennett base cases.

In general, the high mass-flux TRAC-PD2 test predictions (Run 5442) agreed better with the data than the TRAC-PlA results, whereas the low mass-flux runs showed slightly worse agreement with the data. Overall, the Biasi CHF correlation agreed better with the data than the Bowring CHF correlation, which was not included in TRAC-PD2. The low mass-flux runs were too sensitive to the boiling-curve interpolation.

After studying these results, we recommend two code improvements. First, the boiling curve should be examined and changed so that the results are not affected significantly by the interpolation method. Second, the wall friction-factor models should be examined to determine the best model, and only this model should be included in future code versions.

TABLE X

COMPUTER REQUIREMENTS FOR BENNETT PREDICTIONS

<u>Run Number</u>	<u>CPU Time (s)</u>	<u>SCM^a (words)</u>	<u>LCM^b (words)</u>
5336	274	3920	11055
5431	118	2696	9831
5442	201	2696	9831

^aSmall core memory.

^bLarge core memory.

VII. CREARE COUNTERCURRENT-FLOW EXPERIMENTS

A. Experiment Description

We used the Creare countercurrent-flow experiments to examine the effects of countercurrent steam-flow rate, downcomer wall superheating, and liquid subcooling on ECC penetration to the lower plenum. For this assessment, the Creare test facility was a 1/15-scale (linear dimension), multiloop, cylindrical model of a PWR downcomer region. Reference 14 describes this facility and its operation. The Creare vessel can be arranged in at least six geometrical configurations. The tests that we analyzed had a base-line configuration with a 0.0127-m (0.5-in.) downcomer gap and a deep-plenum geometry.

Four cold legs penetrated the outer surface of the vessel at 90° intervals. Three intact-loop cold legs were connected to the ECC-injection lines. One broken-loop cold leg was connected to a pressure-suppression tank. In these assessment tests, the four hot legs were blocked.

The procedures for the countercurrent-flow tests established a constant steam-flow rate through the vessel and purged air from the vessel. Steam entered at the top of the vessel, then flowed down the interior core region into the lower plenum, up the downcomer, and out the broken cold leg. After the desired steady steam-flow rate was established, water was injected simultaneously into the three intact-loop cold legs at a constant, preset flow rate. After a short transient period, the plenum began to fill. The test was run until the lower plenum was full or until the fill rate was determined from the strip-chart records. A complete penetration curve was generated by a series of such tests with fixed liquid-injection rates and temperatures but with varied steam-flow rates. The ECC penetration into the lower plenum ranged from complete delivery to complete bypass for each test series.

B. TRAC-PD2 Model

Figure 75 shows the TRAC model of the Creare vessel. The vessel was modeled with seven axial levels. Each level was subdivided into 2 radial and 8 azimuthal zones for a total of 112 mesh cells. Because level 6 had four sources (PIPES), we selected eight rather than four azimuthal zones. Thus, an ECC-injection source did not connect directly to each cell at this level. We chose one radial segment in the downcomer because this was typical of the TRAC full-scale PWR model. The axial-level dimensions allowed resolution of several important phenomena. Levels 1 and 2 allowed pooling of the liquid in the lower plenum where the results were insensitive to the relative height of each cell. Level 3 allowed flow-pattern resolution near the bottom of the downcomer. Levels 4, 5, and 6 allowed flow-pattern resolution in the downcomer region, and level 7 provided resolution of any liquid stored in the upper part of the downcomer.

The calculational sequence was parallel to that of the Creare experiment. The steam was injected into eight PIPES connected to cells 1-8 at level 7 by FILLS. The intact-loop cold legs were isolated by zero-velocity FILLS. The broken-loop cold leg was connected to a BREAK and the pressure was chosen to give the correct lower-plenum pressure. Thus, the correct ECC subcooling was ensured. A generalized steady-state calculation established a constant, reverse steam flow and lower-plenum pressure. The transient calculation was started from the steady-state dump. The FILLS connected to the three intact-loop cold legs ensured the correct ECC-injection flow rate and temperature.

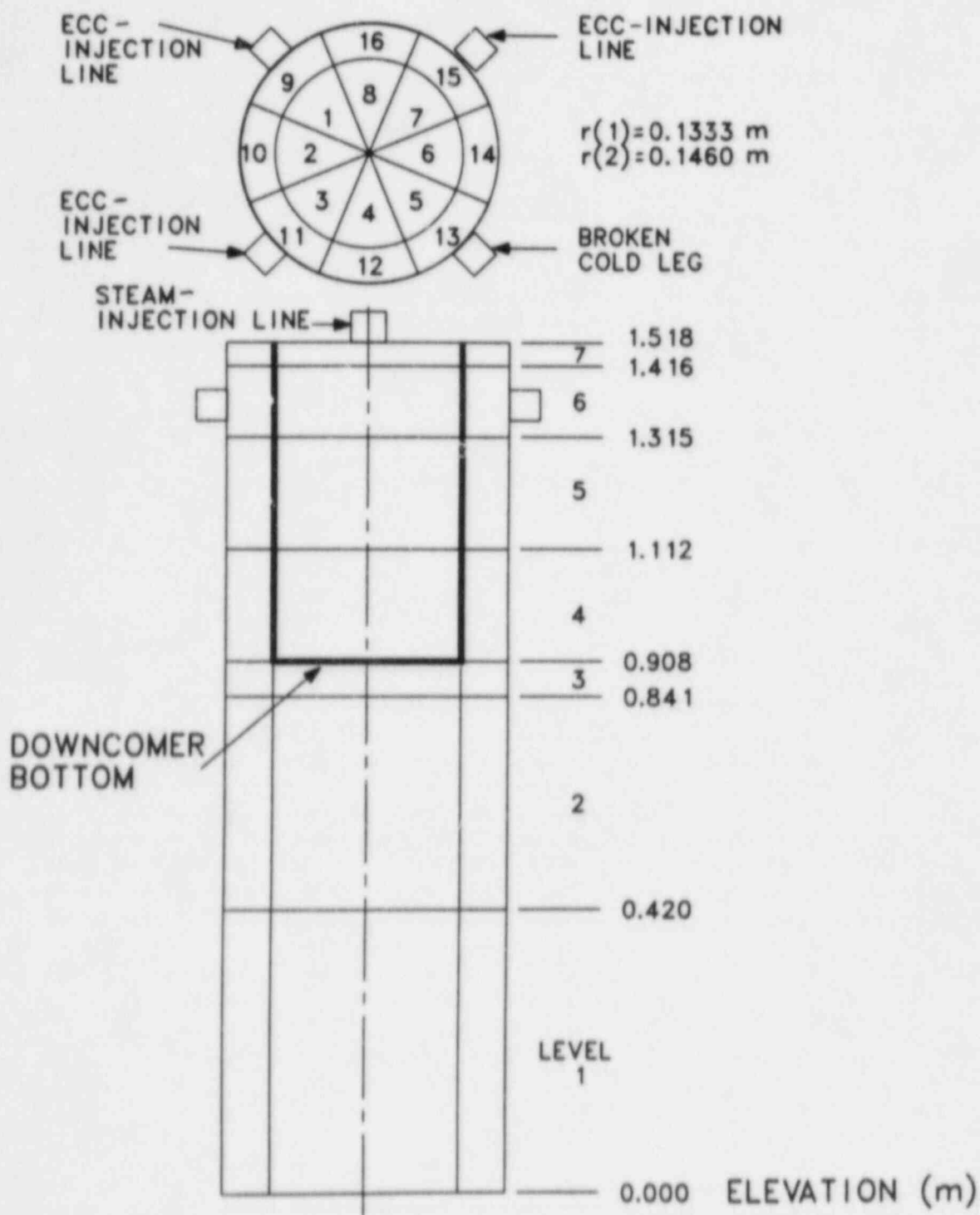


Fig. 75.
TRAC noding for Creare 1/15-scale vessel.

The instantaneous values of J_{gc}^* (the dimensionless steam flow) and J_{fd}^* (the dimensionless liquid flow) at the bottom of the downcomer, the liquid mass in the lower plenum, and the liquid mass stored in the downcomer were plotted as functions of time. The value of J_{gc}^* underwent an initial transient following ECC injection and perhaps never returned to its initial value because of steam condensation. The calculated value of J_{fd}^* was determined from the average lower-plenum fill rate just as it was in the experiment.

C. Data Comparisons

The Creare countercurrent-flow experiments covered a wide range of ECC flow rates and subcoolings. We made six TRAC calculations to generate two complete penetration curves for the following liquid injections: $1.86 \times 10^{-3} \text{ m}^3 \cdot \text{s}^{-1}$ flow rate and 373 K (30 gal/min and 212°F) and $3.78 \times 10^{-3} \text{ m}^3 \cdot \text{s}^{-1}$ flow rate and 339 K (60 gal/min and 150°F). The reactor-scale injection-flow rate was $3.78 \times 10^{-3} \text{ m}^3 \cdot \text{s}^{-1}$ (60 gal/min).

We selected these curves to study two basic phenomena that are important in determining whether ECC bypass or delivery occurs. In the first case, the injected ECC was subcooled slightly; the system pressure ranged from 1-3 atm. Thus, the interfacial drag between the steam and the liquid was the major determinant of bypass. The calculated penetration curve for this case allowed an appraisal of the constitutive relationships that described interfacial momentum transfer. Moreover, because the calculations covered the ECC delivery from complete bypass to complete dumping, flow regimes in the downcomer at the bypass point differed from those at the complete delivery point.

Figure 76 compares the calculated and measured flooding curves for the low-subcooling case. Near the complete delivery steam flow, $J_{gc}^* = 0.053$, the calculated liquid flow, $J_{fd}^* = 0.047$, agreed well with the measured value of 0.051. At a higher steam-flow rate, $J_{gc}^* = 0.14$, there was almost complete bypass of the injected liquid in the experiment. At this steam-flow rate, TRAC-PD2 also predicted nearly complete bypass. The calculated steam flow was 0.005, whereas the measured value was 0.004. In the second set of tests, ECC was injected at 60 gal/min and 150°F. In this case, the ECC was subcooled significantly and the interfacial heat transfer was a significant factor in determining the quantity of ECC delivered to the lower plenum. Moreover, the penetration curves became much flatter as the ECC subcooling was raised (see Ref. 14); that is, the system tended to operate either in a complete-bypass or in a complete-delivery mode. Thus, operation in the intermediate delivery/bypass range was difficult to achieve in the experiment because the change in the steam-flow rate needed to cause a transition from complete delivery to complete bypass was very small.

Figure 77 compares the calculated and measured results for the high-subcooling case. The complete dumping location at $J_{gc}^* = 0.10$ again agreed well with the calculated results. The calculation showed that almost all of the injected liquid was delivered to the lower plenum. At a steam flow of $J_{gc}^* = 0.21$, essentially all of the liquid was bypassed both in the experiment and in the TRAC calculation. Thus, the critical end points for this relatively high-subcooling penetration case were predicted well. The calculated values for J_{gc}^* and J_{fd}^* may have oscillated during the transient. Figure 78 shows the calculated value of the downcomer liquid mass for the case with high subcooling and nearly complete delivery. Because the liquid in the downcomer was delivered periodically to the lower plenum, an oscillatory flooding rate occurred. Figure 79 shows the time-integrated delivery to the lower plenum that represented the actual quantity of liquid delivered to the lower plenum.

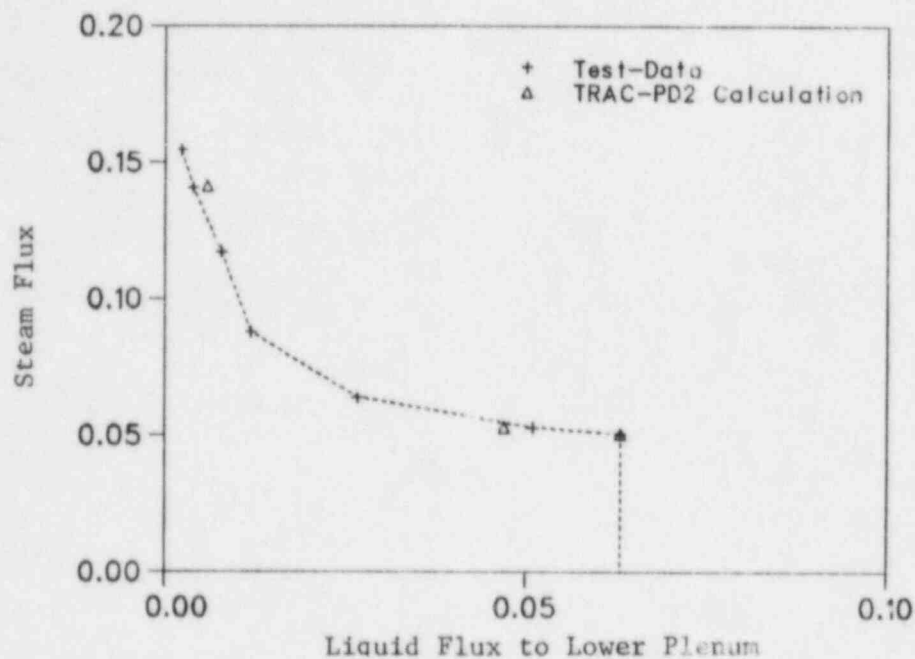


Fig. 76.

Comparison of calculated and measured flooding curves for Creare low-subcooling tests.

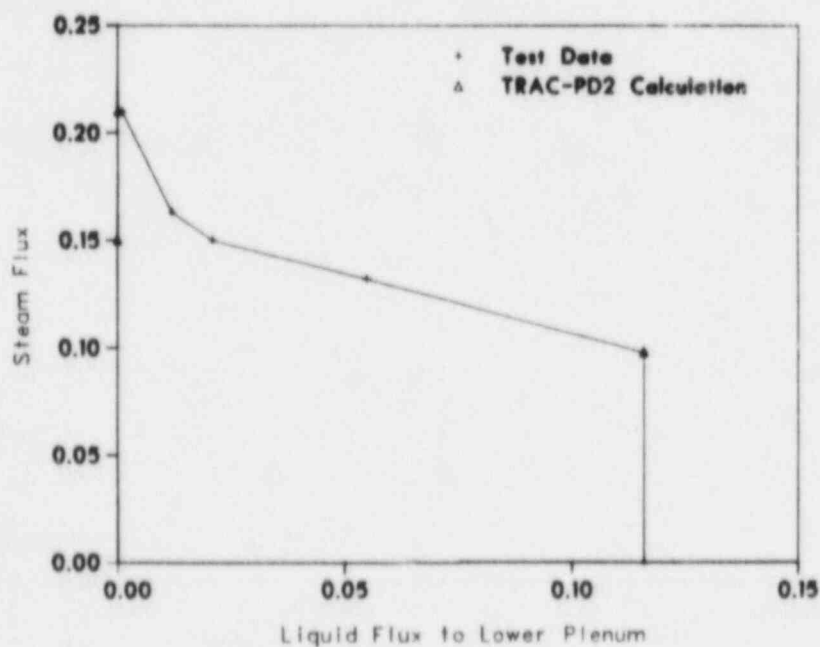


Fig. 77.

Comparison of calculated and measured flooding curves for Creare high-subcooling tests.

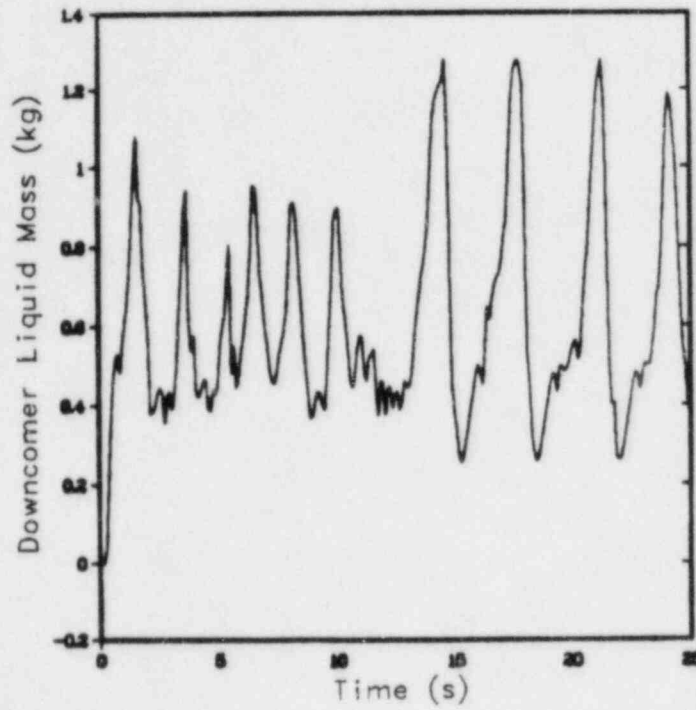


Fig. 78.

Calculated Creare downcomer liquid mass for the high-subcooling, high steam-flow test.

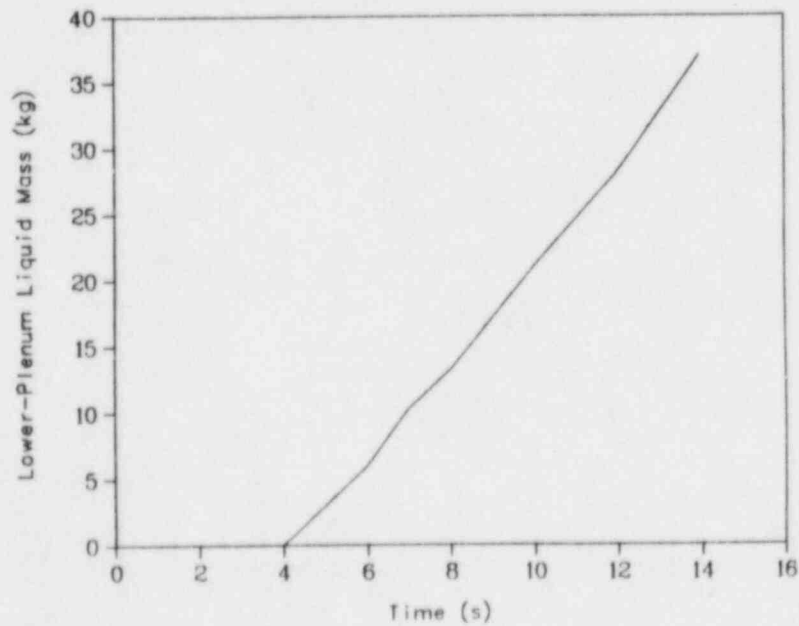


Fig. 79.

Lower-plenum liquid level for the high-subcooling, high steam-flow test.

Thus, even though the instantaneous liquid delivery to the lower plenum was erratic, the resulting collapsed water level in the lower plenum was a monotonically increasing value.

D. TRAC-PD2 Features Tested

Our calculations assessed the interfacial-momentum and heat-transfer constitutive relationships in the three-dimensional VESSEL. The comparisons between the test data and the TRAC-PD2 calculations were in good overall agreement, which indicated that TRAC-PD2 can predict satisfactorily ECC bypass and penetration in annular downcomer geometries at this scale.

E. Input Data Decks

Appendix F.I lists a typical Creare steady-state input deck used to generate the steady-state steam flow. Components 11-18 (FILLS) specified the inlet steam conditions. Component 8 (BREAK) specified the boundary pressure needed at the broken-loop cold leg to produce the correct lower-plenum pressure. Appendix F.II lists the restart input deck for the ECC-injection calculation. Only components 6, 7, and 9, which were connected to the three intact-loop cold legs, were replaced. The new FILLS specified the ECC-injection conditions. The CPU times for the steady-state, initial-condition runs ranged from 2.5-15 min; the CPU time required was sensitive to the steam velocity. The CPU times for the transient calculations with ECC-injection varied from 20-60 min; the CPU time required was determined by the steam-flow rate and the ECC temperature.

VIII. FLECHT FORCED-FLOODING TESTS

A. Experiment Description

The FLECHT program is a series of reflood heat-transfer simulation experiments to evaluate separate effects in PWR emergency core-cooling-system (ECCS) heat transfer. We selected two of these tests for the TRAC-PD2 developmental assessment. Test 4831 had a low flooding rate ($3.8 \text{ cm} \cdot \text{s}^{-1}$) and an axial-cosine power profile,¹⁵ whereas Test 17201 had a higher flooding rate ($7.6 \text{ cm} \cdot \text{s}^{-1}$) and a skewed-axial power profile.¹⁶

The operating procedure for both tests was similar. The lower plenum of the test vessel housing was filled with water to the bottom of the heated rods. Electrical power was supplied to the simulated fuel rods until the initial rod-cladding temperatures were attained. Then, flooding at the specified rate was initiated, while rod power was decreased according to the desired decay curve. Rod-cladding temperatures and fluid conditions were recorded until the bundle was quenched completely.

Test 4831 was conducted in a massive, square vessel. A square rod bundle with 100 full-scale nuclear fuel-rod simulators was placed in the vessel. Ninety-one of these rods were heated electrically to produce a stepped approximation to an axial-cosine power profile. The radial-power peaking varied from 0.95 to 1.1 of the average rod power across the rod bundle.

Because of the housing mass effects in earlier tests, a cylindrical, low-mass housing was designed. Test 17201 used this new geometry. In this test, the rod bundle consisted of 105 heated rods with 7 unheated thimbles and solid spacers to reduce the flow area. Again, a radial power profile was simulated. However, an axial power profile skewed toward the top of the heated section was used.

Liquid effluents from the flooding test were separated and collected in a carryover tank, and the dry steam was exhausted to the atmosphere through an orifice to measure the liquid carryover and the vapor flow from the core. Also, a series of differential-pressure cells provided an approximate void-fraction profile of the test section. Thermocouples measured the rod-cladding and housing temperatures. A data-acquisition system recorded most of the data and provided time history plots.

B. TRAC-PD2 Model

The TRAC model for the FLECHT tests used a constant-velocity FILL, connected by a short PIPE to the VESSEL lower plenum, to inject ECC. An effluent PIPE connected the VESSEL upper plenum to a constant-pressure BREAK that modeled the carryover tank. The VESSEL was divided into 13 axial levels to facilitate the modeling of the rod axial power profile (Fig. 80). This noding necessitated some interpolation of the measured initial rod-cladding temperatures. Thus, some slight disagreement between the measured and the initial temperatures occurred at a few points. Figure 81 compares the TRAC axial power distribution to the test value. The TRAC VESSEL used heat slabs to model the housing walls.

The TRAC calculation paralleled the test procedure. The lower plenum was filled completely and the rods were heated to the initial temperature. Then, the FILL was actuated to simulate forced flooding. The calculation continued until all rods had quenched fully, as determined by the rod-cladding temperature vs time plots.

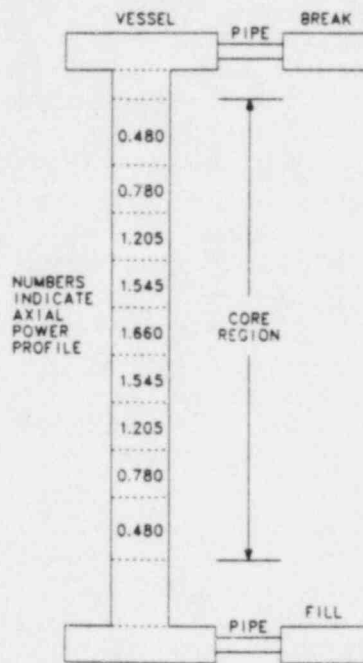


Fig. 80.
TRAC noding diagram of FLECHT forced-flooding experiments.

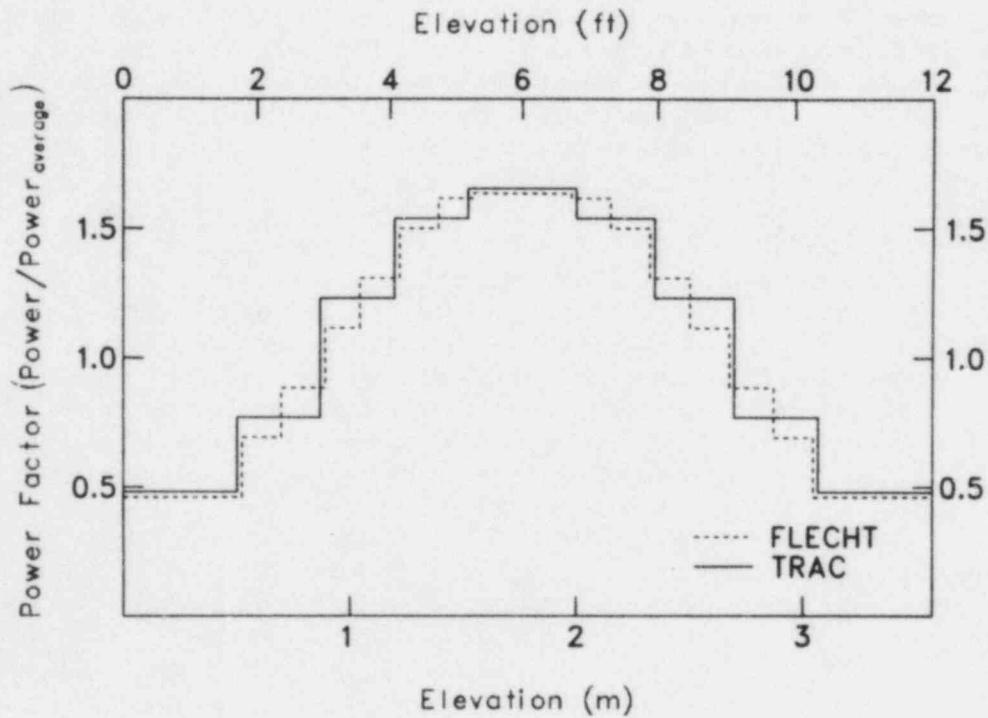


Fig. 81.
Axial power profile for FLECHT Test 4831.

C. Results

We compared the rod-cladding temperatures vs time and the carryover rates into the moisture separator. Our comparisons indicated the accuracy of the TRAC reflood and entrainment models.

In general, the TRAC-PD2 rod-cladding temperatures tended to reverse direction and to quench late. Radiation heat transfer between rods and between the rods and the housing may have caused this discrepancy. This can be an important effect, accounting for 25-30% of the total heat transfer in some cases.¹⁵ A TRAC model that accounts for the radiation heat transfer between the rods and the wall was developed to investigate the effect caused by these phenomena. A calculation, based on a surface-to-surface radiation heat-transfer model,¹⁷ indicated that modeling such an effect could account for most of the discrepancies between the calculated and measured quench times.

Figures 82 and 83 illustrate rod-cladding temperature traces for two levels in Test 17201. At each level, the calculated rod temperature peaked at a much higher value than in the test data. This result may have been caused partially by radiation effects, because the calculated temperature reversed direction much later than the measured temperature. Another possible error may have been an inaccurate precooling rate caused by the carryover or steam precooling models. After the temperature reversed direction, the TRAC-PD2 temperature traces usually showed a higher rod-cooling rate than the test data. Calculated quench times tended to occur 30-40 s after those in the test data; the hottest elevations had the largest discrepancies. In most cases, TRAC-PD2 predicted a quench temperature close to that in the test data, indicating a good film-boiling temperature prediction.

Figures 84 and 85 show the rod-cladding temperatures for two important elevations in Test 4831. Again, the calculated rod temperatures reverse direction and quench late. The radiation effect and the difference between the calculated and test quench temperatures readily account for this discrepancy.

The calculated total effluent mass flows agreed very well with the measured flows for both tests. Figure 86 compares the data for Test 4831 with the TRAC results. Analyzing the data from Test 17201 required greater care. In this test, much of the liquid that was removed from the core was stored in the upper plenum and, thus, was not included in the measured effluent. The TRAC-PD2 input does not model this upper-plenum storage but models the total core effluent, which is determined by including the mass stored in the upper plenum as well as the mass collected in the carryover tank.

Figure 86 shows good agreement between the measured and calculated total effluent masses for Test 4831. However, this agreement is misleading. In fact, much of the time the two-phase mixture that reached the upper plenum was virtually dry steam, because most of the liquid had evaporated or fallen into the vessel. The liquid mass flow did indicate that some liquid slugs were ejected throughout the transient. The TRAC calculation indicated that the integrated liquid mass ejected was ~70 kg at 350 s. The test liquid effluent, including the mass stored in the steam probes and the upper plenum, was 72.6 kg \pm 10.8. The measured mass flow varied more smoothly than the calculated flow but the integrated results were remarkably close.

The TRAC-PD2 calculations for both FLECHT assessment problems compared quite well with the test data. This agreement indicates acceptable TRAC-PD2 reflood and entrainment models.

Appendix G lists the TRAC transient input deck for Test 17201. The input deck for Test 4831 may be found in the TRAC-PIA developmental assessment report.³

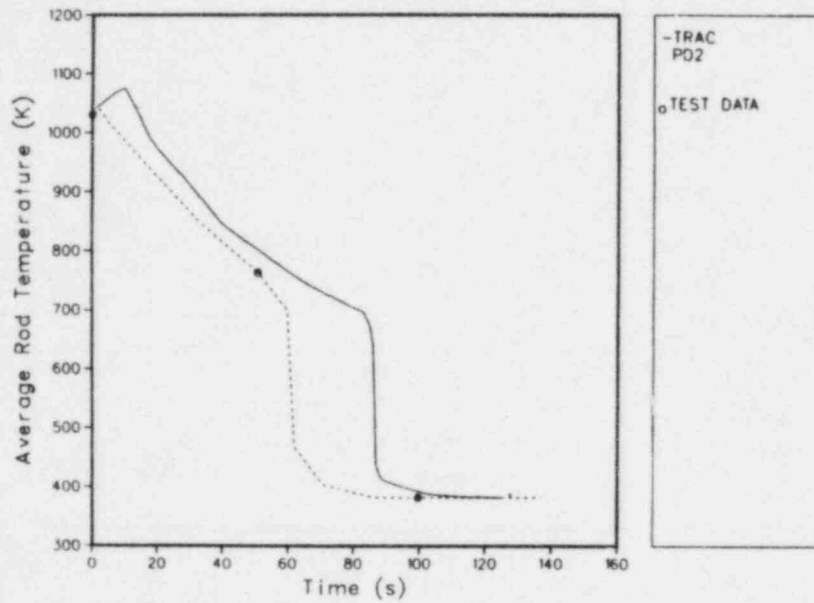


Fig. 82.

FLECHT Test 17201 rod-cladding temperatures at the 6-ft elevation compared with the TRAC-calculated temperatures.

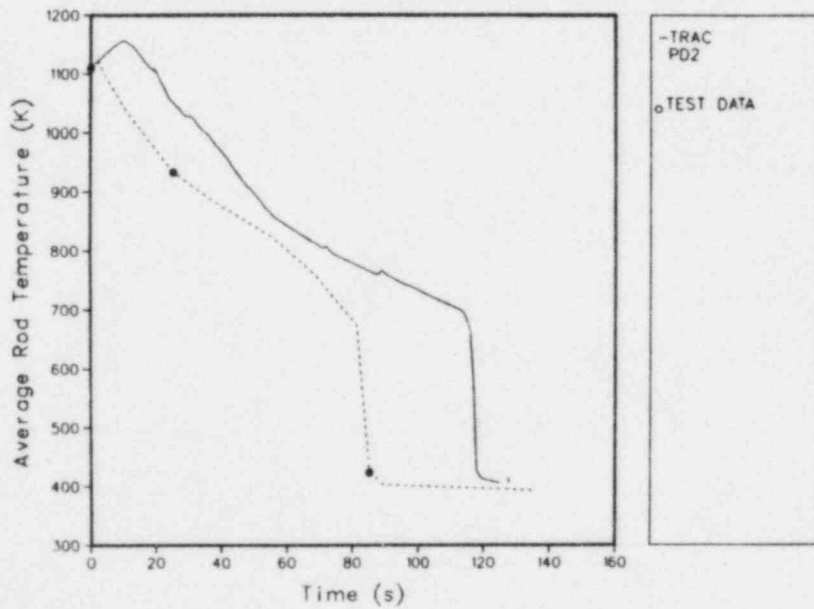


Fig. 83.

FLECHT Test 17201 rod-cladding temperatures at the 8-ft elevation compared with the TRAC-calculated temperatures.

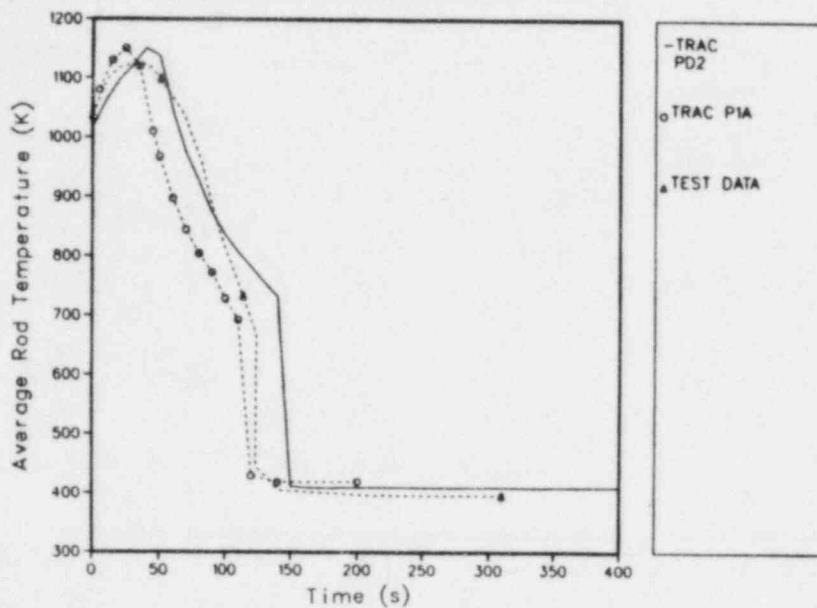


Fig. 84.

FLECHT Test 4831 rod-cladding temperatures at the 4-ft elevation compared with the TRAC-calculated temperatures.

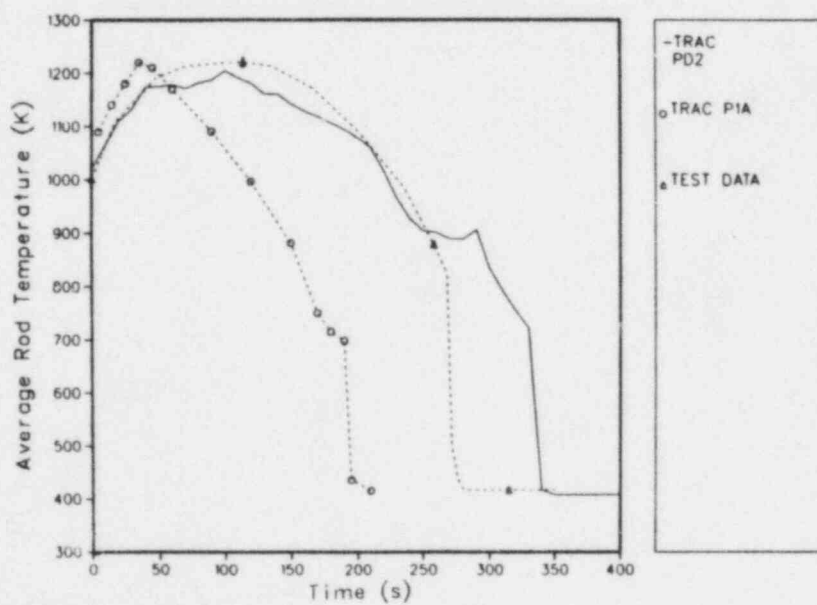


Fig. 85.

FLECHT Test 4831 rod-cladding temperatures at the 6-ft elevation compared with the TRAC-calculated temperatures.

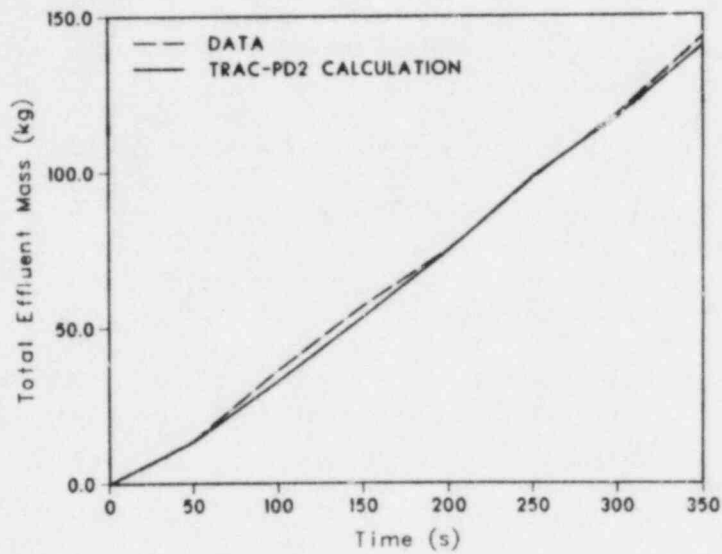


Fig. 86.

FLECHT Test 4831 total effluent mass compared with the TRAC-calculated effluent mass.

IX. SEMISCALE MOD-1 TEST S-02-8

A. Experiment Description

The Semiscale Mod-1 test apparatus¹⁸ was an improved version of the Semiscale isothermal system. In the Mod-1 system, a core, comprised of 40 electrically heated rods with the power and volume scaled to a typical PWR in a ratio of 1 to ~2000, simulated nuclear heating.

Figure 87 shows an isometric view of the test apparatus, which consisted of a pressure vessel with simulated reactor internals; an intact loop with an active steam generator, pump, and pressurizer; a broken loop with a simulated steam generator, a simulated pump, and pipe rupture assemblies; and a pressure-suppression system with header, auxiliary steam supply, and suppression tanks. Test S-02-8 simulated a double-ended offset-shear (200%) cold-leg break. This test differed from other Mod-1 tests because the resistance of the simulated pump was reduced by a factor of ~4 below the typical value.

Before the test, the system was brought to steady-state conditions. Table XI lists the calculated and measured initial parameters. Blowdown was initiated by rupturing the two rupture disks.

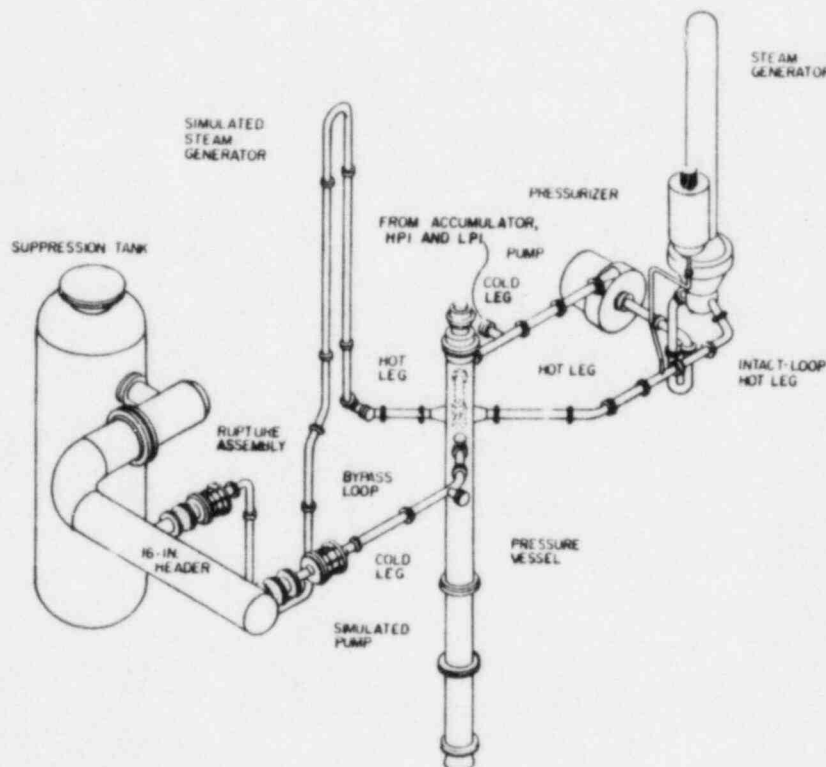


Fig. 87.

Isometric view of the Semiscale Mod-1 test apparatus (adapted from Ref. 18).

TABLE XI

CALCULATED AND MEASURED INITIAL PARAMETERS FOR SEMISCALE MOD-1 TEST S-02-8

<u>Parameter</u>	<u>Test Data</u>	<u>TRAC-PD2 Results</u>
Core power (MW)	1.59	1.59
Intact-loop cold-leg fluid temperature (K)	556.5	556.4
Hot- to cold-leg temperature differential (K)	37.8	38.4
Pressurizer pressure (MPa)	15.60	15.596
Pump mass flow ($\text{kg} \cdot \text{s}^{-1}$)	7.35	7.43
Pump speed ($\text{rad} \cdot \text{s}^{-1}$)	295.3	302.4
Pump differential pressure (kPa)	283.	284.35

B. TRAC-PD2 Model

The TRAC-PD2 best-estimate model of the Semiscale Mod-1 Test S-02-8 contained every component modeled by the code except an accumulator; thus, it was a good example to use in our data comparisons. As shown in Figs. 88 and 89, the system model contained 120 fluid cells in the one-dimensional components and 52 fluid cells in the VESSEL component.

Several modeling techniques were used in the TRAC model of this test to obtain a good representation of the test apparatus and to minimize the computer time needed for the calculations. In the following paragraphs, the methods used in the TRAC-PIA analysis³ of Test S-02-8 are discussed. Then, improvements in the input description used in the TRAC-PD2 analysis of Test S-02-8 are listed.

A flow resistance, instead of a reduced flow area, was used to represent the flow distribution plates at the bottom of the core. In extremely long, thin fluid cells, such as those needed to model the Semiscale core, the large dynamic pressure head needed to reduce the flow area of the flow distribution plate could cause unwanted circulation patterns within the core.

In the blowdown loop, a series of progressively shorter cell lengths was used near the break-nozzle expansion section because the flow conditions changed more rapidly near this section in the constant-area portion of the Semiscale nozzle (Fig. 89). Thus, the change in fluid conditions from cell to cell were more nearly equal than they would have been with equal-length fluid cells.

The line to the pressurizer was calculated by the fully implicit method to eliminate Courant limits on time-step size. Because the junction between the surge line and the pressurizer was placed in the large-area section of the pressurizer (that is, a low fluid-velocity region), the fluid cells at the bottom of the semi-implicit pressurizer could be very small without using small time steps; the small cells improved the TRAC-calculated pressurizer-discharge fluid conditions.

We made the following improvements in the TRAC-PD2 analysis. The break-nozzle expansion sections were more finely noded than in the TRAC-PIA analysis. Parametric studies (Sec. VII) indicated that this finer noding produced a better calculation of the subcooled blowdown section of the transient.

In the TRAC-PIA analysis the addition of the additive-friction terms accounted for the extra flow resistance caused by the orifices in the simulated pump of the broken-loop hot leg. These terms were not multiplied by the

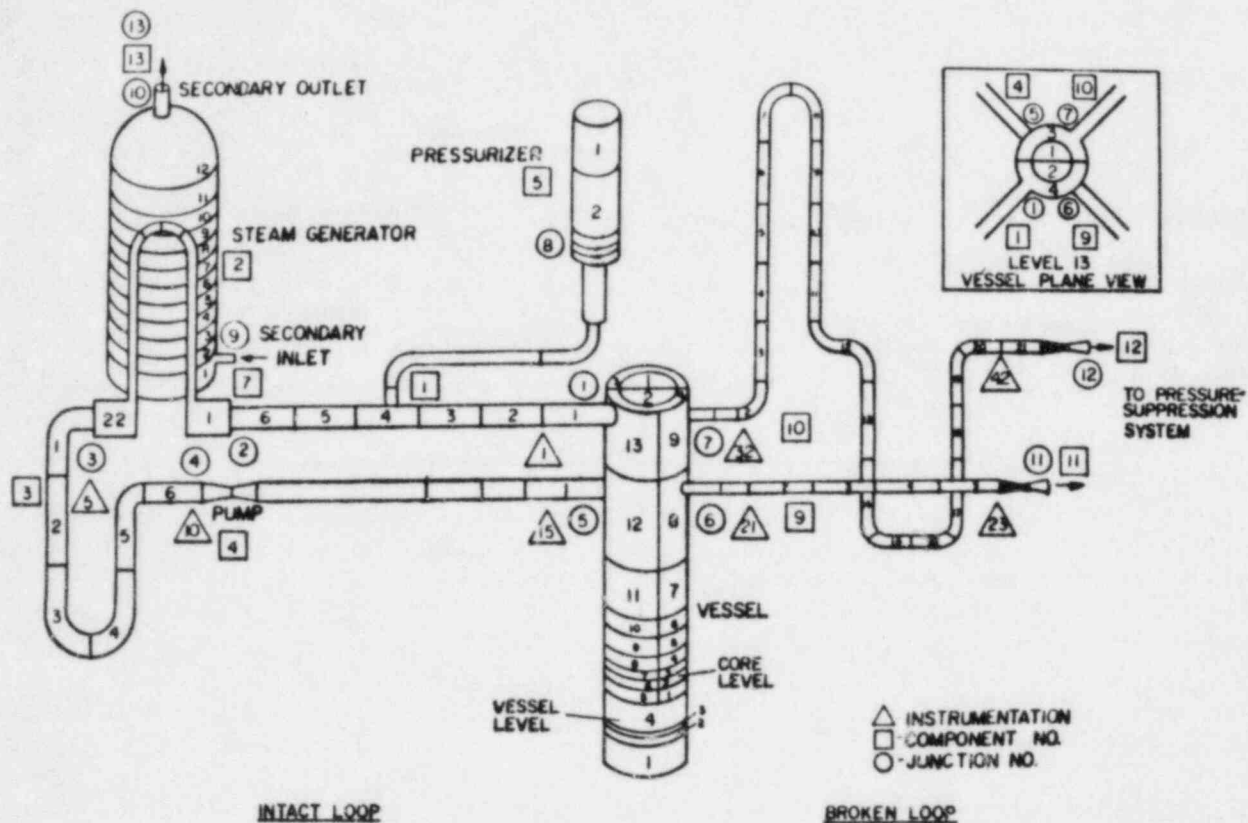


Fig. 88.
TRAC noding and component diagram for Semiscale Mod-1 system.

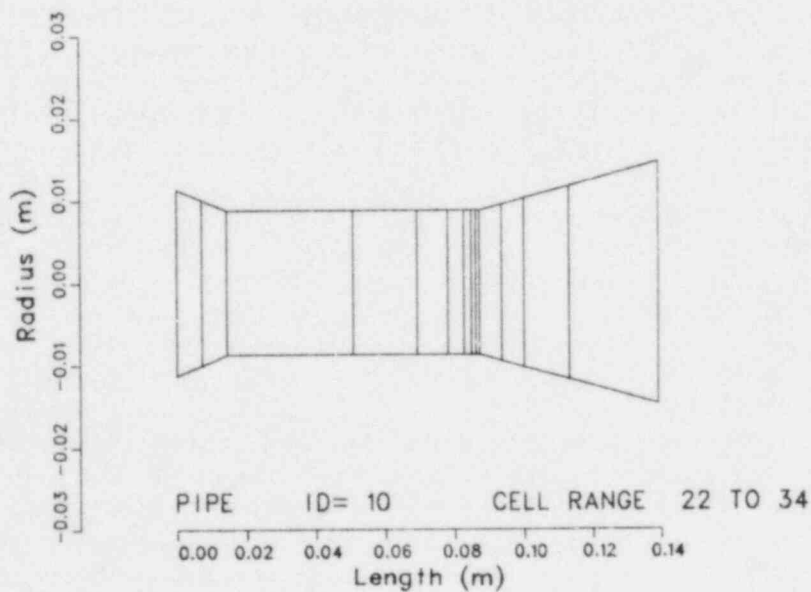


Fig. 89.
Semiscale Mod-1 nozzle noding diagram.

two-phase friction-factor multipliers; however, it seemed reasonable to expect that the orifices would exhibit two-phase flow effects. Therefore, in the TRAC-PD2 input, we deleted the additive-friction terms and decreased some of the hydraulic diameters in the broken-loop hot leg until the single-phase resistance value was the same as that reported in Test S-02-8 to account for this additional flow resistance.

We slightly increased the flow resistance of the intact-loop cold leg to account for the two turbine flow meters; thus, the calculated steady-state pressure drops in this line compared better with those in test data.

To finish the test analysis quickly, we reduced the VESSEL fluid cells from 152 to 52 by decreasing the theta segments from 4 to 2 and by reducing the number of axial levels. Because the Semiscale test apparatus performed like a one-dimensional system, it could be modeled by fewer radial and theta segments than a PWR. The axial segments were reduced from 19 to 13 by using coarser noding in the core and by decreasing the levels in the lower plenum from 4 to 3. To keep the number of levels in the lower plenum to a minimum and to prevent excessive mixing between the top and bottom of the lower plenum, we added a small amount of axial friction in the input descriptions of these levels.

The fuel-rod length was extended into the upper plenum by including the unpowered sections of the rods. We felt that this was a better way to handle the stored heat in the rods than to include the mass in the heat-slab description.

C. Data Comparisons

Differences between the calculated and measured initial conditions generally were caused by inconsistencies in the test data. For example, if the Semiscale homologous curves are correct, TRAC results for the pump head, flow rate, and speed were not totally compatible with those in the test data. These inconsistencies did not affect seriously the results of the transient analysis. Therefore, further refinement of the TRAC steady-state run was not necessary to obtain a good TRAC calculation of the blowdown transient.

The overall performance of a LOCA analysis code is determined partially by its ability to predict system pressure decay. Figure 90 compares the TRAC-calculated lower-plenum pressure (the solid line) with the Semiscale Mod-1 Test S-02-8 data¹⁹ (the dashed line with circles). The comparison in this figure indicates that TRAC predicts system performance well. The slightly underpredicted pressure beyond 10 s probably was caused by the underpredicted superheat in the upper part of the core. These underpredictions also occurred in the TRAC-PlA analysis of this test. Figures 91 and 92 compare the calculated and measured mass flows at the inlet and the outlet of the broken-loop hot leg. At both locations the calculated results generally were within the uncertainty of the test data. The main difference between the TRAC results and the test data was that TRAC underpredicted the magnitude of the flow spike, which started at 7 s and corresponded to the intact-loop pump degradation. The TRAC-PlA predictions of these flow rates generally were similar to the TRAC-PD2 results. Figure 93 shows that both TRAC-PD2 and TRAC-PlA predicted well the broken-loop cold-leg break flows. Figure 94 compares the TRAC-PD2 and TRAC-PlA mass flows in the intact-loop pump to those for Test S-02-8. Except for a slightly advanced pump degradation, both codes calculated these flows well.

Figure 95 compares the calculated and measured mass flows into the intact-loop hot leg. Because TRAC underpredicted the magnitude both during the

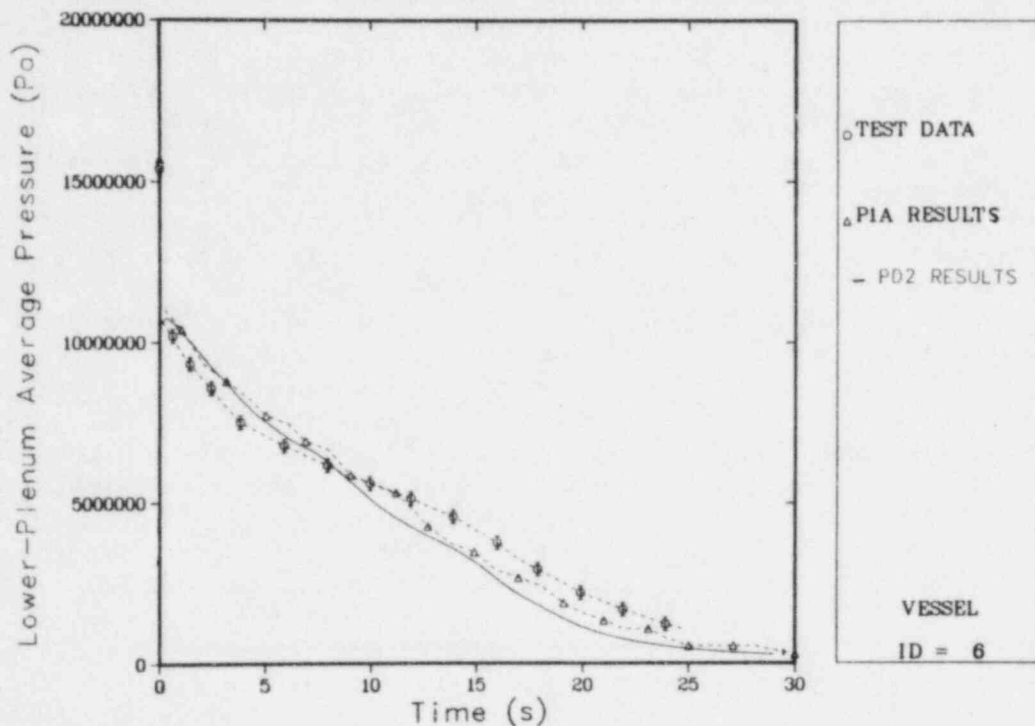


Fig. 90.

Comparison of the calculated and measured lower-plenum pressures for Semiscale Mod-1 Test S-02-8.

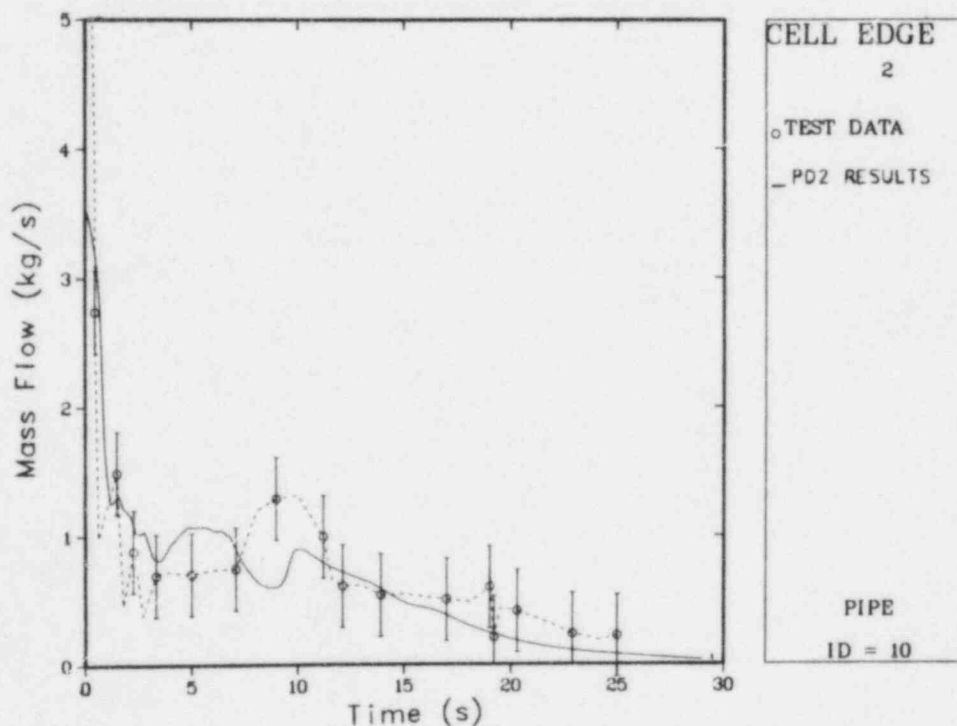


Fig. 91.

Comparison of the calculated and measured mass flows at the inlet of the broken-loop hot leg for Semiscale Mod-1 Test S-02-8.

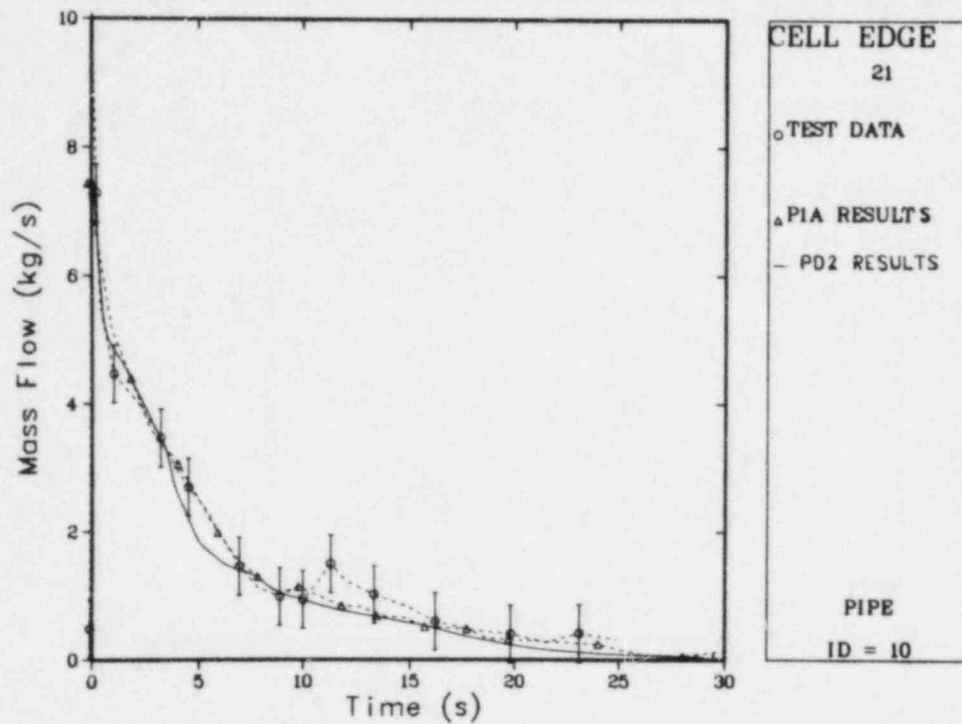


Fig. 92.

Comparison of the calculated and measured mass flows at the outlet of the broken-loop hot leg for Semiscale Mod-1 Test S-02-8.

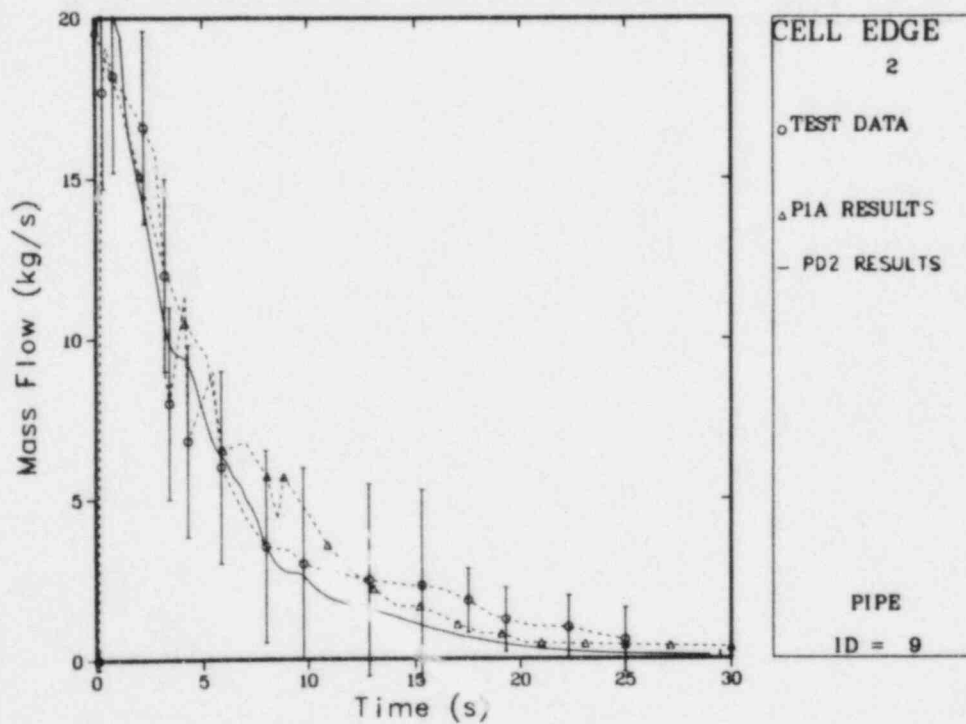


Fig. 93.

Comparison of the calculated and measured broken-loop cold-leg break flows for Semiscale Mod-1 Test S-02-8.

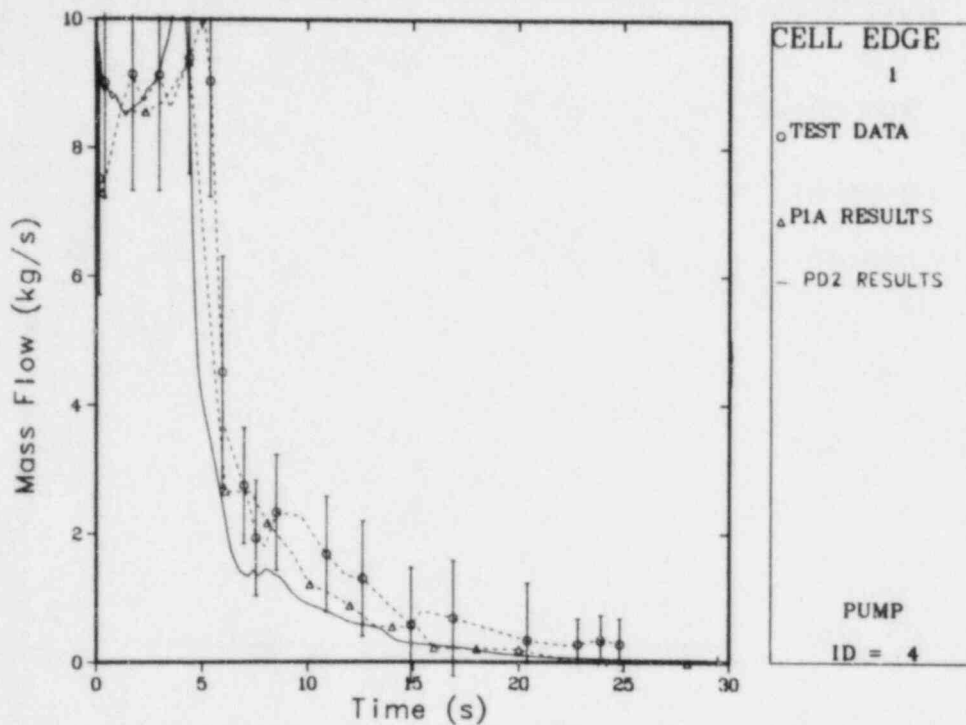


Fig. 94.

Comparison of the calculated and measured mass flows in the intact-loop pump for Semiscale Mod-1 Test S-02-8.

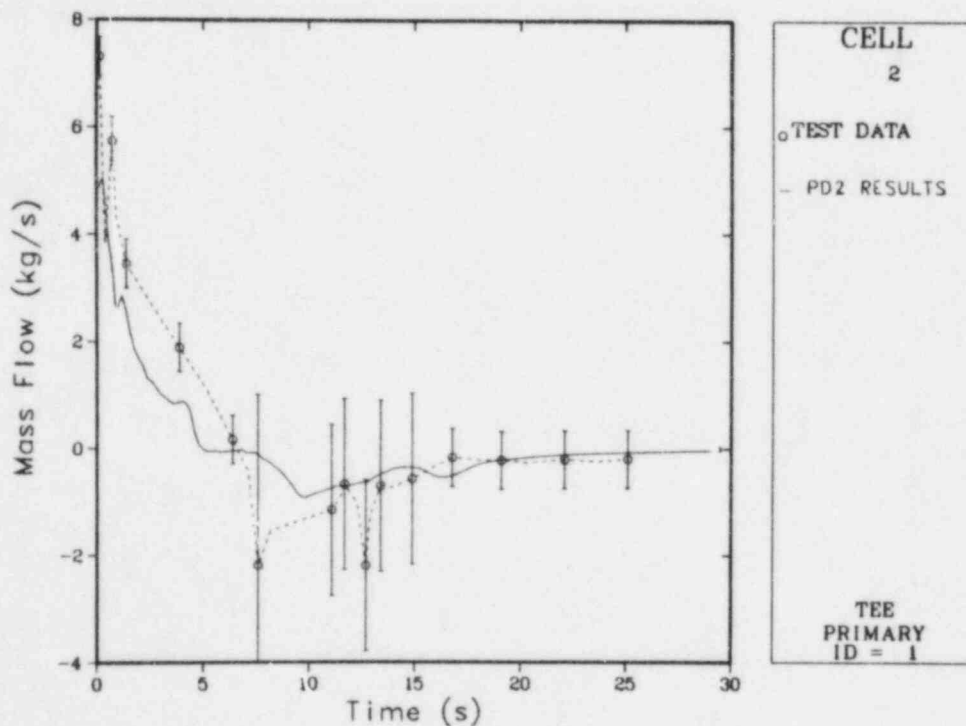


Fig. 95.

Comparison of the calculated and measured mass flows into the intact-loop hot leg for Semiscale Mod-1 Test S-02-8.

positive and the negative flows, it appears that the code underpredicted fluid density in this pipe. The timing of the flow reversal was predicted well.

Figure 96 indicates that both the TRAC-PD2 and the TRAC-PlA calculations of the pressurizer flows were very good.

In general, the TRAC predictions of the mass flows in the one-dimensional components were very good.

Figure 97 compares the calculated and measured mass flows at the entrance to the core. Although the agreement generally was good, TRAC did not predict the flow spike seen in the test data at 1.5 s. Inspection of the piping flows revealed no apparent reason for this discrepancy. Comparison of the calculated and measured temperature profiles in the lower plenum indicated that the TRAC predictions matched the test data well.

Figures 98-100 compare the calculated and measured cladding temperatures in the lower, middle, and upper core, respectively. The TRAC predictions matched the test data well at all three locations, although the calculated time to dryout at the lower and middle core was late. There was a general trend to make predictions that were in the lower range of the test data in the upper core and that were in the upper range of the test data in the lower core. These comparisons did not explain the spike at ~1.5 s in the core inlet flow in the test data. Perhaps, some physical phenomena in the Semiscale Mod-1 core or lower plenum were not modeled.

In general, both TRAC-PD2 and TRAC-PlA calculated well the response of the Semiscale Mod-1 system to a blowdown transient.

D. Conclusions

Semiscale Test S-02-8 assessed the ability of the TRAC-PD2 code to predict accurately the thermal-hydraulic response of a PWR system without ECC injection during blowdown. Except for an accumulator (ACCUM), all TRAC components were included in this problem. The results of this analysis were comparable to those obtained with TRAC-PlA; in general, both codes produced very good results.

Running times on a CDC 7600 computer for the steady-state and blowdown calculations were 10 and 19 min, respectively. These running times were reasonable based on the complexity of the model and were an order of magnitude faster than those for the TRAC-PlA calculations. Approximately half of this increased speed was caused by TRAC-PD2 improvements, which allowed larger time steps to be used.

Appendix H lists the steady-state and transient restart data decks for Semiscale Mod-1 Test S-02-8.

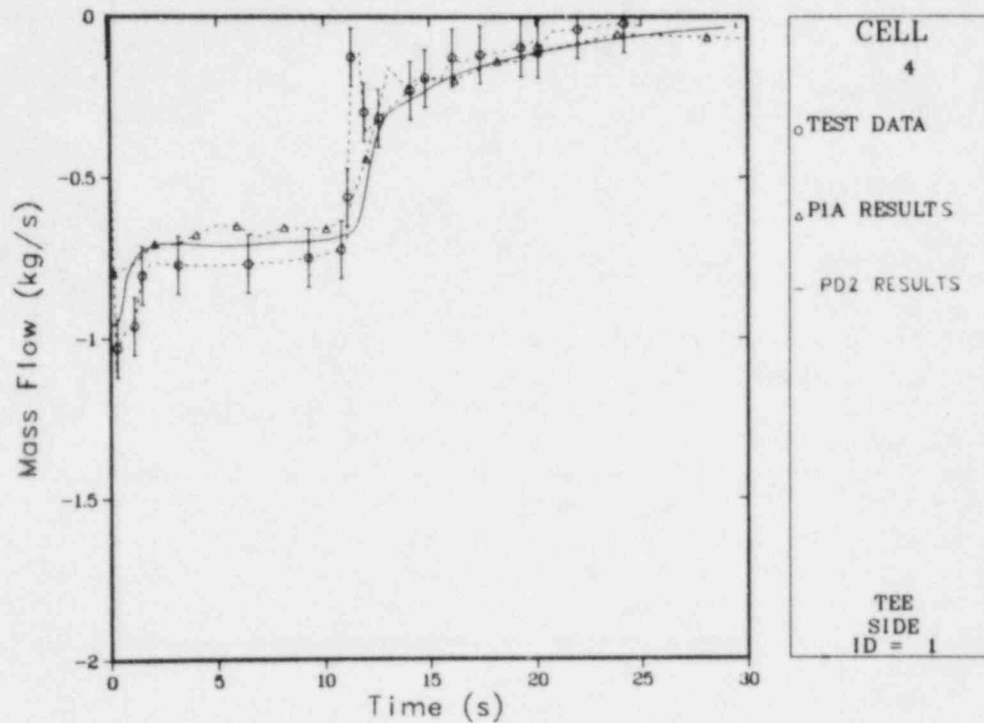


Fig. 96.

Comparison of the calculated and measured pressurizer flows for Semiscale Mod-1 Test S-02-8.

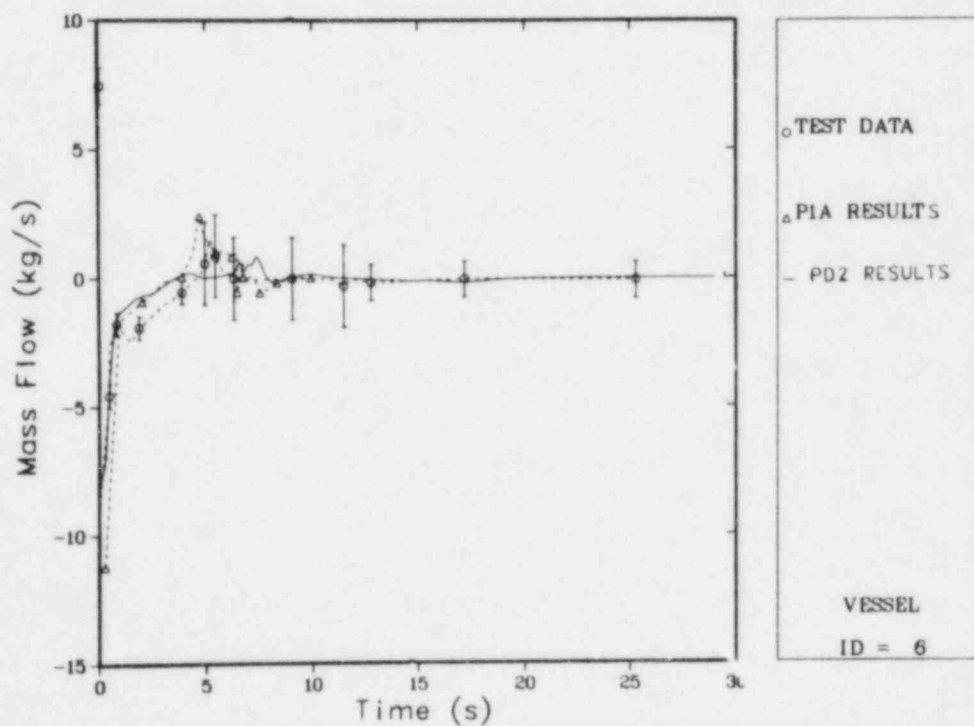


Fig. 97.

Comparison of the calculated and measured mass flows at the entrance to the core for Semiscale Mod-1 Test S-02-8.

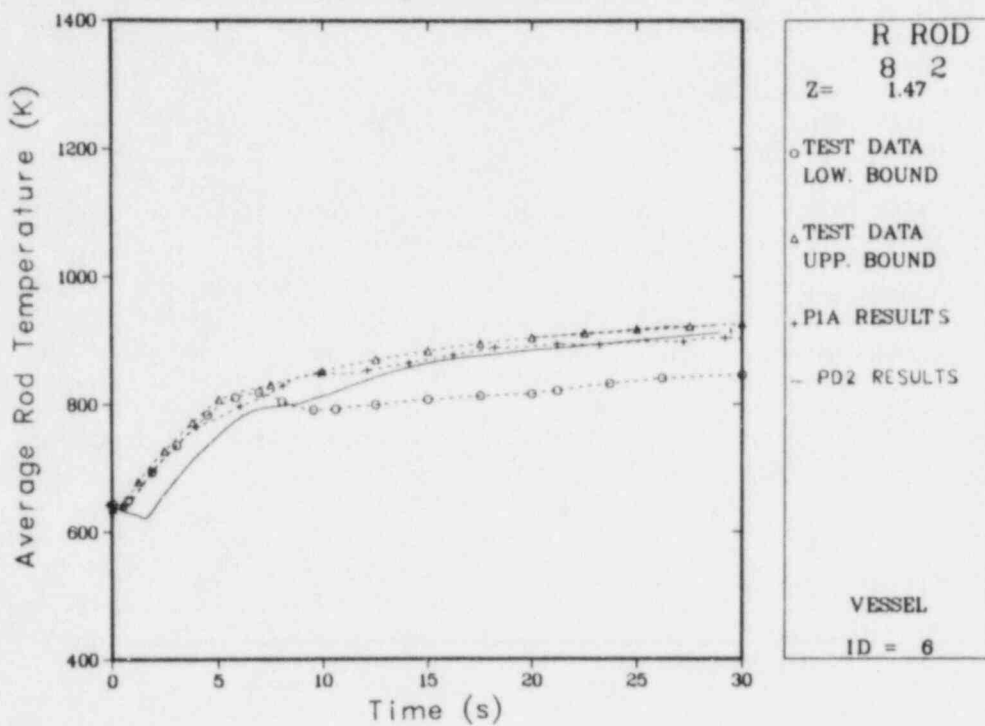


Fig. 98.

Comparison of the calculated and measured cladding temperatures in the lower core for Semiscale Mod-1 Test S-02-8.

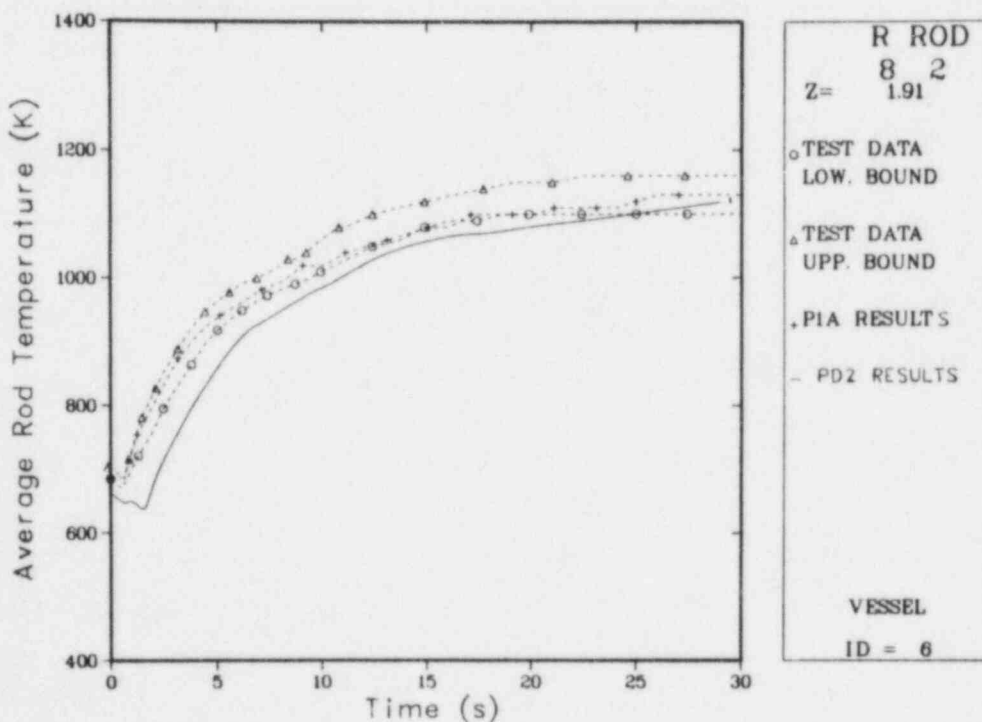


Fig. 99.

Comparison of the calculated and measured cladding temperatures in the middle core for Semiscale Mod-1 Test S-02-8.

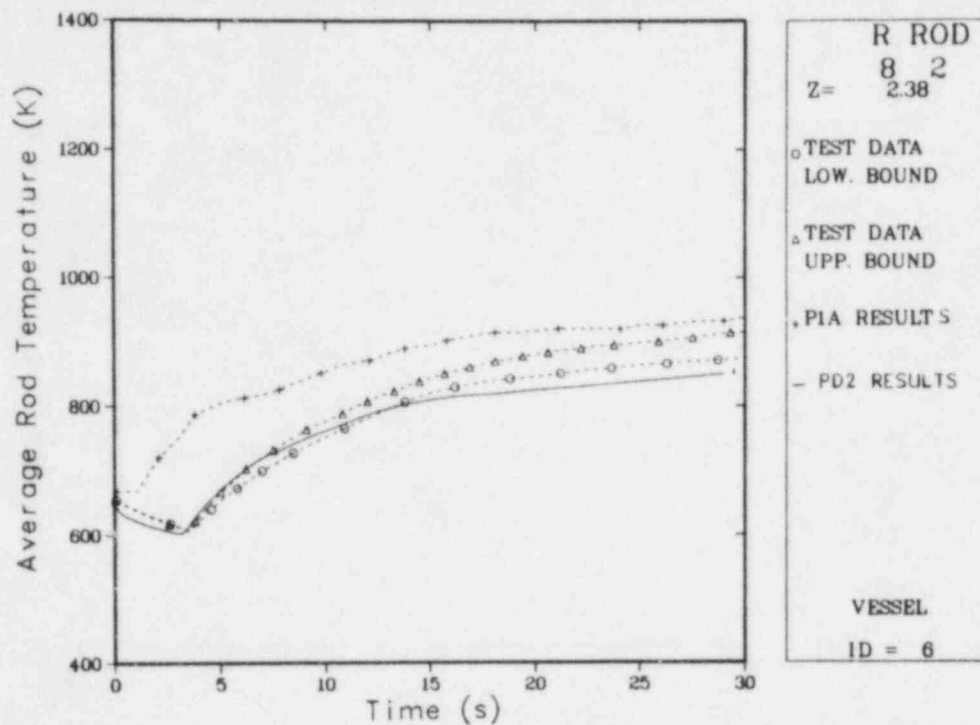


Fig. 100.

Comparison of the calculated and measured cladding temperatures in the upper core for Semiscale Mod-1 Test S-02-8.

X. SEMISCALE NOZZLE

Section IX described the Semiscale system. For our data comparisons the Semiscale broken-loop cold-leg nozzle was isolated from the rest of the system and test data were used for the boundary conditions in the TRAC input. We used the S-02-8 data as a basis for a detailed look at critical flow through a nozzle.

A. TRAC-PD2 Model

Figure 101 illustrates the TRAC PIPE noding used to describe the broken-loop cold-leg nozzle for this study. The volume was divided progressively more finely as it approached the end of the constant flow-area section of the nozzle. This method allowed a reasonable number of very small cells as the fluid reached the critical velocity, whereas an evenly divided nozzle would have required an exorbitant number of volumes. The noding of the nozzle-exit section also was important. A sensitivity study showed that at least four volumes in the exit section improved the predictions for the subcooled portion of the blowdown.

The input boundary conditions were the pressure, temperature, void fraction at the nozzle entrance, and pressure at the nozzle exit. Although the boundary conditions were obtained from the data for the cold-leg entrance, they were applied at the nozzle entrance. We excluded the remainder of the cold leg in the TRAC model because we wanted to minimize the numerical diffusion of sharp changes in the fluid conditions. The time delay between flow entering and exiting the cold-leg piping was very small and did not affect the data

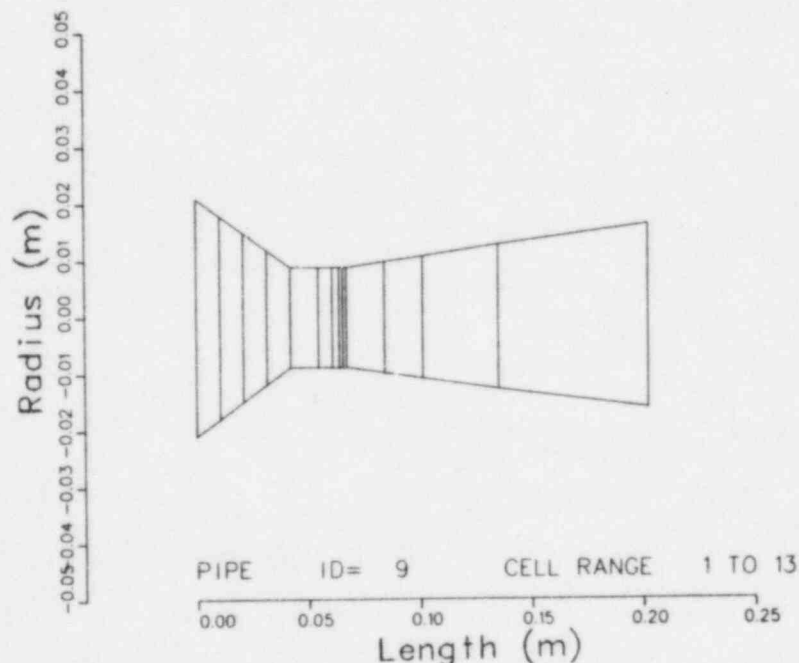


Fig. 101.

Volume diagram of Semiscale Test S-02-8 broken-loop cold-leg nozzle.

significantly. Figures 102-104 compare some of the boundary conditions for the cold-leg nozzle entrance to the test data. Figure 104 shows the density used to obtain the void fraction in Fig. 103. The test density was not totally compatible with the fluid temperature; thus, the test density was less than that used as a boundary condition by TRAC in the first ~2.5 s.

B. Results

Figures 105 and 106 compare the TRAC-calculated mass flow and mixture velocity at the nozzle entrance to the test data. Although these data comparisons were almost equivalent for most of the transient, the mixture-velocity comparison was superior to the mass-flow comparison, especially during the first 2 s of the transient, because the inaccuracy in the measured density was excluded. Figure 106 shows excellent agreement between the TRAC results and the test data during the first 1.5 s, if one accounts for the response time of the turbine flow meter. Thus, the TRAC model predicted mass flows well in a highly subcooled situation. From ~2-3 s, TRAC increasingly underpredicted the mass flows, whereas the test data did not indicate the beginning of boiling in the nozzle until vapor appeared at its entrance. A TRAC nucleation time-delay model is needed to predict this part of the transient precisely. When the void fraction was between 0.05-0.2 (3.5-6.0 s into the transient), the TRAC results agreed well with the test data. When the entrance void fraction varied from 0.2-0.95 (6.0-13.0 s), the TRAC results indicated a higher mixture velocity than the test data. If this discrepancy was caused by a TRAC overprediction rather than by an error in the test data, then the causes probably were associated with the interfacial heat-transfer or the slip correlations. At

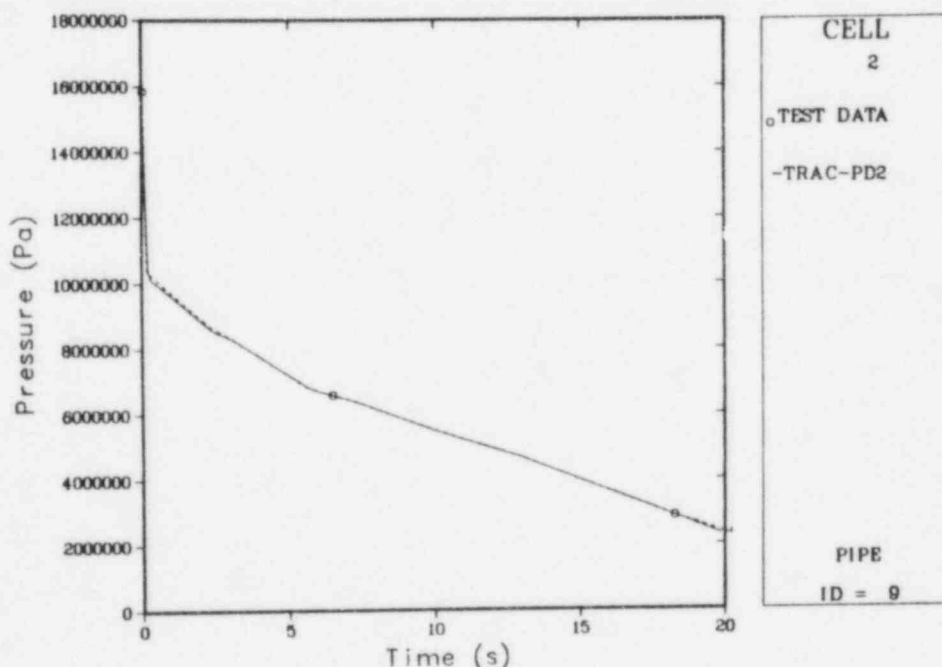


Fig. 102.

Comparison of the upstream pressure boundary condition and the measured pressure for the Semiscale nozzle study.

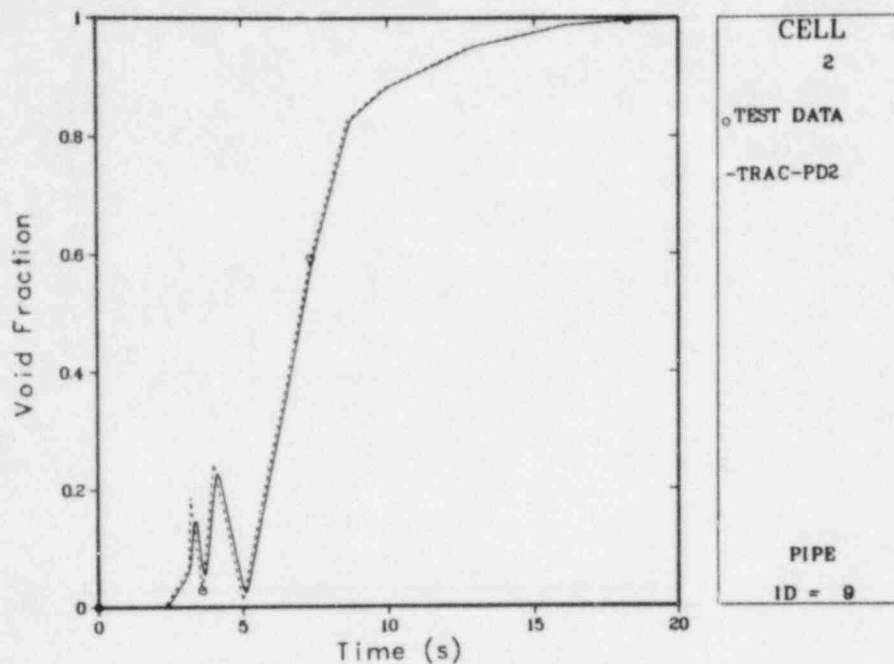


Fig. 103.

Comparison of the upstream void-fraction boundary condition and the measured void fraction for the Semiscale nozzle study.

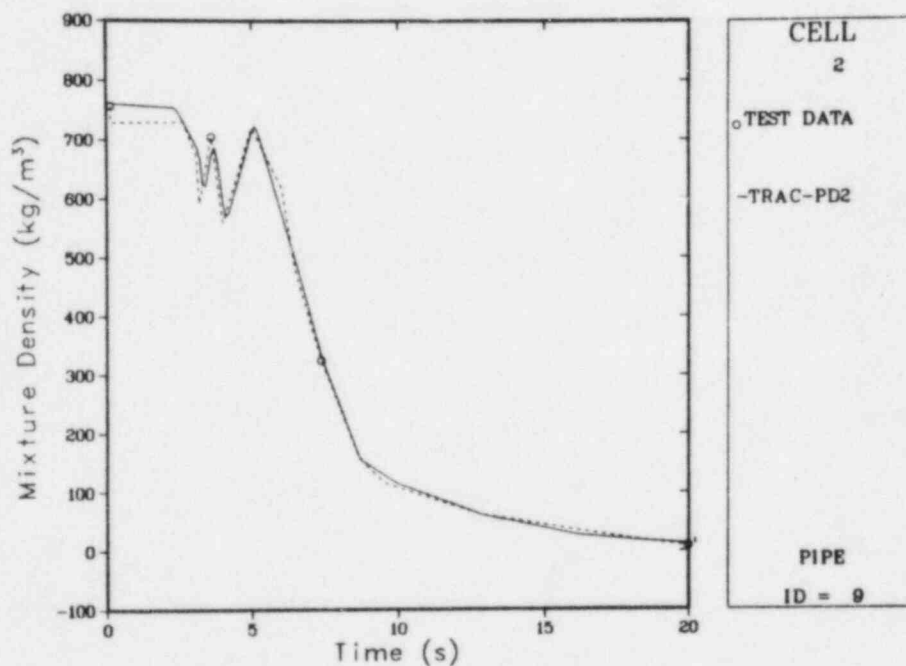


Fig. 104.

Comparison of the upstream density boundary condition and the measured mixture density for the Semiscale nozzle study.

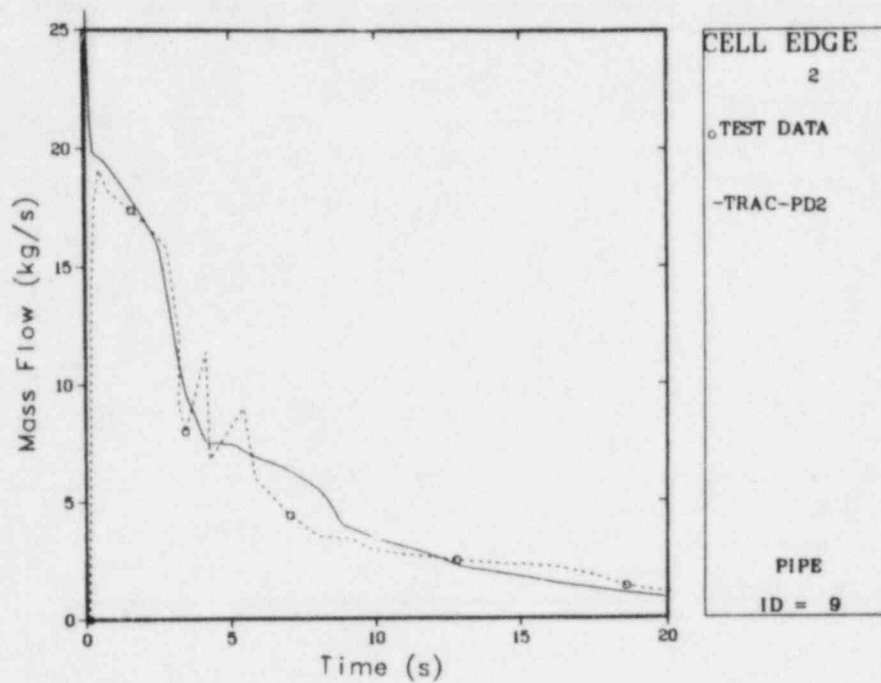


Fig. 105.

Comparison of the calculated and measured mass flows for the Semiscale nozzle study.

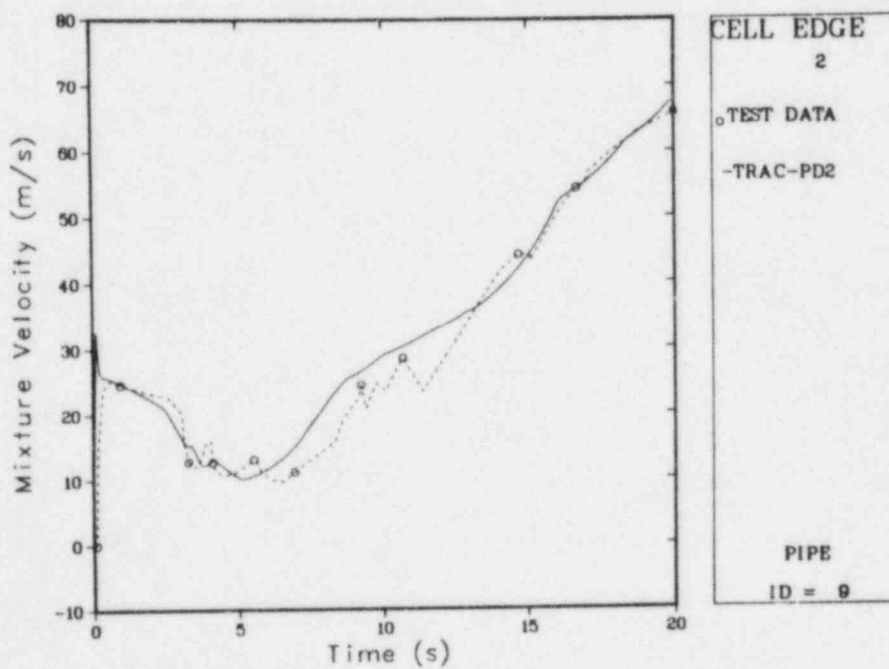


Fig. 106.

Comparison of the calculated and measured mixture velocities for the Semiscale nozzle study.

10 s, the TRAC-calculated temperatures for the fluid, vapor, and interface indicated that the fluids were very close to thermal equilibrium. Because minimum flow generally results from thermal equilibrium, the slip correlations probably were responsible for the overpredicted fluid velocities.

When the entrance void fractions were above 0.95 (after 13 s), the calculated mixture velocities compared well with the test values. The fluid velocity at these high void fractions was very dependent on the input void fraction and, thus, very sensitive to small inaccuracies in the measured density. Consequently, deviations of up to 30% between the TRAC-calculated velocities and the test values might have been caused by the error limits of the density data and would have been acceptable.

C. Conclusions

We conclude that TRAC calculates mass flows well for nozzles similar in size and area ratio to the Semiscale Test S-02-8 nozzle. More specifically, TRAC calculates highly subcooled flow very well, underpredicts flows with low subcooling, predicts well fluid flows with void fractions between 0.05-0.2 and over 0.95, and slightly overpredicts fluid flows with void fractions between 0.2-0.95. The overall predicted break flow appeared adequate to model a Semiscale test blowdown accurately.

Our sensitivity studies indicated that the nozzle section before the end of the constant-area section must be finely noded to predict the saturated blowdown accurately, whereas the expansion section of the nozzle must have at least four nodes to calculate the subcooled portion of the blowdown accurately. The TRAC calculations required 10.69 s of CPU time on a CDC 7600 computer.

XI. SEMISCALE MOD-1 TEST S-06-3

A. Experiment Description

The system used for Semiscale Test S-06-3 (Ref. 20) essentially was the same as that described in Sec. VI except that an accumulator, a high-pressure injection system (HPIS), and a low-pressure injection system (LPIS) to the intact-loop cold leg were added. Other system differences were a higher resistance in the simulated pump and in the active steam generator and a core that consisted of 4 high-power rods (1.485 times the average power), 32 low-power rods (0.939 times the average power), and 4 unpowered rods.

B. TRAC-PD2 Model

The input description used to model Test S-06-3 essentially was the same as that described for Test S-02-8 (Sec. VI) except for the additions needed to model the accumulator and the HPIS and LPIS. Figure 107 shows a noding diagram of Semiscale Test S-06-3.

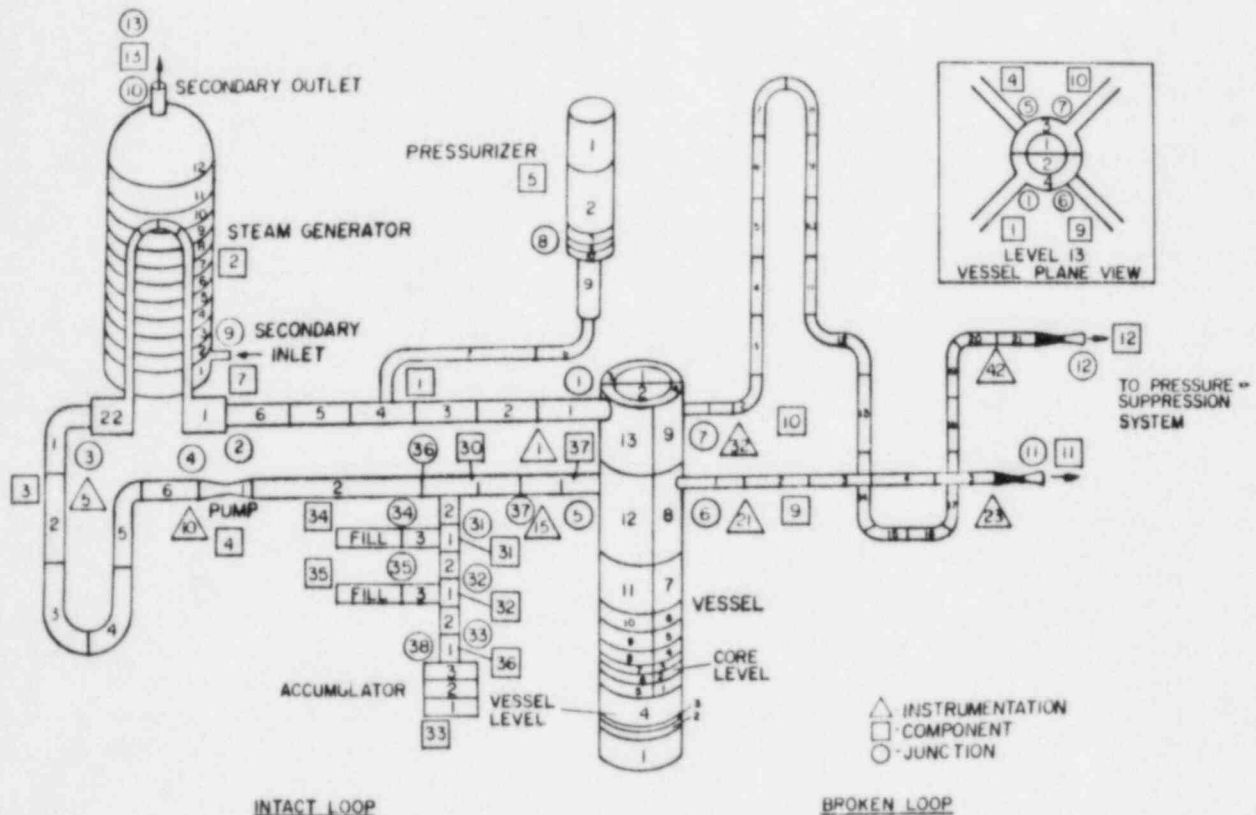


Fig. 107.
TRAC noding diagram of Semiscale Test S-06-3.

We made five changes to the input description for Test S-02-8 to model Test S-06-3.

1. The resistance of the intact-loop steam generator was increased to account for the high-resistance orifice (3.43 cm) used in Test S-06-3.
2. The resistance of the broken-loop simulated pump was changed from 48 to 147 units.
3. Several nodes were combined to increase the length of the node at the pump exit to make the pump less sensitive to ECC backup.
4. The number of nodes in the pressurizer was increased to model the stratified temperature profile in Test S-06-3.
5. The system power level was lowered from 1.59 to 1.004 MW. The number of active rods per theta segment was changed from 19.5 to 18, and hot rods were included to predict both the higher and lower than average rod temperature histories.

We originally modeled the HPIS and LPIS by adding FILL components. However, we discovered that the FILLs acted as dead-end pipes; thus, a high-pressure spike anywhere in the system caused a reflection that decreased the pressure in the volume connected to the FILL below the range of the TRAC thermal-properties routines. We solved this problem by adding a flow resistance between this volume and the rest of the system.

During the transient calculation, we found that the detailed noding of the cold-leg break nozzle necessary to predict the blowdown break flows accurately caused calculational difficulties when the system and break pressures became equal. However, this finely detailed noding was not needed when the pressures were equal because the break flows were subsonic. Consequently, after ~36 s, the finely noded nozzle (Fig. 108) for the broken-loop cold leg was replaced by the coarsely noded nozzle shown in Fig. 109; this new noding includes some of the upstream piping volume to increase cell volume.

C. Data Comparisons

Table XII compares the TRAC-calculated and measured initial conditions for the start of the blowdown. The correlation between the two was sufficient to allow an accurate transient analysis.

Because different time scales were needed to present the calculational results clearly, our transient analysis was limited to curves representing only the blowdown and to curves representing both the blowdown and the reflood.

Figure 110 compares the TRAC-calculated and measured lower-plenum pressures. During the first 5 s, there clearly was a faster rate of pressure decay in the TRAC calculation than in the test data. To determine the reason for this discrepancy, we compared TRAC-calculated mass and volumetric flows in and out of the core with the test values; our results indicated that the TRAC predictions were sufficient to allow an accurately predicted lower-plenum pressure. The temperature profiles of the heater rods also did not indicate any reason for this discrepancy. Heat-slab masses and the water volume in the core were reasonable. During this same 5-s interval, the TRAC-calculated pressure decay for Test S-02-8 also was accurate. In summary, we could not determine any reason for the discrepancy between the TRAC results and the test data.

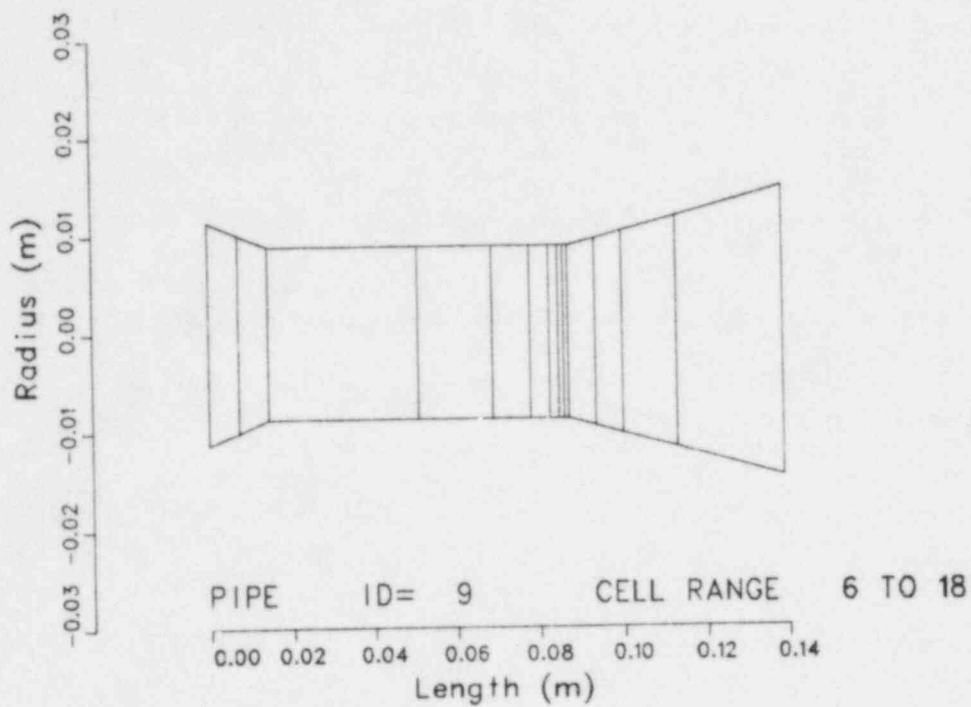


Fig. 108.
Finely noded break nozzle for Semiscale Test S-06-3.

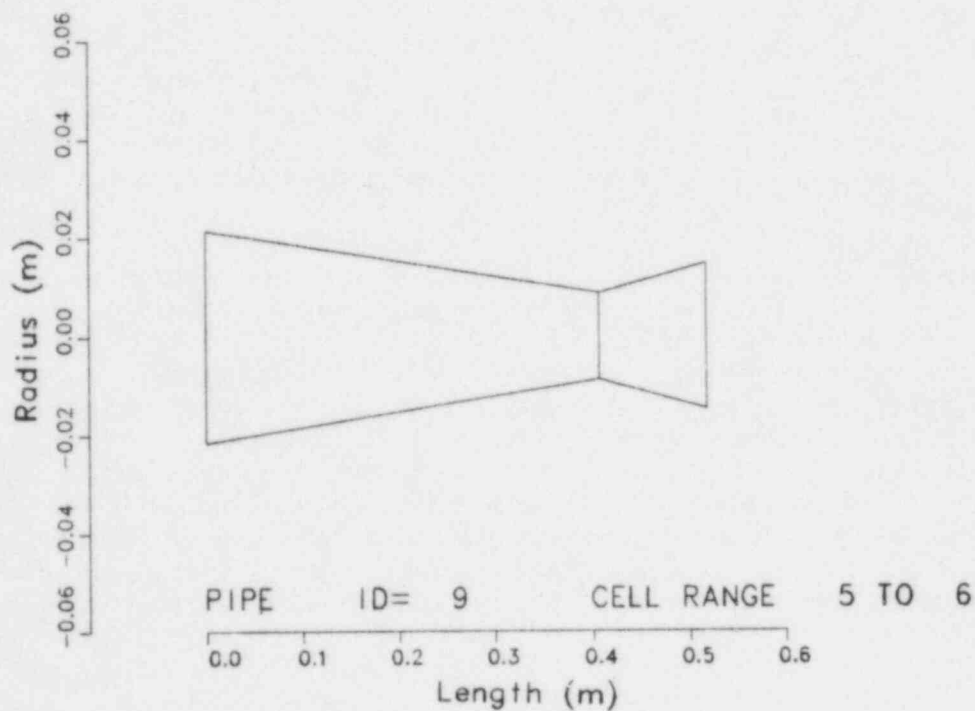


Fig. 109.
Coarsely noded cold-leg break nozzle for Semiscale Test S-06-3.

TABLE XII

CALCULATED AND MEASURED INITIAL CONDITIONS FOR SEMISCALE MOD-1 TEST S-06-3

<u>Parameter</u>	<u>Test Data</u>	<u>TRAC-PD2 Results</u>
Core power (MW)	1.004	1.004
Intact-loop cold-leg temperature (K)	563.	562.4
Hot- to cold-leg temperature differential (K)	34.1	33.7
Pressurizer pressure (MPa)	15.77	15.769
Pump mass flow ($\text{kg} \cdot \text{s}^{-1}$)	5.02	5.208
Pump speed ($\text{rad} \cdot \text{s}^{-1}$)	169.5	170.
Pump differential pressure (kPa)	80.	72.99

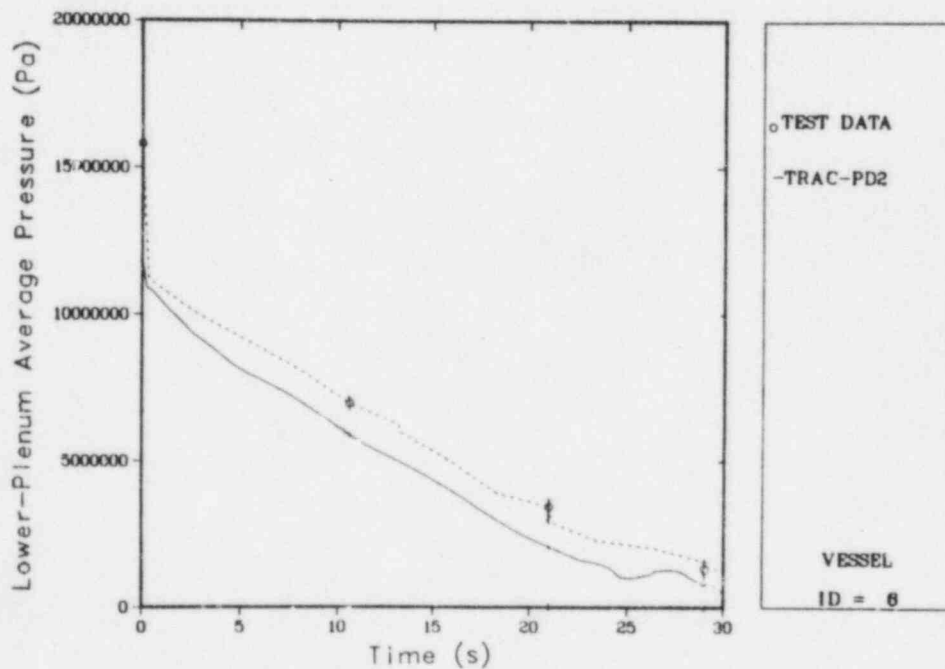


Fig. 110.

Comparison of the TRAC-calculated and measured lower-plenum pressures for Semiscale Test S-06-3.

Figures 111 and 112 compare the mass and volumetric flows at the entrance to the broken-loop cold leg. The comparisons between the TRAC calculations and the test data were remarkably good.

Figure 113 compares the mass flows at the entrance to the broken-loop hot leg. Again, the comparisons between the TRAC results and the test data were very good and well within the accuracy of the experiment data. Figure 114 shows the calculated volumetric flow into the broken-loop hot leg. In Test S-02-8 the inclusion of two-phase flow effects in the simulated pump had little effect on the TRAC predictions; however, their inclusion in Test S-06-3 markedly improved the the TRAC results and, thus, the comparisons with the test data.

Figures 115 and 116 compare the mass and volumetric flows at the inlet to the intact-loop hot leg. The agreement between the TRAC results and the test data was excellent. Because this TRAC calculation used finer detail in the pressurizer component, better agreement was obtained for Test S-06-3 than for Test S-02-8.

Figure 117 compares the TRAC-calculated and measured mass flows at the pressurizer exit. The averaging of the flow rate shown by the calculation probably was caused by the numerically induced mixing of the hot and cold fluids within the pressurizer during blowdown.

Figures 118 and 119 compare the mass and volumetric flows at the pump exit. The TRAC calculations matched the test data well. The most noticeable difference between the two figures was that the calculated pump degradation, indicated by the decrease in mass flow at ~5 s in Fig. 117, occurred earlier than indicated by the test data.

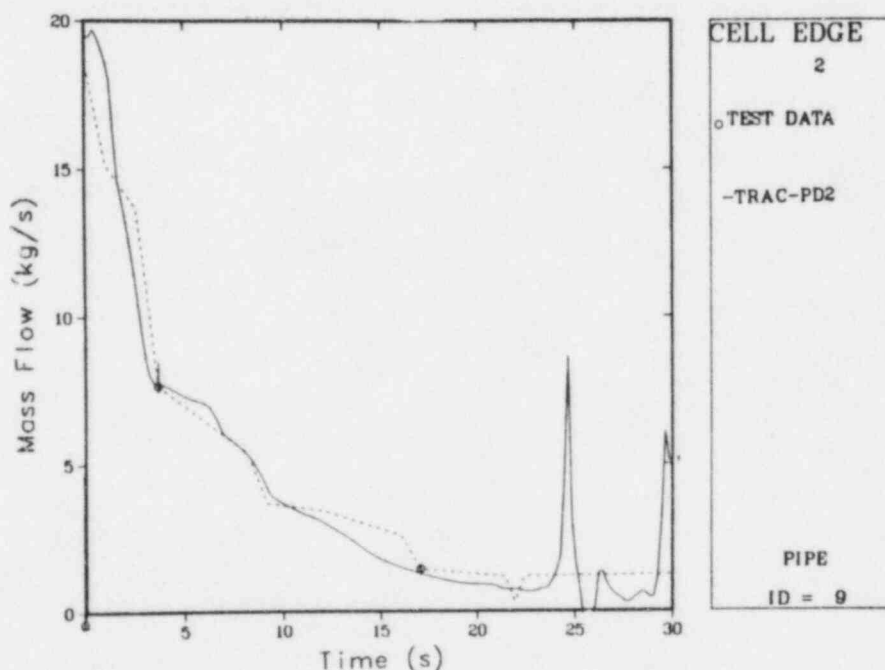


Fig. 111.

Comparison of the TRAC-calculated and measured mass flows at the entrance to the broken-loop cold leg for Semiscale Test S-06-3.

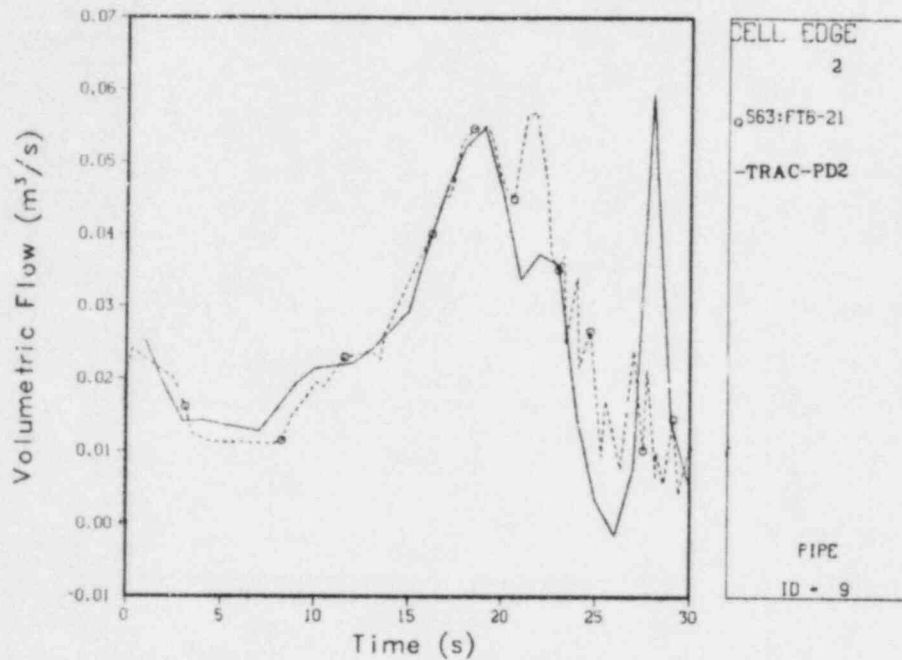


Fig. 112.

Comparison of the TRAC-calculated and measured volumetric flows at the entrance to the broken-loop cold leg for Semiscale Test S-06-3.

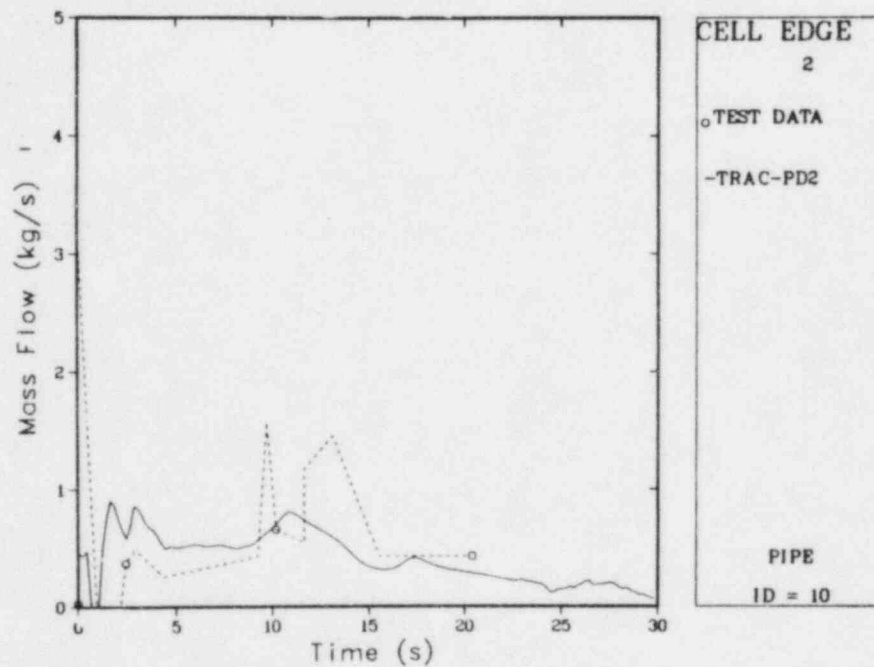


Fig. 113.

Comparison of the TRAC-calculated and measured mass flows at the entrance to the broken-loop hot leg for Semiscale Test S-06-3.

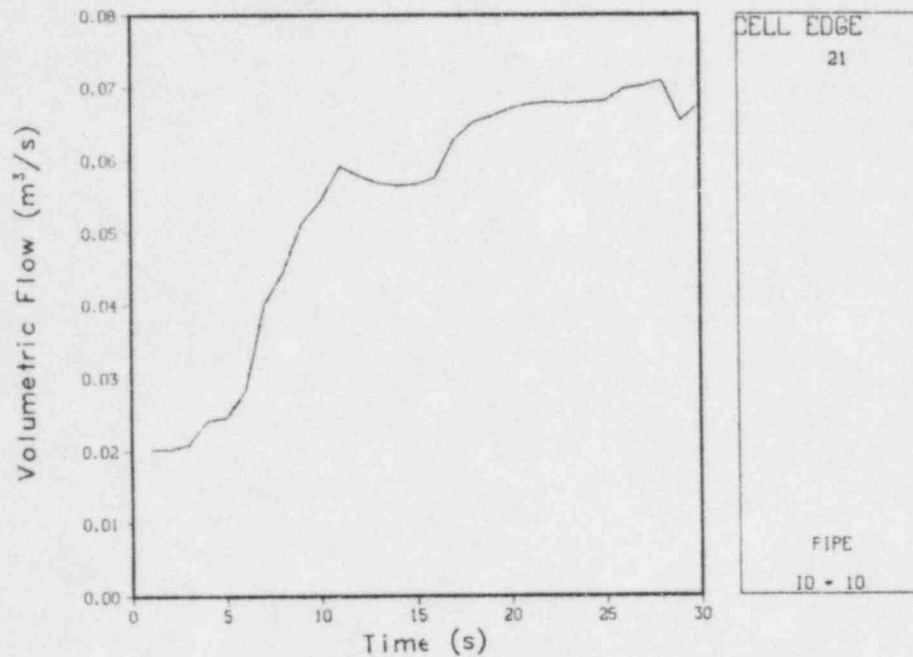


Fig. 114.

Volumetric flow at the entrance to the broken-loop hot leg for Semiscale Test S-06-3.

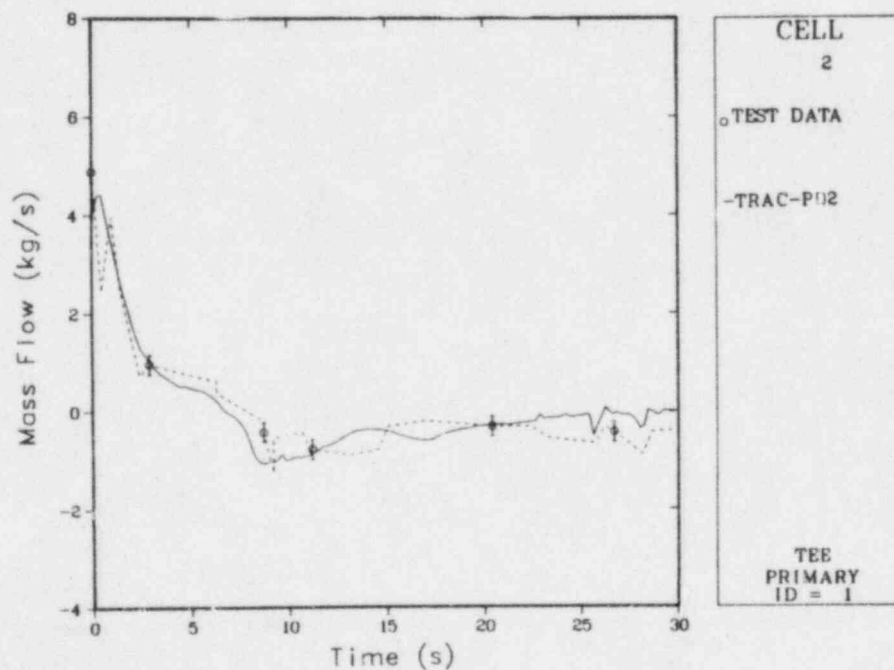


Fig. 115.

Comparison of the TRAC-calculated and measured mass flows at the entrance to the intact-loop hot leg for Semiscale Test S-06-3.

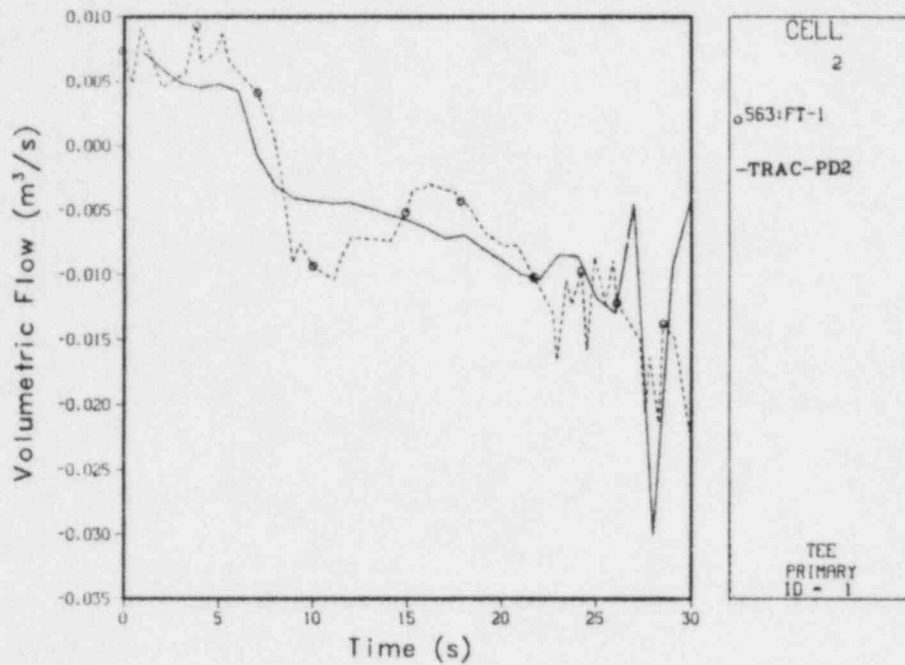


Fig. 116.

Comparison of the TRAC-calculated and measured volumetric flows at the entrance to the intact-loop hot leg for Semiscale Test S-06-3.

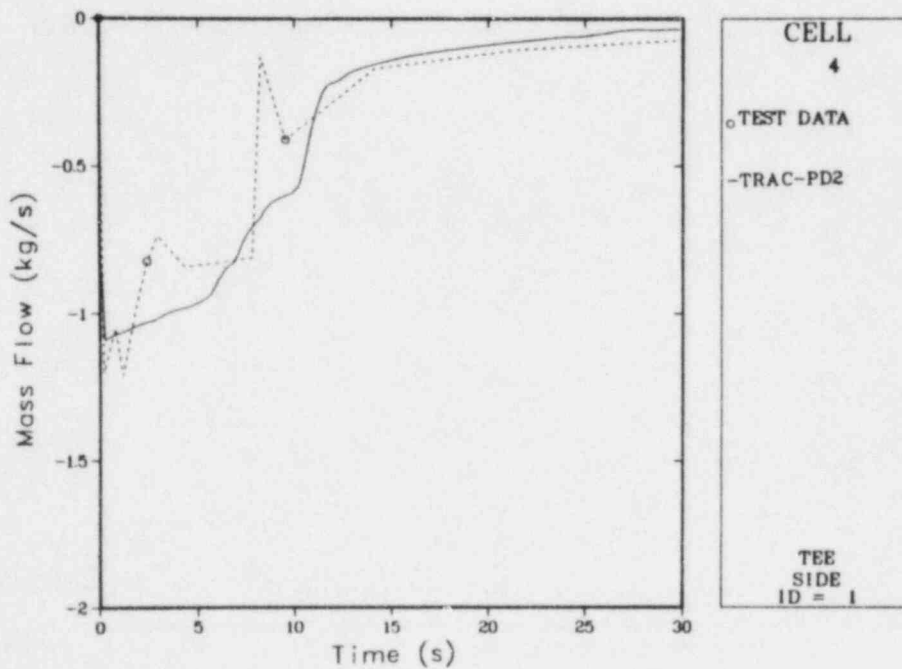


Fig. 117.

Comparison of the TRAC-calculated and measured mass flows at the pressurizer exit for Semiscale Test S-06-3.

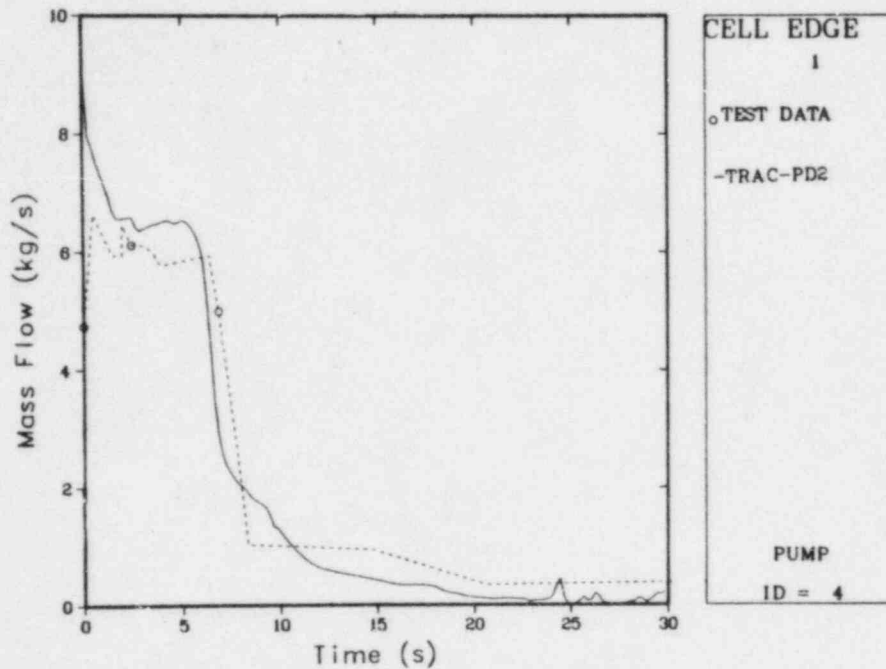


Fig. 118.

Comparison of the TRAC-calculated and measured mass flows at the pump exit for Semiscale Test S-06-3.

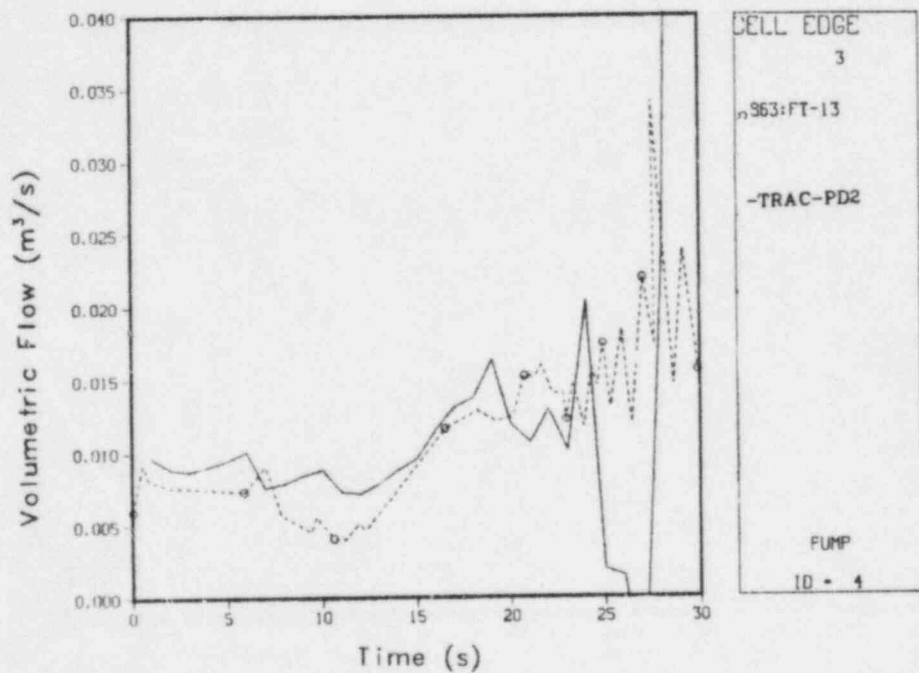


Fig. 119.

Comparison of the TRAC-calculated and measured volumetric flows at the pump exit for Semiscale Test S-06-3.

In summary, the TRAC-calculated pipe flows during the blowdown transient showed excellent agreement with the test data, and any improvements in TRAC probably would affect the predicted rod-cladding temperatures insignificantly.

Figure 120 compares the mixture velocities from the accumulator. Two factors may have caused the deviation between the calculation and the test data. The initial fluctuation in the calculated results at 10 s was caused by flashing of the liquid in the pressure-dependent valve that controls the flow from the accumulator. The steep increase in velocity that occurred at ~20 s in the experiment was calculated at ~15 s by TRAC because of the more rapid decrease in the calculated system pressure between 0 and 5 s than was measured in the test. The overall flow rate and the voiding time of the accumulator were calculated well by TRAC.

Figure 121 compares the mass flows at the core entrance. Although the calculated pipe flows in the hot and cold legs to the vessel and the heat transfer within the core agreed well with the test data, the TRAC calculations for Semiscale Tests S-02-8 and S-06-3 tended to underpredict the degree of negative core flow between 1 and 6 s. We could find no apparent cause for this TRAC underprediction in either test.

The cladding temperature data were plotted for different core levels both for the low-power rods (0.939 times the average power) and for the high-power rods (1.485 times the average power). The core hydraulics were linked to a set of average-power rods. Because there was no direct feedback from the low- or the high-power rods to the hydraulics, a CHF in the high-power rods did not affect the rate of steam generation within the core unless it was matched by a CHF in the average-power rods.

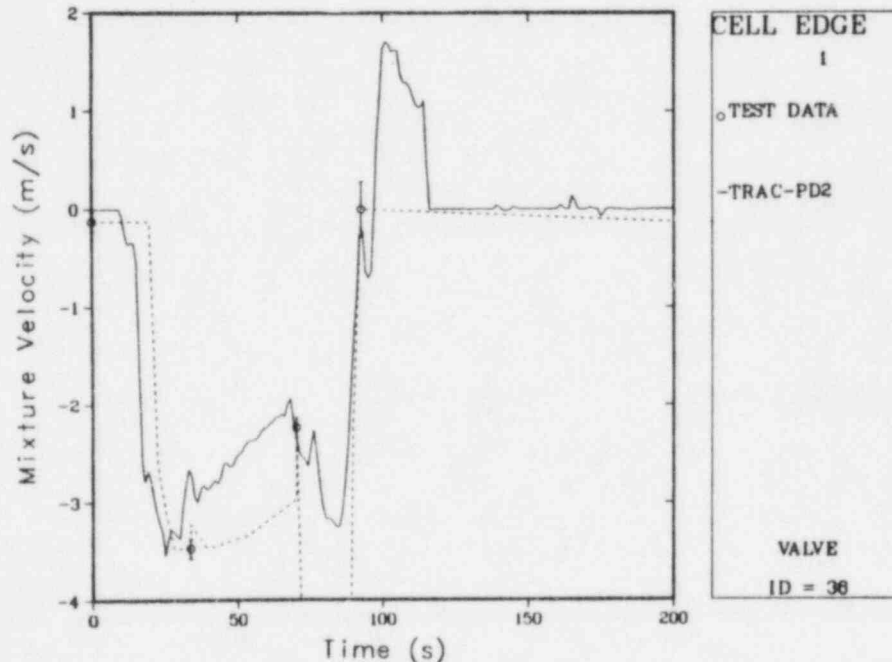


Fig. 120.

Comparison of the TRAC-calculated and measured mixture velocities at the accumulator exit for Semiscale Test S-06-3.

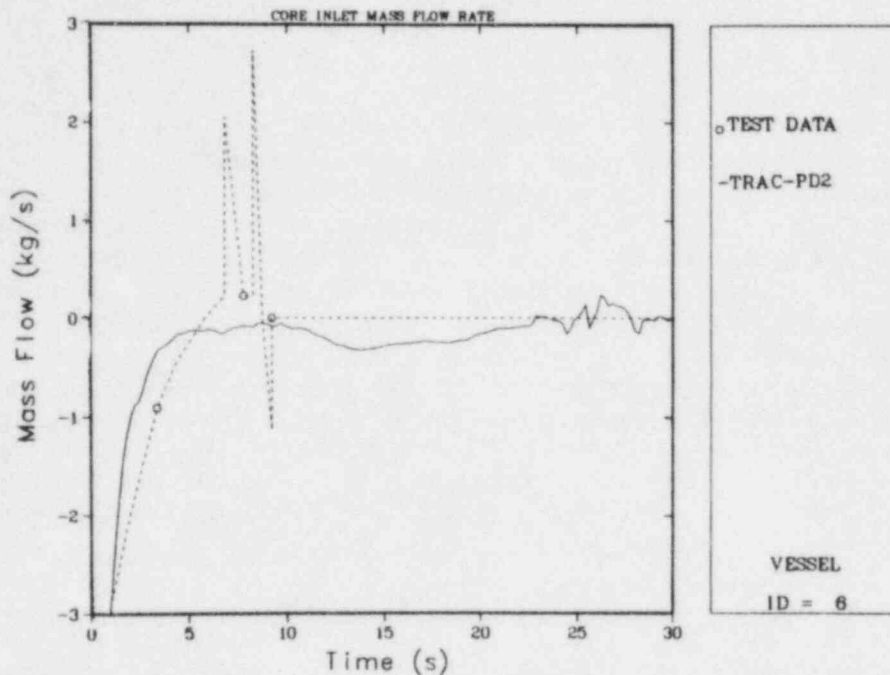


Fig. 121.

Comparison of the TRAC-calculated and measured mass flows at the core entrance for Semiscale Test S-06-3.

Figures 122-124 compare the calculated and measured cladding temperatures for the 32 low-power rods located in the lower, middle, and upper core. The comparisons for all three levels were good.

Figures 125-127 compare the cladding temperatures for the high-power rods in the lower, middle, and upper core. The highest power region of the core was located between $z = 1.7856$ m and $z = 2.03961$ m. For the elevations below the middle of the high-power core region (Figs. 122-124), TRAC predicted the CHF at the correct time, underpredicted the peak cladding temperature from 70-90 K, calculated the quench time within ~ 10 s, and predicted the general trend of the temperature profile well. The calculated CHF in the upper core (Fig. 127) occurred ~ 4 s later than the CHF in the test. The calculated peak cladding temperature was ~ 140 K below the test value, the quench time occurred ~ 40 s earlier than in the test, and the temperature profile diverged from the test data. In the TRAC model of the Semiscale core, one of the two theta segments contained slightly more liquid than the other after the initial voiding of the core and the upper plenum. This difference in liquid volume produced a pressure differential that caused most of the flow through the core to pass through the theta segment with the least liquid. Thus, this theta segment did not void completely. The TRAC-PD2 program contains CHF and transition boiling correlations that are very sensitive to small amounts of water when the void fraction is close to 1.0. Therefore, the rod-cladding temperature in one theta segment may vary greatly from that of a rod in another segment. In our analysis of Test S-06-3, the hot rod was located in the theta segment in which a small amount of water remained. Thus, the calculated hot-rod temperature profiles were not as good as the profiles for the low-power

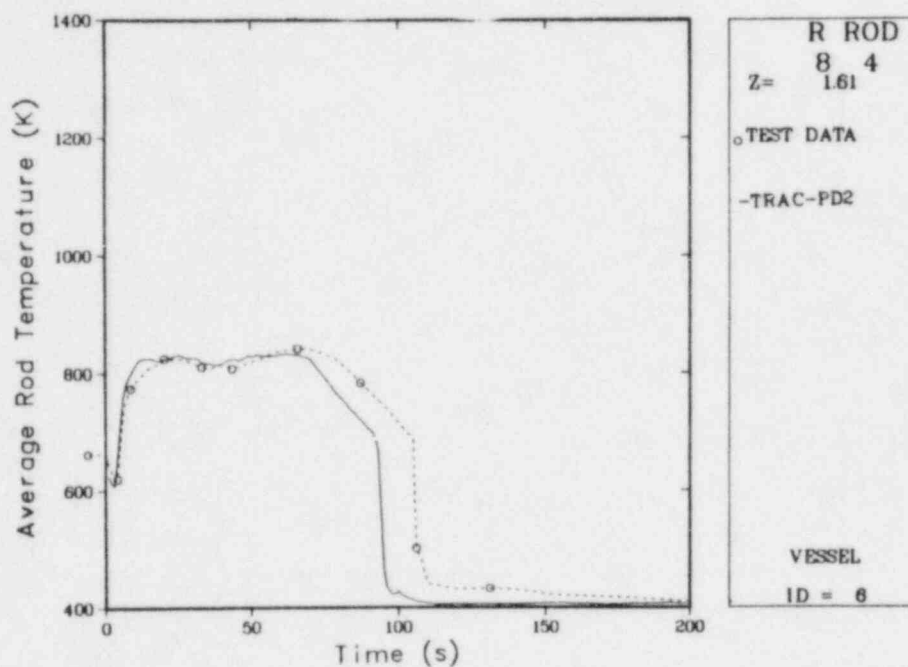


Fig. 122.

Comparison of the TRAC-calculated and measured cladding temperatures for the 32 low-power rods in the lower core.

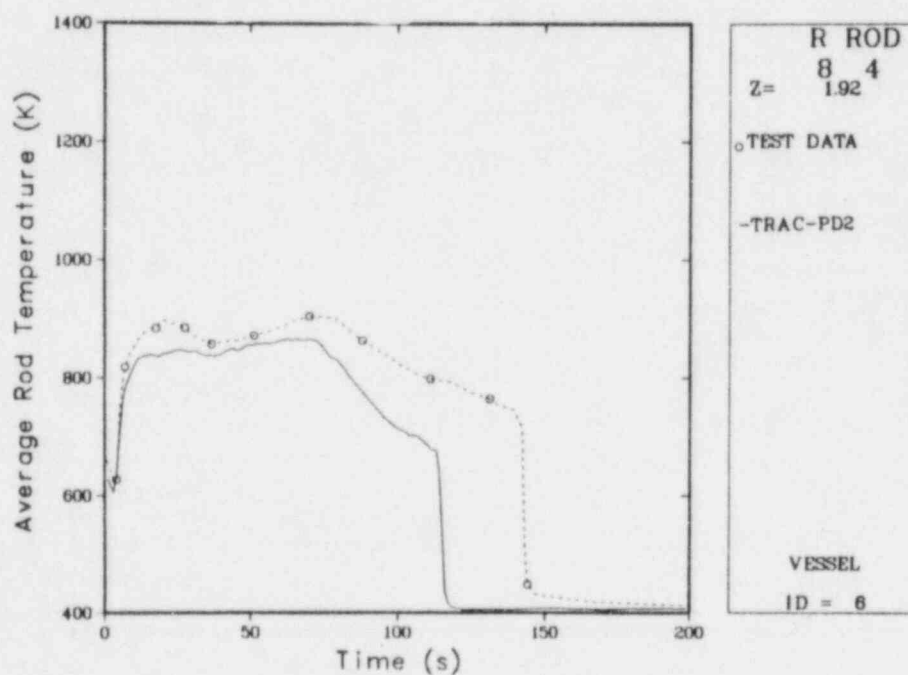


Fig. 123.

Comparison of the TRAC-calculated and measured cladding temperatures for the 32 low-power rods in the midcore.

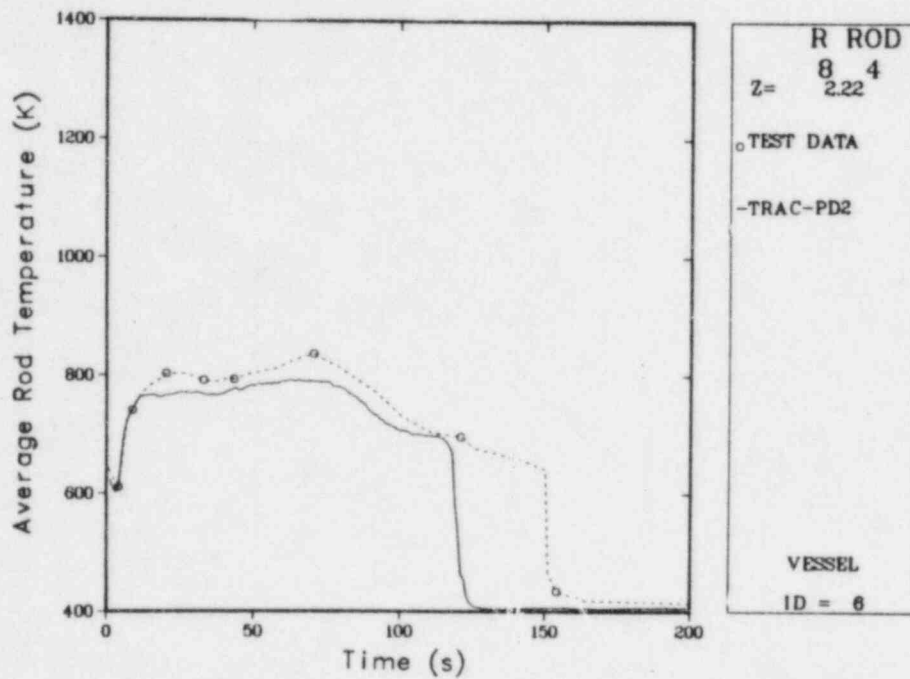


Fig. 124.

Comparison of the TRAC-calculated and measured cladding temperatures for the 32 low-power rods in the upper core.

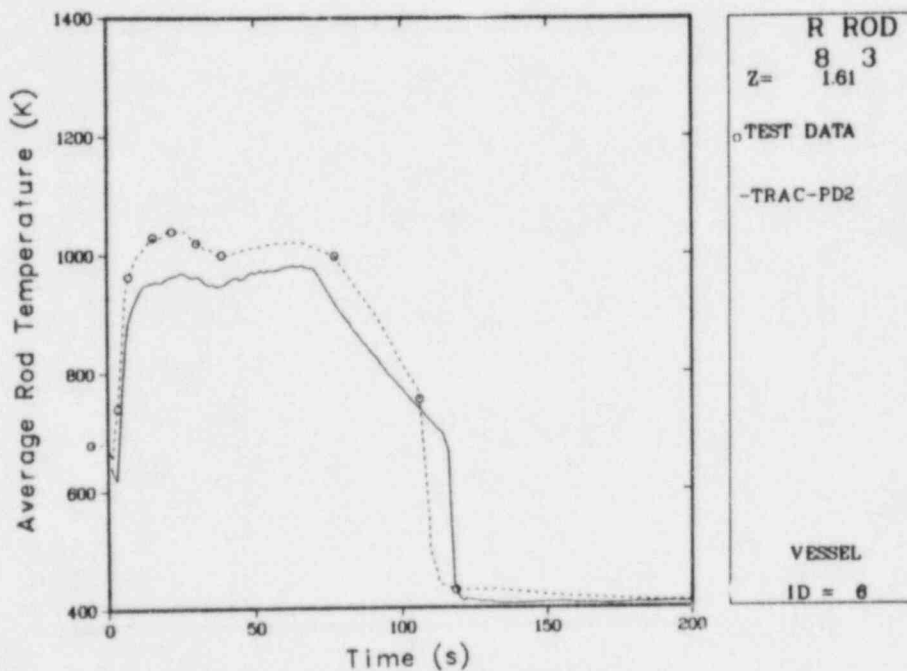


Fig. 125.

Comparison of the TRAC-calculated and measured cladding temperatures for the high-power rods in the lower core for Semiscale Test S-06-3.

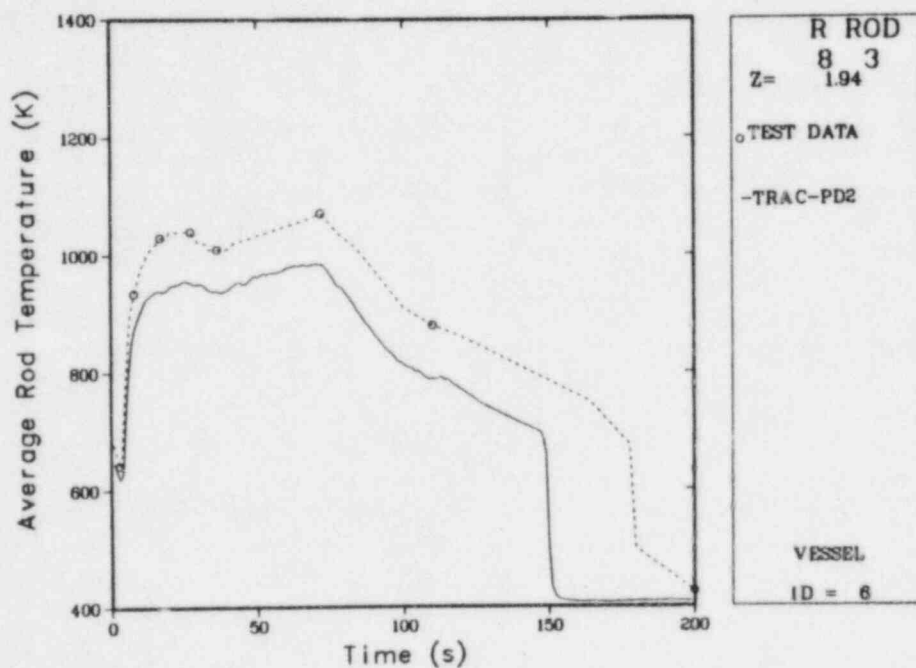


Fig. 126.

Comparison of the TRAC-calculated and measured cladding temperatures for the high-power rods in the midcore for Semiscale Test S-06-3.

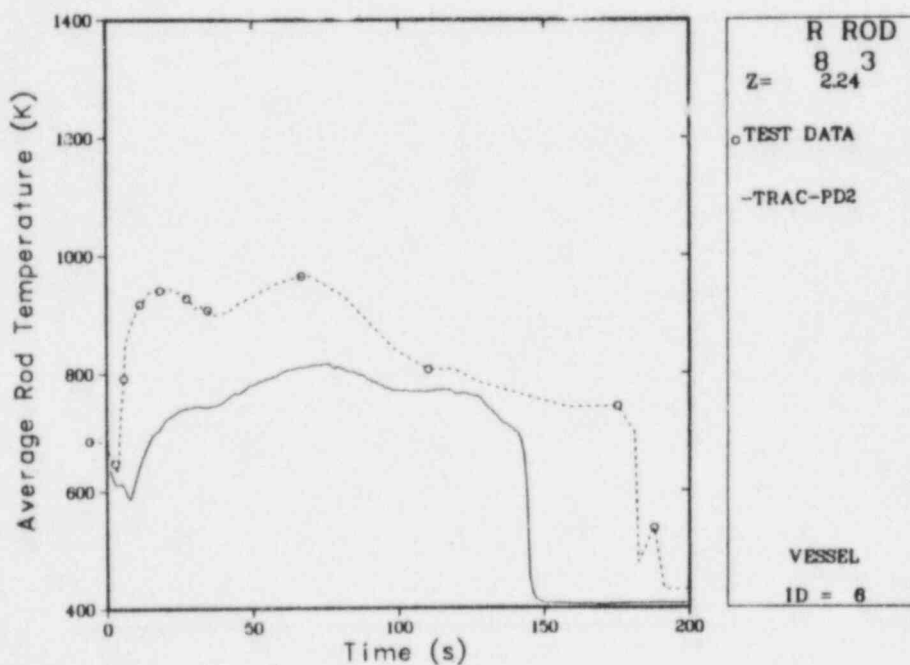


Fig. 127.

Comparison of the TRAC-calculated and measured cladding temperatures for the high-power rods in the upper core for Semiscale Test S-06-3.

rods. Also, because there were only four high-power rods in the core, it was unreasonable to model a separate, small flow channel for the hot rods. Therefore, the code based the core-hydraulics calculations on the average rod power, which was more typical of the low-power rods than the high-power rods.

Semiscale Test S-06-3 was run with a 5-, 6-, and 12-level core. We found that the use of the 6- and 12-level cores produced similar results, but the use of the 5-level core lowered the maximum cladding temperature over 100 K. After further investigation we concluded that the highest powered step of the heater rod should be modeled with two axial core levels.

D. Conclusions

In general, the TRAC-calculated results for Semiscale Test S-06-3 were good. The TRAC results for the one-dimensional components were excellent. The fluid flow in the vessel was predicted well. The cladding temperatures were predicted well for the low- and high-power rods below the middle of the high-power core region. Newly developed input description techniques produced noticeable improvements in the calculated results.

The steady-state and transient calculations required ~6 min and ~317 min, respectively, of CPU time on a CDC 7600 computer.

Appendix I lists the steady-state and transient-restart input decks for Semiscale Mod-1 Test S-06-3.

XII. LOFT NONNUCLEAR EXPERIMENT L1-4

A. Experiment Description

The LOFT facility²¹ is a scale model of a large PWR. The volume-scale ratio between the LOFT system and the large PWR is approximately 1:60; flow and break areas also are scaled using the same ratio. The LOFT L1-4 system consisted of a pressure vessel; an intact loop with a pressurizer, steam generator, and two pumps; a blowdown loop with a simulated steam generator, a simulated pump, and two quick-opening valves (17.5 ms to open fully); and a pressure-suppression system. Figure 128 shows the major LOFT components.

The pressure vessel contained upper and lower plenums, a downcomer, and a core support barrel. For Test L1-4 a hydraulic core simulator provided the flow resistance of the fuel-rod bundles. The blowdown loop was a volume-scale representation of one loop in a large four-loop PWR. The simulated steam generator and pump consisted of piping containing many orifice plates to achieve the desired hydraulic resistance. The intact loop had a volume approximately three times larger than the blowdown loop and represented three intact loops of a large four-loop PWR. The intact loop had a U-tube steam generator, two centrifugal pumps, and a pressurizer. The pressure-suppression system simulated the large volume and the back pressure of the large PWR containment building and contained the blowdown effluent.

Test L1-4, the fourth in a series of five nonnuclear isothermal blowdown experiments performed as part of the LOFT integral test program, is US Standard Problem 7. The purposes of Test L1-4 were to obtain data on the delayed HPIS and LPIS cold-leg injection, to obtain data for the evaluation of downcomer

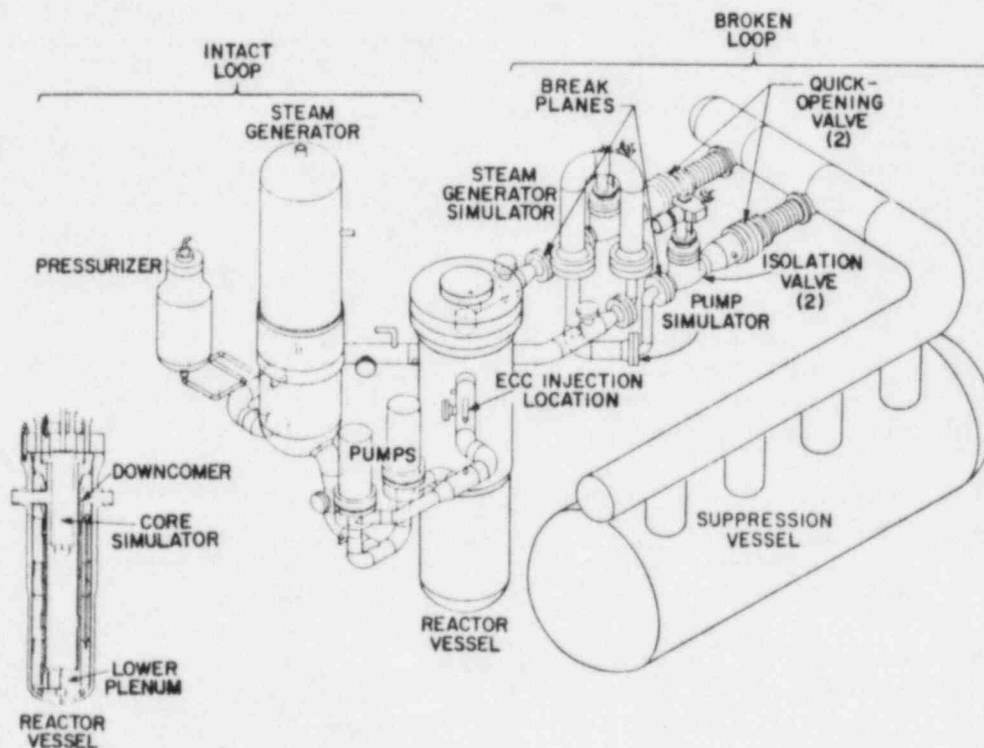


Fig. 128.
Major LOFT components.

bypass and mixing of the ECC with the primary coolant, and to obtain thermal-hydraulic data for comparison with test predictions and other test data for code assessment purposes.

Before the blowdown test, the primary system was brought to its initial temperature (552 K), pressure (15.75 MPa), and flow rate ($268.4 \text{ kg} \cdot \text{s}^{-1}$), using the work energy addition of the primary-coolant pumps. Isothermal conditions were obtained in the nonflowing blowdown loop by recirculation lines connected to the intact loop. Before the system temperature exceeded 366.3 K, the steam-generator secondary side was drained to the zero-power water level (2.59 m from the top of the tube sheet).

Immediately before blowdown, the pressurizer heaters were de-energized and the blowdown was initiated by opening the two quick-opening valves, which simulated a 200% (that is, a 100% break area in each leg), double-ended, offset-shear break in the cold leg. Electrical power to the primary-system motor generator was terminated within 1 s after blowdown initiation; this power loss allowed the flywheels and the fluid-dynamic forces to slow the pumps.

The ECC was injected into the intact-loop cold leg during blowdown. Accumulator injection was initiated at a system low-pressure trip of 4.24 MPa. The HPIS pump was preset to inject at $1.085 \times 10^{-3} \text{ m}^3 \cdot \text{s}^{-1}$ and to initiate at 22 s after blowdown. The LPIS pump was initiated no sooner than 35.5 s after the blowdown began; its flow rate, dependent upon the LOFT system pressure, varied from 0-0.01 $\text{m}^3 \cdot \text{s}^{-1}$.

The TRAC calculations predicted the system thermal-hydraulic response for 70 s after the blowdown began.

B. TRAC-PD2 Model

Figure 128 shows the LOFT components, interconnected in series and in parallel branches. The system was complicated further by area changes and orifice plates. The TRAC program used one-dimensional components to model the blowdown and intact loops and a three-dimensional VESSEL (Fig. 129) to model the reactor vessel.

The TRAC model used 28 components with 29 junctions for a total of 205 fluid cells. Figures 130-136 display the component noding diagrams for the LOFT system. The reactor vessel was divided into 9 axial, 2 radial, and 4 azimuthal segments for a total of 72 fluid cells. The upper and lower plenums contained six and eight fluid cells, respectively. Typical cell dimensions were ~0.2-2.0 m, except near the breaks where the length varied from 0.0127-0.1 m. The semi-implicit option was used for all the components except the broken pipes where the fully implicit option was used. The TRAC ECC system (Fig. 136) consisted of an accumulator (ACCUM) connected to a series of two TEEs. These TEEs were connected to two FILLS that specified the HPIS and LPIS flows. The HPIS was set to initiate at 22 s, whereas the LPIS began at a 14.4-bar pressure. The accumulator VALVE (component 27) tripped open at a 42.6-bar pressure.

Because of the simplicity of the TRAC-PD2 PUMP module, the pump speeds were constrained to agree with the test data through input.

C. TRAC-Calculated Results

1. Steady-State Results. The TRAC calculation for LOFT L1-4 was performed in two stages. First, steady-state conditions were obtained by running a generalized steady-state calculation starting from an initial zero-flow rate, with a uniform pressure and temperature and with the two quick-opening valves closed. Figures 137 and 138 show that the initiation of the two

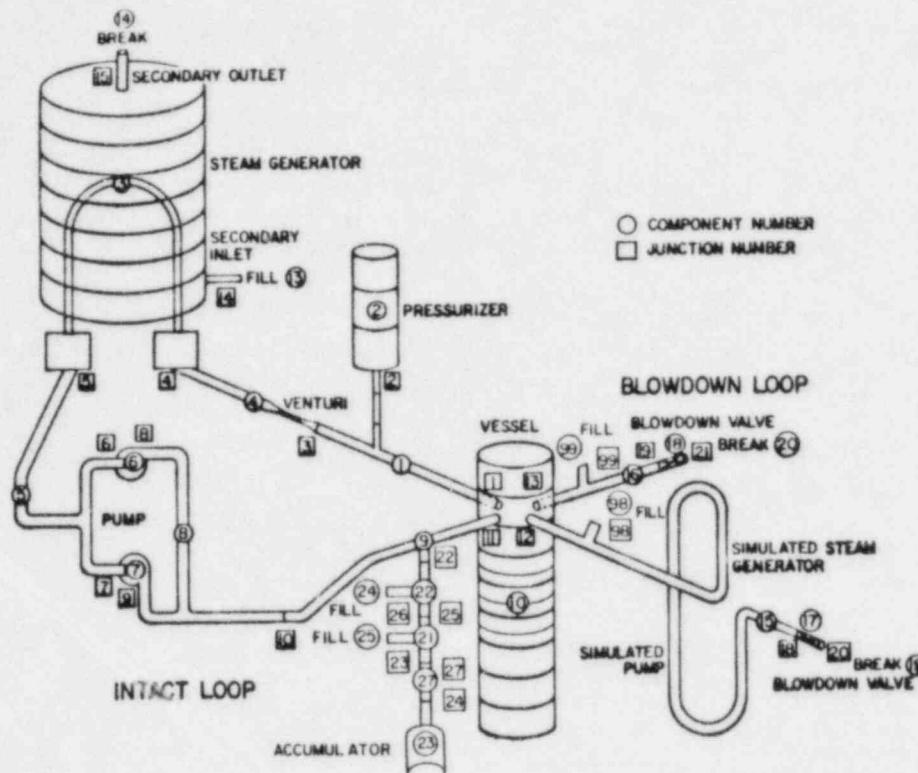


Fig. 129.
TRAC model of LOFT L1-4.

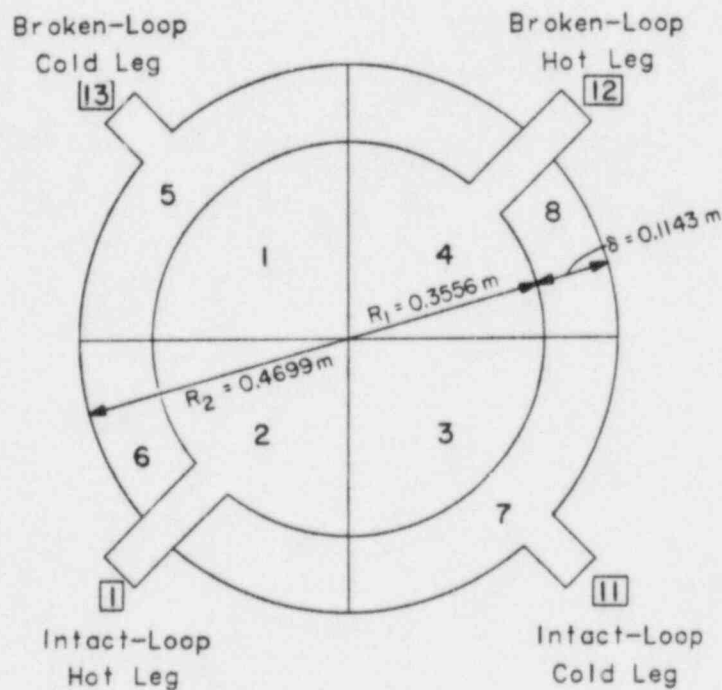


Fig. 130.
LOFT L1-4 reactor-vessel horizontal noding diagram for level 8.

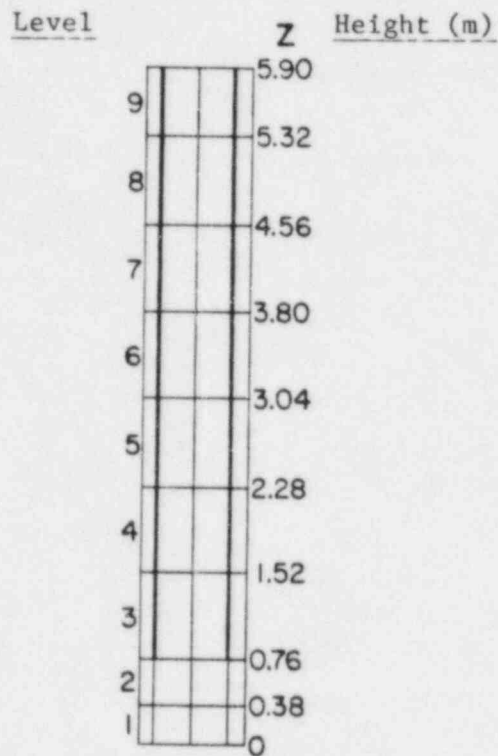


Fig. 131.
LOFT L1-4 reactor-vessel axial noding diagram.

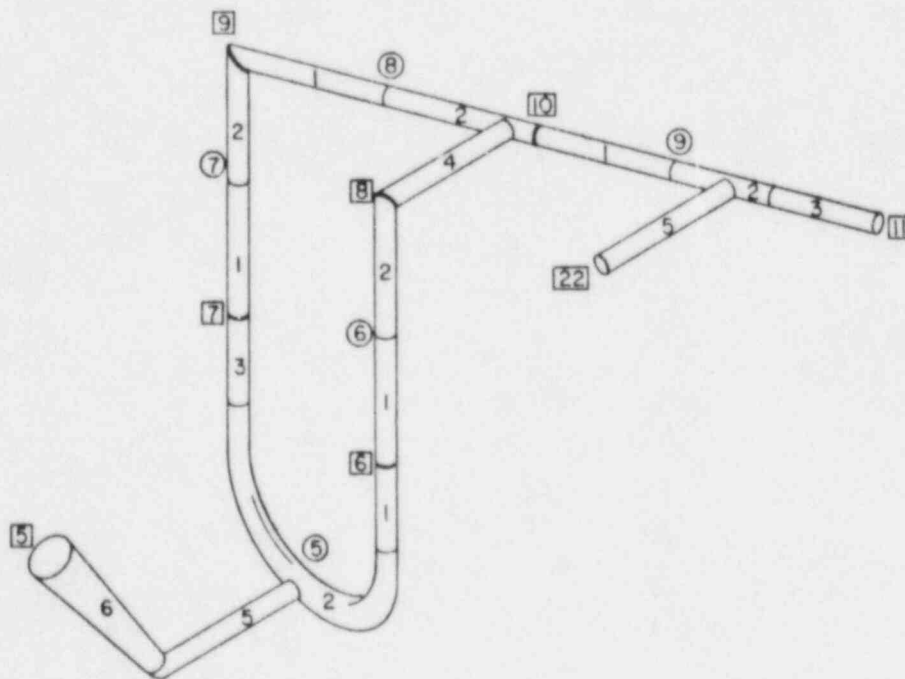


Fig. 132.
LOFT L1-4 intact-loop cold-leg noding diagram.

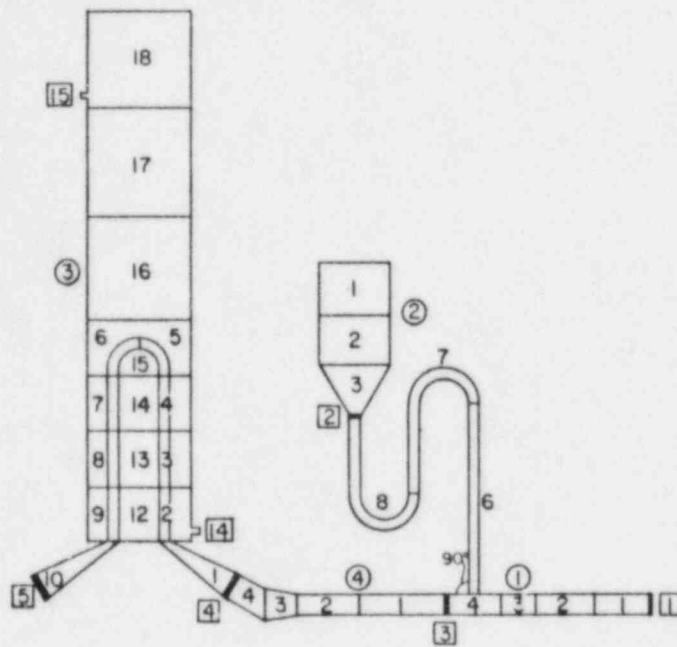


Fig. 133.
LOFT L1-4 intact-loop hot-leg noding diagram.



Fig. 134.
LOFT L1-4 broken-loop hot-leg noding diagram.

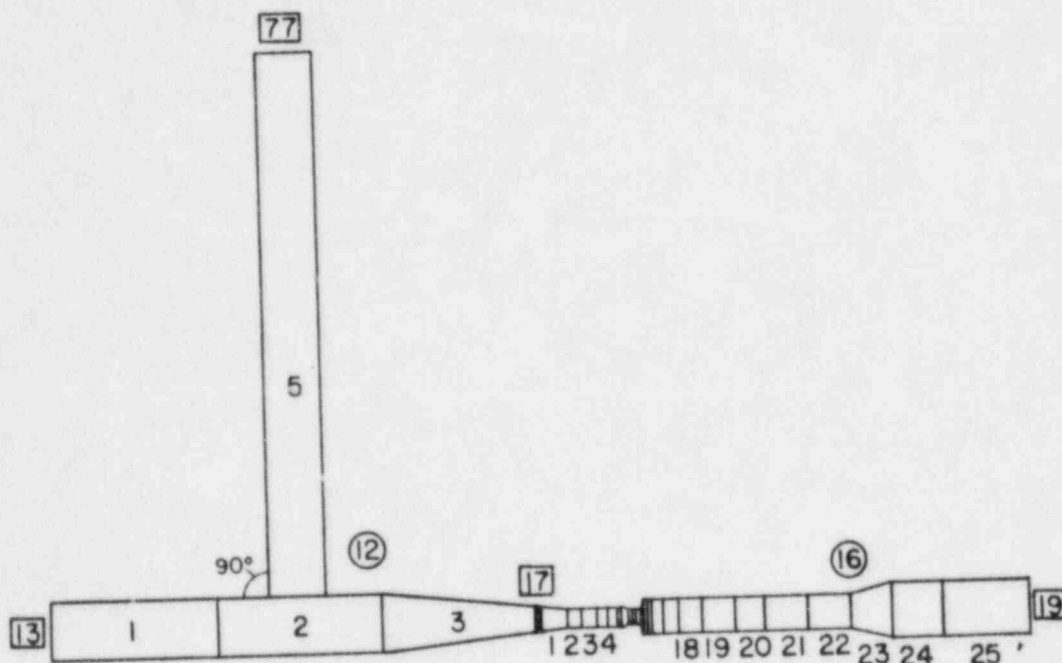


Fig. 135.
LOFT L1-4 broken-loop cold-leg noding diagram.

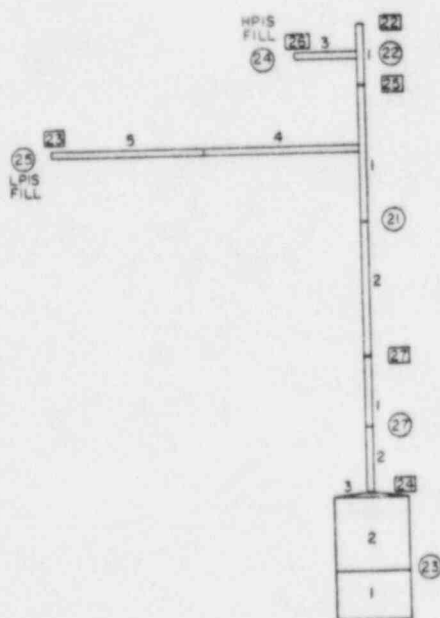


Fig. 136.
LOFT L1-4 ECCS noding diagram.

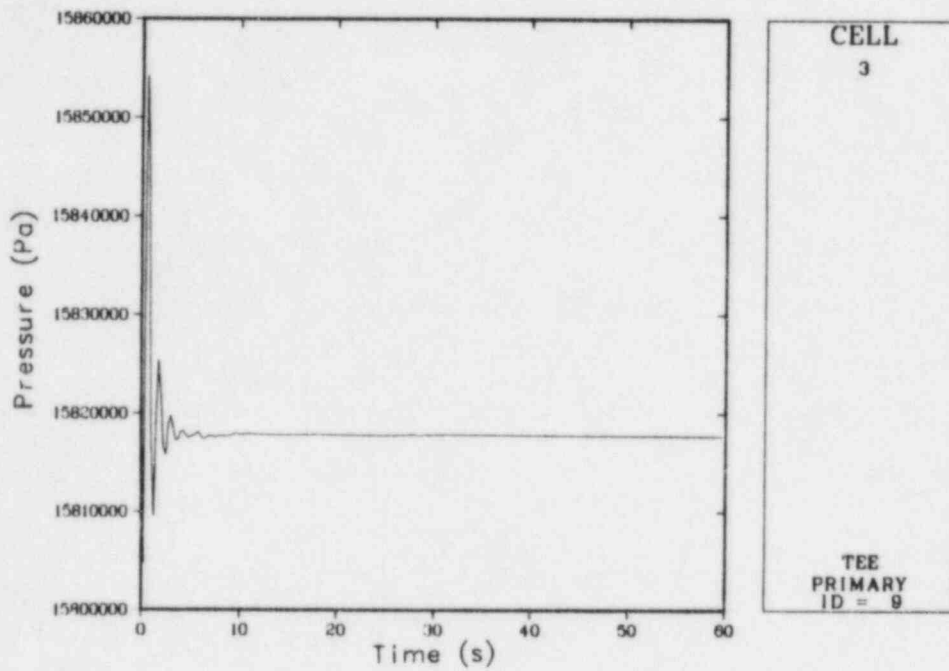


Fig. 137.
LOFT L1-4 steady-state intact-loop pressure.

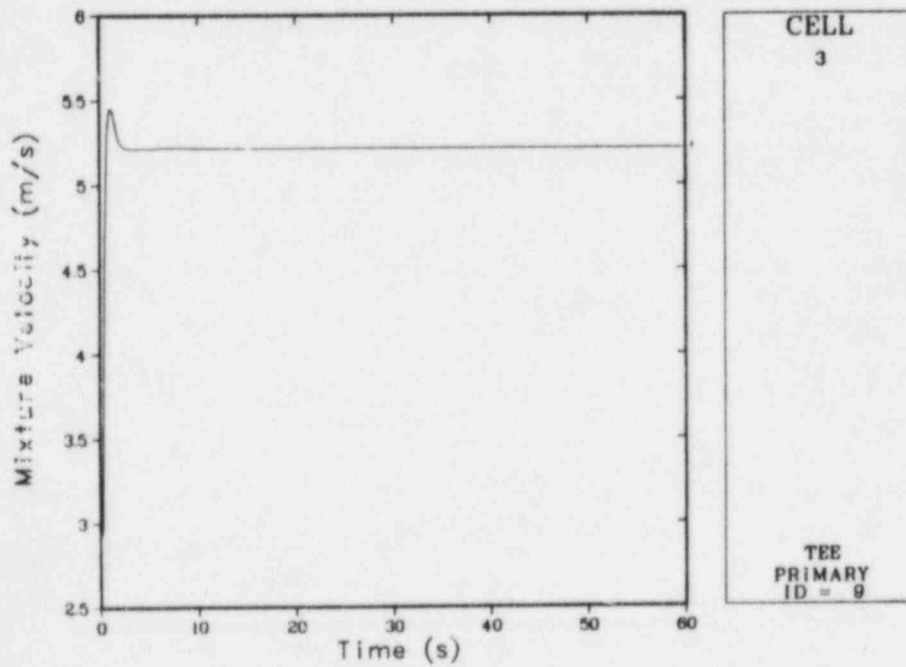


Fig. 138.
LOFT L1-4 steady-state intact-loop mixture velocity.

pumps at time zero caused the system pressure and flow rate to approach their steady-state values quickly after one loop cycle time (3-4 s). The liquid temperature, however, continued to oscillate (Fig. 139) and was driven by the slow approach to steady state in the steam-generator secondary side (Fig. 140). As can be seen in Fig. 140, the secondary-side conditions had not converged fully at 60 s, but they were close enough to convergence that they did not affect the transient results seriously. The steady-state calculation used 6.2 min of CPU time, which was negligible compared to the time used by the transient calculation (168.5 min). The average time-step size for the steady-state calculation was 70 ms. Table XIII shows that all of the calculated steady-state parameters were close to the measured values.

2. Transient Results. The transient calculation was initiated by activating the two quick-opening VALVES (components 17 and 18) at the restart from the steady-state dump. In this section we compare the results of a TRAC-PD2 calculation with test data and a TRAC-PlA/NEWS1 (Ref. 13) calculation. The test results were obtained by digitizing curves from the LOFT L1-4 data report.²²

The most important parameters in any LOFT blowdown experiment are the broken-loop mass and enthalpy flow rates. As can be seen in Figs. 141 and 142, the TRAC-PD2 results for mass flows in the broken loop agreed well with the test data. A fine mesh, not a choking model, was used at choking locations to resolve steep pressure gradients. Figure 141 indicates ECC bypass to the broken-loop cold leg. Figure 143 also indicates ECC bypass and shows the average mass density in the broken-loop cold leg. The TRAC-PD2 results did not predict liquid flow in the broken-loop hot leg at ~23 s. Figure 144 shows a

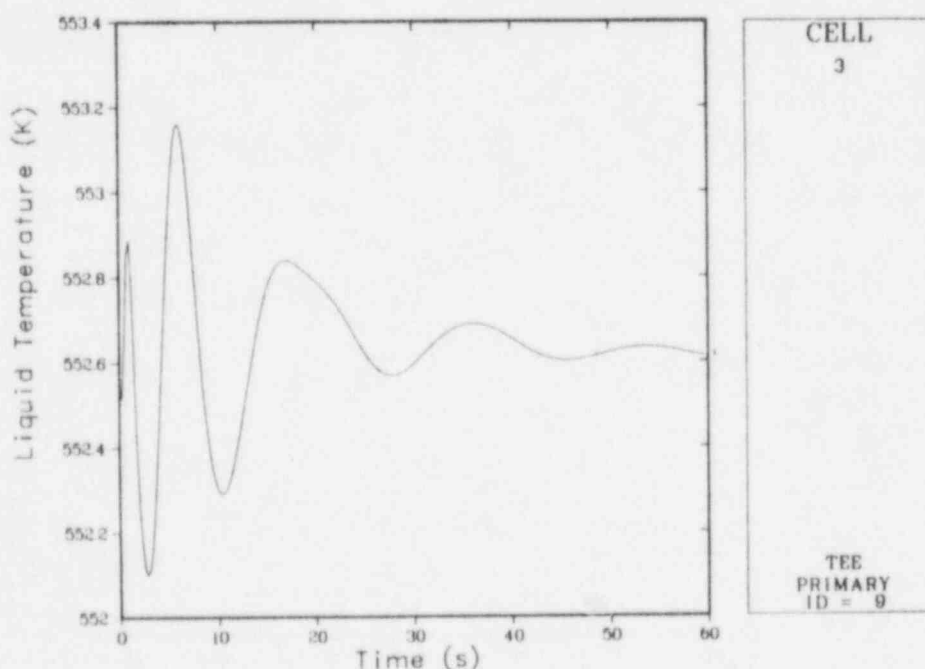


Fig. 139.
LOFT L1-4 steady-state intact-loop liquid temperature.

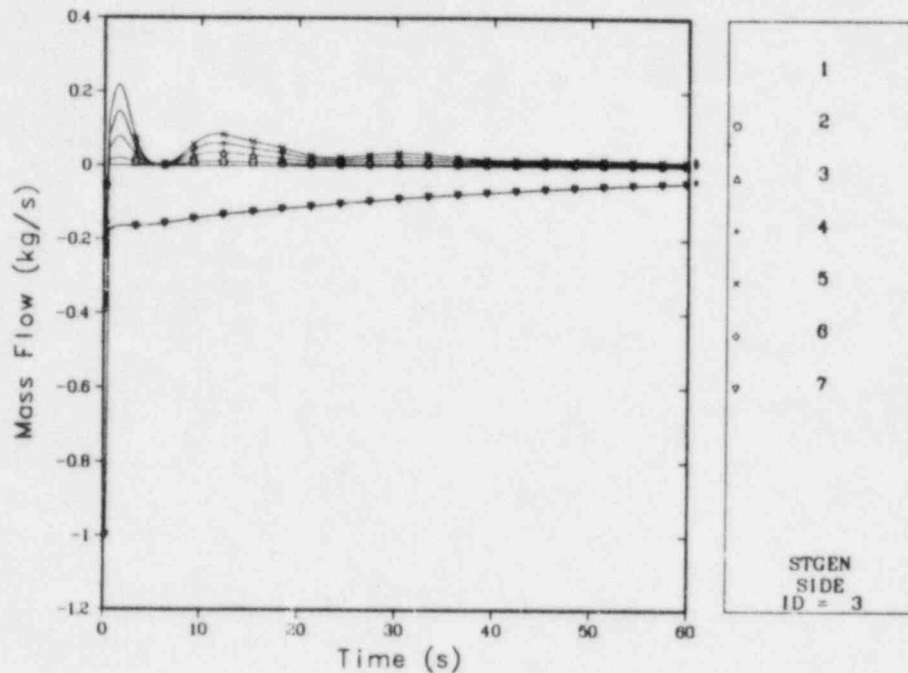


Fig. 140.

Comparison of the LOFT L1-4 steady-state mass flows on the steam-generator secondary side.

TABLE XIII

CALCULATED AND MEASURED INITIAL CONDITIONS FOR LOFT L1-4

<u>Parameters</u>	<u>TRAC-Calculated</u>	<u>Measured</u>
Intact-loop mass-flow rate ($\text{kg} \cdot \text{s}^{-1}$)	255.4	268.40
Pressurizer pressure (MPa)	15.75	15.75
Pressurizer liquid mass (kg)	435.2	418.80
Pressurizer liquid level (m)	1.17	1.16
Steam-generator primary-side pressure (MPa)	15.72	15.75
Steam-generator primary-side inlet temperature (K)	552.6	554.00
Steam-generator primary-side outlet temperature (K)	552.6	552.00
Steam-generator secondary-side temperature (K)	552.4	552.00
Steam-generator secondary-side pressure (MPa)	6.66	6.65
Core inlet temperature (K)	552.6	552.00
Core outlet temperature (K)	552.6	554.00
Differential pressure in intact loop across primary pumps 1 and 2 (MPa)	0.155	0.140

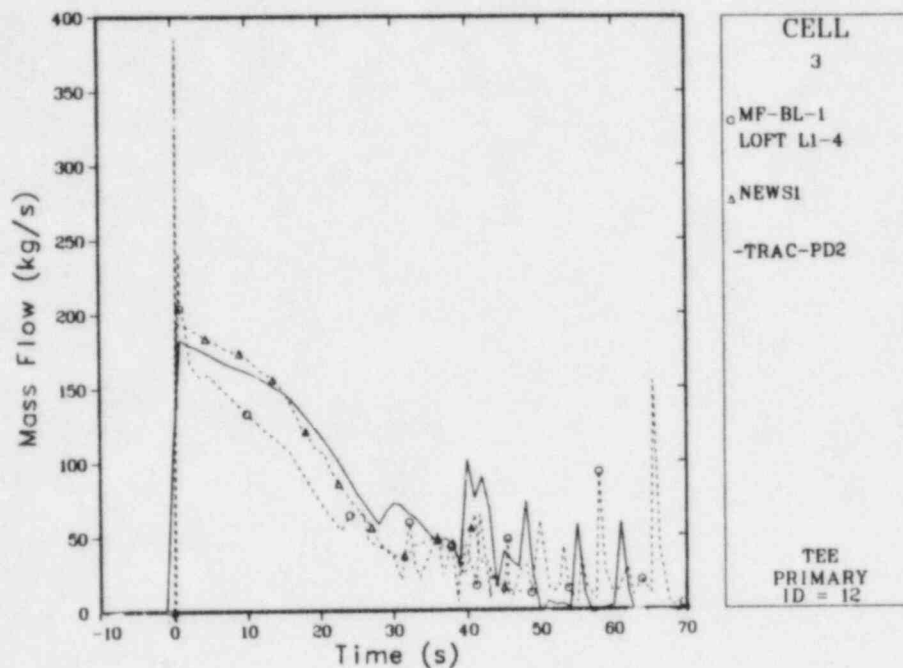


Fig. 141.

Comparison of the TRAC-calculated and measured broken-loop cold-leg mass flows for LOFT L1-4.

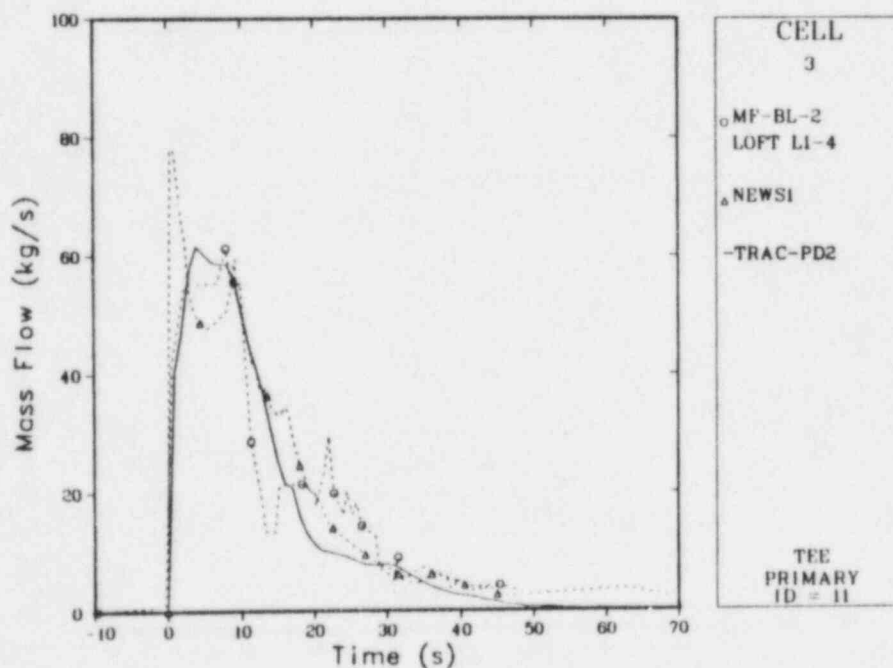


Fig. 142.

Comparison of the TRAC-calculated and measured broken-loop hot-leg mass flows for LOFT L1-4.

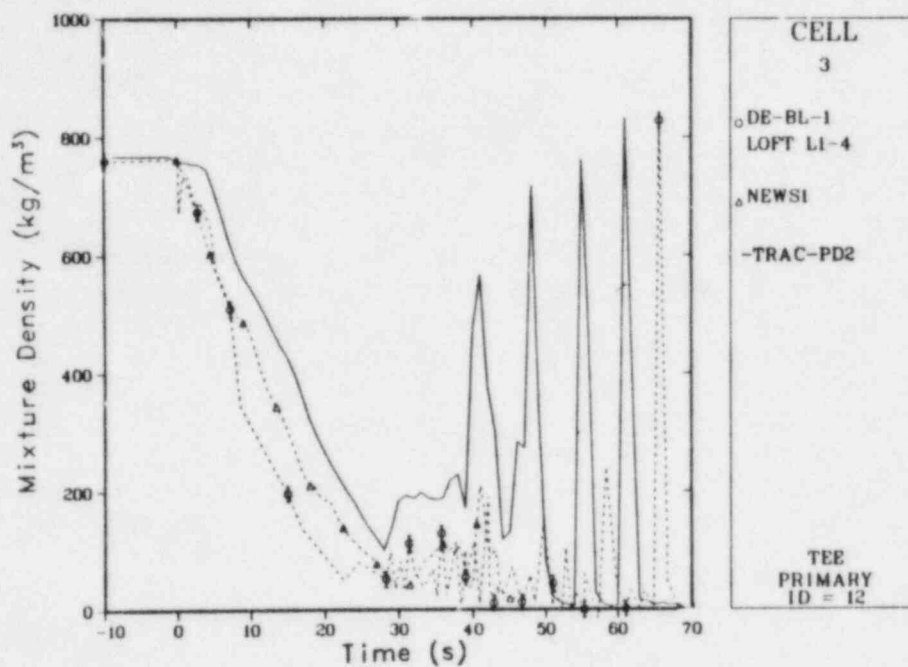


Fig. 143.

Comparison of the TRAC-calculated and measured broken-loop cold-leg average densities for LOFT L1-4.

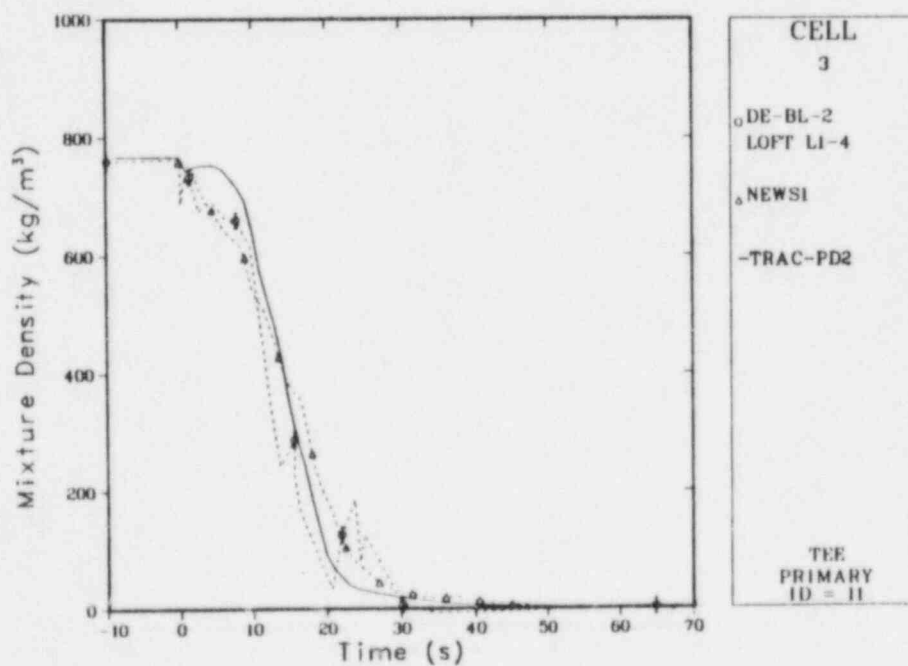


Fig. 144.

Comparison of the TRAC-calculated and measured broken-loop hot-leg average densities for LOFT L1-4.

measured increase in density at this time in the broken-loop hot leg. Figure 145 compares the TRAC-calculated and measured liquid temperatures in the broken-loop cold leg. The data agreed well with the TRAC-PD2 results until 35 s, when the TRAC-calculated pressure (Fig. 146) decreased below the measured value. Because the fluid tended to remain near saturation in this test, the lower calculated liquid temperature was predictable.

Figures 147 and 148 compare the predicted and measured pressures in the pressurizer and intact-loop cold leg. Again, TRAC-PD2 predicted lower pressures later in the transient than measured in the test. A possible cause of these discrepancies might have been the lumped-parameter model used in the VESSEL for structural heat transfer. To keep the heat flux at reasonable levels early in the transient, the effective thickness of the heat slab was limited to 2 cm. However, late in the transient, this thickness resulted in lower heat fluxes, which probably caused the lower pressures and temperatures.

Figure 149 compares the measured and predicted water levels in the pressurizer. The calculation predicted an initial faster voiding but a later retention of some system liquid for a longer period than the experiment showed. An underestimated surge-line flow resistance possibly caused these discrepancies between the calculated and measured results.

Flow resistance in the broken legs was predicted well by TRAC. Figures 150-152 show the differential pressures across the steam-generator simulator, the pump simulator, and the cold-leg break plane, respectively.

Figures 153-155 show that TRAC-PD2 predicted the refilling of the core simulator well. Figures 153 and 154 compare the downcomer liquid levels near the broken- and intact-loop cold legs, respectively. The measurements were

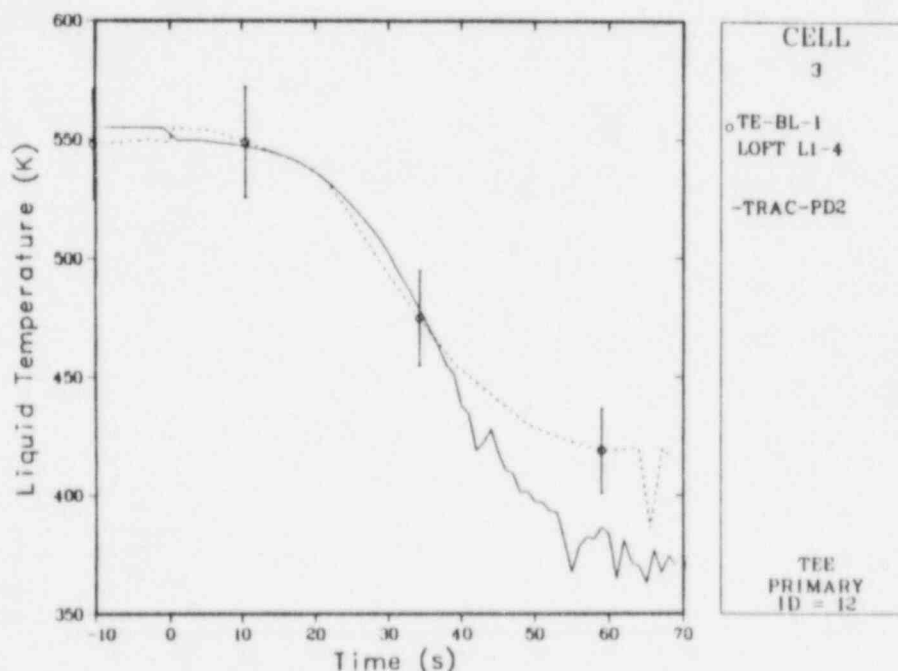


Fig. 145.

Comparison of the TRAC-calculated and measured broken-loop cold-leg liquid temperatures for LOFT L1-4.

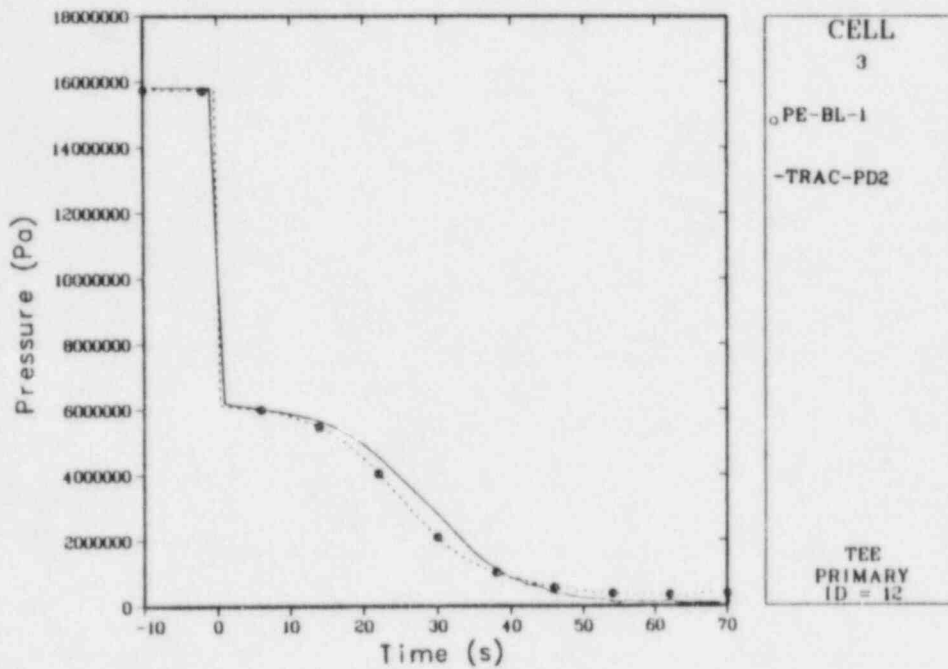


Fig. 146.

Comparison of the TRAC-calculated and measured broken-loop cold-leg pressures for LOFT L1-4.

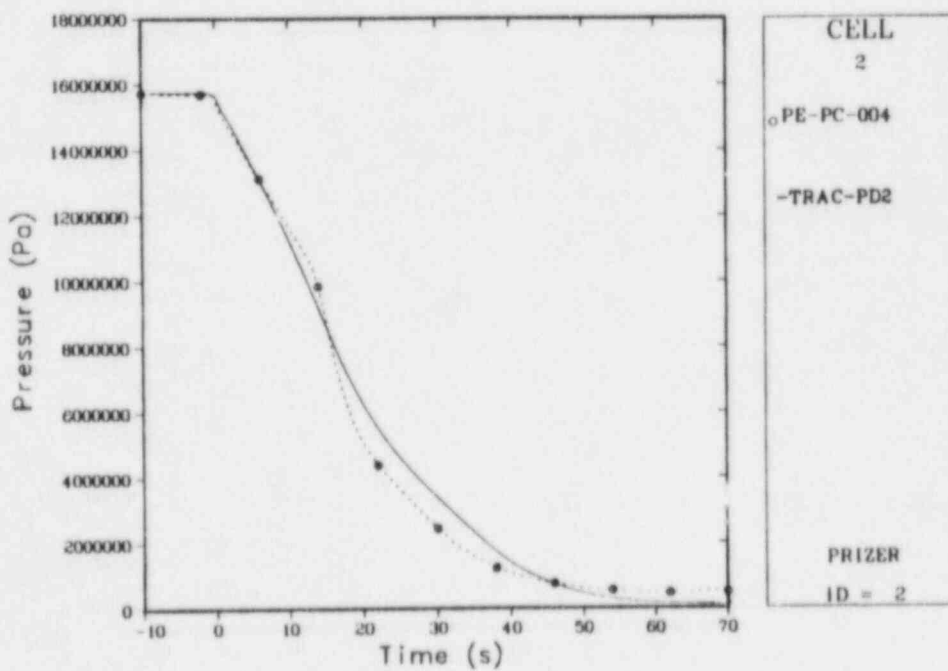


Fig. 147.

Comparison of the TRAC-calculated and measured pressurizer pressures for LOFT L1-4.

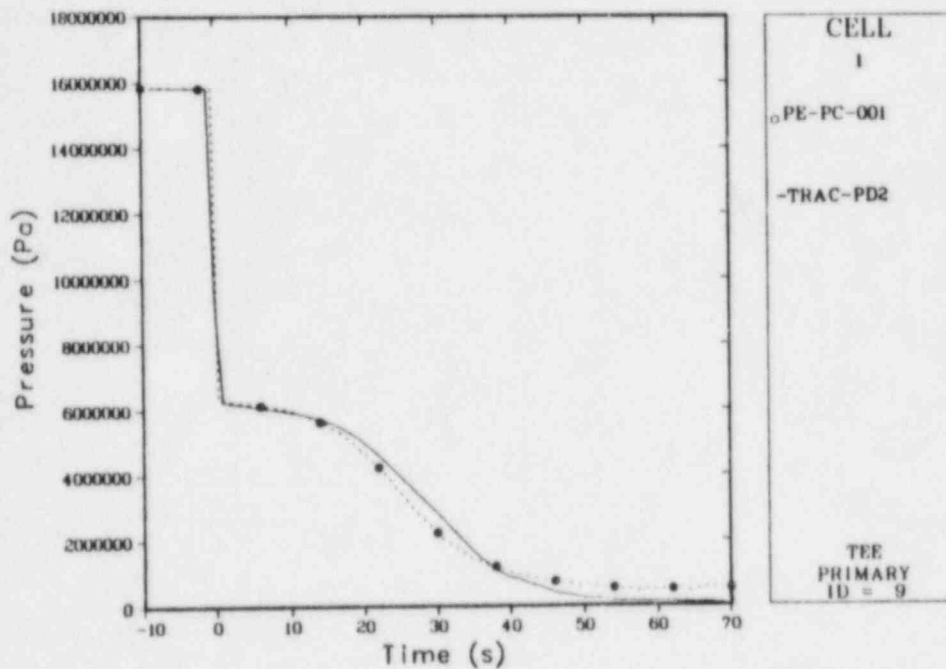


Fig. 148.

Comparison of the TRAC-calculated and measured intact-loop cold-leg pressures for LOFT L1-4.

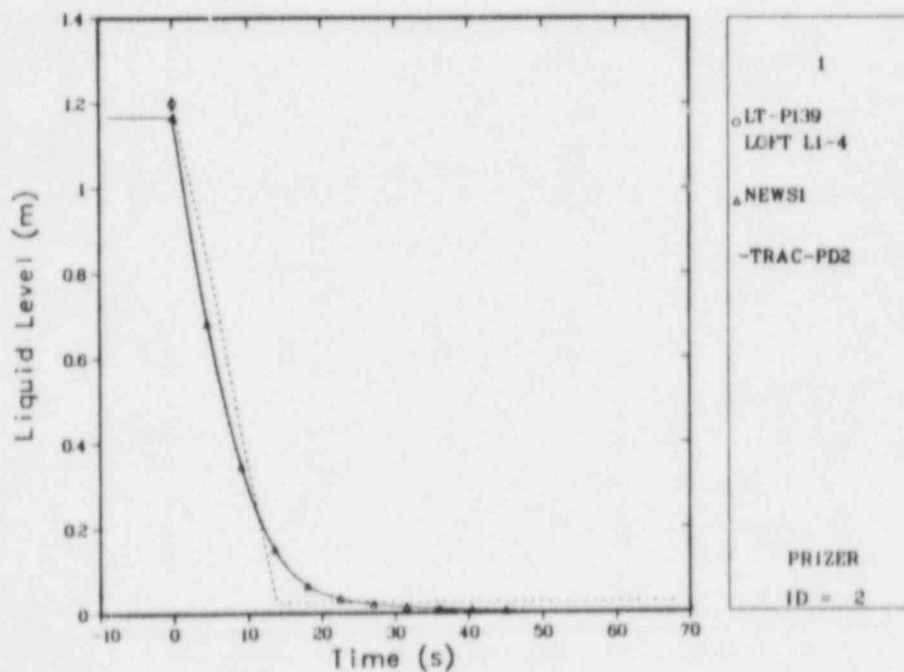


Fig. 149.

Comparison of the TRAC-calculated and measured pressurizer liquid levels for LOFT L1-4.

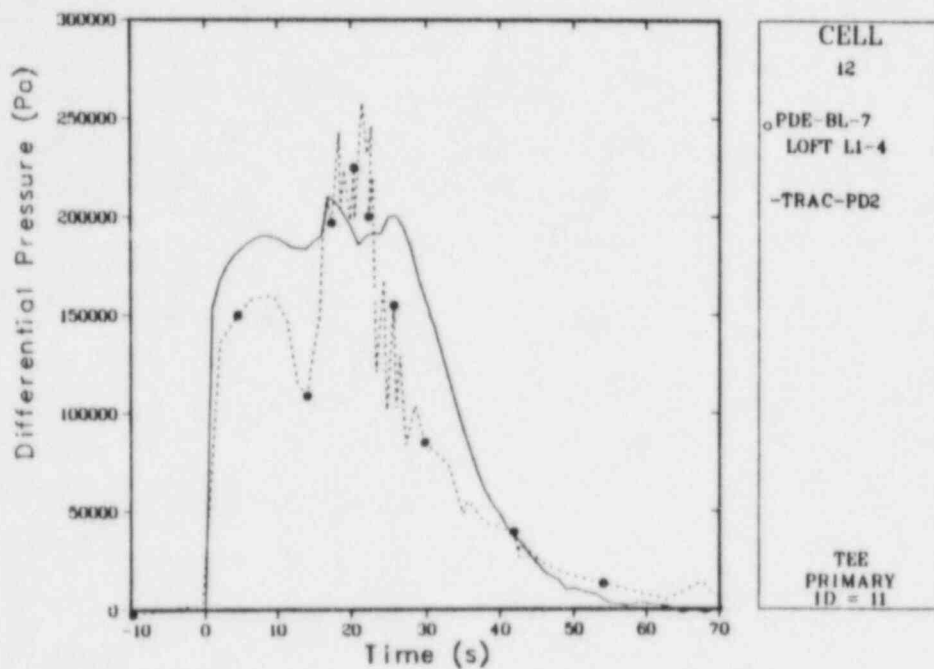


Fig. 150.

Comparison of the TRAC-calculated and measured differential pressures across the steam-generator simulator for LOFT L1-4.

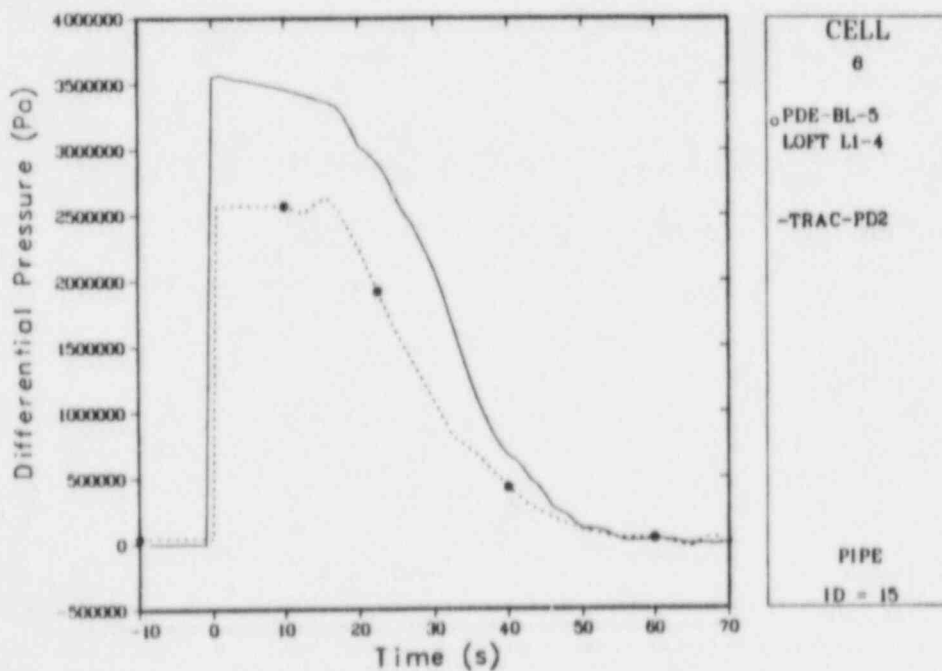


Fig. 151.

Comparison of the TRAC-calculated and measured differential pressures across the pump simulator for LOFT L1-4.

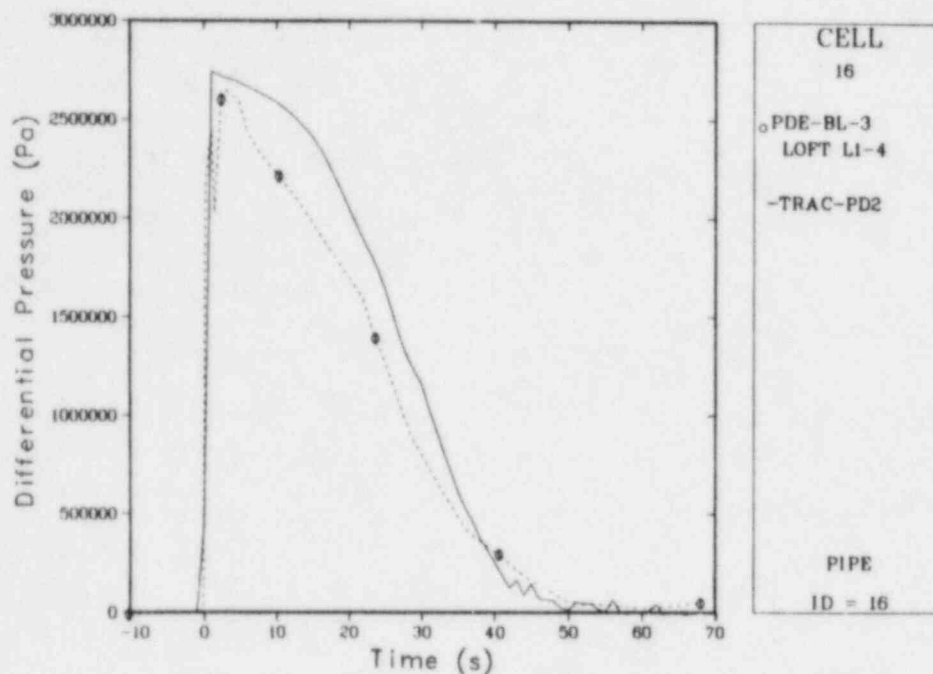


Fig. 152.

Comparison of the TRAC-calculated and measured differential pressures across the cold-leg break plane for LOFT L1-4.

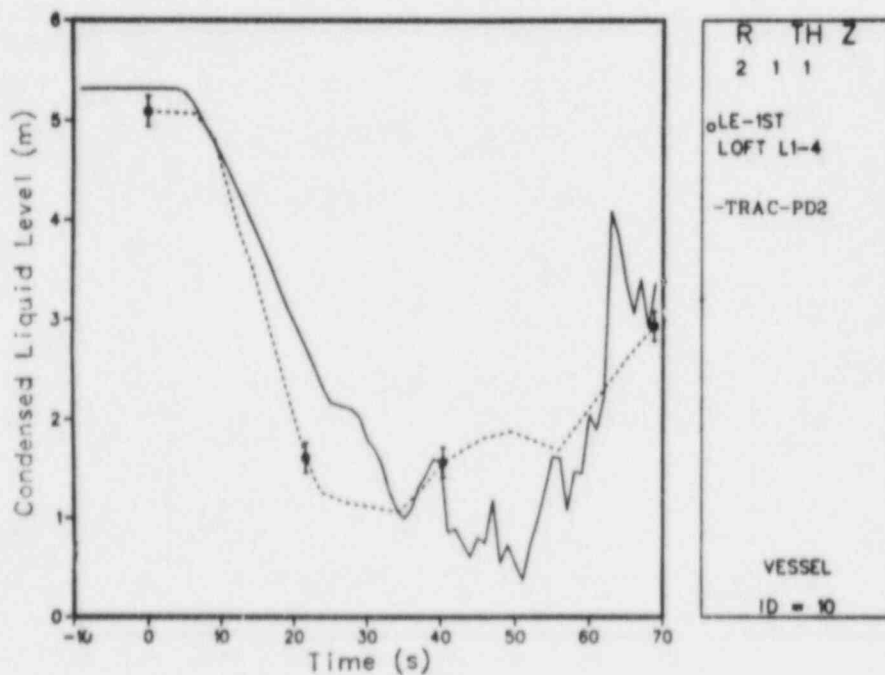


Fig. 153.

Comparison of the TRAC-calculated and measured downcomer liquid levels near the broken-loop cold leg for LOFT L1-4.

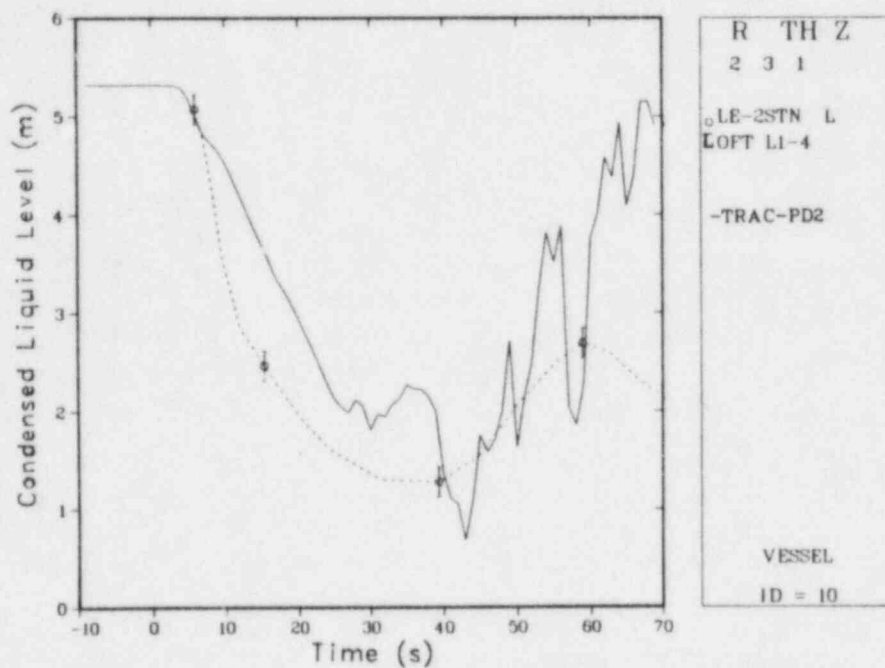


Fig. 154.

Comparison of the TRAC-calculated and measured downcomer liquid levels near the intact-loop cold leg for LOFT L1-4.

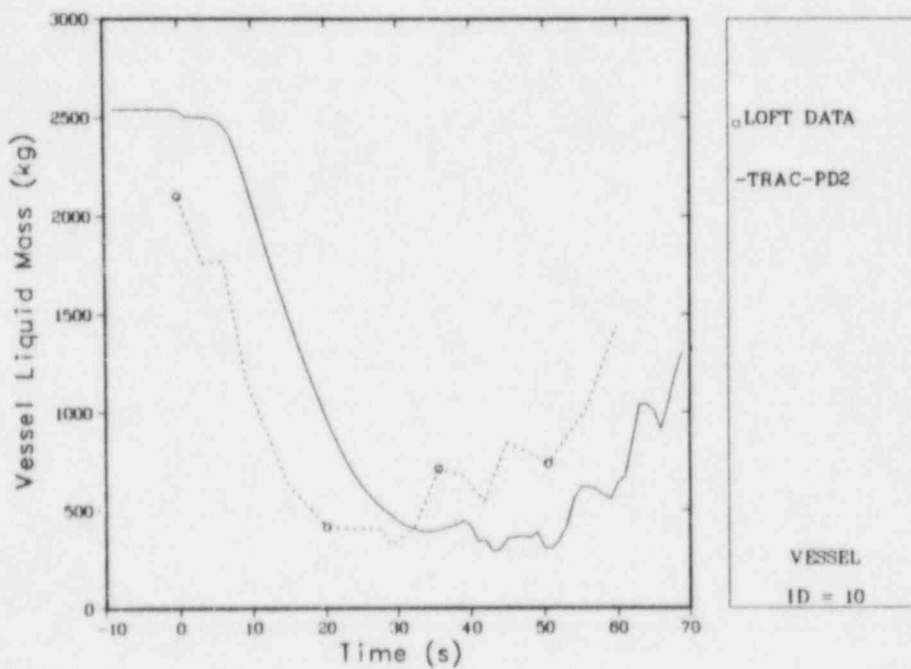


Fig. 155.

Comparison of the TRAC-calculated and measured vessel liquid mass inventories for LOFT L1-4.

performed with conductivity probes and, therefore, were subjective. Figure 155 compares the TRAC-calculated and measured total vessel liquid mass inventories. Data for Fig. 155 were obtained from the LOFT L1-4 quick-look report.²³

D. Parametric Studies

To test the hypothesis that reduced heat-slab thickness accounted for the observed lower pressures and temperatures late in the L1-4 blowdown, we performed a calculation with the correct structural mass. (In some cells this mass was an order of magnitude greater than that used in the best-estimate model.) The calculated pressures were substantially higher than the test values; therefore, we concluded that this reduced thickness probably caused the differences in pressure between the TRAC results and the test data late in the transient.

E. TRAC-PD2 Features Tested

The LOFT L1-4 experiment assessed the ability of TRAC-PD2 to represent the geometry of a PWR system under blowdown and ECC injection conditions. The fuel-rod heat-transfer and reflood models were not used to analyze this experiment.

The generally good agreement between the TRAC-PD2 results and the experiment increased our confidence that TRAC can analyze PWR blowdown accidents and ECC injection well. However, the inability of the lumped-parameter heat-slab model to represent the time history of energy added to the system from structural materials in the VESSEL is a shortcoming in the TRAC code.

F. Input Data Decks

Appendix J lists the steady-state and transient input decks for LOFT L1-4. The transient includes the L1-4 blowdown and refill. All component data were retrieved from the dump at the end of the steady-state calculation.

The CPU times on a CDC 7600 were 6.2 min for the 60-s steady-state calculation and 168.5 min for the 70-s transient calculation.

XIII. LOFT NUCLEAR EXPERIMENT L2-2

A. Experiment Description

Test L2-2 (Ref. 24) not only was the first test in the LOFT power-ascension test series but also was the first nuclear-power test in the LOFT facility. The test was run at 50% maximum power ($26.25\text{-kW} \cdot \text{m}^{-1}$ maximum linear heat generation) and simulated a 200% double-ended cold-leg-break LOCA. Test L2-2 differed from Test L1-4 in that it had a nuclear core at power and, consequently, had a core ΔT of $\sim 23\text{ K}$ at blowdown initiation. The purpose of Test L2-2 was to investigate the behavior of the LOFT system during blowdown, refill, and reflood under these conditions.

The LOFT nuclear core contained 1300 unpressurized fuel rods arranged in five-square and four-triangular fuel modules (Fig. 156). The rods had an active 1.68-m length and an 0.0107-m o.d. The core had thermocouples externally mounted on selected fuel rods and self-powered neutron detectors. Figure 156 designates the instrumented rods.

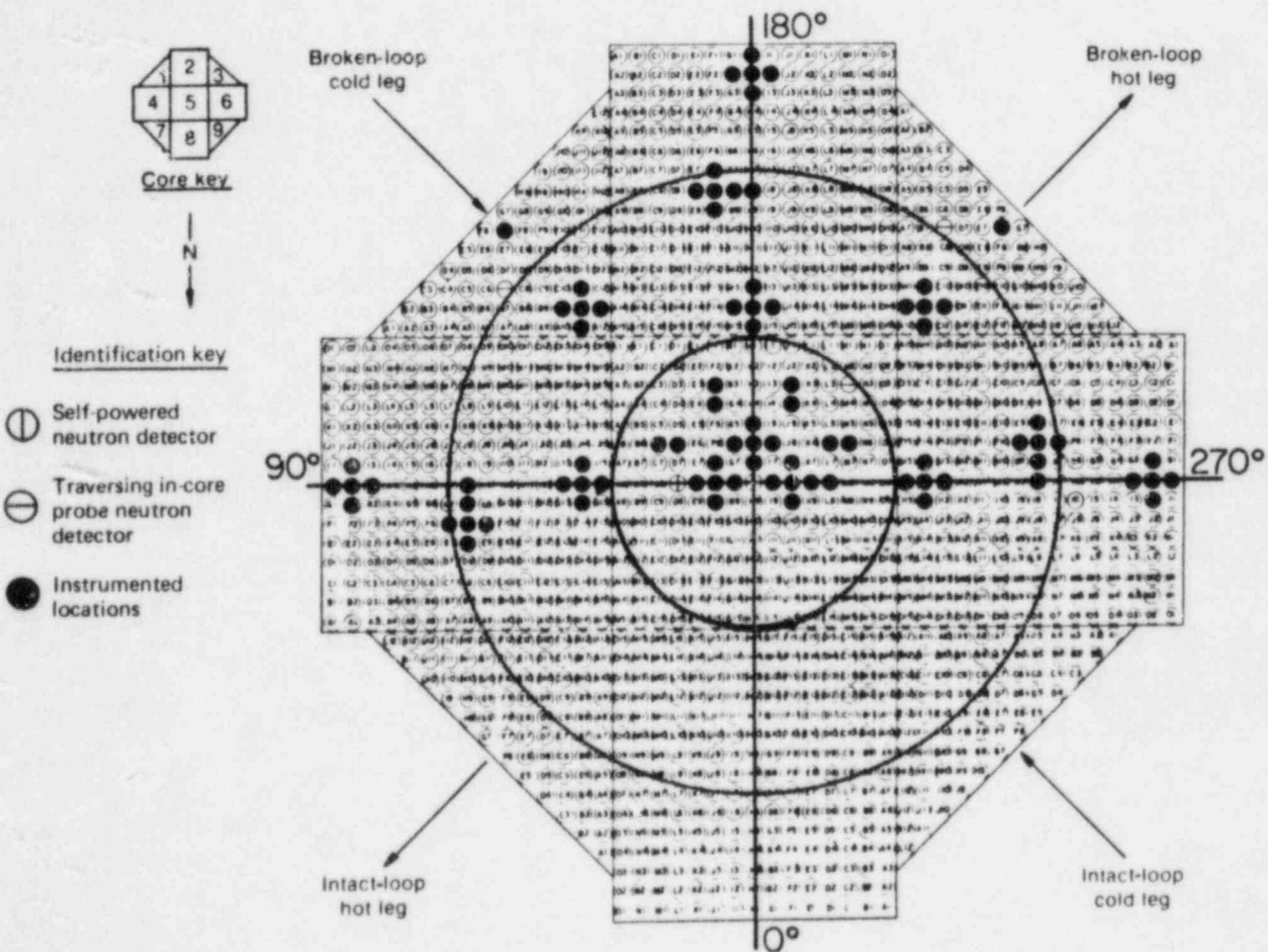


Fig. 156.

LOFT core 1 configuration showing the instrumented rod designations and the TRAC noding.

The sections outside of the core were not modified between Tests L1-4 and L2-2; however, instrumentation was added to some of the external pipes.

At the start of Test L2-2, the intact-loop mass flow was $194.2 \text{ kg} \cdot \text{s}^{-1}$, the steam control valves were closed, and the control rods were inserted into the core. The resulting power transient followed the predicted decay curve. The pressurizer heaters were not energized during this test. The fuel-rod temperatures were especially important. During Test L2-2, the rod-surface temperatures were expected to go through DNB, and this proved to be the case. The surprising test result was how quickly all the fuel rods were rewet after DNB. Before the test, rewet was expected to occur during reflood, at least in the high-power section of the core; however, the test showed that all the rods rewet during the blowdown phase. Consequently, the maximum cladding temperature in this experiment was considerably below the predictions.

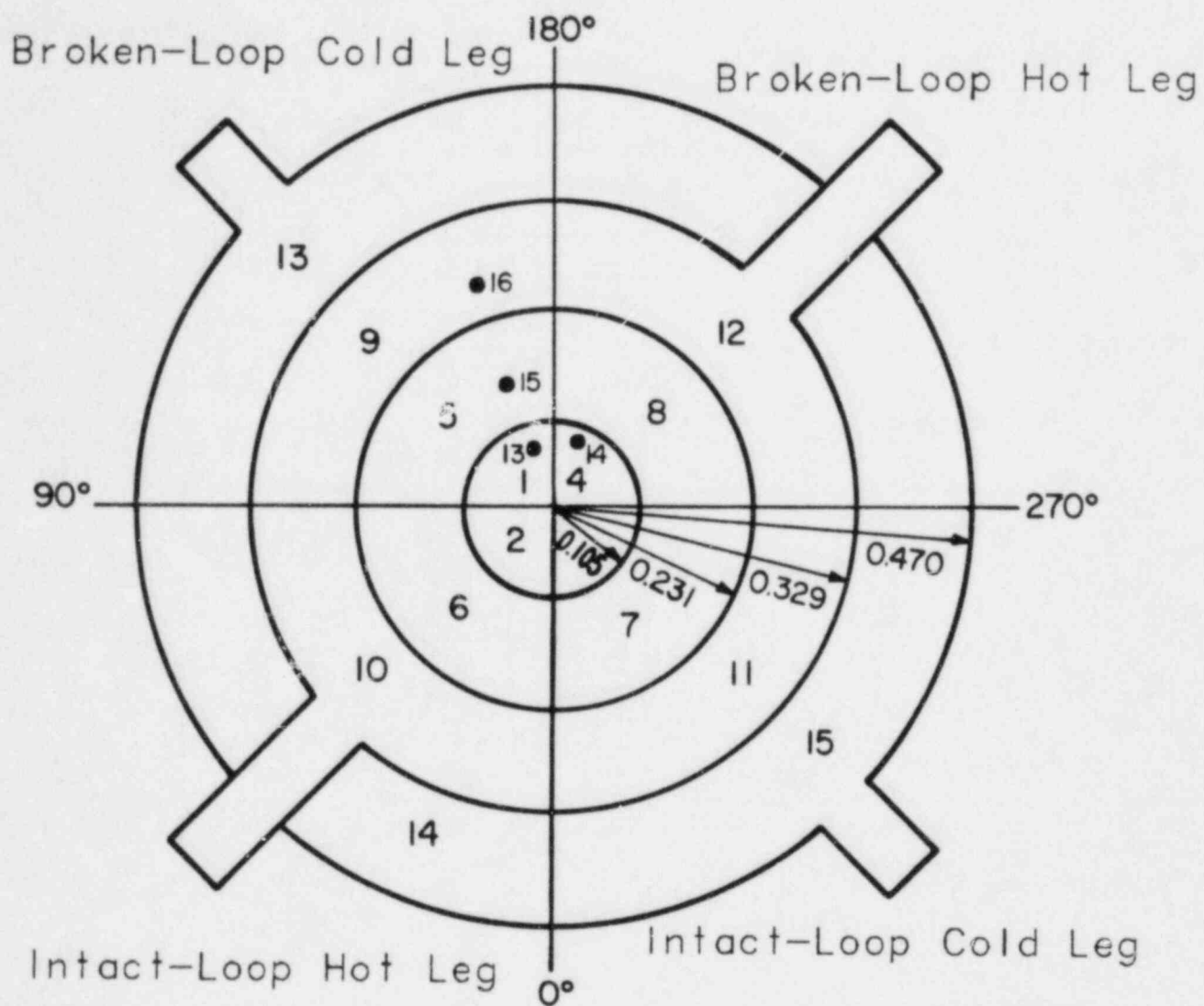
B. TRAC-PD2 Model

The TRAC-PD2 model for Test L2-2 was similar to that used for Test L1-4 except for the VESSEL noding. The HPIS and LPIS FILLs were reversed from those in the L1-4 model; that is, component 24 was the LPIS and component 25 was the HPIS for Test L2-2. The broken legs were modeled with single TEEs, components 15 and 16, rather than the combination of TEEs and PIPEs used in Test L1-4. Figures 157 and 158 show the L2-2 VESSEL noding. The radial subdivisions of the core region were selected to approximate the three regions of the LOFT power distribution. As shown in Fig. 156, the innermost radial region corresponded to the central fuel bundle; the second, to the middle power region; and the third, to the outer, low-power region. In addition to the average-power rods required by TRAC, the L2-2 model also included auxiliary rods that modeled specific instrumented rods. Figure 157 shows these auxiliary rods and their peaking factors. Note that some instrumented rods had peaking factors below 1.

The axial VESSEL division (Fig. 158) was similar to that used for Test L1-4, except that it included finer noding in the core region (levels 4-8). These levels were chosen to allow representation of the LOFT rod axial power profile. Figure 159 compares the TRAC-PD2 axial power profile with the L2-2 test profile and shows the noding used in the core conduction calculation before reflood.

There was considerable uncertainty about the state of the fuel pellets before the test began. This uncertainty arose because it was difficult to account for the fuel-pin behavior during the power variations that preceded the test. We studied this uncertainty effect by conducting a parametric study that used varying fuel radial geometries. Figure 160 shows the base-case fuel radial noding. The geometric variations were made by changing only the location of the fuel-pellet surface. The interior nodes and the cladding geometry were not changed.

The ECCS for Test L2-2 was modeled by an accumulator (ACCUM), a VALVE, two TEEs, and two FILLs. The VALVE controlled the ACCUM flow. The VALVE was programmed to open instantaneously when the local pressure fell below 42.2 bar. The HPIS and LPIS were modeled with FILLs. The HPIS FILL started to inject at $1.58 \times 10^{-3} \text{ m}^3 \cdot \text{s}^{-1}$, 3 s after the pressurizer level fell below 0.23 m. The LPIS model was a pressure-dependent FILL that had a zero-flow rate for local pressures above 15.2 bar.



Rod Number

Rod Peaking Factor

13

1.064

14

1.064

15

1.151

16

0.592

Fig. 157.
LOFT L2-2 VESSEL noding diagram (level 11) and rod locations.

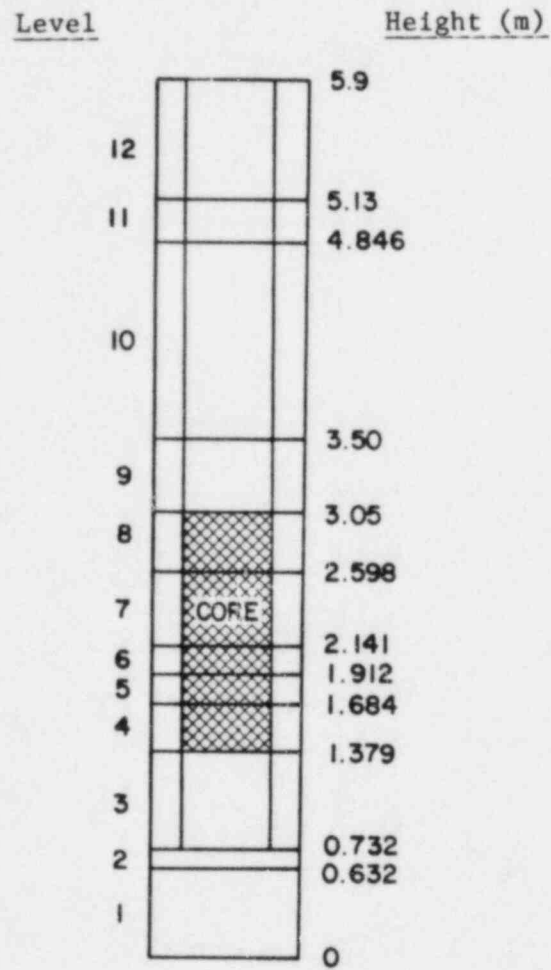


Fig. 158.
LOFT L2-2 VESSEL axial noding diagram.

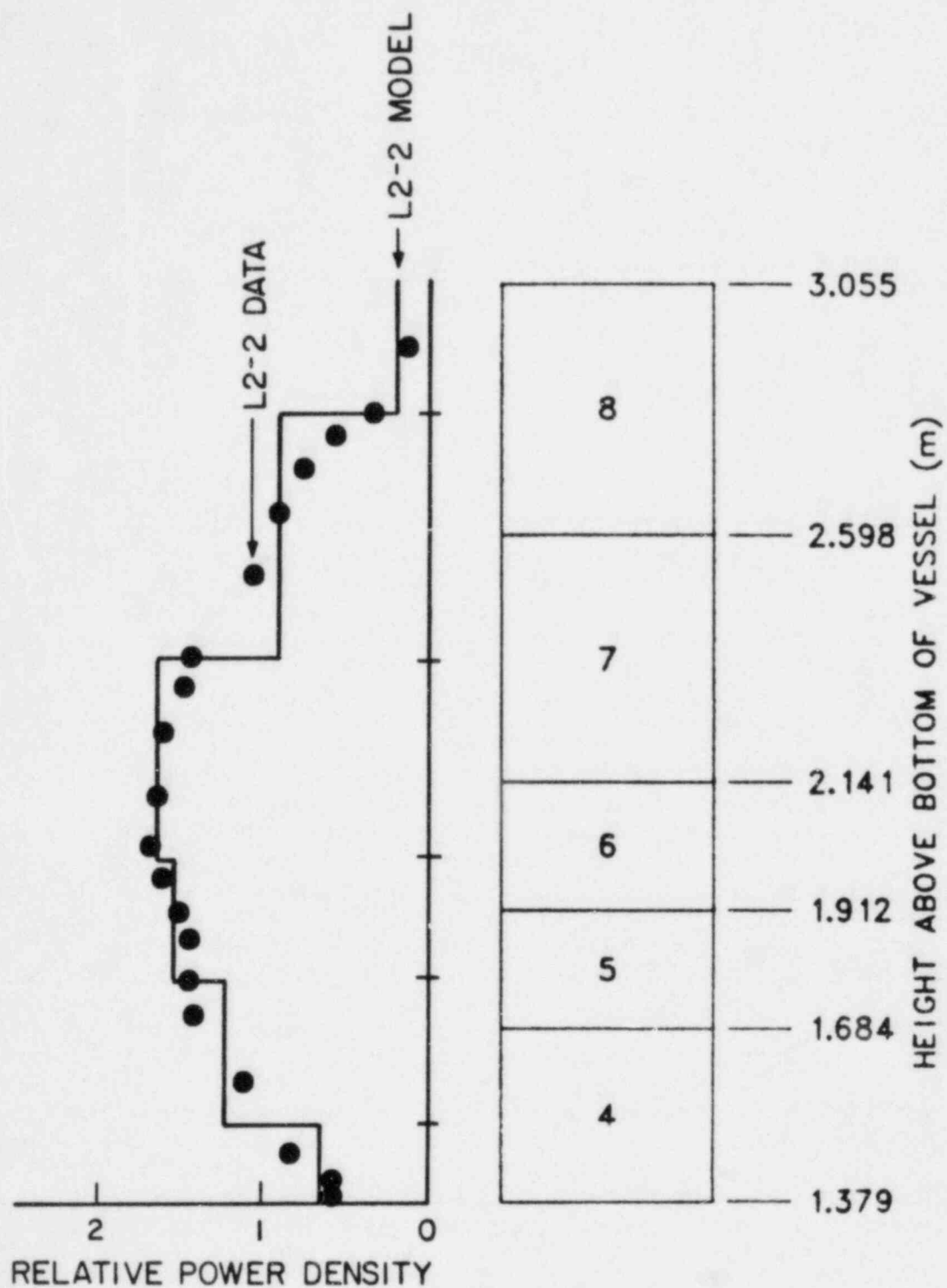


Fig. 159.
LOFT L2-2 core axial noding diagram and power profile.

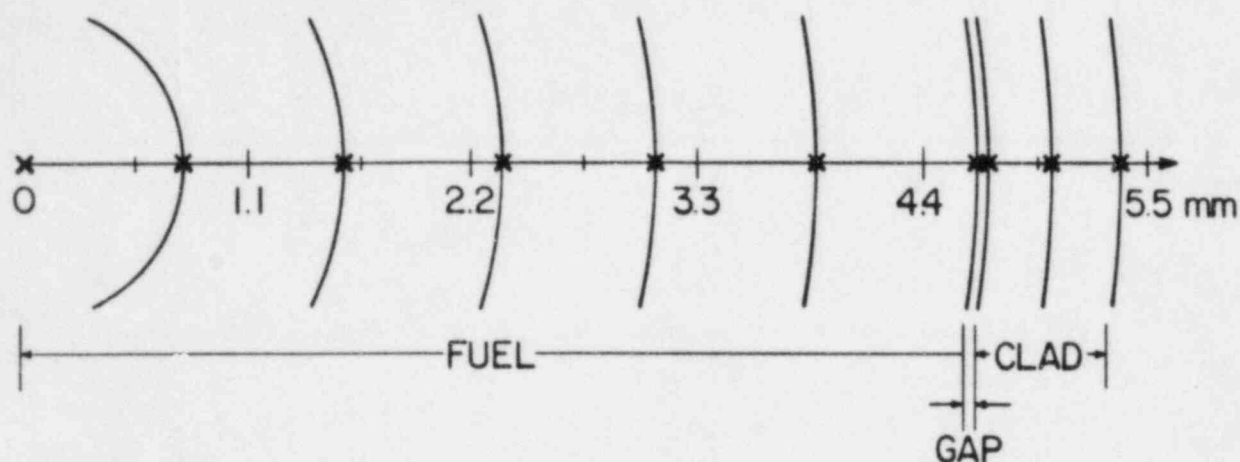


Fig. 160.
LOFT L2-2 fuel-rod radial noding diagram.

C. TRAC-Calculated Results

1. Steady-State Results. The base-case calculation for Test L2-2 was performed in two stages. The steady-state calculation used the generalized steady-state option. The transient began from the resulting dump. Figures 161-171 display the calculated steady-state results for the important parameters. These figures show that the steady-state solution was approximated closely after 30 s. However, convergence did not occur in the 55.7-s calculation because there were mass balance problems on the steam-generator secondary side (Fig. 169). Table XIV compares the steady-state TRAC-calculated results and the test measurements. Closer agreement could have been obtained by adjusting the pump speeds and the steam-generator secondary-side conditions, but the accuracy achieved was sufficient for this large-break loss-of-coolant experiment (LOCE). The differences between the calculated and measured maximum heat-generation rates and the maximum cladding temperatures did not indicate disagreement necessarily between the experiment and the calculation. The heat-generation rates differed because we averaged the nodes in the calculation and the measured peak cladding temperature reflected only thermocouple locations.

The CPU time for the first 30 s of the steady-state calculation was 20.7 min, whereas the CPU time for the complete 55.7-s calculation was 28.3 min. The average time step for the calculation was 22 ms. The problem required 94203 words of LCM and a maximum SCM dynamic area of 7278 words.

2. Transient Results. We divided the calculated transient results into two sections, fluid and rod temperature, to make the information more understandable. The test results in this section were retrieved primarily from tapes provided by the NRC Reactor Safety Research Data Bank at EG&G Idaho, Inc. The data retrieval and error estimation, based on Table XXXVI in Ref. 25, were performed automatically to prevent mistakes.

The 69-s transient calculation required 5.5 h of CPU time on a CDC 7600, used an average 5.8-ms time step, and accessed the same memory as the steady-state calculation. Table XV lists statistics for subsections of the calculation. The code encountered some water-packing problems and occasional convergence problems that required smaller time-step sizes; however, these

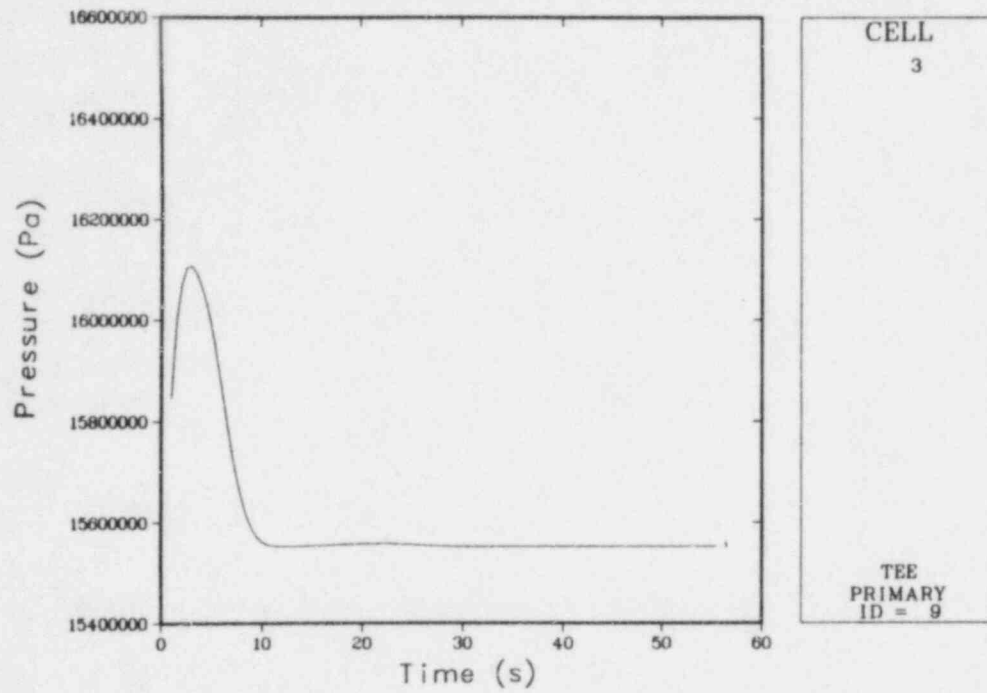


Fig. 161.
LOFT L2-2 steady-state pressure in the intact-loop cold leg.

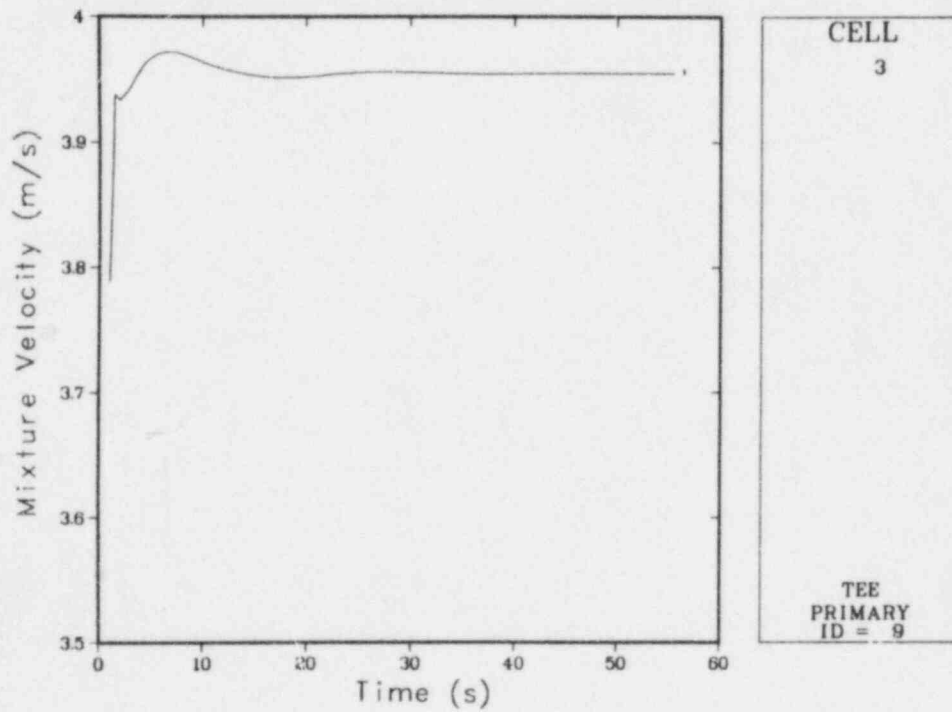


Fig. 162.
LOFT L2-2 steady-state mixture velocity in the intact-loop cold leg.

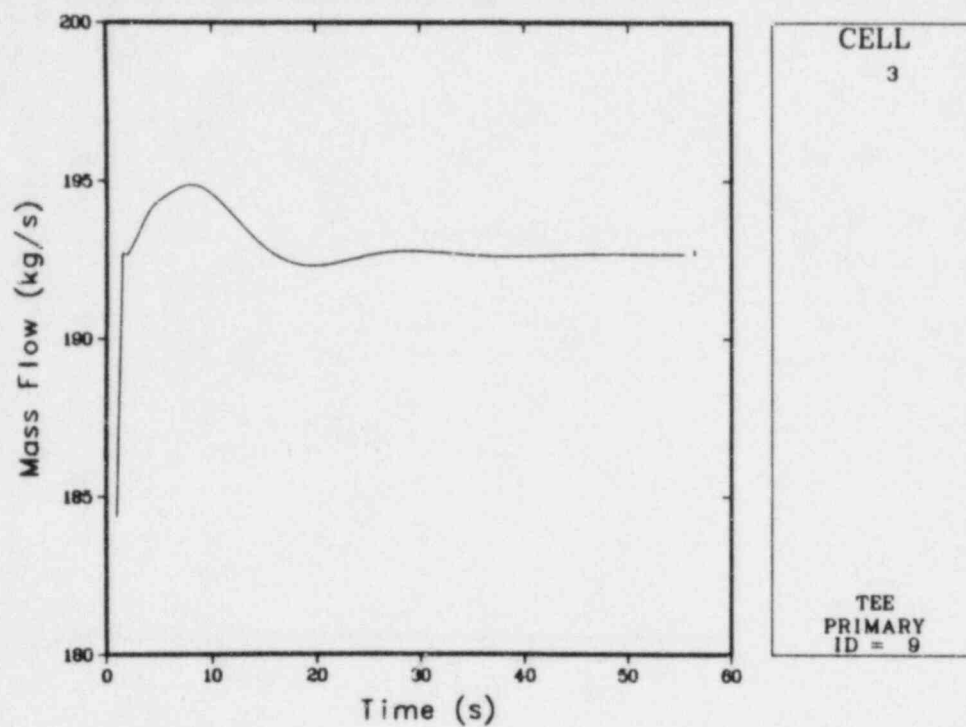


Fig. 163.
LOFT L2-2 steady-state mass flow in the intact-loop cold leg.

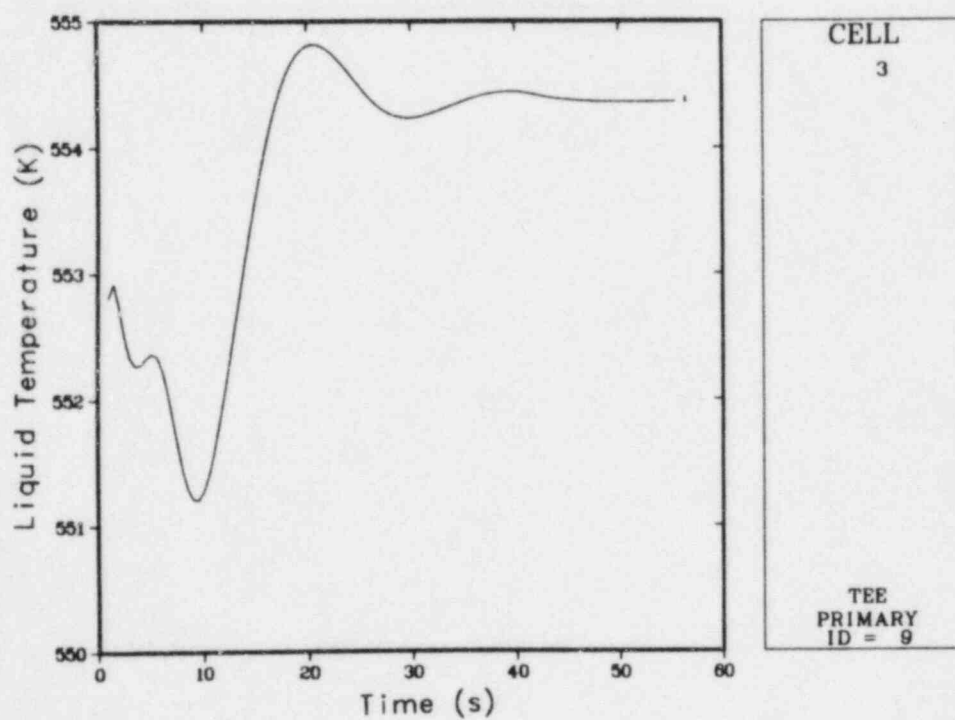


Fig. 164.
LOFT L2-2 steady-state liquid temperature in the intact-loop cold leg.

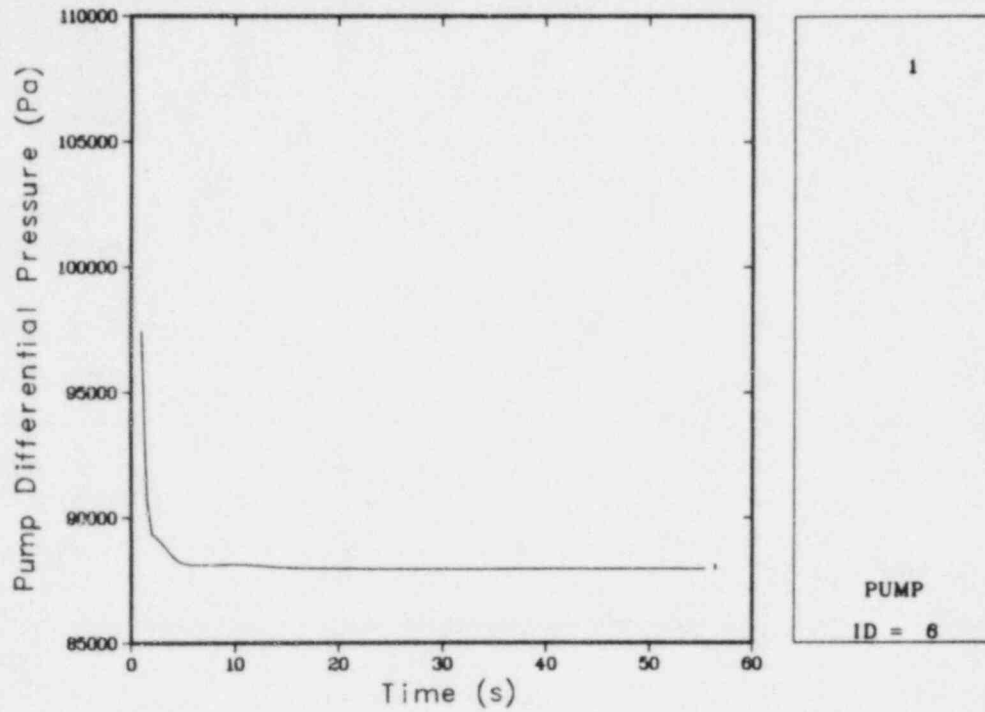


Fig. 165.
LOFT L2-2 steady-state pressure differential across pump 6.

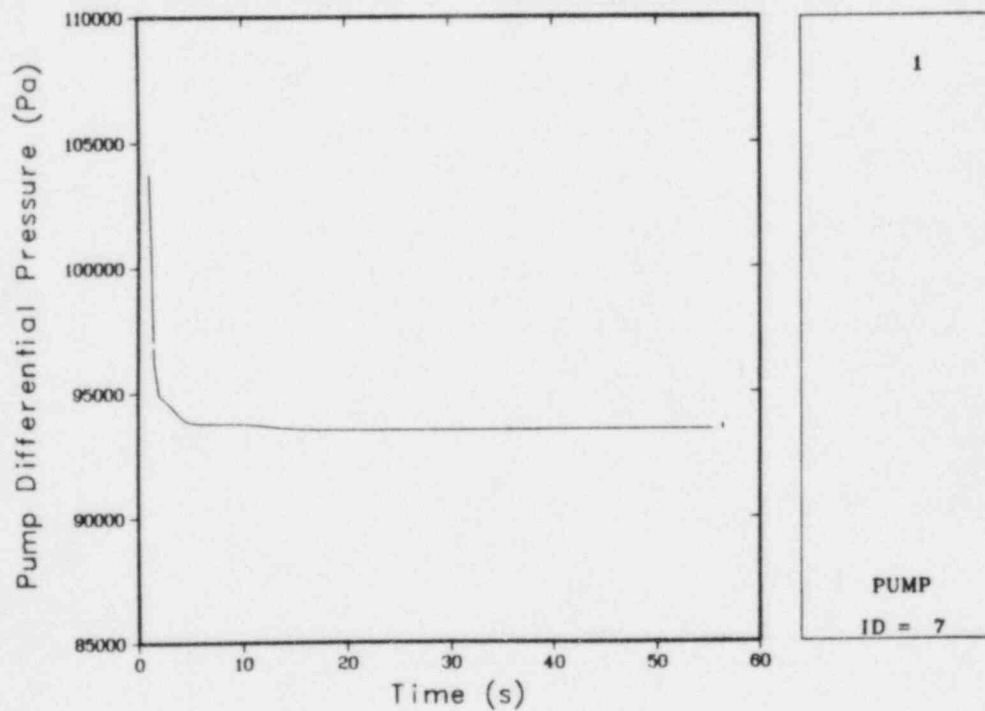


Fig. 166.
LOFT L2-2 steady-state pressure differential across pump 7.

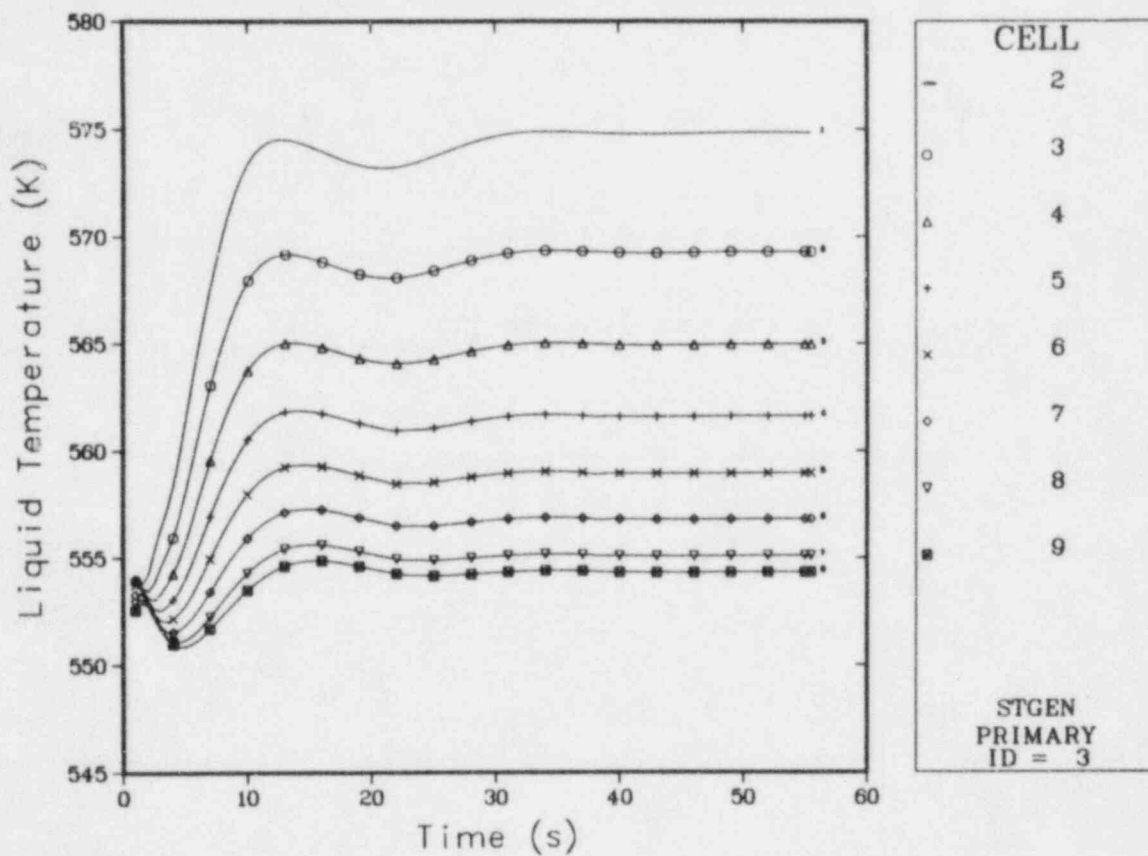


Fig. 167.
LOFT L2-2 steady-state steam-generator primary-side liquid temperatures.

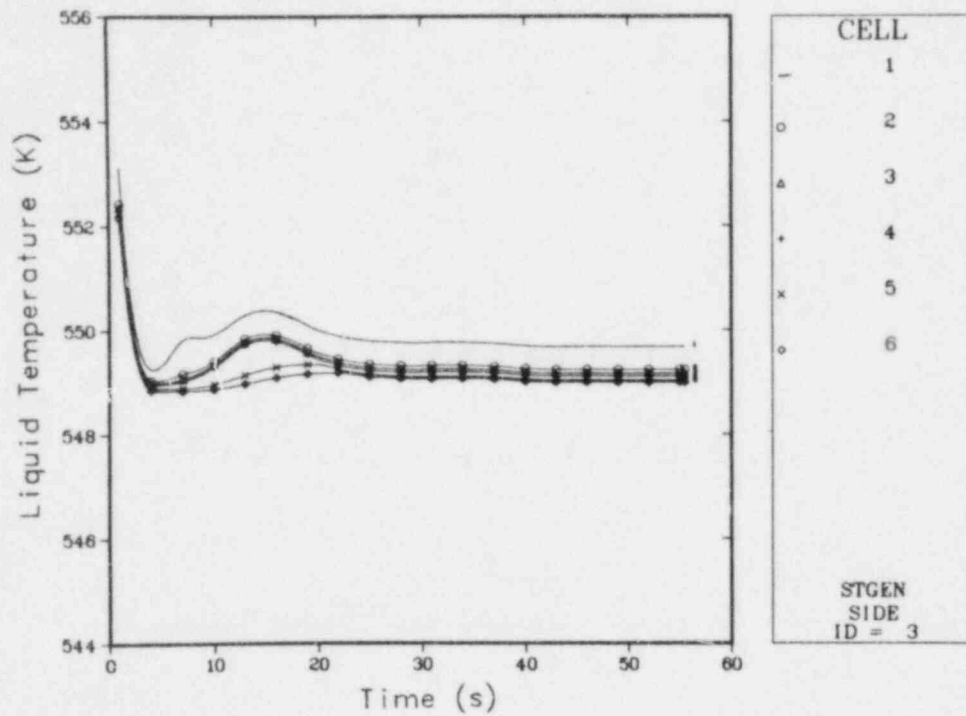


Fig. 168.

LOFT L2-2 steady-state steam-generator secondary-side liquid temperatures.

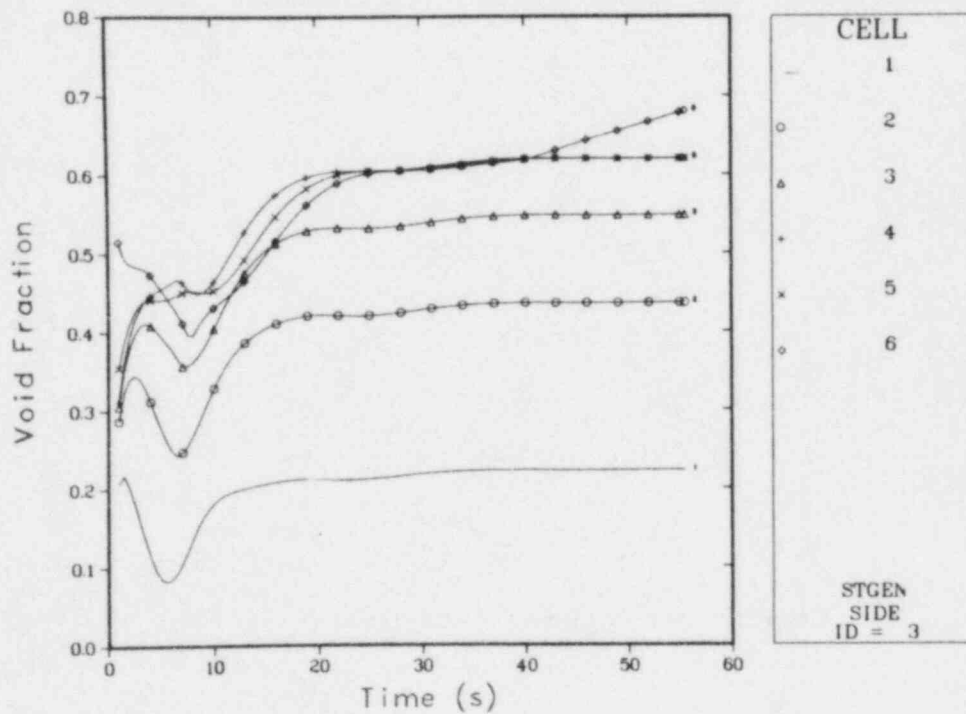


Fig. 169.

LOFT L2-2 steady-state steam-generator secondary-side void fractions.

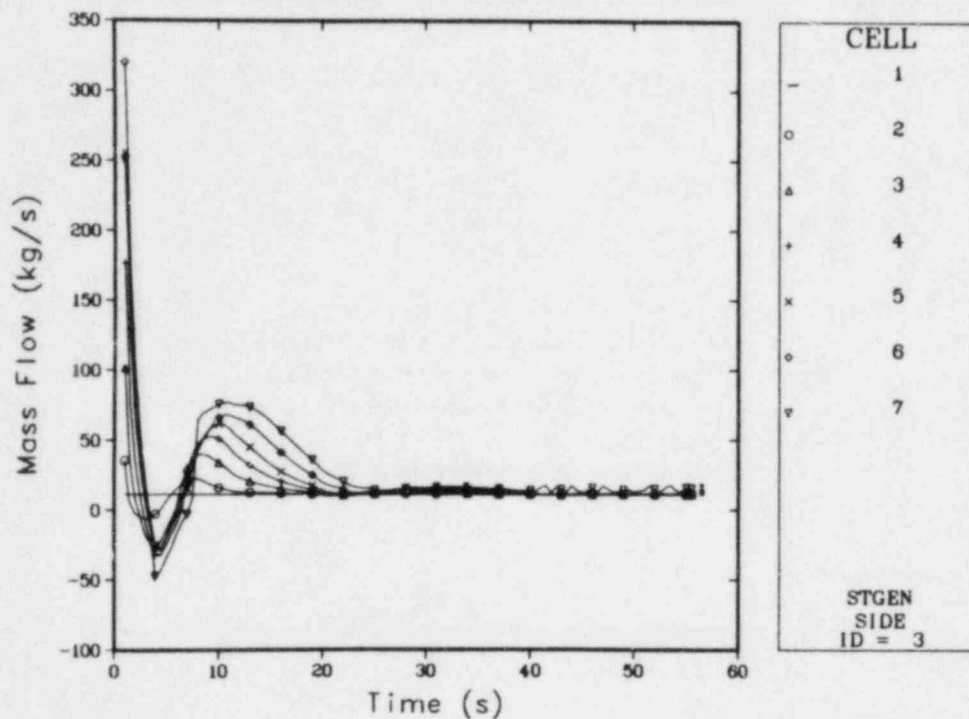


Fig. 170.
LOFT L2-2 steady-state steam-generator secondary-side mass flows.

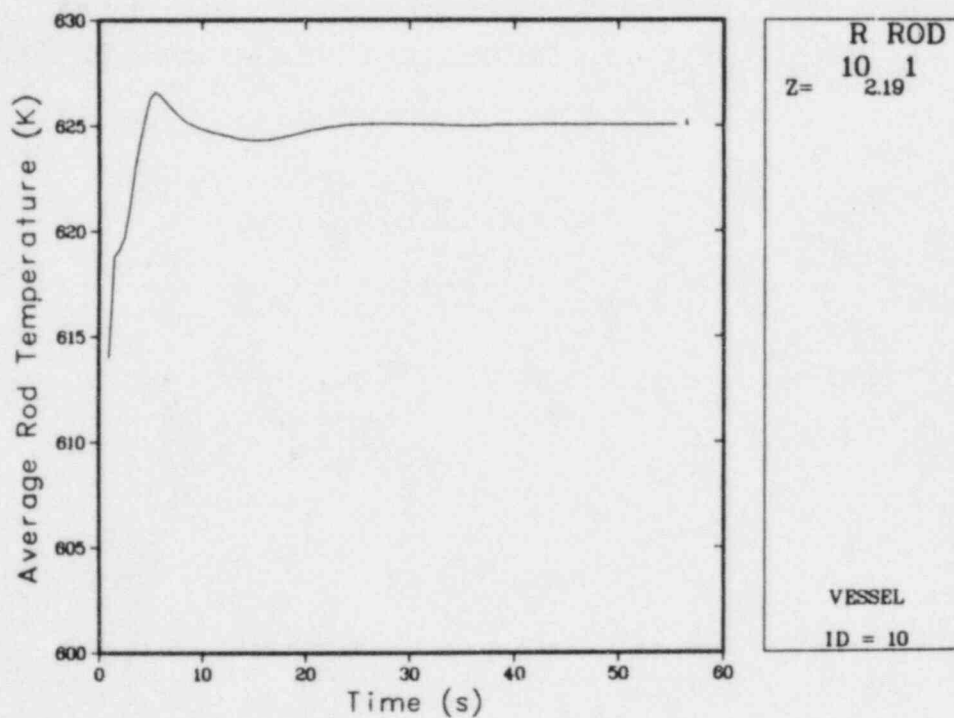


Fig. 171.
LOFT L2-2 steady-state fuel-rod cladding-surface temperatures.

TABLE XIV

CALCULATED AND MEASURED INITIAL CONDITIONS FOR LOFT L2-2

<u>Parameters</u>	<u>TRAC-Calculated</u>	<u>Measured</u>
Intact-loop mass flow rate ($\text{kg} \cdot \text{s}^{-1}$)	192.7	194.2
Pressurizer pressure (MPa)	15.5	15.6
Pressurizer liquid level (m)	1.10	1.09
Steam-generator primary-side inlet temperature (K)	578.7	580.4
Steam-generator primary-side outlet temperature (K)	554.3	557.7
Steam-generator secondary-side temperature (K)	549	553
Steam-generator secondary-side inlet mass flow ($\text{kg} \cdot \text{s}^{-1}$)	11.2	12.7
Steam-generator secondary-side outlet mass flow ($\text{kg} \cdot \text{s}^{-1}$)	14.7	12.7
Intact-loop differential pressure across primary pump 6 (kPa)	88.0	88.0
Intact-loop differential pressure across primary pump 7 (kPa)	94.0	93.0
Core power (MW)	24.88	24.88
Maximum linear heat-generation rate ($\text{kW} \cdot \text{m}^{-1}$)	23.76	26.37
Maximum cladding temperature (K)	626.5	610 ^a
Accumulator pressure (MPa)	4.11	4.11
Accumulator temperature (K)	300.8	300.8

^aThe temperature was affected by its location in the thermal boundary layer on the rod.

TABLE XV

LOFT L2-2 STATISTICS

<u>Time Period (s)</u>	<u>Number of Time Steps</u>	<u>CPU Time (s)</u>	<u>Final Time-Step Size (ms)</u>	<u>Average Time-Step Size (ms)</u>	<u>CPU Time/Time Step (s)</u>
0 + 15.	2853	3395	1.85	4.42	1.19
15. + 38.8	2585	3572	7.10	9.21	1.38
38.8 + 47.6	1809	3680	2.04	4.86	2.03
47.6 + 52.0	1590	3709	4.42	2.77	2.33
52.0 + 55.3	949	1922	2.97	3.48	2.03
55.3 + 69.0	2210	3628	20.0	6.20	1.64
<hr/>					
0 + 69	11996	19906		5.75	1.66

difficulties, which were overcome by the code automatically, insignificantly degraded the code performance.

a. Fluid Results. In general, agreement was excellent between the measured and TRAC-calculated fluid conditions for this LOFT test. For Tests L1-4 and L2-2, TRAC calculated a low system pressure late in the transient. Again, we believe that the TRAC-PD2 structural heat-transfer models for the VESSEL were inadequate.

Table XVI lists the major calculated and observed sequence of events for LOFT L2-2. The primary discrepancy between the calculation and the data was the behavior of the accumulator. The TRAC calculation injected the accumulator inventory over a longer period of time than was observed experimentally. Thus, the accumulator did not empty during the calculation, whereas the LOFT accumulator emptied at 49 s. Consequently, TRAC calculated the filling of the lower plenum later in the transient than shown in the data but predicted the filling of the core reasonably well. Also, TRAC predicted the time of the maximum cladding temperature later than shown in the data because of delayed liquid flow through the core. The calculated peak cladding temperature (~795 K) was quite close to the observed value (~780 K); however, this parameter was dependent on the selection of initial fuel-rod conditions.

i. Intact-Loop Results. Figures 172-178 compare the TRAC-calculated and measured parameters of the intact-loop components. Figures 172 and 175 also show the low system pressure late in the transient. The cold ECCS injection from 25-40 s significantly affected the measured cold-leg temperature (Fig. 177) but insignificantly affected the calculated result. This discrepancy was caused by measurement problems. The higher wall temperatures at low void fractions greatly affected the thermocouples. The increased

TABLE XVI
SEQUENCE OF EVENTS FOR LOFT L2-2

<u>Event</u>	<u>Time (s)</u>	
	<u>Calculated</u>	<u>Observed</u>
Blowdown initiation	0	0
End of subcooled blowdown	0.1	0.07
HPIS initiation	12	12
Pressurizer emptied	15	15
Accumulator flow initiation	17	18
LPIS initiation	29	29
Lower plenum filled with liquid	~50	35
End of saturated blowdown	~45	44
Accumulator emptied	--	49
Core filled with liquid	~60	55
Maximum cladding-temperature time	7	4

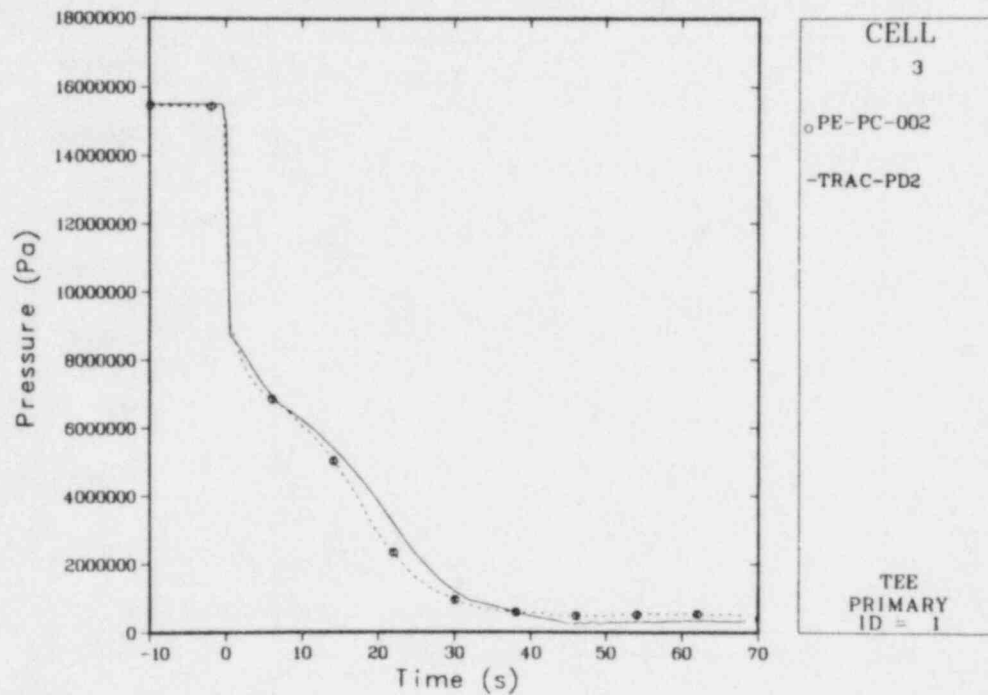


Fig. 172.

Comparison of the TRAC-calculated and measured intact-loop hot-leg pressures for LOFT L2-2.

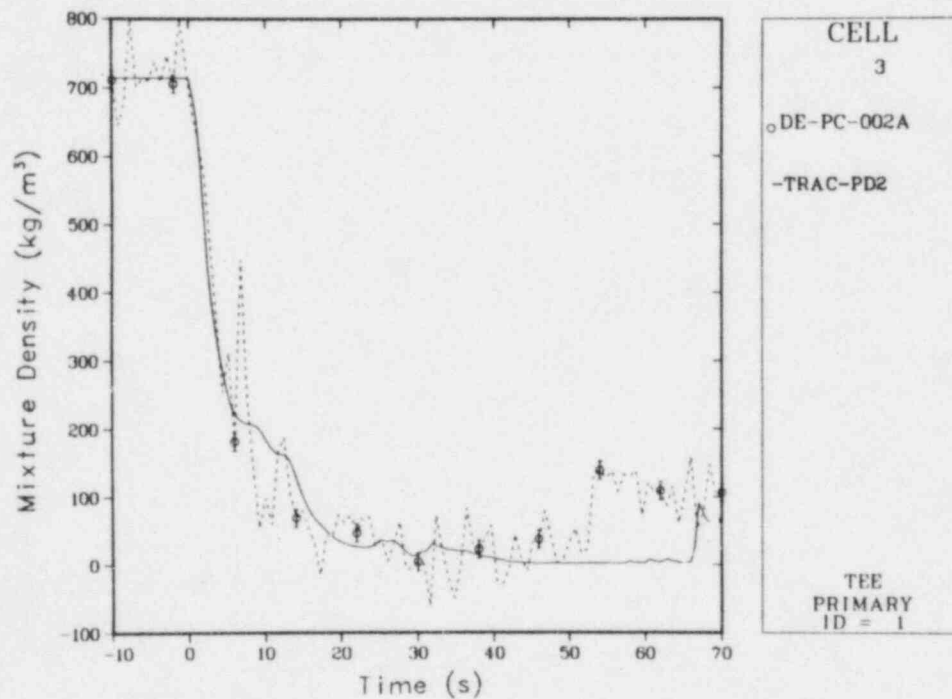


Fig. 173.

Comparison of the TRAC-calculated and measured intact-loop hot-leg mixture densities for LOFT L2-2.

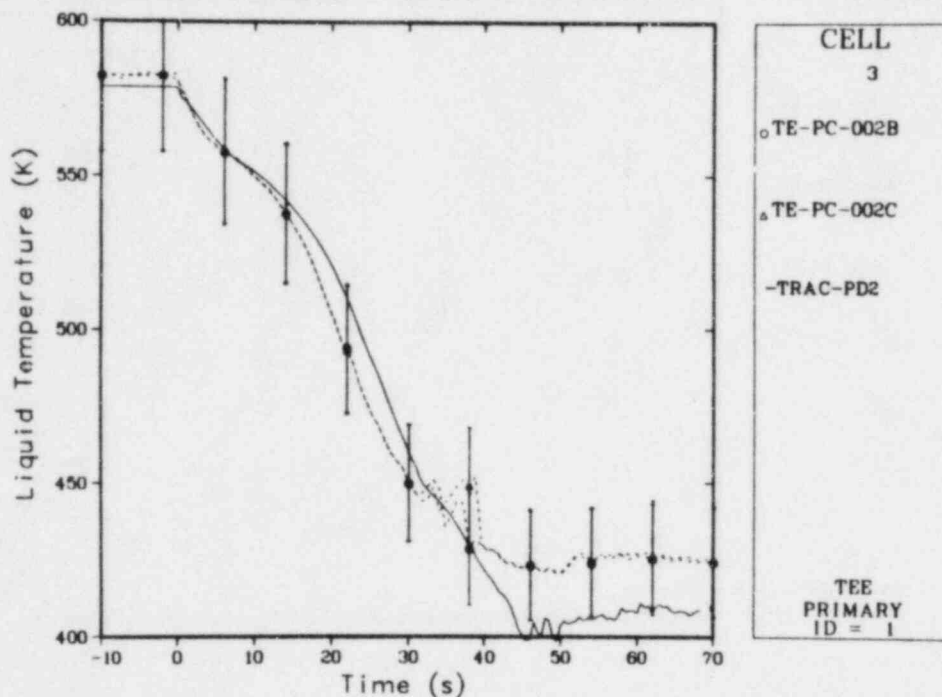


Fig. 174.

Comparison of the TRAC-calculated and measured intact-loop hot-leg liquid temperatures for LOFT L2-2.

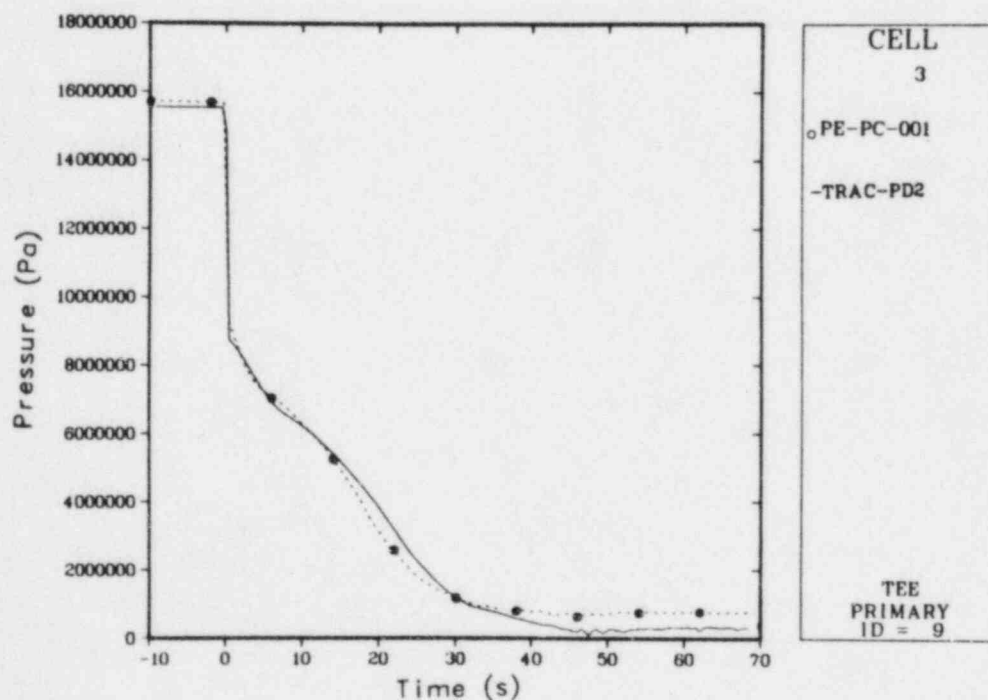


Fig. 175.

Comparison of the TRAC-calculated and measured intact-loop cold-leg pressures for LOFT L2-2.

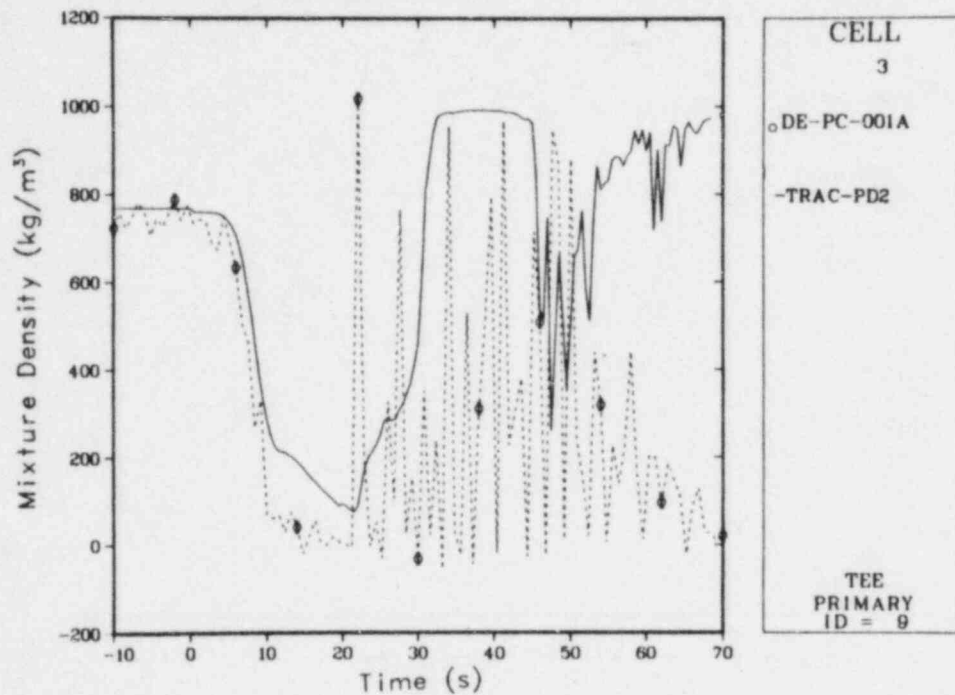


Fig. 176.

Comparison of the TRAC-calculated and measured intact-loop cold-leg mixture densities for LOFT L2-2.

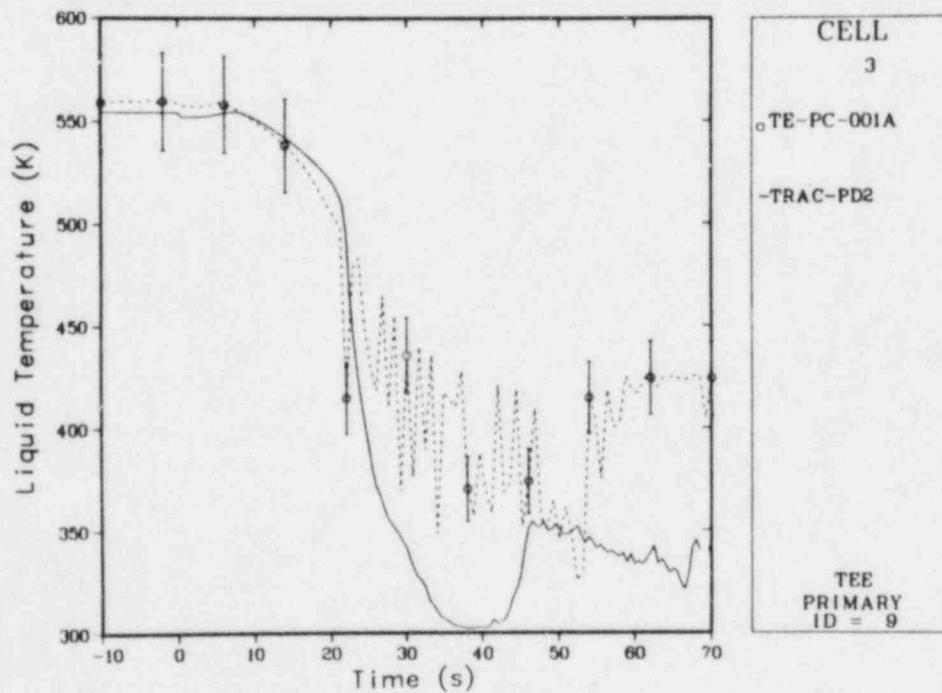


Fig. 177.

Comparison of the TRAC-calculated and measured intact-loop cold-leg liquid temperatures for LOFT L2-2.

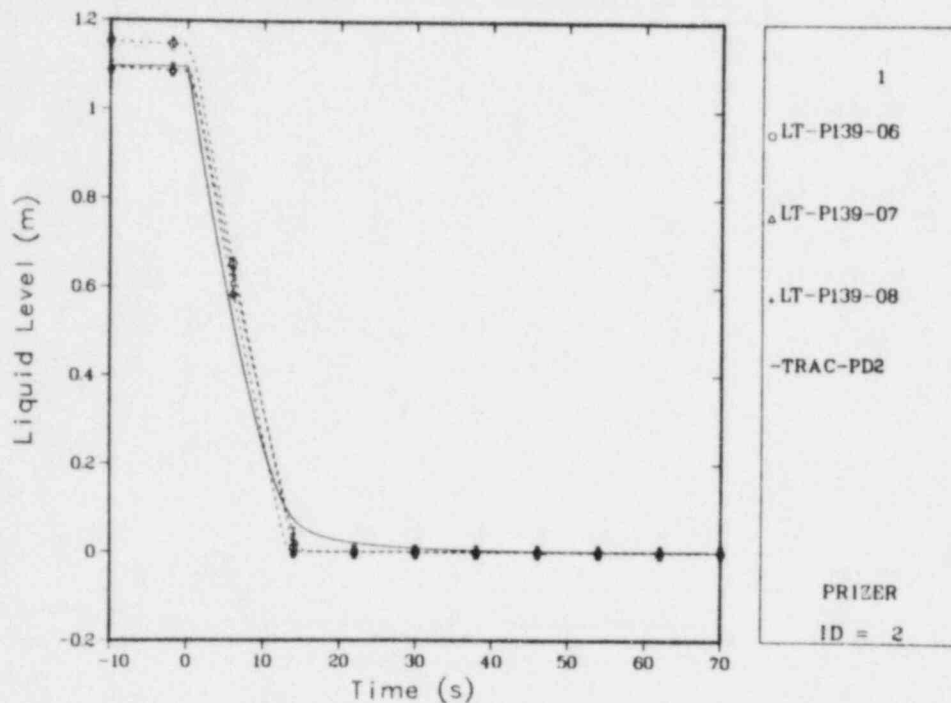


Fig. 178.

Comparison of the TRAC-calculated and measured pressurizer liquid levels for LOFT L2-2.

hot-leg fluid density (Fig. 173) measured at ~53 s, but not calculated until later in the transient, was caused by the filling of the downcomer at this time. The fluctuations in the calculated densities were smoothed by mesh-cell averaging. The large discrepancy between the mixture densities (Fig. 176) after 50 s in the intact-loop cold leg was caused by the continuation of accumulator flow in the calculation. The difference between the TRAC-calculated and measured fluid temperatures after 53 s in the intact-loop cold leg (Fig. 177) again was caused by the thermocouple measurement of the wall temperatures when the void fraction was high.

Figure 178 compares the TRAC-calculated and measured pressurizer water levels. Agreement was excellent, although there was a small discrepancy when the pressurizer emptied because the donor-cell technique used an average void fraction for convection out of the bottom pressurizer component.

ii. ECCS Results Figures 179-183 compare the TRAC-calculated and measured HPIS, LPIS, and accumulator flows; the accumulator pressures; and the accumulator liquid levels. The data in Figs. 179-180 were evaluated by dividing the measured volumetric flow rates by the appropriate flow area. Because they were modeled with variable FILLS, the TRAC HPIS and LPIS reacted in exact accordance with the LOFT specifications. Thus, the differences in Figs. 179-180 reflect errors in the calculated local pressures and the specified performance. These differences did not influence the overall results significantly; the ECCS for Test L2-2 was dominated by the behavior of the accumulator. As we mentioned previously and as Fig. 181 shows, the TRAC accumulator model did not represent accurately the test system. Before ~48 s, the calculated mass flow was ~320 kg less than the test value; after 48 s, TRAC

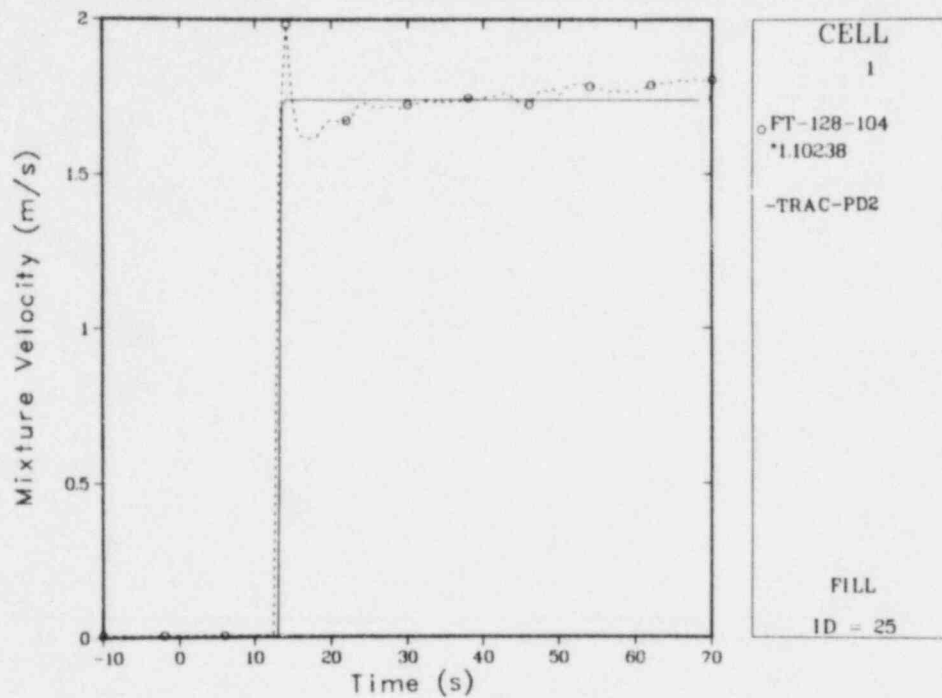


Fig. 179.
Comparison of the TRAC-calculated and measured HPIS flows for LOFT L2-2.

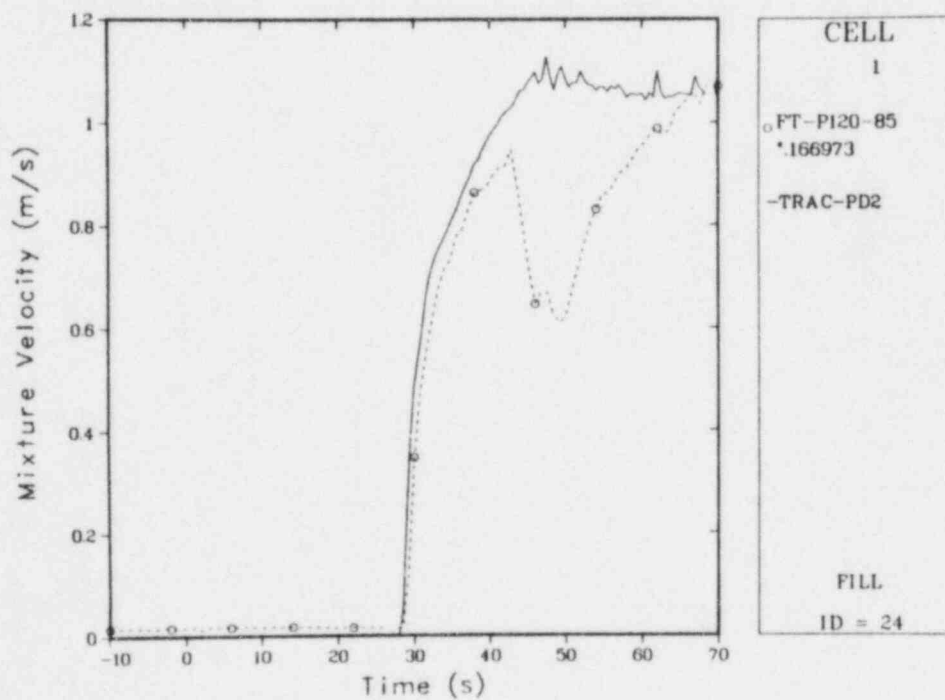


Fig. 180.
Comparison of the TRAC-calculated and measured LPIS flows for LOFT L2-2.

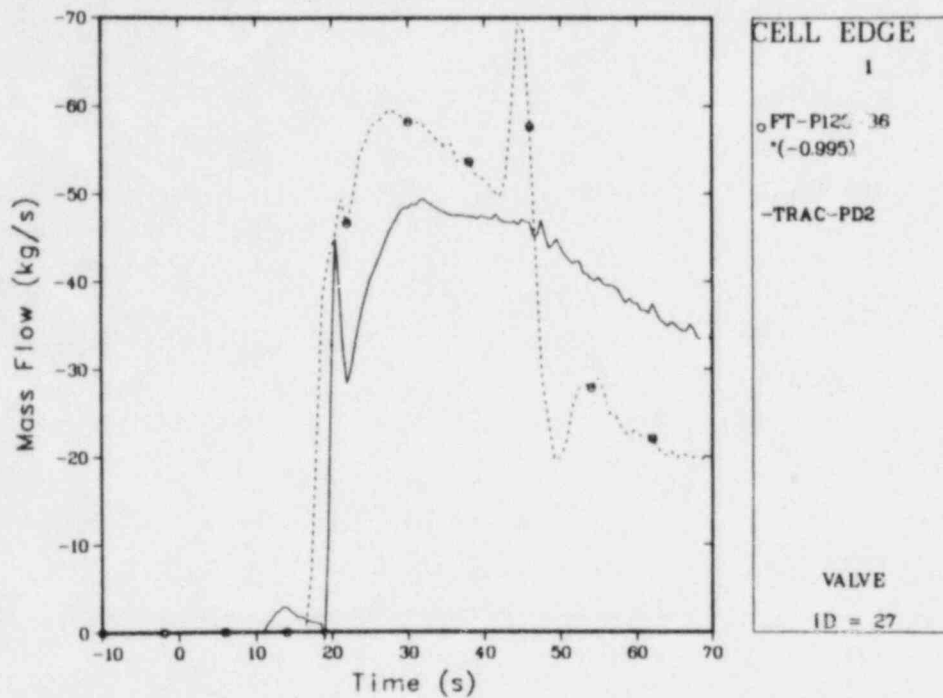


Fig. 181.

Comparison of the TRAC-calculated and measured accumulator flows for LOFT L2-2.

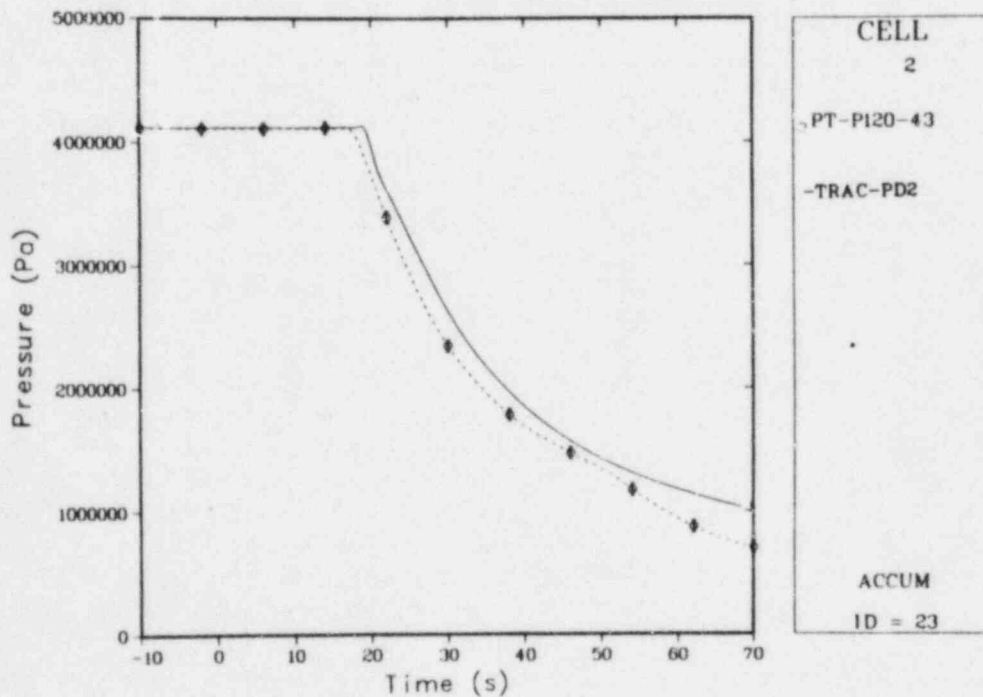


Fig. 182.

Comparison of the TRAC-calculated and measured accumulator pressures for LOFT L2-2.

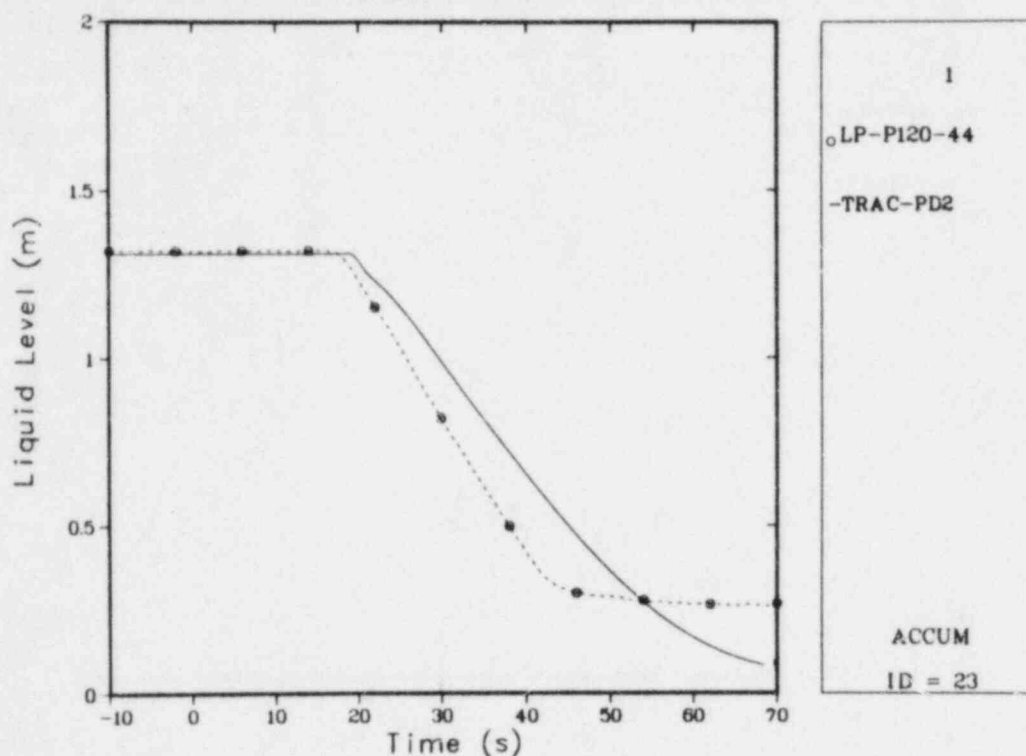


Fig. 183.

Comparison of the TRAC-calculated and measured accumulator liquid levels for LOFT L2-2.

added the 320 kg to the system mass flow. The low initial flow and the resulting long flow period markedly changed the refill and reflood portions of the calculation. The test data in Fig. 181 were evaluated by multiplying the measured volumetric flow rate by the calculated density of the accumulator fluid, $995 \text{ kg} \cdot \text{m}^{-3}$. The underpredicted calculated accumulator mass flows resulted from a low driving-pressure difference (accumulator pressure minus the intact-loop cold-leg pressure) and uncertainty in the flow resistance of the ECC line. Figure 183 compares the TRAC-calculated and measured accumulator liquid levels. In the experiment, this level was inferred from a pressure differential whose lower level was at $\sim 0.25 \text{ m}$. This fact may explain why the data failed to show the emptying of the accumulator; however, Fig. 181 infers the emptying. Because this measurement was made downstream from the accumulator, a small flow continued after the accumulator emptied.

iii. Broken-Loop Results. Figures 184-193 plot the fluid conditions in the broken-loop legs. The broken-loop hot-leg mixture-density comparison (Fig. 184) showed the delayed filling of the reactor core; in Fig. 185, the delayed filling was exhibited by the lower calculated mass flow through the broken-loop hot leg. The high temperatures measured later in the transient (Fig. 186) reflected vapor superheat and possibly some effect of the hot piping walls; because this figure compares the calculated liquid temperature to the data, the superheat did not appear in the calculated curve.

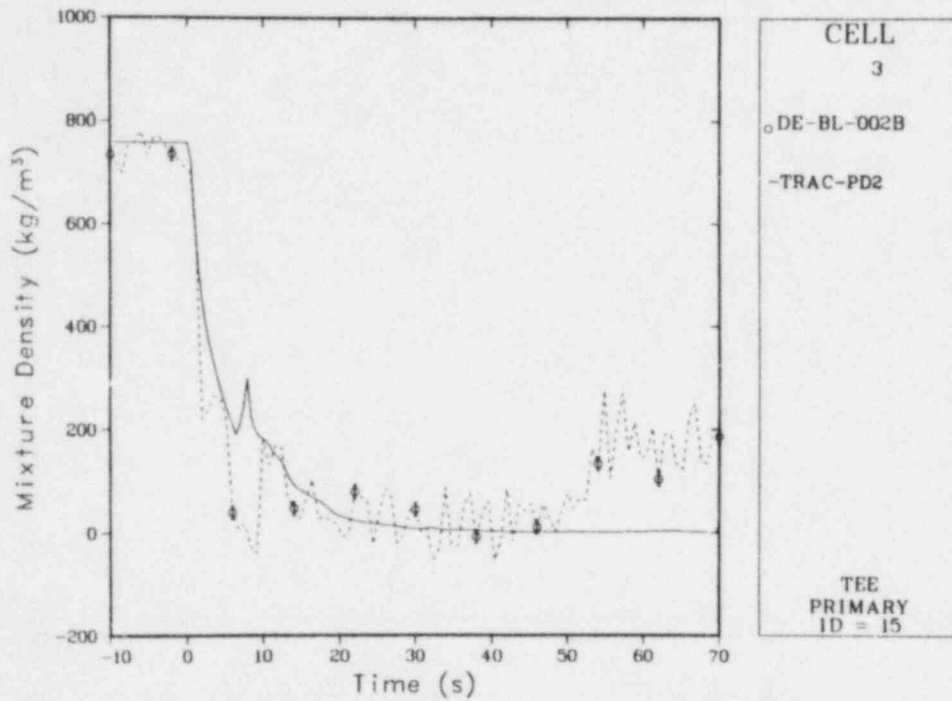


Fig. 184.

Comparison of the TRAC-calculated and measured broken-loop hot-leg mixture densities for LOFT L2-2.

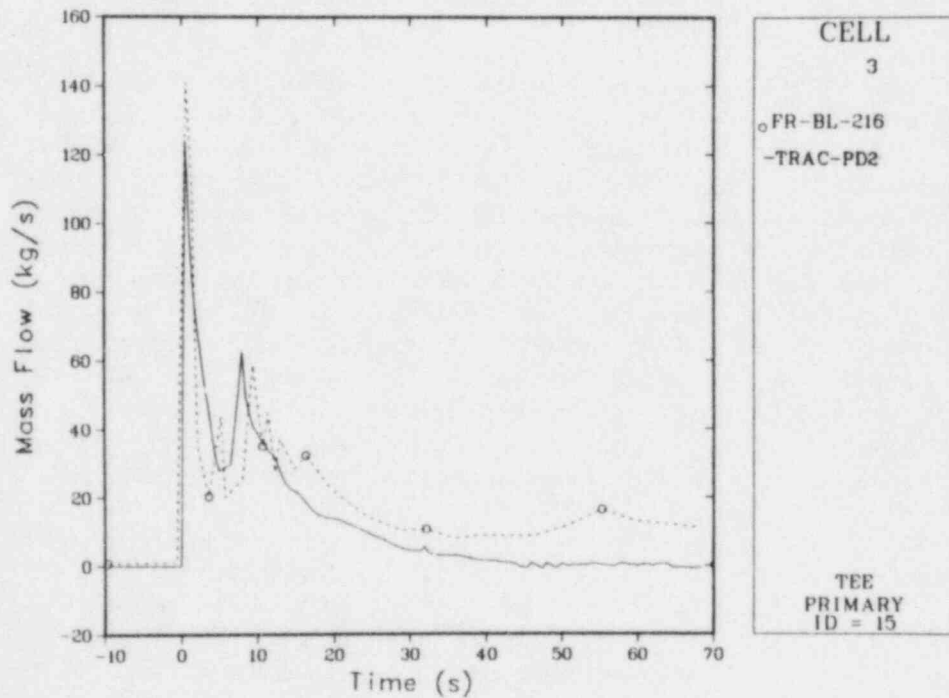


Fig. 185.

Comparison of the TRAC-calculated and measured broken-loop hot-leg mass flows for LOFT L2-2.

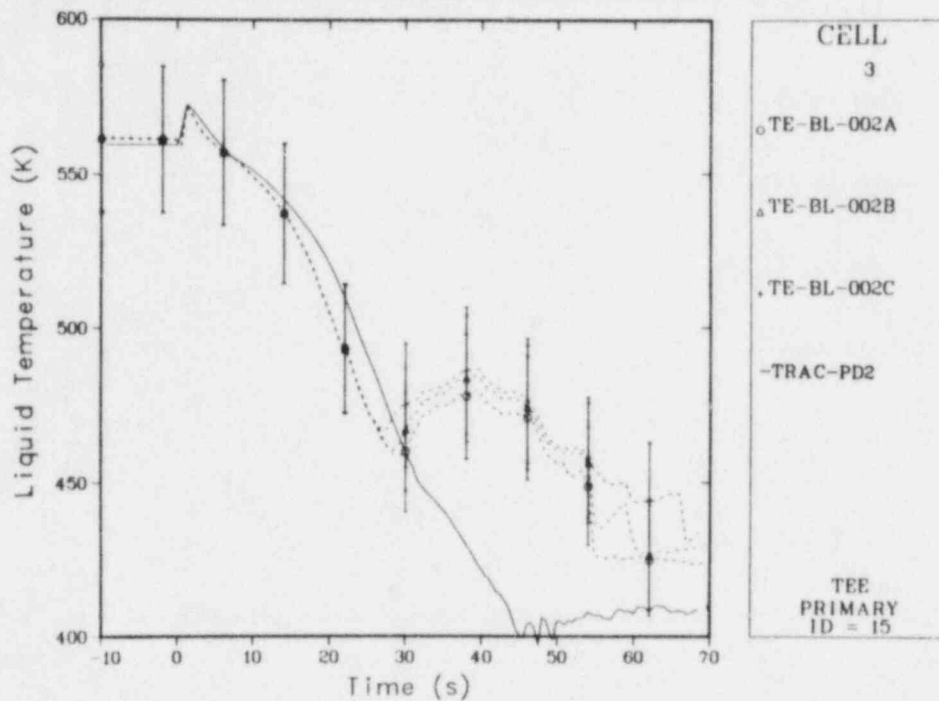


Fig. 186.

Comparison of the TRAC-calculated and measured broken-loop hot-leg liquid temperatures for LOFT L2-2.

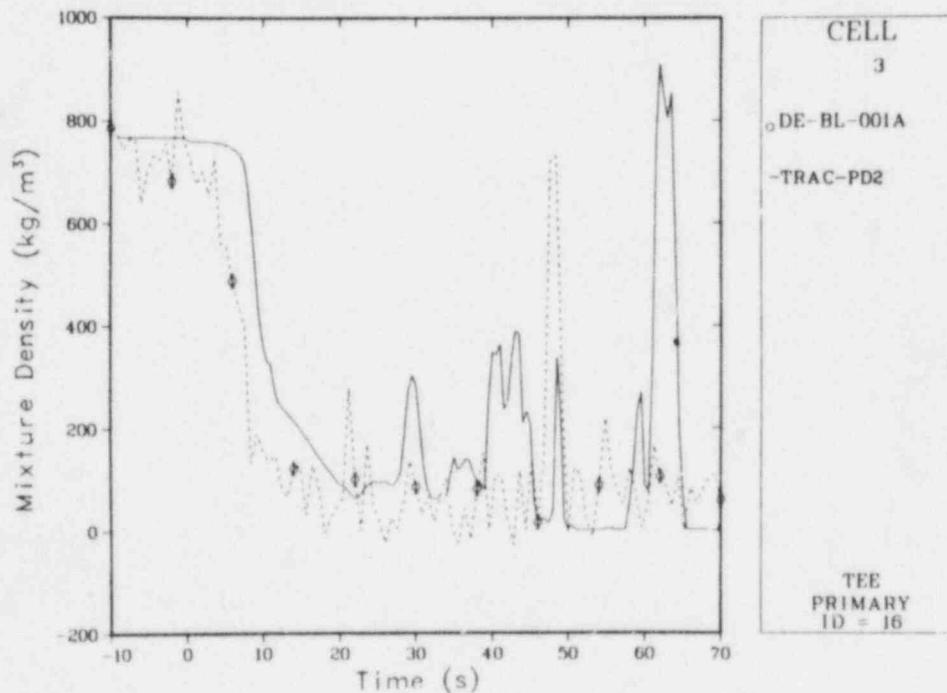


Fig. 187.

Comparison of the TRAC-calculated and measured broken-loop cold-leg mixture densities for LOFT L2-2.

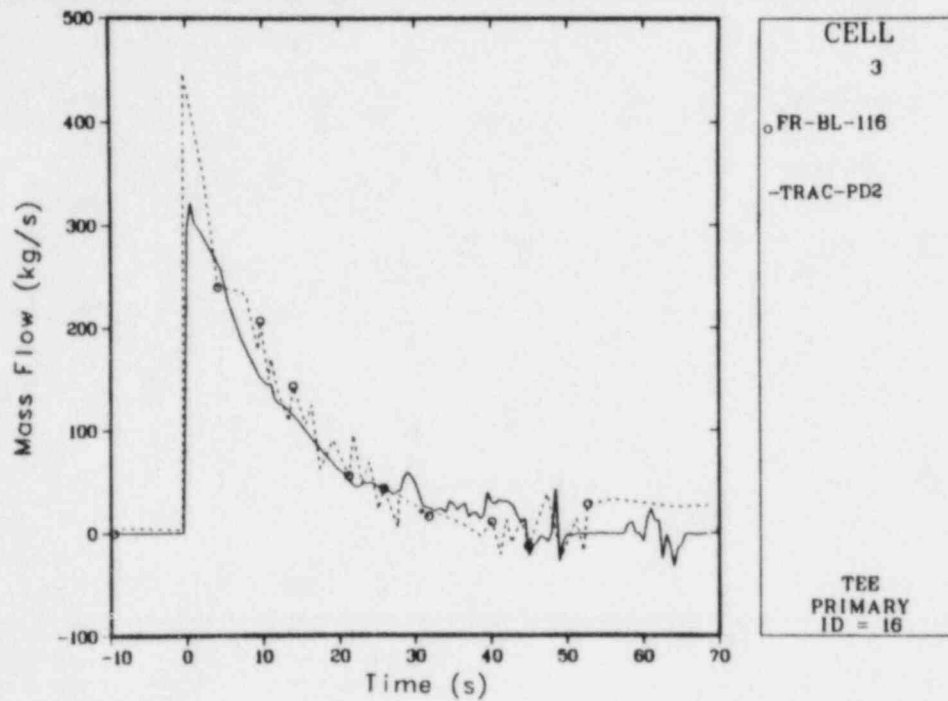


Fig. 188.

Comparison of the TRAC-calculated and measured broken-loop cold-leg mass flows for LOFT L2-2.

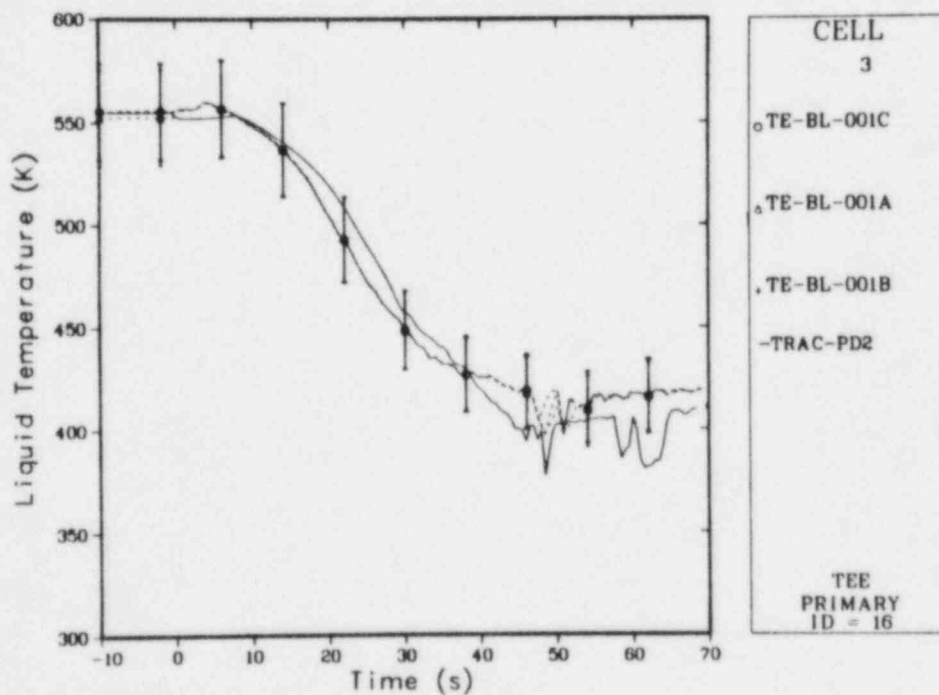


Fig. 189.

Comparison of the TRAC-calculated and measured broken-loop cold-leg liquid temperatures for LOFT L2-2.

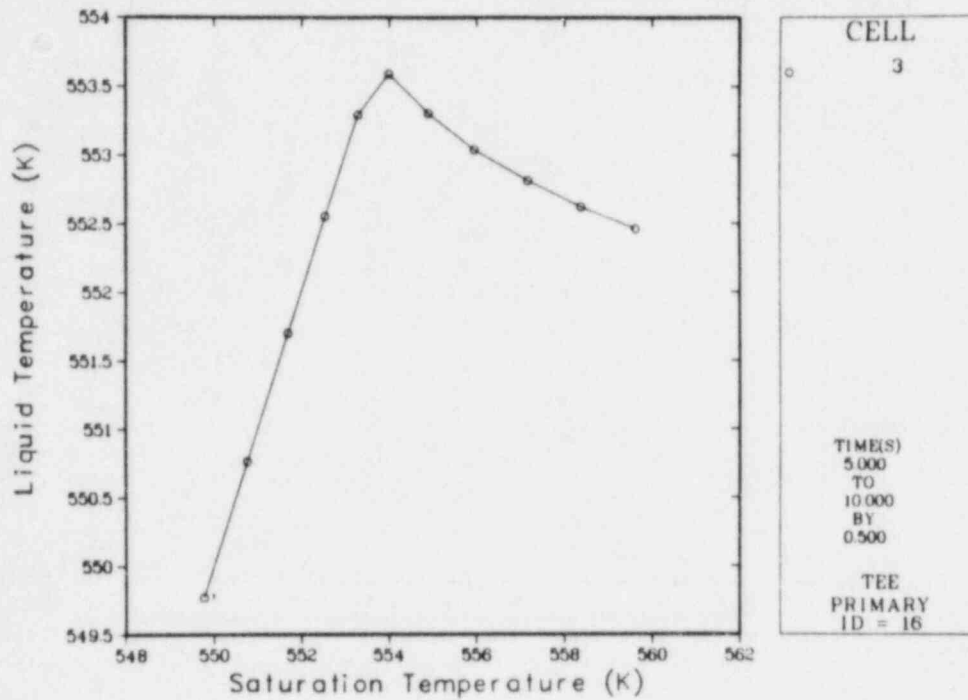


Fig. 190.

The calculated broken-loop cold-leg liquid vs the calculated saturation temperatures for LOFT L2-2.

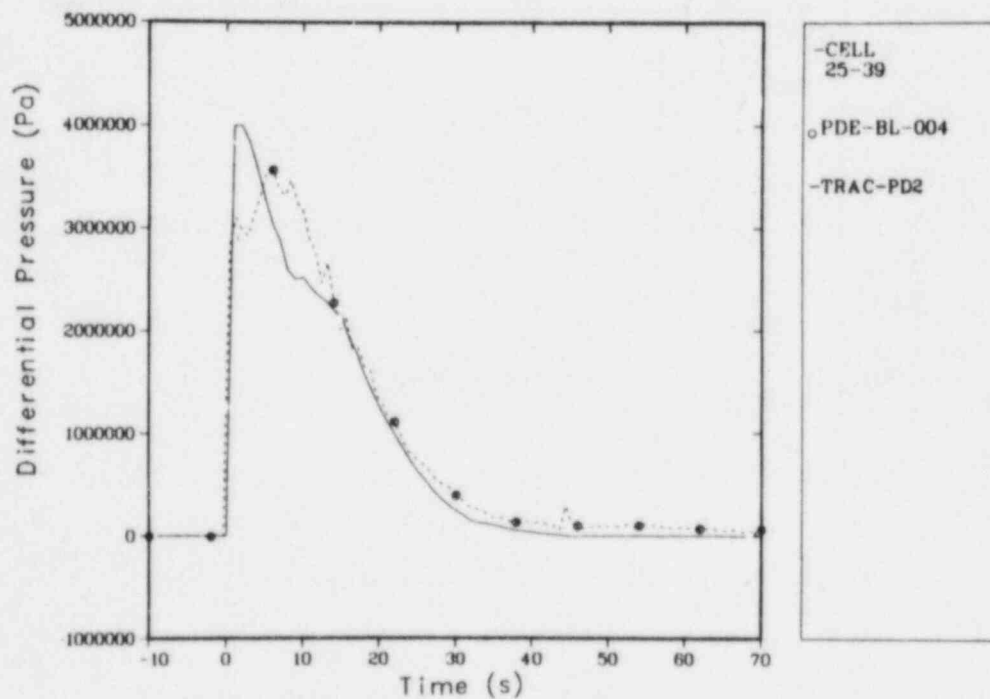


Fig. 191.

Comparison of the pressure differentials across the hot-leg break plane for LOFT L2-2.

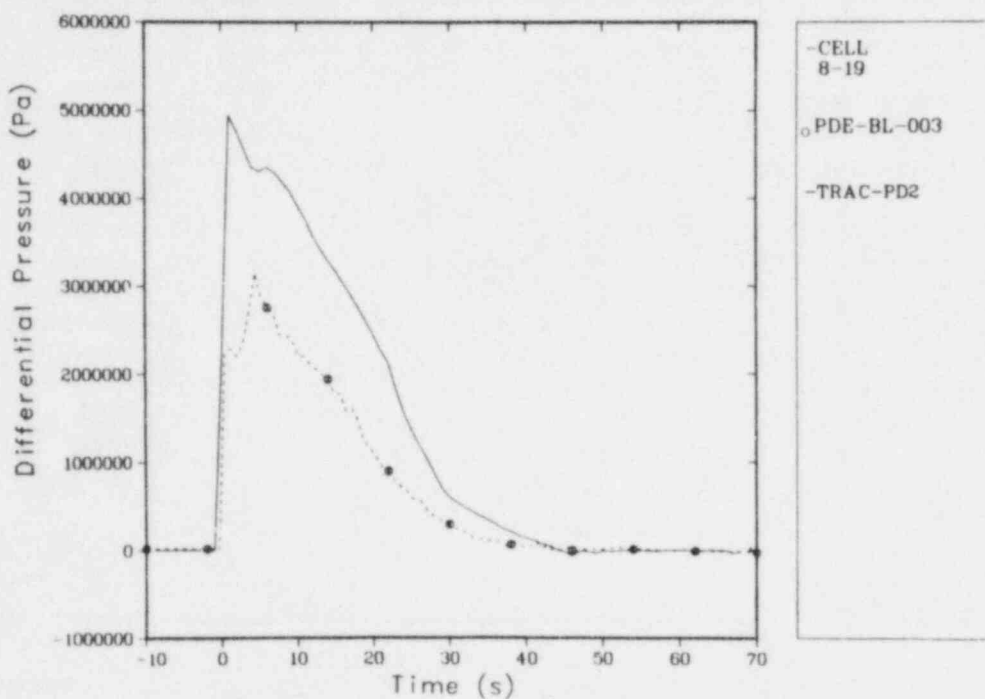


Fig. 192.

Comparison of the pressure differentials across the cold-leg break plane for LOFT L2-2.

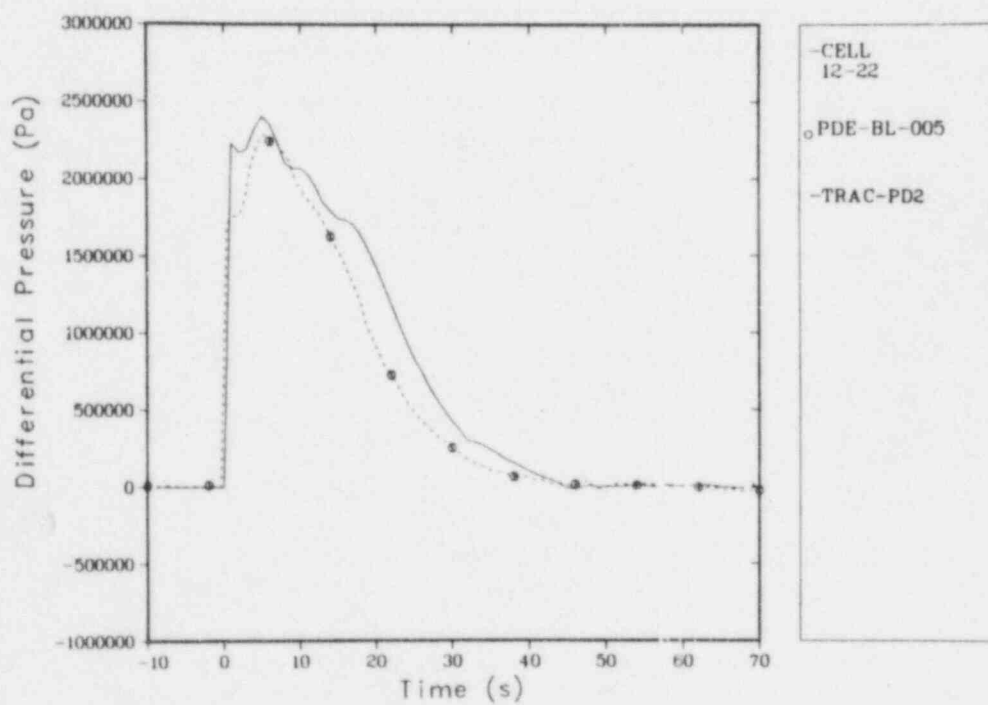


Fig. 193.

Comparison of the pressure differentials across the pump simulator for LOFT L2-2.

Figures 187-189 compare the broken-loop cold-leg conditions. Figure 187 shows ECC bypass in the calculated and measured broken-loop cold-leg mixture densities. The density spikes did not correlate well between the experiment and the calculation, but they showed similar behavior. The calculated broken-loop cold-leg mass flow (Fig. 188) agreed well with the measurement, except for the first 10 s of the transient. Figure 190 shows that this period corresponded to the subcooled critical flow at this location and that the fluid entering the broken-loop cold leg reached saturation at 8 s. During the period of subcooled critical flow, TRAC substantially underpredicted the mass flow because the code lacked an accurate bubble nucleation model.²⁶ Figures 191-193 compare the TRAC-calculated and the measured differential pressures in the broken loops. Agreement was excellent across the hot-leg break plane (Fig. 191) and across the pump simulator (Fig. 193); however, the pressure differential calculated across the cold-leg break plane was considerably below the measured value. In Fig. 188 this difference did not affect the mass flow rate beyond 10 s, because the flow was choked at this location even with the lower pressure differential. The error may have occurred because the modeling of the flow path downstream of the break plane did not reflect accurately the pressure tap location and the nozzle jet.

iv. Additional Calculated Results. To augment the comparisons with test data provided previously, we have included some interesting calculated results for which there were no comparable test data. Figures 194 and 195 show the calculated total liquid mass in the vessel and core, respectively. The vessel had not refilled completely at 70 s, because the cold liquid was more dense than the original liquid in the vessel; thus, the ultimate total mass would have been 2500 kg. We continued the TRAC calculation until 100 s, at which point liquid was still filling the vessel. Figure 195 shows the total liquid mass in the VESSEL core section. The liquid pulse at ~10 s caused the early fuel-rod quenching. This plot also displays the filling of the lower plenum (at ~50 s when the core mass began its abrupt increase) and the complete reflooding of the core (between 60 and 70 s when the mass became stable). Figures 196 and 197 display the total heat transfer to the fluid from the fuel rods and vessel structural material. In Fig. 196 the pulse at ~10 s resulted from the rod quenching associated with the liquid pulse in Fig. 195. The pulses at ~50 s corresponded to the final quenching of the core during reflood. The large nonphysical spikes (Fig. 197) resulted from the inadequate structural heat-transfer models (Sec. XII.C.2). Figure 198 shows the void fraction at each axial level within the core. Both the fluid pulse from Fig. 195 and the eventual reflooding of the core are more detailed in this figure.

b. Rod Temperature Results. To determine the correct fuel-rod geometry for this calculation, we performed a parametric study, which is discussed further in Sec. XIII.B. In this section we compare the TRAC-calculated and measured temperatures at the surface of the fuel-rod cladding and present some fluid results that affect the comparisons. The results discussed in this section were obtained from the base-case calculation performed with the optimum rod geometry.

The comparison of the TRAC-calculated and measured fuel-rod temperatures must be considered carefully. The data showed that local effects strongly influenced the temperature of the rods and caused wide variations in the measured temperatures. The TRAC calculations did not account for these local variations and, therefore, must be compared to a variety of data. Agreement or disagreement of the TRAC-calculated fuel-rod temperatures with specific data did not invalidate the calculation. Meaningful TRAC results existed only at a

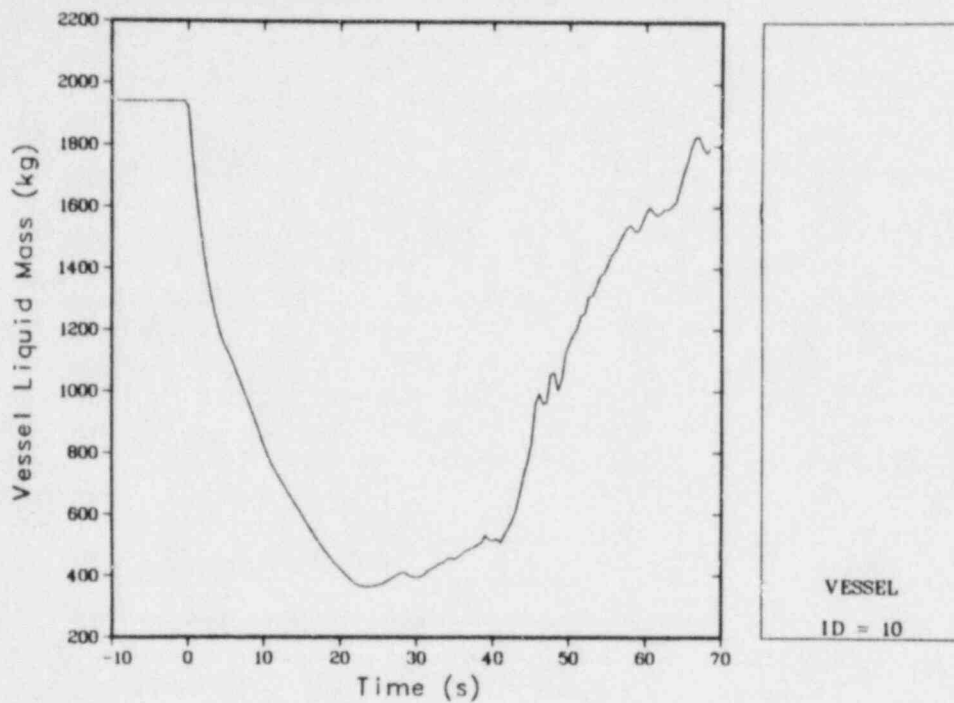


Fig. 194.
LOFT L2-2 calculated vessel liquid mass.

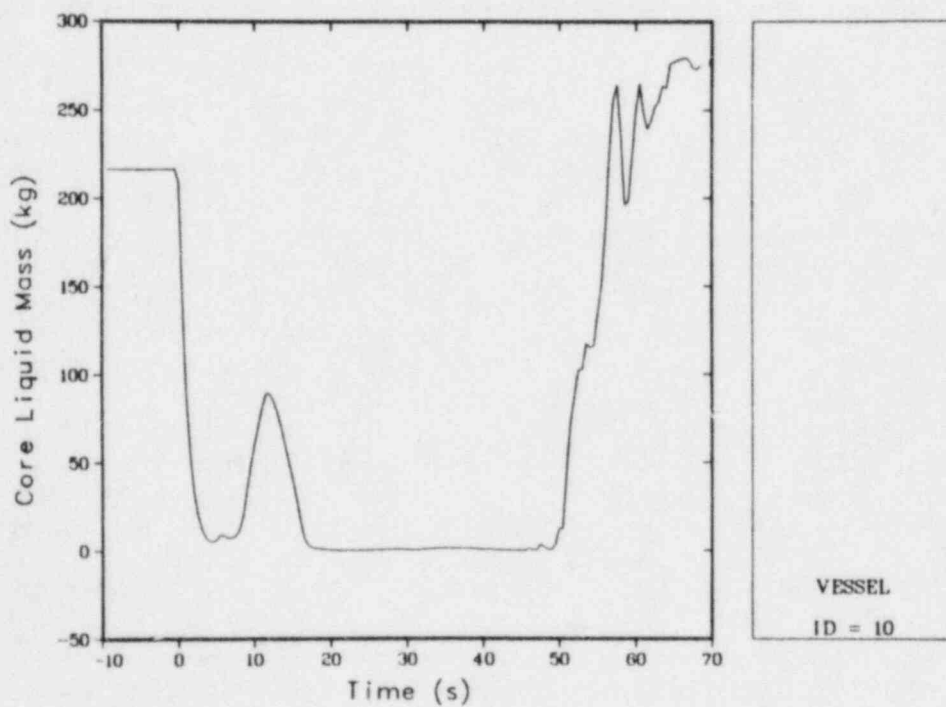


Fig. 195.
LOFT L2-2 calculated core liquid mass.

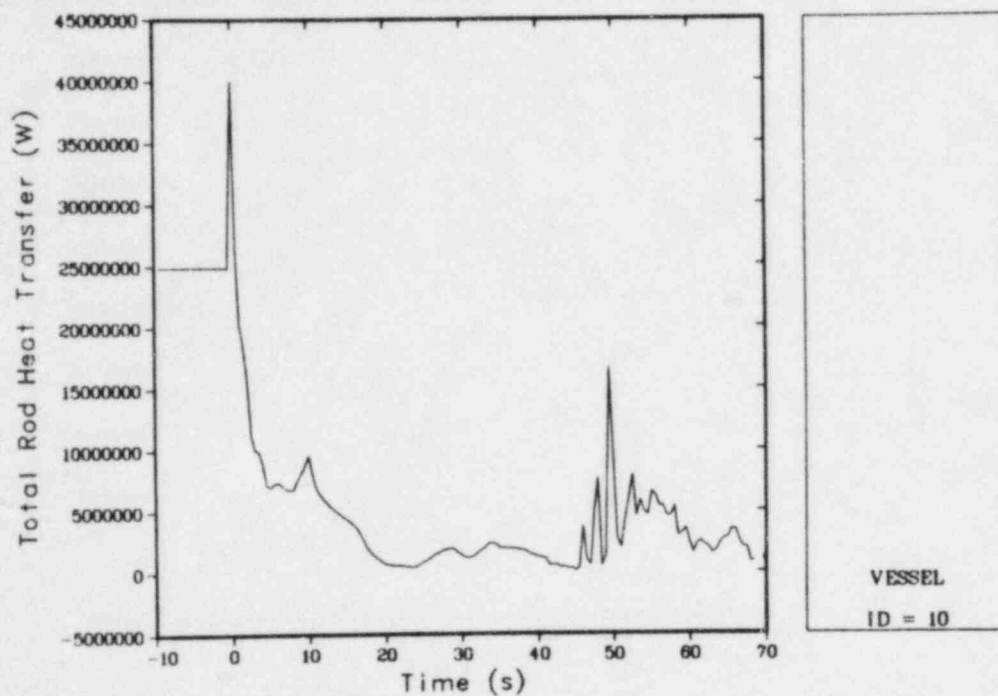


Fig. 196.
LOFT L2-2 calculated total rod heat transfer.

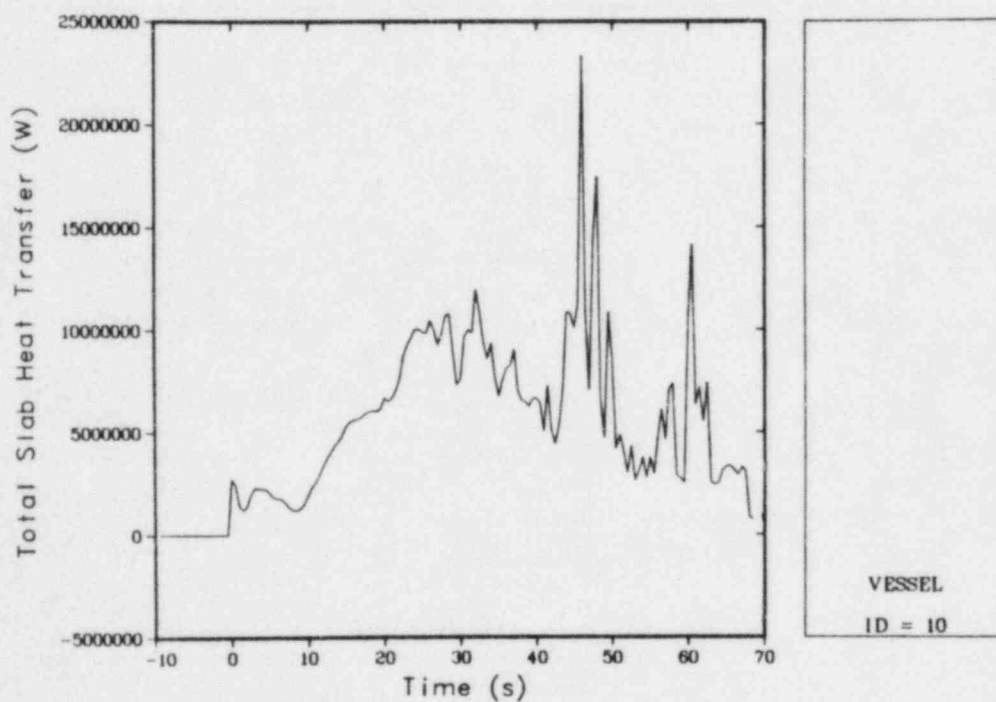


Fig. 197.
LOFT L2-2 calculated total slab heat transfer.

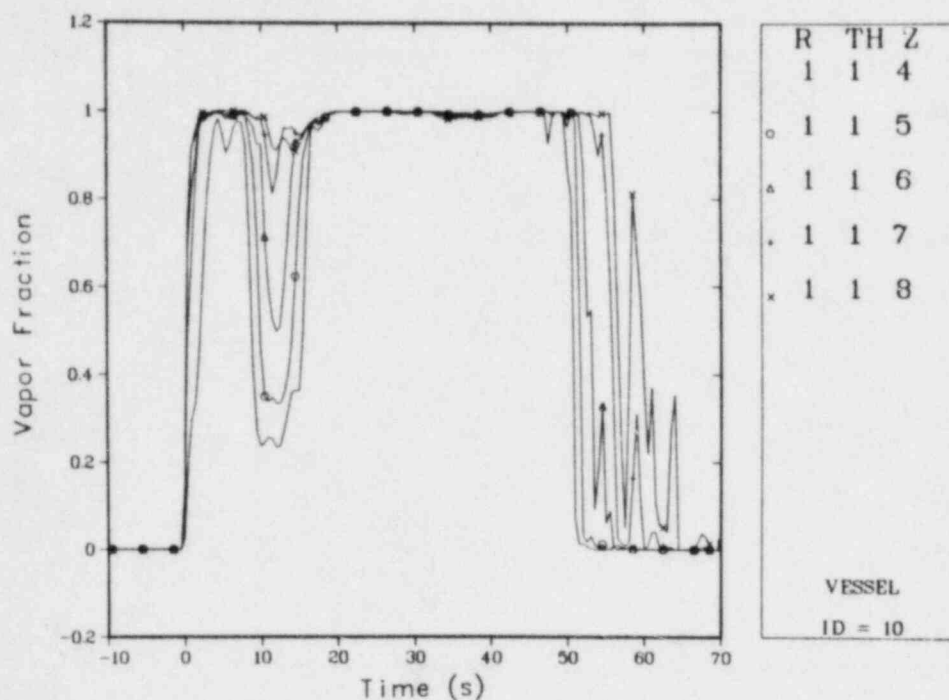


Fig. 198.
LOFT L2-2 calculated core vapor fractions.

few specific axial locations before the reflood portion of the calculation. To alleviate the misleading nature of the test results, we compared the measurements taken at nearby axial and horizontal points. Table XVII specifies the measurements by their group number and their TRAC-PD2 and measurement axial location. Separate plots compare the calculated results with the individual groups.

1. Central Fuel Module. Figures 199-205 compare the calculated and measured results for the central fuel module. Figure 199 compares the calculated cladding-surface temperatures at six axial locations for TRAC-PD2 fuel rod 1. Several important features are evident in this plot. The rod-surface temperature changed during the dryouts and rewets that occurred before the core reflood at ~50 s. These dryouts and rewets occurred simultaneously throughout the axial length of this rod, although the magnitude of the temperature excursions differed depending on the axial position. The variations in magnitude (Fig. 159) primarily resulted from the change in power along the rod. The calculation predicted the peak fuel-rod cladding-surface temperature during the blowdown phase, immediately before the first rewet; thus, the TRAC prediction agreed with the test data. Thereafter, the rod temperatures decreased regularly, with occasional increases caused by subsequent dryouts. Figure 200 compares the calculated rod-surface temperatures at the axial midplane for rods 1-4, 13, and 14. These were the only rods in the central radial zone represented in the calculation. Generally, these calculated results showed little azimuthal variation. The variations caused by the auxiliary-rod peaking factors were small. The results agreed between rods 1 and 13 and between rods 4 and 14; however, the two rods in the fourth azimuthal segment (rods 4 and 14) did not experience the second

TABLE XVII
FUEL-ROD TEMPERATURE MEASUREMENTS

<u>Group Number</u>	<u>TRAC-PD2 Axial Location</u>	<u>Rod^a</u>	<u>Measurement Axial Location</u>
1	2.14	5D6	2.14
		5D6	2.19
		5F4	2.14
2	2.14	5F8	2.09
		5F8	2.19
		5F9	2.14
3	2.14	5G6	2.14
		5H6	2.09
		5H6	2.19
4	2.14	5J7	2.14
		5J8	2.09
		5J8	2.19
5	2.14	5J4	2.14
		5L6	2.14
		5L6	2.19
6	1.65	5F9	1.66
		5G6	1.66
		5J7	1.66
7	2.95	5F9	2.95
		5G6	2.95
		5J7	2.95
8	2.14	1B11	2.09
		1B11	2.19
9	2.14	4E8	2.14
		4F8	2.19
10	2.14	4G14	2.14
		4F8	2.19
11	2.14	2E8	2.14
		2F8	2.09
		2F8	2.19
12	2.14	2G14	2.14
		2H14	2.09
		2H14	2.19

^aThe first digit of the rod identifier specifies the fuel module; the following letter and digit specify the rod row and column (Fig. 156).

TABLE XVII (cont.)

Group Number	TRAC-PD2 Axial Location	Rod ^a	Measurement Axial Location
13	2.14	3B11	2.09
14	2.14	6F8	2.09
		6F8	2.19
		6E8	2.14
15	2.14	6G14	2.14
		6H14	2.09
		6H14	2.19
16	2.03	2H3	2.04
		4H3	2.04
		6H3	2.04
		1F7	2.04
		3F7	2.04

^aThe first digit of the rod identifier specifies the fuel module; the following letter and digit specify the rod row and column (Fig. 156).

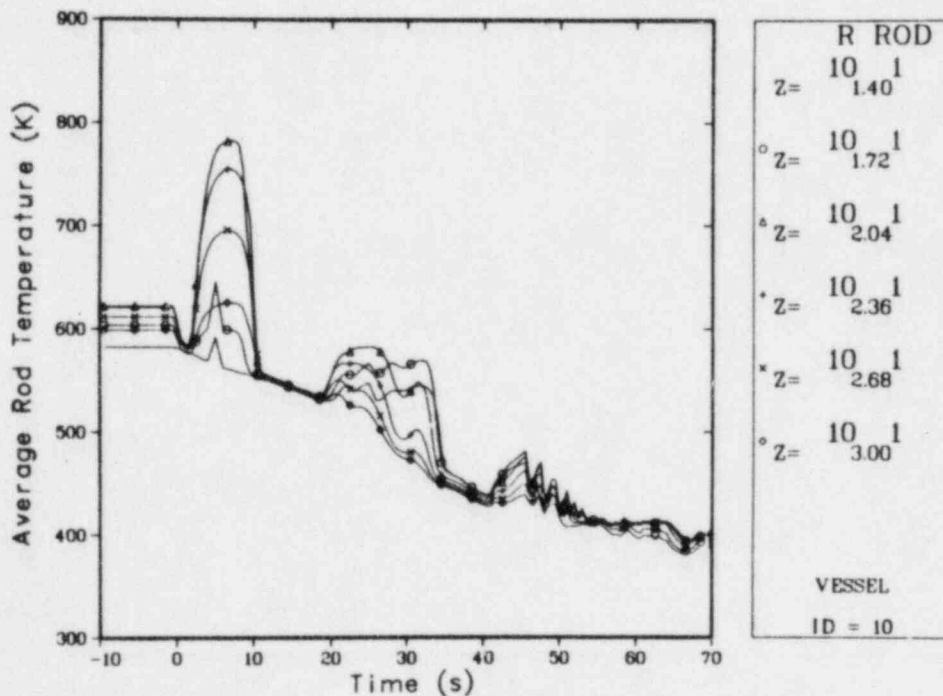


Fig. 199.

Axial comparison of the calculated central-rod cladding-surface temperatures for LOFT L2-2.

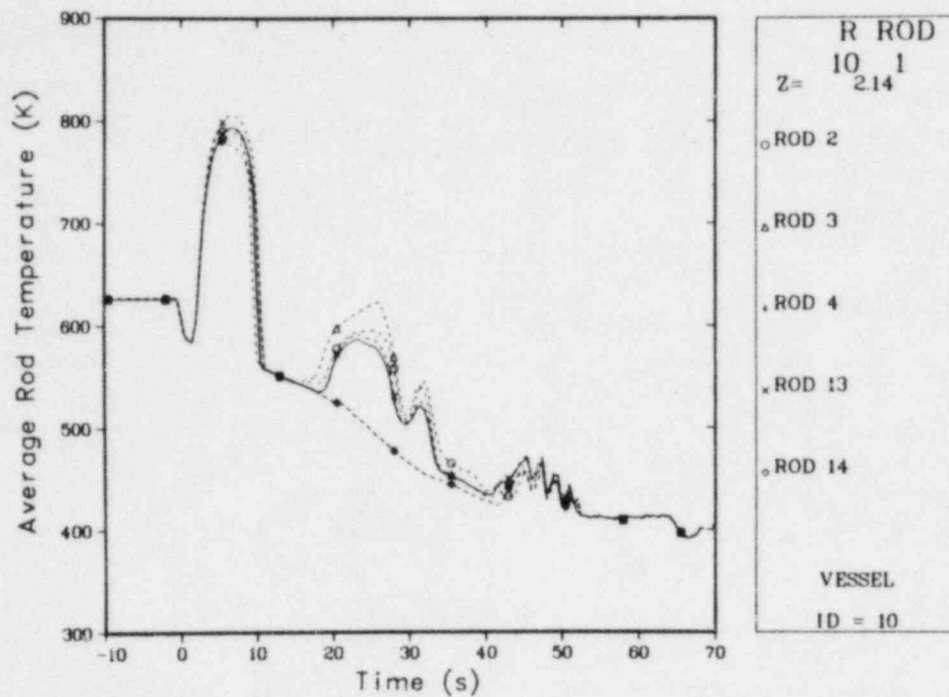


Fig. 200.

Azimuthal comparison of the calculated central-rod midplane cladding-surface temperatures for LOFT L2-2.

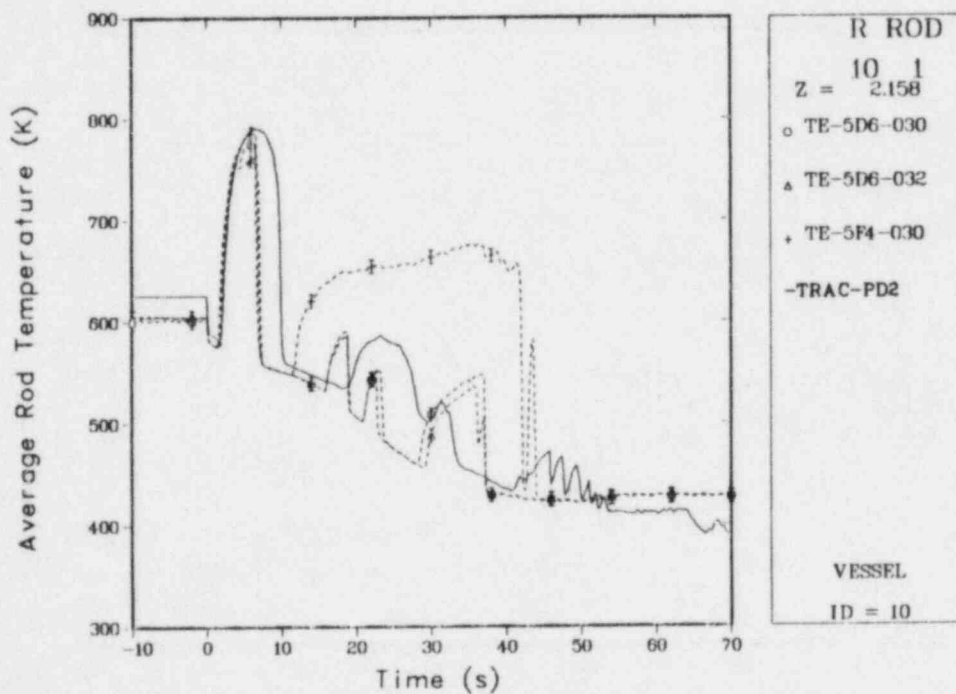


Fig. 201.

Comparison of the calculated central-rod midplane cladding-surface temperatures and group 1 data for LOFT L2-2.

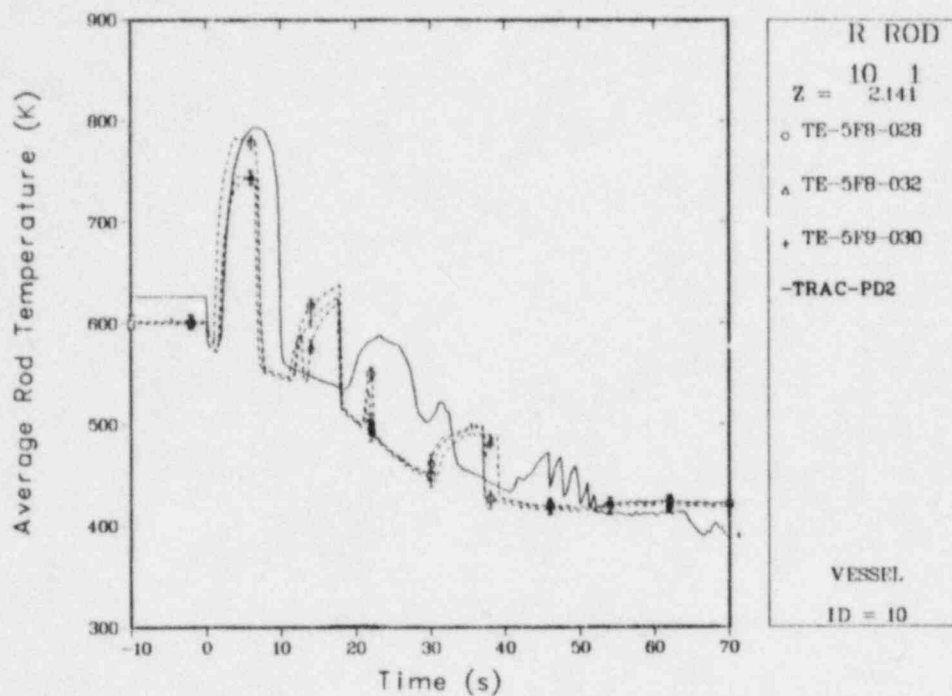


Fig. 202.

Comparison of the calculated central-rod midplane cladding-surface temperatures and group 2 data for LOFT L2-2.

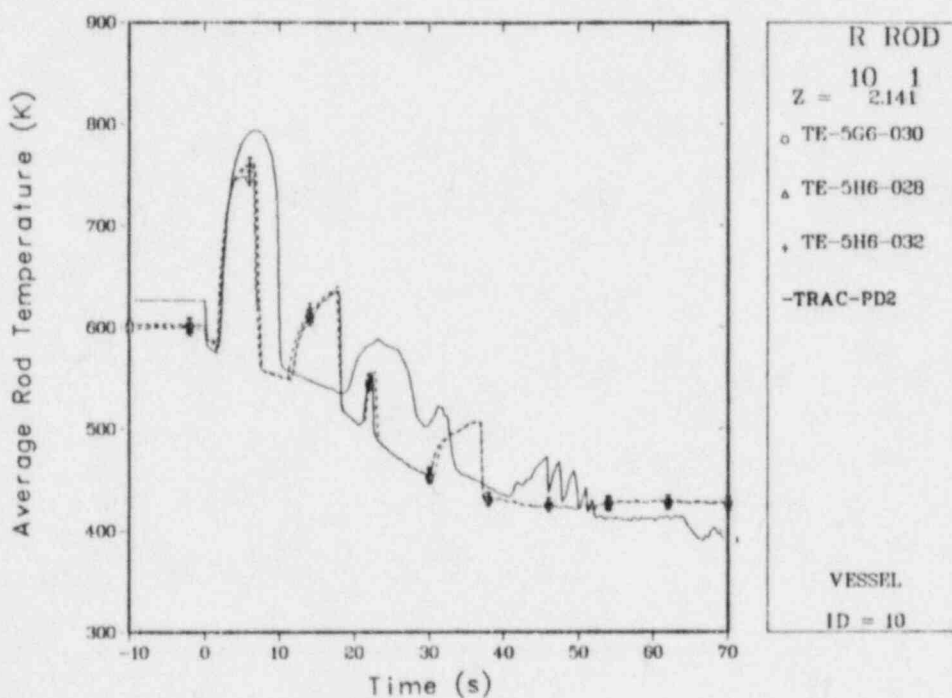


Fig. 203.

Comparison of the calculated central-rod midplane cladding-surface temperatures and group 3 data for LOFT L2-2.

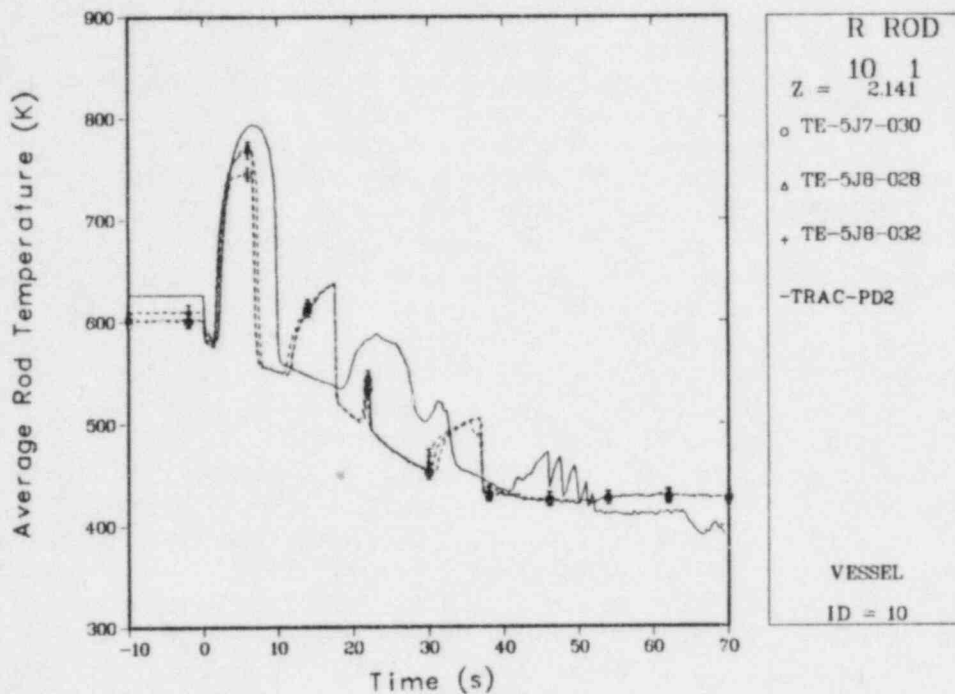


Fig. 204.

Comparison of the calculated central-rod midplane cladding-surface temperatures and group 4 data for LOFT L2-2.

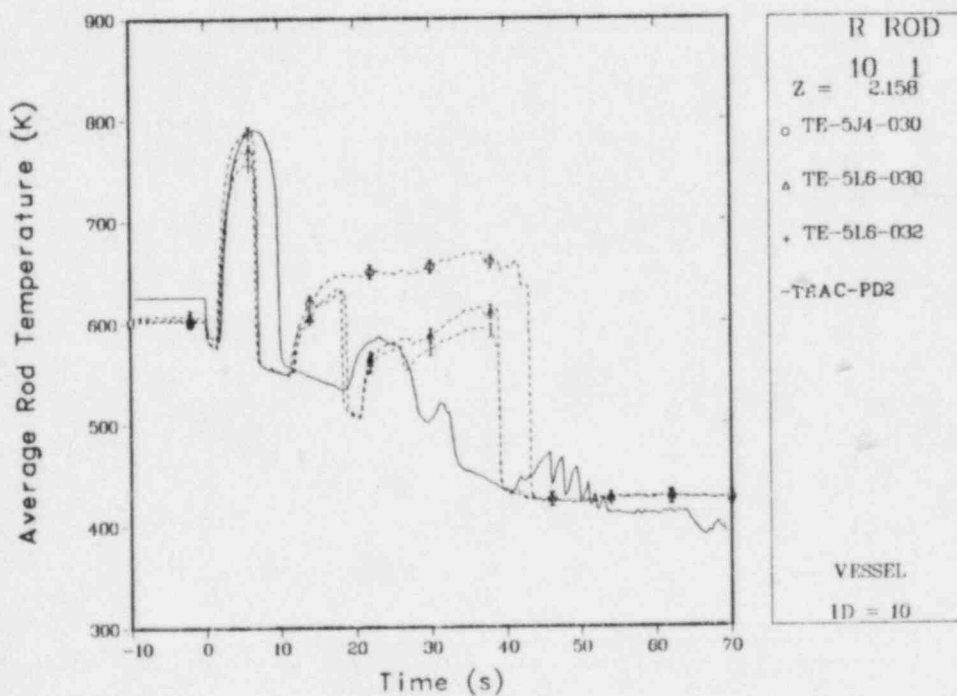


Fig. 205.

Comparison of the calculated central-rod midplane cladding-surface temperatures and group 5 data for LOFT L2-2.

dryout because the flow out of the adjacent broken-loop hot leg decreased the void fraction in azimuthal region 4 (Fig. 206).

Figures 201-205 compare the calculated results for rod 1 with the test data from groups 1-5. The wide variations in the test data were attributed to local effects (for example, adjacent rod power, grid spacer locations, local fluid conditions). Some general trends were apparent. The dryouts and rewets occurred similarly in the calculation and the data. The first rewet and subsequent dryouts and rewets occurred later in the calculation than in the data. Figure 198 shows the cause of the first rewet. The decrease in vapor fraction during the interval 8-18 s was caused by the liquid surging from the downcomer through the lower plenum and up into the core region. This surge was caused by the relative magnitudes of the intact- and broken-loop cold-leg mass flows and by flashing of liquid in the downcomer and lower plenum. We found that the pressure differential across the vessel diminished when the cold-leg temperature saturated at ~8 s (Fig. 190) because the system pressure decreased. The calculated saturation was delayed because of the reduced broken-loop cold-leg mass flow, which we ascribed to the inadequate subcooled critical-flow model.

Figures 207-210 compare the rod cladding-surface temperatures at axial levels below and above the midplane. These results were similar to those obtained at the midplane. However, low in the core, the code calculated a delayed DNB, which seemed to coincide with a delayed loss of fluid from the bottom level of the core (Fig. 198). Again, this discrepancy probably was caused by the reduced broken-loop cold-leg mass flow. The comparatively small computed temperature increases probably were caused by the inadequate TRAC fuel-rod model. The initial stored energy in the fuel rods was critical in

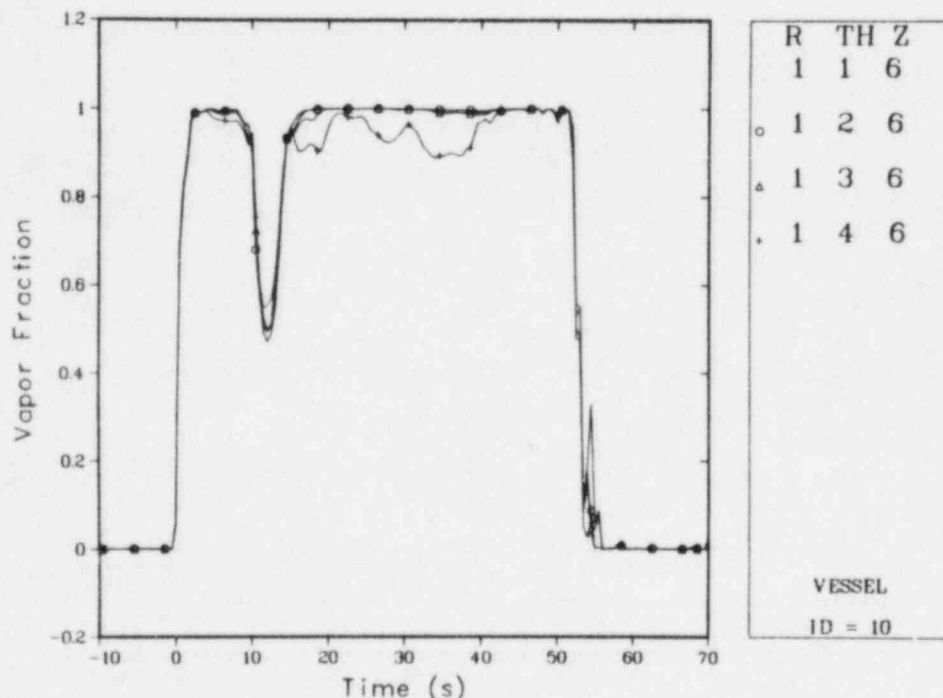


Fig. 206.

Comparison of the calculated vessel void fractions for LOFT L2-2.

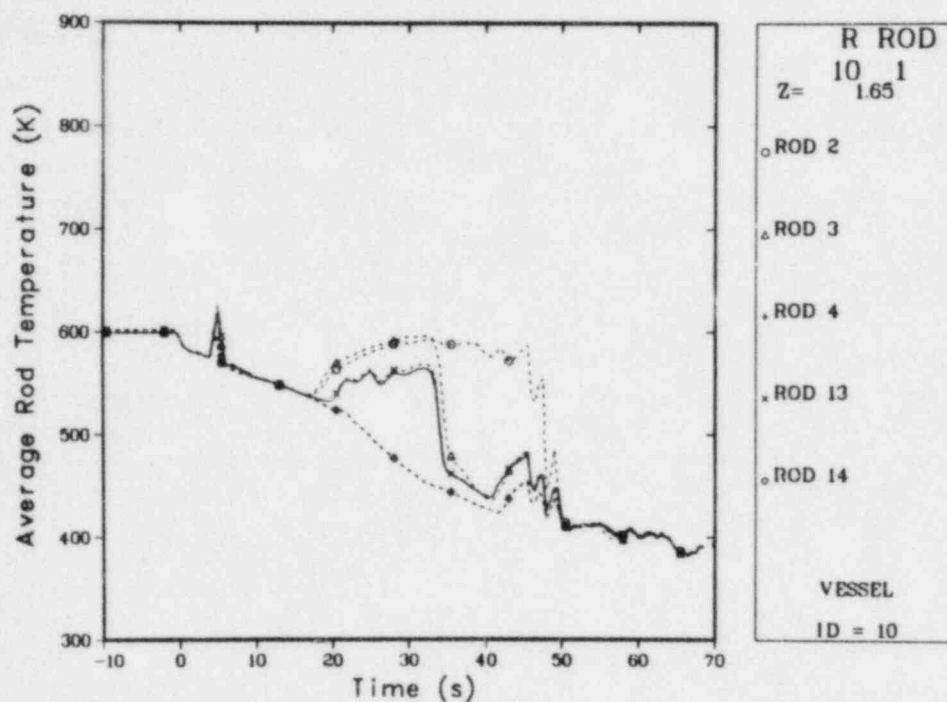


Fig. 207.

Azimuthal comparison of the calculated central-rod low-plane cladding-surface temperatures for LOFT L2-2.

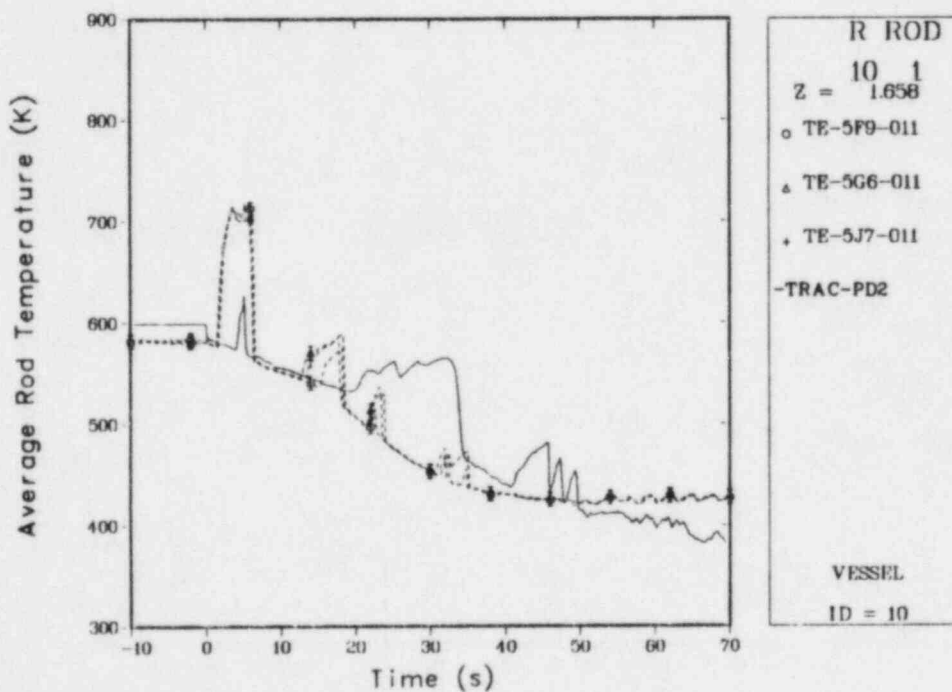


Fig. 208.

Comparison of the calculated central-rod low-plane cladding-surface temperatures and the group 6 data for LOFT L2-2.

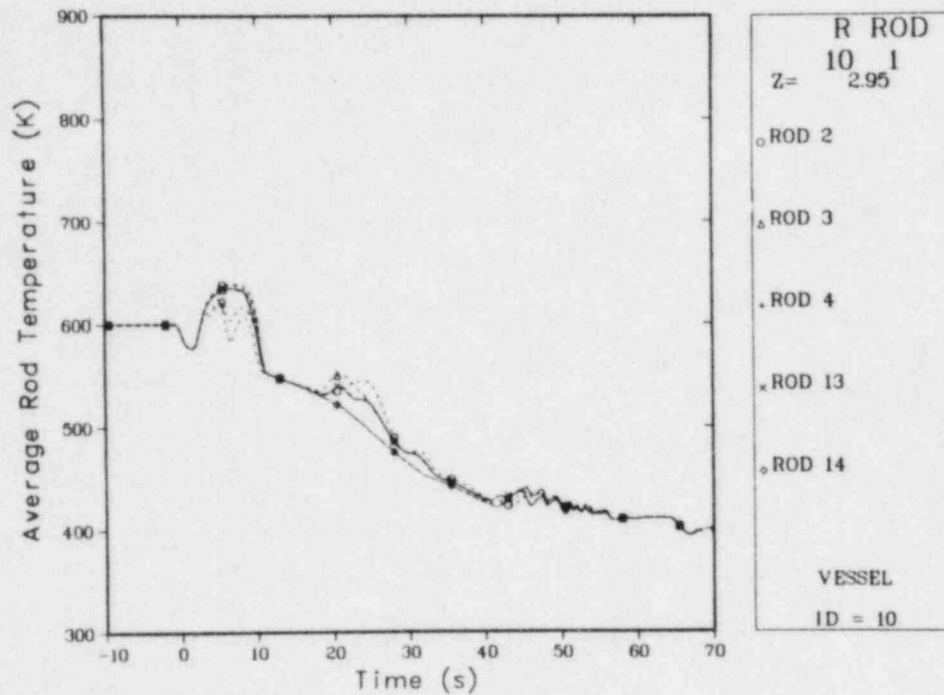


Fig. 209.

Azimuthal comparison of the calculated central-rod high-plane cladding-surface temperatures for LOFT L2-2.

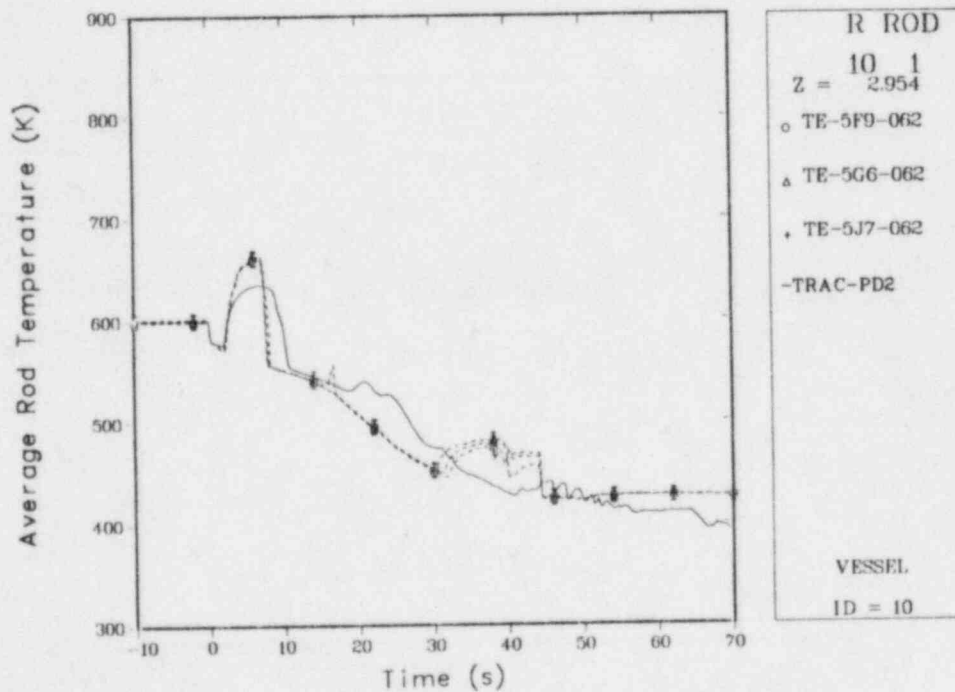


Fig. 210.

Comparison of the calculated central-rod high-plane cladding-surface temperatures and the group 7 data for LOFT L2-2.

determining the magnitude of the first rod-temperature maximum. Unfortunately, the TRAC-PD2 fuel-rod model did not permit axial variation of the fuel-cladding gap size. Therefore, it was impossible to predict accurately the maximum cladding temperature along the entire length of the fuel rods. We chose to match the midplane temperature in the base-case calculation, which resulted in low temperatures above and below that location.

ii. Second Radial Zone. Figures 211-219 compare the calculated and test results at the axial midplane of rods in the second TRAC radial zone of the core (Fig. 157). Figure 211 compares the calculated results for the four average rods and the one hot rod in the second radial zone. Again, the rod in the fourth azimuthal zone behaved differently from the others. The comparisons between the data and the calculations in Figs. 212-219 agreed better than those in the central module. The first calculated rewet occurred earlier in the second ring than in the first, in good agreement with the data, and the timing of the second dryout and rewet was better in the second zone.

Figures 220 and 221 compare the calculated and measured rod cladding-surface temperatures in the outermost radial core ring. The results were similar to those for the second radial ring.

D. Parametric Studies

Before Test L2-2, the LOFT facility had been operated at power for long periods of time. This type of operation modifies the state of the fuel rods by cracking and relocating the fuel. Reasonable modifications to the TRAC fuel-rod description can cause significant changes in the energy stored in the fuel rods before the transient begins and, thus, can cause large differences in the

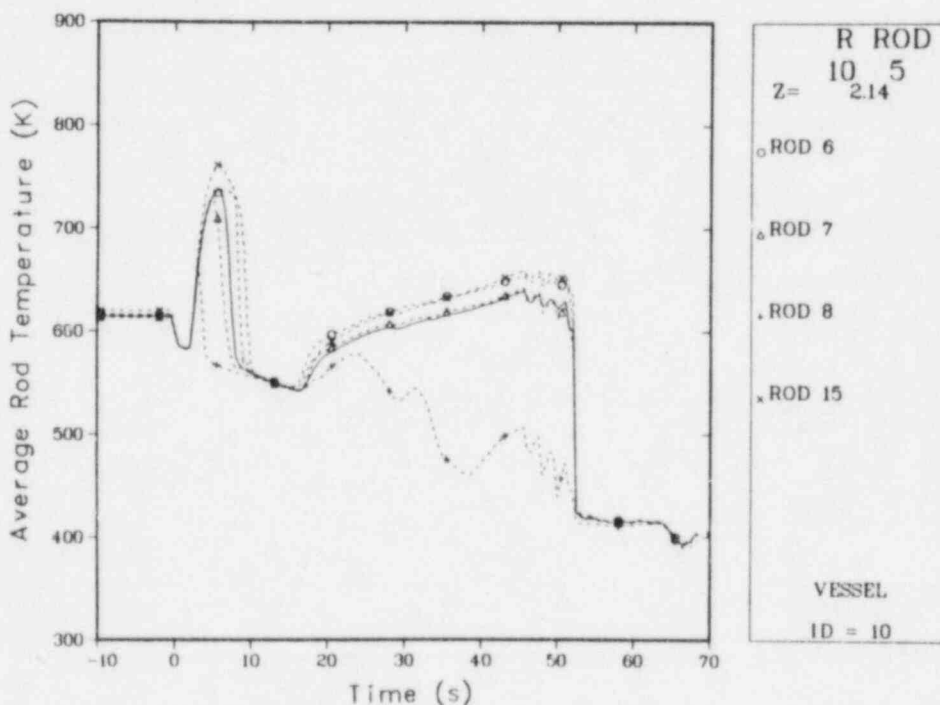


Fig. 211.

Comparison of the calculated second radial-zone midplane cladding-surface temperatures for LOFT L2-2.

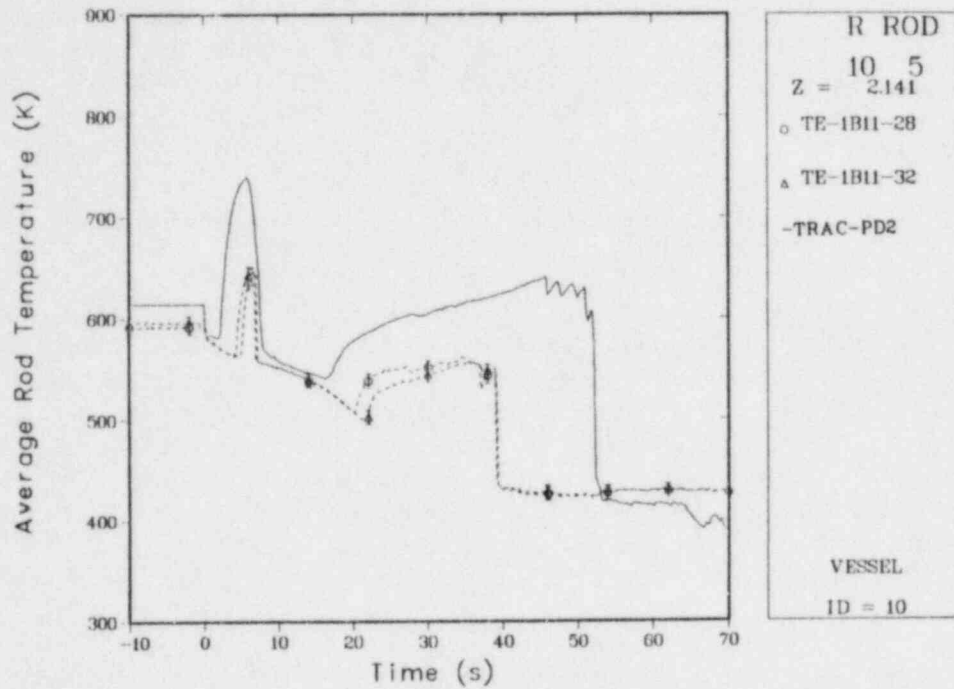


Fig. 212.

Comparison of the calculated second radial-zone midplane cladding-surface temperatures and group 8 data for LOFT L2-2.

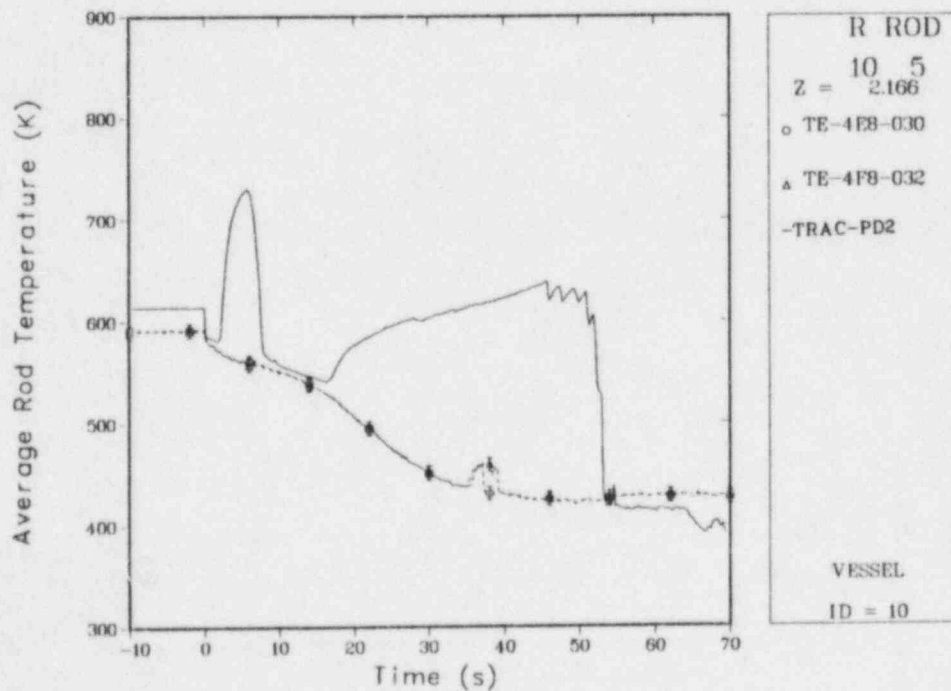


Fig. 213.

Comparison of the calculated second radial-zone midplane cladding-surface temperatures and group 9 data for LOFT L2-2.

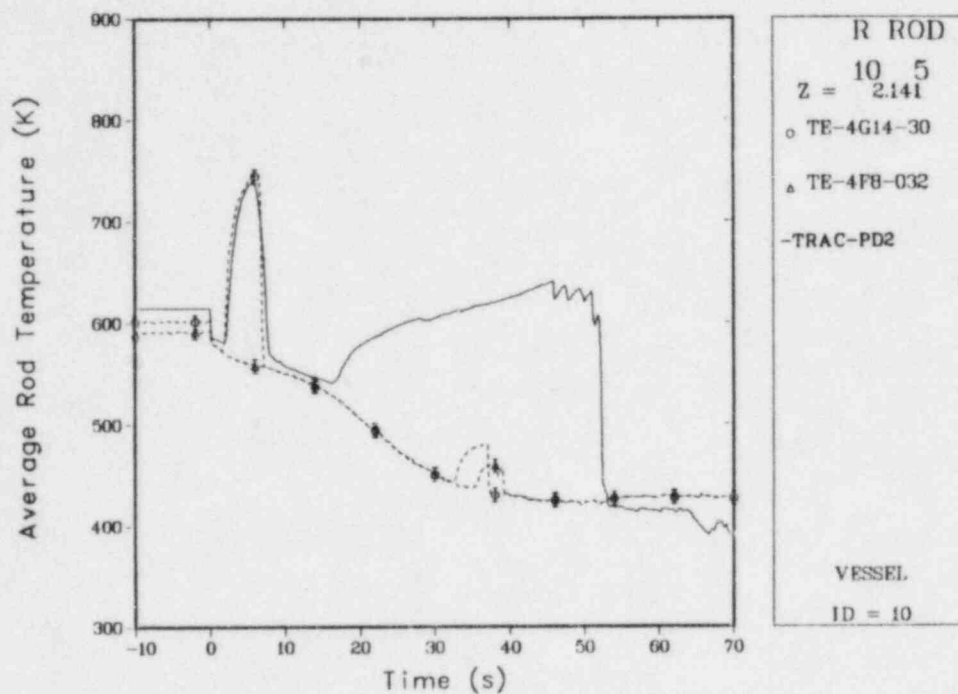


Fig. 214.

Comparison of the calculated second radial-zone midplane cladding-surface temperatures and group 10 data for LOFT L2-2.

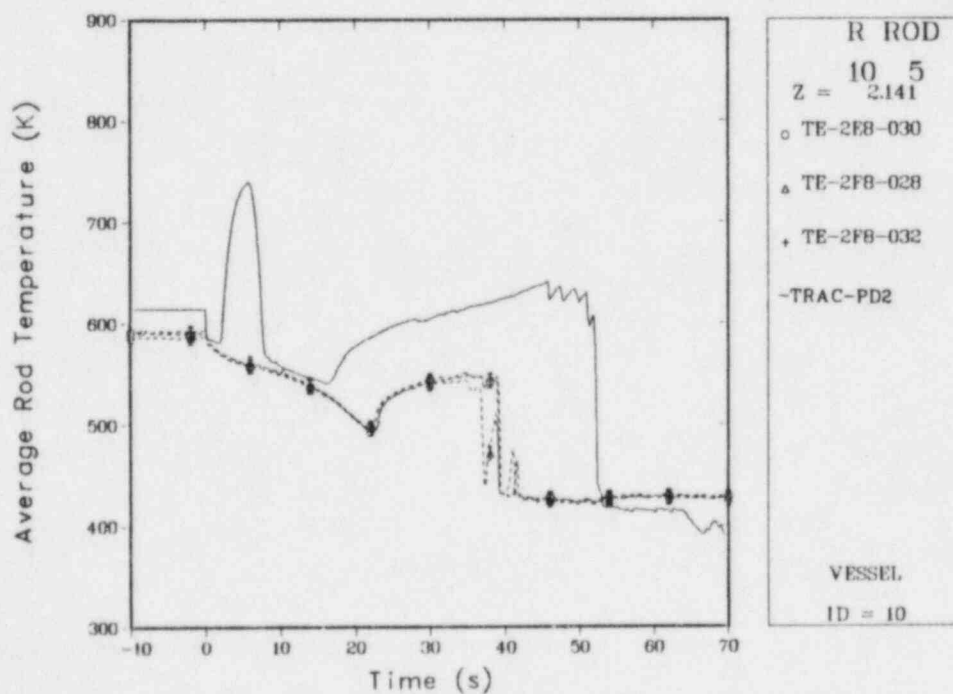


Fig. 215.

Comparison of the calculated second radial-zone midplane cladding-surface temperatures and group 11 data for LOFT L2-2.

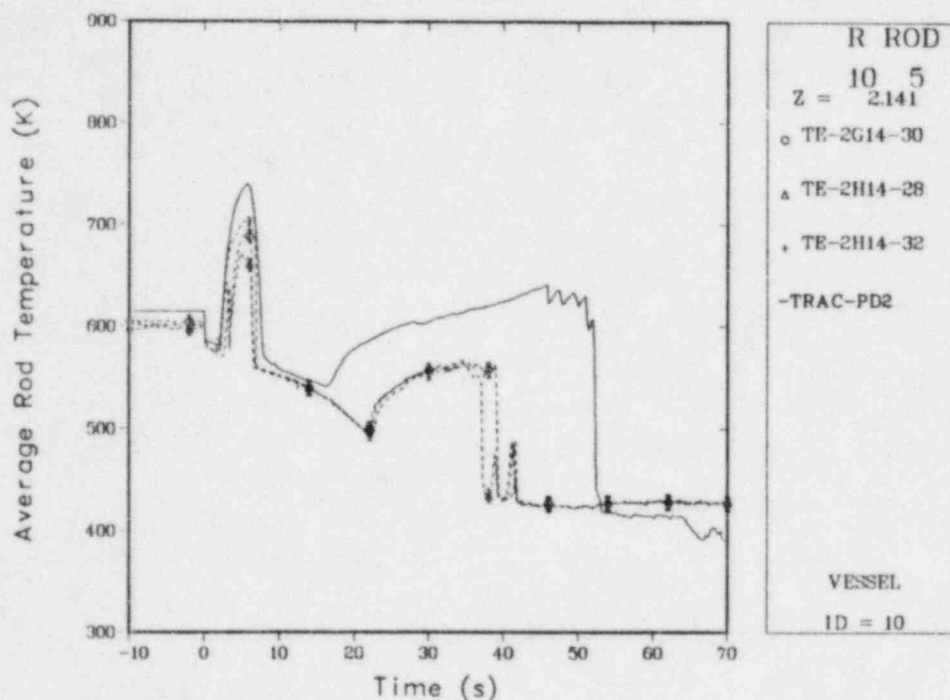


Fig. 216.

Comparison of the calculated second radial-zone midplane cladding-surface temperatures and group 12 data for LOFT L2-2.

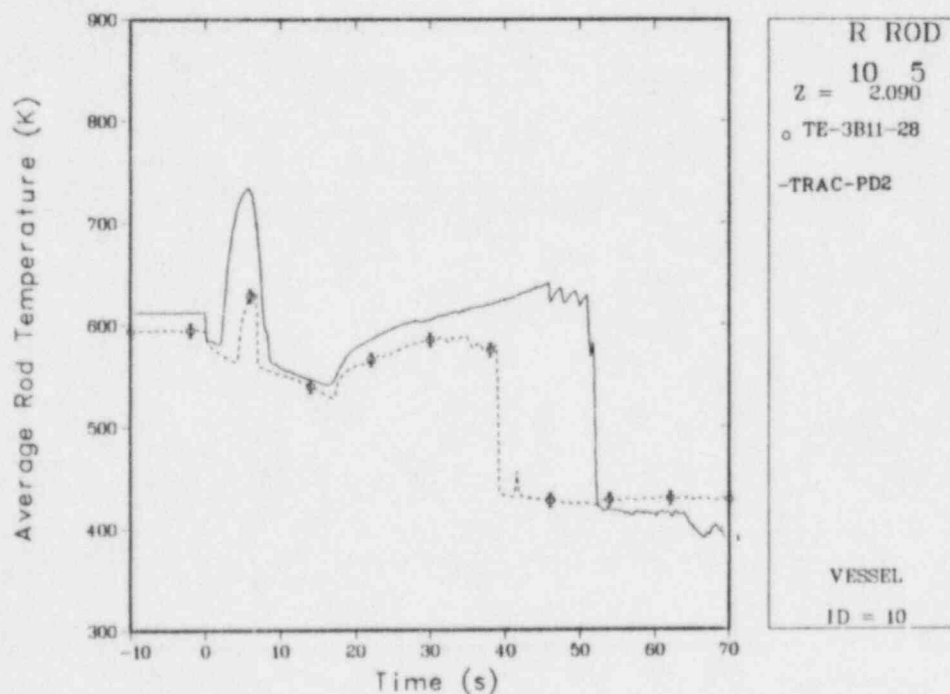


Fig. 217.

Comparison of the calculated second radial-zone midplane cladding-surface temperatures and group 13 data for LOFT L2-2.

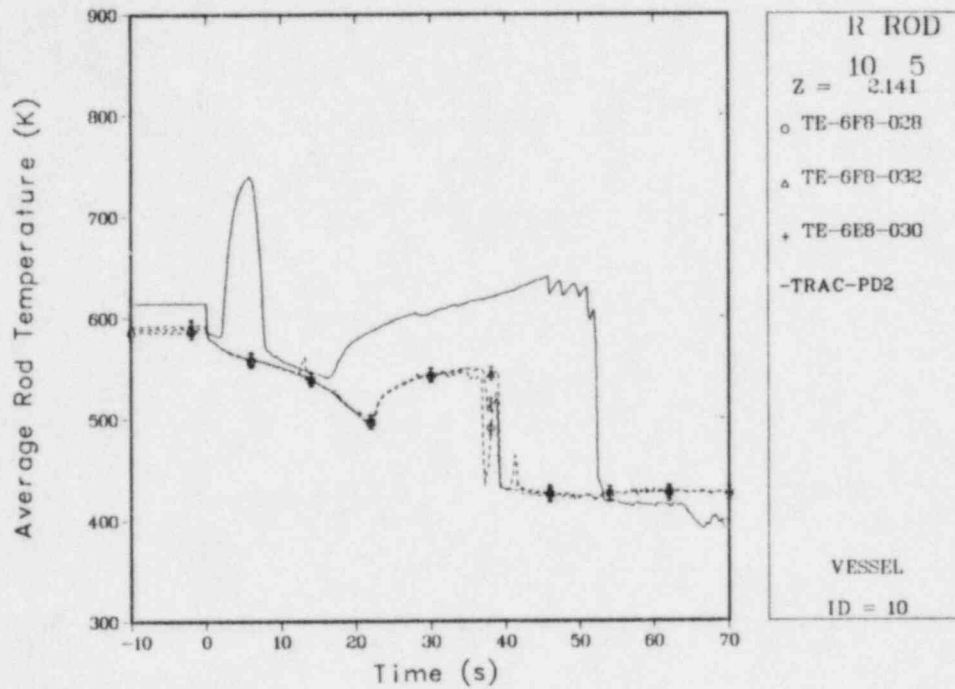


Fig. 218.

Comparison of the calculated second radial-zone midplane cladding-surface temperatures and group 14 data for LOFT L2-2.

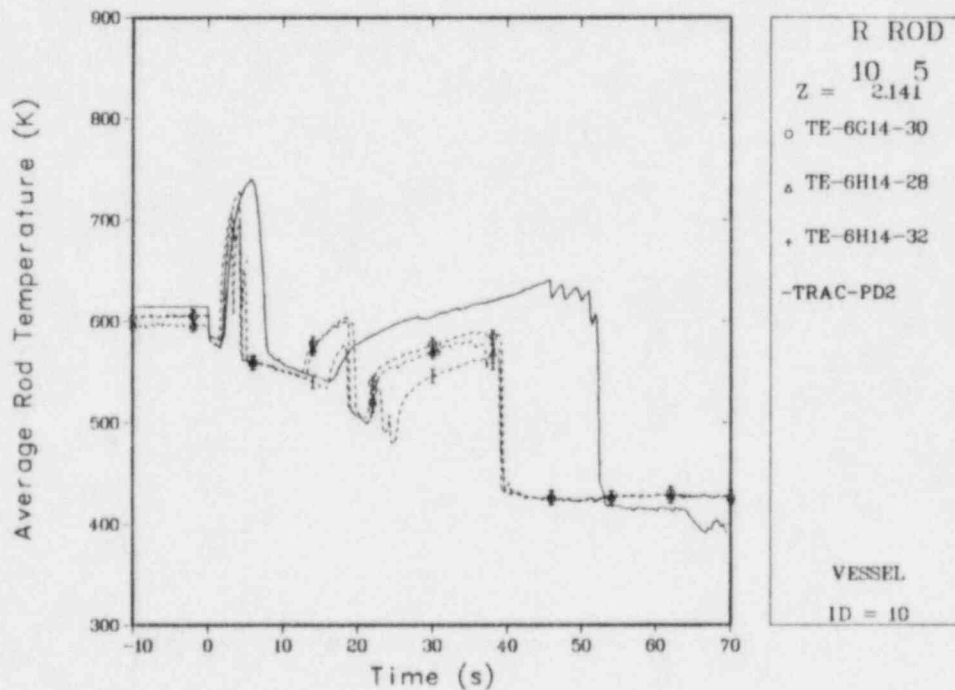


Fig. 219.

Comparison of the calculated second radial-zone midplane cladding-surface temperatures and group 15 data for LOFT L2-2.

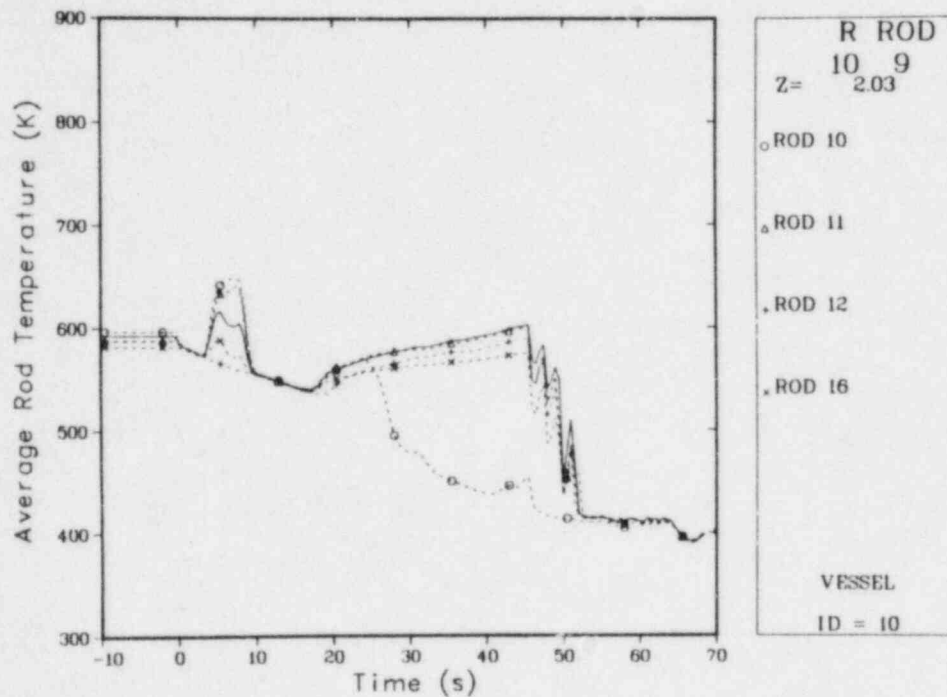


Fig. 220.

Azimuthal comparison of calculated outer radial-zone midplane cladding-surface temperatures for LOFT L2-2.

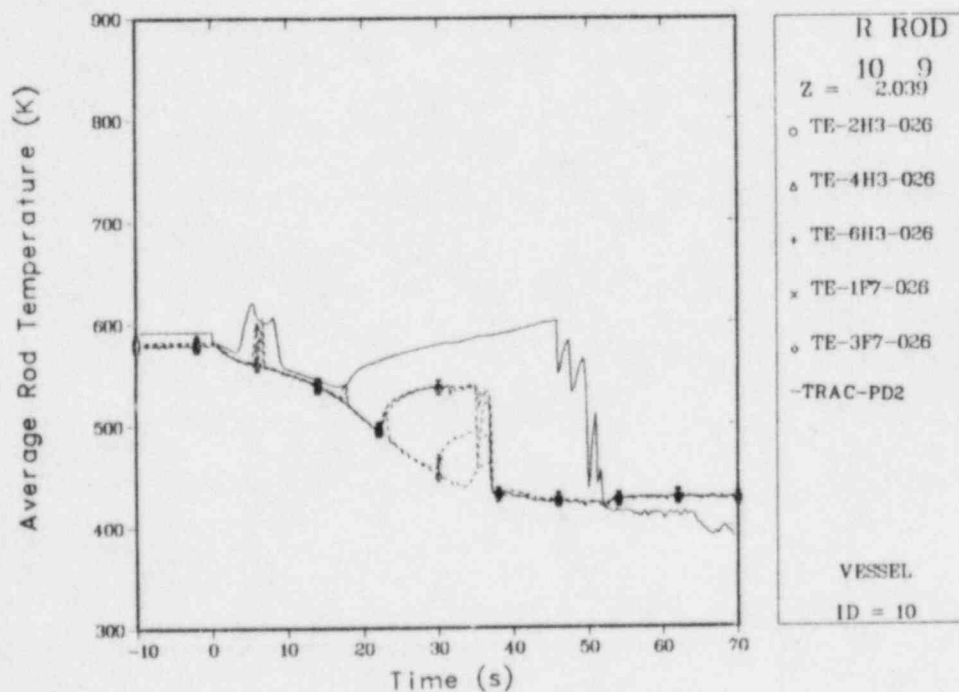


Fig. 221.

Comparison of calculated outer radial-zone midplane cladding-surface temperatures and group 16 data for LOFT L2-2.

maximum cladding temperature. This result agreed with the previously published results.^{27,28} Unfortunately, we did not know the state of the fuel rods because they were sealed within the test vessel, nor did we know the initial fuel stored energy because thermocouples were located only on the outer cladding-surface in LOFT. Therefore, we conducted a study of four fuel-rod descriptions to choose the optimum for the TRAC-PD2 base-case calculation.

In this report we discuss only four of the rod descriptions that we investigated. Table XVIII lists these models. Three models used the capabilities of the standard TRAC-PD2 program. The fourth required a simple modification to the code itself. In the first three models, the location of the fuel-pellet surface differed. Model 1 placed the fuel-pellet surface at the location required in the LOFT fuel-rod manufacturing specifications; thus, it had a 0.0953-mm fuel-cladding gap. The second model arbitrarily set the gap dimension to 0.0796 mm and the third, to 0.0002 mm. A FRAPCON-1 (Ref. 29) calculation was the basis for determining the size of the third model. INEL personnel developed the FRAPCON-1 code* to simulate the behavior of fuel rods during operational power transients. We used a calculation that followed the LOFT power history up to the initiation of Test L2-2. As we examined the results of the FRAPCON-1 calculation, we noticed another effect, the variation of the fuel conductivity, which strongly influenced the initial rod stored energy. Because TRAC-PD2 evaluated metal conductivities from MATPRO³⁰ without accounting for cracking, we had to modify the code to adjust for this change in the fuel. The fourth calculation was performed with the fuel conductivity corrected to 74% of its theoretical value and with a 0.0002-mm gap; thus, these parameters agreed with those in the FRAPCON-1 calculation.

Figures 222-224 compare the calculated pressures, mass flows, and void fractions in the intact-loop cold leg for the four models. The results were essentially identical, indicating that the fuel-rod description did not affect the hydraulic response of the calculation.

Table XVIII compares the calculated steady-state gap conductance for the four calculations at the midplane of rod 1 with the FRAPCON-1 results. Figure 225 shows the radial temperature distribution calculated at the same spot. Case 4, which used the corrected conductivity and a 0.0002-m gap, agreed better with the FRAPCON-1 results than cases 1-3. Figure 226 compares the four calculated transient responses of the fuel-rod surface at the axial midplane of rod 1 with some typical data for this location. As we expected, the model using the FRAPCON-1 conditions gave the best overall agreement with the data. Because this model required a modified code, it could not be used as the base case for the TRAC-PD2 developmental assessment. Therefore, we chose the 0.0796-mm gap model for our base-case calculation.

However, Figs. 208 and 210 show that this gap did not give good results below or above the midplane. This conclusion was reasonable because the fuel power history at these locations differed from that at the midplane. Because TRAC-PD2 did not allow for axial changes in the fuel-rod geometry, we had to choose which of the three gap sizes to apply uniformly. Because the peak cladding temperature occurred at the midplane, we felt that it was most important to match the fuel-rod conditions there. Similarly, the fuel rods located outside of module 5 experienced a different history from the central rods. Again, TRAC-PD2 did not permit variation of fuel-rod geometry from rod

*W. Driscoll and G. Berna of INEL provided copies of FRAPCON-1 and the FRAPCON LOFT input deck. The input format for FRAPCON-1 is given in Ref. 29.

TABLE XVIII

LOFT L2-2 FUEL-ROD MODELS FOR SENSITIVITY STUDY

Model	Outside Fuel Pellet Radius (mm)	Gap Width (mm)	Conductance Gap ($W \cdot m^{-2} \cdot K^{-1}$)	Fuel Conductivity Factor
1	4.6469	0.0953	3926	1.0
2	4.6626	0.0796	4741	1.0
3	4.7420	0.0002	28370	1.0
4	4.7420	0.0002	28370	0.74
FRAPCON	--	--	37000	0.74

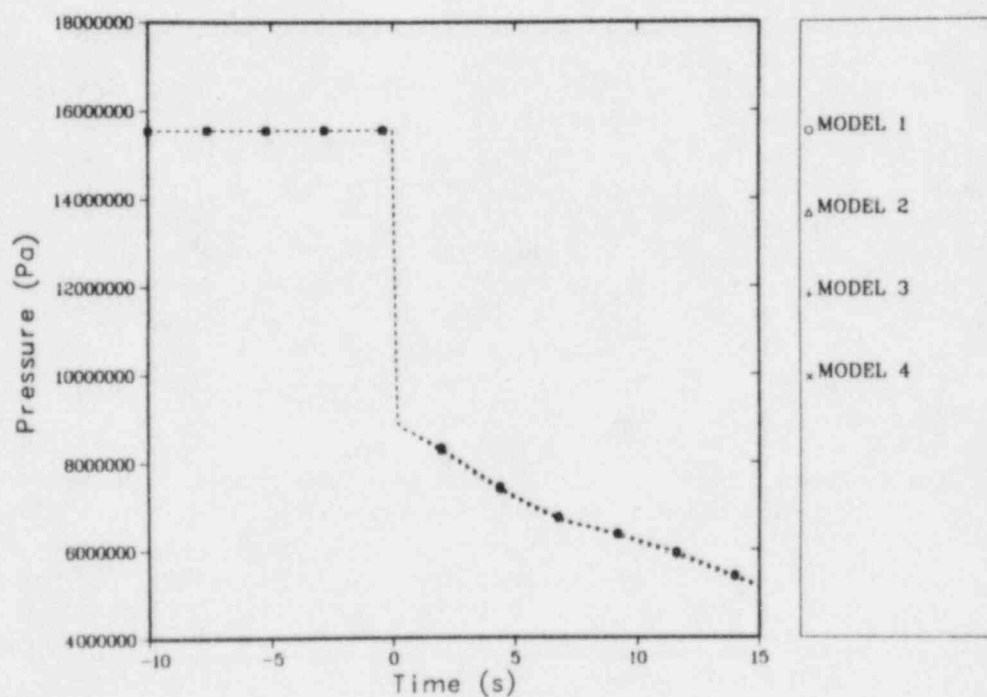


Fig. 222.
LOFT L2-2 parametric-study pressures.

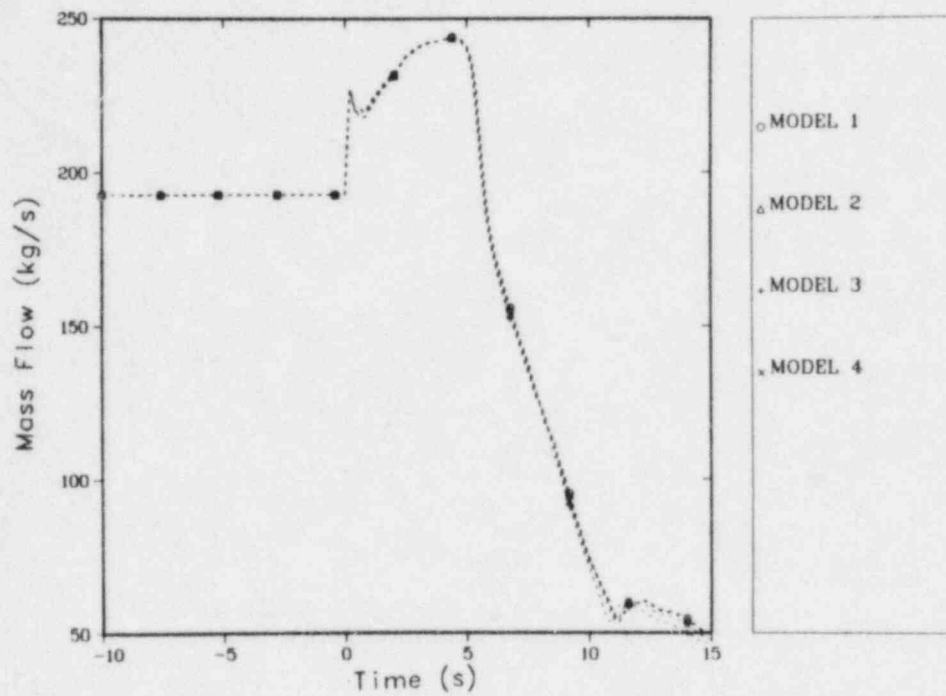


Fig. 223.
LOFT L2-2 parametric-study mass flows.

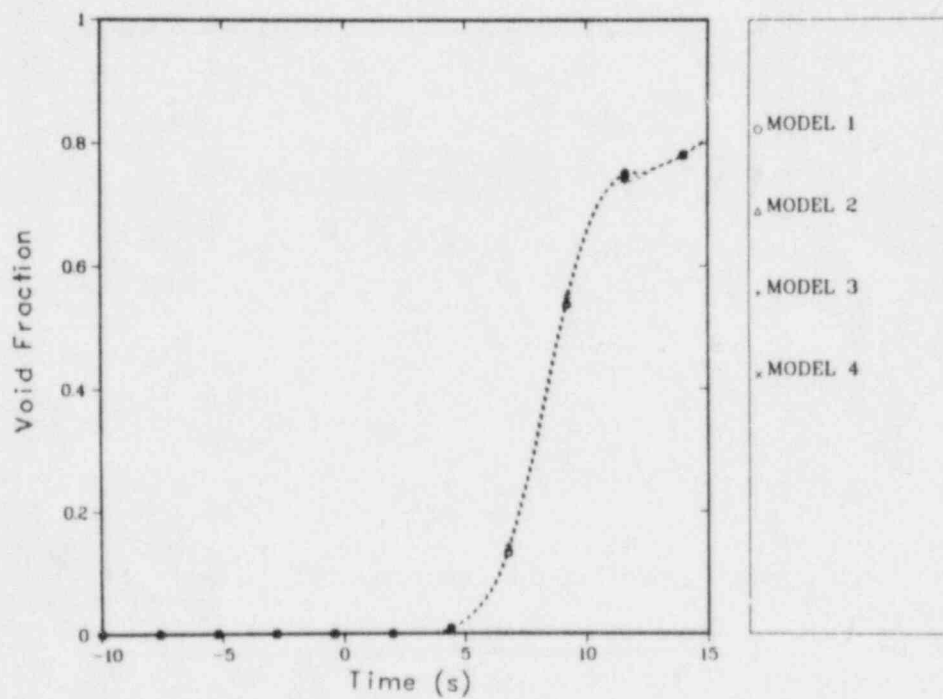


Fig. 224.
LOFT L2-2 parametric-study void fractions.

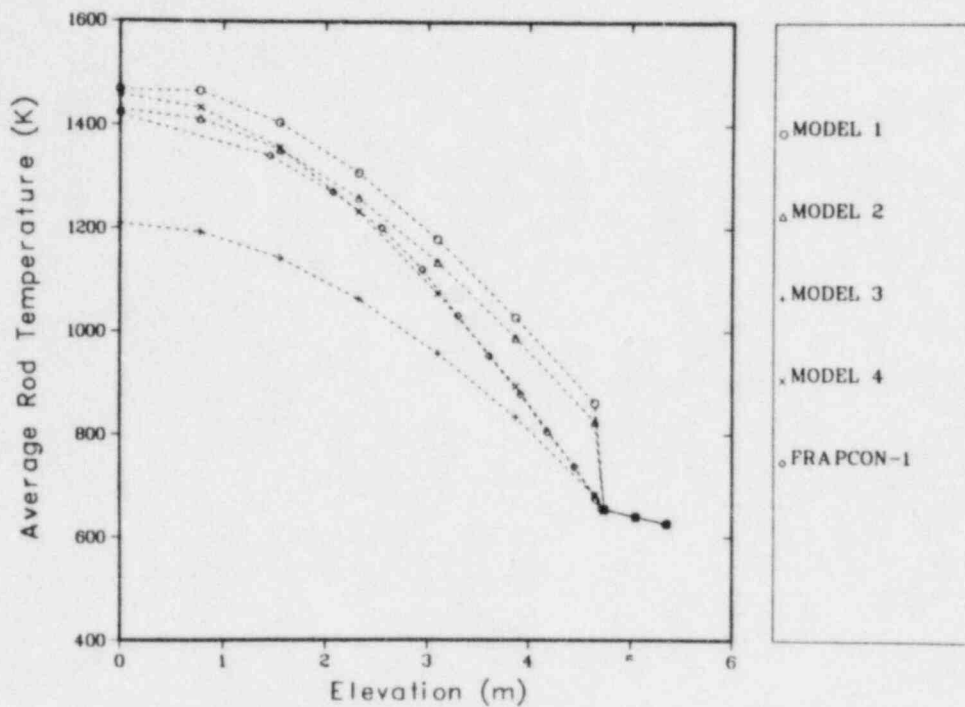


Fig. 225.

LOFT L2-2 calculated radial temperature distribution at the midplane of rod 1.

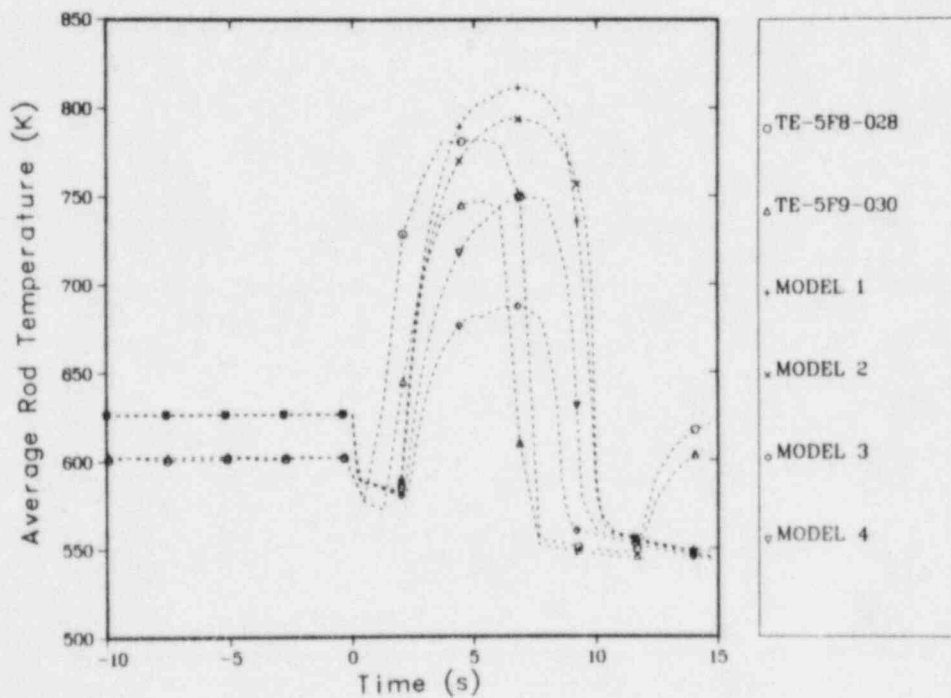


Fig. 226.

LOFT L2-2 transient response of the fuel-rod surface at the axial midplane of rod 1.

to rod and we were forced to retain the 0.0796-mm gap. The results in Figs. 212-219 and Fig. 221 did not deteriorate appreciably from the use of this gap size, but this may have been fortuitous.

E. TRAC-PD2 Features Tested

The LOFT L2-2 calculation tested all TRAC-PD2 features that were necessary to perform a large-break LOCA calculation for a full-scale PWR. Only this calculation included nuclear-power fuel rods. No other assessment calculation showed significant effects caused by subcooled critical flow. Finally, LOFT L2-2 provided the most physical example of the interaction between cold ECC liquid and a complete system, including mixing phenomena, core bypass, and eventual reflood.

F. Conclusions and Recommendations

The agreement between the TRAC-PD2 calculations and the data for LOFT Test L2-2 generally was quite good. In the cases where there was a large discrepancy between the calculated and measured results, we have identified possible test difficulties or suggested TRAC modifications to improve the agreement. Our recommendations are

- improve the treatment of heat transfer from structural materials in the vessel by eliminating the lumped-parameter heat-slab model (also suggested because of the LOFT L1-4 results);
- improve the treatment of bubble nucleation, particularly in the case of subcooled critical flow; and
- allow variations in the fuel-rod geometry and fuel conductivity, both axially within a rod and between rods in different core regions.

This final recommendation might be extended to provide an automated method of coupling TRAC with a fuel-rod simulation code, such as FRAPCON-1, to obtain accurate initial conditions.

G. Input Data Decks

Appendix K lists the steady-state and transient input decks for LOFT L2-2. All component and trip data were obtained from the dump taken at the conclusion of the steady-state calculation.

XIV. CONCLUSIONS

The tests described briefly in Table I and subsequently analyzed in this report have served a dual purpose for TRAC-PD2. First, the tests constitute a minimal set of calculations that, in the final analyses presented here, represent the initial independent assessment of the code, covering the full range of LOCA phenomena and demonstrating the integral-system calculational capability. Second, the tests and their analyses with earlier, developmental versions of TRAC-PD2 have formed the basis of quality assurance for the code, that is, developmental assessment. Toward the end of the development process resulting in TRAC-PD2, we ran these analyses many times as changes were made to the code. Through the repeated analyses of the same tests, we found and corrected many code errors and improved some of the code models and constitutive relations. Although we do not claim that the code is free of errors, this process has reduced substantially the errors and made the code more robust and easier to use, at least in terms of code failures and error messages indicating calculational difficulties.

The code calculated many things very well. The results from the separate-effects tests, including the Edwards' pipe blowdown, the two CISE tests, the two Marviken critical-flow tests, and the Bennett tube experiments, generally compared very well with the test data and did not indicate problems with the components and constitutive equations that are important to the large-break LOCA analysis. In particular, these tests indicated that the calculation of critical flow and wall heat transfer is good.

The analyses of the Creare tests demonstrated that TRAC-PD2 can calculate well the ECC-bypass phenomena under conditions of high or low flows and high or low subcooling of the injected ECC liquid. We ran two complete flooding curves from complete bypass to total delivery. The curve based on low-subcooling injection showed that the three-dimensional VESSEL component can calculate accurately the coarse, overall multidimensional flows important to downcomer penetration. In addition to verifying the three-dimensional numerics and field equations in the code, the low-subcooling case also yielded indirect evidence that the interfacial-drag model in the code is adequate for this purpose. The high-subcooling case further verified the results of the low-subcooling case and indicated that the interfacial-condensation model in TRAC-PD2 also is adequate for calculating downcomer penetration.

The two FLECHT tests demonstrated the validity of the new dynamic fine mesh in the fuel-rod conduction model for tracking quench fronts during the reflood phase of a large-break LOCA. The results for Tests S-06-3 and L2-2 also support this conclusion. Not only does the fine-mesh scheme work, but it can track accurately the quench fronts during both slow and fast refloods. This major change in TRAC-PD2 resolved problems with the reflood analysis in TRAC-PLA (Ref. 3) associated with fast refloods. We no longer observe in the calculations the quench front artificially stalling at axial cell boundaries in the core.

The results of the separate-effects analyses of critical flow (the two Marviken tests and the Semiscale-nozzle study) demonstrated the validity of the TRAC-PD2 scheme for calculating critical flow using the fully implicit, one-dimensional numerics together with a detailed noding scheme. The fully implicit one-dimensional numerics allow the code to exceed the material Courant limit on time steps and, therefore, do not affect adversely the execution time when short cells are used. The detailed noding scheme permits representation of flow-area changes leading to the choking plane and resolution of large

pressure gradients upstream of the choking plane. This detail is necessary for calculating correctly the fluid conditions at the choking plane. The results for Marviken Test 24, with its low L/D ratio, suggested that this scheme as it is implemented in TRAC-PD2 may break down in cases where nonequilibrium effects are important. In such cases, appreciable superheat exists in the liquid upstream of the choking plane. The analyses for Test L1-4 and L2-2 confirm the problem, although the results were not affected adversely. The superheat in the liquid upstream of the choking plane works through the TRAC-PD2 constitutive models to generate vapor unrealistically and to drive the calculation toward equilibrium. Although this problem is not important to large-break LOCA analyses, it can have a significant impact on small-break LOCA analyses where the period of subcooled critical flow is very long. The resolution of this problem with TRAC-PD2 lies in alternate noding schemes for critical flow in small-break LOCA analyses and comparisons of calculated results to existing critical-flow models. The long-term resolution of the problem requires that a delayed-nucleation model and/or a critical-flow model be included in the code.

The analyses for LOFT L1-4 and L2-2 indicated that the lumped-parameter heat slabs in the TRAC-PD2 VESSEL are inadequate in that the stored energy in the slabs is allowed to dissipate too rapidly into the adjacent fluid. This problem is not overly significant for large-break LOCA analyses because the problem time is short and because the active portion of the vessel structural mass can be estimated and modeled. For small-break LOCA analyses this problem can have significant impact on the calculated course of the transient by adversely affecting the time history of the energy content of the fluid in the primary system. Resolution of the problem requires the implementation of at least a one-dimensional heat slab in the VESSEL similar to those in the one-dimensional components.

Many of the analyses demonstrated the capability of the code to initialize itself to the correct steady-state conditions by running a generalized steady-state calculation. The resulting steady-state conditions are consistent with the models and numerics that are used for transient analyses. The analysis of Semiscale Test S-06-3 demonstrated that the user can renode and otherwise change components on restart at any point in the calculational sequence. The analyses for LOFT L1-4 and L2-2 showed that it is unnecessary to change components at any time after the beginning of the steady-state calculation; in particular, for these two tests we input at the beginning of the steady-state calculation all of the components necessary for the transient calculation, and we started the transient calculation from the steady-state restart dump with the most simple input deck possible.

The analyses of Semiscale Tests S-02-8 and S-06-3 and LOFT L1-4 and L2-2 have demonstrated the capability of the TRAC-PD2 code to perform integral calculations with complete representations of the primary systems through all phases of the large-break LOCA scenario (steady state, blowdown, refill, and reflood). The calculations of these tests compared well with the appropriate data. All of the analyses in this report indicate that TRAC-PD2 is a very versatile, flexible, robust thermal-hydraulic code that is well suited to large-break LOCA analyses and that may be applied to a large variety of other thermal-hydraulic problems.

REFERENCES

1. "TRAC-PD2, An Advanced Best-Estimate Computer Program for Pressurized Water Reactor Loss-of-Coolant Accident Analysis," Los Alamos National Laboratory report LA-8709-MS, NUREG/CR-2054 (April 1981).
2. A. R. Edwards and T. P. O'Brien, "Studies of Phenomena Connected with the Depressurization of Water Reactors," J. of Brit. Nucl. Ener. Soc. 9, 125-135 (April 1970).
3. "TRAC-PLA Developmental Assessment," Los Alamos Scientific Laboratory report LA-8056-MS, NUREG/CR-1059 (October 1979).
4. R. W. Garner, "Comparative Analyses of Standard Problems--Standard Problem One (Straight Pipe Depressurization Experiments)," Aerojet Nuclear Company report I-212-74-5.1 (October 1973).
5. A. Premoli and W. T. Hancox, "An Experimental Investigation of Subcooled Blowdown with Heat Addition," Specialists Meeting on Transient Two-Phase Flow, S. Banerjee and K. R. Weaver, Eds., (Atomic Energy of Canada, Ltd., Mississauga, Ontario, 1978) pp. 550-579.
6. W. T. Hancox and A. Premoli, "Standard Problem 3: Subcooled Blowdown with Heat Addition," Submission to Committee on the Safety of Nuclear Installations Ad Hoc Group on Emergency Core Cooling, Bethesda, Maryland (Revised March 1976).
7. "Results from Test 4, The Marviken Full-Scale Critical Flow Tests," Joint Reactor Safety Experiments in the Marviken Power Station, Sweden, Marviken report MXC-204 (September 1979).
8. "Results from Test 24, The Marviken Full-Scale Critical Flow Tests," Joint Reactor Safety Experiments in the Marviken Power Station, Sweden, Marviken report MXC-224 (September 1979).
9. C. B. Mullins, C. R. Hyman, W. G. Craddick, T. M. Anklam, and R. A. Hedrick, "PWR Blowdown Heat-Transfer Separate-Effects Program Data Evaluation Report--THTF Test Series II," Oak Ridge National Laboratory report ORNL/NUREG-53, NUREG/CR-0539 (April 1979).
10. O. C. Iloeje, D. N. Plummer, P. Griffith, and W. M. Rohsenow, "An Investigation of the Collapse and Surface Rewet in Film Boiling in Forced Vertical Flow," J. Heat Trans. 97, 166-172 (May 1975). Note that this reference has several misprints in Eq. (5): 0.217 should be 0.127 and g_c should be g in the $1/3$ power term.
11. A. W. Bennett, G. F. Hewitt, H. A. Kearsey, and R. K. F. Keeys, "Heat Transfer to Steam-Water Mixtures Flowing in Uniformly Heated Tubes in which the Critical Heat Flux Has Been Exceeded," Atomic Energy Research Establishment, Harwell, England, report AERE-R5373 (1967).

12. "TRAC-PIA: An Advanced Best-Estimate Computer Program for PWR LOCA Analysis," Los Alamos Scientific Laboratory report LA-7777-MS, NUREG/CR-0665 (May 1979).
13. "TRAC Newsletter No. 1," Los Alamos Scientific Laboratory publication (July 1979).
14. C. J. Crowley, J. A. Block, and C. N. Cary, "Downcomer Effects in a 1/15-Scale PWR Geometry--Experimental Data Report," Creare, Inc. report NUREG-0281 (May 1977).
15. E. R. Rosal, L. E. Hochreiter, M. F. McGuire, and M. C. Krepinevich, "FLECHT Low Flooding Rate Cosine Test Series Data Report," Westinghouse Electric Corporation report WCAP-8651 (1975).
16. E. R. Rosal, C. E. Conway, and M. C. Krepinevich, "FLECHT Low Flooding Rate Skewed Test Series Data Report," Westinghouse Electric Corporation report WCAP-9108 (May 1977).
17. E. M. Sparrow and R. D. Cess, Radiation Heat Transfer (Brooks/Cole Publishing Co., Belmont, California, 1966).
18. L. J. Ball, D. J. Hanson, K. A. Dietz, and D. J. Olson, "Semiscale Program Description," Idaho National Engineering Laboratory report TREE-NUREG-1210 (May 1978).
19. H. S. Crapo and K. E. Sackett, "Experimental Data Report for Semiscale Mod-1 Test S-02-8 (Blowdown Heat Transfer Test)," Aerojet Nuclear Company report ANCR-NUREG-1238 (August 1976).
20. B. L. Collins, M. L. Patton, Jr., K. E. Sackett, and K. Stanger, "Experimental Data Report for Semiscale Mod-1 Test S-06-3 (LOFT Counterpart Test)," EG&G Idaho, Inc. report NUREG/CR-0251 (July 1978).
21. H. C. Robinson, "LOFT System and Test Description (Loss-of-Coolant Experiments Using a Core Simulator)," Idaho National Engineering Laboratory report TREE-NUREG-1019 (November 1976).
22. D. L. Batt, "Experiment Data Report for LOFT Nonnuclear Test L1-4," Idaho National Engineering Laboratory report TREE-NUREG-1084 (July 1977).
23. H. C. Robinson, "Quick-Look Report on LOFT Nonnuclear Experiment L1-4," Idaho National Engineering Laboratory report QLR-L1-4 (June 1977).
24. M. McCormick-Barger, "Experiment Data Report for LOFT Power Ascension Test L2-2," Idaho National Engineering Laboratory report NUREG/CR-0492, TREE-1322 (1979).
25. D. L. Reeder, "LOFT System and Test Description (5.5-ft Nuclear Core 1 Locs)," EG&G Idaho, Inc. report NUREG/CR-0247, TREE-1208 (July 1978).

26. James F. Jackson and M. G. Stevenson, "Nuclear Reactor Safety: October 1-December 31, 1979," Los Alamos Scientific Laboratory report LA-8299-PR, NUREG/CR-1516 (May 1980).
27. D. A. Niebruegge, E. L. Tolman, and C. W. Solbrig, "Best-Estimate Fuel Rod Modeling Techniques," Nucl. Sci. Eng. 68, 363-368 (1978).
28. E. L. Tolman, W. E. Driskell, and E. W. Coryell, "Fuel Rod Stored-Energy Estimates for the LOFT LOCA Tests," Amer. Nucl. Soc. Trans. 34, 484 (1980).
29. G. A. Berna, M. P. Bohn, and D. R. Coleman, "FRAPCON-1: A Computer Code for the Steady State Analysis of Oxide Fuel Rods," Idaho National Engineering Laboratory report CDAP-TR-78-032-R1 (1978).
30. D. L. Hagerman, G. A. Reymann, and R. E. Mason, "MATPRO-Version 11 (Rev. 1): A Handbook of Material Properties for Use in the Analysis of Light Water Reactor Fuel Behavior," EG&G Idaho, Inc. report NUREG/CR-0497, TREE-1280, Rev. 1 (February 1980).

APPENDIX A

TRAC INPUT DECK FOR EDWARDS' BLOWDOWN EXPERIMENT

CARD	1	2	3	4	5	6	7
1	123456789012345678901234567890123456789012345678901234567890						
2	EDWARDS BLOWDOWN EXPERIMENT MODEL NO. 1						
3	Q9CA 25.4 GOPD2						
4	0 0.						
5	0 1 4 3 0						
6	.100000E-02 .100000E-02 .100000E+01 0.						
7	10 20 20 0 0						
8	0 1 0 2 0 3 0 4 0 0						
9	FILL 4 4						
10	3						
11	1.205000E-01 5.060000E-04 5.148000E+02						
12	6.996100E+06						
13	PIPE 2 2						
14	16 0 1 2 6						
15	0 1						
16	0. 0. 0. 0. 0.						
17	0.						
18	R 6 5.0917E-03R 9 3.0550E-02R 1 4.1000E-02E						
19	R 6 2.1400E-05R 9 1.2840E-04R 1 1.7230E-04E						
20	R 1 3.6566E-03R16 4.2030E-03E						
21	R 1 1.4360E+00R16 0. E						
22	F 0. E						
23	F 7.3152E-02E						
24	F 4E						
25	F 0. E						
26	F 0. E						
27	4.9830E+02 4.9827E+02 4.9823E+02 4.9820E+02 4.9817E+02						
28	4.9813E+02 4.9810E+02 4.9807E+02 4.9803E+02 4.9800E+02						
29	4.9797E+02 4.9793E+02 4.9790E+02 4.9787E+02 4.9783E+02						
30	4.9780E+02E						
31	4.9830E+02 4.9827E+02 4.9823E+02 4.9820E+02 4.9817E+02						
32	4.9813E+02 4.9810E+02 4.9807E+02 4.9803E+02 4.9800E+02						
33	4.9797E+02 4.9793E+02 4.9790E+02 4.9787E+02 4.9783E+02						
34	4.9780E+02E						
35	F 6.9961E+06E						
36	PIPE 3 3						
37	30 0 2 3 6						
38	0 0						
39	0. 0. 0. 0. 0.						
40	0.						

	1	2	3	4	5	6	7
CARD	1234567890123456789012345678901234567890123456789012345678901234567890						
41	R29 1.2515E-01R 1	1.2050E-01E					
42	R29 5.2600E-04R 1	5.0600E-04E					
43	F 4.2030E-03E						
44	F 0. E						
45	F 0. E						
46	F 7.3152E-02E						
47	F 4E						
48	F 0. E						
49	F 0. E						
50	R 1 4.9780E+02R 1	4.9908E+02R 1	5.0037E+02R 1	5.0165E+02R 1	5.0293E+02		
51	R 1 5.0422E+02R 2	5.0550E+02R 1	5.0528E+02R 1	5.0507E+02R 1	5.0485E+02		
52	R 1 5.0463E+02R 1	5.0442E+02R 2	5.0420E+02R 1	5.0453E+02R 1	5.0485E+02		
53	R 1 5.0518E+02R 2	5.0550E+02R 1	5.0597E+02R 1	5.0643E+02R 2	5.0690E+02		
54	R 1 5.0645E+02R 1	5.0600E+02R 1	5.0555E+02R 1	5.0510E+02R 1	5.0465E+02		
55	R 1 5.0420E+02E						
56	R 1 4.9780E+02R 1	4.9908E+02R 1	5.0037E+02R 1	5.0165E+02R 1	5.0293E+02		
57	R 1 5.0422E+02R 2	5.0550E+02R 1	5.0528E+02R 1	5.0507E+02R 1	5.0485E+02		
58	R 1 5.0463E+02R 1	5.0442E+02R 2	5.0420E+02R 1	5.0453E+02R 1	5.0485E+02		
59	R 1 5.0518E+02R 2	5.0550E+02R 1	5.0597E+02R 1	5.0643E+02R 2	5.0690E+02		
60	R 1 5.0645E+02R 1	5.0600E+02R 1	5.0555E+02R 1	5.0510E+02R 1	5.0465E+02		
61	R 1 5.0420E+02E						
62	F 6.9961E+06E						
63	BREAK	1	1				
64	1						
65	5.091700E-03	0.214000E-04	1.000000E+00	3.731500E+02	1.013535E+05		
66	1.0E-5	0.1	15.1E-3				
67	1.0E-3	1.0E-4	1.0				
68	1.0E-5	0.1	0.6				
69	0.05	0.005	1.0				
70	-1.000000E+00						

APPENDIX B

TRAC INPUT DECKS FOR CISE BLOWDOWN EXPERIMENTS (TESTS 4 AND R)

I. TRAC INPUT DECK FOR CISE UNHEATED BLOWDOWN EXPERIMENT (TEST 4)

CARD	1	2	3	4	5	6	7
1	1234567890	1234567890	1234567890	1234567890	1234567890	1234567890	1234567890
2	CISE UNHEATED BLOWDOWN EXPERIMENT MODEL NO. 1						
3	Q9CA 25.4 GOPD2						
4	0 0.						
5	0	1	6	5	0		
6	.100000E-02	.100000E-02	.100000E+01	0.			
7	10	20	20	0	0		
8	0	1 0	2 0	3 0	4 0	5	
9	0	6 0	0 0	0 0	0 0	0	
10	FILL	1	1				
11	1						
12	1.010300E+00	5.364000E-04				5.835000E+02	
13	9.820000E+06						
14	PIPE	2	2				
15	10	2	1	2	6		
16	0	0					
17	1.300000E-02	2.000000E-03	0.	0.	3.000000E+02		
18	3.000000E+02						
19	F 1.0103E+00E						
20	F 5.3640E-04E						
21	R10 5.3093E-04R	1 3.4636E-04E					
22	F 0. E						
23	R10-1.4300E-01R	1-1.0000E+00E					
24	R10 2.6000E-02R	1 2.1000E-02E					
25	F 4E						
26	F 0. E						
27	R10-1.3000E+00R	1-1.9930E+00E					
28	F 5.4400E+02E						
29	F 5.4400E+02E						
30	9.7800E+06	9.7822E+06	9.7844E+06	9.7867E+06	9.7889E+06		
31	9.7911E+06	9.7933E+06	9.7956E+06	9.7978E+06	9.8000E+06E		
32	F 0. E						
33	F 5.4400E+02E						
34	PIPE	3	3				
35	10	5	2	3	6		
36	0	0					
37	1.050000E-02	2.000000E-03	0.	5.000000E+01	3.000000E+02		
38	3.000000E+02						
39	F 4.0000E-01E						
40	F 1.3854E-04E						

CARD	1	2	3	4	5	6	7
41	R10 3.4636E-04R	1 2.2698E-04E					
42	F 0.	E					
43	F -1.0000E+00E						
44	R10 2.1000E-02R	1 1.7000E-02E					
45	F	4E					
46	F 0.	E					
47	R10-1.9930E+00R	1-3.0410E+00E					
48	F 5.4400E+02E						
49	F 5.4400E+02E						
50	9.8000E+06	9.8067E+06	9.8133E+06	9.8200E+06	9.8267E+06		
51	9.8333E+06	9.8400E+06	9.8467E+06	9.8533E+06	9.8600E+06E		
52	F 0.	E					
53	F 5.4400E+02E						
54	PIPE		4	4			
55		10	2	3	4	6	
56		0	0				
57	8.500000E-03	1.500000E-03	0.	0.		3.000000E+02	
58	3.000000E+02						
59	F 9.5570E-01E						
60	F 2.1690E-04E						
61	F 2.2698E-04E						
62	F 0.	E					
63	R 1-1.0000E+00R	10-3.6600E-01E					
64	F 1.7000E-02E						
65	F	4E					
66	F 0.	E					
67	F -3.0410E+00E						
68	F 5.4400E+02E						
69	F 5.4400E+02E						
70	9.8600E+06	9.8667E+06	9.8733E+06	9.8800E+06	9.8867E+06		
71	9.8933E+06	9.9000E+06	9.9067E+06	9.9133E+06	9.9200E+06E		
72	F 0.	E					
73	F 5.4400E+02E						
74	PIPE		5	5			
75		8	2	4	5	6	
76		0	1				
77	8.500000E-03	1.500000E-03	0.	0.		3.000000E+02	
78	3.000000E+02						
79	R 3 1.0000E-01R	5 2.0000E-02E					
80	R 3 2.2700E-05R	5 4.5400E-06E					
81	F 2.2698E-04E						
82	F 0.	E					
83	R 1-3.6600E-01R	8 0.	E				
84	F 1.7000E-02E						
85	F	4E					

	1	2	3	4	5	6	7
CARD	123456789012345678901234567890123456789012345678901234567890						

86	F	0.	E				
87	R	1-3.0410E+00R 8 0.	E				
88	F	5.4400E+02E					
89	F	5.4400E+02E					
90	F	9.9200E+06E					
91	F	0.	E				
92	F	5.4400E+02E					
93	BREAK		6		6		
94		5					
95		2.000000E-02	4.540000E-06	1.000000E+00	3.730000E+02	1.000000E+05	
96		1.000000E-05	1.000000E-01	1.000000E-01			
97		1.000000E-02	1.000000E-02	1.000000E+00			
98		1.000000E-05	5.000000E-03	5.000000E-01			
99		1.000000E-01	1.000000E-02	1.000000E+00			
100		1.000000E-05	1.000000E-02	6.000000E+00			
101		2.000000E-01	2.000000E-02	1.000000E+01			
102		-1.000000E+00					

II. TRAC INPUT DECK FOR CISE HEATED BLOWDOWN EXPERIMENT (TEST R)

CARD	1	2	3	4	5	6	7
1	2	0					
2	CISE HEATED BLOWDOWN EXPERIMENT MODEL NO. 1						
3	Q9CA 25.4 GOPD2						
4	0	0.					
5	0	1	6		5		0
6	.100000E-02	.100000E-02	.100000E+01	0.			
7	10	20	20		0		0
8	0	1 0	2 0	3 0	4 0		5
9	0	6 0	0 0	0 0	0 0		0
10	FILL		1	1			
11	1						
12	1.010300E+00	5.364000E-04				5.835000E+02	
13	9.820000E+06						
14	PIPE		2	2			
15	10	2	1		2		6
16	0	0					
17	1.300000E-02	2.000000E-03	0.		0.	3.000000E+02	
18	3.000000E+02						
19	F 1.0103E+00E						
20	F 5.3640E-04E						
21	R10 5.3093E-04R	1 3.4636E-04E					
22	F 0.	E					
23	R10-1.4300E-01R	1-1.0000E+00E					
24	R10 2.6000E-02R	1 2.1000E-02E					
25	F	4E					
26	F 0.	E					
27	R10-1.3000E+00R	1-1.9930E+00E					
28	F 5.7900E+02E						
29	F 5.7900E+02E						
30	9.7800E+06	9.7822E+06	9.7844E+06	9.7867E+06	9.7889E+06		
31	9.7911E+06	9.7933E+06	9.7956E+06	9.7978E+06	9.8000E+06E		
32	F 0.	E					
33	F 5.7900E+02E						
34	PIPE		3	3			
35	10	5	2		3		6
36	1	0					
37	1.050000E-02	2.000000E-03	0.		5.000000E+01	3.000000E+02	
38	3.000000E+02						
39	F 4.0000E-01E						
40	F 1.3854E-04E						
41	R10 3.4636E-04R	1 2.2698E-04E					
42	F 0.	E					
43	F -1.0000E+00E						
44	R10 2.1000E-02R	1 1.7000E-02E					
45	F	4E					

	1	2	3	4	5	6	7
CARD	123456789012345678901234567890123456789012345678901234567890						
46	F 0.	E					
47	R10-1.9930E+00R	1-3.0410E+00E					
48	5.7900E+02	5.7500E+02	5.7100E+02	5.6700E+02	5.6300E+02		
49	5.5900E+02	5.5500E+02	5.5100E+02	5.4700E+02	5.4300E+02E		
50	5.7900E+02	5.7500E+02	5.7100E+02	5.6700E+02	5.6300E+02		
51	5.5900E+02	5.5500E+02	5.5100E+02	5.4700E+02	5.4300E+02E		
52	9.8000E+06	9.8067E+06	9.8133E+06	9.8200E+06	9.8267E+06		
53	9.8333E+06	9.8400E+06	9.8467E+06	9.8533E+06	9.8600E+06E		
54	F 1.8940E+08E						
55	5.9600E+02	6.0100E+02	6.0600E+02	6.1100E+02	6.1600E+02		
56	5.9500E+02	6.0000E+02	6.0500E+02	6.1000E+02	6.1500E+02		
57	5.9500E+02	6.0000E+02	6.0500E+02	6.1000E+02	6.1500E+02		
58	5.9500E+02	6.0000E+02	6.0500E+02	6.1000E+02	6.1500E+02		
59	5.9500E+02	6.0000E+02	6.0500E+02	6.1000E+02	6.1500E+02		
60	5.9200E+02	5.9700E+02	6.0200E+02	6.0700E+02	6.1200E+02		
61	5.8700E+02	5.9200E+02	5.9700E+02	6.0200E+02	6.0700E+02		
62	5.8100E+02	5.8600E+02	5.9100E+02	5.9600E+02	6.0100E+02		
63	5.7800E+02	5.8300E+02	5.8800E+02	5.9300E+02	5.9800E+02		
64	5.7500E+02	5.8000E+02	5.8500E+02	5.9000E+02	5.9500E+02E		
65	PIPE		4	4			
66		10	2	3	4	6	
67		0	0				
68	8.500000E-03	1.500000E-03	0.	0.		3.000000E+02	
69	3.000000E+02						
70	F 9.5570E-01E						
71	F 2.1690E-04E						
72	F 2.2698E-04E						
73	F 0.	E					
74	R 1-1.0000E+00R10-3.6600E-01E						
75	F 1.7000E-02E						
76	F 4E						
77	F 0.	E					
78	F -3.0410E+00E						
79	5.4300E+02	5.4333E+02	5.4367E+02	5.4400E+02	5.4433E+02		
80	5.4467E+02	5.4500E+02	5.4533E+02	5.4567E+02	5.4600E+02E		
81	5.4300E+02	5.4333E+02	5.4367E+02	5.4400E+02	5.4433E+02		
82	5.4467E+02	5.4500E+02	5.4533E+02	5.4567E+02	5.4600E+02E		
83	9.8600E+06	9.8667E+06	9.8733E+06	9.8800E+06	9.8867E+06		
84	9.8933E+06	9.9000E+06	9.9067E+06	9.9133E+06	9.9200E+06E		
85	F 0.	E					
86	F 5.4400E+02E						
87	PIPE		5	5			
88		8	2	4	5	6	
89		0	1				
90	8.500000E-03	1.500000E-03	0.	0.		3.000000E+02	

	1	2	3	4	5	6	7
CARD	123456789012345678901234567890123456789012345678901234567890						
91	3.000000E+02						
92	R 3 1.0000E-01R 5 2.0000E-02E						
93	R 3 2.2700E-05R 5 4.5400E-06E						
94	F 2.2698E-04E						
95	F 0. E						
96	R 1-3.6600E-01R 8 0. E						
97	F 1.7000E-02E						
98	F 4E						
99	F 0. E						
100	R 1-3.0410E+00R 8 0. E						
101	5.4460E+02	5.4200E+02	5.3970E+02	5.3800E+02	5.3450E+02		
102	5.2900E+02	5.2350E+02	5.1850E+02E				
103	5.4460E+02	5.4200E+02	5.3970E+02	5.3800E+02	5.3450E+02		
104	5.2900E+02	5.2350E+02	5.1850E+02E				
105	F 9.9200E+06E						
106	F 0. E						
107	F 5.4400E+02E						
108	BREAK	6	6				
109	5						
110	2.000000E-02	4.540000E-06	1.000000E+00	3.730000E+02	1.000000E+05		
111	1.000000E-05	1.000000E-05	1.000000E-05				
112	1.000000E-05	1.000000E-05	1.000000E+10				
113	1.000000E-05	1.000000E-04	1.000000E-02				
114	1.000000E-03	1.000000E-03	1.000000E+10				
115	1.000000E-04	1.000000E-04	1.000000E-01				
116	1.000000E-02	1.000000E-02	1.000000E+10				
117	5.000000E-04	5.000000E-04	5.000000E-01				
118	1.000000E-01	1.000000E-01	1.000000E+10				
119	5.000000E-04	1.000000E-02	6.000000E+00				
120	1.000000E-01	1.000000E-01	1.000000E+10				
121	-1.000000E+00						

APPENDIX C

TRAC INPUT DECKS FOR MARVIKEN TESTS 4 AND 24

I. TRAC INPUT DECK FOR MARVIKEN TEST 4

CARD	1	2	3	4	5	6	7
1	12345678901234567890123456789012345678901234567890						
2	MARVIKEN III TEST 4 DETAILED NODING MODEL NO. 1						
3	Q9CA 25.4 GOPD2						
4	0 0.						
5	0	1	4	3	0		
6	.100000E-02	.100000E-02	.100000E-01	.100000E+00			
7	30	80	80	0	0		
8	0	1 0	2 0	3 0	4 0	0	
9	FILL	1	128				
10	1	1	0	0			
11	1.550	2.7391	1.0	.0	535.6		
12	4940000.						
13	PIPE	2	128				
14	15	0	1	2	1		
15	1	0					
16	2.610000E+00	1.000000E-01	0.	0.	3.000000E+02		
17	3.000000E+02						
18	R 1 1.5500E+00R 1 1.6000E+00R 1 1.0000E+00R 2 1.4000E+00R10 1.5000E+00E						
19	R 1 2.7391E+00R 1 2.8274E+00R 1 9.5118E+00R 2 2.9005E+01R10 3.1076E+01E						
20	R 3 1.7671E+00R13 2.0718E+01E						
21	F 0. E						
22	F -1.0000E+00E						
23	R 3 1.5000E+00R13 5.1360E+00E						
24	F 4E						
25	R 5 1.0000E+00R10 0. E						
26	F 0. E						
27	R10 5.3620E+02R 1 5.2300E+02R 1 5.1000E+02R 2 5.0600E+02R 1 5.0100E+02E						
28	R10 5.3620E+02R 1 5.2300E+02R 1 5.1000E+02R 2 5.0600E+02R 1 5.0100E+02E						
29	R 1 4.9340E+06R 3 4.9350E+06R 2 4.9360E+06R 1 4.9490E+06R 1 4.9610E+06						
30	R 1 4.9730E+06R 1 4.9850E+06R 1 4.9970E+06R 1 5.0090E+06R 1 5.0220E+06						
31	R 1 5.0340E+06R 1 5.0460E+06E						
32	PIPE	3	128				
33	45	0	2	3	1		
34	1	1					
35	2.550000E-01	1.000000E-01	0.	0.	3.000000E+02		
36	3.000000E+02						
37	R 1 6.0000E-01R 8 5.0000E-01R 1 7.9000E-01R 1 6.1000E-01R 1 6.0000E-01						
38	R 1 5.6800E-01R 2 5.0000E-01R10 2.5000E-02R 7 2.0000E-01R10 2.5000E-02						
39	R 1 2.0000E-02R 2 2.8000E-02E						
40	R 1 1.2104E+01R 1 9.4300E+00R 1 7.7925E+00R 1 4.9886E+00R 1 1.5474E+00						

	1	2	3	4	5	6	7
CARD	123456789012345678901234567890123456789012345678901234567890						
41	R 4 2.2210E-01R 1	3.5090E-01R 1	2.8110E-01R 1	2.8670E-01R 1	2.6180E-01		
42	R 2 2.2210E-01R 1	1.0213E-02R 1	8.5590E-03R 1	7.3090E-03R 1	6.4930E-03		
43	R 1 5.8340E-03R 1	5.3000E-03R 4	5.0870E-03R 7	4.0696E-02R 4	5.0870E-03		
44	R 1 5.5610E-03R 1	6.5520E-03R 4	7.0690E-03R 1	5.6550E-03R 1	8.7490E-03		
46	R 1 2.0718E+01R 1	1.9635E+01R 1	1.8096E+01R 1	1.3203E+01R 1	7.0686E+00		
47	R 6 4.4410E-01R 2	4.7780E-01R 3	4.4410E-01R 1	3.7390E-01R 1	3.1170E-01		
48	R 1 2.7340E-01R 1	2.4630E-01R 1	2.2060E-01R 16	2.0350E-01R 1	2.4190E-01		
49	R 6 2.8270E-01R 1	3.4320E-01R 1	4.0940E-01E				
50	F .0000E						
51	F -1.0000E+00E						
52	R 1 5.1360E+00R 1	5.0000E+00R 1	4.8000E+00R 1	4.1000E+00R 1	3.0000E+00		
53	R 6 7.5200E-01R 2	7.8000E-01R 3	7.5200E-01R 1	6.9000E-01R 1	6.3000E-01		
54	R 1 5.9000E-01R 1	5.6000E-01R 1	5.3000E-01R 16	5.0900E-01R 1	5.5500E-01		
55	R 6 6.0000E-01R 1	6.6100E-01R 1	7.2200E-01E				
56	F 4E						
57	F 0. E						
58	F 0. E						
59	R 5 4.9900E+02R 1	4.9800E+02R 2	4.9700E+02R 1	4.9600E+02R 1	4.9500E+02		
60	R 1 4.9400E+02R 1	4.9200E+02R 1	4.8400E+02R 1	4.7900E+02R 1	4.7600E+02		
61	R30 4.7500E+02E						
62	R 5 4.9900E+02R 1	4.9800E+02R 2	4.9700E+02R 1	4.9600E+02R 1	4.9500E+02		
63	R 1 4.9400E+02R 1	4.9200E+02R 1	4.8400E+02R 1	4.7900E+02R 1	4.7600E+02		
64	R30 4.7500E+02E						
65	R 1 5.0550E+06R 1	5.0600E+06R 1	5.0640E+06R 1	5.0680E+06R 1	5.0720E+06		
66	R 1 5.0760E+06R 1	5.0810E+06R 1	5.0850E+06R 1	5.0890E+06R 1	5.0940E+06		
67	R 1 5.1000E+06R 1	5.1050E+06R 1	5.1100E+06R 1	5.1150E+06R 1	5.1190E+06		
68	R 2 5.1210E+06R 4	5.1220E+06R 4	5.1230E+06R 1	5.1240E+06R 1	5.1260E+06		
69	R 1 5.1280E+06R 1	5.1290E+06R 1	5.1310E+06R 1	5.1330E+06R 1	5.1340E+06		
70	R 1 5.1350E+06R 4	5.1360E+06R 5	5.1370E+06R 3	5.1380E+06E			
71	BREAK	4	128				
72	3	0	0	0			
73	.028	.010522	1.0	373.	101700.		
74	.00001	.050	5.0				
75	.1	.1	5.0				
76	.00001	.050	56.				
77	1.0	.1	10.				
78	-1.0						

II. TRAC INPUT DECK FOR MARVIKEN TEST 24

CARD	1	2	3	4	5	6	7
1	2	0					
2	MARVIKEN III TEST 24 MODEL NO. 1						
3	Q9CA 25.4 GOPD2						
4	0	0.					
5	0	1	4	3	0		
6	.100000E-02	.100000E-02	.100000E-01	.100000E+00			
7	30	80	80	0	0	0	
8	0	1	0	2	0	4	0
9	FILL	1	128				
10	1	1	0	0			
11	1.550	2.7391	1.0	.0	536.56		
12	4960000.						
13	PIPE	2	128				
14	15	0	1	2	1		
15	1	0					
16	2.568000E+00	1.000000E-01	0.	0.	3.000000E+02		
17	3.000000E+02						
18	R 1 1.5500E+00R	1 1.6000E+00R	1 1.0000E+00R	1 5.2000E-01R	1 1.9800E+00		
19	R 1 1.6000E+00R	1 1.7000E+00R	8 1.5000E+00E				
20	R 1 2.7391E+00R	1 2.8274E+00R	1 9.5118E+00R	1 1.0773E+01R	1 4.1021E+01		
21	R 1 3.3148E+01R	1 3.5220E+01R	8 3.1076E+01E				
22	R 3 1.7671E+00R	13 2.0718E+01E					
23	F 4.0000E-02E						
24	F -1.0000E+00E						
25	R 3 1.5000E+00R	13 5.1360E+00E					
26	F 4E						
27	R 4 1.0000E+00R	11 0.	E				
28	F 0.	E					
29	R 5 5.3656E+02R	1 5.3300E+02R	1 5.0740E+02R	1 5.0661E+02R	1 5.0655E+02		
30	R 1 5.0648E+02R	1 5.0641E+02R	1 5.0634E+02R	1 5.0628E+02R	1 5.0621E+02		
31	R 1 5.0610E+02E						
32	R 5 5.3656E+02R	1 5.3300E+02R	1 5.0740E+02R	1 5.0661E+02R	1 5.0655E+02		
33	R 1 5.0648E+02R	1 5.0641E+02R	1 5.0634E+02R	1 5.0628E+02R	1 5.0621E+02		
34	R 1 5.0610E+02E						
35	R 4 4.9600E+06R	1 4.9604E+06R	1 4.9755E+06R	1 4.9892E+06R	1 5.0027E+06		
36	R 1 5.0153E+06R	1 5.0277E+06R	1 5.0400E+06R	1 5.0524E+06R	1 5.0646E+06		
37	R 1 5.0769E+06R	1 5.0892E+06E					
38	PIPE	3	128				
39	27	0	2	3	1		
40	1	1					
41	2.500000E-01	1.000000E-01	0.	0.	3.000000E+02		
42	3.000000E+02						
43	R 1 6.0000E-01R	1 4.0000E-01R	1 6.0000E-01R	6 5.0000E-01R	1 7.9000E-01		
44	R 1 6.1000E-01R	1 6.0000E-01R	1 5.6800E-01R	2 5.0000E-01R	4 5.0000E-02		
45	R 6 2.5000E-02R	1 2.0000E-02R	1 2.1000E-02E				

CARD	1	2	3	4	5	6	7
46	R 1 1.2104E+01R	1 7.5440E+00R	1 9.3509E+00R	1 4.9886E+00R	1 1.5474E+00		
47	R 4 2.2210E-01R	1 3.5090E-01R	1 2.8110E-01R	1 2.8670E-01R	1 2.6180E-01		
48	R 2 2.2210E-01R	1 1.9601E-02R	1 1.5116E-02R	1 1.2234E-02R	1 1.0784E-02		
49	R 1 5.0270E-03R	5 4.9090E-03R	1 3.9270E-03R	1 4.1230E-03E			
50	R 1 2.0718E+01R	1 1.9635E+01R	1 1.8096E+01R	1 1.3203E+01R	1 7.0686E+00		
51	R 6 4.4410E-01R	2 4.7780E-01R	3 4.4410E-01R	1 3.4210E-01R	1 2.6420E-01		
52	R 1 2.2560E-01R	1 2.0590E-01R	8 1.9630E-01E				
53	F 0.	E					
54	F -1.0000E+00E						
55	R 1 5.1360E+00R	1 5.0000E+00R	1 4.8000E+00R	1 4.1000E+00R	1 3.0000E+00		
56	R 6 7.5200E-01R	2 7.8000E-01R	3 7.5200E-01R	1 6.6000E-01R	1 5.8000E-01		
57	R 1 5.3600E-01R	1 5.1200E-01R	8 5.0000E-01E				
58	F	4E					
59	F 0.	E					
60	F 0.	E					
61	R 1 5.0573E+02R	1 5.0522E+02R	1 5.0444E+02R	1 5.0318E+02R	1 5.0011E+02		
62	R 1 4.9701E+02R	1 4.9382E+02R	1 4.9037E+02R	1 4.8692E+02R	1 4.8246E+02		
63	R 1 4.7758E+02R	1 4.7331E+02R	1 4.6920E+02R	1 4.6544E+02R	1 4.6191E+02		
64	R12 4.6015E+02E						
65	R 1 5.0573E+02R	1 5.0522E+02R	1 5.0444E+02R	1 5.0318E+02R	1 5.0011E+02		
66	R 1 4.9701E+02R	1 4.9382E+02R	1 4.9037E+02R	1 4.8692E+02R	1 4.8246E+02		
67	R 1 4.7758E+02R	1 4.7331E+02R	1 4.6920E+02R	1 4.6544E+02R	1 4.6191E+02		
68	R12 4.6015E+02E						
69	5.0978E+06	5.1019E+06	5.1060E+06	5.1105E+06	5.1146E+06		
70	5.1187E+06	5.1229E+06	5.1270E+06	5.1312E+06	5.1367E+06		
71	5.1426E+06	5.1478E+06	5.1528E+06	5.1574E+06	5.1618E+06		
72	5.1642E+06	5.1646E+06	5.1651E+06	5.1655E+06	5.1658E+06		
73	5.1660E+06	5.1663E+06	5.1665E+06	5.1667E+06	5.1669E+06		
74	5.1671E+06	5.1673E+06E					
75	BREAK		4	128			
76		3	0	0	0		
77	.021	.004123		1.0	373.25	101700.	
78	.00001	.020		5.			
79	.1	.1		5.			
80	.00001	.050		80.			
81	1.	.1		80.			

APPENDIX D

TRAC STEADY-STATE AND TRANSIENT INPUT DECKS FOR THTF TEST 177

I. TRAC STEADY-STATE INPUT DECK FOR THTF TEST 177

CARD	1	2	3	4	5	6	7
	123456789012345678901234567890123456789012345678901234567890						
1	5						
2	*						
3	*						
4	ORNL THTF MODEL NO. 1						
5	Q9CA 25.4 GOPD2						
6	*						
7	0	0.0					
8	1	0	11	10			0
9	1.E-03	1.0E-05	1.0E-02	1.0E-01			
10	10	0	10	0			0
11	1	2	3	4			5
12	6	7	8	9			10
13	11E						
14	VESSEL	1	1				
15	18	2	1	4			
16	15	1	1	14			2
17	1						
18	0	0	0	1			
19	5.0	50.0	0.005				
20	8009.2	4023988.6	15.6	0.0		100000.	
21	1.334						
22	15	12	6				
23	0	0	0	0		100	
24	3695850.	0.0	0.0				
25	0.0475	0.2666	0.4952	0.9524		1.1810	
26	1.4858	1.7906	2.0954	2.4002		2.7050	
27	3.0098	3.2384	3.6956	3.9242		4.1338	
28	4.2002	4.3331	4.6897E				
29	.1728	.27440E					
30	.1010E						
31	15	2	3	1			
32	14	2	3	3			
33	18	2	3	6			
34	18	1	2	10			
35	0.0	0.0	0.0	1.0		1.0	
36	1.0	0.0	0.0	0.0		0.0	
37	0.0	0.0	0.0	0.0		0.0E	
38	1.0E						
39	0.422	0.422	0.597	1.065		1.285	
40	1.670	1.670	1.670	1.285		1.065	

CARD	1	2	3	4	5	6	7
41	0.597	0.422	0.422E				
42	45.0E						
43	0.0	0.0012813	0.0025626	0.002830519	0.003098438		
44	0.003521805	0.003945172	0.004368539	0.00455902	0.004749501		
45	0.004939982	0.005130463	0.00513201	0.005258997	0.005385984E		
46	4	4	10	10	4		
47	4	4	7	7	7		
48	7	3	7	7E			
49	0.0	3695850.	1.38	1000000.S			
50	1.5	500000.	2.0	500000.S			
51	3.5	750000.	4.0	750000.S			
52	4.5	2000000.	5.0	2250000.S			
53	7.0	2250000.	7.5	900000.S			
54	8.5	750000.	10.5	0.E			
55	F 0E						
56	F 0.0E						
57	F 0.0E						
58	F 0.0E						
59	F 0.0E						
60	F 0.0E						
61	F 0.0E						
62	F 0.0E						
63	F 0.0E						
64	.0836	.0836E					
65	1.7917	419.E					
66	0.0	0.0E					
67	.33	.15E					
68	0.0	0.0E					
69	0.0	0.0E					
70	0.0	0.0E					
71	0.0	0.0E					
72	.5717	1.0E					
73	0.0	0.0E					
74	.5717	1.0E					
75	1.0	0.0E					
76	0.0	0.0E					
77	.05	.05E					
78	1.0	0.0E					
79	550.7	550.7E					
80	0.0	0.0E					
81	0.0	0.0E					
82	0.0	0.0E					
83	0.0	0.0E					
84	0.0	0.0E					
85	0.0	0.0E					

	1	2	3	4	5	6	7
CARD	123456789012345678901234567890123456789012345678901234567890	123456789012345678901234567890123456789012345678901234567890	123456789012345678901234567890123456789012345678901234567890	123456789012345678901234567890123456789012345678901234567890	123456789012345678901234567890123456789012345678901234567890	123456789012345678901234567890123456789012345678901234567890	123456789012345678901234567890123456789012345678901234567890
86	-4.5		0.0E				
87	550.7		550.7E				
88	550.7		550.7E				
89	15.9E06		15.9E06E				
90	.089		.144E				
91	19.25		117.E				
92	0.0		0.0E				
93	.386		0.0E				
94	0.0		0.0E				
95	0.0		0.0E				
96	.386		0.0E				
97	0.0		0.0E				
98	.5717		1.0E				
99	0.0		0.0E				
100	.5717		1.0E				
101	0.0		0.0E				
102	0.0		0.0E				
103	.0063		.0546E				
104	0.0		0.0E				
105	550.7		550.7E				
106	0.0		0.0E				
107	0.0		0.0E				
108	0.0		0.0E				
109	0.0		0.0E				
110	0.0		0.0E				
111	4.84		-1.6E				
112	0.0		0.0E				
113	550.7		550.7E				
114	550.7		550.7E				
115	15.9E06		15.9E06E				
116	.093		.1595E				
117	20.05		36.15E				
118	0.0		0.0E				
119	.2285		0.0E				
120	0.0		0.0E				
121	0.0		0.0E				
122	.2285		0.0E				
123	0.0		0.0E				
124	.5717		1.0E				
125	0.0		0.0E				
126	.5717		1.0E				
127	0.0		0.0E				
128	0.0		0.0E				
129	.0063		.0546E				
130	0.0		0.0E				

	1	2	3	4	5	6	7
CARD	1234567890123456789012345678901234567890123456789012345678901234567890						
131	551.		550.7E				
132	0.0		0.0E				
133	0.0		0.0E				
134	0.0		0.0E				
135	0.0		0.0E				
136	0.0		0.0E				
137	4.84		-1.6E				
138	0.0		0.0E				
139	551.		550.7E				
140	551.		550.7E				
141	15.9E06		15.9E06E				
142	.185		.317E				
143	40.1		72.5E				
144	0.0		0.0E				
145	.464		0.0E				
146	0.0		0.0E				
147	0.0		0.0E				
148	.464		0.0E				
149	0.0		0.0E				
150	.5717		1.0E				
151	0.0		0.0E				
152	.5717		1.0E				
153	0.0		0.0E				
154	0.0		0.0E				
155	.0063		.0546E				
156	0.0		0.0E				
157	554.		550.7E				
158	0.0		0.0E				
159	0.0		0.0E				
160	0.0		0.0E				
161	0.0		0.0E				
162	0.0		0.0E				
163	4.84		-1.6E				
164	0.0		0.0E				
165	554.		550.7E				
166	554.		550.7E				
167	15.9E06		15.9E06E				
168	.092		.159E				
169	20.0		36.10E				
170	0.0		0.0E				
171	.298		0.0E				
172	0.0		0.0E				
173	0.0		0.0E				
174	.298		0.0E				
175	0.0		0.0E				

	1	2	3	4	5	6	7
CARD	123456789012345678901234567890123456789012345678901234567890						
176	.5717		1.0E				
177	0.0		0.0E				
178	.5717		1.0E				
179	0.0		0.0E				
180	0.0		0.0E				
181	.0063		.0546E				
182	0.0		0.0E				
183	557.		550.7E				
184	0.0		0.0E				
185	0.0		0.0E				
186	0.0		0.0E				
187	0.0		0.0E				
188	0.0		0.0E				
189	4.84		-1.6E				
190	0.0		0.0E				
191	557.		550.7E				
192	557.		550.7E				
193	15.9E06		15.9E06E				
194	.123		.178E				
195	26.7		48.25E				
196	0.0		0.0E				
197	.348		0.0E				
198	0.0		0.0E				
199	0.0		0.0E				
200	.348		0.0E				
201	0.0		0.0E				
202	.5717		1.0E				
203	0.0		0.0E				
204	.5717		1.0E				
205	0.0		0.0E				
206	0.0		0.0E				
207	.0063		.0546E				
208	0.0		0.0E				
209	560.		550.7E				
210	0.0		0.0E				
211	0.0		0.0E				
212	0.0		0.0E				
213	0.0		0.0E				
214	0.0		0.0E				
215	4.84		-1.6E				
216	0.0		0.0E				
217	560.		550.7E				
218	560.		550.7E				
219	15.9E06		15.9E06E				
220	.123		.178E				

	1	2	3	4	5	6	7
CARD	123456789012345678901234567890123456789012345678901234567890						
221	26.7		48.25E				
222	0.0		0.0E				
223	.348		0.0E				
224	0.0		0.0E				
225	0.0		0.0E				
226	.348		0.0E				
227	0.0		0.0E				
228	.5717		1.0E				
229	0.0		0.0E				
230	.5717		1.0E				
231	0.0		0.0E				
232	0.0		0.0E				
233	.0063		.0546E				
234	0.0		0.0E				
235	563.		550.7E				
236	0.0		0.0E				
237	0.0		0.0E				
238	0.0		0.0E				
239	0.0		0.0E				
240	0.0		0.0E				
241	4.84		-1.6E				
242	0.0		0.0E				
243	563.		550.7E				
244	563.		550.7E				
245	15.9E06		15.9E06E				
246	.123		.178E				
247	26.7		48.25E				
248	0.0		0.0E				
249	.348		0.0E				
250	0.0		0.0E				
251	0.0		0.0E				
252	.348		0.0E				
253	0.0		0.0E				
254	.5717		1.0E				
255	0.0		0.0E				
256	.5717		1.0E				
257	0.0		0.0E				
258	0.0		0.0E				
259	.0063		.0546E				
260	0.0		0.0E				
261	566.		550.7E				
262	0.0		0.0E				
263	0.0		0.0E				
264	0.0		0.0E				
265	0.0		0.0E				

	1	2	3	4	5	6	7
CARD	12345678901234567890123456789012345678901234567890						
266		0.0	0.0E				
267		4.84	-1.6E				
268		0.0	0.0E				
269		566.	550.7E				
270		566.	550.7E				
271	15.9E06		15.9E06E				
272		.123	.178E				
273		26.7	48.25E				
274		0.0	0.0E				
275		.348	0.0E				
276		0.0	0.0E				
277		0.0	0.0E				
278		.348	0.0E				
279		0.0	0.0E				
280		.5717	1.0E				
281		0.0	0.0E				
282		.5717	1.0E				
283		0.0	0.0E				
284		0.0	0.0E				
285		.0063	.0546E				
286		0.0	0.0E				
287		569.	550.7E				
288		0.0	0.0E				
289		0.0	0.0E				
290		0.0	0.0E				
291		0.0	0.0E				
292		0.0	0.0E				
293		4.84	-1.6E				
294		0.0	0.0E				
295		569.	550.7E				
296		569.	550.7E				
297	15.9E06		15.9E06E				
298		.123	.178E				
299		26.7	48.25E				
300		0.0	0.0E				
301		.348	0.0E				
302		0.0	0.0E				
303		0.0	0.0E				
304		.348	0.0E				
305		0.0	0.0E				
306		.5717	1.0E				
307		0.0	0.0E				
308		.5717	1.0E				
309		0.0	0.0E				
310		0.0	0.0E				

	1	2	3	4	5	6	7
CARD	123456789012345678901234567890123456789012345678901234567890						
311	.0063		.0546E				
312	0.0		0.0E				
313	572.		550.7E				
314	0.0		0.0E				
315	0.0		0.0E				
316	0.0		0.0E				
317	0.0		0.0E				
318	0.0		0.0E				
319	4.84		-1.6E				
320	0.0		0.0E				
321	572.		550.7E				
322	572.		550.7E				
323	15.9E06		15.9E06E				
324	.175		.211E				
325	26.6		48.10E				
326	0.0		0.0E				
327	.398		0.0E				
328	0.0		0.0E				
329	0.0		0.0E				
330	.398		0.0E				
331	0.0		0.0E				
332	.5717		1.0E				
333	0.0		0.0E				
334	.5717		1.0E				
335	0.0		0.0E				
336	0.0		0.0E				
337	.0063		.0546E				
338	0.0		0.0E				
339	575.		550.7E				
340	0.0		0.0E				
341	0.0		0.0E				
342	0.0		0.0E				
343	0.0		0.0E				
344	0.0		0.0E				
345	4.84		-1.6E				
346	0.0		0.0E				
347	575.		550.7E				
348	575.		550.7E				
349	15.9E06		15.9E06E				
350	.093		.159E				
351	20.1		36.3E				
352	0.0		0.0E				
353	.305		0.0E				
354	0.0		0.0E				
355	0.0		0.0E				

	1	2	3	4	5	6	7
CARD	123456789012345678901234567890123456789012345678901234567890	123456789012345678901234567890123456789012345678901234567890	123456789012345678901234567890123456789012345678901234567890	123456789012345678901234567890123456789012345678901234567890	123456789012345678901234567890123456789012345678901234567890	123456789012345678901234567890123456789012345678901234567890	123456789012345678901234567890123456789012345678901234567890
356	.305		0.0E				
357	0.0		0.0E				
358	.5717		1.0E				
359	0.0		0.0E				
360	.5717		1.0E				
361	0.0		0.0E				
362	0.0		0.0E				
363	.0063		.0546E				
364	0.0		0.0E				
365	578.		550.7E				
366	0.0		0.0E				
367	0.0		0.0E				
368	0.0		0.0E				
369	0.0		0.0E				
370	0.0		0.0E				
371	4.84		-1.6E				
372	0.0		0.0E				
373	578.		550.7E				
374	578.		550.7E				
375	15.9E06		15.9E06E				
376	.186		.319E				
377	40.1		72.3E				
378	0.0		0.0E				
379	.29		0.0E				
380	0.0		0.0E				
381	0.0		0.0E				
382	.29		0.0E				
383	0.0		0.0E				
384	.5717		1.0E				
385	0.0		0.0E				
386	.5717		1.0E				
387	0.0		0.0E				
388	0.0		0.0E				
389	.0063		.0546E				
390	0.0		0.0E				
391	581.		550.7E				
392	0.0		0.0E				
393	0.0		0.0E				
394	0.0		0.0E				
395	0.0		0.0E				
396	0.0		0.0E				
397	4.84		-1.6E				
398	0.0		0.0E				
399	581.		550.7E				
400	581.		550.7E				

	1	2	3	4	5	6	7
CARD	12345678901234567890123456789012345678901234567890						
401	15.9E06		15.9E06E				
402	.093		.1595E				
403	20.05		36.15E				
404	0.0		0.0E				
405	.2285		0.0E				
406	0.0		0.0E				
407	0.0		0.0E				
408	.2285		0.0E				
409	0.0		0.0E				
410	.5717		1.0E				
411	0.0		0.0E				
412	.5717		1.0E				
413	0.0		0.0E				
414	0.0		0.0E				
415	.0063		.0546E				
416	0.0		0.0E				
417	582.		550.7E				
418	0.0		0.0E				
419	0.0		0.0E				
420	0.0		0.0E				
421	0.0		0.0E				
422	0.0		0.0E				
423	4.84		-1.6E				
424	0.0		0.0E				
425	582.		550.7E				
426	582.		550.7E				
427	15.9E06		15.9E06E				
428	.085		.11E				
429	18.3		24.9E				
430	0.0		0.0E				
431	.2055		0.0E				
432	0.0		0.0E				
433	0.0		0.0E				
434	.2055		0.0E				
435	0.0		0.0E				
436	.5717		1.0E				
437	0.0		0.0E				
438	.5717		0.0E				
439	0.0		0.0E				
440	0.0		0.0E				
441	.0063		.0546E				
442	0.0		0.0E				
443	582.		550.70E				
444	0.0		0.0E				
445	0.0		0.0E				

CARD	1	2	3	4	5	6	7
	123456789012345678901234567890123456789012345678901234567890						
446	0.0		0.0E				
447	0.0		0.0E				
448	0.0		0.0E				
449	4.84		-1.6E				
450	0.0		0.0E				
451	582.		550.70E				
452	582.		550.70E				
453	15.9E06		15.9E06E				
454	0.0		.054E				
455	0.0		12.12E				
456	0.0		0.0E				
457	0.0		0.0E				
458	0.0		0.0E				
459	0.0		0.0E				
460	0.0		0.0E				
461	0.0		0.0E				
462	.5717		1.0E				
463	0.0		0.0E				
464	.5717		1.0E				
465	1.0		0.0E				
466	0.0		0.0E				
467	.0063		.0546E				
468	1.0		0.0E				
469	582.		582.E				
470	0.0		0.0E				
471	0.0		0.0E				
472	0.0		0.0E				
473	0.0		0.0E				
474	0.0		0.0E				
475	3.0		3.0E				
476	0.0		0.0E				
477	582.		582.E				
478	582.		582.E				
479	15.9E06		15.9E06E				
480	0.0		.107E				
481	0.0		24.24E				
482	0.0		0.0E				
483	0.0		0.0E				
484	0.0		0.0E				
485	0.0		0.0E				
486	0.0		0.0E				
487	0.0		0.0E				
488	.5717		1.0E				
489	0.0		0.0E				
490	.5717		1.0E				

	1	2	3	4	5	6	7
CARD	123456789012345678901234567890123456789012345678901234567890						
491	1.0		0.0E				
492	0.0		0.0E				
493	.0063		.0546E				
494	1.0		0.0E				
495	582.		582.E				
496	0.0		0.0E				
497	0.0		0.0E				
498	0.0		0.0E				
499	0.0		0.0E				
500	0.0		0.0E				
501	4.84		1.6E				
502	0.0		0.0E				
503	582.		582.E				
504	582.		582.E				
505	15.9E06		15.9E06E				
506	0.0		.23E				
507	0.0		51.2E				
508	0.0		0.0E				
509	0.0		0.0E				
510	0.0		0.0E				
511	0.0		0.0E				
512	0.0		0.0E				
513	0.0		0.0E				
514	.5717		1.0E				
515	0.0		0.0E				
516	0.0		0.0E				
517	0.0		0.0E				
518	0.0		0.0E				
519	0.0063		0.0546E				
520	0.0		0.0E				
521	582.		582.E				
522	0.0		0.0E				
523	0.0		0.0E				
524	0.0		0.0E				
525	0.0		0.0E				
526	0.0		0.0E				
527	0.0		3.13439E				
528	0.0		0.0E				
529	582.		582.E				
530	582.		582.E				
531	15.9E06		15.9E06E				
532	F 0.0i						
533	F 558.58L						
534	PIPE		2	2			
535	10		0	1	2		6

	1	2	3	4	5	6	7
CARD	123456789012345678901234567890123456789012345678901234567890						
536	0		1				
537							
538							
539	F 0.024129E						
540	F 0.00014976E						
541	F 0.0062068E						
542	F 0.0E						
543	F 0.0E						
544	F 0.08889E						
545	F 4E						
546	F 0.0E						
547	F 0.0E						
548	F 558.58E						
549	F 558.58E						
550	F 1.5887E07E						
551	FILL		3	3			
552	2		1	0	0		
553	0.024129	0.00014976		0.0	0.0	619.90	
554	1.5887E07	0.0					
555	PIPE		4	4			
556	10	10		4	3	6	
557	3	1					
558	0.04445	0.0127		0.0	0.0	560.0	
559	300.0						
560	F 0.07765E						
561	F 0.000482E						
562	F 0.00621E						
563	F 0.0E						
564	F 1.0E						
565	F 0.0889E						
566	F 4E						
567	F 0.0E						
568	F 4.4113E						
569	F 550.70E						
570	F 550.70E						
571	F 1.5887E07E						
572	F 0.0E						
573	F 300.0E						
574	PIPE		5	5			
575	10	10		5	4	6	
576	3	1					
577	0.04445	0.007314		0.0	0.0	560.0	
578	300.0						
579	F 0.09143E						
580	F 0.00056747E						

CARD		1	2	3	4	5	6	7
		12345678901	2345678901	2345678901	2345678901	2345678901	2345678901	234567890
581	F	0.00621E						
582	F	0.0E						
583	F	1.0E						
584	F	0.0889E						
585	F	4E						
586	F	0.0E						
587	F	4.4113E						
588	F	550.70E						
589	F	550.70E						
590	F	1.5887E07E						
591	F	0.0E						
592	F	300.0E						
593	BREAK			6		6		
594		5		0		0	0	
595		0.09143	0.00056747		0.0	550.70	1.6036E07	
596	FILL			7		7		
597		8		1		0	0	
598		0.09143	0.00056747		0.0	-5.1711	581.43	
599		1.5679E07	-2.2757E+01					
600	PIPE			8		8		
601		10	10		6	7		6
602		3	1					
603		0.0445	0.007366		0.0	0.0	560.0	
604		300.0						
605	F	0.15251E						
606	F	0.000947E						
607	F	0.00621E						
608	F	0.0E						
609	F	0.0E						
610	F	0.0889E						
611	F	4E						
612	F	0.0E						
613	F	5.1711E						
614	F	581.43E						
615	F	581.43E						
616	F	1.5679E07E						
617	F	0.0E						
618	F	300.0E						
619	PIPE			9		9		
620		10	10		7	8		6
621		3	1					
622		0.0445	0.012700		0.0	0.0	560.0	
623		300.0						
624	F	0.09143E						
625	F	0.00056747E						

CARD	1	2	3	4	5	6	7
123456789012345678901234567890123456789012345678901234567890							

626	F	0.00621E					
627	F	0.0E					
628	F	-1.0E					
629	F	0.0889E					
630	F	4E					
631	F	0.0E					
632	F	5.1711E					
633	F	581.43E					
634	F	581.43E					
635	F	1.5679E07E					
636	F	0.0E					
637	F	300.0E					
638	FILL		10	10			
639		9	1	0	0		
640		0.635	0.00002011	0.0	0.0	550.70	
641		1.5887E07	0.0				
642	PIPE		11	11			
643		1	0	9	10	6	
644		0	1				
645							
646							
647	F	0.635E					
648	F	0.00002011E					
649	F	0.00003167E					
650	F	0.0E					
651	F	-1.0E					
652	F	0.00635E					
653	F	4E					
654	F	0.0E					
655	F	0.0E					
656	F	550.70E					
657	F	550.70E					
658	F	1.5887E07E					
659		1.0E-3	0.01	20.0	1000.0		
660		1.0E+1	1.0E+1	20.0	1.0		
661		-1.0					

II. TRAC TRANSIENT INPUT DECK FOR THTF TEST 177

CARD	1	2	3	4	5	6	7
1	123456789012345678901234567890123456789012345678901234567890						
2		2					
3		THTF TEST 177 MODEL NO. 1					
4		Q9CA 26.0 GOPD2					
5		-1	0.0				
6		0	1	11	10		0
7		1.E-03	1.0E-05	1.0E-02	1.0E-01		
8		100	0	10	0		0
9		1	2	3	4		5
10		6	7	8	9		10
11		11E					
12	FILL		6	6			
13		5	2	0	47		
14		0.09143	0.00056747	0.0	4.7120		550.70
15		1.6036E07	2.2703E+01				
16		0.0	4.7120	0.2	-0.5537S		
17		0.5	-2.2149	1.0	-2.7143S		
18		2.0	-2.9097	3.0	-2.9640S		
19		4.00	-2.703	4.25	-2.277S		
20		4.50	-1.532	4.75	-1.630S		
21		5.00	-1.543	5.25	-1.619S		
22		5.50	-1.575	5.75	-1.369S		
23		6.00	-1.054	6.25	-0.869S		
24		6.50	-0.869	6.75	-0.869S		
25		7.00	-0.869	7.25	-1.206S		
26		7.50	-1.836	7.75	-2.401S		
27		8.00	-1.760	8.25	-1.119S		
28		8.50	-1.032	8.75	-0.891S		
29		9.00	-0.869	9.25	-1.401S		
30		9.50	-2.716	9.75	-3.477S		
31		10.00	-2.347	10.25	-2.390S		
32		10.50	-1.662	10.75	-1.260S		
33		11.00	-1.325	11.25	-1.510S		
34		11.50	-1.184	11.75	-0.891S		
35		12.00	-0.869	12.25	-1.021S		
36		12.50	-1.184	12.75	-2.216S		
37		13.00	-2.173	13.25	-2.249S		
38		13.50	-1.836	13.75	-2.564S		
39		14.00	-1.825E				
40	FILL		7	7			
41		8	2	0	112		
42		0.09143	0.00056747	0.0	-5.1711		581.43
43		1.5679E07	-2.2757E+01				
44		0.0	-5.171	0.10	-4.813S		
45		0.15	-4.205	0.20	-3.661S		
46		0.25	-3.454	0.30	-3.488S		

	1	2	3	4	5	6	7
CARD	123456789012345678901234567890123456789012345678901234567890	123456789012345678901234567890123456789012345678901234567890	123456789012345678901234567890123456789012345678901234567890	123456789012345678901234567890123456789012345678901234567890	123456789012345678901234567890123456789012345678901234567890	123456789012345678901234567890123456789012345678901234567890	123456789012345678901234567890123456789012345678901234567890
46	0.35	-3.553		0.40	-3.748S		
47	0.50	-4.161		0.55	-4.313S		
48	0.60	-4.443		0.65	-4.519S		
49	0.70	-4.563		0.75	-4.563S		
50	0.80	-4.476		0.85	-4.357S		
51	0.90	-4.086		0.95	-3.824S		
52	1.00	-3.488		1.05	-3.086S		
53	1.10	-2.802		1.15	-2.347S		
54	1.20	-2.152		1.25	-1.847S		
55	1.30	-1.424		1.35	-1.358S		
56	1.40	-1.151		1.45	-0.869S		
57	1.50	-0.869		1.55	-0.869S		
58	1.60	-0.869		1.65	-0.869S		
59	1.70	-0.869		1.75	-0.869S		
60	1.80	-0.869		1.85	-0.869S		
61	1.90	-0.869		2.30	-0.869S		
62	2.35	-0.869		2.40	-0.869S		
63	2.45	-0.880		2.50	-0.955S		
64	2.55	-1.163		2.60	-1.466S		
65	2.65	-1.554		2.70	-1.554S		
66	2.75	-1.608		2.80	-1.750S		
67	2.85	-1.934		2.90	-2.118S		
68	2.95	-2.270		3.00	-2.314S		
69	3.05	-3.509		3.10	-2.705S		
70	3.15	-2.749		3.20	-2.716S		
71	3.25	-2.987		3.30	-3.563S		
72	3.35	-3.955		3.40	-4.064S		
73	3.45	-4.454		3.50	-4.574S		
74	3.55	-4.498		3.60	-4.302S		
75	3.65	-4.270		3.70	-4.357S		
76	3.75	-4.498		3.80	-4.519S		
77	3.85	-4.367		3.90	-4.390S		
78	3.95	-4.769		4.00	-4.802S		
79	4.25	-4.465		4.50	-5.161S		
80	4.75	-6.030		5.00	-6.573S		
81	5.25	-7.409		5.50	-8.246S		
82	5.75	-9.050		6.00	-10.071S		
83	6.25	-10.397		6.50	-10.386S		
84	6.75	-10.473		7.00	-10.549S		
85	7.25	-8.213		7.50	-5.367S		
86	7.75	-5.834		8.00	-4.052S		
87	8.25	-5.150		8.50	-6.062S		
88	8.75	-5.204		9.00	-5.193S		
89	9.25	-3.118		9.50	-2.205S		
90	9.75	-2.032		10.00	-2.564S		

	1	2	3	4	5	6	7
CARD	123456789012345678901234567890123456789012345678901234567890						
91	10.25	-3.096		10.50	-3.542S		
92	10.75	-3.618		11.00	-3.085S		
93	11.25	-3.585		11.50	-3.998S		
94	11.75	-4.411		12.00	-4.932S		
95	12.25	-5.595		12.50	-5.823S		
96	12.75	-5.258		13.00	-4.509S		
97	13.25	-4.183		13.50	-4.204S		
98	13.75	-4.020		14.00	-3.553E		
99	FILL	10		10			
100	9	1		0	0		
101	0.635	0.00002011		0.0	0.0	619.90	
102	1.5887E07	0.0					
103	END						
104	1.0E-3	0.01		14.0	1000.0		
105	5.0E-1	1.0E-2		14.0	1.0		
106	-1.0						

APPENDIX E

TRAC STEADY-STATE INPUT DECKS FOR BENNETT RUNS 5442, 5431, AND 5336

I. TRAC STEADY-STATE INPUT DECK FOR BENNETT RUN 5442

CARD	1	2	3	4	5	6	7
1	1	0	0				
2	DATA COMPARISONS - TRAC-PD2 VS BENNETT VERTICAL TUBE - RUN 5442						
3	0	0.					
4	0	1	3	2			0
5	.100000E-02	.100000E-04	.100000E-01	.100000E+00			
6	10	20	10	1			0
7	0	1	0	2	0	0	0
8	1	0	0.0	0.0			
9	0	0	0	0			
10	FILL	1	01				
11	1	8	1	3			
12	0.1542	1.910E-05	0.0	0.0			541.5
13	6.895E06						
14	0.0	0.0	0.01	.60175			100.0
15	.60175						
16	PIPE	2	2				
17	24	5	1	2			10
18	1	0					
19	6.310000E-03	1.620000E-03	0.	0.			2.000000E+02
20	2.000000E+02						
21	F 1.5240E-01E						
22	F 1.9100E-05E						
23	F 1.2500E-04E						
24	F 0. E						
25	F 1.0000E+00E						
26	F 1.2600E-02E						
27	F 1E						
28	F 0. E						
29	F 0. E						
30	F 5.3740E+02E						
31	F 5.3740E+02E						
32	F 6.8900E+06E						
33	F 1.1340E+09E						
34	F 5.3740E+02E						
35	BREAK	3	03				
36	2	0	0	0			
37	0.1524	1.910E-05	1.0	557.9			6.89E06
38	0.00001	1.0	25.0	0.0			
39	1.0	0.1	25.0				
40	-1.0						

II. TRAC STEADY-STATE INPUT DECK FOR BENNETT RUN 5431

CARD	1	2	3	4	5	6	7
1	1	0	0				
2	DATA COMPARISONS - TRAC-PD2 VS BENNETT VERTICAL TUBE - RUN 5431						
3	0	0.					
4	0	1	3	2			0
5	.100000E-02	.100000E-04	.100000E-01	.100000E+00			
6	10	20	10	1			0
7	0	1	0	2	0	0	0
8	1	0	0.0	0.0			
9	0	0	0	0			
10	FILL	1	01				
11	1	8	1	3			
12	0.1524	1.910E-05	0.0	0.0			534.0
13	6.895E06						
14	0.0	0.0	0.01	.081375			100.0
15	.081375						
16	PIPE	2	2				
17	24	5	1	2			10
18	1	0					
19	6.310000E-03	1.620000E-03	0.	0.			2.000000E+02
20	2.000000E+02						
21	F	1.5240E-01E					
22	F	1.9100E-05E					
23	F	1.2500E-04E					
24	F	0. E					
25	F	1.0000E+00E					
26	F	1.2600E-02E					
27	F	1E					
28	F	0. E					
29	F	0. E					
30	F	5.3400E+02E					
31	F	5.3400E+02E					
32	F	6.8900E+06E					
33	F	4.3500E+08E					
34	F	5.3400E+02E					
35	BREAK	3	03				
36	2	0	0	0			
37	0.1524	1.910E-05	1.0	557.9			6.89E06
38	0.00001	1.0	25.0	0.0			
39	1.0	0.1	25.0				
40	-1.0						

III. TRAC STEADY-STATE INPUT DECK FOR BENNETT RUN 5336

CARD	1	2	3	4	5	6	7
1	1	0	0				
2	DATA COMPARISONS - TRAC-PD2 VS BENNETT VERTICAL TUBE - RUN 5431						
3	0	0.					
4	0	1	3	2			0
5	.100000E-02	.100000E-04	.100000E-01	.100000E+00			
6	10	20	10	1			0
7	0	1	0	2	0	0	0
8	1	0	0.0	0.0			
9	0	0	0	0			
10	FILL	1	01				
11	1	8	1	3			
12	0.1524	1.910E-05	0.0	0.0			534.0
13	6.895E06						
14	0.0	0.0	0.01	.081375			100.0
15	.081375						
16	PIPE	2	2				
17	24	5	1	2			10
18	1	0					
19	6.310000E-03	1.620000E-03	0.	0.			2.000000E+02
20	2.000000E+02						
21	F 1.5240E-01E						
22	F 1.9100E-05E						
23	F 1.2500E-04E						
24	F 0. E						
25	F 1.0000E+00E						
26	F 1.2600E-02E						
27	F 1E						
28	F 0. E						
29	F 0. E						
30	F 5.3400E+02E						
31	F 5.3400E+02E						
32	F 6.8900E+06E						
33	F 4.3500E+08E						
34	F 5.3400E+02E						
35	BREAK	3	03				
36	2	0	0				
37	0.1524	1.910E-05	1.0	557.9			6.89E06
38	0.00001	1.0	25.0	0.0			
39	1.0	0.1	25.0				
40	-1.0						

APPENDIX F

TYPICAL TRAC STEADY-STATE AND RESTART INPUT DECKS FOR CREARE COUNTERCURRENT-FLOW EXPERIMENTS

I. TYPICAL TRAC INPUT DECK FOR CREARE STEADY-STATE RUN

CARD	1	2	3	4	5	6	7
1	1						
2	CREARE CCFLOW WITH 30GPM 215K ECC AND J*GC=.043 LPP=1.04 BAR						
3							
4	1	0	25	24	1		
5	1.0E-3	1.E-5	1.0E-3				
6	10	50	10	1			
7	11	2	3	4	5		
8	6	7	8	9	10		
9	12	13	14	15	16		
10	17	18	19	20	21		
11	22	23	24	25	1		
12	2000	0	99.0	0.0			
13							
14	VESSEL	1	1				
15	7	2	8	12			
16	7	3	1				
17							
18							
19							
20	8026.0	502.0	17.3	0.6	1.0		
21	1.0						
22							
23							
24							
25	0.420	0.841	0.908	1.112	1.315		
26	1.416	1.518E					
27	0.1333	0.1460E					
28	0.7854	1.5710	2.3500	3.1420	3.927		
29	4.712	5.4980	6.2830E				
30	6	9	3	1			
31	6	11	3	2			
32	6	13	3	3			
33	6	15	3	4			
34	7	5	2	9			
35	7	1	2	60			
36	7	2	2	61			
37	7	3	2	62			
38	7	4	2	63			
39	7	6	2	64			
40	7	7	2	65			

	1	2	3	4	5	6	7
CARD	123456789012345678901234567890123456789012345678901234567890						

41		7	8	2	66
42	F	0.0E			
43	F	0.0E			
44	F	0.0E			
45	F	0.0E			
46	F	0.0E			
47	F	0.0E			
48	F	0.0E			
49	F	0.0E			
50	F	1.0E			
51	F	1.0E			
52	F	1.0E			
53	F	1.0E			
54	F	0.01E			
55	F	0.01E			
56	F	0.01E			
57	F	395.0E			
58	F	1.0E			
59	F	0.0E			
60	F	0.0E			
61	F	0.0E			
62	F	0.0E			
63	F	0.0E			
64	F	0.0E			
65	F	395.0E			
66	F	395.0E			
67	F	1.1E05E			
68	F	0.0E			
69	F	0.0E			
70	F	0.0E			
71	F	0.0E			
72	F	0.0E			
73	F	0.0E			
74	F	0.0E			
75	F	0.0E			
76	F	1.0E			
77	F	1.0E			
78	F	1.0E			
79	F	1.0E			
80	F	0.01E			
81	F	0.01E			
82	F	0.01E			
83	F	395.0E			
84	F	1.0E			
85	F	0.0E			

	1	2	3	4	5	6	7
CARD	123456789012345678901234567890123456789012345678901234567890						

86	F	0.0E					
87	F	0.0E					
88	F	0.0E					
89	F	0.0E					
90	F	0.0E					
91	F	395.0E					
92	F	395.0E					
93	F	1.1E05E					
94	F	0.0 E					
95	F	0.0 E					
96	F	0.0E					
97	F	0.0E					
98	F	0.0E					
99	F	0.0E					
100	F	0.0E					
101	F	0.0E					
102	F	1.0E					
103	F	1.0E					
104	F	1.0E					
105	F	1.0E					
106	F	0.01E					
107	F	0.01E					
108	F	0.01E					
109	F	395.0E					
110	F	1.C					
111	F	0.0E					
112	F	0.0E					
113	F	0.0E					
114	F	0.0E					
115	F	0.0E					
116	F	0.0E					
117	F	395.0E					
118	F	395.0E					
119	F	1.1E05E					
120	F	0.0 E					
121	F	0.0 E					
122	F	0.0E					
123	F	0.0E					
124	F	0.0E					
125	F	0.0E					
126	F	0.0E					
127	F	0.0E					
128	R 8	1.00R 8	1.0E				
129	F	1.0E					
130	F	1.0E					

		1	2	3	4	5	6	7
CARD		123456789012345678901234567890123456789012345678901234567890						
131	F	1.0E						
132	F	0.01E						
133	F	0.01E						
134	F	0.01E						
135	F	395.0E						
136	F	1.0E						
137	F	0.0E						
138	F	0.0E						
139	F	0.0E						
140	F	0.0E						
141	F	0.0E						
142	F	0.0E						
143	F	395.0E						
144	F	395.0E						
145	F	1.1E05E						
146	F	0.0 E						
147	F	0.0 E						
148	F	0.0E						
149	F	0.0E						
150	F	0.0E						
151	F	0.0E						
152	F	0.0E						
153	F	0.0E						
154	R 8	1.00R 8	1.0E					
155	F	1.0E						
156	F	1.0E						
157	F	1.0E						
158	F	0.01E						
159	F	0.01E						
160	F	0.01E						
161	F	395.0E						
162	F	1.0E						
163	F	0.0E						
164	F	0.0E						
165	F	0.0E						
166	F	0.0E						
167	F	0.0E						
168	F	0.0E						
169	F	395.0E						
170	F	395.0E						
171	F	1.1E05E						
172	F	0.0 E						
173	F	0.0 E						
174	F	0.0E						
175	F	0.0E						

		1	2	3	4	5	6	7
CARD		123456789012345678901234567890123456789012345678901234567890						
176	F	0.0E						
177	F	0.0E						
178	F	0.0E						
179	F	0.0E						
180	R 8	1.00		1.0	0.59		1.0	0.59
181		1.0		0.59	1.0		0.59E	
182	R 8	1.0		1.0	0.25		1.0	0.25
183		1.0		0.25	1.0		0.25E	
184	R 8	1.0		1.0	0.31		1.0	0.31
185		1.0		0.3	1.0		0.31E	
186	F	1.0E						
187	F	0.01E						
188	F	0.01E						
189	F	0.01E						
190	F	395.0E						
191	F	1.0E						
192	F	0.0E						
193	F	0.0E						
194	F	0.0E						
195	F	0.0E						
196	F	0.0E						
197	F	0.0E						
198	F	395.0E						
199	F	395.0E						
200	F	1.1E05E						
201	F	0.0 E						
202	F	0.0 E						
203	F	0.0E						
204	F	0.0E						
205	F	0.0E						
206	F	0.0E						
207	F	0.0E						
208	F	0.0E						
209	R 8	1.00R 8		1.0E				
210	F	1.0E						
211	F	1.0E						
212	F	1.0E						
213	F	0.01E						
214	F	0.01E						
215	F	0.01E						
216	F	395.0E						
217	F	1.0E						
218	F	0.0E						
219	F	0.0E						
220	F	0.0E						

	1	2	3	4	5	6	7
CARD	123456789012345678901234567890123456789012345678901234567890						
221	F	0.0E					
222	F	0.0E					
223	F	0.0E					
224	F	395.0E					
225	F	395.0E					
226	F	1.1E05E					
227	PIPE		10	10			
228		1	0	9		10	
229		0	1				
230							
231							
232	F	2.0E					
233	F	2.40E-2E					
234	F	2.53E-4E					
235	F	0.1E					
236	F	0.0E					
237	F	0.1E					
238	F	0E					
239	F	1.0E					
240	F	0.0E					
241	F	395.00E					
242	F	395.0E					
243	F	1.05E05E					
244	PIPE		19	19			
245		1	0	50		60	
246		0	1				
247							
248							
249	F	2.0E					
250	F	2.40E-2E					
251	F	2.53E-4E					
252	F	0.1E					
253	F	0.0E					
254	F	0.1E					
255	F	0E					
256	F	1.0E					
257	F	0.0E					
258	F	395.00E					
259	F	395.0E					
260	F	1.05E05E					
261	PIPE		20	20			
262		1	0	51		61	
263		0	1				
264							
265							

		1	2	3	4	5	6	7
CARD		1234567890123456789012345678901234567890123456789012345678901234567890						
266	F	2.0E						
267	F	2.40E-2E						
268	F	2.53E-4E						
269	F	0.1E						
270	F	0.0E						
271	F	0.1E						
272	F	0E						
273	F	1.0E						
274	F	0.0E						
275	F	395.00E						
276	F	395.0E						
277	F	1.05E05E						
278	PIPE			21		21		
279		1		0		52		62
280		0		1				
281								
282								
283	F	2.0E						
284	F	2.40E-2E						
285	F	2.53E-4E						
286	F	0.1E						
287	F	0.0E						
288	F	0.1E						
289	F	0E						
290	F	1.0E						
291	F	0.0E						
292	F	395.00E						
293	F	395.0E						
294	F	1.05E05E						
295	PIPE			22		22		
296		1		0		53		63
297		0		1				
298								
299								
300	F	2.0E						
301	F	2.40E-2E						
302	F	2.53E-4E						
303	F	0.1E						
304	F	0.0E						
305	F	0.1E						
306	F	0E						
307	F	1.0E						
308	F	0.0E						
309	F	395.00E						
310	F	395.0E						

CARD	1	2	3	4	5	6	7
	123456789012345678901234567890123456789012345678901234567890						
311	F	1.05E05E					
312	PIPE		23	23			
313		1	0	54		64	
314		0	1				
315							
316							
317	F	2.0E					
318	F	2.40E-2E					
319	F	2.53E-4E					
320	F	0.1E					
321	F	0.0E					
322	F	0.1E					
323	F	0E					
324	F	1.0E					
325	F	0.0E					
326	F	395.00E					
327	F	395.0E					
328	F	1.05E05E					
329	PIPE		24	24			
330		1	0	55		65	
331		0	1				
332							
333							
334	F	2.0E					
335	F	2.40E-2E					
336	F	2.53E-4E					
337	F	0.1E					
338	F	0.0E					
339	F	0.1E					
340	F	0E					
341	F	1.0E					
342	F	0.0E					
343	F	395.00E					
344	F	395.0E					
345	F	1.05E05E					
346	PIPE		25	25			
347		1	0	56		66	
348		0	1				
349							
350							
351	F	2.0E					
352	F	2.40E-2E					
353	F	2.53E-4E					
354	F	0.1E					
355	F	0.0E					

CARD		1	2	3	4	5	6	7
		123456789012345678901234567890123456789012345678901234567890						
356	F	0.1E						
357	F	0E						
358	F	1.0E						
359	F	0.0E						
360	F	395.00E						
361	F	395.0E						
362	F	1.05E05E						
363	FILL		11		11			
364		10						
365		0.1	0.1		1.0	28.2		375.0
366		1.05E05						
367	FILL		12		12			
368		50						
369		0.1	0.1		1.0	28.2		375.0
370		1.05E05						
371	FILL		13		13			
372		51						
373		0.1	0.1		1.0	28.2		375.0
374		1.05E05						
375	FILL		14		14			
376		52						
377		0.1	0.1		1.0	28.2		375.0
378		1.05E05						
379	FILL		15		15			
380		53						
381		0.1	0.1		1.0	28.2		375.0
382		1.05E05						
383	FILL		16		16			
384		54						
385		0.1	0.1		1.0	28.2		375.0
386		1.05E05						
387	FILL		17		17			
388		55						
389		0.1	0.1		1.0	28.2		375.0
390		1.05E05						
391	FILL		18		18			
392		56						
393		0.1	0.1		1.0	28.2		375.0
394		1.05E05						
395	PIPE		2		2			
396		1	0		1	5		1
397		0	0					
398								
399								
400	F	0.1E						

CARD	1	2	3	4	5	6	7
123456789012345678901234567890123456789012345678901234567890							
401 F	1.78E-4E						
402 F	1.78E-3E						
403 F	0.1E						
404 F	0.0E						
405 F	4.76E-2E						
406 F	0E						
407 F	1.0E						
408 F	0.0E						
409 F	395.0E						
410 F	395.0E						
411 F	1.12E5E						
412 PIPE			3	3			
413	1		0	2		6	1
414	0		0				
415							
416							
417 F	0.1E						
418 F	1.78E-4E						
419 F	1.78E-3E						
420 F	0.1E						
421 F	0.0E						
422 F	4.76E-2E						
423 F	0E						
424 F	1.0E						
425 F	0.0E						
426 F	395.0E						
427 F	395.0E						
428 F	1.12E5E						
429 PIPE			4	4			
430	1		0	3		7	1
431	0		0				
432							
433							
434 F	1.6E						
435 F	2.84E-3E						
436 F	1.78E-3E						
437 F	0.001E						
438 F	0.0E						
439 F	4.76E-2E						
440 F	0E						
441 F	1.0E						
442 F	0.0E						
443 F	395.0E						
444 F	395.0E						
445 F	1.12E5E						

		1	2	3	4	5	6	7
CARD		123456789012345678901234567890123456789012345678901234567890						
446	PIPE			5	5			
447		1		0	4		8	1
448		0		0				
449								
450								
451	F	0.1E						
452	F	1.78E-4E						
453	F	1.78E-3E						
454	F	0.1E						
455	F	0.0E						
456	F	4.76E-2E						
457	F	0E						
458	F	1.0E						
459	F	0.0E						
460	F	395.0E						
461	F	395.0E						
462	F	1.12E5E						
463	FILL		6		6			
464		5						
465		.1	0.1		0.0		0.0	395.0
466		1.05E05						
467	FILL		7		7			
468		6						
469		.1	0.1		0.0		0.0	395.0
470		1.05E05						
471	FILL		9		9			
472		8						
473		.1	0.1		0.0		0.0	395.0
474		1.05E05						
475	BREAK		8		8			
476		7					3	
477		0.1	0.1		1.0		380.0	1.05E05
478		0.1E-4	0.1		50.0			
479		5.00	0.10		5.0			
480	-1.0							

II. TYPICAL TRAC RESTART INPUT DECK FOR CREARE TRANSIENT RUN

	1	2	3	4	5	6	7
CARD	123456789012345678901234567890123456789012345678901234567890						
1	1						
2	CREARE CCFLOW	30	GPM ECC FLOW	RESTART DECK			
3	-9342		20.0				
4			1	25		24	1
5	1.0E-3		1.0E-5	1.0E-2			
6	10		50			1	
7	11		2	3		4	5
8	6		7	8		9	10
9	12		13	14		15	16
10	17		18	19		20	21
11	22		23	24		25	1
12	2000		0	99.0		0.0	
13							
14	FILL		6	6			
15	5						
16	.1		0.1	0.0		0.3545	374.0
17	1.12E5						
18	FILL		7	7			
19	6						
20	.1		0.1	0.0		0.3545	374.0
21	1.12E5						
22	FILL		9	9			
23	8						
24	.1		0.1	0.0		0.3545	374.0
25	1.12E5						
26	END						
27	1.0E-4		0.1	50.0			
28	5.00		0.10	5.0			
29	-1.0						

APPENDIX G

TRAC TRANSIENT INPUT DECK FOR FLECHT TEST 17201

CARD	1	2	3	4	5	6	7	8
1	2							
2	FLECHT SKEWED PROFILE LOW FLOODING RATE TEST NO. 17201	01/08/79						
3	(V = 6 IN/SEC	TIN = 127.0 F	TCLAD = 1630 F)					
4	0	0.0						
5	0	1	5	4	0			
6	1.0E-03	1.0E-05	1.0E-02	1.0E-1				
7	10	0	10	1	0			
8	1	2	3	4	5E			
9	1001	0	1.0E-05	0.0				
10	0	0	0					
11	FILL	1	01					
12	1	2	0	3				
13	3.048E-01	3.956E-03	0.0	0.0	326.0			
14	3.100E+05							
15	0.0	0.0	1.0E-05	0.1524	1.0E03			
16	0.1524E							
17	PIPE	2	02				INLET	
18	1	0	1	2	6			
19	0	0						
20	8.890E-02	4.775E-03	0.0	0.0	300.0			
21	300.0							
22	F 3.048E-01E							
23	F 3.956E-03E							
24	F 1.293E-02E							
25	F 0.0E							
26	F 0.0E							
27	F 1.544E-02E							
28	F 1E							
29	F 0.0E							
30	F 0.0E							

CARD	1	2	3	4	5	6	7	8
	1234567890123456789012345678901234567890123456789012345678901234567890							
31	F	326.0E						
32	F	326.0E						
33	F	3.10E+05E						
34	PIPE		3	03				OUTLET
35		1	0	3		4	6	
36		0	0					
37		8.890E-02	4.775E-03	0.0		0.0	300.0	
38		300.0						
39	F	3.048E-01E						
40	F	3.956E-03E						
41	F	1.298E-02E						
42	F	0.0E						
43	F	0.0E						
44	F	1.544E-02E						
45	F	1E						
46	F	1.0E						
47	F	0.0E						
48	F	403.9E						
49	F	403.9E						
50	F	2.758E05E						
51	BREAK		4	04				
52		4	0	0		0		
53		3.048E-01	3.956E-03	1.0		403.9	2.758E05	
54	VESSEL		5	05				
55		16	1	1		2		
56		0	0	0		15	2	
57		1						
58		0	0	0		1		
59		4.0E+00	5.0E+01	5.0E-03				
60		7.8488E03	4.663E02	4.33E01		0.80	6.0E04	
61		1.336						
62		9	12	7		1001		
63		1001	0	0		0	100	
64		0.00E05	0.0	0.0				
65		0.1524	0.4064	0.8636		1.1684	1.4732	

CARD	1	2	3	4	5	6	7	8
66	1.7780	2.0828	2.3876	2.6924	2.9972			
67	3.2258	3.5306	3.6830	3.8354	4.0640			
68	4.2164E							
69	0.1576E							
70	0.1576E							
71	1	1	-2	2				
72	16	1	2	3				
73 R 2	0.0R 3	1.0R 4	0.0E					
74 F	1.0E							
75	0.48	0.52	0.59	0.66	0.71			
76	0.77	0.83	0.89	0.95	1.00			
77	1.00	0.90	0.66	0.53E				
78	100.0E							
79	0.0	4.445E-04	8.890E-04	1.397E-03	1.905E-03			
80	3.328E-03	4.750E-03	5.055E-03	5.359E-03E				
81	4	4	5	5	4			
82	4	8	8E					
83	0.0	0.000E05	10.0	0.000E05	20.0			
84	0.000E05	30.0	5.538E05	50.0	5.277E05			
85	70.0	5.084E05	100.0	4.867E05	150.0			
86	4.608E05	200.0	4.326E05	300.0	3.945E05			
87	500.0	3.499E05	1000.0	2.963E05E				
88 R13	3E							
89 F	0.0E							
90 F	0.0E							
91 F	0.0E							
92 F	0.0E							
93 F	0.0E							
94 F	0.0E							
95 F	0.0E							
96 F	0.0E							
97 F	0.0E							
98 F	0.0E							
99 F	0.0E							
100 F	0.0E							

LEVEL 1
(LOWER
PLENUM)

		1	2	3	4	5	6	7	8
CARD		12345678901234567890123456789012345678901234567890123456789012345678901234567890							
101	F		0.0E						
102	F		0.0E						
103	F		0.0E						
104	F		0.0E						
105	F	5.228E-01E							
106	F		0.0E						
107	F	5.228E-01E							
108	F		0.0E						
109	F		0.0E						
110	F	1.544E-02E							
111	F		0.0E						
112	F		0.0E						
113	F		0.0E						
114	F		0.0E						
115	F		0.0E						
116	F		0.0E						
117	F		0.0E						
118	F		0.0E						
119	F		0.0E						
120	F	405.0E							
121	F	350.0E							
122	F	2.758E05E							
123	F		0.0E						
124	F		0.0E						
125	F		0.0E						
126	F		0.0E						
127	F		0.0E						
128	F		0.0E						
129	F		0.0E						
130	F		0.0E						
131	F	5.228E-01E							
132	F		0.0E						
133	F	5.228E-01E							
134	F		0.0E						
135	F		0.0E						

LEVEL 2
(UNHEATED
SECTION)

		1	2	3	4	5	6	7	8
CARD		12345678901	23456789012	34567890123	45678901234	56789012345	67890123456	78901234567	8901234567890
136	F	1.544E-02E							
137	F	0.0E							
138	F	0.0E							
139	F	0.0E							
140	F	0.0E							
141	F	0.0E							
142	F	0.0E							
143	F	0.0E							
144	F	0.0E							
145	F	0.0E							
146	F	405.0E							
147	F	400.0E							
148	F	2.7580E05E							
149	F	0.0E							
150	F	0.0E							
151	F	0.0E							
152	F	0.0E							
153	F	0.0E							
154	F	0.0E							
155	F	0.0E							
156	F	0.0E							
157	F	5.228E-01E							
158	F	0.0E							
159	F	5.228E-01E							
160	F	0.0E							
161	F	0.0E							
162	F	1.544E-02E							
163	F	0.0E							
164	F	425.0E							
165	F	1.0E							
166	F	0.0E							
167	F	0.0E							
168	F	0.0E							
169	F	0.0E							
170	F	0.0E							

LEVEL 3
(FIRST
HEATED
SECTION)

		1	2	3	4	5	6	7	8
CARD		1234567890123456789012345678901234567890123456789012345678901234567890							
171	F		0.0E						
172	F		630.0E						
173	F		405.0E						
174	F		2.7580E05E						
175	F		0.0E						
176	F		0.0E						
177	F		0.0E						
178	F		0.0E						
179	F		0.0E						
180	F		0.0E						
181	F		0.0E						
182	F		0.0E						
183	F		5.228E-01E						
184	F		0.0E						
185	F		5.228E-01E						
186	F		0.0E						
187	F		0.0E						
188	F		1.544E-02E						
189	F		0.0E						
190	F		425.0E						
191	F		1.0E						
192	F		0.0E						
193	F		0.0E						
194	F		0.0E						
195	F		0.0E						
196	F		0.0E						
197	F		0.0E						
198	F		675.0E						
199	F		405.0E						
200	F		2.7580E05E						
201	F		0.0E						
202	F		0.0E						
203	F		0.0E						
204	F		0.0E						
205	F		0.0E						

CARD		1	2	3	4	5	6	7	8
		1234567890123456789012345678901234567890123456789012345678901234567890							
206	F		0.0E						
207	F		0.0E						
208	F		0.0E						
209	F	5.228E-01E							
210	F		0.0E						
211	F	5.228E-01E							
212	F		0.0E						
213	F		0.0E						
214	F	1.544E-02E							
215	F		0.0E						
216	F	430.0E							
217	F		1.0E						
218	F		0.0E						
219	F		0.0E						
220	F		0.0E						
221	F		0.0E						
222	F		0.0E						
223	F		0.0E						
224	F	720.0E							
225	F	405.0E							
226	F	2.7580E05E							
227	F		0.0E						
228	F		0.0E						
229	F		0.0E						
230	F		0.0E						
231	F		0.0E						
232	F		0.0E						
233	F		0.0E						
234	F		0.0E						
235	F	5.228E-01E							
236	F		0.0E						
237	F	5.228E-01E							
238	F		0.0E						
239	F		0.0E						
240	F	1.544E-02E							

		1	2	3	4	5	6	7	8
CARD		12345678901234567890123456789012345678901234567890123456789012345678901234567890							
241	F		0.0E						
242	F		435.0E						
243	F		1.0E						
244	F		0.0E						
245	F		0.0E						
246	F		0.0E						
247	F		0.0E						
248	F		0.0E						
249	F		0.0E						
250	F		775.0E						
251	F		405.0E						
252	F		2.7580E05E						
253	F		0.0E						
254	F		0.0E						
255	F		0.0E						
256	F		0.0E						
257	F		0.0E						
258	F		0.0E						
259	F		0.0E						
260	F		0.0E						
261	F		5.228E-01E						
262	F		0.0E						
263	F		5.228E-01E						
264	F		0.0E						
265	F		0.0E						
266	F		1.544E-02E						
267	F		0.0E						
268	F		440.0E						
269	F		1.0E						
270	F		0.0E						
271	F		0.0E						
272	F		0.0E						
273	F		0.0E						
274	F		0.0E						
275	F		0.0E						

CARD		1	2	3	4	5	6	7	8
		12345678901	2345678901	2345678901	2345678901	2345678901	2345678901	2345678901	234567890
276	F		805.0E						
277	F		405.0E						
278	F		2.7580E05E						
279	F		0.0E						
280	F		0.0E						
281	F		0.0E						
282	F		0.0E						
283	F		0.0E						
284	F		0.0E						
285	F		0.0E						
286	F		0.0E						
287	F		5.228E-01E						
288	F		0.0E						
289	F		5.228E-01E						
290	F		0.0E						
291	F		0.0E						
292	F		1.544E-02E						
293	F		0.0E						
294	F		455.0E						
295	F		1.0E						
296	F		0.0E						
297	F		0.0E						
298	F		0.0E						
299	F		0.0E						
300	F		0.0E						
301	F		0.0E						
302	F		840.0E						
303	F		405.0E						
304	F		2.7580E05E						
305	F		0.0E						
306	F		0.0E						
307	F		0.0E						
308	F		0.0E						
309	F		0.0E						
310	F		0.0E						

		1	2	3	4	5	6	7	8
CARD		12345678901234567890123456789012345678901234567890123456789012345678901234567890							
311	F		0.0E						
312	F		0.0E						
313	F		5.228E-01E						
314	F		0.0E						
315	F		5.228E-01E						
316	F		0.0E						
317	F		0.0E						
318	F		1.544E-02E						
319	F		0.0E						
320	F		480.0E						
321	F		1.0E						
322	F		0.0E						
323	F		0.0E						
324	F		0.0E						
325	F		0.0E						
326	F		0.0E						
327	F		0.0E						
328	F		875.0E						
329	F		405.0E						
330	F		2.7580E05E						
331	F		0.0E						
332	F		0.0E						
333	F		0.0E						
334	F		0.0E						
335	F		0.0E						
336	F		0.0E						
337	F		0.0E						
338	F		0.0E						
339	F		5.228E-01E						
340	F		0.0E						
341	F		5.228E-01E						
342	F		0.0E						
343	F		0.0E						
344	F		1.544E-02E						
345	F		0.0E						

		1	2	3	4	5	6	7	8
CARD		1234567890123456789012345678901234567890123456789012345678901234567890							
346	F	497.0E							
347	F	1.0E							
348	F	0.0E							
349	F	0.0E							
350	F	0.0E							
351	F	0.0E							
352	F	0.0E							
353	F	0.0E							
354	F	925.0E							
355	F	405.0E							
356	F	2.7580E05E							
357	F	0.0E							
358	F	0.0E							
359	F	0.0E							
360	F	0.0E							
361	F	0.0E							
362	F	0.0E							
363	F	0.0E							
364	F	0.0E							
365	F	5.228E-01E							
366	F	0.0E							
367	F	5.228E-01E							
368	F	0.0E							
369	F	0.0E							
370	F	1.544E-02E							
371	F	0.0E							
372	F	490.0E							
373	F	1.0E							
374	F	0.0E							
375	F	0.0E							
376	F	0.0E							
377	F	0.0E							
378	F	0.0E							
379	F	0.0E							
380	F	975.0E							

		1	2	3	4	5	6	7	8
CARD		12345678901234567890123456789012345678901234567890123456789012345678901234567890							
381	F		405.0E						
382	F	2.7580E05E							
383	F		0.0E						
384	F		0.0E						
385	F		0.0E						
386	F		0.0E						
387	F		0.0E						
388	F		0.0E						
389	F		0.0E						
390	F		0.0E						
391	F	5.228E-01E							
392	F		0.0E						
393	F	5.228E-01E							
394	F		0.0E						
395	F		0.0E						
396	F	1.544E-02E							
397	F		0.0E						
398	F		470.0E						
399	F		1.0E						
400	F		0.0E						
401	F		0.0E						
402	F		0.0E						
403	F		0.0E						
404	F		0.0E						
405	F		0.0E						
406	F	1015.0E							
407	F		405.0E						
408	F	2.7580E05E							
409	F		0.0E						
410	F		0.0E						
411	F		0.0E						
412	F		0.0E						
413	F		0.0E						
414	F		0.0E						
415	F		0.0E						

CARD	1	2	3	4	5	6	7	8
	1234567890123456789012345678901234567890123456789012345678901234567890							
416	F	0.0E						
417	F	5.228E-01E						
418	F	0.0E						
419	F	5.228E-01E						
420	F	0.0E						
421	F	0.0E						
422	F	1.544E-02E						
423	F	0.0E						
424	F	450.0E						
425	F	1.0E						
426	F	0.0E						
427	F	0.0E						
428	F	0.0E						
429	F	0.0E						
430	F	0.0E						
431	F	0.0E						
432	F	990.0E						
433	F	405.0E						
434	F	2.7580E05E						
435	F	0.0E						
436	F	0.0E						
437	F	0.0E						
438	F	0.0E						
439	F	0.0E						
440	F	0.0E						
441	F	0.0E						
442	F	0.0E						
443	F	5.228E-01E						
444	F	0.0E						
445	F	5.228E-01E						
446	F	0.0E						
447	F	0.0E						
448	F	1.544E-02E						
449	F	0.0E						
450	F	435.0E						

		1	2	3	4	5	6	7	8
CARD		1234567890	1234567890	1234567890	1234567890	1234567890	1234567890	1234567890	1234567890
451	F			1.0E					
452	F			0.0E					
453	F			0.0E					
454	F			0.0E					
455	F			0.0E					
456	F			0.0E					
457	F			0.0E					
458	F			940.0E					
459	F			405.0E					
460	F		2.7580E05E						
461	F			0.0E					
462	F			0.0E					
463	F			0.0E					
464	F			0.0E					
465	F			0.0E					
466	F			0.0E					
467	F			0.0E					
468	F			0.0E					
469	F		5.228E-01E						
470	F			0.0E					
471	F		5.228E-01E						
472	F			0.0E					
473	F			0.0E					
474	F		1.544E-02E						
475	F			0.0E					
476	F		419.0E						
477	F			1.0E					
478	F			0.0E					
479	F			0.0E					
480	F			0.0E					
481	F			0.0E					
482	F			0.0E					
483	F			0.0E					
484	F			800.0E					
485	F			405.0E					

CARD	1	2	3	4	5	6	7	8
486	F	2.7580E05E						
487	F	0.0E						LEVEL 16
488	F	0.0E						(UPPER
489	F	0.0E						PLENUM)
490	F	0.0E						
491	F	0.0E						
492	F	0.0E						
493	F	0.0E						
494	F	0.0E						
495	F	5.228E-01E						
496	F	0.0E						
497	F	5.228E-01E						
498	F	0.0E						
499	F	0.0E						
500	F	1.544E-02E						
501	F	0.0E						
502	F	0.0E						
503	F	1.0E						
504	F	0.0E						
505	F	0.0E						
506	F	0.0E						
507	F	0.0E						
508	F	0.0E						
509	F	0.0E						
510	F	405.0E						
511	F	405.0E						
512	F	2.7580E05E						
513	F	0.0E						VESSEL
514	R 9	800.0R 9	824.9R 9	866.6R 9	922.1R 9	966.6	ROD	
515	R 9	1011.0R 9	1052.7R 9	1094.3R 9	1122.1R 9	1138.8	DATA	
516	R 9	1094.3R 9	1027.7R 9	922.1R 9	800.0E			
517		1.0E-06	1.0E+00	18.0E+00				
518		3.0E+00	1.0E-02	3.0E+00				
519		-1.0						

APPENDIX H

TRAC STEADY-STATE AND TRANSIENT INPUT DECKS FOR SEMISCALE MOD-1 TEST S-02-8

I. TRAC STEADY-STATE INPUT DECK FOR SEMISCALE MOD-1 TEST S-02-8

CARD	1	2	3	4	5	6	7	8
1	3	0						
2	SP5 SS USING TRAC VER 26.0							
3	SP5SPD26 S63 TYPE VESSEL ,AND PUMP							
4	STEADY STATE							
5	0	0.						
6	1	0	13		13		01	
7	1.00000E-02	1.00000E-05	1.00000E-03	0.				
8	10	00	10		3		0	
9	0	1 0	2 0	3 0	4 0		5	
10	0	7 0	8 0	9 0	10 0		11	
11	0	12 0	13 0	6 0	0 0		0	
12	100	0	.100000E+04	0.				
13	0	0	0		0			
14	1000	0	.100000E+04	0.				
15	0	0	0		0			
16	900	0	.10000E+04		0			
17	0	0	0		0			
18	TEE	1	0					
19	4	1	7 0.				3	
20	0	6	1		2		0	
21	3.335020E-02	1.112520E-02	0.	0.		2.950000E+02		
22	2.950000E+02							
23	1	5	8					
24	9.425000E-03	3.911600E-03	0.	0.		2.950000E+02		
25	2.950000E+02							
26	F 5.1480E-01E							
27	F 1.7986E-03E							
28	3.4942E-02F	3.4942E-03E						
29	F 0.	E						
30	R 6 0.	R 1 1.0000E+00E						

CARD		1	2	3	4	5	6	7	8
31	F	6.6700E-02E							
32	F		4E						
33	F	0.	E						
34	F	0.	E						
35	F	5.9640E+02E							
36	F	5.9640E+02E							
37	F	1.5596E+07E							
38	F	0.	E						
39	F	5.9640E+02E							
40		5.0000E-02	1.6720E+00	7.2000E-01	2.0300E-01	4.0000E-03E			
41		1.7471E-04	7.1745E-05	3.0895E-05	7.0930E-04	9.1040E-05E			
42		3.4942E-03R 3	4.2910E-05R 1	3.4940E-03	2.2760E-02E				
43	F	6.8000E-03E							
44	F	1.0000E+00E							
45		6.6700E-02R 3	7.3900E-03R 1	6.6700E-02R 1	1.7000E-01E				
46	F		4E						
47	F	0.	E						
48	F	0.	E						
49	F	5.9640E+02E							
50	F	5.9640E+02E							
51	F	1.5596E+07E							
52	F	0.	E						
53	F	5.9640E+02E							
54	STGEN		2	0					
55		22	3	2	3	10			
56		1	0	0	1				
57		5.100000E-03	1.200000E-03						
58		12	9	10					
59	R 1	4.6000E-01R20	2.5680E-01R 1	4.6000E-01E					
60	R 1	9.6278E-03R20	1.1398E-03R 1	9.6278E-03E					
61	R 1	3.4942E-03R21	4.4000E-03R 1	3.4942E-03E					
62	R 1	0.	R21 9.3000E-02R 1	0.	E				
63	R11	1.0000E+00R 1	0.	R11-1.0000E+00E					
64	R 1	6.6700E-02R21	1.0200E-02R 1	6.6700E-02E					
65	R 1		4R21	1R 1	4E				

CARD		1	2	3	4	5	6	7	8
66	F	0.	E						
67	F	0.	E						
68		5.9640E+02	5.9440E+02	5.9240E+02	5.9040E+02	5.8840E+02			
69		5.8640E+02	5.8440E+02	5.8240E+02	5.8040E+02	5.7840E+02			
70		5.7640E+02	5.7440E+02	5.7240E+02	5.7040E+02	5.6840E+02			
71		5.6640E+02	5.6440E+02	5.6240E+02	5.6040E+02	5.5840E+02			
72		5.5640E+02	5.5440E+02E						
73		5.9640E+02	5.9440E+02	5.9240E+02	5.9040E+02	5.8840E+02			
74		5.8640E+02	5.8440E+02	5.8240E+02	5.8040E+02	5.7840E+02			
75		5.7640E+02	5.7440E+02	5.7240E+02	5.7040E+02	5.6840E+02			
76		5.6640E+02	5.6440E+02	5.6240E+02	5.6040E+02	5.5840E+02			
77		5.5640E+02	5.5440E+02E						
78	F	1.5596E+07E							
79	F	5.5000E+02E							
80	F	2.5680E-01E							
81	R10	1.1210E-02R	2 7.5000E-02E						
82	R11	4.3830E-02R	2 9.2000E-03E						
83	F	0.	E						
84	F	1.0000E+00E							
85	F	1.8800E-02E							
86	F		4E						
87	R 2	0.	R 1 3.0300E-01R	1 3.6722E-01R	1 4.3144E-01R	1 4.9567E-01			
88	R 1	5.5989E-01R	1 6.2411E-01R	1 6.8833E-01R	1 7.5256E-01R	1 8.1678E-01			
89	R 1	8.8100E-01E							
90		5.0000E-03	5.2400E-03	5.5000E-03	7.9000E-01	9.0222E-01			
91		1.0144E+00	1.1267E+00	1.2389E+00	1.3511E+00	1.4633E+00			
92		1.5756E+00	1.6878E+00	1.8000E+00E					
93	R 1	5.1700E+02R	1 5.3820E+02R	10 5.4430E+02E					
94	R 1	5.1700E+02R	1 5.3820E+02R	10 5.4430E+02E					
95		5.5700E+06	5.5691E+06	5.5682E+06	5.5673E+06	5.5664E+06			
96		5.5655E+06	5.5645E+06	5.5636E+06	5.5627E+06	5.5618E+06			
97		5.5609E+06	5.5600E+06E						
98	R 1	0.	R20 4.0000E-01R	1 0.					E
99	F	5.5330E-01E							
100	PIPE			3		0			

CARD	1	2	3	4	5	6	7	8
101		6	1	3		4	7	
102		3	0					
103	3.324800E-02	1.112520E-02	0.		0.		2.950000E+02	
104	2.950000E+02							
105	R 3 5.1000E-01R	3 4.6140E-01E						
106	R 3 1.7820E-03R	3 1.6122E-03E						
107	F 3.4942E-03E							
108	F 0.	E						
109	R 1-1.0000E+00R	1 0.	R 1-1.0000E+00R	2 1.0000E+00R	2 0.		E	
110	F 6.6700E-02E							
111	F 4E							
112	F 0.	E						
113	F 0.	E						
114	F 5.5440E+02E							
115	F 5.5440E+02E							
116	F 1.5596E+07E							
117	F 0.	E						
118	F 5.5440E+02E							
119	PUMP		4	0				
120		7	1	4		5	7	
121		0	0	1		0	1	
122		0	0					
123	3.324800E-02	1.112520E-02	0.		0.		2.945000E+02	
124	2.950000E+02							
125	5.739000E+02	4.345000E+01	1.148000E-02	1.000000E+03		3.728000E+02		
126	2.662000E+00	0.	3.730000E+00	3.024000E+02				
127	1							
128	R 2 5.8350E-01R	5 4.8430E-01E						
129	R 2 2.0388E-03R	5 1.6922E-03E						
130	F 3.4942E-03E							
131	F 0.	E						
132	F 0.	E						
133	F 6.6700E-02E							
134	F 4E							
135	F 0.	E						

CARD	1	2	3	4	5	6	7	8
136	F	0.	E					
137	F	5.5440E+02E						
138	F	5.5440E+02E						
139	F	1.5596E+07E						
140	F	0.	E					
141	F	5.5440E+02E						
142	PRIZER		5	0				
143		4	8					
144		8.000000E+03	1.559600E+07	1.000000E+05	1.000000E-01			
145	R 2	5.0000E-01R	1 1.2840E-01R	1 2.0000E-02E				
146	R 2	1.1730E-02R	1 3.0125E-03R	1 4.6920E-04E				
147	F	2.2760E-02E						
148	F	0.	E					
149	F	-1.0000E+00E						
150	F	1.7000E-01E						
151	F	4E						
152	R 1	1.0000E+00R	3 0.	E				
153	F	0.	E					
154	F	5.9640E+02E						
155	F	5.9640E+02E						
156	F	1.5596E+07E						
157	VESSEL		6					
158		13	2	2		4		
159		12	3	1		13		4
160		1						
161		0	0	0		2		
162		10.0	20.0	5.0000E-03				
163		8026.	502.	17.3		.6	60000.	
164		1.334						
165		10	7	07		1000		
166		900	0	0		0		150
167		1.590 E+6	0	0E				
168		.3659	.6098	.7318		1.2522		1.6585
169		1.849	1.9759	2.1664		2.4203		2.9282
170		3.955	4.981	6.2220				

CARD	1	2	3	4	5	6	7	8
	12345678901	2345678901	2345678901	2345678901	2345678901	2345678901	2345678901	2345678901
171	.0750572	.0857252						
172	3.1415926	6.2831853 E						
173		13	4	3		1		
174		13	3	3		7		
175		12	4	3		6		
176		12	3	3		5		
177		0.	1.	1.		1.F	0.	
178	F 1.							
179	4.983	17.667	19.	19.		17.667		
180	9.933	.187 F	0.0 E					
181	19.5	19.5 E						
182	0.0	.0008001	.0013462	.0018923		.0027178		
183	.0035433	.0043688	.0047105	.0050523		.0053594		
184	R 1	4R 2	5R 3	4R 3	8E			
185	0.	1.59E+6	.1	1.59E+6		.63		
186	1.10229E6	1.9	1.05505 E+6	8.1	.39997 E+6	PWTB		
187	20.	.0803 E+6	1000.	.0803 E+6		PWTB		
188	F	3				NFAX		
189	F 0.					FPUO2		
190	F 1.					FTD		
191	F 0.					GMIX		
192	F 0.					GMLES		
193	F 0.					PGAPT		
194	F 0.					PLVOL		
195	F 0.					PSLEN		
196	F 0.					CLENN		
197	R 2 .0088	R 2 .1012	E					
198	R 2 .44	R 2 5.06	E					
199	F .005					LEVEL 1		
200	F 50.0					LEVEL 1		
201	F .005					LEVEL 1		
202	F .005					LEVEL 1		
203	F 50.0					LEVEL 1		
204	F .005					LEVEL 1		
205	F 1.					LEVEL 1		

CARD	1	2	3	4	5	6	7	8
206	F	1.						LEVEL 1
207	F	1.						LEVEL 1
208	F	1.						LEVEL 1
209	R 2	0.0750R 2	0.0107E					
210	R 2	0.0750R 2	0.0107E					
211	R 2	0.0750R 2	0.0107E					
212	F	554.4E						
213	F	0.						LEVEL 1
214	F	0.						LEVEL 1
215	F	0.						LEVEL 1
216	F	0.						LEVEL 1
217	F	0.						LEVEL 1
218	F	0.						LEVEL 1
219	F	0.						LEVEL 1
220	F	562.0						LEVEL 1
221	F	562.0						LEVEL 1
222	F	1.5596 E+7						LEVEL 1
223	R 2	0.0	R 2 .0656	E				
224	R 2	0.0	R 2 3.2800	E				
225	F	.005						LEVEL 2
226	F	50.0						LEVEL 2
227	F	.005						LEVEL 2
228	F	.005						LEVEL 2
229	F	50.0						LEVEL 2
230	F	.005						LEVEL 2
231	F	1.						LEVEL 2
232	F	1.						LEVEL 2
233	F	.91468						LEVEL 2
234	F	1.						LEVEL 2
235	R 2	0.0750R 2	0.0107E					
236	R 2	0.0750R 2	0.0107E					
237	R 2	0.0750R 2	0.0107E					
238	R 2	0.	R 2 562.0	E				
239	F	0.						LEVEL 2
240	F	0.						LEVEL 2

CARD	1	2	3	4	5	6	7	8
241	F	0.						LEVEL 2
242	F	0.						LEVEL 2
243	F	0.						LEVEL 2
244	F	0.						LEVEL 2
245	F	0.						LEVEL 2
246	F	562.0						LEVEL 2
247	F	562.0						LEVEL 2
248	F	1.5596 E+7						LEVEL 2
249	R 2	0.0	P 2 .0328	E				
250	R 2	0.0	R 2 1.640	E				
251	F	.005						LEVEL 3
252	F	.005						LEVEL 3
253	F	.005						LEVEL 3
254	F	.005						LEVEL 3
255	F	.005						LEVEL 3
256	F	.005						LEVEL 3
257	F	1.						LEVEL 3
258	F	1.						LEVEL 3
259	F	.91468						LEVEL 3
260	F	1.						LEVEL 3
261	R 2	0.0750R 2	0.0107E					
262	R 2	0.0750R 2	0.0107E					
263	R 2	0.0750R 2	0.0107E					
264	R 2	0.	R 2 562.0	E				
265	F	0.						LEVEL 3
266	F	0.						LEVEL 3
267	F	0.						LEVEL 3
268	F	0.						LEVEL 3
269	F	0.						LEVEL 3
270	F	0.						LEVEL 3
271	F	0.						LEVEL 3
272	F	562.0						LEVEL 3
273	F	562.0						LEVEL 3
274	F	1.5596 E+7						LEVEL 3
275	R 4	.2628	E					

CARD	1	2	3	4	5	6	7	8
276	R 4	13.14	E					
277	F	.005						LEVEL 4
278	R 2	23.	F	0.				
279	F	.005						
280	F	.005						
281	R 2	23.	F	0.				
282	F	.005						LEVEL 4
283	R 2	.61160	R 2	1.0				LEVEL 4
284	R 2	.91468	R 2	1.0				LEVEL 4
285	R 2	.2758	R 2	1.				LEVEL 4
286	F	1.						LEVEL 4
287	R 2	0.0750	R 2	0.0213E				
288	R 2	0.0750	R 2	0.0213E				
289	R 2	0.0750	R 2	0.0213E				
290	F	554.2E						
291	F	0.						LEVEL 4
292	F	0.						LEVEL 4
293	F	0.						LEVEL 4
294	F	0.						LEVEL 4
295	F	0.						LEVEL 4
296	F	0.						LEVEL 4
297	F	0.						LEVEL 4
298	F	562.0						LEVEL 4
299	F	562.0						LEVEL 4
300	F	1.5596	E+7					LEVEL 4
301	R 4	.20544	E					
302	R 4	10.272	E					
303	F	.005						LEVEL 5
304	F	.005						LEVEL 5
305	F	.005						LEVEL 5
306	F	.005						LEVEL 5
307	F	.005						LEVEL 5
308	F	.005						LEVEL 5
309	R 2	.2758	P 1.					LEVEL 5
310	R 2	.38	1.					LEVEL 5

CARD	1	2	3	4	5	6	7	8
311	R 2	.2758	R 2	1.				LEVEL 5
312	F	0.						LEVEL 5
313	R 2	.010719R 2		0.0213E				
314	R 2	.010719R 2		0.0213E				
315	R 2	.010719R 2		0.0213E				
316	R 2	0.	R 2	562.0	E			
317	F	0.						LEVEL 5
318	F	0.						LEVEL 5
319	F	0.						LEVEL 5
320	F	0.						LEVEL 5
321	F	0.						LEVEL 5
322	F	0.						LEVEL 5
323	F	0.						LEVEL 5
324	R 2	562.0	R 2	562.0				LEVEL 5
325	R 2	562.0	R 2	562.0				LEVEL 5
326	F	1.5596 E+7						LEVEL 5
327	R 4	.0963	E					
328	R 4	4.815	E					
329	F	.005						LEVEL 6
330	F	.005						LEVEL 6
331	F	.005						LEVEL 6
332	F	.005						LEVEL 6
333	F	.005						LEVEL 6
334	F	.005						LEVEL 6
335	R 2	.2758	R 2	1.				LEVEL 6
336	R 2	.38	R 2	1.				LEVEL 6
337	R 2	.2758	R 2	1.				LEVEL 6
338	F	0.						LEVEL 6
339	R 2	.010719R 2		0.0213E				
340	R 2	.010719R 2		0.0213E				
341	R 2	.010719R 2		0.0213E				
342	R 2	0.	R 2	562.0	E			
343	F	0.						LEVEL 6
344	F	0.						LEVEL 6
345	F	0.						LEVEL 6

CARD	1	2	3	4	5	6	7	8
346	F	0.						LEVEL 6
347	F	0.						LEVEL 6
348	F	0.						LEVEL 6
349	F	0.						LEVEL 6
350	R 2	562.0	R 2	562.0				LEVEL 6
351	R 2	562.0	R 2	562.0				LEVEL 6
352	F	1.5596	E+7					LEVEL 6
353	R 4	.0642	E					
354	R 4	1.284	E					
355	F	.005						LEVEL 7
356	F	.005						LEVEL 7
357	F	.005						LEVEL 7
358	F	.005						LEVEL 7
359	F	.005						LEVEL 7
360	F	.005						LF' 7
361	R 2	.2758	R 2	1.				LEVEL 7
362	R 2	.38	R 2	1.				LEVEL 7
363	R 2	.2758	R 2	1.				LEVEL 7
364	F	0.						LEVEL 7
365	R 2	.010719	R 2	0.0213E				LEVEL 7
366	R 2	.010719	R 2	0.0213E				LEVEL 7
367	R 2	.010719	R 2	0.0213E				LEVEL 7
368	R 2	0.	R 2	562.0	E			LEVEL 7
369	F	0.						LEVEL 7
370	F	0.						LEVEL 7
371	F	0.						LEVEL 7
372	F	0.						LEVEL 7
373	F	0.						LEVEL 7
374	F	0.						LEVEL 7
375	F	0.						LEVEL 7
376	R 2	562.0	R 2	562.0				LEVEL 7
377	R 2	562.0	R 2	562.0				LEVEL 7
378	F	1.5596	E+7					LEVEL 7
379	R 4	.0963	E					
380	R 4	4.1926	E					

CARD	1	2	3	4	5	6	7	8
381	F	.005						LEVEL 8
382	F	.005						LEVEL 8
383	F	.005						LEVEL 8
384	F	.005						LEVEL 8
385	F	.005						LEVEL 8
386	F	.005						LEVEL 8
387	R 2	.2758	R 2	1.				LEVEL 8
388	R 2	.38	R 2	1.				LEVEL 8
389	R 2	.2758	R 2	1.				LEVEL 8
390	F	0.						LEVEL 8
391	R 2	.010719	R 2	0.0213E				LEVEL 8
392	R 2	.010719	R 2	0.0213E				LEVEL 8
393	R 2	.010719	R 2	0.0213E				LEVEL 8
394	R 2	0.	R 2	562.0	E			LEVEL 8
395	F	0.						LEVEL 8
396	F	0.						LEVEL 8
397	F	0.						LEVEL 8
398	F	0.						LEVEL 8
399	F	0.						LEVEL 8
400	F	0.						LEVEL 8
401	F	0.						LEVEL 8
402	R 2	562.0	R 2	562.0				LEVEL 8
403	R 2	562.0	R 2	562.0				LEVEL 8
404	F	1.5596	E+7					LEVEL 8
405	R 4	.284	E					
406	R 4	6.42	E					
407	F	.005						LEVEL 9
408	F	.005						LEVEL 9
409	F	.005						LEVEL 9
410	F	.005						LEVEL 9
411	F	.005						LEVEL 9
412	F	.005						LEVEL 9
413	R 2	.2758	R 2	1.				LEVEL 9
414	R 2	.38	R 2	1.				LEVEL 9
415	R 2	.2758	R 2	1.				LEVEL 9

CARD	1	2	3	4	5	6	7	8
416	F	0.						LEVEL 9
417	R 2	.010719R 2	0.0213E					LEVEL 9
418	R 2	.010719R 2	0.0213E					LEVEL 9
419	R 2	.010719R 2	0.0213E					LEVEL 9
420	R 2	0.	R 2 562.0	E				LEVEL 9
421	F	0.						LEVEL 9
422	F	0.						LEVEL 9
423	F	0.						LEVEL 9
424	F	0.						LEVEL 9
425	F	0.						LEVEL 9
426	F	0.						LEVEL 9
427	F	0.						LEVEL 9
428	R 2	562.0	R 2 562.0					LEVEL 9
429	R 2	562.0	R 2 562.0					LEVEL 9
430	F	1.5596 E+7						LEVEL 9
431	R 4	.2568	E					
432	R 4	12.84	E					
433	F	.005						LEVEL 10
434	F	.005						LEVEL 10
435	F	.005						LEVEL 10
436	F	.005						LEVEL 10
437	F	.005						LEVEL 10
438	F	.005						LEVEL 10
439	R 2	.2758	R 2 1.					LEVEL 10
440	R 2	.38	R 2 1.					LEVEL 10
441	R 2	.2758	R 2 1.					LEVEL 10
442	F	0.						LEVEL 10
443	R 2	.010719R 2	0.0213E					LEVEL 10
444	R 2	.010719R 2	0.0213E					LEVEL 10
445	R 2	.010719R 2	0.0213E					LEVEL 10
446	R 2	0.	R 2 562.0	E				LEVEL 10
447	F	0.						LEVEL 10
448	F	0.						LEVEL 10
449	F	0.						LEVEL 10
450	F	0.						LEVEL 10

CARD	1	2	3	4	5	6	7	8
451	F	0.						LEVEL 10
452	F	0.						LEVEL 10
453	F	0.						LEVEL 10
454	R 2	562.0	R 2	562.0				LEVEL 10
455	R 2	562.0	R 2	562.0				LEVEL 10
456	F	1.5596	E+7					LEVEL 10
457	R 4	.5134	E					
458	R 4	25.67	E					
459	F	.005						LEVEL 11
460	F	.005						LEVEL 11
461	F	.005						LEVEL 11
462	F	.005						LEVEL 11
463	F	.005						LEVEL 11
464	F	.005						LEVEL 11
465	R 2	.2758	R 2	1.				LEVEL 11
466	R 2	.38	R 2	1.				LEVEL 11
467	R 2	.2758	R 2	1.				LEVEL 11
468	F	0.						LEVEL 11
469	R 2	0.1576	R 2	0.0213E				LEVEL 11
470	R 2	0.1576	R 2	0.0213E				LEVEL 11
471	R 2	0.1576	R 2	0.0213E				LEVEL 11
472	R 2	596.4	R 2	555.4	E			LEVEL 11
473	F	0.						LEVEL 11
474	F	0.						LEVEL 11
475	F	0.						LEVEL 11
476	F	0.						LEVEL 11
477	F	0.						LEVEL 11
478	F	0.						LEVEL 11
479	F	0.						LEVEL 11
480	F	596.4						LEVEL 11
481	F	596.4						LEVEL 11
482	F	1.5596	E+7					LEVEL 11
483	R 4	.513	E					
484	R 4	25.65	E					
485	F	.005						LEVEL 12

CARD	1	2	3	4	5	6	7	8
486	F	.005						LEVEL 12
487	F	.005						LEVEL 12
488	F	.005						LEVEL 12
489	F	.005						LEVEL 12
490	F	.005						LEVEL 12
491	R 2	.2758	R 2	1.719				LEVEL 12
492	R 2	.38	R 2	1.				LEVEL 12
493	R 2	.2758	R 2	0.0				LEVEL 12
494	F	0.						LEVEL 12
495	R 2	0.1576	R 2	0.0213E				LEVEL 12
496	R 2	0.1576	R 2	0.0213E				LEVEL 12
497	R 2	0.1576	R 2	0.0213E				LEVEL 12
498	R 2	596.4	R 2	555.4	E			LEVEL 12
499	F	0.						LEVEL 12
500	F	0.						LEVEL 12
501	F	0.						LEVEL 12
502	F	0.						LEVEL 12
503	F	0.						LEVEL 12
504	F	0.						LEVEL 12
505	F	0.						LEVEL 12
506	F	596.4						LEVEL 12
507	F	596.4						LEVEL 12
508	F	1.5596	E+7					LEVEL 12
509	R 2	.63735	R 2	.356	E			
510	R 2	31.87	R 2	17.80	E			
511	F	.005						LEVEL 13
512	F	.005						LEVEL 13
513	F	.005						LEVEL 13
514	F	.005						LEVEL 13
515	F	.005						LEVEL 13
516	F	.005						LEVEL 13
517	R 2	.4947	R 2	.56	E			
518	R 2	.38	R 2	.56				LEVEL 13
519	F	0.						LEVEL 13
520	R 2	.0155	R 2	0.0	E			

CARD	1	2	3	4	5	6	7	8
521	R 2	0.0750R 2	0.0107E				LEVEL 13	
522	R 2	0.0750R 2	0.0107E				LEVEL 13	
523	R 2	0.0750R 2	0.0107E				LEVEL 13	
524	F	596.4E					LEVEL 13	
525	F	0.					LEVEL 13	
526	F	0.					LEVEL 13	
527	F	0.					LEVEL 13	
528	F	0.					LEVEL 13	
529	F	0.					LEVEL 13	
530	F	0.					LEVEL 13	
531	F	0.					LEVEL 13	
532	F	596.4					LEVEL 13	
533	F	596.4					LEVEL 13	
534	F	1.5596 E+7					LEVEL 13	
535	F	0.					ROD DATA	
536	F	640.0						
537	F	0.					ROD DATA	
538	F	640.0						
539	FILL		7					
540		9	4	100		3		
541		.26	.01	0.	.05		490.5	
542		55.7 E+5						
543		0.	.05	.1	0.		1000.	
544		0.						
545	BREAK		8					
546		13						
547		.26	2.0 E-3	.93	543.8		55.6 E+5	
548	PIPE		9		0			
549		1	0		6	11	7	
550		0	0					
551	0.	0.	0.	0.	0.	0.		
552	0.							
553	F	5.0000E-01E						
554	F	5.0000E-03E						
555	F	1.0000E-03E						

CARD	1	2	3	4	5	6	7	8
556	F	0.	E					
557	F	0.	E					
558	F	3.6000E-02E						
559	F		4E					
560	F	0.	E					
561	F	0.	E					
562	F	5.5440E+02E						
563	F	5.5440E+02E						
564	F	1.5596E+07E						
565	PIPE		10	0				
566		1	0	7		12	7	
567		0	0					
568	0.	0.	0.	0.	0.	0.		
569	0.							
570	F	5.0000E-01E						
571	F	5.0000E-03E						
572	F	1.0000E-03E						
573	F	0.	E					
574	F	0.	E					
575	F	3.6000E-02E						
576	F		4E					
577	F	0.	E					
578	F	0.	E					
579	F	5.5440E+02E						
580	F	5.5440E+02E						
581	F	1.5596E+07E						
582	FILL		11					
583		11	1					
584	.1	.001	0.	0.		554.4		
585		1.5596E+7						
586	FILL		12					
587		12	1					
588	.1	.001	0.	0.		596.4		
589		1.5596E+7						
590	VALVE		13	0				

	1								2								3								4								5								6								7								8							
CARD	1	2	3	4	5	6	7	8	1	2	3	4	5	6	7	8	1	2	3	4	5	6	7	8	1	2	3	4	5	6	7	8	1	2	3	4	5	6	7	8	1	2	3	4	5	6	7	8	1	2	3	4	5	6	7	8								
591																																																																
592																																																																
593	0.								0.								0.								0.								0.								0.																							
594	0.																																																															
595																																																																
596	9.200000E-03								1.880000E-02								0.																																															
597	F	5.0000E-01E																																																														
598	F	4.6000E-03E																																																														
599	F	9.2000E-03E																																																														
600	F	0.	E																																																													
601	F	0.	E																																																													
602	F	1.8800E-02E																																																														
603	F	4E																																																														
604	F	8.8100E-01E																																																														
605	F	1.8000E+00E																																																														
606	F	5.4430E+02E																																																														
607	F	5.4430E+02E																																																														
608	F	5.5600E+06E																																																														
609		0.							1.0000E+00								1.0000E-01							0.								1.0000E+03																																
610		0.	E																																																													
611		.000105							0.10								588.							1000.																																								
612		4.0															4.0															1.																																
613		-1.																																																														

II. TRAC TRANSIENT RESTART INPUT DECK FOR SEMISCALE MOD-1 TEST S-02-8

CARD	1	2	3	4	5	6	7	8
1	3	0						
2	SP5 USING TRAC VER 26.0							
3	SP5TPD27 FINAL RUN ?							
4	RESTART USING SP5SPD2R6							
5	-1	0.						
6	0	1	13	13	01			
7	.100000E-02	.500000E-05	0.	0.				
8	10	000	20	3	0			
9	0	1 0	2 0	3 0	4 0	5		
10	0	6 0	7 0	8 0	9 0	10		
11	0	11 0	12 0	13 0	0 0	0		
12	100	0	.100000E+01	0.				
13	0	0	0	0				
14	1000	0 0.	0.					
15	0	0	0	0				
16	900	0	0.0	0.				
17	0	0	0	0				
18	PIPE	9	0					
19	18	1	6	11	7			
20	01	1						
21	3.335000E-02	1.112520E-02	0.	0.	2.930000E+02			
22	2.930000E+02							
23	R 1 5.3486E-01R	2 4.0399E-01R	2 4.0747E-01R	2 7.2070E-03R	1 3.6417E-02			
24	R 1 1.8208E-02R	1 9.1040E-03R	1 4.5520E-03R	1 2.2760E-03R	2 1.1380E-03			
25	R 2 6.4756E-03R	1 1.2951E-02R	1 2.5903E-02E					
26	R 1 1.8689E-03R	2 1.4116E-03R	2 7.0990E-04R	1 2.5906E-06R	1 2.0151E-06			
27	R 1 8.8202E-06R	1 4.4101E-06R	1 2.2050E-06R	1 1.1025E-06R	1 5.5126E-07			
28	R 2 2.7563E-07S							
29	R 1 1.7065E-06R	1 1.9942E-06R	1 4.9523E-06R	1 1.4434E-05E				
30	3.4942E-02S							

CARD	1	2	3	4	5	6	7	8
31	R 2	3.4942E-03R	2 1.4455E-03R	1 4.0190E-04R	1 3.1700E-04R	8 2.4218E-04		
32	R 1	2.8487E-04R	1 3.3103E-04R	1 4.3374E-04R	1 6.8072E-04E			
33	F	0.	E					
34	F	0.	E					
35	R 1	4.8260E-02R	2 6.6700E-02R	2 4.2900E-02R	1 2.2620E-02R	1 2.0090E-02		
36	R 8	1.7560E-02S						
37	R 1	1.9045E-02R	1 2.0530E-02R	1 2.3500E-02R	1 2.9440E-02E			
38	F		4E					
39	F	0.0000E+00E						
40	F	0.	E					
41	I 2	555.3	553.2	F 553.2	E			
42	I 2	555.3	553.2	F 553.2	E			
43	F	1.5596E+07E						
44	F	0.	E					
45	I 2	555.3	553.2	F 553.2	E			
46	PIPE		10	0				
47		34	3	7	12	7		
48		01	1					
49		3.335000E-02	1.112520E-02	0.	0.	2.930000E+02		
50		2.930000E+02						
51	R 1	5.1690E-01R	1 3.8570E-01R	10 5.1530E-01R	2 6.4260E-01R	1 4.5840E-01		
52	R 2	4.0640E-01R	2 5.2780E-01R	2 3.2790E-01R	2 7.2070E-03R	1 3.6417E-02		
53	R 1	1.8208E-02R	1 9.1040E-03R	1 4.5520E-03R	1 2.2760E-03R	2 1.1380E-03		
54	R 2	6.4756E-03R	1 1.2951E-02R	1 2.5903E-02E				
55	R 1	1.8066E-03R	1 1.3479E-03R	10 1.5843E-03R	2 9.2880E-04R	1 6.6261E-04		
56	R 2	7.4050E-04R	2 6.0175E-04R	2 4.9514E-04R	1 2.5906E-06R	1 2.0151E-06		
57	R 1	8.8202E-06R	1 4.4101E-06R	1 2.2050E-06R	1 1.1025E-06R	1 5.5126E-07		
58	R 2	2.7563E-07S						
59	R 1	1.7065E-06R	1 1.9942E-06R	1 4.9523E-06R	1 1.4434E-05E			
60	R 1	3.4942E-02R	2 3.4949E-03R	9 3.7378E-03R	3 1.4455E-03R	3 2.4475E-04		
61	R 3	1.1401E-03R	1 4.0190E-04R	1 3.1700E-04R	8 2.4218E-04S			
62	R 1	2.8487E-04R	1 3.3103E-04R	1 4.3374E-04R	1 6.8072E-04E			
63	R 2	1.1000E+01R	11 1.2500E+00R	1 1.3000E+00R	6 .05600E-02R	15 0.	E	
64	R 1	0.	R 1 5.0000E-01R	5 1.0000E+00R	4-1.0000E+00R	1-5.0000E-01		
65	R 2	-1.0000E+00R	2 0.	R 3 1.0000E+00R	16 0.	E		

CARD	1	2	3	4	5	6	7	8
66	R 1 4.8260E-02R	2 6.6700E-02R	9 6.8990E-02R	3 4.2900E-02R	3 .99323E-02			
67	R 3 3.8100E-02R	1 2.2620E-02R	1 2.0090E-02R	8 1.7560E-02S				
68	R 1 1.9045E-02R	1 2.0530E-02R	1 2.3500E-02R	1 2.9440E-02E				
69	F	4E						
70	F 0.	E						
71	F 0.	E						
72	R14 592.1	I 4 592.1	585.9	F 585.9				
73	R14 592.1	I 4 592.1	585.9	F 585.9				
74	F 1.5596E+07E							
75	F 0.	E						
76	R14 592.1	I 4 592.1	585.9	F 585.9				
77	BREAK		11					
78		11						
79	.13589	7.13949 E-5	1.000000E+00	396.7		2.206 E+05		
80	BREAK		12					
81		12						
82	.13589	7.13949 E-5	1.000000E+00	396.7		2.206 E+05		
83	PRIZER		5	0				
84		4	8					
85	8.000000E+03	1.559600E+07	1.000000E+05	1.000000E-01				
86	R 2 5.0000E-01R	1 1.2840E-01R	1 2.0000E-02E					
87	R 2 1.1730E-02R	1 3.0125E-03R	1 4.6920E-04E					
88	F 2.2760E-02E							
89	F 0.	E						
90	F -1.0000E+00E							
91	F 1.7000E-01E							
92	F	4E						
93	R 1 1.0000E+00R	3 0.	E					
94	R 4 0.	R 1 4.2524E-03E						
95	F 6.1840E+02E							
96	F 6.1840E+02E							
97	F 1.5596E+07E							
98	END							
99	1.0E-5	2.0E-2	.01	.01				
100	.01	.005	2.	.5				

	1					2					3					4					5					6					7					8				
CARD	1	2	3	4	5	1	2	3	4	5	1	2	3	4	5	1	2	3	4	5	1	2	3	4	5	1	2	3	4	5	1	2	3	4	5					
101		1.0E-5					2.0E-2							.10						.10																				
102		.10					.05							2.						.5																				
103		1.0E-5					2.0E-2							1.0						1.0																				
104		1.0					2.0E-1							2.						.5																				
105		1.0E-5					2.0E-2							10.						10.																				
106		2.0					2.0E-1							2.						.5																				
107		1.0E-5					2.0E-2							29.1						1.0																				
108		5.0					2.0E-1							5.						.5																				
109	-1.																																							

APPENDIX I

TRAC STEADY-STATE AND TRANSIENT INPUT DECKS FOR SEMISCALE MOD-1 TEST S-06-3

I. TRAC STEADY-STATE INPUT DECK FOR SEMISCALE MOD-1 TEST S-06-3

CARD	1	2	3	4	5	6	7	8
1	3	0						
2	S63 SS USING TRAC VER 26.0							
3	S63SPD31 INCREASE FRIC IN INT. LOOP							
4	STEADY STATE							
5	0 0.							
6	1	0	21	21	1			
7	1.00000E-02	1.00000E-05	01.00000E-03	0.				
8	10	0	20	4	0			
9	0	1 0	2 0	3 0	4 0	105		
10	0	7 0	8 0	9 0	10 0	11		
11	0	12 0	13 0	30 0	31 0	32		
12	0	33 0	34 0	35 0	36 0	37		
13	0	6E 0	0 0	0 0	0 0	0		
14	100	0	.100000E+04	0.				
15	0	0	0	0	0			
16	1000	0	.100000E+04	0.				
17	0	0	0	0	0			
18	900	0	.100000E+04	0.				
19	0	0	0	0	0			
20	2000	-1	.423800E+07	0.				
21	32	2	1	0	0			
22	TEE	1	0					
23	4	1	7	3.000000E-06	0			
24	0	6	1	2	0			
25	3.335020E-02	1.112520E-02	0.	0.	2.950000E+02			
26	2.950000E+02							
27	1	5	8					
28	9.425000E-03	3.911600E-03	0.	0.	2.950000E+02			
29	2.950000E+02							
30	F 5.1480E-01E							

CARD	1	2	3	4	5	6	7	8
31	F	1.7986E-03E						
32		3.4942E-02F	3.4942E-03E					
33		0.0	00.00	00.00	F	0.0	E	
34	R 6	0.	R 1	1.0000E+00E				
35	F	6.6700E-02E						
36	F		4E					
37	F	0.	E					
38	F	0.	E					
39	F	5.9640E+02E						
40	F	5.9640E+02E						
41	F	1.5596E+07E						
42	F	0.	E					
43	F	5.9640E+02E						
44		5.0000E-02	1.6720E+00	7.2000E-01	2.0300E-01	4.0000E-03E		
45		1.7471E-04	7.1745E-05	3.0895E-05	7.0930E-04	9.1040E-05E		
46		3.4942E-03R	3 4.2910E-05R	1 3.4940E-03	2.2760E-02E			
47	F	6.8000E-03E						
48	F	1.0000E+00E						
49		6.6700E-02R	3 7.3900E-03R	1 6.6700E-02R	1 1.7000E-01E			
50	F		4E					
51	F	0.	E					
52	F	0.	E					
53	F	5.9640E+02E						
54	F	5.9640E+02E						
55	F	1.5596E+07E						
56	F	0.	E					
57	F	5.9640E+02E						
58	STGEN		2	0				
59		22	3	2	3	10		
60		1	0	0	1			
61		5.100000E-03	1.200000E-03					
62		12	9	10				
63	R 1	4.6000E-01R	20 2.5680E-01R	1 4.6000E-01E				
64	R 1	9.6278E-03R	20 1.1398E-03R	1 9.6278E-03E				
65	R 1	3.4942E-03R	21 4.4000E-03R	1 3.4942E-03E				

CARD	1	2	3	4	5	6	7	8
66	R 1 0.	R21 2.4400E-02R 1 0.						E
67	R11 1.0000E+00R 1 0.							R11-1.0000E+00E
68	R 1 6.6700E-02R21 1.0200E-02R 1 6.6700E-02E							
69	R 1	4R21	1R 1					4E
70	F 0.	E						
71	F 0.	E						
72	5.9640E+02	5.9440E+02	5.9240E+02	5.9040E+02	5.8840E+02			
73	5.8640E+02	5.8440E+02	5.8240E+02	5.8040E+02	5.7840E+02			
74	5.7640E+02	5.7440E+02	5.7240E+02	5.7040E+02	5.6840E+02			
75	5.6640E+02	5.6440E+02	5.6240E+02	5.6040E+02	5.5840E+02			
76	5.5640E+02	5.5440E+02E						
77	5.9640E+02	5.9440E+02	5.9240E+02	5.9040E+02	5.8840E+02			
78	5.8640E+02	5.8440E+02	5.8240E+02	5.8040E+02	5.7840E+02			
79	5.7640E+02	5.7440E+02	5.7240E+02	5.7040E+02	5.6840E+02			
80	5.6640E+02	5.6440E+02	5.6240E+02	5.6040E+02	5.5840E+02			
81	5.5640E+02	5.5440E+02E						
82	F 1.5596E+07E							
83	F 5.5000E+02E							
84	F 2.5680E-01E							
85	R10 1.1210E-02R 2 7.5000E-02E							
86	R11 4.3830E-02R 2 9.2000E-03E							
87	F 0.	E						
88	F 1.0000E+00E							
89	F 1.8800E-02E							
90	F	4E						
91	R 2 0.	R 1 3.0300E-01R 1 3.6722E-01R 1 4.3144E-01R 1 4.9567E-01						
92	R 1 5.5989E-01R 1 6.2411E-01R 1 6.8833E-01R 1 7.5256E-01R 1 8.1678E-01							
93	R 1 8.8100E-01E							
94	5.0000E-03	5.2400E-03	5.5000E-03	7.9000E-01	9.0222E-01			
95	1.0144E+00	1.1267E+00	1.2389E+00	1.3511E+00	1.4633E+00			
96	1.5756E+00	1.6878E+00	1.8000E+00E					
97	R 1 5.1700E+02R 1 5.3820E+02R10 5.4430E+02E							
98	R 1 5.1700E+02R 1 5.3820E+02R10 5.4430E+02E							
99	5.5700E+06	5.5691E+06	5.5682E+06	5.5673E+06	5.5664E+06			
100	5.5655E+06	5.5645E+06	5.5636E+06	5.5627E+06	5.5618E+06			

CARD	1	2	3	4	5	6	7	8
101	5.5609E+06	5.5600E+06E						
102	R 1 0.	R20 4.0000E-01R 1 0.		E				
103	F 5.5330E-01E							
104	PIPE		3	0				
105		6	1	3		4		7
106		3	0					
107	3.324800E-02	1.112520E-02	0.		0.		2.950000E+02	
108	2.950000E+02							
109	R 3 5.1000E-01R 3 4.6140E-01E							
110	R 3 1.7820E-03R 3 1.6122E-03E							
111	F 3.4942E-03E							
112	F 0.	E						
113	R 1-1.0000E+00R 1 0.		R 1-1.0000E+00R 2 1.0000E+00R 2 0.				E	
114	F 6.6700E-02E							
115	F 4E							
116	F 0.	E						
117	F 0.	E						
118	F 5.5440E+02E							
119	F 5.5440E+02E							
120	F 1.5596E+07E							
121	F 0.	E						
122	F 5.5440E+02E							
123	PUMP		4	0				
124		2	1	4		36		7
125		0	0	1		0		1
126		0	0					
127	3.324800E-02	1.112520E-02	0.		0.		2.945000E+02	
128	2.950000E+02							
129	5.739000E+02	4.345000E+01	1.148000E-02	1.000000E+03	3.728000E+02			
130	2.662000E+00	0.	3.730000E+00	1.700000E+02				
131	1							
132	11.670E-01	14.529E-01E						
133	4.0776E-03	5.0766E-03E						
134	F 3.4942E-03E							
135	0.0	.0076	E					

CARD	1	2	3	4	5	6	7	8
136	F	0.	E					
137	F	6.6700E-02E						
138	F		4E					
139	F	0.	E					
140	F	0.	E					
141	F	5.5440E+02E						
142	F	5.5440E+02E						
143	F	1.5596E+07E						
144	F	0.	E					
145	F	5.5440E+02E						
146	PIPE		37	0				
147		1	1	37		5		7
148		0	0					
149		3.224800E-02	1.112500E-02	0.	0.			2.950000E+02
150		2.950000E+02						
151	F	4.8430E-01E						
152	F	1.6922E-03E						
153	F	3.4942E-03E						
154		0.0	.0076	E				
155	F	0.	E					
156	F	6.6700E-02E						
157	F		4E					
158	F	0.	E					
159	F	0.	E					
160	F	5.5440E+02E						
161	F	5.5440E+02E						
162	F	1.5596E+07E						
163	F	0.	E					
164	F	5.5440E+02E						
165	VESSEL		6					
166		13	2	2		4		
167		12	3	1		13		4
168		1						
169		0	0	0		4		
170		10.0	20.0	5.0000E-03				

CARD	1	2	3	4	5	6	7	8
	12345678901	2345678901	2345678901	2345678901	2345678901	2345678901	2345678901	234567890
171	8026.	502.	17.3	.6	60000.			
172	1.334							
173	10	22	7	1000				
174	900	0	0	0	150			
175	1.004 E+6	0	0E					
176	.3659	.6098	.7318	1.2522	1.6585			
177	1.849	1.9759	2.1664	2.4203	2.9282			
178	3.955	4.981	6.2220					
179	.0750572	.0857252						
180	3.1415926	6.2831853 E						
181	13	4	3	1				
182	13	3	3	7				
183	12	4	3	6				
184	12	3	3	5				
185	0.	1.	1.	1.F	0.			
186	F 1.							
187	1	2						
188	1.4850	.9390 E						
189	4.983	17.667	19.	19.	17.667			
190	9.933	.187 F	0.0 E					
191	18.0	18.0 E						
192	0.0	.0008001	.0013462	.0018923	.0027178			
193	.0035433	.0043688	.0047105	.0050523	.0053594			
194	R 1	4R 2	5R 3	4R 3	8E			
195	0.0	1.0040E+06	2.0	.60000E+06S				
196	2.5	.5750E+06	3.0	.60000E+06S				
197	3.3	1.0000E+06	5.1	1.00000E+06S				
198	6.0	.5000E+06	7.3	.20000E+06S				
199	11.0	.2000E+06	11.6	.17500E+06S				
200	15.0	.1700E+06	16.0	.08000E+06S				
201	17.2	.0800E+06	17.8	.15500E+06S				
202	19.5	.1550E+06	20.0	.05000E+06S				
203	26.8	.0500E+06	27.2	.02000E+06S				
204	36.0	.0200E+06	40.0	.05000E+06S				
205	100.	.0400E+06	300.	.04000E+06E				

CARD	1	2	3	4	5	6	7	8
206	F		3					NFAX
207	F	0.						FPUO2
208	F	1.						FTD
209	F	0.						GMIX
210	F	0.						GMLES
211	F	0.						PGAPT
212	F	0.						PLVOL
213	F	0.						PSLEN
214	F	0.						CLENN
215	R 2	.0088	R 2 .1012	E				
216	R 2	.44	R 2 5.06	E				
217	F	.005						LEVEL 1
218	F	50.0						LEVEL 1
219	F	.005						LEVEL 1
220	F	.005						LEVEL 1
221	F	50.0						LEVEL 1
222	F	.005						LEVEL 1
223	F	1.						LEVEL 1
224	F	1.						LEVEL 1
225	F	1.						LEVEL 1
226	F	1.						LEVEL 1
227	R 2	0.0750R 2	0.0107E					
228	R 2	0.0750R 2	0.0107E					
229	R 2	0.0750R 2	0.0107E					
230	F	554.4E						
231	F	0.						LEVEL 1
232	F	0.						LEVEL 1
233	F	0.						LEVEL 1
234	F	0.						LEVEL 1
235	F	0.						LEVEL 1
236	F	0.						LEVEL 1
237	F	0.						LEVEL 1
238	F	562.0						LEVEL 1
239	F	562.0						LEVEL 1
240	F	1.5596 E+7						LEVEL 1

CARD	1	2	3	4	5	6	7	8
241	R 2 0.0	R 2 .0656	E					
242	R 2 0.0	R 2 3.2800	E					
243	F .005						LEVEL	2
244	F 50.0						LEVEL	2
245	F .005						LEVEL	2
246	F .005						LEVEL	2
247	F 50.0						LEVEL	2
248	F .005						LEVEL	2
249	F 1.						LEVEL	2
250	F 1.						LEVEL	2
251	F .91468						LEVEL	2
252	F 1.						LEVEL	2
253	R 2 0.0750R 2	0.0107E						
254	R 2 0.0750R 2	0.0107E						
255	R 2 0.0750R 2	0.0107E						
256	R 2 0.	R 2 562.0	E					
257	F 0.						LEVEL	2
258	F 0.						LEVEL	2
259	F 0.						LEVEL	2
260	F 0.						LEVEL	2
261	F 0.						LEVEL	2
262	F 0.						LEVEL	2
263	F 0.						LEVEL	2
264	F 562.0						LEVEL	2
265	F 562.0						LEVEL	2
266	F 1.5596 E+7						LEVEL	2
267	R 2 0.0	R 2 .0328	E					
268	R 2 0.0	R 2 1.640	E					
269	F .005						LEVEL	3
270	F .005						LEVEL	3
271	F .005						LEVEL	3
272	F .005						LEVEL	3
273	F .005						LEVEL	3
274	F .005						LEVEL	3
275	F 1.						LEVEL	3

CARD	1	2	3	4	5	6	7	8
276	F	1.						LEVEL 3
277	F	.91468						LEVEL 3
278	F	1.						LEVEL 3
279	R 2	0.0750R 2	0.0107E					
280	R 2	0.0750R 2	0.0107E					
281	R 2	0.0750R 2	0.0107E					
282	R 2	0.	R 2 562.0	E				
283	F	0.						LEVEL 3
284	F	0.						LEVEL 3
285	F	0.						LEVEL 3
286	F	0.						LEVEL 3
287	F	0.						LEVEL 3
288	F	0.						LEVEL 3
289	F	0.						LEVEL 3
290	F	562.0						LEVEL 3
291	F	562.0						LEVEL 3
292	F	1.5596 E+7						LEVEL 3
293	R 4	.2628	E					
294	R 4	13.14	E					
295	F	.005						LEVEL 4
296	R 2	23.	F 0.					
297	F	.005						
298	F	.005						
299	R 2	23.	F 0.					
300	F	.005						LEVEL 4
301	R 2	.61160	R 2 1.0					LEVEL 4
302	R 2	.91468	R 2 1.0					LEVEL 4
303	R 2	.2758	R 2 1.					LEVEL 4
304	F	1.						LEVEL 4
305	R 2	0.0750R 2	0.0213E					
306	R 2	0.0750R 2	0.0213E					
307	R 2	0.0750R 2	0.0213E					
308	F	554.2E						
309	F	0.						LEVEL 4
310	F	0.						LEVEL 4

CARD	1	2	3	4	5	6	7	8
311	F	0.						LEVEL 4
312	F	0.						LEVEL 4
313	F	0.						LEVEL 4
314	F	0.						LEVEL 4
315	F	0.						LEVEL 4
316	F	562.0						LEVEL 4
317	F	562.0						LEVEL 4
318	F	1.5596	E+7					LEVEL 4
319	R 4	.20544		E				
320	R 4	10.272		E				
321	F	.005						LEVEL 5
322	F	.005						LEVEL 5
323	F	.005						LEVEL 5
324	F	.005						LEVEL 5
325	F	.005						LEVEL 5
326	F	.005						LEVEL 5
327	R 2	.2758		R 2	1.			LEVEL 5
328	R 2	.38		R 2	1.			LEVEL 5
329	R 2	.2758		R 2	1.			LEVEL 5
330	F	0.						LEVEL 5
331	R 2	.010719	R 2		0.0213E			
332	R 2	.010719	R 2		0.0213E			
333	R 2	.010719	R 2		0.0213E			
334	R 2	0.		R 2	562.0			
335	F	0.						LEVEL 5
336	F	0.						LEVEL 5
337	F	0.						LEVEL 5
338	F	0.						LEVEL 5
339	F	0.						LEVEL 5
340	F	0.						LEVEL 5
341	F	0.						LEVEL 5
342	R 2	562.0		R 2	562.0			LEVEL 5
343	R 2	562.0		R 2	562.0			LEVEL 5
344	F	1.5596	E+7					LEVEL 5
345	R 4	.0963		E				

CARD	1	2	3	4	5	6	7	8
346	R 4	4.815	E					
347	F	.005					LEVEL	6
348	F	.005					LEVEL	6
349	F	.005					LEVEL	6
350	F	.005					LEVEL	6
351	F	.005					LEVEL	6
352	F	.005					LEVEL	6
353	R 2	.2758	R 2	1.			LEVEL	6
354	R 2	.38	R 2	1.			LEVEL	6
355	R 2	.2758	R 2	1.			LEVEL	6
356	F	0.					LEVEL	6
357	R 2	.010719	R 2	0.0213E				
358	R 2	.010719	R 2	0.0213E				
359	R 2	.010719	R 2	0.0213E				
360	R 2	0.	R 2	562.0	E			
361	F	0.					LEVEL	6
362	F	0.					LEVEL	6
363	F	0.					LEVEL	6
364	F	0.					LEVEL	6
365	F	0.					LEVEL	6
366	F	0.					LEVEL	6
367	F	0.					LEVEL	6
368	R 2	562.0	R 2	562.0			LEVEL	6
369	R 2	562.0	R 2	562.0			LEVEL	6
370	F	1.5596	E+7				LEVEL	6
371	R 4	.0642	E					
372	R 4	1.284	E					
373	F	.005					LEVEL	7
374	F	.005					LEVEL	7
375	F	.005					LEVEL	7
376	F	.005					LEVEL	7
377	F	.005					LEVEL	7
378	F	.005					LEVEL	7
379	R 2	.2758	R 2	1.			LEVEL	7
380	R 2	.38	R 2	1.			LEVEL	7

CARD	1	2	3	4	5	6	7	8
381	R 2	.2758	R 2	1.				LEVEL 7
382	F	0.						LEVEL 7
383	R 2	.010719R 2		0.0213E				LEVEL 7
384	R 2	.010719R 2		0.0213E				LEVEL 7
385	R 2	.010719R 2		0.0213E				LEVEL 7
386	R 2	0.	R 2	562.0	E			LEVEL 7
387	F	0.						LEVEL 7
388	F	0.						LEVEL 7
389	F	0.						LEVEL 7
390	F	0.						LEVEL 7
391	F	0.						LEVEL 7
392	F	0.						LEVEL 7
393	F	0.						LEVEL 7
394	R 2	562.0	R 2	562.0				LEVEL 7
395	R 2	562.0	R 2	562.0				LEVEL 7
396	F	1.5596 E+7						LEVEL 7
397	R 4	.0963	E					
398	R 4	4.1926	E					
399	F	.005						LEVEL 8
400	F	.005						LEVEL 8
401	F	.005						LEVEL 8
402	F	.005						LEVEL 8
403	F	.005						LEVEL 8
404	F	.005						LEVEL 8
405	R 2	.2758	R 2	1.				LEVEL 8
406	R 2	.38	R 2	1.				LEVEL 8
407	R 2	.2758	R 2	1.				LEVEL 8
408	F	0.						LEVEL 8
409	R 2	.010719R 2		0.0213E				LEVEL 8
410	R 2	.010719R 2		0.0213E				LEVEL 8
411	R 2	.010719R 2		0.0213E				LEVEL 8
412	R 2	0.	R 2	562.0	E			LEVEL 8
413	F	0.						LEVEL 8
414	F	0.						LEVEL 8
415	F	0.						LEVEL 8

	1	2	3	4	5	6	7	8
CARD	1234567890123456789012345678901234567890123456789012345678901234567890							
416	F	0.						LEVEL 8
417	F	0.						LEVEL 8
418	F	0.						LEVEL 8
419	F	0.						LEVEL 8
420	R 2	562.0	R 2	562.0				LEVEL 8
421	R 2	562.0	R 2	562.0				LEVEL 8
422	F	1.5596	E+7					LEVEL 8
423	R 4	.284	E					
424	R 4	6.42	E					
425	F	.005						LEVEL 9
426	F	.005						LEVEL 9
427	F	.005						LEVEL 9
428	F	.005						LEVEL 9
429	F	.005						LEVEL 9
430	F	.005						LEVEL 9
431	R 2	.2758	R 2	1.				LEVEL 9
432	R 2	.38	R 2	1.				LEVEL 9
433	R 2	.2758	R 2	1.				LEVEL 9
434	F	0.						LEVEL 9
435	R 2	.010719	R 2	0.0213E				LEVEL 9
436	R 2	.010719	R 2	0.0213E				LEVEL 9
437	R 2	.010719	R 2	0.0213E				LEVEL 9
438	R 2	0.	R 2	562.0	E			LEVEL 9
439	F	0.						LEVEL 9
440	F	0.						LEVEL 9
441	F	0.						LEVEL 9
442	F	0.						LEVEL 9
443	F	0.						LEVEL 9
444	F	0.						LEVEL 9
445	F	0.						LEVEL 9
446	R 2	562.0	R 2	562.0				LEVEL 9
447	R 2	562.0	R 2	562.0				LEVEL 9
448	F	1.5596	E+7					LEVEL 9
449	R 4	.2568	E					
450	R 4	12.84	E					

CARD	1	2	3	4	5	6	7	8
451	F	.005						LEVEL 10
452	F	.005						LEVEL 10
453	F	.005						LEVEL 10
454	F	.005						LEVEL 10
455	F	.005						LEVEL 10
456	F	.005						LEVEL 10
457	R 2	.2758	R 2	1.				LEVEL 10
458	R 2	.38	R 2	1.				LEVEL 10
459	R 2	.2758	R 2	1.				LEVEL 10
460	F	0.						LEVEL 10
461	R 2	.010719	R 2	0.0213E				LEVEL 10
462	R 2	.010719	R 2	0.0213E				LEVEL 10
463	R 2	.010719	R 2	0.0213E				LEVEL 10
464	R 2	0.	R 2	562.0	E			LEVEL 10
465	F	0.						LEVEL 10
466	F	0.						LEVEL 10
467	F	0.						LEVEL 10
468	F	0.						LEVEL 10
469	F	0.						LEVEL 10
470	F	0.						LEVEL 10
471	F	0.						LEVEL 10
472	R 2	562.0	R 2	562.0				LEVEL 10
473	R 2	562.0	R 2	562.0				LEVEL 10
474	F	1.5596	E+7					LEVEL 10
475	R 4	.5134	E					
476	R 4	25.67	E					
477	F	.005						LEVEL 11
478	F	.005						LEVEL 11
479	F	.005						LEVEL 11
480	F	.005						LEVEL 11
481	F	.005						LEVEL 11
482	F	.005						LEVEL 11
483	R 2	.2758	R 2	1.				LEVEL 11
484	R 2	.38	R 2	1.				LEVEL 11
485	R 2	.2758	R 2	1.				LEVEL 11

CARD	1	2	3	4	5	6	7	8
486	F	0.						LEVEL 11
487	R 2	0.1576R 2	0.0213E					LEVEL 11
488	R 2	0.1576R 2	0.0213E					LEVEL 11
489	R 2	0.1576R 2	0.0213E					LEVEL 11
490	R 2	596.4	R 2 555.4	E				LEVEL 11
491	F	0.						LEVEL 11
492	F	0.						LEVEL 11
493	F	0.						LEVEL 11
494	F	0.						LEVEL 11
495	F	0.						LEVEL 11
496	F	0.						LEVEL 11
497	F	0.						LEVEL 11
498	F	596.4						LEVEL 11
499	F	596.4						LEVEL 11
500	F	1.5596 E+7						LEVEL 11
501	R 4	.513	E					
502	R 4	25.65	E					
503	F	.005						LEVEL 12
504	F	.005						LEVEL 12
505	F	.005						LEVEL 12
506	F	.005						LEVEL 12
507	F	.005						LEVEL 12
508	F	.005						LEVEL 12
509	R 2	.2758	R 2 1.719					LEVEL 12
510	R 2	.38	R 2 1.					LEVEL 12
511	R 2	.2758	R 2 0.0					LEVEL 12
512	F	0.						LEVEL 12
513	R 2	0.1576R 2	0.0213E					LEVEL 12
514	R 2	0.1576R 2	0.0213E					LEVEL 12
515	R 2	0.1576R 2	0.0213E					LEVEL 12
516	R 2	596.4	R 2 555.4	E				LEVEL 12
517	F	0.						LEVEL 12
518	F	0.						LEVEL 12
519	F	0.						LEVEL 12
520	F	0.						LEVEL 12

CARD	1	2	3	4	5	6	7	8
521	F	0.						LEVEL 12
522	F	0.						LEVEL 12
523	F	0.						LEVEL 12
524	F	596.4						LEVEL 12
525	F	596.4						LEVEL 12
526	F	1.5596 E+7						LEVEL 12
527	R 2	.63735	R 2	.356	E			
528	R 2	31.87	R 2	17.80	E			
529	F	.005						LEVEL 13
530	F	.005						LEVEL 13
531	F	.005						LEVEL 13
532	F	.005						LEVEL 13
533	F	.005						LEVEL 13
534	F	.005						LEVEL 13
535	R 2	.4947	R 2	.56	E			
536	R 2	.38	R 2	.56				LEVEL 13
537	F	0.						LEVEL 13
538	R 2	.0155	R 2	0.0	E			
539	R 2	0.0750	R 2	0.0107	E			LEVEL 13
540	R 2	0.0750	R 2	0.0107	E			LEVEL 13
541	R 2	0.0750	R 2	0.0107	E			LEVEL 13
542	F	596.4E						LEVEL 13
543	F	0.						LEVEL 13
544	F	0.						LEVEL 13
545	F	0.						LEVEL 13
546	F	0.						LEVEL 13
547	F	0.						LEVEL 13
548	F	0.						LEVEL 13
549	F	0.						LEVEL 13
550	F	596.4						LEVEL 13
551	F	596.4						LEVEL 13
552	F	1.5596 E+7						LEVEL 13
553	F	0.						ROD DATA
554	F	640.0						
555	F	0.						ROD DATA

CARD	1	2	3	4	5	6	7	8
556	F	640.0						
557	F	0.						ROD DATA
558	F	640.0						
559	F	0.						ROD DATA
560	F	640.0						
561	FILL		7					
562		9	4	100		3		
563		.26	.01	0.	.05		497.0	
564		68.3 E+5						
565		0.	.05	.1	0.		1000.	
566		0.						
567	BREAK		8					
568		13						
569		.26	2.0 E-3	.93	543.8		6.85 E+6	
570	PIPE		9		0			
571		1	0		6	11	7	
572		0	0					
573	0.	0.	0.		0.	0.		
574	0.							
575	F	5.0000E-01E						
576	F	5.0000E-03E						
577	F	1.0000E-03E						
578	F	0. E						
579	F	0. E						
580	F	3.6000E-02E						
581	F	4E						
582	F	0. E						
583	F	0. E						
584	F	5.5440E+02E						
585	F	5.5440E+02E						
586	F	1.5596E+07E						
587	PIPE		10		0			
588		1	0		7	12	7	
589		0	0					
590	0.	0.	0.		0.	0.		

CARD	1	2	3	4	5	6	7	8
591	0.							
592	F	5.0000E-01E						
593	F	5.0000E-03E						
594	F	1.0000E-03E						
595	F	0.	E					
596	F	0.	E					
597	F	3.6000E-02E						
598	F		4E					
599	F	0.	E					
600	F	0.	E					
601	F	5.5440E+02E						
602	F	5.5440E+02E						
603	F	1.5596E+07E						
604	FILL		11					
605		11	1					
606	.1	.001	0.		0.		562.0	
607		1.5596E+7						
608	FILL		12					
609		12	1					
610	.1	.001	0.		0.		596.4	
611		1.5596E+7						
612	VALVE		13		0			
613		2	0		10		13	0
614		0	0					
615	0.	0.	0.		0.		0.	
616	0.							
617		3	100		3		0	2
618	9.200000E-03	1.880000E-02	0.					
619	F	5.0000E-01E						
620	F	4.6000E-03E						
621	F	9.2000E-03E						
622	F	0.	E					
623	F	0.	E					
624	F	1.8800E-02E						
625	F		4E					

CARD	1	2	3	4	5	6	7	8
626	F	8.8100E-01E						
627	F	1.8000E+00E						
628	F	5.4430E+02E						
629	F	5.4430E+02E						
630	F	5.5600E+06E						
631		0.	1.0000E+00	1.0000E-01	0.		1.0000E+03	
632		0.	E					
633	TEE		30	0				
634		1	1	7	0.		0	
635		0	1	36		37	0	
636		3.324800E-02	1.112500E-02	0.	0.		2.945000E+02	
637		2.950000E+02						
638		0	1	31				
639		1.215000E-02	5.500000E-04	0.	0.		2.945000E+02	
640		2.950000E+02						
641	F	4.8430E-01E						
642	F	1.6922E-03E						
643	F	3.4942E-03E						
644	F	.0076	E					
645	F	0.	E					
646	F	6.6700E-02E						
647	F		4E					
648	F	0.	E					
649	F	0.	E					
650	F	5.5440E+02E						
651	F	5.5440E+02E						
652	F	1.5596E+07E						
653	F	0.	E					
654	F	5.5440E+02E						
655	F	1.5000E+00E						
656	F	6.9612E-04E						
657	F	4.6408E-04E						
658	F	3.3000E-01E						
659	F	0.	E					
660	F	2.4300E-02E						

CARD	1	2	3	4	5	6	7	8
661	F		4E					
662	F	0.	E					
663	F	0.	E					
664	F	5.5440E+02E						
665	F	5.5440E+02E						
666	F	1.5596E+07E						
667	F	0.	E					
668	F	5.5440E+02E						
669	TEE		31		0			
670		1	1		7	0.		0
671		0	2		31		32	0
672		1.215000E-02	5.500000E-04	0.		0.		2.945000E+02
673		2.950000E+02						
674		0	1		35			
675		1.215000E-02	5.500000E-04	0.		0.		2.945000E+02
676		2.950000E+02						
677	F	1.5000E+00E						
678	F	6.9612E-04E						
679	F	4.6408E-04E						
680	F	3.3000E-01E						
681	F	0.	E					
682	F	2.4300E-02E						
683	F		4E					
684	F	0.	E					
685	F	0.	E					
686	F	5.5440E+02E						
687	F	5.5440E+02E						
688	F	1.5596E+07E						
689	F	0.	E					
690	F	5.5440E+02E						
691	F	1.5000E+00E						
692	F	6.9612E-04E						
693	F	4.6408E-04E						
694		225.6	0.0	E				
695	F	0.	E					

CARD	1	2	3	4	5	6	7	8
696	F	2.4300E-02E						
697	F		4E					
698	F	0.	E					
699	F	0.	E					
700	F	5.5440E+02E						
701	F	5.5440E+02E						
702	F	1.5596E+07E						
703	F	0.	E					
704	F	5.5440E+02E						
705	TEE		32		0			
706		1	1		7	0.		0
707		0	2		32		33	0
708		1.215000E-02	5.500000E-04	0.		0.		2.945000E+02
709		2.950000E+02						
710		0	1		34			
711		1.215000E-02	5.500000E-04	0.		0.		2.945000E+02
712		2.950000E+02						
713		1.5000E+00	3.0000E+00E					
714		6.9612E-04	1.3922E-03E					
715	F	4.6408E-04E						
716	F	3.3000E-01E						
717		0.	1.0000E+00	0.	E			
718	F	2.4300E-02E						
719	F		4E					
720	F	0.	E					
721	F	0.	E					
722	F	5.5440E+02E						
723	F	5.5440E+02E						
724	F	1.5596E+07E						
725	F	0.	E					
726	F	5.5440E+02E						
727	F	1.5000E+00E						
728	F	6.9612E-04E						
729	F	4.6408E-04E						
730		34.5	0.0	E				

CARD	1	2	3	4	5	6	7	8
766	F	2.4300E-02E						
767	F		4E					
768	F	0.	E					
769	F	0.	E					
770		5.5440E+02	3.0000E+02E					
771		5.5440E+02	3.0000E+02E					
772		1.5596E+07	4.2382E+06E					
773	ACCUM		33		0			
774		3	38					
775		5.2680E-01	7.9140E-01	1.5000E-01E				
776		3.4600E-02	5.1900E-02	9.8363E-03E				
777	R 3	6.5575E-02R 1	4.6408E-04E					
778	F	0.	E					
779	F	-1.0000E+00E						
780	R 3	2.8895E-01R 1	2.4300E-02E					
781	F		4E					
782	R 1	1.0000E+00R 2	0.	E				
783	F	0.	E					
784	F	3.0000E+02E						
785	F	3.0000E+02E						
786	F	4.2382E+06E						
787	BREAK		105		REPLACES PRIZER			
788		8	0	0		0		
789		.004	9.1040E-05	0.0	588.		1.5596E+07	
790		1.0E-4	0.10	380.10	1000.			
791		4.0	.09	4.0		1.		
792		-1.						

II. TRAC TRANSIENT RESTART INPUT DECK FOR SEMISCALE MOD-1 TEST S-06-3

CARD	1	2	3	4	5	6	7	8
1	3	0						
2	S63 TRANS. USING TRAC VER 26.0							
3	S63TPD32 COR. PRIZER MASS							
4	USED WITH S63SPD3R1							
5	-1	0.						
6	0	1	21		21		1	
7	.100000E-02	.500000E-05	.100000E-02	0.				
8	10	0	20		4		0	
9	0	1 0	2 0	3 0	4 0		5	
10	0	7 0	8 0	9 0	10 0		11	
11	0	12 0	13 0	30 0	31 0		32	
12	0	33 0	34 0	35 0	36 0		37	
13	0	6E 0	0 0	0 0	0 0		0	
14	100	0	.100000E+01	0.				
15	0	0	0		0			
16	1000	0 0.	0.					
17	0	0	0		0			
18	900	0	0.0	0.				
19	0	0	0		0			
20	2000	-1	.423800E+07	0.				
21	36	0	1		0			
22	PIPE	9	0					
23	18	1	6		11		7	
24	01	1						
25	3.335000E-02	1.112520E-02	0.	0.		2.930000E+02		
26	2.930000E+02							
27	R 1 5.3486E-01R	2 4.0399E-01R	2 4.0747E-01R	2 7.2070E-03R	1 3.6417E-02			
28	R 1 1.8208E-02R	1 9.1040E-03R	1 4.5520E-03R	1 2.2760E-03R	2 1.1380E-03			
29	R 2 6.4756E-03R	1 1.2951E-02R	1 2.5903E-02E					
30	R 1 1.8689E-03R	2 1.4116E-03R	2 7.0990E-04R	1 2.5906E-06R	1 2.0151E-06			

CARD	1	2	3	4	5	6	7	8
31	R 1	8.8202E-06R	1 4.4101E-06R	1 2.2050E-06R	1 1.1025E-06R	1 5.5126E-07		
32	R 2	2.7563E-07S						
33	R 1	1.7065E-06R	1 1.9942E-06R	1 4.9523E-06R	1 1.4434E-05E			
34		3.4942E-02S						
35	R 2	3.4942E-03R	2 1.4455E-03R	1 4.0190E-04R	1 3.1700E-04R	8 2.4218E-04		
36	R 1	2.8487E-04R	1 3.3103E-04R	1 4.3374E-04R	1 6.8072E-04E			
37	F	0.	E					
38	F	0.	E					
39	R 1	4.8260E-02R	2 6.6700E-02R	2 4.2900E-02R	1 2.2620E-02R	1 2.0090E-02		
40	R 8	1.7560E-02S						
41	R 1	1.9045E-02R	1 2.0530E-02R	1 2.3500E-02R	1 2.9440E-02E			
42	F		4E					
43	F	0.0000E+00E						
44	F	0.	E					
45	I 2	555.	562.	F 562.	E			
46	I 2	555.	562.	F 562.	E			
47	F	1.5610E+07E						
48	F	0.	E					
49	I 2	555.	562.	F 562.	E			
50	PIPE		10	0				
51		34	3	7	12	7		
52		01	1					
53		3.335000E-02	1.112520E-02	0.	0.	2.930000E+02		
54		2.930000E+02						
55	R 1	5.1690E-01R	1 3.8570E-01R	10 5.1530E-01R	2 6.4260E-01R	1 4.5840E-01		
56	R 2	4.0640E-01R	2 5.2780E-01R	2 3.2790E-01R	2 7.2070E-03R	1 3.6417E-02		
57	R 1	1.8208E-02R	1 9.1040E-03R	1 4.5520E-03R	1 2.2760E-03R	2 1.1380E-03		
58	R 2	6.4756E-03R	1 1.2951E-02R	1 2.5903E-02E				
59	R 1	1.8066E-03R	1 1.3479E-03R	10 1.5843E-03R	2 9.2880E-04R	1 6.1261E-04		
60	R 2	7.4050E-04R	2 6.0175E-04R	2 4.9514E-04R	1 2.5906E-06R	1 2.0151E-06		
61	R 1	8.8202E-06R	1 4.4101E-06R	1 2.2050E-06R	1 1.1025E-06R	1 5.5126E-07		
62	R 2	2.7563E-07S						
63	R 1	1.7065E-06R	1 1.9942E-06R	1 4.9523E-06R	1 1.4434E-05E			
64	R 1	3.4942E-02R	2 3.4949E-03R	9 3.7378E-03R	3 1.4455E-03R	3 2.4475E-04		
65	R 3	1.1401E-03R	1 4.0190E-04R	1 3.1700E-04R	8 2.4218E-04S			

CARD	1	2	3	4	5	6	7	8
66	R 1 2.8487E-04R	1 3.3103E-04R	1 4.3374E-04R	1 6.8072E-04E				
67	R 2 1.1000E+01R11	1.2500E+00R	1 1.3000E+00R	6 .05600E-02R15	0.		E	
68	R 1 0.	R 1 5.0000E-01R	5 1.0000E+00R	4-1.0000E+00R	1-5.0000E-01			
69	R 2-1.0000E+00R	2 0.	R 3 1.0000E+00R16	0.		E		
70	R 1 4.8260E-02R	2 6.6700E-02R	9 6.8990E-02R	3 4.2900E-02R	3 .38190E-02			
71	R 3 3.8100E-02R	1 2.2620E-02R	1 2.0090E-02R	8 1.7560E-02S				
72	R 1 1.9045E-02R	1 2.0530E-02R	1 2.3500E-02R	1 2.9440E-02E				
73	F	4E						
74	F 0.	E						
75	F 0.	E						
76	R14 596.	I 4 596.	591.	F 591.				
77	R14 596.	I 4 596.	591.	F 591.				
78	F 1.5610E+07E							
79	F 0.	E						
80	R14 596.	I 4 596.	591.	F 591.				
81	BREAK		11					
82		11						
83	.13589	7.13949 E-5	1.000000E+00	396.7		2.420 E+05		
84	BREAK		12					
85		12						
86	.13589	7.13949 E-5	1.000000E+00	396.7		2.420 E+05		
87	PRIZER		5	0				
88		12	8					
89	8.000000E+03	1.576900E+07	1.000000E+05	1.000000E-01				
90	5.6340E-01R10	.0597	4.0000E-03E					
91	1.7664E-02R10	1.3587E-03	9.1040E-05E					
92	F 2.2760E-02E							
93	F 0.	E						
94	F -1.0000E+00E							
95	F 1.7000E-01E							
96	F	4E						
97	R 2 1.0000E+00	.283	F 0.	E				
98	F 0.	E						
99	R 4 6.1840E+02F	558.	E					
100	F 6.1840E+02E							

CARD	1	2	3	4	5	6	7	8
101	F	1.5769E+07E						
102	TEE		1	0				
103		4	1	7	3.000000E-06		0	
104		0	6	1		2	0	
105		3.335020E-02	1.112520E-02	0.	0.		2.950000E+02	
106		2.950000E+02						
107		1	5	8				
108		9.425000E-03	3.911600E-03	0.	0.		2.950000E+02	
109		2.950000E+02						
110	F	5.1480E-01E						
111	F	1.7986E-03E						
112	R 1	3.4942E-02R	6	3.4942E-03E				
113	F	0.	E					
114	R 6	0.	R 1	1.0000E+00E				
115	F	6.6700E-02E						
116	F	4E						
117		9.0373E-14	9.3488E-14	9.3197E-14	9.2786E-14	9.2622E-14		
118		9.2442E-14E						
119	R 1	2.2299E-01R	3	2.2299E+00R	3	2.2281E+00E		
120	F	5.9605E+02E						
121	R 1	6.1855E+02R	5	6.1853E+02E				
122	R 1	1.5617E+07R	5	1.5613E+07E				
123	F	0.	E					
124	F	5.9605E+02E						
125		5.0000E-02	1.6720E+00	7.2000E-01	2.0300E-01	4.0000E-03E		
126		1.7471E-04	7.1745E-05	3.0895E-05	7.0930E-04	9.1040E-05E		
127	R 1	3.4942E-03R	3	4.2910E-05R	1	3.4940E-03R	1	2.2760E-02E
128	F	6.8000E-03E						
129	F	1.0000E+00E						
130	R 1	6.6700E-02R	3	7.3900E-03R	1	6.6700E-02R	1	1.7000E-01E
131	F	4E						
132		9.6632E-14	9.6801E-14	9.6752E-14	7.8755E-14	7.5607E-14E		
133	R 1	1.7329E-03R	3	1.4111E-01R	1	1.7329E-03R	1	2.6603E-04E
134	F	515.	E					
135	R 1	6.1853E+02R	1	6.1850E+02R	1	6.1845E+02R	2	6.1843E+02E

CARD	1	2	3	4	5	6	7	8
136	1.5613E+07	1.5608E+07	1.5600E+07	1.5597E+07	1.5596E+07E			
137	F 0.	E						
138	F 515.	E						
139	END							
140	1.0E-5	2.0E-2	.01	.01				
141	.01	.005	2.	.5				
142	1.0E-5	2.0E-2	.10	.10				
143	.10	.05	2.	.5				
144	1.0E-5	2.0E-2	1.0	1.0				
145	1.0	2.0E-1	2.	.5				
146	1.0E-5	2.0E-2	10.	10.				
147	2.0	2.0E-1	2.	.5				
148	1.0E-5	2.0E-2	36.	1.0				
149	5.0	2.0E-1	5.	.5				
150	-1.							

III. TRAC TRANSIENT RESTART INPUT DECK WITH RENODED BROKEN-LOOP COLD LEG
FOR SEMISCALE MOD-1 TEST S-06-3

CARD	1	2	3	4	5	6	7	8
1		3	0					
2	S63 TRANS. USING TRAC VER 26.0							
3	S63NPD32							
4	USED WITH S63TPD3R2							
5		-1	0.					
6		0	1	21		21		1
7	.100000E-02	.500000E-05	.100000E-02	0.				
8		10	0	20		4		0
9	0	1 0	2 0	3 0		4 0		5
10	0	7 0	8 0	9 0		10 0		11
11	0	12 0	13 0	30 0		31 0		32
12	0	33 0	34 0	35 0		36 0		37
13	0	6E 0	0 0	0 0		0 0		0
14		-1						
15								
16	PIPE		9	0				
17		6	1	6		11		7
18		3	1					
19	3.335000E-02	1.112520E-02	0.	0.		2.930000E+02		
20	2.930000E+02							
21	.53486	.40399	.40399	.40747		.40747		
22	.11	E						
23	F -1.0	E						
24	F -1.0	E						
25	R 5 0.0	.0339	0.0	E				
26	F 0.	E						
27	.04826	.0667	.0667	.0429		.0429		
28	.01756	.02944	E					
29	F	4E						
30	.1909	.0585	.02032	.01187		.007603		

CARD	1	2	3	4	5	6	7	8
31	.5	E						
32	.09688		.9974	.9516	2.275	2.275		
33	12.0	E						
34	402.2		396.8	393.6	395.7	395.6		
35	395.1	E						
36	407.1		407.1	407.0	406.9	406.2		
37	394.3	E						
38	3.12387E+05		3.12446E+05	3.12026E+05	3.10825E+05	3.04822E+05		
39	2.10433E+05E							
40	F 0.0							
41	464.4		470.2	467.4	461.3	438.5		
42	432.6	E						
43	END							
44	1.0E-5		2.0E-2	200.	1.0			
45	5.0		2.0E-1	5.	.5			
46	-1.							

APPENDIX J

TRAC STEADY-STATE AND TRANSIENT INPUT DECKS FOR LOFT NONNUCLEAR EXPERIMENT L1-4

I. TRAC STEADY-STATE INPUT DECK FOR LOFT NONNUCLEAR EXPERIMENT L1-4

CARD	1	2	3	4	5	6	7	8
1	2	0	0					
2	LOFT TEST L1-4						(INITIAL INPUT)	
3	STEADY STATE							
4	-1	0.0					MCC 1	
5	1	0	28		29	1	MCC 2	
6	1.0E-03	1.0E-05	1.0E-04				MCC 3	
7	10	50	20		3		MCC 4	
8	1	2	3		4	5	IORDER	
9	6	7	8		9	11	IORDER	
10	12	13	14		15	16	IORDER	
11	17	18	19		20	21	IORDER	
12	22	23	24		25	27	IORDER	
13	77	99	10E				IORDER	
14	1	0	1.0				TRIPS	
15							TRIPS	
16	2	0	0.0				TRIPS	
17							TRIPS	
18	3	-1	424.01E4		0.0		TRIPS	
19	27	0	1		0		TRIPS	
20	TEE	1					CAKD 1	
21	4	1	7		0.0	0	CARD 2	
22	0	4	1		3		CARD 3	
23	1.420000E-01	3.650000E-02	0.0		0.0	2.950000E02	CARD 4	
24	2.950000E2						CARD 5	
25	0	3	2				CARD 6	
26	2.330050E-02	8.696800E-03	0.0		0.0	2.950000E02	CARD 7	
27	2.950000E2						CARD 8	
28	R 2 666.75E-03	41.91E-02	66.01E-02E				DX 1	
29	R 24233.39E-05	266.18E-04	4190.92E-05E				VOL 1	
30	F 6342.53E-05E						FA 1	

CARD	1	2	3	4	5	6	7	8
31	F	0.0E						FRIC 1
32	F	0.0E						GRAV 1
33	F	2.84E-1E						HD 1
34	F	+4E						NFF 1
35	F	0.0E						ALP 1
36	F	0. E						VM 1
37	F	5.52E+02E						TL 1
38	F	5.52E+02E						TV 1
39	F	15.75E+06E						P 1
40	F	0.0E						QPPP 1
41	F	5.52E+02E						TW 1
42		2149.85E-3	2642.77E-03	2221.69E-3E				DX 2
43		3114.87E-6	3695.37E-6	5705.88E-6E				VOL 2
44	R 3	1449.29E-6	5732.12E-6E					FA 2
45		1652.98E-4	5503.15E-6	4668.77E-6	0.0E+00E			FRIC 2
46		1.00E0R 2	0.0	1.00E0E				GRAV 2
47	R 3	4295.68E-5	8543.04E-5E					HD 2
48	R 2	+4R 2	+4E					NFF 2
49	F	0.0E						ALP 2
50	F	0.0E						VM 2
51	F	5.52E+02E						TL 2
52	F	5.52E+02E						TV 2
53	F	15.75E+06E						P 2
54	F	0.0E						QPPP 2
55	F	5.52E+02E						TW 2
56	PIPE		4					CARD 1
57		4	1	3		4	7	CARD 2
58		0	0					CARD 3
59		1.505690E-01	3.761400E-02	0.0		0.0	2.950000E02	CARD 4
60		2.950000E+02						CARD 5
61		10.16E-01	73.66E-02	35.56 E-02	53.34E-02E			DX
62		4955.48E-05	4672.31E-05	2605.16E-05	433.26E-004E			VOL
63	R	36342.53E-05R	28319.46E-05E					FA
64	F	0.0E						FRIC
65	R 4	0.0	7071.07E-04E					GRAV

CARD	1	2	3	4	5	6	7	8
66	R 3	2.84E-01R	23254.64E-04E					HD
67	R 2	+4R 2	+4	+4E				NFF
68	F	0.0E						ALP
69	F	0.0E						VM
70	F	5.54E+02E						TL
71	F	5.54E+02E						TV
72	F	15.75E+06E						P
73	F	0.0E						QPPP
74	F	5.54E+02E						TW
75	PRIZER		2					CARD 1
76		3	2					CARD 2
77		0.000000E+00	1.565000E+07	1.378020E+05	1.167600E00			CARD 3
78		5307.32E-04R 2	58.38E-02E					DX
79		0.30E00R 2	0.33E00E					VOL
80	R 3	35652.63E-04	5732.12E-06E					FA
81	R 3	0.0	4668.77E-6E					FRIC
82	F	-1.00E00E						GRAV
83	R 3	848.36E-03	8543.04E-05E					HD
84	R 3	4	+4E					NFF
85		1.00E00R 2	0.0E					ALP
86	F	0.0E						VM
87	F	6.19E+02E						TL
88	F	6.19E+02E						TV
89	F	15.75E+06E						P
90	STGEN		3					CARD 1
91		10	3	4	5	10		CARD 2
92		1	0	0	1			CARD 3
93		5.105400E-03	1.244600E-03					CARD 4
94		7	14	15				CARD 5
95		1.0000R	86419.85E-04	1.0000E				DX 1
96		3354.06E-04R	89698.57E-05	3354.06E-04E				VOL 1
97		8319.46E-05R	91511.71E-04	8319.46E-05E				FA 1
98		.00	R 9 0.0168	.00	E			FRIC 1
99		7071.07E-04R 4	1.00E00	0.0R 4	-1.00E00	-7071.07E-4E		GRAV 1
100		3254.64E-04R	91021.08E-05	3254.64E-04E				HD 1

CARD	1	2	3	4	5	6	7	8
101		4	+1R 7	1	+1		4E NFF 1	
102	F	0.0E					ALP 1	
103	F	0.0E					VM 1	
104	R 5	5.54E+02R 5	5.52E+02E				TL 1	
105	R 5	5.54E+02R 5	5.52E+02E				TV 1	
106	F	15.75E+06E					P 1	
107	F	5.52E2E					TW	
108	R	46419.85E-04R	31170.23E-03E				DX 2	
109		4008.61E-04R	37355.19E-04R	31157.07E-03E			VOL 2	
110		8107.32E-6R 6	1.15E00	1824.15E-5E			FA 2	
111	F	0.0E					FRIC 2	
112	F	1.00E00E					GRAV 2	
113		10.16E-2R 6	1210.06E-3	15.24E-2E			HD 2	
114		+4R 5	4	+4E			NFF 2	
115	R 4	0.0	2631.54E-4R 2	1.0E			ALP 2	
116	F	0.0E					VM 2	
117	F	5.52E2E					TL 2	
118	F	5.52E2E					TV 2	
119	F	66.50E5E					P 2	
120		0.0	17.60000000R 6	3802.86E-2	17.60000000		0.0E WA 1	
121		22.00CR 3	4729.93E-2R 3	0.0E			WA 2	
122	TEE		5				CARD 1	
123		2	1	7	0.0	0	CARD 2	
124		0	3	6	7		CARD 3	
125		1.420870E-1	3.572600E-2	0.0	0.0	2.950000E+2	CARD 4	
126		2.950000E+2					CARD 5	
127		0	2	5			CARD 6	
128		1.420870E-1	3.572600E-2	0.0	0.0	2.950000E+2	CARD 7	
129		2.950000E+2					CARD 8	
130		6.35E-1	167.64E-2	6.35E-1E			DX 1	
131		2746.75E-5	1124.88E-4	2746.75E-5E			VOL 1	
132		3661.31E-5R 2	6342.49E-5	3.66131E-2E			FA 1	
133	F	0.0E					FRIC 1	
134	R 2	-1.00E0R 2	1.00E0E				GRAV 1	
135		215.91E-3R 2	2841.74E-4	215.91E-3E			HD 1	

CARD	1	2	3	4	5	6	7	8
136	F	+4E						NFF 1
137	F	0.0E						ALP 1
138	F	0.0E						VM 1
139	F	5.52E2E						TL 1
140	F	5.52E2E						TV 1
141	F	15.75E6E						P 1
142	F	0.0E						QPPP 1
143	F	5.52E2E						TW 1
144		131.41 E-2	124.46E-2E					DX 2
145		834.66E-4	9004.81E-5E					VOL 2
146	R 2	6342.49E-5	8319.46E-5E					FA 2
147	F	0.0E						FRIC 2
148		0.0	1.00E0	7071.07E-4E				GRAV 2
149	R 2	2841.74E-4	3254.64E-4E					HD 2
150	F	+4E						NFF 2
151	F	0.0E						ALP 2
152	F	0.0E						VM 2
153	F	5.52E2E						TL 2
154	F	5.52E2E						TV 2
155	F	15.75E6E						P 2
156	F	0.0E						QPPP 2
157	F	5.52E2E						TW 2
158	PUMP		6					CARD 1
159		2	1	6	8		7	CARD 2
160		0	0	1	1		1	CARD 3
161		1	9					CARD 4
162		1.079550E-1	2.835930E-2	0.0	0.0	2.950000E2		CARD 5
163		2.950000E2						CARD 6
164		941.54	500.	.315	614.	369.661		CARD 7
165		3.174380E2	3.68125000	2.311860E2	1.884960E2			CARD 8
166		0						CARD 9
167		7	10	11	11		13	NDATA
168		10	14	6	12		8	NDATA
169		4	6	2	2		2	NDATA
170		2	11	7				NDATA

	1	2	3	4	5	6	7	8
CARD	1234567890123456789012345678901234567890123456789012345678901234567890							
206	1.00E0	2.46E0E						HTP4
207	-1.00E0	2.00E0	-0.80E0	1.40E0	-0.70E0	TSP1		
208	1.20E0	-0.60E0	1.03E0	-0.40E0	0.80E0	TSP1		
209	-0.20E0	0.66E0	-0.10E0	0.61E0	0.0	TSP1		
210	0.60E0	0.10E0	0.61E0	0.20E0	0.63E0	TSP1		
211	0.60E0	0.83E0	1.00E0	1.00E0E		TSP1		
212	-1.00E0	-1.00E0	-0.30E0	-0.90E0	-0.20E0	TSP2		
213	-0.87E0	-0.10E0	-0.81E0	0.0	-0.68E0	TSP2		
214	0.40E0	-0.27E0	0.50E0	0.15E0	1.00E0	TSP2		
215	1.00E0E					TSP2		
216	-1.00E0	2.00E0	-0.10E0	1.35E0	0.50E0	TSP3		
217	0.83E0	1.00E0	0.34E0E			TSP3		
218	-1.00E0	-1.00E0	-0.30E0	-0.90E0	-0.10E0	TSP4		
219	-0.52E0	0.40E0	-0.27E0	0.50E0	0.0	TSP4		
220	1.00E0	0.34E0E				TSP4		
221	-1.00E0	0.0	1.00E0	0.0E		TTP1		
222	-1.00E0	0.0	1.00E0	0.0E		TTP2		
223	-1.00E0	0.0	1.00E0	0.0E		TTP3		
224	-1.00E0	0.0	1.00E0	0.0E		TTP4		
225	0.0	0.0	0.10E0	0.0	0.15E0	HDM		
226	0.05E0	0.24E0	0.80E0	0.30E0	0.96E0	HDM		
227	0.40E0	0.98E0	0.60E0	0.97E0	0.80E0	HDM		
228	0.90E0	0.90E0	0.80E0	0.96E0	0.50E0	HDM		
229	1.00E0	0.0E				HDM		
230	0.	0.	.1	0.	.15	TDM		
231	0.48E-1	0.22E0	5.64E-1	0.80E0	5.64E-1	TDM		
232	0.96E0	4.54E-1	1.00E0	0.76E-1E		TDM		
233	0.0	188.496	4.00	157.08	9.00	SPTBL		
234	131.95	19.00	94.25	29.00	68.07	SPTBL		
235	31.50	63.36	46.50	78.54	64.00	SPTBL		
236	62.83	69.00	48.17 E			SPTBL		
237	F 1352.13E-3E					DX		
238	F 4955.48E-5E					VOL		
239	F 3661.31E-5E					FA		
240	F 0.0E					FRIC		

CARD	1	2	3	4	5	6	7	8
241	F	+1.00E0E						GRAV
242	F	215.91E-3E						HD
243	F	4E						NFF
244	F	0.0E						ALP
245	F	0.0E						VM
246	F	5.53E2E						TL
247	F	5.53E2E						TV
248	F	15.75E6E						P
249	F	0.0E						QPPP
250	F	5.53E2E						TW
251	PUMP		7					CARD 1
252		2	1	7	9		7	CARD 2
253		0	0	1	1		1	CARD 3
254		1	8					CARD 4
255		1.079550E-1	2.835930E-2	0.0	0.0	2.950000E2		CARD 5
256		2.950000E2						CARD 6
257		941.54	500.	.315	614.	369.661		CARD 7
258		317.438	3.68125	231.186	170.693			CARD 8
259		0						CARD 9
260		7	10	11	11		13	NDATA
261		10	14	6	12		8	NDATA
262		4	6	2	2		2	NDATA
263		2	11	7				NDATA
264		-1.00E0	2.44E0	-0.80E0	2.03E0	-0.40E0		HSP1
265		1.60E0	-0.20E0	1.47E0	0.0	1.40E0		HSP1
266		0.40E0	1.30E0	1.00E0	1.00E0E			HSP1
267		-1.00E0	-1.00E0	-0.40E0	-0.88E0	-0.30E0		HSP2
268		-0.83E0	0.0	-0.68E0	0.20E0	-0.51E0		HSP2
269		0.40E0	-0.28E0	0.60E0	0.0	0.70E0		HSP2
270		0.18E0	0.80E0	0.40E0	1.00E0	1.00E0E		HSP2
271		-1.00E0	2.44E0	-0.83E0	2.00E0	-0.70E0		HSP3
272		1.70E0	-0.65E0	1.60E0	-0.45E0	1.32E0		HSP3
273		-0.17E0	1.10E0	0.0	0.93E0	0.50E0		HSP3
274		0.83E0	0.78E0	0.83E0	0.95E0	0.93E0		HSP3
275		1.00E0	1.00E0E					HSP3

	1	2	3	4	5	6	7	8
CARD	12345678901234567890123456789012345678901234567890123456789012345678901234567890	12345678901234567890123456789012345678901234567890123456789012345678901234567890	12345678901234567890123456789012345678901234567890123456789012345678901234567890	12345678901234567890123456789012345678901234567890123456789012345678901234567890	12345678901234567890123456789012345678901234567890123456789012345678901234567890	12345678901234567890123456789012345678901234567890123456789012345678901234567890	12345678901234567890123456789012345678901234567890123456789012345678901234567890	12345678901234567890123456789012345678901234567890123456789012345678901234567890
276	-1.00E0	-1.00E0	-0.80E0	-0.60E0	-0.60E0	HSP4		
277	-0.30E0	-0.44E0	-0.10E0	-0.23E0	0.10E0	HSP4		
278	-0.05E0	0.23E0	3.90E-1	0.33E0	0.40E0	HSP4		
279	0.27E0	0.62E0	0.48E00	0.90E0	0.83E0	HSP4		
280	1.00E0	1.00E0E				HSP4		
281	-1.00E0	3.61E0	-0.90E00	3.49E0	-0.80E0	HTP1		
282	3.83E0	-0.60E0	4.62E00	-0.50E0	4.63E0	HTP1		
283	-0.40E0	4.27E0	-0.20E00	2.82E0	0.0	HTP1		
284	1.45E0	0.12E0	0.55E00	0.20E0	0.26E0	HTP1		
285	0.40E0	0.25E0	0.90E00	0.22E0	1.00E0	HTP1		
286	0.0E					HTP1		
287	0.0	-0.68E0	0.10E0	-0.58E0	0.20E0	HTP2		
288	-0.51E0	0.30E0	-0.49E0	0.40E0	-0.48E0	HTP2		
289	0.60E0	-0.43E0	0.70E0	-0.37E0	0.80E0	HTP2		
290	-0.26E0	0.90E0	-0.07E0	1.00F0	0.0E	HTP2		
291	-1.00E0	3.61E0	-0.83E0	2.60E0	-0.70E0	HTP3		
292	2.03E0	-0.65E0	1.85E0	-0.45E0	1.37E0	HTP3		
293	-0.17E0	1.05E0	0.0	0.83E0	0.20E0	HTP3		
294	0.76E0	0.40E0	0.73E0	0.50E0	0.76E0	HTP3		
295	0.60E0	0.88E0	0.78E0	1.31E0	0.95E0	HTP3		
296	2.08E0	1.00E0	2.46E0E			HTP3		
297	0.0	0.24E0	3.99E-1	0.82E0	0.40E0	HTP4		
298	0.77E0	0.62E0	1.58E0	0.90E0	2.18E0	HTP4		
299	1.00E0	2.46E0E				HTP4		
300	-1.00E0	2.00E0	-0.80E0	1.40E0	-0.70E0	TSP1		
301	1.20E0	-0.60E0	1.03E0	-0.40E0	0.80E0	TSP1		
302	-0.20E0	0.66E0	-0.10E0	0.61E0	0.0	TSP1		
303	0.60E0	0.10E0	0.61E0	0.20E0	0.63E0	TSP1		
304	0.60E0	0.83E0	1.00E0	1.00E0E		TSP1		
305	-1.00E0	-1.00E0	-0.30E0	-0.90E0	-0.20E0	TSP2		
306	-0.87E0	-0.10E0	-0.81E0	0.0	-0.68E0	TSP2		
307	0.40E0	-0.27E0	0.50E0	0.15E0	1.00E0	TSP2		
308	1.00E0E					TSP2		
309	-1.00E0	2.00E0	-0.10E0	1.35E0	0.50E0	TSP3		
310	0.83E0	1.00E0	0.34E0E			TSP3		

CARD	1	2	3	4	5	6	7	8
	1234567890123456789012345678901234567890123456789012345678901234567890123456789012345678901234567890							
311	-1.00E0	-1.00E0	-0.30E0	-0.90E0	-0.10E0	TSP4		
312	-0.52E0	0.40E0	-0.27E0	0.50E0	0.0	TSP4		
313	1.00E0	0.34E0E				TSP4		
314	-1.00E0	0.0	1.00E0	0.0E		TTP1		
315	-1.00E0	0.0	1.00E0	0.0E		TTP2		
316	-1.00E0	0.0	1.00E0	0.0E		TTP3		
317	-1.00E0	0.0	1.00E0	0.0E		TTP4		
318	0.0	0.0	0.10E0	0.0	0.15E0	HDM		
319	0.05E0	0.24E0	0.80E0	0.30E0	0.96E0	HDM		
320	0.40E0	0.98E0	0.60E0	0.97E0	0.80E0	HDM		
321	0.90E0	0.90E0	0.80E0	0.96E0	0.50E0	HDM		
322	1.00E0	0.0E				HDM		
323	0.	0.	.1	0.	.15	TDM		
324	0.48E-1	0.22E0	5.64E-1	0.80E0	5.64E-1	TDM		
325	0.96E0	4.54E-1	1.00E0	0.76E-1E		TDM		
326	0.0	1706.93E-01	4.00E0	142.42E0	9.00E0	SPTBL		
327	118.33	19.00	78.54	28.00	54.45	SPTBL		
328	46.50	78.54	64.00	62.83	69.00	SPTBL		
329	40.32 E					SPTBL		
330	F 1352.13E-3E					DX		
331	F 4955.48E-5E					VOL		
332	F 3661.31E-5E					FA		
333	F 0.0E					FRIC		
334	F 1.00E0E					GRAV		
335	F 215.91-3E					HD		
336	F 4E					NFF		
337	F 0.0E					ALP		
338	F 0.0E					VM		
339	F 5.53E2E					TL		
340	F 5.53E2E					TV		
341	F 15.75E6E					P		
342	F 0.0E					QPPP		
343	F 5.53E2E					TW		
344	TEE		8			CARD	1	
345		2	1	7	0.0	0	CARD	2

299

CARD	1	2	3	4	5	6	7	8
381	2	1	7	0.0	0	CARD	2	
382	0	3	10	11		CARD	3	
383	1.420870E-1	3.572600E-2	0.0	0.0	295.0	CARD	4	
384	295.00					CARD	5	
385	0	1	22			CARD	6	
386	4.366260E-2	1.348740E-2	0.0	0.0	295.0	CARD	7	
387	295.0					CARD	8	
388	116.84E-2R	2 7087.35E-4E				DX 1		
389	7419.05E-5R	2 4474.09E-5E				VOL 1		
390	F 6342.4E-5E					FA 1		
391	F 0.000E					FRIC 1		
392	F 0.0E					GRAV 1		
393	F 2841.74E-4E					HD 1		
394	F 4E					NFF 1		
395	F 0.0E					ALP 1		
396	F 0.0E					VM 1		
397	F 552.5 E					TL 1		
398	F 552.5 E					TV 1		
399	F 15.79E6E					P 1		
400	F 0.0E					QPPP 1		
401	F 552.00E					TW 1		
402	1.500E					DX 2		
403	8983.81E-6E					VOL 2		
404	F 598.92E-5E					FA 2		
405	F 0.0E					FRIC 2		
406	F 0.0E					GRAV 2		
407	F 8732.52E-5E					HD 2		
408	F 4E					NFF 2		
409	F 0.0E					ALP 2		
410	F 0.0E					VM 2		
411	F 552.5 E					TL 2		
412	F 552.5 E					TV 2		
413	F 15.79E6E					P 2		
414	F 0.0E					QPPP 2		
415	F 552.00E					TW 2		

CARD	1	2	3	4	5	6	7	8
416	VESSEL		10					CARD 1
417		9	2	4		4		CARD 2
418		9	2	1		0	0	CARD 3
419		0						CARD 4
420		0	0	0		0		CARD 5
421		0.0E+00	0.0E+00	0.0E+00				CARD 6
422		0.007800E6	0.557668E3	0.016206E3	0.600000E0		0.0	CARD 7
423		1.500000E0	0.0E+00					CARD 8
424		0	0	1				CARD 9
425		0	0	0		0	0	CARD 10
426		0.0	0.0	0.0				CARD 11
427		0.38E0	0.76E0	1.52E0	2.28E0		3.04E0	Z
428		3.80E0	4.56E0	5.32E0	59.02E-1E			Z
429		35.56E-2	46.99E-2E					RAD
430		1570.80E-3	3141.59E-3	4712.39E-3	6283.19E-3E			TH
431		8	5	3		13		SOURCE
432		8	2	3		1		SOURCE
433		8	7	3		11		SOURCE
434		8	4	3		12		SOURCE
435	*							LEVEL 1
436	F	1.99E-01E						
437	F	6.23E+01E						
438	F	0.0E						CFZL-T
439	F	0.0E						CFZL-Z
440	F	0.0E						CFZL-R
441	F	0.0E						CFZV-T
442	F	0.0E						CFZV-Z
443	F	0.0E						CFZV-R
444	R 4	9735.62E-4R 4	0.577E					VOL
445	F	1.00EOE						FA-T
446	F	1.00EOE						FA-Z
447	R 4	1.00EOR 4	0.0E					FA-R
448	R 4	3673.95E-4R 4	1757.43E-4E					HD-T
449	R 4	3128.57E-4R 4	194.34E-3E					HD-Z
450	R 4	45.23E-2R 4	0.0E					HD-R

CARD	1	2	3	4	5	6	7	8
451	F	555.	E					HSTN
452	F		0.0E					ALPN
453	F		0.0E					VVN-T
454	F		0.0E					VVN-Z
455	F		0.0E					VVN-R
456	F		0.0E					VLN-T
457	F		0.0E					VLN-Z
458	F		0.0E					VLN-R
459	F		5.55E2E					TVN
460	F		5.55E2E					TLN
461	F		15.75E6E					PN
462	*							LEVEL 2
463	F		1.99E-01E					
464	F		6.23E+01E					
465	F		0.0E					CFZL-T
466	F		0.0E					CFZL-Z
467	F		0.0E					CFZL-R
468	F		0.0E					CFZV-T
469	F		0.0E					CFZV-Z
470	F		0.0E					CFZV-R
471	R 4	9735.62E-4R 4		0.577E				VOL
472	F		1.00E0E					FA-T
473	R 4	0.25 R 4		1.00E				FA-Z
474	R 4	1.00E0R 4		0.0E				FA-R
475	R 4	3673.95E-4R 4	1757.43E-4E					HD-T
476	R 4	3128.57E-4R 4	194.34E-3E					HD-Z
477	R 4	45.23E-2R 4		0.0E				HD-R
478	F	555.	E					HSTN
479	F		0.0E					ALPN
480	F		0.0E					VVN-T
481	F		0.0E					VVN-Z
482	F		0.0E					VVN-R
483	F		0.0E					VLN-T
484	F		0.0E					VLN-Z
485	F		0.0E					VLN-R

CARD	1	2	3	4	5	6	7	8
486	F	5.55E2E						TVN
487	F	5.55E2E						TLN
488	F	15.75E6E						PN
489	*							LEVEL 3
490	F	3.98E-01E						
491	F	1.25E+02E						
492	F	0.0E						CFZL-T
493	F	0.0E						CFZL-Z
494	F	0.0E						CFZL-R
495	F	0.0E						CFZV-T
496	F	0.0E						CFZV-Z
497	F	0.0E						CFZV-R
498	R 4	9735.62E-4R 4	0.577E					VOL
499	R 4	7775.16E-4R 4	0.50E0E					FA-T
500	R 4	1.0R 4	0.57700E					FA-Z
501	F	0.0E						FA-R
502	R 4	2087.61E-4R 4	1063.06E-4E					HD-T
503	R 4	1353.69E-4R 4	4574.89E-5E					HD-Z
504	F	0.0E						HD-R
505	F	552. E						HSTN
506	F	0.0E						ALPN
507	F	0.0E						VVN-T
508	F	0.0E						VVN-Z
509	F	0.0E						VVN-R
510	F	0.0E						VLN-T
511	F	0.0E						VLN-Z
512	F	0.0E						VLN-R
513	F	5.52E2E						TVN
514	F	5.52E2E						TLN
515	F	15.75E6E						PN
516	*							LEVEL 4
517	F	3.98E-01E						
518	F	1.25E+02E						
519	F	0.0E						CFZL-T
520	F	0.0E						CFZL-Z

CARD	1	2	3	4	5	6	7	8
521	F	0.0E						CFZL-R
522	F	0.0E						CFZV-T
523	F	0.0E						CFZV-Z
524	F	0.0E						CFZV-R
525	R 4	9735.62E-4R 4	0.577E					VOL
526	R 4	1.00E0R 4	0.50E0E					FA-T
527	R 4	1.00E0R 4	0.577E0E					FA-Z
528	F	0.0E						FA-R
529	R 4	4845.03E-4R 4	1063.06E-4E					HD-T
530	R 4	3128.57E-4R 4	4574 89E-5E					HD-Z
531	F	0.0E						HD-R
532	F	552. E						HSTN
533	F	0.0E						ALPN
534	F	0.0E						VVN-T
535	F	0.0E						VVN-Z
536	F	0.0E						VVN-R
537	F	0.0E						VLN-T
538	F	0.0E						VLN-Z
539	F	0.0E						VLN-R
540	F	5.52E2E						TVN
541	F	5.52E2E						TLN
542	F	15.75E6E						PN
543	*							LEVEL 5
544	F	3.98E-01E						
545	F	1.25E+02E						
546	F	0.0E						CFZL-T
547	F	0.0E						CFZL-Z
548	F	0.0E						CFZL-R
549	F	0.0E						CFZV-T
550	F	0.0E						CFZV-Z
551	F	0.0E						CFZV-R
552	R 4	9735.62E-4R 4	0.577E					VOL
553	R 4	1.00E0R 4	0.50E0E					FA-T
554	R 4	1.00E0R 4	0.577E0E					FA-Z
555	F	0.0E						FA-R

CARD	1	2	3	4	5	6	7	8
556	R 4	4845.03E-4R	4	1063.06E-4E				HD-T
557	R 4	3128.57E-4R	4	4574.89E-5E				HD-Z
558	F	0.0E						HD-R
559	F	552.	E					HSTN
560	F	0.0E						ALPN
561	F	0.0E						VVN-T
562	F	0.0E						VVN-Z
563	F	0.0E						VVN-R
564	F	0.0E						VLN-T
565	F	0.0E						VLN-Z
566	F	0.0E						VLN-R
567	F	5.52E2E						TV
568	F	5.52E2E						TLN
569	F	15.75E6E						PN
570	*							LEVEL 6
571	F	3.98E-01E						
572	F	1.25E+02E						
573	F	0.0E						CFZL-T
574	F	0.0E						CFZL-Z
575	F	0.0E						CFZL-R
576	F	0.0E						CFZV-T
577	F	0.0E						CFZV-Z
578	F	0.0E						CFZV-R
579	R 4	9735.62E-4R	4	0.577E				VOL
580	R 4	1.00E0R	4	0.50E0E				FA-T
581	R 4	0.18400R	4	0.57700E				FA-Z
582	F	0.0E						FA-R
583	R 4	4845.03E-4R	4	1063.06E-4E				HD-T
584	R 4	3128.57E-4R	4	4574.89E-5E				HD-Z
585	F	0.0E						HD-R
586	F	552.	E					HSTN
587	F	0.0E						ALPN
588	F	0.0E						VVN-T
589	F	0.0E						VVN-Z
590	F	0.0E						VVN-R

CARD	1	2	3	4	5	6	7	8
591	F	0.0E						VLN-T
592	F	0.0E						VLN-Z
593	F	0.0E						VLN-R
594	F	5.52E2E						TVN
595	F	5.52E2E						TLN
596	F	15.75E6E						PN
597	*							LEVEL 7
598	F	3.98E-01E						
599	F	1.25E+02E						
600	F	0.0E						CFZL-T
601	F	0.0E						CFZL-Z
602	F	0.00E						CFZL-R
603	F	0.0E						CFZV-T
604	F	0.00E						CFZV-Z
605	F	0.00E						CFZV-R
606	R 4	9735.62E-4R 4	0.577E					VOL
607	R 4	1.00E0R 4	0.50E0E					FA-T
608	R 4	0.1038R 4	0.57700E					FA-Z
609	F	0.0E						FA-R
610	R 4	4845.03E-4R 4	1063.06E-4E					HD-T
611	R 4	30.48E-2R 4	4574.89E-5E					HD-Z
612	F	0.0E						HD-R
613	R 4	552. R 4	5.55E2E					HSTN
614	F	0.0E						ALPN
615	F	0.0E						VVN-T
616	F	0.0E						VVN-Z
617	F	0.0E						VVN-R
618	F	0.0E						VLN-T
619	F	0.0E						VLN-Z
620	F	0.0E						VLN-R
621	R 4	5.52E2R 4	5.55E2E					TVN
622	R 4	5.52E2R 4	5.55E2E					TLN
623	F	15.75E6E						PN
624	*							LEVEL 8
625	F	3.98E-01E						

CARD	1	2	3	4	5	6	7	8
626	F	1.25E+02E						
627	F	0.0E						CFZL-T
628	F	0.0E						CFZL-Z
629	F	0.0E						CFZL-R
630	F	0.0E						CFZV-T
631	F	0.0E						CFZV-Z
632	F	0.0E						CFZV-R
633	R 4	9735.62E-4R 4	0.577E					VOL
634	R 4	1.00E0R 4	0.50E0E					FA-T
635	R 4	1.00R 4	0.577E					FA-Z
636		0.0	1494.06E-4	0.0	1494.06E-4	1130.64E-4		FA-R
637		0.0	1130.64E-4	0.0E				FA-R
638	R 4	4845.03E-4R 4	1063.06E-4E					HD-T
639	R 4	8669.01E-5R 4	4574.89E-5E					HD-Z
640		0.0	2.84E-1	0.0	2.84E-1	2.84E-1		HD-R
641		0.0	2.84E-1	0.0E				HD-R
642	R 4	555. R 4	5.55E02E					HSTN
643	F	0.0E						ALPN
644	F	0.0E						VVN-T
645	F	0.0E						VVN-Z
646	F	0.0E						VVN-R
647	F	0.0E						VLN-T
648	F	0.0E						VLN-Z
649	F	0.0E						VLN-R
650	R 4	5.52E2R 4	5.55E2E					TVN
651	R 4	5.52E2R 4	5.55E2E					TLN
652	F	15.75E6E						PN
653	*							LEVEL 9
654	F	3.04E-01E						
655	F	9.56E+01E						
656	F	0.0E						CFZL-T
657	F	0.0E						CFZL-Z
658	F	0.0E						CFZL-R
659	F	0.0E						CFZV-T
660	F	0.0E						CFZV-Z

CARD	1	2	3	4	5	6	7	8
661	F	0.0E						CFZV-R
662	R 4	9735.62E-4R 4	0.577E					VOL
663	R 4	1.00E0R 4	0.50E0E					FA-T
664	F	0.0E						FA-Z
665	F	0.0E						FA-R
666	R 4	4845.03E-4R 4	1063.06E-4E					HD-T
667	F	0.0E						HD-Z
668	F	0.0E						HD-R
669	R 4	552. R 4	552.0 E					HSTN
670	F	0.0E						ALPN
671	F	0.0E						VVN-T
672	F	0.0E						VVN-Z
673	F	0.0E						VVN-R
674	F	0.0E						VLN-T
675	F	0.0E						VLN-Z
676	F	0.0E						VLN-R
677	R 4	5.52E2R 4	5.55E2E					TVN
678	R 4	5.52E2R 4	5.55E2E					TLN
679	F	15.75E6E						PN
680	FILL		13					CARD 1
681		14						CARD 2
682		1.00E0	1.00E0	0.0	0.0	5.53E2		CARD 3
683		15.75E6						CARD 4
684	BREAK		14					CARD 1
685		15	0					CARD 2
686		1.00E0	1.00E0	1.00E0	5.53E2	66.50E5		CARD 3
687	TEE		12					CARD 1
688		2	1	7	0.0	1		CARD 2
689		0	3	13	17			CARD 3
690		0.142000E0	3.571240E-2	0.0	0.0	2.950000E2		CARD 4
691		2.950000E2						CARD 5
692		0	1	77				CARD 6
693		0.11115	3.57E-2	0.0	0.0	295.0		CARD 7
694		295.0						CARD 8
695	F	5583.76E-4E						DX 1

CARD	1	2	3	4	5	6	7	8
696	F	35.44E-3E						VOL 1
697	R 3	6342.53E-5	1387.58E-5E					FA 1
698		0.0	2671.89E-3	44.38E-3	0.0E			FRIC 1
699	F	0.0E						GRAV 1
700	R 3	2.84E-1	1329.18E-4E					HD 1
701	F	4E						NFF 1
702	F	0.0E						ALP 1
703	F	0.0E						VM 1
704	F	5.55E2E						TL 1
705	F	5.55E2E						TV 1
706	F	15.75E6E						P 1
707	F	0.0E						QPPP 1
708	F	5.52E2E						TW 1
709	F	7.9845E						DX 2
710	F	0.3098E						VOL 2
711	F	3.88E-2E						FA 2
712	F	0.0E						FRIC 2
713	F	1.0E						GRAV 2
714	F	0.2223E						HD 2
715	F	4E						NFF 2
716	F	0.0E						ALP 2
717	F	0.0E						VM 2
718	F	5.55E2E						TL 2
719	F	5.55E2E						TV 2
720	F	15.75E6E						P 2
721	F	0.0E						QPPP 2
722	F	5.55E2E						TW 2
723	PIPE		16					CARD 1
724		25	1	17	19		7	CARD 2
725		0	1					CARD 3
726		0.958804E-1	0.159919E0	0.0	0.0	2.950000E2		CARD 4
727		2.950000E2						CARD 5
728		1.27E-1	9925.54E-5	7444.15E-5R 2	4962.77E-5R 2	2481.39E-5		DX
729	R 6	1.27E-2R 2	2579.69E-5	5159.38E-5	7739.06E-5	1183.93E-4		DX
730		1851.91E-4R 3	2160.57E-4	2063.75E-4	3460.75E-4	46.99E-2E		DX

CARD	1	2	3	4	5	6	7	8
731	1479.66E-6	9355.59E-7	701.67E-6R 2	467.78E-6R 2	233.89E-6	VOL		
732	R 6 1062.32E-7R 2	6067.41E-7	1213.48E-6	1820.22E-6	2284.08E-6	VOL		
733	4355.69E-6R 3	5081.64E-6	4853.93E-6	1798.07E-5	2441.41E-5E	VOL		
734	1387.58E-5R 6	9425.75E-6R 6	8364.71E-6R10	2351.98E-5R 3	5195.56E-5E	FA		
735	R 7 0.0R 7	1.6R 8	0.0R 4	0.20E		FRIC		
736	F 0.0E					GRAV		
737	1329.18E-4R 6	109.55E-3R 6	10.32E-2R10	173.05E-3R 3	25.72E-2E	HD		
738	F 4E					NFF		
739	F 0.0E					ALP		
740	F 0.0E					VM		
741	R19 5.55E2R06	5.45E2E				TL		
742	R19 5.55E2R06	5.45E2E				TV		
743	F 15.75E6E					P		
744	F 0.0E					QPPP		
745	R19 5.55E2R06	5.45E2E				TW		
746	TEE	11				CARD	1	
747	2	1	7	0.0	0	CARD	2	
748	0	16	12	16		CARD	3	
749	0.144514E0	0.758863E-1	0.0	0.0	2.950000E2	CARD	4	
750	2.950000E2					CARD	5	
751	0	1	99			CARD	6	
752	0.11115	3.57E-2	0.0	0.0	295.0	CARD	7	
753	295.0					CARD	8	
754	R 3 5583.76E-4	525.78E-3	4674.87E-4	558.61E-3	1987.49E-3	DX	1	
755	R 2 1077.21E-3	1987.49E-3	5102.86E-4	5462.91E-4	4862.83E-4	DX	1	
756	2.54E-1	171.45E-3	1746.25E-4E			DX	1	
757	R 3 35.44E-3	4728.01E-6	3757.89E-6	4660.33E-6	1968.55E-4	VOL	1	
758	R 2 1138.34E-4	1968.55E-4	4072.76E-6	4063.49E-6	317.15E-5	VOL	1	
759	1611.49E-5	7091.63E-6	1107.57E-5E			VOL	1	
760	R 3 6342.53E-5	139.13E-4R 2	8364.71E-6	1914.12E-5R 2	1056.26E-4	FA	1	
761	1914.12E-5	1056.26E-4R 2	8364.71E-6	6342.53E-5R 2	9462.37E-6	FA	1	
762	6342.53E-5E					FA	1	
763	0.0	2671.89E-3R 3	0.0	2614.89E-5	0.0	FRIC	1	
764	111.08E-2	3234.17E-5	2273.55E-5	111.08E-2R 3	0.0	FRIC	1	
765	1302.49E-4	1700.00E-3	0.0E			FRIC	1	

CARD	1	2	3	4	5	6	7	8
766	R 5	0.0R 3	1.00E0	0.0R 5	-1.00E0R 3	0.0E	GRAV 1	
767	R 3	2.84E-1	1330.96E-4R 2	10.32E-2	1756.41E-5R 2	3667.25E-4	HD 1	
768		1756.41E-5R 3	10.32E-2	2.84E-1R 2	1197.61E-5	2.84E-1E	HD 1	
769	F	4E					NFF 1	
770	F	0.0E					ALP 1	
771	F	0.0E					VM 1	
772	F	5.55E2E					TL 1	
773	F	5.55E2E					TV 1	
774	F	15.75E6E					P 1	
775	F	0.0E					QPPP 1	
776	F	5.54E2E					TW 1	
777	F	7.54640E					DX 2	
778	F	0.2928E					VOL 2	
779	F	3.88E-2E					FA 2	
780	F	0.0E					FRIC 2	
781	F	1.0E					GRAV 2	
782	F	.2223E					HD 2	
783	F	4E					NFF 2	
784	F	0.0E					ALP 2	
785	F	0.0E					VM 2	
786	F	5.55E2E					TL 2	
787	F	5.55E2E					TV 2	
788	F	15.75E6E					P 2	
789	F	0.0E					QPPP 2	
790	F	5.55E2E					TW 2	
791	PIPE		15				CARD 1	
792		25	1	16		7	CARD 2	
793		0	1				CARD 3	
794		8331.79E-5	164.79E-3	0.0	0.0	2.95E2	CARD 4	
795		2.95E2					CARD 5	
796		27.94E-2R 2	2118.36E-4R 4	1871.66E-4R 2	1496.06E-4	8413.75E-5	DX	
797		5609.17E-5	2804.58E-5R 6	1.27E-2	2716.39E-5	5432.78E-5	DX	
798	R 2	8149.17E-5R 3	19.05E-2E				DX	
799		6860.64E-6R 2	1766.69E-6R 4	1567.35E-6R 2	1245.95E-6	703.79E-6	VOL	
800		4691.93E-7	2345.97E-7R 6	1062.32E-7	1411.33E-6	2822.65E-6	VOL	

CARD		1	2	3	4	5	6	7	8
		12345678901234567890123456789012345678901234567890123456789012345678901234567890							
801	R 2	4233.99E-6R 3	9897.61E-6E						VOL
802		6342.53E-5R18	8364.71E-6R 7	5195.56E-5E					FA
803	R 3	0.0	4396.98E-5R 5	0.0	4396.98E-5R16			0.0E	FRIC
804	R 3	0.0R 5	1.00E0	7071.07E-4R17	0.0E				GRAV
805		2.84E-01R18	10.32E-2R 7	25.72E-2E					HD
806	F	4E							NFF
807	F	0.0E							ALP
808	F	0.0E							VM
809	R13	5.55E2R12	5.45E2E						TL
810	R13	5.55E2R12	5.45E2E						TV
811	F	15.75E6E							P
812	F	0.0E							QPPP
813	R13	5.55E2R12	5.45E2E						TW
814	VALVE		18						CARD 1
815		2	1	19	21			7	CARD 2
816		0	0						CARD 3
817		0.128600E0	0.277813E-1	0.0	0.0	2.950000E2			CARD 4
818		2.950000E2							CARD 5
819		4	2	2				2	CARD 6
820		5.273E-2	9.525E-2						CARD 7
821		1.5E0	2.00E0E						DX
822		3282.71E-5	6058.79E-5E						VOL
823		5195.56E-5	5272.92E-5	5855.64E-5E					FA
824		1.0	1.0	1.0E					FRIC
825	F	0.0E							GRAV
826		25.72E-2	9524.99E-5	273.05E-3E					HD
827	F	4E							NFF
828		0.0	1.00E0E						ALP
829	F	0.0E							VM
830		545.0	373.0E						TL
831		545.0	373.0E						TV
832		59.00E5	1.01E5E						P
833	F	0.0E							QPPP
834		545.0	373.0E						TW
835		0.0	0.00001	1.75E-2	1.00E0E				VLTL

CARD	1	2	3	4	5	6	7	8
836	VALVE		17					CARD 1
837		2	1	18		20	7	CARD 2
838		0	0					CARD 3
839		0.128600E0	0.277813E-1	0.0	0.0	2.950000E2		CARD 4
840		2.950000E2						CARD 5
841		4	2	2			2	CARD 6
842		0.05272920	0.09525000					CARD 7
843		1.500	2.000000E					DX
844		3282.71E-5	6058.79E-5E					VOL
845		5195.56E-5	5272.92E-5	5855.64E-5E				FA
846	F	1.0E						FRIC
847	F	0.0E						GRAV
848		25.72E-2	9524.99E-5	273.05E-3E				HD
849	F	4E						NFF
850		0.0	1.00E0E					ALP
851	F	0.0E						VM
852		545.0	374.0 E					TL
853		545.0	374.0 E					TV
854		15.75E6	1.01E5E					P
855	F	0.0E						QPPP
856		545.0	374.0 E					TW
857		0.0	0.000001	1.75E-2	1.00E0E			VLTBL
858	FILL		99					CARD 1
859		99	1					CARD 2
860		2.50	0.226783E-2	0.0	0.0	0.297440E3		CARD 3
861		4.24E6						CARD 4
862	FILL		77					CARD 1
863		77	1					CARD 2
864		2.50	0.226783E-2	0.0	0.0	0.297440E3		CARD 3
865		4.24E6						CARD 4
866	BREAK		19					CARD 1
867		20	0					CARD 2
868		0.822325E0	0.605879E-1	1.00E0	3.73E2	101.33E3		CARD 3
869	BREAK		20					CARD 1
870		21	0					CARD 2

CARD	1	2	3	4	5	6	7	8
871	.2	.06	1.0	373.0	1.01E5	CARD	3	
872	TEE	21	0					
873	1	0	7	-1.000000E+00	0			
874	0	2	25	27	0			
875	4.366260E-02	3.487400E-03	0.	0.	2.950000E+02			
876	2.950000E+02							
877	0	2	23					
878	1.699260E-02	7.137400E-03	0.	0.	2.950000E+02			
879	2.950000E+02							
880	F 2.1844E+00E							
881	F 5.2331E-02E							
882	R 2 5.9890E-03R 1	5.5470E-02E						
883	F 4.5000E-01E							
884	F 0. E							
885	R 2 8.7330E-02R 1	2.6360E-01E						
886	F 4E							
887	F 0. E							
888	F 0. E							
889	F 5.5244E+02E							
890	F 5.5244E+02E							
891	F 1.5600E+07E							
892	F 2.5000E+00E							
893	F 2.2678E-03E							
894	F 9.0713E-04E							
895	F 0. E							
896	F 0. E							
897	F 3.3985E-02E							
898	F 4E							
899	F 0. E							
900	F 0. E							
901	F 5.5244E+02E							
902	F 5.5244E+02E							
903	F 1.5600E+07E							
904	TEE	22	0					
905	1	0	7	1.000000E+00	0			

CARD	1	2	3	4	5	6	7	8
906		1	1	25	22		0	
907	0.	0.	0.	0.	0.	0.		
908	0.							
909		1	1	26				
910	0.	0.	0.	0.	0.	0.		
911	0.							
912	F	1.0000E+00E						
913	F	5.9890E-03E						
914	F	5.9890E-03E						
915	F	0. E						
916	F	0. E						
917	F	8.7330E-02E						
918	F	4E						
919	F	0. E						
920	F	0. E						
921	F	5.5240E+02E						
922	F	5.5240E+02E						
923	F	1.5600E+07E						
924	F	1.0000E+00E						
925	F	5.9890E-03E						
926	F	5.9890E-03E						
927	F	0. E						
928	F	0. E						
929	F	8.7330E-02E						
930	F	4E						
931	F	0. E						
932	F	0. E						
933	F	5.5240E+02E						
934	F	5.5240E+02E						
935	F	1.5600E+07E						
936	ACCUM		23	0				
937		3	24					
938		8.8633E-01	1.2886E+00	2.2500E-02E				
939		9.6000E-01	1.6760E+00	2.0000E-02E				
940	R 3	1.2460E+00R 1	3.2852E-02E					

CARD	1	2	3	4	5	6	7	8
941	F	4.5000E-01E						
942	F	-1.0000E+00E						
943	R 3	1.2595E+00R	1 2.0452E-01E					
944	F	4E						
945	R 1	1.0000E+00R	2 0.	E				
946	F	0.	E					
947	F	3.0080E+02E						
948	F	3.0080E+02E						
949	F	4.1100E+06E						
950	FILL		25		LPIS PUMP EQUIVALENT			CARD 1
951		23	3		11			CARD 2
952		1.50	8.983810E-3	0.0	0.421345E0	0.297440E3		CARD 3
953		4.24E6						CARD 4
954		1.00E+04	7.72E+00	1.38E+05	7.40E+00S			FLTBL
955		3.97E+05	6.68E+00	5.89E+05	5.98E+00S			FLTBL
956		7.93E+05	5.19E+00	9.74E+05	4.41E+00S			FLTBL
957		1.13E+06	3.43E+00	1.25E+06	2.47E+00S			FLTBL
958		1.35E+06	1.39E+00	1.44E+06	0.00E+00S			FLTBL
959		2.00E+07	0.00E+00E					FLTBL
960	FILL		24		HPIS PUMP EQUIVALENT			CARD 1
961		26	2		4			CARD 2
962		2.50	0.226783E-2	0.0	0.0	0.297440E3		CARD 3
963		4.24E6						CARD 4
964		0.0	0.0	22.0	0.0S			FLTBL
965		22.10E0	1.84E-01	1.00E3	1.84E-01E			FLTBL
966	VALVE		27	0				
967		2	0	27	24	7		
968		0	0					
969		4.366260E-02	3.487400E-03	0.	0.	2.950000E+02		
970		2.950000E+02						
971		2	3	0	0	2		
972		5.989200E-02	8.732520E-01	0.				
973	F	1.0922E+00E						
974	F	2.6166E-02E						
975	R 2	5.5470E-02R	1 3.2852E-02E					

	1					2					3					4					5					6					7					8				
CARD	1	2	3	4	5	1	2	3	4	5	1	2	3	4	5	1	2	3	4	5	1	2	3	4	5	1	2	3	4	5	1	2	3	4	5					
976	F			4.5000E-01E																																				
977	F			0.	E																																			
978	R	2		2.6360E-01R	1				2.0452E-01E																															
979	F				4E																																			
980	F			0.	E																																			
981	F			0.	E																																			
982				5.5250E+02					3.0567E+02E																															
983				5.5250E+02					3.0567E+02E																															
984				1.5600E+07					4.2400E+06E																															
985				1.0E-4					0.100					100.0																	1.0E+03									
986				5.0					0.10					5.0																										
987				-1.																																				

CARD	1	2	3	4	5	6	7	8
1	2							
2	LOFT TEST L1-4						(INITIAL INPUT)	
3	BLOWDOWN							
4	-1	0.0						MCC 1
5	0		1	28		29		1 MCC 2
6	2.0e-3	1.0e-5		1.0e-2				MCC 3
7	10	50		10		3		MCC 4
8	1	2		3		4		5 IORDER
9	6	7		8		9		11 IORDER
10	12	13		14		15		16 IORDER
11	17	18		19		20		21 IORDER
12	22	23		24		25		27 IORDER
13	77	99		10e				IORDER
14	-1							
15								
16	END							
17	1.0e-4	0.1		70.0				TIMSTP
18	5.0	0.05		5.0				TIMSTP
19	-1.							TIMSTP
20	P							

APPENDIX 8

TRAC STEADY-STATE AND TRANSIENT INPUT DECKS FOR LOFT EXPERIMENT L2-2

I. TRAC STEADY-STATE INPUT DECK FOR LOFT EXPERIMENT L2-2

CARD	1	2	3	4	5	6	7	8
1	3			1				
2	LOFT STEADY STATE TEST (INITIAL INPUT)							
3	L2-2 INCLUDING UPPER PLENUM BLOCKAGE							
4	GAP WIDTH = 0.0953 MM							
5	-1	0.						
6	1	0		27		28		1
7	1.00000E-03	5.00000E-06		1.00000E-04		0.00000E+00		
8	10	100		20		7		1
9	1	2		3		4		5
10	6	7		8		9		10
11	13	14		15		16		17
12	18	19		20		21		22
13	23	24		25		27		50
14	77	99E						
15	333E							
16	1	0	.100000E+01	0.				
17	0	0		0		0		
18	2	0	0.		0.			
19	0	0		0		0		
20	3000	-1	.422000E+07	0.				
21	27	0		1		0		
22	4	-7	.230000E+00		.300000E+01			
23	2	0		1		0		
24	555	0	0.		0.			
25	0	0		0		0		
26	333	0		35.0		0.0		
27	0	0		0		0		
28	2000	0	0.		0.			
29	0	0		0		0		
30	TEE	1		0				

CARD	1	2	3	4	5	6	7	8
31		4	1	7	0.		0	
32		0	4	1		3	0	
33	1.420000E-01	3.650000E-02	0.		0.		2.950000E+02	
34	2.950000E+02							
35		0	3	2				
36	2.330050E-02	8.696800E-03	0.		0.		2.950000E+02	
37	2.950000E+02							
38	R 2 6.6675E-01R	1 4.1910E-01R	1 6.6010E-01E					
39	R 2 4.2334E-02R	1 2.6618E-02R	1 4.1909E-02E					
40	F 6.3425E-02E							
41	F 0.	E						
42	F 0.	E						
43	F 2.8400E-01E							
44	F 4E							
45	F 0.	E						
46	F 0.	E						
47	F 5.5200E+02E							
48	F 5.5200E+02E							
49	F 1.5750E+07E							
50	F 0.	E						
51	F 5.5200E+02E							
52	2.1499E+00	2.6423E+00	2.2217E+00E					
53	3.1149E-03	3.6954E-03	5.7059E-03E					
54	P 3 1.4493E-03R	1 5.7321E-03E						
55	1.6530E-01	5.5032E-03	4.6688E-03	0.		E		
56	R 1 5.0000E-01R	2 0.	R 1 5.0000E-01E					
57	R 3 4.2957E-02R	1 8.5430E-02E						
58	F 4E							
59	F 0.	E						
60	F 0.	E						
61	F 5.5200E+02E							
62	F 5.5200E+02E							
63	F 1.5750E+07E							
64	F 0.	E						
65	F 5.5200E+02E							

	1	2	3	4	5	6	7	8
CARD	1234567890123456789012345678901234567890123456789012345678901234567890							
66	PIPE		4	0				
67		4	1	3		4	7	
68		0	0					
69	1.505690E-01	3.761400E-02	0.	0.		2.950000E+02		
70	2.950000E+02							
71	1.0160E+00	7.3660E-01	3.5560E-01	5.3340E-01E				
72	4.9555E-02	4.6723E-02	2.6052E-02	4.3326E-02E				
73	6.3430E-02	3.3300E-02	6.3430E-02	8.3190E-02	5.1600E-02E			
74	R 4 0.	R 1 2.5000E-02E						
75	F 0.	E						
76	R 3 2.8400E-01R	1 3.2546E-01R	1 2.5600E-01E					
77	F	4E						
78	F 0.	E						
79	F 0.	E						
80	F 5.5400E+02E							
81	F 5.5400E+02E							
82	F 1.5750E+07E							
83	F 0.	E						
84	F 5.5400E+02E							
85	STGEN		3	0				
86		10	3	4		5	12	
87		1	0	0		1		
88	5.105400E-03	1.244600E-03						
89		7	14	15				
90	R 1 1.0000E+00R	8 6.4199E-01R	1 1.0000E+00E					
91	R 1 3.3541E-01R	8 9.7000E-02R	1 3.3541E-01E					
92	R 1 5.1605E-02R	9 1.5117E-01R	1 5.1605E-02E					
93	R 1 2.5000E-02R	9 0.	R 1 2.5000E-02E					
94	R 1 0.	R 4 1.0000E+00R	1 0.	R 4-1.0000E+00R	1 0.			
95	R 1 2.5600E-01R	9 1.0211E-02R	1 2.5600E-01E					
96	R 1	4R 9	1R 1	4E				
97	F 0.	E						
98	F 0.	E						
99	R 5 5.5400E+02R	5 5.5200E+02E						
100	R 5 5.5400E+02R	5 5.5200E+02E						

	1	2	3	4	5	6	7	8
CARD	1234567890123456789012345678901234567890123456789012345678901234567890							
101	F	1.5750E+07E						
102	F	5.4600E+02E						
103	R 4	6.4199E-01R 3	1.0502E+00E					
104	R 1	4.7450E-01R 3	8.7060E-01R 3	1.1894E+00E				
105	R 7	1.3560E+00R 1	1.8200E-02E					
106	F	0.	E					
107	F	1.0000E+00E						
108	R 1	1.0200E-01R 6	3.5700E-02R 1	1.5240E-01E				
109	F		4E					
110	R 4	0.	R 1	2.6315E-01R 2	1.0000E+00E			
111	F	0.	E					
112	F	5.5800E+02E						
113	F	5.5800E+02E						
114	F	6.3340E+06E						
115	R 1	0.	R 1	2.4040E+01R 6	4.4100E+01R 1	2.4040E+01R 1	0.	E
116	R 1	2.5780E+01R 3	4.7300E+01R 3	0.	E			
117	TEE		5		0			
118		2	1		7	0.		0
119		0	3		6		7	0
120		1.420870E-01	3.572600E-02	0.		0.		2.950000E+02
121		2.950000E+02						
122		0	2		5			
123		1.420870E-01	3.572600E-02	0.		0.		2.950000E+02
124		2.950000E+02						
125		6.3500E-01	1.6764E+00		6.3500E-01E			
126		2.7468E-02	1.1249E-01		2.7468E-02E			
127	R 1	3.6613E-02R 2	6.3425E-02R 1	3.6613E-02E				
128	F	0.	E					
129		-1.2380E-01	-1.0000E+00	1.0000E+00		1.2380E-01E		
130	R 1	2.1591E-01R 2	2.8417E-01R 1	2.1591E-01E				
131	F		4E					
132	F	0.	E					
133	F	0.	E					
134	F	5.5200E+02E						
135	F	5.5200E+02E						

CARD	1	2	3	4	5	6	7	8
136	F	1.5750E+07E						
137	F	0.	E					
138	F	5.5200E+02E						
139		1.3141E+00	1.2446E+00E					
140		8.3466E-02	9.0048E-02E					
141	R 2	6.3425E-02R 1	5.1605E-02E					
142	F	0.	E					
143		0.	1.0000E+00	0.	E			
144	R 2	2.8417E-01R 1	2.5600E-01E					
145	F		4E					
146	F	0.	E					
147	F	0.	E					
148	F	5.5200E+02E						
149	F	5.5200E+02E						
150	F	1.5750E+07E						
151	F	0.	E					
152	F	5.5200E+02E						
153	PUMP		6	0				
154		2	1	6		8		7
155		0	0	1		1		1
156		0	0					
157		1.079550E-01	2.835930E-02	0.	0.		2.950000E+02	
158		2.950000E+02						
159		941.54	500.	.315		614.		369.661 CARD 7
160		3.174380E+02	3.681250E+00	2.311860E+02	1.370000E+02			
161		0						
162		7	10	11		11		13
163		10	14	6		12		8
164		4	6	2		2		2
165		2	11	7				
166	R 1	-1.0000E+00R 1	2.4400E+00R 1	-8.0000E-01R 1	2.0300E+00R 1	-4.0000E-01		
167	R 1	1.6000E+00R 1	-2.0000E-01R 1	1.4700E+00R 1	0.	R 1 1.4000E+00		
168	R 1	4.0000E-01R 1	1.3000E+00R 2	1.0000E+00E				
169	R 2	-1.0000E+00R 1	-4.0000E-01R 1	-8.8000E-01R 1	-3.0000E-01R 1	-8.3000E-01		
170	R 1	0.	R 1 -6.8000E-01R 1	2.0000E-01R 1	-5.1000E-01R 1	4.0000E-01		

CARD	1	2	3	4	5	6	7	8
171	R 1-2.8000E-01R 1 6.0000E-01R 1 0.				R 1 7.0000E-01R 1 1.8000E-01			
172	R 1 8.0000E-01R 1 4.0000E-01R 2 1.0000E+00E							
173	R 1-1.0000E+00R 1 2.4400E+00R 1-8.3000E-01R 1 2.0000E+00R 1-7.0000E-01							
174	R 1 1.7000E+00R 1-6.5000E-01R 1 1.6000E+00R 1-4.5000E-01R 1 1.3200E+00							
175	R 1-1.7000E-01R 1 1.1000E+00R 1 0.				R 1 9.3000E-01R 1 5.0000E-01			
176	R 1 8.3000E-01R 1 7.8000E-01R 1 8.3000E-01R 1 9.5000E-01R 1 9.3000E-01							
177	R 2 1.0000E+00E							
178	R 2-1.0000E+00R 1-8.0000E-01R 2-6.0000E-01R 1-3.0000E-01R 1-4.4000E-01							
179	R 1-1.0000E-01R 1-2.3000E-01R 1 1.0000E-01R 1-5.0000E-02R 1 2.3000E-01							
180	R 1 3.9000E-01R 1 3.3000E-01R 1 4.0000E-01R 1 2.7000E-01R 1 6.2000E-01							
181	R 1 4.8000E-01R 1 9.0000E-01R 1 8.3000E-01R 2 1.0000E+00E							
182	-1.0000E+00	3.6100E+00	-9.0000E-01	3.4900E+00	-8.0000E-01			
183	3.8300E+00	-6.0000E-01	4.6200E+00	-5.0000E-01	4.6300E+00			
184	-4.0000E-01	4.2700E+00	-2.0000E-01	2.8200E+00	0.			
185	1.4500E+00	1.2000E-01	5.5000E-01	2.0000E-01	2.6000E-01			
186	4.0000E-01	2.5000E-01	9.0000E-01	2.2000E-01	1.0000E+00			
187	0.	E						
188	0.	-6.8000E-01	1.0000E-01	-5.8000E-01	2.0000E-01			
189	-5.1000E-01	3.0000E-01	-4.9000E-01	4.0000E-01	-4.8000E-01			
190	6.0000E-01	-4.3000E-01	7.0000E-01	-3.7000E-01	8.0000E-01			
191	-2.6000E-01	9.0000E-01	-7.0000E-02	1.0000E+00	0.	E		
192	-1.0000E+00	3.6100E+00	-8.3000E-01	2.6000E+00	-7.0000E-01			
193	2.0300E+00	-6.5000E-01	1.8500E+00	-4.5000E-01	1.3700E+00			
194	-1.7000E-01	1.0500E+00	0.	8.3000E-01	2.0000E-01			
195	7.6000E-01	4.0000E-01	7.3000E-01	5.0000E-01	7.6000E-01			
196	6.0000E-01	8.8000E-01	7.8000E-01	1.3100E+00	9.5000E-01			
197	2.0800E+00	1.0000E+00	2.4600E+00E					
198	0.	2.4000E-01	3.9900E-01	8.2000E-01	4.0000E-01			
199	7.7000E-01	6.2000E-01	1.5800E+00	9.0000E-01	2.1800E+00			
200	1.0000E+00	2.4600E+00E						
201	R 1-1.0000E+00R 1 2.0000E+00R 1-8.0000E-01R 1 1.4000E+00R 1-7.0000E-01							
202	R 1 1.2000E+00R 1-6.0000E-01R 1 1.0300E+00R 1-4.0000E-01R 1 8.0000E-01							
203	R 1-2.0000E-01R 1 6.6000E-01R 1-1.0000E-01R 1 6.1000E-01R 1 0.							
204	R 1 6.0000E-01R 1 1.0000E-01R 1 6.1000E-01R 1 2.0000E-01R 1 6.3000E-01							
205	R 1 6.0000E-01R 1 8.3000E-01R 2 1.0000E+00E							

CARD	1	2	3	4	5	6	7	8
206	R 2-1.0000E+00R	1-3.0000E-01R	1-9.0000E-01R	1-2.0000E-01R	1-8.7000E-01			
207	R 1-1.0000E-01R	1-8.1000E-01R	1 0.	R 1-6.8000E-01R	1 4.0000E-01			
208	R 1-2.7000E-01R	1 5.0000E-01R	1 1.5000E-01R	2 1.0000E+00E				
209	-1.0000E+00	2.0000E+00	-1.0000E-01	1.3500E+00	5.0000E-01			
210	8.3000E-01	1.0000E+00	3.4000E-01E					
211	R 2-1.0000E+00R	1-3.0000E-01R	1-9.0000E-01R	1-1.0000E-01R	1-5.2000E-01			
212	R 1 4.0000E-01R	1-2.7000E-01R	1 5.0000E-01R	1 0.	R 1 1.0000E+00			
213	R 1 3.4000E-01E							
214	-1.0000E+00	0.	1.0000E+00	0.	E			
215	-1.0000E+00	0.	1.0000E+00	0.	E			
216	-1.0000E+00	0.	1.0000E+00	0.	E			
217	-1.0000E+00	0.	1.0000E+00	0.	E			
218	R 2 0.	R 1 1.0000E-01R	1 0.	R 1 1.5000E-01R	1 5.0000E-02			
219	R 1 2.4000E-01R	1 8.0000E-01R	1 3.0000E-01R	1 9.6000E-01R	1 4.0000E-01			
220	R 1 9.8000E-01R	1 6.0000E-01R	1 9.7000E-01R	1 8.0000E-01R	2 9.0000E-01			
221	R 1 8.0000E-01R	1 9.6000E-01R	1 5.0000E-01R	1 1.0000E+00R	1 0.	E		
222	R 2 0.	R 1 1.0000E-01R	1 0.	R 1 1.5000E-01R	1 4.8000E-02			
223	R 1 2.2000E-01R	1 5.6400E-01R	1 8.0000E-01R	1 5.6400E-01R	1 9.6000E-01			
224	R 1 4.5400E-01R	1 1.0000E+00R	1 7.6000E-02E					
225	F 1.3521E+00E							
226	F 4.9555E-02E							
227	F 3.6613E-02E							
228	F 0.	E						
229	R 1 1.2380E-01R	2 0.	E					
230	F 2.1591E-01E							
231	F 4E							
232	F 0.	E						
233	F 0.	E						
234	F 5.5300E+02E							
235	F 5.5300E+02E							
236	F 1.5750E+07E							
237	F 0.	E						
238	F 5.5300E+02E							
239	PUMP		7	0				
240		2	1	7	9		7	

CARD	1	2	3	4	5	6	7	8
	12345678901234567890123456789012345678901234567890123456789012345678901234567890							
241	0	0	1	1	1			
242	0	0						
243	1.079550E-01	2.835930E-02	0.	0.		2.950000E+02		
244	2.950000E+02							
245	941.54	500.	.315	614.	369.661	CARD 7		
246	3.174380E+02	3.681250E+00	2.311860E+02	1.370000E+02				
247	0							
248	7	10	11	11	13			
249	10	14	6	12	8			
250	4	6	2	2	2			
251	2	11	7					
252	R 1-1.0000E+00R 1 2.4400E+00R 1-8.0000E-01R 1 2.0300E+00R 1-4.0000E-01							
253	R 1 1.6000E+00R 1-2.0000E-01R 1 1.4700E+00R 1 0.				R 1 1.4000E+00			
254	R 1 4.0000E-01R 1 1.3000E+00R 2 1.0000E+00E							
255	R 2-1.0000E+00R 1-4.0000E-01R 1-8.8000E-01R 1-3.0000E-01R 1-8.3000E-01							
256	R 1 0.	R 1-6.8000E-01R 1 2.0000E-01R 1-5.1000E-01R 1 4.0000E-01						
257	R 1-2.8000E-01R 1 6.0000E-01R 1 0.		R 1 7.0000E-01R 1 1.8000E-01					
258	R 1 8.0000E-01R 1 4.0000E-01R 2 1.0000E+00E							
259	R 1-1.0000E+00R 1 2.4400E+00R 1-8.3000E-01R 1 2.0000E+00R 1-7.0000E-01							
260	R 1 1.7000E+00R 1-6.5000E-01R 1 1.6000E+00R 1-4.5000E-01R 1 1.3200E+00							
261	R 1-1.7000E-01R 1 1.1000E+00R 1 0.		R 1 9.3000E-01R 1 5.0000E-01					
262	R 1 8.3000E-01R 1 7.8000E-01R 1 8.3000E-01R 1 9.5000E-01R 1 9.3000E-01							
263	R 2 1.0000E+00E							
264	R 2-1.0000E+00R 1-8.0000E-01R 2-6.0000E-01R 1-3.0000E-01R 1-4.4000E-01							
265	R 1-1.0000E-01R 1-2.3000E-01R 1 1.0000E-01R 1-5.0000E-02R 1 2.3000E-01							
266	R 1 3.9000E-01R 1 3.3000E-01R 1 4.0000E-01R 1 2.7000E-01R 1 6.2000E-01							
267	R 1 4.8000E-01R 1 9.0000E-01R 1 8.3000E-01R 2 1.0000E+00E							
268	-1.0000E+00	3.6100E+00	-9.0000E-01	3.4900E+00	-8.0000E-01			
269	3.8300E+00	-6.0000E-01	4.6200E+00	-5.0000E-01	4.6300E+00			
270	-4.0000E-01	4.2700E+00	-2.0000E-01	2.8200E+00	0.			
271	1.4500E+00	1.2000E-01	5.5000E-01	2.0000E-01	2.6000E-01			
272	4.0000E-01	2.5000E-01	9.0000E-01	2.2000E-01	1.0000E+00			
273	0.	E						
274	0.	-6.8000E-01	1.0000E-01	-5.8000E-01	2.0000E-01			
275	-5.1000E-01	3.0000E-01	-4.9000E-01	4.0000E-01	-4.8000E-01			

CARD	1	2	3	4	5	6	7	8
	1234567890123456789012345678901234567890123456789012345678901234567890123456789012345678901234567890							
276	6.0000E-01	-4.3000E-01	7.0000E-01	-3.7000E-01	8.0000E-01			
277	-2.6000E-01	9.0000E-01	-7.0000E-02	1.0000E+00	0.		E	
278	-1.0000E+00	3.6100E+00	-8.3000E-01	2.6000E+00	-7.0000E-01			
279	2.0300E+00	-6.5000E-01	1.8500E+00	-4.5000E-01	1.3700E+00			
280	-1.7000E-01	1.0500E+00	0.	8.3000E-01	2.0000E-01			
281	7.6000E-01	4.0000E-01	7.3000E-01	5.0000E-01	7.6000E-01			
282	6.0000E-01	8.8000E-01	7.8000E-01	1.3100E+00	9.5000E-01			
283	2.0800E+00	1.0000E+00	2.4600E+00E					
284	0.	2.4000E-01	3.9900E-01	8.2000E-01	4.0000E-01			
285	7.7000E-01	6.2000E-01	1.5800E+00	9.0000E-01	2.1800E+00			
286	1.0000E+00	2.4600E+00E						
287	R 1-1.0000E+00R 1 2.0000E+00R 1-8.0000E-01R 1 1.4000E+00R 1-7.0000E-01							
288	R 1 1.2000E+00R 1-6.0000E-01R 1 1.0300E+00R 1-4.0000E-01R 1 8.0000E-01							
289	R 1-2.0000E-01R 1 6.6000E-01R 1-1.0000E-01R 1 6.1000E-01R 1 0.							
290	R 1 6.0000E-01R 1 1.0000E-01R 1 6.1000E-01R 1 2.0000E-01R 1 6.3000E-01							
291	R 1 6.0000E-01R 1 8.3000E-01R 2 1.0000E+00E							
292	R 2-1.0000E+00R 1-3.0000E-01R 1-9.0000E-01R 1-2.0000E-01R 1-8.7000E-01							
293	R 1-1.0000E-01R 1-8.1000E-01R 1 0. R 1-6.8000E-01R 1 4.0000E-01							
294	R 1-2.7000E-01R 1 5.0000E-01R 1 1.5000E-01R 2 1.0000E+00E							
295	-1.0000E+00 2.0000E+00 -1.0000E-01 1.3500E+00 5.0000E-01							
296	8.3000E-01 1.0000E+00 3.4000E-01E							
297	R 2-1.0000E+00R 1-3.0000E-01R 1-9.0000E-01R 1-1.0000E-01R 1-5.2000E-01							
298	R 1 4.0000E-01R 1-2.7000E-01R 1 5.0000E-01R 1 0. R 1 1.0000E+00							
299	R 1 3.4000E-01E							
300	-1.0000E+00 0. 1.0000E+00 0. E							
301	-1.0000E+00 0. 1.0000E+00 0. E							
302	-1.0000E+00 0. 1.0000E+00 0. E							
303	-1.0000E+00 0. 1.0000E+00 0. E							
304	R 2 0. R 1 1.0000E-01R 1 0. R 1 1.5000E-01R 1 5.0000E-02							
305	R 1 2.4000E-01R 1 8.0000E-01R 1 3.0000E-01R 1 9.6000E-01R 1 4.0000E-01							
306	R 1 9.8000E-01R 1 6.0000E-01R 1 9.7000E-01R 1 8.0000E-01R 2 9.0000E-01							
307	R 1 8.0000E-01R 1 9.6000E-01R 1 5.0000E-01R 1 1.0000E+00R 1 0. E							
308	R 2 0. R 1 1.0000E-01R 1 0. R 1 1.5000E-01R 1 4.8000E-02							
309	R 1 2.2000E-01R 1 5.6400E-01R 1 8.0000E-01R 1 5.6400E-01R 1 9.6000E-01							
310	R 1 4.5400E-01R 1 1.0000E+00R 1 7.6000E-02E							

CARD	1	2	3	4	5	6	7	8
311	F	1.3521E+00E						
312	F	4.9555E-02E						
313	F	3.6613E-02E						
314	F	0.	E					
315	R 1	1.2380E-01R	2 0.	E				
316	F	2.1591E-01E						
317	F		4E					
318	F	0.	E					
319	F	0.	E					
320	F	5.5300E+02E						
321	F	5.5300E+02E						
322	F	1.5750E+07E						
323	F	0.	E					
324	F	5.5300E+02E						
325	TEE		8	0				
326		2	1	7 0.			0	
327		0	2	9	10		0	
328		1.079550E-01	2.835930E-02	0.	0.		2.950000E+02	
329		2.950000E+02						
330		0	1	8				
331		1.079550E-01	2.835930E-02	0.	0.		2.950000E+02	
332		2.950000E+02						
333		1.3081E+00	1.1176E+00E					
334		4.7856E-02	6.6308E-02E					
335	R 2	3.6613E-02R	1 6.3425E-02E					
336	F	0.	E					
337	F	0.	E					
338	R 2	2.1591E-01R	1 2.8417E-01E					
339	F		4E					
340	F	0.	E					
341	F	0.	E					
342	F	5.5300E+02E						
343	F	5.5300E+02E						
344	F	1.5750E+07E						
345	F	0.	E					

CARD	1	2	3	4	5	6	7	8
346	F	5.5300E+02E						
347	F	5.4292E-01E						
348	F	2.5439E-02E						
349	F	3.6613E-02E						
350	F	0.	E					
351	F	0.	E					
352	F	2.1591E-01E						
353	F		4E					
354	F	0.	E					
355	F	0.	E					
356	F	5.5300E+02E						
357	F	5.5300E+02E						
358	F	1.5750E+07E						
359	F	0.	E					
360	F	5.5300E+02E						
361	TEE		9		0			
362		2	1		7 0.			0
363		0	3		10	11		0
364		1.420870E-01	3.572600E-02	0.				2.950000E+02
365		2.950000E+02						
366		0	1		22			
367		4.366260E-02	1.348740E-02	0.				2.950000E+02
368		2.950000E+02						
369	R 1	1.1684E+00R	2 7.0874E-01E					
370	R 1	7.4191E-02R	2 4.4741E-02E					
371	F	6.3424E-02E						
372	F	0.	E					
373	F	0.	E					
374	F	2.8417E-01E						
375	F		4E					
376	F	0.	E					
377	F	0.	E					
378	F	5.5250E+02E						
379	F	5.5250E+02E						
380	F	1.5790E+07E						

CARD	1	2	3	4	5	6	7	8
381	F	0.	E					
382	F	5.5200E+02E						
383	F	1.5000E+00E						
384	F	8.9838E-03E						
385	F	5.9892E-03E						
386	F	0.	E					
387	F	0.	E					
388	F	8.7325E-02E						
389	F		4E					
390	F	0.	E					
391	F	0.	E					
392	F	5.5250E+02E						
393	F	5.5250E+02E						
394	F	1.5790E+07E						
395	F	0.	E					
396	F	5.5200E+02E						
397	TEE		16		0	BROKEN LOOP COLD LEG		
398		1	1	7		0.0		0
399		1	28	13		19		
400		9.588040E-02	1.599190E-01	0.	0.		2.950000E+02	
401		2.950000E+02						
402		0	1	77				
403		9.588040E-02	1.599190E-01	0.	0.		2.950000E+02	
404		2.950000E+02						
405	R 3	5.5837E-01R	1 1.2700E-01R	1 9.9255E-02R	1 7.4442E-02R	2 4.9628E-02		
406	R 2	2.4814E-02R	5 1.2700E-02R	2 2.5797E-02R	1 5.1594E-02R	1 7.7391E-02		
407	R 1	1.1839E-01R	1 1.8519E-01R	3 2.1606E-01R	1 2.0638E-01R	1 3.4608E-01		
408	R 1	4.6990E-01E						
409	R 3	3.5440E-02R	1 1.4797E-03R	1 9.3556E-04R	1 7.0167E-04R	2 4.6778E-04		
410	R 2	2.3389E-04R	6 1.0623E-04R	2 6.0674E-04R	1 1.2135E-03R	1 1.8202E-03		
411	R 1	2.2841E-03R	1 4.3557E-03R	3 5.0816E-03R	1 4.8539E-03R	1 1.7981E-02		
412	R 1	2.4414E-02E						
413	R 3	6.3425E-02R	1 1.3876E-02R	6 9.4258E-03R	6 8.3647E-03R	10 2.3520E-02		
414	R 3	5.1956E-02E						
415	R 1	0.	R 1 2.6719E+00R	1 4.4380E-02R	7 0.		R 7 1.6000E+00	

	1	2	3	4	5	6	7	8
CARD	1234567890123456789012345678901234567890123456789012345678901234567890							
416	R 8 0.	R 4 2.0000E-01E						
417	F 0.	E						
418	R 3 2.8400E-01R 1	1.3292E-01R 6	1.0955E-01R 6	1.0320E-01R 10	1.7305E-01			
419	R 3 2.5720E-01E							
420	F	4E						
421	F 0.	E						
422	F 0.	E						
423	R 4 5.5500E+02R 1	5.5429E+02R 1	5.5358E+02R 1	5.5288E+02R 1	5.5217E+02			
424	R 1 5.5146E+02R 1	5.5075E+02R 1	5.5004E+02R 1	5.4933E+02R 1	5.4863E+02			
425	R 1 5.4792E+02R 1	5.4721E+02R 1	5.4650E+02R 1	5.4579E+02R 1	5.4508E+02			
426	R 1 5.4438E+02R 1	5.4367E+02R 1	5.4296E+02R 1	5.4225E+02R 1	5.4154E+02			
427	R 1 5.4083E+02R 1	5.4013E+02R 1	5.3942E+02R 1	5.3871E+02R 1	5.3800E+02E			
428	R 4 5.5500E+02R 1	5.5429E+02R 1	5.5358E+02R 1	5.5288E+02R 1	5.5217E+02			
429	R 1 5.5146E+02R 1	5.5075E+02R 1	5.5004E+02R 1	5.4933E+02R 1	5.4863E+02			
430	R 1 5.4792E+02R 1	5.4721E+02R 1	5.4650E+02R 1	5.4579E+02R 1	5.4508E+02			
431	R 1 5.4438E+02R 1	5.4367E+02R 1	5.4296E+02R 1	5.4225E+02R 1	5.4154E+02			
432	R 1 5.4083E+02R 1	5.4013E+02R 1	5.3942E+02R 1	5.3871E+02R 1	5.3800E+02E			
433	F 1.5750E+07E							
434	F 0.	E						
435	R 3 5.5500E+02R 1	5.4350E+02R 1	5.4327E+02R 1	5.4304E+02R 1	5.4281E+02			
436	R 1 5.4258E+02R 1	5.4235E+02R 1	5.4212E+02R 1	5.4190E+02R 1	5.4167E+02			
437	R 1 5.4144E+02R 1	5.4121E+02R 1	5.4098E+02R 1	5.4075E+02R 1	5.4052E+02			
438	R 1 5.4029E+02R 1	5.4006E+02R 1	5.3983E+02R 1	5.3960E+02R 1	5.3937E+02			
439	R 1 5.3915E+02R 1	5.3892E+02R 1	5.3869E+02R 1	5.3846E+02R 1	5.3823E+02			
440	R 1 5.3800E+02E							
441	F 7.9845E+00E							
442	F 3.0980E-01E							
443	F 3.8800E-02E							
444	F 0.0000E+00E							
445	F 1.0000E+00E							
446	F 2.2230E-01E							
447	F	4E						
448	F 0.0000E+00E							
449	F 0.0000E+00E							
450	F 5.5500E+02E							

CARD	1	2	3	4	5	6	7	8
451	F	5.5500E+02E						
452	F	1.5750E+07E						
453	F	0.0000E+00E						
454	F	5.5500E+02E						
455	TEE		15		0	BROKEN LOOP HOT LEG		
456		1	1	7		0.0		0
457		1	41	12		18		
458		8.331790E-02	1.647900E-01	0.	0.		2.950000E+02	
459		2.950000E+02						
460		0	1	99				
461		8.331790E-02	1.647900E-01	0.	0.		2.950000E+02	
462		2.950000E+02						
463	R 3	5.5838E-01R 1	5.2578E-01R 1	4.6749E-01R 1	5.5861E-01R 1	1.9875E+00		
464	R 2	1.0772E+00R 1	1.9875E+00R 1	5.1029E-01R 1	5.4629E-01R 1	4.8628E-01		
465	R 1	2.5400E-01R 1	1.7145E-01R 1	3.0000E-01R 1	2.7940E-01R 2	2.1184E-01		
466	R 4	1.8717E-01R 2	1.4961E-01R 1	8.4138E-02R 1	5.6092E-02R 1	2.8046E-02		
467	R 6	1.2700E-02R 1	2.7164E-02R 1	5.4328E-02R 2	8.1492E-02R 3	1.9050E-01E		
468	R 3	3.5440E-02R 1	4.7280E-03R 1	3.7579E-03R 1	4.6603E-03R 1	1.9686E-01		
469	R 2	1.1383E-01R 1	1.9686E-01R 1	4.0728E-03R 1	4.0635E-03R 1	3.1715E-03		
470	R 1	2.7500E-02R 1	1.8500E-02R 1	1.8900E-02R 1	6.8606E-03R 2	1.7667E-03		
471	R 4	1.5674E-03R 2	1.2460E-03R 1	7.0379E-04R 1	4.6919E-04R 1	2.3460E-04		
472	R 6	1.0623E-04R 1	1.4113E-03R 1	2.8227E-03R 2	4.2340E-03R 3	9.8976E-03E		
473	R 3	6.3425E-02R 1	1.3913E-02R 3	8.3647E-03R 3	1.9141E-02R 3	8.3647E-03		
474	R 1	6.3425E-02R 2	9.4624E-03R 1	6.3425E-02R 18	8.3647E-03R 7	5.1956E-02E		
475	R 1	0.	R 4 2.6400E-01R 1	0.	R 1 7.7200E-03R 3	1.4000E-02		
476	R 1	1.9300E-02R 3	0.	R 1 1.4000E-01R 1	1.7000E-01R 1	1.1200E-01		
477	R 2	0.	R 1 4.3970E-02R 5	0.	R 1 4.3970E-02R 3	0.		
478	R 7	2.2000E+00R 6	0.	E				
479	R 5	0.	R 3 1.0000E+00R 1	0.	R 5-1.0000E+00R 5	0.		
480	R 5	1.0000E+00R 1	7.0711E-01R 17	0.	E			
481	R 3	2.8400E-01R 1	1.3300E-01R 3	1.0300E-01R 3	1.7500E-02R 3	1.0300E-01		
482	R 1	2.8400E-01R 2	1.1900E-02R 1	2.8400E-01R 18	1.0320E-01R 7	2.5770E-01E		
483	F		4E					
484	F	0.	E					
485	F	0.	E					

CARD		1	2	3	4	5	6	7	8	
486	R 1	5.6100E+02R	1	5.6033E+02R	1	5.5967E+02R	1	5.5900E+02R	1	5.5833E+02
487	R 1	5.5767E+02R	1	5.5700E+02R	1	5.5633E+02R	1	5.5567E+02R	1	5.5500E+02
488	R 1	5.5433E+02R	1	5.5367E+02R	1	5.5300E+02R	1	5.5233E+02R	1	5.5167E+02
489	R 2	5.5100E+02R	1	5.5067E+02R	1	5.5033E+02R	1	5.5000E+02R	1	5.4967E+02
490	R 1	5.4933E+02R	1	5.4900E+02R	1	5.4867E+02R	1	5.4833E+02R	1	5.4800E+02
491	R 1	5.4767E+02R	1	5.4733E+02R	1	5.4700E+02R	1	5.4667E+02R	1	5.4633E+02
492	R 1	5.4600E+02R	1	5.4567E+02R	1	5.4533E+02R	1	5.4500E+02R	1	5.4467E+02
493	R 1	5.4433E+02R	1	5.4400E+02R	1	5.4367E+02R	1	5.4333E+02R	1	5.4300E+02E
494	R 1	5.6100E+02R	1	5.6033E+02R	1	5.5967E+02R	1	5.5900E+02R	1	5.5833E+02
495	R 1	5.5767E+02R	1	5.5700E+02R	1	5.5633E+02R	1	5.5567E+02R	1	5.5500E+02
496	R 1	5.5433E+02R	1	5.5367E+02R	1	5.5300E+02R	1	5.5233E+02R	1	5.5167E+02
497	R 2	5.5100E+02R	1	5.5067E+02R	1	5.5033E+02R	1	5.5000E+02R	1	5.4967E+02
498	R 1	5.4933E+02R	1	5.4900E+02R	1	5.4867E+02R	1	5.4833E+02R	1	5.4800E+02
499	R 1	5.4767E+02R	1	5.4733E+02R	1	5.4700E+02R	1	5.4667E+02R	1	5.4633E+02
500	R 1	5.4600E+02R	1	5.4567E+02R	1	5.4533E+02R	1	5.4500E+02R	1	5.4467E+02
501	R 1	5.4433E+02R	1	5.4400E+02R	1	5.4367E+02R	1	5.4333E+02R	1	5.4300E+02E
502	F	1.5750E+07E								
503	F	0.	E							
504	R 1	5.6100E+02R	1	5.6033E+02R	1	5.5967E+02R	1	5.5900E+02R	1	5.5833E+02
505	R 1	5.5767E+02R	1	5.5700E+02R	1	5.5633E+02R	1	5.5567E+02R	1	5.5500E+02
506	R 1	5.5433E+02R	1	5.5367E+02R	1	5.5300E+02R	1	5.5233E+02R	1	5.5167E+02
507	R 2	5.5100E+02R	1	5.5067E+02R	1	5.5033E+02R	1	5.5000E+02R	1	5.4967E+02
508	R 1	5.4933E+02R	1	5.4900E+02R	1	5.4867E+02R	1	5.4833E+02R	1	5.4800E+02
509	R 1	5.4767E+02R	1	5.4733E+02R	1	5.4700E+02R	1	5.4667E+02R	1	5.4633E+02
510	R 1	5.4600E+02R	1	5.4567E+02R	1	5.4533E+02R	1	5.4500E+02R	1	5.4467E+02
511	R 1	5.4433E+02R	1	5.4400E+02R	1	5.4367E+02R	1	5.4333E+02R	1	5.4300E+02E
512	F	7.5464E+00E								
513	F	2.9280E-01E								
514	F	3.8800E-02E								
515	F	0.0000E+00E								
516	F	1.0000E+00E								
517	F	2.2230E-01E								
518	F		4E							
519	F	0.0000E+00E								
520	F	0.0000E+00E								

CARD	1	2	3	4	5	6	7	8
521	F	5.6100E+02E						
522	F	5.6100E+02E						
523	F	1.5750E+07E						
524	F	0.0000E+00E						
525	F	5.6100E+02E						
526	PRIZER		2		0			
527		3	2					
528	0.	0.		1.000000E+00	0.			
529		5.3073E-01	1.1500E+00	2.0000E-01E				
530		3.4000E-01	6.1000E-01	1.0000E-02E				
531	R 3	5.6526E-01R 1	5.7321E-03E					
532	R 3	0. R 1	4.6688E-03E					
533	F	-1.0000E+00E						
534	R 3	8.4836E-01R 1	8.5430E-02E					
535	F	4E						
536	R 1	1.0000E+00R 2	0. E					
537	F	0. E						
538	F	6.1900E+02E						
539	F	6.1900E+02E						
540	F	1.5500E+07E						
541	VALVE		18	0				
542		2	1	19		21		7
543		0	0					
544		1.286000E-01	2.778130E-02	0.	0.		2.950000E+02	
545		2.950000E+02						
546		4	2	2		0		2
547		5.273000E-02	9.525000E-02	0.				
548		1.5000E+00	2.0000E+00E					
549		7.7930E-02	1.1700E-01E					
550		5.1956E-02	5.2729E-02	5.8556E-02E				
551	F	5.0000E-02E						
552	F	0. E						
553		2.5720E-01	9.5250E-02	2.7305E-01E				
554	F	4E						
555		0.	1.0000E+00E					

	1	2	3	4	5	6	7	8
CARD	1234567890123456789012345678901234567890123456789012345678901234567890							
556	F	0.	E					
557		5.3800E+02	3.7300E+02E					
558		5.3800E+02	3.7300E+02E					
559		1.5500E+07	1.0100E+05E					
560	F	0.	E					
561		5.6100E+02	3.7300E+02E					
562		0.	1.0000E-05	1.7500E-02	1.0000E+00E			
563	VALVE		17	0				
564		2	1	18	20		7	
565		0	0					
566		1.286000E-01	2.778130E-02	0.	0.	2.950000E+02		
567		2.950000E+02						
568		4	2	2	0		2	
569		5.272920E-02	9.525000E-02	0.				
570		1.5000E+00	2.0000E+00E					
571		7.7930E-02	1.1700E-01E					
572		5.1956E-02	5.2729E-02	5.8556E-02E				
573	F	5.0000E-02E						
574	F	0.	E					
575		2.5720E-01	9.5250E-02	2.7305E-01E				
576	F	4E						
577		0.	1.0000E+00E					
578	F	0.	E					
579		5.4300E+02	3.7400E+02E					
580		5.4300E+02	3.7400E+02E					
581		1.5500E+07	1.0100E+05E					
582	F	0.	E					
583		5.8000E+02	3.7400E+02E					
584		0.	1.0000E-06	1.7500E-02	1.0000E+00E			
585	TEE		21	0	HPIS INJECTION TEE			
586		1	0	7	-1.000000E+00		0	
587		0	2	25	27		0	
588		4.366260E-02	3.487400E-03	0.	0.	2.950000E+02		
589		2.950000E+02						
590		0	2	23				

CARD	1	2	3	4	5	6	7	8
591	1.699260E-02	7.137400E-03	0.		0.		2.950000E+02	
592	2.950000E+02							
593	F 2.1844E+00E							
594	F 5.2331E-02E							
595	R 2 5.9890E-03R	1 5.5470E-02E						
596	F 4.5000E-01E							
597	F 0.	E						
598	R 2 8.7330E-02R	1 2.6360E-01E						
599	F	4E						
600	F 0.	E						
601	F 0.	E						
602	F 5.5244E+02E							
603	F 5.5244E+02E							
604	F 1.5600E+07E							
605	F 2.5000E+00E							
606	F 2.2678E-03E							
607	F 9.0713E-04E							
608	F 0.	E						
609	F 0.	E						
610	F 3.3985E-02E							
611	F	4E						
612	F 0.	E						
613	F 0.	E						
614	F 5.5244E+02E							
615	F 5.5244E+02E							
616	F 1.5600E+07E							
617	TEE		22		0 LPIS INJECTION TEE			
618		1	0		7 1.000000E+00		0	
619		1	1		25 22		0	
620	0.	0.	0.		0.	0.		
621	0.							
622		1	1		26			
623	0.	0.	0.		0.	0.		
624	0.							
625	F 1.0000E+00E							

		1	2	3	4	5	6	7	8
CARD		1234567890123456789012345678901234567890123456789012345678901234567890							
626	F	5.9890E-03E							
627	F	5.9890E-03E							
628	F	0.	E						
629	F	0.	E						
630	F	8.7330E-02E							
631	F		4E						
632	F	0.	E						
633	F	0.	E						
634	F	5.5240E+02E							
635	F	5.5240E+02E							
636	F	1.5600E+07E							
637	F	1.0000E+00E							
638	F	5.9890E-03E							
639	F	5.9890E-03E							
640	F	0.	E						
641	F	0.	E						
642	F	8.7330E-02E							
643	F		4E						
644	F	0.	E						
645	F	0.	E						
646	F	5.5240E+02E							
647	F	5.5240E+02E							
648	F	1.5600E+07E							
649	ACCUM			23		0			
650			3	24					
651		8.8633E-01	1.2886E+00		2.2500E-02E				
652		9.6000E-01	1.6760E+00		2.0000E-02E				
653	R 3	1.2460E+00R	1 3.2852E-02E						
654	F	4.5000E-01E							
655	F	-1.0000E+00E							
656	R 3	1.2595E+00R	1 2.0452E-01E						
657	F		4E						
658	R 1	1.0000E+00R	2 0.	E					
659	F	0.	E						
660	F	3.0080E+02E							

CARD	1	2	3	4	5	6	7	8
661	F	3.0080E+0E						
662	F	4.1100E+06E						
663	FILL		24		LPIS FILL			
664		26	3			13		
665		1.50	8.983810E-3	0.0	0.421345E0		0.297440E3	
666		4.24E6						
667		0.1	1.21	8.5E4	1.17		4.3E5	
668		1.02	7.7E5	0.840	9.47E5		0.730	
669		11.2E5	0.591	11.9E5	0.529		12.6E5	
670		0.449	13.3E5	0.361	13.9E5		0.255	
671		14.6E5	0.120	15.2E5	0.0		100.0E6	
672		0.000E						
673	FILL		25		HPIS FILL			
674		23	4	4		2		
675		2.50	0.226783E-2	0.0		0.0	0.297440E3	
676		4.24E6						
677		0.00E0	1.74	1.00E3	1.74	E		
678	VALVE		27	0				
679		2	0	27		24		7
680		0	0					
681		4.366260E-02	3.487400E-03	0.	0.		2.950000E+02	
682		2.950000E+02						
683		2	3000	0		0		2
684		5.989200E-02	8.732520E-01	0.				
685	F	1.0922E+00E						
686	F	2.6166E-02E						
687	R 2	5.5470E-02R	1 3.2852E-02E					
688	F	4.5000E-01E						
689	F	0.	E					
690	R 2	2.6360E-01R	1 2.0452E-01E					
691	F	4E						
692	F	0.	E					
693	F	0.	E					
694		5.5250E+02	3.0567E+02E					
695		5.5250E+02	3.0567E+02E					

	1				2				3				4				5				6				7				8			
CARD	1	2	3	4	1	2	3	4	1	2	3	4	1	2	3	4	1	2	3	4	1	2	3	4	1	2	3	4	1	2	3	4
696		1.5600E+07				4.2400E+06E																										
697	BREAK						20																									
698		21				1				8				3																		
699		1.0				.1			1.0				410.0											1.0E5								
700		0.0				1.05E5			1.0				2.0E5S																			
701		20.0				3.00E5			30.0				2.8E5S																			
702		50.0				2.80E5			70.0				3.5E5S																			
703		90.0				3.30E5			150.0				3.2E5E																			
704	BREAK						19																									
705		20				1			8				3																			
706		1.0				.1			1.0				410.0											1.0E5								
707		0.0				1.05E5			1.0				2.0E5S																			
708		20.0				3.00E5			30.0				2.8E5S																			
709		50.0				2.80E5			70.0				3.5E5S																			
710		90.0				3.30E5			150.0				3.2E5E																			
711	BREAK						14																									
712		80				0																										
713		1.00E0				1.00E0			1.00E0				5.59E2											60.00E5								
714	VALVE					50			0																							
715		2				0			15				80											0								
716		0				0																										
717	0.		0.				0.			0.				0.																		
718	0.																															
719		3				2			2				0											2								
720		1.820000E-02				1.500000E-01	0.																									
721	F	1.0000E+00E																														
722	F	1.8200E-02E																														
723	F	1.8200E-02E																														
724	F	0.				E																										
725	F	0.				E																										
726	F	1.5240E-01E																														
727	F					4E																										
728	F	9.2000E-01E																														
729	F	1.6800E+01E																														
730	F	5.5700E+02E																														

CARD		1	2	3	4	5	6	7	8
		12345678901234567890123456789012345678901234567890123456789012345678901234567890							
731	F	5.5700E+02E							
732	F	6.8240E+06E							
733		0.	1.0000E+00	1.0000E+01	0.	E			
734	FILL		13						
735		14							
736		1.00E0	1.00E0	0.0	1.07E-02	5.45E2			
737		6.36E6							
738	VESSEL		10						CARD 1
739		12	4	4	4				CARD 2
740		12	2	3	8			3	CARD 3
741		3							CARD 4
742					16				CARD 5
743		4.0E+00	5.0E+01	1.0E-03					CARD 6
744		7800.0	558.0	16.2	0.7	1.0E03			CARD 7
745		1.336	0.7						CARD 8
746		10	19	7	555				CARD 9
747		333	1	1	1			50	CARD 10
748		24.88E6							CARD 11
749		.632	.732	1.379	1.684	1.912	Z		
750		2.141	2.598	3.055	3.500	4.846	Z		
751		5.130	5.900E				Z		
752		0.105	0.231	0.329	0.470E		RADIUS		
753		1.571	3.142	4.712	6.283E		THETA		
754		11	15	3	11		SOURCE		
755		11	12	3	12		SOURCE		
756		11	13	3	13		SOURCE		
757		11	10	3	1		SOURCE		
758		0.955	0.960	0.965	0.975	0.990	RDPWR		
759		1.016	1.060R 3	0.000E			RDPWR		
760	R 4	1.4312R 4	1.1191R 4	0.7295E			CPOWR		
761		1	4	5	9E		IDROD		
762	R 2	1.0640R 1	1.1510R 1	0.5922E			RPKF		
763		0.652	1.227	1.504	1.516	0.912	ZPOWR		
764		0.178E					ZPOWR		
765	R 4	40.50R 4	152.7R 4	131.8E			RDX		

CARD	1	2	3	4	5	6	7	8
	1234567890123456789012345678901234567890123456789012345678901234567890							
766		0.0	7.7449E-4	1.5489E-3	2.3235E-3	3.0979E-3	RADRD	
767		3.8725E-3	4.64690E-3	4.74220E-3	5.0508E-3	5.3594E-3	RADRD	
768	R 6	1	3R 2	2E			MATRD	
769		0.0	24.80E6	0.1	1.736E6S		PWTB	
770		1.0	1.495E6	2.0	1.438E6S		PWTB	
771		5.0	1.339E6	10.0	1.240E6S		PWTB	
772		15.0	1.166E6	20.0	1.116E6S		PWTB	
773		50.0	9.424E5	75.0	8.680E5S		PWTB	
774		100.0	8.184E5	125.0	7.936E5S		PWTB	
775		150.0	7.688E5	200.0	7.192E5S		PWTB	
776		300.0	6.448E5	400.0	5.952E5S		PWTB	
777		500.0	5.456E5	600.0	5.208E5S		PWTB	
778		1000.0	4.464E5E				PWTB	
779	F	0E					NFAX	
780	F	0.0E					FPU02	
781	F	0.93E					FTD	
782		9.8101E-01	0.0000E+00	1.0103E-02	1.7830E-03	0.0000E+00	GMIX	
783		7.0991E-03	0.0000E+00S	S	S		GMIX	
784		9.8101E-01	0.0000E+00	1.0103E-02	1.7830E-03	0.0000E+00	GMIX	
785		7.0991E-03	0.0000E+00S	S	S		GMIX	
786		9.8101E-01	0.0000E+00	1.0103E-02	1.7830E-03	0.0000E+00	GMIX	
787		7.0991E-03	0.0000E+00S	S	S		GMIX	
788		9.8101E-01	0.0000E+00	1.0103E-02	1.7830E-03	0.0000E+00	GMIX	
789		7.0991E-03	0.0000E+00S	S	S		GMIX	
790		9.8101E-01	0.0000E+00	1.0103E-02	1.7830E-03	0.0000E+00	GMIX	
791		7.0991E-03	0.0000E+00S	S	S		GMIX	
792		9.8101E-01	0.0000E+00	1.0103E-02	1.7830E-03	0.0000E+00	GMIX	
793		7.0991E-03	0.0000E+00S	S	S		GMIX	
794		9.8101E-01	0.0000E+00	1.0103E-02	1.7830E-03	0.0000E+00	GMIX	
795		7.0991E-03	0.0000E+00S	S	S		GMIX	
796		9.8101E-01	0.0000E+00	1.0103E-02	1.7830E-03	0.0000E+00	GMIX	
797		7.0991E-03	0.0000E+00S	S	S		GMIX	
798		9.8101E-01	0.0000E+00	1.0103E-02	1.7830E-03	0.0000E+00	GMIX	
799		7.0991E-03	0.0000E+00S	S	S		GMIX	
800		9.8101E-01	0.0000E+00	1.0103E-02	1.7830E-03	0.0000E+00	GMIX	

CARD		1	2	3	4	5	6	7	8
		12345678901234567890123456789012345678901234567890123456789012345678901234567890							
801		7.0991E-03	0.0000E+00S		S		S		GMIX
802		9.8101E-01	0.0000E+00	1.0103E-02	1.7830E-03	0.0000E+00			GMIX
803		7.0991E-03	0.0000E+00S		S		S		GMIX
804		9.8101E-01	0.0000E+00	1.0103E-02	1.7830E-03	0.0000E+00			GMIX
805		7.0991E-03	0.0000E+00E						GMIX
806	F	1.0E							GMILES
807	F	3.13E5E							PGAPT
808	F	0.0E							PLVOL
809	F	0.0E							PSLEN
810	F	0.0E							CLENN
811	R 4	0.0087R 4	0.0333R 4	0.0431R 4	0.344E				LEVEL 1
812	R 4	1.36R 4	.519R 4	.672R 4	53.66E				
813	F	0.0E							
814	F	0.0E							
815	F	0.0E							
816	F	0.0E							
817	F	0.0E							
818	F	0.0E							
819	F	1.0E							
820	F	1.0E							
821	F	1.0E							
822	F	1.0E							
823	F	0.1E							
824	F	0.1E							
825	F	0.1E							
826	F	553.0E							
827	F	0.0E							
828	F	0.0E							
829	F	0.0E							
830	F	0.0E							
831	F	0.0E							
832	F	0.0E							
833	F	0.0E							
834	F	553.0E							
835	F	553.0E							

CARD		1	2	3	4	5	6	7	8
836	F	155.8E05E							
837	R12	0.0R 4	0.0956E					LEVEL 2	
838	R12	0.0R 4	1.491E						
839	F	.0E							
840	F	0.0E							
841	F	0.0E							
842	F	0.0E							
843	F	0.0E							
844	F	0.0E							
845	F	1.0E							
846	F	1.0E							
847	R12	.409R 4	.401E						
848	F	1.0E							
849	F	.1E							
850	F	.1E							
851	F	.1E							
852	F	553.0E							
853	F	0.0E							
854	F	0.0E							
855	F	0.0E							
856	F	0.0E							
857	F	0.0E							
858	F	0.0E							
859	F	0.0E							
860	F	553.0E							
861	F	553.0E							
862	F	155.8E05E							
863	R 4	0.1526R 4	0.5868R 4	0.7606R 4	0.9407E			LEVEL 3	
864	R 4	23.81R 4	91.54R 4	118.65R 4	146.75E				
865	F	0.0E							
866	F	0.0E							
867	F	0.0E							
868	F	0.0E							
869	F	0.0E							
870	F	0.0E							

CARD		1	2	3	4	5	6	7	8
		1234567890123456789012345678901234567890123456789012345678901234567890							
871	R12		.932R 4		0.375E				
872	R12		.9R 4		.362E				
873	R12		0.481R 4		.401E				
874	F		.9E						
875	R12		1.22E-2R 4		0.100E				
876	R12		1.22E-2R 4		0.100E				
877	R12		1.22E-2R 4		0.100E				
878	F		553.0E						
879	F		0.0E						
880	F		0.0E						
881	F		0.0E						
882	F		0.0E						
883	F		0.0E						
884	F		0.0E						
885	F		0.0E						
886	F		553.0E						
887	F		553.0E						
888	F		155.8E05E						
889	R12		0.0R 4		0.4435E				LEVEL 4
890	R12		0.0R 4		69.19E				
891	F		0.0E						
892	F		0.0E						
893	F		0.0E						
894	F		0.0E						
895	F		0.0E						
896	F		.0E						
897	R12		.518R 4		.375E				
898	R12		0.251R 4		.362E				
899	R12		0.481R 4		.401E				
900	F		.251E						
901	R12		1.22E-2R 4		0.100E				
902	R12		1.22E-2R 4		0.100E				
903	R12		1.22E-2R 4		0.100E				
904	F		553.0E						
905	F		0.0E						

		1	2	3	4	5	6	7	8
CARD		1234567890123456789012345678901234567890123456789012345678901234567890							
906	F		0.0E						
907	F		0.0E						
908	F		0.0E						
909	F		0.0E						
910	F		0.0E						
911	F		0.0E						
912	F		553.0E						
913	F		553.0E						
914	F	155.8E05E							
915	R12		0.0R 4	0.3315E				LEVEL 5	
916	R12		0.0R 4	51.71E					
917	F		0.0E						
918	F		0.0E						
919	F		0.0E						
920	F		0.0E						
921	F		0.0E						
922	F		.0E						
923	R12		.518R 4	.375E					
924	R12		0.251R 4	.362E					
925	R12		0.481R 4	.401E					
926	F		.251E						
927	R12		1.22E-2R 4	0.100E					
928	R12		1.22E-2R 4	0.100E					
929	R12		1.22E-2R 4	0.100E					
930	F		553.0E						
931	F		0.0E						
932	F		0.0E						
933	F		0.0E						
934	F		0.0E						
935	F		0.0E						
936	F		0.0E						
937	F		0.0E						
938	F		553.0E						
939	F		553.0E						
940	F	155.8E05E							

CARD		1	2	3	4	5	6	7	8
941	R12	.0R	4	0.3330E				LEVEL 6	
942	R12	0.0R	4	51.95E					
943	F	0.0E							
944	F	0.0E							
945	F	0.0E							
946	F	0.0E							
947	F	0.0E							
948	F	.0E							
949	R12	.518R	4	.375E					
950	R12	0.251R	4	.362E					
951	R12	0.481R	4	.401E					
952	F	.251E							
953	R12	1.22E-2R	4	0.100E					
954	R12	1.22E-2R	4	0.100E					
955	R12	1.22E-2R	4	0.100E					
956	F	553.0E							
957	F	0.0E							
958	F	0.0E							
959	F	0.0E							
960	F	0.0E							
961	F	0.0E							
962	F	0.0E							
963	F	0.0E							
964	F	553.0E							
965	F	553.0E							
966	F	155.8E05E							
967	R12	0.0R	4	0.6645E				LEVEL 7	
968	R12	0.0R	4	103.66E					
969	F	0.0E							
970	F	0.0E							
971	F	0.0E							
972	F	0.0E							
973	F	0.0E							
974	F	.0E							
975	R12	.518R	4	.375E					

CARD		1	2	3	4	5	6	7	8
976	R12	0.251R	4		.362E				
977	R12	0.481R	4		.401E				
978	F	.251E							
979	R12	1.22E-2R	4		0.100E				
980	R12	1.22E-2R	4		0.100E				
981	R12	1.22E-2R	4		0.100E				
982	F	553.0E							
983	F	0.0E							
984	F	0.0E							
985	F	0.0E							
986	F	0.0E							
987	F	0.0E							
988	F	0.0E							
989	F	0.0E							
990	F	553.0E							
991	F	553.0E							
992	F	155.8E05E							
993	R12	0.0R	4		0.6645E				LEVEL 8
994	R12	0.0R	4		103.66E				
995	F	0.0E							
996	F	0.0E							
997	F	0.0E							
998	F	0.0E							
999	F	0.0E							
1000	F	.0E							
1001	R12	.518R	4		.375E				
1002	R12	0.251R	4		.362E				
1003	R12	0.481R	4		.401E				
1004	F	.251E							
1005	R12	1.22E-2R	4		0.100E				
1006	R12	1.22E-2R	4		0.100E				
1007	R12	1.22E-2R	4		0.100E				
1008	F	553.0E							
1009	F	0.0E							
1010	F	0.0E							

CARD		1	2	3	4	5	6	7	8
		1234567890123456789012345678901234567890123456789012345678901234567890							
1011	F	0.0E							
1012	F	0.0E							
1013	F	0.0E							
1014	F	0.0E							
1015	F	0.0E							
1016	F	553.0E							
1017	F	553.0E							
1018	F	155.8E05E							
1019	R 4	0.7208R 4	2.7708R 4	3.5916R 4	1.2243E			LEVEL 9	
1020	R 4	24.76R 4	95.12R 4	123.31R 4	190.99E				
1021	F	0.0E							
1022	R 4	0.0R 4	1.2R 4	0.5R 4	0.0E				
1023	F	0.0E							
1024	F	0.0E							
1025	R 4	0.0R 4	1.2R 4	0.5R 4	0.0E				
1026	F	0.0E							
1027	R12	0.951R 4	.375E						
1028	R12	0.366R 4	.362E						
1029	R 4	0.85R 8	0.366R 4	0.4010E					
1030	F	0.3660E							
1031	R12	1.22E-2R 4	0.100E						
1032	R12	1.22E-2R 4	0.100E						
1033	R12	1.22E-2R 4	0.100E						
1034	F	553.0E							
1035	F	0.0E							
1036	F	0.0E							
1037	F	0.0E							
1038	F	0.0E							
1039	F	0.0E							
1040	F	0.0E							
1041	F	0.0E							
1042	F	553.0E							
1043	F	553.0E							
1044	F	155.8E05E							
1045	R 4	0.6641R 4	2.5528R 4	3.3090R 4	1.2228E			LEVEL 10	

CARD		1	2	3	4	5	6	7	8
		1234567890123456789012345678901234567890123456789012345678901234567890							
1046	R 4	15.99R 4	61.50R 4	79.71R 4	190.76E				
1047	F	0.0E							
1048	F	0.0E							
1049	F	0.0E							
1050	F	0.0E							
1051	F	0.0E							
1052	F	0.0E							
1053	R12	0.951R 4	.375E						
1054	R 4	1.0R 8	0.0R 4	.3620E					
1055	R 4	0.85R 4	0.0R 4	.250R 4	.401E				
1056	F	0.0000E							
1057	R12	1.22E-2R 4	0.100E						
1058	R12	1.22E-2R 4	0.100E						
1059	R12	1.22E-2R 4	0.100E						
1060	F	580.0E							
1061	F	0.0E							
1062	F	0.0E							
1063	F	0.0E							
1064	F	0.0E							
1065	F	0.0E							
1066	F	0.0E							
1067	F	0.0E							
1068	F	580.0E							
1069	F	580.0E							
1070	F	155.8E05E							
1071	R 4	.3948R 4	1.5176R 4	1.9672R 4	1.6500E			LEVEL 11	
1072	R 4	9.51R 4	36.56R 4	47.39R 4	257.40E				
1073	F	0.0E							
1074	F	0.0E							
1075	F	0.0E							
1076	F	0.0E							
1077	F	0.0E							
1078	F	0.0E							
1079	R12	0.951R 4	1.25E						
1080	R12	0.366R 4	.362E						

CARD	1	2	3	4	5	6	7	8
	1234567890123456789012345678901234567890123456789012345678901234567890							
1081	R12	0.365R 4	.000E					
1082	F	0.3660E						
1083	R12	1.22E-2R 4	0.100E					
1084	R12	1.22E-2R 4	0.100E					
1085	R12	1.22E-2R 4	0.100E					
1086	F	553.0E						
1087	F	0.0E						
1088	F	0.0E						
1089	F	0.0E						
1090	F	0.0E						
1091	F	0.0E						
1092	F	0.0E						
1093	F	0.0E						
1094	F	553.0E						
1095	F	553.0E						
1096	F	155.8E05E						
1097	R 4	0.5227R 4	2.0093R 4	2.6046R 4	0.0E			LEVEL 12
1098	R 4	12.59R 4	48.40R 4	62.74R 4	0.0E			
1099	F	0.0E						
1100	F	0.0E						
1101	F	0.0E						
1102	F	0.0E						
1103	F	0.0E						
1104	F	0.0E						
1105	R12	0.951R 4	.000E					
1106	R12	0.366R 4	.362E					
1107	R12	0.365R 4	.401E					
1108	F	0.3660E						
1109	R12	1.22E-2R 4	0.100E					
1110	R12	1.22E-2R 4	0.100E					
1111	R12	1.22E-2R 4	0.100E					
1112	F	553.0E						
1113	F	0.0E						
1114	F	0.0E						
1115	F	0.0E						

CARD	1	2	3	4	5	6	7	8
	1234567890123456789012345678901234567890123456789012345678901234567890							
1116	F	0.0E						
1117	F	0.0E						
1118	F	0.0E						
1119	F	0.0E						
1120	F	553.0E						
1121	F	553.0E						
1122	F	155.8E05E						
1123	F	0.0	E					ROD 1
1124	F	553.0	E					ROD 1
1125	F	0.0	E					ROD 2
1126	F	553.0	E					ROD 2
1127	F	0.0	E					ROD 3
1128	F	553.0	E					ROD 3
1129	F	0.0	E					ROD 4
1130	F	553.0	E					ROD 4
1131	F	0.0	E					ROD 5
1132	F	553.0	E					ROD 5
1133	F	0.0	E					ROD 6
1134	F	553.0	E					ROD 6
1135	F	0.0	E					ROD 7
1136	F	553.0	E					ROD 7
1137	F	0.0	E					ROD 8
1138	F	553.0	E					ROD 8
1139	F	0.0	E					ROD 9
1140	F	553.0	E					ROD 9
1141	F	0.0	E					ROD 10
1142	F	553.0	E					ROD 10
1143	F	0.0	E					ROD 11
1144	F	553.0	E					ROD 11
1145	F	0.0	E					ROD 12
1146	F	553.0	E					ROD 12
1147	F	0.0	E					ROD 13
1148	F	553.0	E					ROD 13
1149	F	0.0	E					ROD 14
1150	F	553.0	E					ROD 14

II. TRAC TRANSIENT INPUT DECK INCLUDING THE BLOWDOWN, REFILL, AND REFLOOD
FOR LOFT EXPERIMENT L2-2

CARD	1	2	3	4	5	6	7	8
1	1234567890123456789012345678901234567890123456789012345678901234567890							
2		2		1				
3		LOFT TEST L2-2 TRANSIENT						
4		ILOEGE TMIN CORRELATION						
5		-1 0.						
6		0	1	27	28		1	
7		1.00000E-03	5.00000E-06	1.00000E-04	0.00000E+00			
8		10	100	20	7		1	
9		1	2	3	4		5	
10		6	7	8	9		10	
11		13	14	15	16		17	
12		18	19	20	21		22	
13		23	24	25	27		50	
14		77	99E					
15		333E						
16		-1						
17		END						
18		1.0E-5	0.005	1.0				
19		5.0	0.01	5.0	5.0			
20		1.0E-5	0.005	10.0				
21		5.0	0.10	5.0	5.0			
22		1.0E-5	0.020	100.0				
23		5.0	0.10	5.0	5.0			
24		-1.						

12055078977 I LAN184
US NRC
ADM-DIV OF TIDC
POLICY & PUB MGT HR-PDR NUREG
8-561
WASHINGTON DC 20555

Los Alamos

Available from

GPO Sales Program
Division of Technical Information and Document Control
US Nuclear Regulatory Commission
Washington, DC 20555

and

National Technical Information Service
Springfield, VA 22161